MONASH UNIVERSITY
THESIS ACCEPTED IN SATISFACTION OF THE
REQUIREMENTS FOR THE DEGREE OF
DOCTOR OF PHILOSOPHY
ON..... 2 December 2003 .....
.....[redacted].....
Sec. Research Graduate School Committee

Free Space Permittivity and Permeability Measurements at Microwave Frequencies

by

Andrew Amiet B.Sc. (Hons.)

A thesis submitted for the degree of Doctor of Philosophy in the Department of Electrical and Computer Systems Engineering, Monash University, Clayton, Australia

Submitted April 2003

Reprinted with amendments November 2003

To the best of my knowledge, this dissertation contains no material previously published or written by another person, except where due reference has been made in the text. I certify that none of the original material reported here has been accepted for the award of any other degree or diploma in any university or institution.

Andrew Amiet

Acknowledgments

I have many people to thank for their help in the completion of this thesis. In particular, my supervisor at DSTO Dr. Peter Jewsbury who was instrumental in getting the project started, providing key advice in the direction of the research and helping me understand the topic more fully. I appreciate all his support.

I would also like to thank Dr. John Bennett who was my supervisor at Monash for the first few years and helped guide the research in its early stages. Special thanks also to Dr. Greg Cambrell who took over from Dr. Bennett, and forced me to be much more careful with my notation of the various vectors fields, and for chasing down the problems with the sign conventions adopted in the thesis. He also spent a lot of time proof reading the thesis – even the more tedious parts; and as a result, this document is a vast improvement on earlier efforts.

Thanks to my friends and who took an interest in this work, and for not being too unkind as to the length of time the project was taking.

My family have been extremely loving and supportive not only during the production of this thesis, but throughout my entire life. I would like to thank them for encouraging my life in the science and (cough) engineering fields.

Finally, my sincere thanks goes to my wife, Sharon, for allowing me to share her life with her. Her love has been a real tower of strength to me as I undertook and finally completed this research.

Summary

In the early 1990s, the Australian Department of Defence called upon its Science and Technology Organisation (DSTO) to set a program in motion to generate an Australian capability for producing radar absorbing materials (RAM). At the time the Materials Division at DSTO had some measurement facilities that could be utilised for this task, but interest in a full scale production, test and measurement facility was low. Nevertheless, with high level backing from the armed services the first steps were taken to investigate the possibilities for research into RAM.

Early materials testing involved the use of a Hewlett-Packard Vector Network Analyser system with candidate materials being cut out and placed into rectangular or coaxial waveguides. Very early it became apparent that this technique was not always the most appropriate or accurate for some materials. Due to the size of the samples, the degree of inhomogeneity and physical properties of likely absorbing materials, the standard method of cutting out very small specimens and placing them in transmission lines was found to be unsuitable. Other methods for testing the electromagnetic properties of the materials needed to be found, so that high performance RAM could be produced.

Due to the large size of the materials and the nature of the absorbing ingredients, it was decided that a measurement in free space using microwave horns would be a better way of determining the permittivity and permeability at microwave frequencies. The free space techniques introduced their own unique errors to the testing process, and these needed to be fully investigated so that the resulting material properties could be accurately extracted.

The measurement procedure involves sampling the reflection and/or transmission components from a microwave source. Conversion of these measured signals into the material's permittivity and/or permeability is performed using a series of novel extraction algorithms. Existing techniques use measured values from both reflection and transmission components; however, these have been extended to give permittivity results for non-magnetic materials from measurements of just one of the components. Furthermore, the standard extraction method is improved by the addition of user-defined mathematical adjustments to the data.

The first chapter in the thesis gives some of the important background theory and formulations, while chapters 2 and 3 describe in more detail the specific aspects of the measurement processes and details of the materials to be tested. In these chapters, the single

parameter (permittivity) extraction algorithms are described and the time domain conversion and gating processes are outlined. Various methods for improving the measurement process are also explained in these chapters, with examples given using invented perfect data.

Chapter 4 introduces the computer programs written specifically for extracting the material properties using the newly constructed algorithms. Computers are an integral part of the measurement process, since they are used to set up and calibrate the equipment, to collect the measured data and to apply any relevant corrections before finally converting the data to the permittivity and/or permeability values.

The data measured using the free space techniques are presented in Chapters 5 to 7. Due to the overwhelming amount of data collected, the results were broken up into smaller sections depending upon the form of the sample tested. Chapter 5 gives the results for the free space testing of the large 445 mm square samples, Chapter 6 presents the intermediate 305 mm square specimens and Chapter 7 is concerned with the small 150 mm square samples. Many of the findings concerning the large samples directly affect the testing procedures of the smaller ones.

Chapters 8 and 9 present results using standard techniques and compares them with the free space techniques. Chapter 9 in particular gives examples of the types of errors one frequently encounters when testing some styles of materials of particular interest to Defence.

Chapter 10 introduces a number of "one-off" measurements that do not fit into the systematic testing procedures of the earlier chapters. Chapter 11 presents an analysis of the measurement techniques, and ties together all the results to form a cohesive picture of the improvements that have been achieved using the various methods outlined in the thesis.

This thesis presents some of the errors associated with the measurement of the electromagnetic properties of materials together with their resolution, so that the accuracy of the techniques may be improved. The effect of diffraction around the specimen was found to be a major source of inaccuracy when measuring the material properties, and techniques were developed to reduce its effects. The removal process developed was very successful, and allowed meaningful results to be extracted even when the error signal was of equal magnitude to that of the specimen.

Abstract

The determination of permittivity and permeability of condensed materials at microwave frequencies using free space techniques has been thoroughly investigated and shown to be superior to standard techniques. It has been shown that often the new techniques developed are not only easier to use, but also provide greater accuracy than the standard techniques normally employed. By investigating the many sources of error that arise from the free space reflection and transmission technique described here, a series of rules has been developed in order to obtain maximum precision for the extracted electromagnetic parameters.

It has been shown that the size of the material under test (MUT) is usually the most important factor for obtaining an accurate determination of the electric and magnetic RF properties of the specimen. When the transmission through the specimen is measured, the signal is typically contaminated by the diffracted wave that travels around the specimen. Using the techniques described in this thesis, the effects from this diffraction signal can be effectively removed even when it is of similar strength to the desired signal.

Novel permittivity extraction algorithms have been developed for single parameter measurements using transmission, reflection or backed reflection techniques. By using computer codes developed by the author, accurate values of the permittivity of the MUT can be obtained in a timely manner.

Errors in property extraction caused by sample thickness inaccuracy, inhomogeneity and position have been investigated, with solutions presented to minimise their effect. Measuring in the near field of the antennas has been shown to have a negligible effect, negating the requirement for lenses or reflecting elements to reduce sphericity of the incident beam.

Chapter 1. Introduction

In this chapter, the basic definitions and relationships between electromagnetic waves and materials will be presented. While a full derivation of the appropriate equations and their consequences is not required as part of this thesis, it is nonetheless useful to introduce a brief overview of the relevant theory and how it relates to the problem at hand.

1.1. Electromagnetic waves

When electromagnetic waves strike the surface of an object, the electronic state of the material is perturbed. The field causes movement in each individual electric charge, moving it slightly from its initial configuration. This movement causes polarisation of the entire region to take place and sets up an electric and sometimes a magnetic field in opposition to the applied field. Either this internal field can repel the applied field from entering the material almost completely, or it can allow the field to pass through the material with almost no loss. Most materials fall somewhere between these two extremes, and material-specific parameters have been devised so as to give an indication of how the material will respond to an applied electromagnetic field. To describe these quantities we need to first introduce the theory of electromagnetic wave propagation.

If we assume the electromagnetic field is time harmonic with the variation represented by $e^{i\omega t}$, Maxwell's equations[1] (shown below) describe how the electric and magnetic fields behave in time and space.

$$\nabla \times \mathbf{E} = -\mathbf{K}_i - i\omega\mathbf{B} \qquad \text{Equation 1-1}$$

$$\nabla \times \mathbf{H} = \mathbf{J}_i + \mathbf{J}_c + i\omega\mathbf{D} \qquad \text{Equation 1-2}$$

$$\nabla \cdot \mathbf{D} = q_{ev} \qquad \text{Equation 1-3}$$

$$\nabla \cdot \mathbf{B} = q_{mv} \qquad \text{Equation 1-4}$$

where ∇ is the gradient operator, defined in cartesian coordinates as

$$\nabla = \mathbf{i}\frac{\partial}{\partial x} + \mathbf{j}\frac{\partial}{\partial y} + \mathbf{k}\frac{\partial}{\partial z}, \qquad \text{Equation 1-5}$$

and **E** is the electric field intensity [V/m], **D** is the electric flux density [C/m^2], **H** is the magnetic field intensity [A/m], **B** is the magnetic flux density [Wb/m^2] or [T], $\mathbf{J}_i$ is the impressed (source) electric current density [A/m^2], $\mathbf{J}_c$ is the conduction electric current density [A/m^2], $\mathbf{K}_i$ is the impressed magnetic current density [V/m^2], q_{ev} is the electric charge density [C/m^3], q_{mv} is the magnetic charge density [Wb/m^3], and ω is the angular frequency equal to 2π times the frequency [Hz]. Boldface letters indicate vectors. The concepts of magnetic charge and current density were introduced to balance the equations, and although not physically realisable, they are useful for describing various situations, such as the magnetic fields induced in an iron core by an applied alternating voltage source.

The response from a material subject to an electromagnetic field is characterised by its complex constitutive parameters[1]: conductivity (associated with static fields on free charges) σ_s, permittivity (associated with alternating fields on bound charges) ε_a, and permeability μ. In general, these values can change depending upon field strength and direction, position and frequency of the applied field.

Materials whose parameters are not functions of the applied field are called linear. Many materials exhibit almost linear behaviour up to a certain field strength, after which non-linear behaviour is observed. An example of this is the dielectric breakdown of air above electric field strengths of about 1 MV/m – below this value air is very close to linear, but above it air is very non-linear.

Homogeneous materials have values that are independent of position; otherwise, they are known as inhomogeneous. Almost all materials are inhomogeneous to some degree but, in most cases, the level of inhomogeneity is small enough to be ignored.

If the response of a material is independent of the direction of the applied field, it is known as isotropic. Materials such as crystals can exhibit a high degree of anisotropy, resulting in property values that are not a single number, but a three-dimensional dyadic (or sometimes inaccurately referred to as a tensor).

The properties of nearly all materials are frequency dependent, commonly known as dispersive. The permittivities and conductivities of dielectric materials and the permeabilities of magnetic materials are usually dispersive to some degree.

For homogeneous isotropic materials the constitutive parameters can be expressed as a single complex number at a given frequency, and relate the electric and magnetic fields by the equations:

$$\mathbf{D} = \varepsilon_a \mathbf{E} = \varepsilon_0 \mathbf{E} + \mathbf{P} \qquad \text{Equation 1-6}$$

$$\mathbf{B} = \mu \mathbf{H} = \mu_0 (\mathbf{H} + \mathbf{M}) \qquad \text{Equation 1-7}$$

$$\mathbf{J}_c = \sigma_s \mathbf{E} \qquad \text{Equation 1-8}$$

where ε_a is the medium's complex alternating field permittivity [Farads/m], ε_0 is the permittivity of free space, μ is the medium's complex permeability [Henries/m], μ_0 is the permeability of free space, σ_s is the static conductivity [Siemens/m], **P** is called the electric polarisation vector [C/m^2], and **M** is known as the magnetic polarisation (magnetisation) vector [A/m].

Using Equation 1-6 we can rearrange Equation 1-2 to form

$$\begin{aligned} \nabla \times \mathbf{H} &= \mathbf{J}_i + \mathbf{J}_c + i\omega\varepsilon_a \mathbf{E} \\ &= \mathbf{J}_i + \sigma_s \mathbf{E} + i\omega(\varepsilon'_a + i\varepsilon''_a)\mathbf{E} \\ &= \mathbf{J}_i + (\sigma_s - \omega\varepsilon''_a)\mathbf{E} + i\omega\varepsilon'_a \mathbf{E} \\ &= \mathbf{J}_i + i\omega\varepsilon_e \mathbf{E} \end{aligned} \qquad \text{Equation 1-9}$$

where the complex permittivity ε_a has been broken up into its real (ε'_a) and imaginary (ε''_a) components. The real and imaginary components of the effective complex permittivity ε_e are found by

$$\begin{aligned} i\omega(\varepsilon'_e + i\varepsilon''_e) &= \sigma_s - \omega\varepsilon''_a + i\omega\varepsilon'_a \\ i\omega\varepsilon'_e - \omega\varepsilon''_e &= \sigma_s - \omega\varepsilon''_a + i\omega\varepsilon'_a \\ \varepsilon'_e = \varepsilon'_a \;\; ; \;\; \varepsilon''_e &= -\frac{\sigma_s}{\omega} + \varepsilon''_a \end{aligned} \qquad \text{Equation 1-10}$$

Note that the sign convention adopted gives positive real and negative imaginary components for permittivity (and permeability). The solutions to Maxwell's equations for any given field are in the form of a second order partial differential equation, usually referred to as the reduced wave equation. In an electromagnetic source free region ($\mathbf{J}_i = q_{ev} = 0$ and $\mathbf{K}_i = q_{mv} = 0$), Maxwell's equations can be expressed as

$$\nabla \times \mathbf{E} = -i\omega\mathbf{B} \qquad \text{Equation 1-11}$$

$$\nabla \times \mathbf{H} = \mathbf{J}_c + i\omega\mathbf{D} \qquad \text{Equation 1-12}$$

$$\nabla \cdot \mathbf{D} = 0 \qquad \text{Equation 1-13}$$

$$\nabla \cdot \mathbf{B} = 0 \qquad \text{Equation 1-14}$$

Taking the curl of Equation 1-11 and using Equations 1-7 and 1-9 gives

$$\nabla \times (\nabla \times \mathbf{E}) = -i\omega\nabla \times (\mu \mathbf{H})$$

$$\nabla(\nabla \cdot \mathbf{E}) - \nabla^2 \mathbf{E} = -i\omega\mu\nabla \times \mathbf{H}$$

$$\frac{1}{\varepsilon_a}\nabla\left(\nabla \cdot \mathbf{D}\right) - \nabla^2 \mathbf{E} = -i\omega\mu\,(i\omega\varepsilon_e \mathbf{E}) \qquad \text{Equation 1-15}$$

$$(0) + \nabla^2 \mathbf{E} = -\omega^2 \mu\varepsilon_e \mathbf{E} = \gamma^2 \mathbf{E}$$

assuming homogeneous media. Similarly, it can be shown that

$$\nabla^2 \mathbf{H} = -\omega^2 \mu\varepsilon_e \mathbf{H} = \gamma^2 \mathbf{H} \qquad \text{Equation 1-16}$$

where $$\gamma^2 = -\omega^2 \varepsilon_e \mu \qquad \text{Equation 1-17}$$

remembering that ε_e is the effective (total) complex permittivity which includes the static conductivity component, and the permeability μ is also complex. The plane wave solution to the reduced wave equation is

$$\mathbf{F} = \mathbf{F}_0 e^{i\omega t - \gamma z} \qquad \text{Equation 1-18}$$

where $\mathbf{F}_0$ is a constant complex vector. The propagation constant γ is usually broken up into its real and imaginary components

$$\gamma = \alpha + i\beta \qquad \text{Equation 1-19}$$

where α is known as the attenuation constant [Np/m] and β is the phase constant [rad/m].

To determine the values of these constants for a material exhibiting both electric and magnetic losses (such as ferrites), we expand the complex permittivity and permeability into their real and imaginary parts.

$$\begin{aligned}\gamma^2 &= -\omega^2(\varepsilon'_e + i\varepsilon''_e)(\mu' + i\mu'') \\ &= -\omega^2(\varepsilon'_e \mu' - \varepsilon''_e \mu'') - i\omega^2(\varepsilon'_e \mu'' + \varepsilon''_e \mu') \\ \gamma &= \sqrt{-\omega^2(\varepsilon'_e \mu' - \varepsilon''_e \mu'') - i\omega^2(\varepsilon'_e \mu'' + \varepsilon''_e \mu')} \\ &= \alpha + i\beta\end{aligned} \qquad \text{Equation 1-20}$$

In order to obtain the square root of a complex number $A + iB$ we write $\sqrt{A+iB} = a + ib$, where

$$a = \pm\frac{1}{\sqrt{2}}\sqrt{A + \sqrt{A^2 + B^2}}, \quad b = \pm\frac{1}{\sqrt{2}}\sqrt{-A + \sqrt{A^2 + B^2}} \qquad \text{Equation 1-21}$$

Using Equation 1-20, for our purposes $A = -\omega^2(\varepsilon'_e \mu' - \varepsilon''_e \mu'')$, $B = -\omega^2(\varepsilon'_e \mu'' + \varepsilon''_e \mu')$ and assuming positive a and b, we substitute into the above equations to find a and b (and hence α and β).

$$\begin{aligned}\alpha = a &= \frac{1}{\sqrt{2}}\sqrt{A + \sqrt{A^2 + B^2}} \\ &= \frac{1}{\sqrt{2}}\sqrt{-\omega^2(\varepsilon'_e \mu' - \varepsilon''_e \mu'') + \sqrt{(-\omega^2(\varepsilon'_e \mu' - \varepsilon''_e \mu''))^2 + (-\omega^2(\varepsilon'_e \mu'' + \varepsilon''_e \mu'))^2}} \\ &= \frac{1}{\sqrt{2}}\omega\sqrt{-(\varepsilon'_e \mu' - \varepsilon''_e \mu'') + \sqrt{\left(\varepsilon'^2_e + \varepsilon''^2_e\right)\left(\mu'^2 + \mu''^2\right)}} \\ &= \frac{1}{\sqrt{2}}\omega\sqrt{-\varepsilon'_e \mu'\left(1 - \frac{\varepsilon''_e}{\varepsilon'_e}\frac{\mu''}{\mu'}\right) + \varepsilon'_e \mu'\sqrt{\left(1 + \left(\frac{\varepsilon''_e}{\varepsilon'_e}\right)^2\right)\left(1 + \left(\frac{\mu''}{\mu'}\right)^2\right)}} \\ &= \omega\sqrt{\frac{\varepsilon'_e \mu'}{2}}\sqrt{-\left(1 - \frac{\varepsilon''_e}{\varepsilon'_e}\frac{\mu''}{\mu'}\right) + \sqrt{\left(1 + \left(\frac{\varepsilon''_e}{\varepsilon'_e}\right)^2\right)\left(1 + \left(\frac{\mu''}{\mu'}\right)^2\right)}}\end{aligned} \qquad \text{Equation 1-22}$$

Similarly

$$\beta = b = \omega\sqrt{\frac{\varepsilon'_e \mu'}{2}}\sqrt{\left(1 - \frac{\varepsilon''_e}{\varepsilon'_e}\frac{\mu''}{\mu'}\right) + \sqrt{\left(1 + \left(\frac{\varepsilon''_e}{\varepsilon'_e}\right)^2\right)\left(1 + \left(\frac{\mu''}{\mu'}\right)^2\right)}} \qquad \text{Equation 1-23}$$

In the case of lossless materials ($\varepsilon''_e = \mu'' = 0$), the attenuation constant $\alpha = 0$, and the phase constant β (often represented by the factor k) becomes

$$\beta = k \equiv \omega\sqrt{\varepsilon'_e \mu'} \qquad \text{Equation 1-24}$$

The ratio of the negative imaginary to the (positive) real component of the permittivity is a dimensionless quantity called the electric loss tangent.

$$\tan\delta_e = -\frac{\varepsilon''_e}{\varepsilon'_e} \qquad \text{Equation 1-25}$$

In magnetic materials, the ratio of the negative imaginary to the real component of the permeability is called the magnetic loss tangent (or tan δ_m). Since the effective permittivity is used exclusively from this point on, the subscript will be dropped to reduce clutter.

The values of ε_0 and μ_0 in free space have been calculated using the convention that the speed of light (c) is fixed at 2.99792458 x 10^8 m/s. In the case of wave transmission in free space, it can be shown[1] that the velocity (v) of the wave is

$$v = \frac{\omega}{\beta} = \frac{\omega}{\omega\sqrt{\varepsilon_0 \mu_0}} \qquad \text{Equation 1-26}$$

$$c = \frac{1}{\sqrt{\varepsilon_0 \mu_0}}$$

where the permeability of free space is defined as

$$\mu_0 = 4\pi \times 10^{-7}\ \text{H/m} \qquad \text{Equation 1-27}$$

and so the permittivity of free space is approximately

$$\varepsilon_0 = 8.854188 \times 10^{-12}\ \text{F/m}. \qquad \text{Equation 1-28}$$

To avoid working with very small numbers, the permittivity and permeability of materials are usually expressed relative to those of free space, shown in the equations below

$$\varepsilon_r = \frac{\varepsilon}{\varepsilon_0} \qquad \text{Equation 1-29}$$

$$\mu_r = \frac{\mu}{\mu_0} \qquad \text{Equation 1-30}$$

where ε_r is the relative permittivity, and μ_r is the relative permeability. Material properties are sometimes also expressed in terms of the wave impedance (Z) where

$$Z = \sqrt{\frac{\mu}{\varepsilon}} \qquad \text{Equation 1-31}$$

Using the values in equations 1-27 and 1-28, we find that the wave impedance of free space (Z_0) is approximately 376.7 ohms.

1.2. Material properties

For homogeneous isotropic materials, the permittivity and permeability can be expressed as a single complex number at a particular frequency. The real component gives a measure of how strongly the material interacts with the applied field; the imaginary component is more concerned with how much dissipation of the wave occurs in the material. Figure 1-1 shows how the real and imaginary components of permittivity typically vary with the frequency of

the applied electromagnetic field. Low frequency behaviour is attributed to free ionic motion in the material, which can occur only if some solvent is present. At microwave frequencies spinning polar molecules cause the Debye relaxation shown in Figure 1-1. At very high frequencies such as in the infra-red and visible regions, resonances related to electronic and atomic polarisations give rise to sharp peaks in ε''.

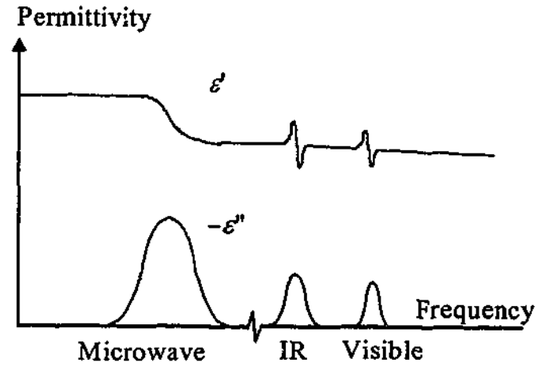

Figure 1-1. A qualitative diagram of how permittivity changes with the frequency of the applied field.

The permittivity and permeability completely define how an electromagnetic wave will be affected if it encounters a material. When the wave crosses a boundary between two media, some will be reflected and some transmitted. Figure 1-2 shows such a case for normal incidence.

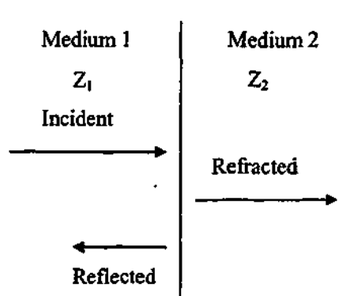

Figure 1-2. Reflection and refraction of an electromagnetic wave at the surface between two media at normal incidence

If the magnitude and phase of a single component of the vector electric field (eg. E_x) of the incident wave at the interface is written as the complex number E_i, then the magnitude and phase of the reflected wave E_r is

$$E_r = \Gamma E_i \qquad \text{Equation 1-32}$$

where Γ is known as the reflection coefficient. The value of Γ is

$$\Gamma = \frac{Z_2 - Z_1}{Z_2 + Z_1} \qquad \text{Equation 1-33}$$

where Z_2 is the impedance of medium 2 and Z_1 is the impedance of medium 1. If medium 1 is air, then equation 1-33 can be rewritten to give

$$\Gamma = \frac{Z_2 - Z_1}{Z_2 + Z_1} = \frac{\sqrt{\frac{\mu_r}{\varepsilon_r}} - 1}{\sqrt{\frac{\mu_r}{\varepsilon_r}} + 1} \qquad \text{Equation 1-34}$$

The amount transmitted into the material is calculated by

$$T = \frac{2Z_2}{Z_1 + Z_2} \qquad \text{Equation 1-35}$$

where T is known as the transmission coefficient.

For finite samples, the amount transmitted through the material is obviously dependent upon the thickness of the material. This is not only because of any lossy behaviour that may occur in the sample, but also because of reflections that can occur within the material from each boundary. Figure 1-3 shows the path of an electromagnetic wave incident upon a sample with permittivity ε_2 and permeability μ_2, with air on both sides.

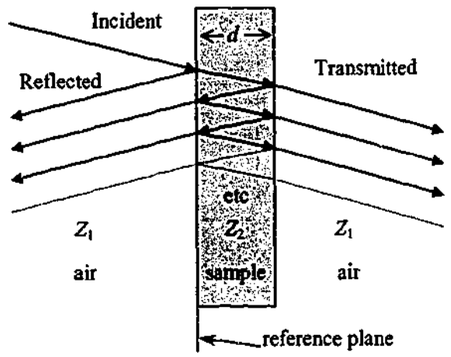

Figure 1-3. Schematic diagram showing electromagnetic wave reflection and transmission pathways when incident on a material

Each constituent reflection is describable by Equation 1-33. The effects of the multiple reflections cause constructive and destructive interferences if the thickness of the material is close to a multiple of a quarter of the wavelength of the field inside that material. Odd quarter wavelengths give rise to destructive interference conditions whereas even multiples cause constructive interference. This affects both the total reflection and transmission.

The overall effective reflection and transmission coefficients can be shown to equal[2]

$$\Gamma_{total} = \frac{(1 - Z_{12})(1 + Z_{21}) + (1 + Z_{12})(1 - Z_{21})e^{-2\gamma_2 d}}{(1 + Z_{12})(1 + Z_{21}) + (1 - Z_{12})(1 - Z_{21})e^{-2\gamma_2 d}} \qquad \text{Equation 1-36}$$

$$T_{total} = \frac{4e^{-\gamma_2 d}}{(1 + Z_{12})(1 + Z_{21}) + (1 - Z_{12})(1 - Z_{21})e^{-2\gamma_2 d}} \qquad \text{Equation 1-37}$$

where

$$Z_{ij} = \frac{\mu_i \gamma_j}{\mu_j \gamma_i} \qquad \text{Equation 1-38}$$

and d is the thickness of the material.

1.3. Measurement procedures

The measurement of permittivity and permeability at microwave frequencies is important for a wide variety of reasons, such as antenna design, electromagnetic shielding, cable manufacture and in electromagnetic radiation absorbers. A measurement technique will ideally possess the following characteristics:

- high accuracy,
- non-destructive sample preparation,
- the ability to test wide frequency ranges with a single measurement,
- the ability to test inhomogeneous materials,
- minimal instrument setting up,
- ease of testing and
- straight-forward permittivity and permeability extraction.

In order to test the performance of a technique, materials whose properties are well known should be measured and compared to the recorded data from other sources. Only by confirming that the technique extracts the correct result for these known materials, can we have confidence in the values obtained from specimens whose properties are not known.

A number of different techniques have been devised over many years to enable accurate testing of the permittivity and permeability. Lynch[3] reviewed much of the literature concerning test procedures up to 1974. Early procedures involved slotted line techniques[4, 5, 6, 7]. A material backed by a metallic short circuit is placed in a waveguide, and the complex impedance of the system is measured. Next, the short circuit is moved a distance of a quarter of the wavelength ($\lambda/4$) of the field to simulate an open circuit, where a second measurement is taken. These two measurements can be used to solve the appropriate equations to extract the permittivity and permeability of the material under test. Each frequency needs to be measured individually and so is time consuming, and the actual measurement itself is difficult to make.

At low frequencies, permittivity and permeability can be measured using standard capacitor and inductor techniques. In the capacitor case, the specimen is placed between two parallel plates and the capacitance of the system[8, 9, 10] is measured. The difference in capacitance and loss factor between the loaded and unloaded fixture is used to determine the electrical properties of the specimen. A similar technique is used to determine permeability[10] by looping a conductor around the sample. However, these methods are only suitable at frequencies below 1 GHz or so, since the radiating fields generated from the structures at higher frequencies interfere with the field incident on the specimen.

Cavity resonators have been used for some time to measure the permittivity of a dielectric material at fixed frequencies[6, 11, 12, 13]. A metal box of any shape is completely closed except for two small holes, one to allow for excitation of the cavity, the other for measuring the response. At certain frequencies the cavity will resonate, with the frequency and magnitude of the oscillation measured. The material under test is then placed inside the cavity and difference in the response of cavity used to determine the permittivity.

More modern techniques involve placing the sample in a waveguide, then measuring the complex reflection and transmission signals. Nicolson and Ross[14] showed how ε and μ could be calculated using network analysis theory with the use of scattering parameter matrix data, abbreviated to S-parameter data. This was later expanded upon[15] to incorporate measurements taken in the frequency domain.

The derivation of S-parameters[16, 17] is shown below, and they are used to characterise the input and output response of a linear network. In a two-port network such as the one shown in Figure 1-4, a_i and b_i are the normalised complex voltage waves incident on and reflected from

the i'th port of the network. They are defined in terms of the terminal voltage V_i, the terminal current I_i, and an arbitrary reference complex impedance Z_i as

$$a_i = \frac{V_i + Z_i I_i}{2\sqrt{|\mathrm{Re}(Z_i)|}} \qquad \text{Equation 1-39}$$

and

$$b_i = \frac{V_i - Z_i^* I_i}{2\sqrt{|\mathrm{Re}(Z_i)|}} \qquad \text{Equation 1-40}$$

where Z^* denotes the complex conjugate of the impedance.

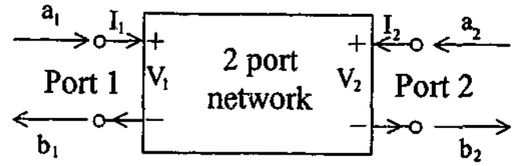

Figure 1-4. General two-port network

The scattering matrix relates the outputs to the inputs as

$$\begin{bmatrix} b_1 \\ b_2 \end{bmatrix} = \begin{bmatrix} S_{11} & S_{12} \\ S_{21} & S_{22} \end{bmatrix} \begin{bmatrix} a_1 \\ a_2 \end{bmatrix} \qquad \text{Equation 1-41}$$

The S-parameters are read as $S_{\text{out in}}$, where the first number refers to the output port where the signal is measured, and the second number refers to the input port from where the signal originated. So in this configuration, the reflected signal is designated S_{11}, the transmitted signal as S_{21}. The values of the S-parameters can be calculated using the following equations:

$$S_{11} = \left.\frac{b_1}{a_1}\right|_{a_2 = 0} \qquad \text{Equation 1-42}$$

$$S_{22} = \left.\frac{b_2}{a_2}\right|_{a_1 = 0} \qquad \text{Equation 1-43}$$

$$S_{21} = \left.\frac{b_2}{a_1}\right|_{a_2 = 0} \qquad \text{Equation 1-44}$$

$$S_{12} = \left.\frac{b_1}{a_2}\right|_{a_1 = 0} \qquad \text{Equation 1-45}$$

S-parameters are more easily measured at microwave frequencies than any other parameter set to characterise linear networks. For this reason, modern vector network analysers use S-parameters exclusively. With a sample of thickness d, reflection coefficient Γ and transmission coefficient T, Nicolson and Ross[14] showed that the S-parameters are given by

$$S_{11}(\omega) = \frac{(1-T^2)\Gamma}{1-T^2\Gamma^2} \qquad \text{Equation 1-46}$$

$$S_{21}(\omega) = \frac{(1-\Gamma^2)T}{1-T^2\Gamma^2} \qquad \text{Equation 1-47}$$

where ω is the angular frequency. Γ has been defined in equation 1-34 as the reflection coefficient when the length of the sample is infinite, and T is the transmission coefficient of the finite material, related to ε_r and μ_r by equation 1-48.

$$T = e^{-\gamma d} = e^{-d\sqrt{-\omega^2\varepsilon\mu}} = e^{-i\left(\frac{\omega}{c}\right)d\sqrt{\varepsilon_r\mu_r}} \qquad \text{Equation 1-48}$$

Once the S-parameters are measured, the complex permittivity and permeability can be extracted using the above equations. Modern vector network analysers such as Agilent Technology's (the former Hewlett-Packard) 8510 system can be configured to output the S-parameters directly to a computer for analysis and permittivity/permeability extraction[18].

In order to extract both real and imaginary permittivity and permeability, one needs to measure the magnitude and phase of the reflected and transmitted signals. In cases where the material under test is known to be non-magnetic at the frequencies of interest, it is possible to fix the permeability equal to that of free space and use only the reflection or transmission signal to find permittivity. This highly useful result will be expanded upon in later chapters.

The waveguides typically used for material property evaluation are either of the coaxial or rectangular/circular type. Coaxial waveguides have the advantage of allowing a very wide frequency band to be measured from a single specimen but have the disadvantage of being difficult to accurately machine to size. Samples for rectangular or circular waveguides can be machined more accurately but can only cover narrow frequency bands[19, 20, 21, 22, 23, 24]. Measurements using either shape are highly sensitive to the specimen's homogeneity, isotropy and size tolerance. The specimen must completely fill the waveguide cross-section or large errors result. An examination of the errors that can occur has been performed by Baker-

Jarvis[25, 26] and others[27, 28, 29]. Direct material comparisons have been performed[30] showing measurements in the coaxial waveguide taken on a number of different homogeneous materials by different researchers. Large variations in measured properties were evident, proving that even on these homogeneous, isotropic materials, uncertainty in the deduced permittivity is still significant.

Waveguide measurements require careful sample preparation; the samples are usually small and must be the correct size (for example the coaxial method requires a 7.00 mm outer diameter and a 3.04 mm inner diameter). The preparation process is a destructive one, and if the material is not homogeneous then the values obtained from the small specimen may not be representative of the whole sheet.

Free space methods using larger samples avoid many of the sample size and contact problems associated with waveguide measurements. Free-space techniques for permittivity and permeability extraction have been used since at least 1984; however, these were either an extension of the slotted line technique using a sliding short at a fixed frequency[31], or simply the placing of horns mouth-to-mouth[32]. Swept frequency measurements were used by Hallikainen et al[33, 34] to measure the dielectric properties of soil and snow, by measuring the transmission only and assuming the permeability was equal to that of free space. This assumption is well founded since there exist only a few materials that retain some magnetic behaviour above 1 GHz. A similar technique of permittivity extraction by measuring transmission alone was undertaken by Capps et al[35]. They measured the transmitted signal through water at two different thicknesses and calculated the real and imaginary permittivity with good accuracy. The method required high precision on the water thickness and was only performed in single frequency steps.

Swept frequency measurements on solid materials using free space techniques have been performed using focussed horn antennas[36, 37, 38, 39, 40]. The researchers used lenses to focus the electromagnetic waves to a spot on the material under test. The reflection and/or transmission was measured and the values of ε_r and μ_r calculated. When both reflection and transmission are tested there is enough data to calculate ε_r and μ_r[37], but when only one of the components is measured, then permittivity values are calculated assuming the permeability is that of free space[36, 38]. Accuracies of ± 2-4% were achievable using this technique, but the method required precise positioning of both the sample and the horns and so was difficult to perform. Moreover, the focussing behaviour of the horns did not allow for an accurate determination of inhomogeneous materials since the area of the material under test is small.

Similar techniques have been used to measure the properties of rocks and building materials over a wide frequency band[41, 42]. Plastics and rubbers have also been measured using this technique over a narrow frequency band[43]. Permittivity extraction using the transmission and reflection signals collected at off-normal angles of incidence has also been demonstrated[44, 45], as have measurements of permittivity using only the amplitudes of the reflection and transmission signals[46]. Other researchers replaced the focussing horn antennas with offset parabolic reflectors to focus the beam with some success[47].

Extracting permittivity using the reflection from materials backed by a metal sheet has also been investigated using techniques similar to standard RCS measurements[48, 49, 50, 51, 52, 53, 54]. In one case[55], a carbon fibre loaded rubber sheet with the fibres aligned linearly, was tested in an anechoic chamber at different angles of rotation to the linearly polarised incident microwave source. The complex permittivity tensor was calculated for this material. The accuracy of this method is difficult to judge since no measurements on known materials were reported. This method can be utilised to test a wide variety of samples, including those that have very large inclusions. As with most methods, accurate thickness determination is required.

A quite different method of determining permittivity is with the use of an open resonator[56, 57, 58, 59, 60, 61]. Two spherical mirrors face each other and resonance is established. Then the sample is placed between the mirrors and the differences measured. There are essentially two procedures; the first involves measuring the resonance frequency with and without the specimen, keeping the length between the mirrors fixed. The second method fixes the frequency while the distance between the mirrors is adjusted to obtain a resonance with and without the specimen. Very accurate measurements are possible using this method (better than 1% for real permittivity); however, the actual measurements are difficult to perform and the components quite expensive. It has also been found that the method is not suitable for highly lossy materials.

A further method related to the open resonator can be used to measure both permittivity and permeability[62, 63]. It requires two spherical mirrors at right angles to each other, into which the specimen is placed at 45 degrees to both, and an ellipsoidal mirror used to direct the beam towards the material. The setup is complex and the accuracy is estimated to be around ± 5%.

Open ended coaxial and waveguide techniques have also been investigated as a method to measure permittivity[64, 65, 66, 67, 68, 69, 70, 71, 72]. The reflection from the surface of the material is

tested only. The model assumes the material under test is infinite in thickness and paramagnetic, and so can solve the necessary equations to extract permittivity. This method has the advantage that thickness measurements are not required, which is usually a major source of inaccuracy when the sample is not exactly flat. To achieve high accuracy, the sample must be smooth, and as such the technique is especially useful for testing liquids. Agilent have marketed a dielectric probe kit (cat # 85070A). Typical accuracies of around 5% are quoted.

The new method proposed in this investigation is to extend the procedure of Ghodgaonkar, Varadan and Varadan.[36] The material under test is supported on a transparent material and the reflection and transmission is measured using microwave horn antennas. This method utilises the same equations as for the waveguide methods, the method is non-destructive and so requires no sample preparation, the size of the material can be very large so inhomogeneous materials can be tested with confidence, and the actual test is quite easy to perform. The lensed horn antennas will be replaced by normal microwave horns. This technique offers an accurate way to obtain the response of materials that are inhomogeneous over distances of a few centimetres, measuring the average transmission over the whole specimen. Samples of up to 500 mm square may be tested non-destructively via this method, with no specimen preparation required. In conjunction with other tests, for instance a measurement similar to that of Hashimoto et al[48], the determination of both permittivity and permeability can be made making two relatively easy measurements.

Chapter 2. Methods of Testing

In this chapter, the various techniques used in the thesis are described in detail so as to obtain a better understanding of the various processes involved. This includes the free space and transmission line microwave measurement techniques, as well as the low frequency dielectric test procedure. The various methods for improving the measured signals are also presented, such as removing stray reflections using time gating, using microwave lenses in the test procedure to reduce near field effects, and employing diffraction removal techniques to reduce errors in the transmission signal.

2.1. Network analyser methods

2.1.1. Network analyser details

An Agilent Technology 8510C vector network analyser system is used to perform all the measurements at microwave frequencies. The 8510C analyser is connected to an 8517A S-Parameter Test Set with an 83651B Synthesized Frequency Source. The frequency range of this system covers 45 MHz to 50 GHz. The network analyser system has a dynamic range of greater than 100 dB, and resolutions of 0.01 dB in magnitude and 0.01 degrees in phase are readily achievable. An IBM compatible computer controls the system, with the software written by the author. Output from the system is usually in the form of S-parameters, which have been defined earlier. These complex quantities can be readily transformed into absolute magnitudes and phases of the reflection and transmission within a network, and permittivity and permeability of a material can be extracted when the appropriate formulas are used.

2.1.2. Coaxial waveguide

Waveguide methods provide a very accurate way of determining both the permittivity and permeability of materials, providing the sample can be machined accurately. When the test sample completely fills the waveguide and the surfaces are perfectly flat, highly accurate measurements of permittivity and permeability can be made. The advantage of using coaxial waveguides is that wide frequency ranges can be measured using just one configuration. For instance, a commonly used waveguide is the so-called 7 mm beadless airline, which is 100 mm long, has an outer diameter of 7.00 mm, and an inner rod conductor with diameter of 3.04 mm. In conjunction with the network analyser system, this airline can be used from 0.045 to

18 GHz using a single swept frequency measurement. Using rectangular waveguides over the same range would require a large number of samples and waveguides of different sizes.

The method is quite simple in theory. A specimen for testing is cut to shape out of the main block and placed in the waveguide. The reflection and transmission S-parameters are measured and, using the equations shown in the introduction, values of permittivity and permeability can be determined. The solution is not unique, because of the cyclic nature of the phase measurements, and so a solution number must be included. Usually the correct answer corresponds to the lowest solution number, and so this is hardly ever a concern.

Figure 2-1 shows a schematic diagram of the setup. The incident microwave signal exits from port 1, travels through a cable and then contacts the surface of the sample inside the airline. Some of the radiation is reflected from the surface and some is transmitted through the sample to be collected at port 2. The analyser measures the signals at each port, and records the complex S-parameters. In this configuration, the reflected signal is designated S_{11}, the transmitted signal as S_{21}.

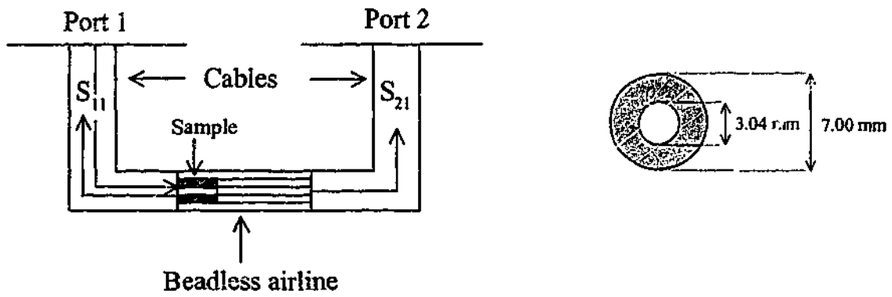

Figure 2-1. Coaxial waveguide holder and sample

The main problem associated with waveguide methods is incomplete filling of the waveguide in the radial direction. (The sample does not need to be exactly 100 mm long because the phase shift through the rest of the waveguide can be easily removed assuming the thickness of the sample is well known.) Coaxial measurements are particularly difficult because it is hard to drill a hole in a sample exactly 3.04 mm in diameter, while making the outer diameter of the sample exactly 7.00 mm. Many algorithms have been devised to correct for inaccuracies of the sample diameters, with varying degrees of success[25]. Added to this problem is that the specimen must be homogeneous for the parameter extraction to work. In some cases, a small doughnut shaped sample will be representative of the whole sample, but there exist many important instances when that assumption is not valid. These include plastics with additives such as carbon fibres, where the length of the fibre is greater than that of the sample, and inhomogeneous materials whose permittivity varies spatially over large distances.

Coaxial waveguide measurements on these types of samples will lead to misleading results. Nevertheless, coaxial waveguide measurements are still one of the most accurate methods of determining the permittivity and permeability of a material at microwave frequencies.

The thickness of the sample is an important factor in the measurement. The sample must be flat, and the thickness well known so that it can be used in both the parameter extraction algorithms, and for removal of the phase shift caused by the empty airline. Also, if the thickness is equal to a quarter of the wavelength of the signal inside the sample, then destructive interference occurs between waves reflected off the front of the sample, and from the rear. This destructive interference magnifies any sample imperfections and leads to errors in the reflected signal. These errors then lead to incorrect determinations of permittivity and permeability for that material.

2.1.3. Dielectric probe

Another method of measuring permittivity is by using a coaxial probe. This is a reflection only technique that relies on the assumption that the sample is infinitely thick. Figure 2-2 shows the probe being placed on the sample and the microwave signal entering the sample. The microwave beam "fringes" into the sample, and the S_{11} reflectivity data is collected at port 1.

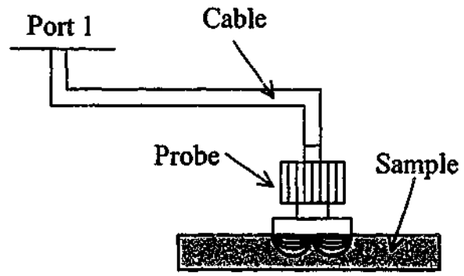

Figure 2-2. Dielectric probe measurement.

Agilent Technology sells a dielectric probe kit (part number 85070B). This connects directly into the 8510C network analyser system, and allows real and imaginary permittivity measurements from 0.5 to 18 GHz. Accuracy is quoted at ± 5% for this method at high frequencies, but is worse at frequencies below 5 GHz. Agilent also supplies a software package to extract the permittivity from the S_{11} measurements. The probe has a great

advantage in that the thickness of the sample does not need to be known. The technique is non-destructive, only relying on the sample having a diameter larger than 20 mm, the surface of the sample being smooth, and the thickness satisfying

$$d > \frac{20}{\sqrt{\varepsilon_r}} \qquad \text{Equation 2-1}$$

where d is the thickness of the sample in millimetres. It main weaknesses are that it is only useful for measuring paramagnetic materials, that the samples must be homogeneous over a very small distance scale, and that any movement in the cable after the system has been calibrated causes large errors. For this latter reason, the probe must be clamped firmly in place and the sample brought up to meet it. The technique is also very sensitive to air gaps between the sample and the end of the probe.

2.1.4. Horn details for free space techniques

The free space measurements are performed using wideband horn antennas to direct the microwave source to the sample under test. Three horns are used to investigate frequency ranges from 1 to 40 GHz. Some specifications of each are given below in Figure 2-3.

	"Gold" horn	"Silver" horn	"Hi-freq" horn
Freq range (GHz)	1 – 18	7.5 – 18	16 – 40
Gain (dBi)	6 – 16 (typical)	15 – 22 (typical)	18 – 24 (typical)
Size (mm)	200 × 241 × 143	203 × 91 × 65	149 × 67 × 50

Figure 2-3. Details of the horns used for free space measurements

Figure 2-4. Photograph of horns used in this study

The horns used were chosen so the widest possible frequency band could be tested using the smallest number of measurements. The horns typically have their lowest gain at low frequencies, since the wavelength of the radiation becomes longer and it is therefore harder to

match the impedance between the coaxial input at the horn to the outside air in a short distance. In order to obtain the very large bandwidths, all these horns are of the "dual-ridged" type. The ridges prevent higher modes forming in the area near the back of the horn, which reduce the amount of effective radiation leaving the mouth of the horn. The ridges are most prominent on the "gold" horn, situated in the centre of the top and bottom plates before flaring out at the ends.

The gain of the horn is directly related to the spread of the radiation leaving the horn, so a low gain is indicative of a wide spread. This means that for a low gain horn there is more chance of diffraction around a small sample, or stray reflections from parts of the measurement equipment interfering with the measurement. For this reason it is better to use the highest gain horns possible. However, if the source is concentrated at a very small area (which can be achieved using lenses or reflectors) an overall picture of the sample as a whole may be lost, especially if the sample under test is inhomogeneous.

2.1.5. Reflection / transmission "wall" technique

The reflection/transmission "wall" technique is a free space version of the coaxial waveguide method. The sample is laid flat on a transparent material (usually lightweight polystyrene foam) between two rectangular microwave horns attached to a slider bar fixed to the wall. The reflection (S_{11}) and transmission (S_{21}) through the material is measured and values of the permittivity and permeability can be extracted using the same formulas as for the coaxial waveguide. This technique assumes the material is large enough so that diffraction around the sample does not occur. Figure 2-5 shows a schematic diagram and a photograph of the test configuration.

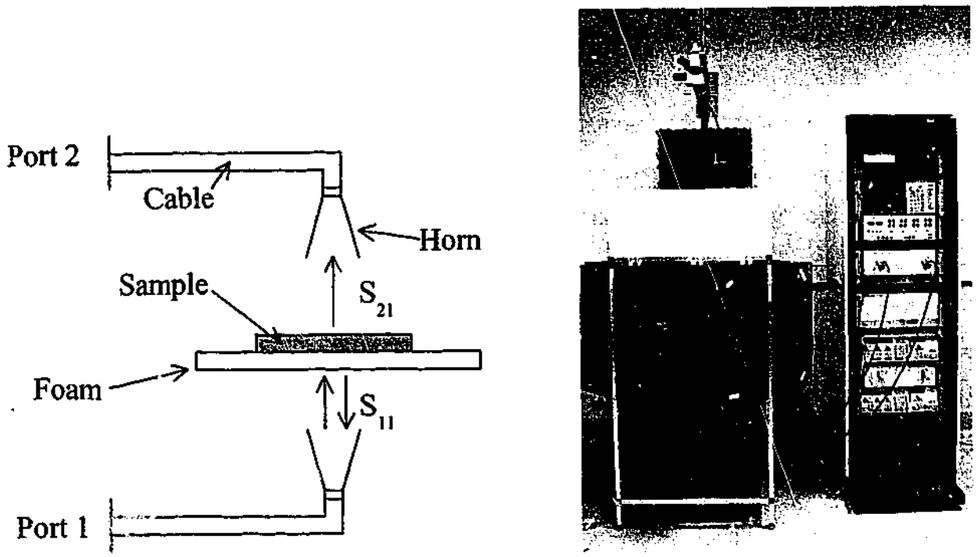

Figure 2-5. Reflection / Transmission wall measurement.

The method has many advantages over conventional techniques, in that no sample preparation is required. The technique is completely non-destructive and so can be used in a quality assurance (QA) role to check the dielectric properties. The material can be inhomogeneous over many wavelengths and the analysis will still yield meaningful average results for the entire sample. Both small areas and the entire sheet can be tested by changing the distance between the horns and the sample, and the technique is easy to perform. The sample needs to be flat over its entire area or the value of thickness used in the determination of permittivity and permeability would not have a well-defined value.

The horn positions can be moved independently so as to allow for testing at different distances. At distances more than a few wavelengths from the mouth of the horn the wavefront is typically spherical in shape, as if from a point source a small distance behind the horn. When the horns are far away from the sample, the wavefront flattens out to be more like a plane wave, and the magnitude variation reduces also. Therefore, it is better to have the horns as far away from the sample as possible so that the closest approximation to plane wave behaviour is met. This reasoning assumes the sample is very large (larger than the diffraction from the horns), and that there are no obstructions between the two horns. Unfortunately, these conditions are not always met in the real world, and compromises must be made to reduce stray reflections from measurement equipment and minimise diffraction around a finite-sized sample. The horns can be moved so that the "best" position for a particular sized sample can be investigated.

The calibration process for reflection is the Response/Isolation type[73]. The send horn is positioned below the transparent foam sheet so that the top surface of the foam is on the calibration plane. The foam sheet is thick enough to prevent it bending under the weight of the reflection standard or the sample. The Response part of the procedure is made by placing a flat metal plate on the transparent foam sheet and the magnitude and phase of S_{11} is measured. The metal sheet is ground flat and the entire system is levelled. One or more convoluted foam absorbers are placed on top of the metal sheet to remove stray reflections from behind it. The plate is then removed and the reflection from the convoluted absorbers is then measured. This makes up the isolation part of the calibration procedure. When measuring the actual sample, the absorbers are again placed on top. The material dimensions must match the size of the calibration plate.

The calibration procedure for transmission is much easier; just a simple response calibration[73] is sufficient. The transparent foam base is positioned between the horns and the magnitude and phase of S_{21} is measured. An isolation measurement is not required.

The most difficult parameter to measure accurately is the phase of S_{11}. Very slight imperfections in the metal reflection standard lead to large errors in the measured phase. If the plate is even only a tenth of a millimetre off being flat, very large errors in the determination of permittivity and permeability are seen. The same effect is observed if the foam sample holder bends even slightly. However, if we can assume the material is non-magnetic at microwave frequencies, the problem of reflection errors can usually be overcome by ignoring the reflected signal altogether, and just using the transmitted signal to calculate the permittivity. No metal sheet is required in this case; the transmission through the sample is measured relative to empty space. This assumption of non-magnetism makes the measurement far easier to perform, although the mathematics involved in extracting the permittivity is more difficult. An iterative technique must be used to solve the equations to find ε. Multiple reflections between the sample and the horns can be eliminated by the use of time gating, which can be set up so that stray reflections are ignored completely. Time gating can introduce errors of its own near the frequency end points, but the magnitude of these errors is not well known.

If the specimen tested is not large enough, the microwave beam can diffract around it giving unwanted contributions which lead to errors in the extracted results. An obvious way of alleviating this problem is to use larger samples, but sometimes this is not possible and one must test the small sample. One method of reducing diffraction around the sample is to place

the material on a metal sheet with a hole cut in the centre. Another method of overcoming the problem is to place an absorbing frame around the sample so that the frame will instead absorb the part of the field that might be diffracted. Figure 2-6 shows how a frame may be placed around the small sample to remove diffraction effects.

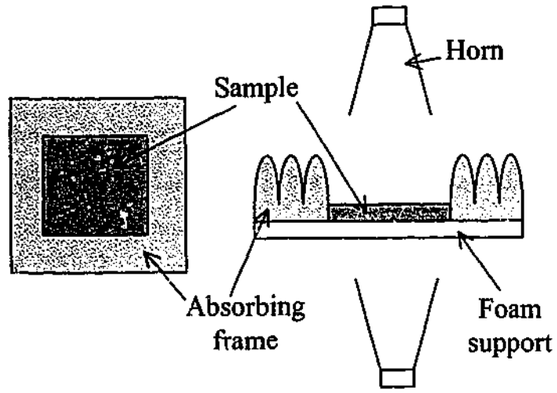

Figure 2-6. Absorbing frame placed around small sample.

The absorber used is a convoluted carbon loaded foam that is commonly used to cover the walls of anechoic chambers.

Absorbing the diffracted wave is not always easy to achieve in practice. Unless the sample fits exactly into the hole in the absorbing frame, the frame must be moved each time a sample is measured. If this is not performed accurately, then repositioning errors will occur and can be larger than those due to the diffraction. However, the diffracted beam can be removed if its magnitude and phase is known. It can be measured by placing a flat metallic sheet that is the same size as the material under test between the horns. Since none of the radiation travels through the plate, only the diffracted wave is seen by the receive horn. This removal technique is the inverse of the previous one, and although the effect can be estimated using Babinet's principle[74], it is more accurate to measure the error signal with the actual equipment. It can then be removed later using the formulation shown in Figure 2-7.

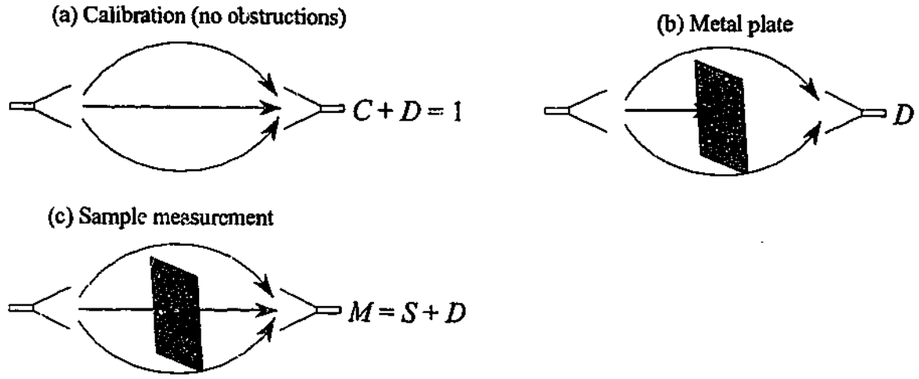

Figure 2-7. Formulation of equation to remove diffracted wave from measurements

Firstly, the system is calibrated using a "Response" type calibration (a). As indicated in the figure, this includes all paths to the receive horn. The measured response from paths that would normally pass through a sample of pre-determined size are given the label "*C*", the response from paths that would travel around that sample without intercepting are labelled "*D*". The value of "*D*" can be measured by placing a metal plate of the same size as the sample between the horns. Only the "*D*" response is measured. When the sample is measured, the receive horn collects the sum "*M*" of the wave that travels through the sample "*S*", and that part that doesn't, the "*D*" component.

Since the parameter we are chasing is the sample (*S*) measurement divided by the calibration (*C*), we can use the values we actually measure (ie *M*, *C* and *D*) to determine the response of the sample alone. The equation used is shown below. This technique will also help to remove stray reflections from other parts of the sample holder.

$$S_{21} = \frac{S}{C} = \frac{M - D}{1 - D} \qquad \text{Equation 2-2}$$

Another refinement to this method that may increase accuracy is the use of absorbing layers in between the horns and the sample. This will help reduce reflections between the horns and the sample. If the foam support shown in Figure 2-6 was made of a lossy foam (which causes say a 10 dB absorption) instead of a lightweight polystyrene, then any reflection between the sample and the end of the receive horn would be 20 dB lower than the direct (unreflected) signal. Such a layer could be seen as a diode, by only allowing the direct transmission and reducing to a very low level any contributions from back reflections.

This technique is useful for frequencies above 1 GHz. Below this value wavelength effects mean that the antennas used to direct the energy become very large and so the samples

must also increase in size. Diffraction effects increase and the overall measurement system becomes unwieldy and difficult to use. Waveguide techniques are better for parameter measurements at these frequencies. However, at frequencies above 18 GHz the technique is extremely useful, since the waveguides required are small and sample preparation becomes difficult.

2.1.6. Range backed reflection technique

Another free space measurement that has many of the benefits of the reflection/transmission wall technique is the backed reflection technique. The technique employed is to place the sample in contact with a metal backing sheet and then measure the reflection from the laminate. A Response/Isolation calibration of the system is performed using the backing sheet alone, and the return from the room is also measured with the backing plate removed. This eliminates many of the cross talk and stray reflections that could lead to measurement error. Figure 2-8 shows a schematic diagram of the setup. This method is based on a standard technique used to measure the effectiveness of radar absorbing materials (RAM).

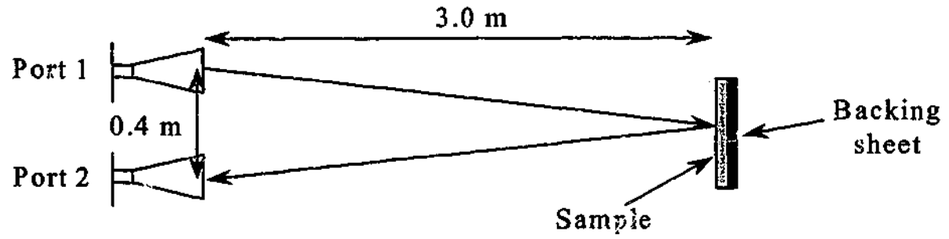

Figure 2-8. Range backed reflection method.

The distance between the horns and the sample is very important. For ease of computation, the permittivity extraction algorithms assume that a plane wave is normally incident upon the surface of the sample. This requires that the sample be in the so-called far field of the microwave beam. True far field behaviour occurs when there is zero phase variation across the target. Since this requires the target to be an infinite distance away from the source, a convention has been introduced which states that the phase variation across the target should be no larger than $\pi/8$ radians, or 22.5 degrees. With this approximation, one can readily calculate the minimum distance required for far field measurements. For a target with maximum diameter d, the distance between the source horns and the target (the range), is

$$R = \frac{2d^2}{\lambda}$$ Equation 2-3

where R is the range, and λ is the wavelength of the radiation. For a 300 mm square sheet, measurements up to 18 GHz should be taken no closer than 21.6 metres away to ensure far field behaviour.

Anechoic chambers with lengths of over 20 metres are extremely expensive and therefore rare. A way of obtaining a plane wave at shorter distances is with the use of a lens. A lens with the correct focal length will be able to flatten out the spherical wave incident on it into a plane wave. Using a setup of this kind should improve measurement accuracy over one where a lens is not used. The steps involved in designing and making such a lens will be discussed later.

The range facility at DSTO is not a fully lined anechoic chamber, and is relatively short at about 4 metres for its longest dimension. Once the equipment is put into place, a useable distance of about 3 metres is available. With the horns approximately 0.4 m apart, the actual angle of incidence is about 4 degrees, but this is assumed to be close enough to normal incidence. A 500 mm square lens has been made with a focal length of 2.8 metres to investigate far-field behaviour. Permittivity measurements are only generally available since only the reflection is measured with this technique. The material is assumed to be paramagnetic.

2.2. Permittivity/permeability extraction algorithms

2.2.1. Reflection/transmission technique

When both reflection and transmission are measured, the formulae for extracting permittivity and permeability using a network analyser are relatively straightforward[18]. Since there are four unknowns (real and imaginary permittivity, real and imaginary permeability), we need four pieces of information to extract them. The information is in the form of complex S_{11} and S_{21}. Repeating the equations from Chapter 1 for convenience, we can relate the measured S-parameters to the reflection and transmission coefficients as shown below.

$$S_{11} = \frac{(1-T^2)\Gamma}{1-T^2\Gamma^2}$$ Equation 2-4

$$S_{21} = \frac{(1-\Gamma^2)T}{1-T^2\Gamma^2}$$ Equation 2-5

where Γ is the complex reflection coefficient between the sample with wave impedance Z_s and the surrounding air has the characteristic impedance Z_0 when the thickness of the sample is infinite

$$\Gamma = \frac{Z_s - Z_0}{Z_s + Z_0} = \frac{\sqrt{\frac{\mu_r}{\varepsilon_r}} - 1}{\sqrt{\frac{\mu_r}{\varepsilon_r}} + 1} \qquad \text{Equation 2-6}$$

and T is the complex transmission coefficient in the sample of finite thickness d

$$T = e^{-i(\omega/c)d\sqrt{\mu_r \varepsilon_r}} \qquad \text{Equation 2-7}$$

where ε_r is the relative permittivity and μ_r is the relative permeability of the sample. By rearranging Equations 2-4 and 2-5, the values of T and Γ can be put in terms of S_{11} and S_{21}.

$$\Gamma = K \pm \sqrt{K^2 - 1} \qquad \text{Equation 2-8}$$

$$T = \frac{S_{11} + S_{21} - \Gamma}{1 - (S_{11} + S_{21})\Gamma} \qquad \text{Equation 2-9}$$

where

$$K = \frac{S_{11}^2 - S_{21}^2 + 1}{2S_{11}} \qquad \text{Equation 2-10}$$

The permittivity and permeability can be determined rearranging equations 2-6 and 2-7 to give

$$\frac{\mu_r}{\varepsilon_r} = \left(\frac{1+\Gamma}{1-\Gamma}\right)^2 = x \qquad \text{Equation 2-11}$$

$$\mu_r \varepsilon_r = -\left(\frac{c}{\omega d}\ln\left[\frac{1}{T}\right]\right)^2 = y \qquad \text{Equation 2-12}$$

then

$$\mu_r = \sqrt{x\,y} \qquad \text{Equation 2-13}$$

$$\varepsilon_r = \sqrt{\frac{y}{x}} \qquad \text{Equation 2-14}$$

The value for Γ in Equation 2-8 is easily chosen by remembering that $|\Gamma| \leq 1$. Of greater concern is the value for the natural logarithm of the complex value $1/T$. Because the form for the logarithm in complex analysis is

$$\ln(A \angle \phi) = \ln(A) + i(\phi + 2\pi n) \qquad \text{Equation 2-15}$$

a suitable value for the non-negative integer n needs to be chosen so that the correct solution is found. The value of n can and frequently does change across a frequency band, especially when the permittivity is large, the frequency high, or when the sample is thick. It is usually clear if the incorrect solution has been chosen by examining the value of permeability. When testing a nonmagnetic material the resulting permeability should equal that of free space, however when the incorrect solution is chosen the resulting values are usually very different. When the extracted values of permittivity and permeability show a sudden jump across a frequency band of interest it usually means that the value of n has not changed to the correct figure. Normally at low frequencies the value of n is zero, but as frequency increases the value typically increases. A computer program can adjust the parameter to keep the permittivity and permeability continuous.

2.2.2. Transmission only technique

It is not always necessary to measure the entire S matrix; for instance, in the case of non-magnetic materials the permeability can be fixed at the free space value and just the permittivity calculated. Usually the easiest measurement to take in free space is the transmission through the sample (S_{21}), so in the case where relative permeability is known to be unity, this measurement is usually sufficient.

However, simply fixing the permeability equal to 1 and ignoring S_{11} doesn't make the equations any easier to solve, in fact quite the opposite. It is impossible to obtain a form of the equations where the permittivity is given explicitly. Instead, an approximation technique such as Newton's method is necessary to solve the implicit equation for permittivity. Newton's method requires the derivative of the equation to be calculated and an initial guess x_0 of the solution. With the equation in the form $f(x) = 0$, the iterative technique works to find the root using the formula

$$x_n = x_{n-1} - \frac{f(x_{n-1})}{f'(x_{n-1})} \qquad \text{Equation 2-16}$$

Once the *n*th estimate has been found, it is then put back into the formula to find the $(n+1)$th estimate and the process is repeated. When the difference between x_n and x_{n-1} is below a user-defined level, the process is stopped and the solution is found to the required degree of accuracy.

The transmission component S_{21} as shown in Equation 2-5 can be expressed in terms of ε_r and μ_r by substituting the values of T and Γ using the expressions shown in Equations 2-6 and 2-7. Appropriate re-arrangement of the equation leads to a fast and stable convergence to the solution. The equation used is shown in Equation 2-17.

$$f_1(\varepsilon_r) \equiv S_{21}\left\{\varepsilon_r \cos\left[\frac{d\omega\sqrt{\varepsilon_r}}{c}\right] + i\sqrt{\frac{\varepsilon_r}{4}}(1+\varepsilon_r)\sin\left[\frac{d\omega\sqrt{\varepsilon_r}}{c}\right]\right\} - \varepsilon_r = 0 \qquad \text{Equation 2-17}$$

Differentiating this equation was made much easier using *Mathematica*, a computer program that specialises in symbolic algebra. Differentiating this equation with respect to ε gives

$$f'_1(\varepsilon_r) \equiv \frac{S_{21}}{4c}\left\{(4c + id\omega(1+\varepsilon_r))\cos\left[\frac{d\omega\sqrt{\varepsilon_r}}{c}\right] + \left(\frac{ic(1+3\varepsilon_r)}{\sqrt{\varepsilon_r}} - 2d\omega\sqrt{\varepsilon_r}\right)\sin\left[\frac{d\omega\sqrt{\varepsilon_r}}{c}\right]\right\} - 1$$

Equation 2-18

The computer program used to calculate the permittivity terminates the iterative process when the values of both real and imaginary parts of permittivity are varying by less than 10^{-7}. The algorithm moves through the 401 frequency data points taking as the initial guess for each new frequency the converged value calculated for the previous one. To calculate all the permittivity values takes less than half a second on a Pentium 3 running at 900 MHz.

2.2.3. Reflection only technique

In the same way that permittivity can be calculated using the transmission signal alone, the reflection signal (S_{11}) can be used by re-arranging Equation 2-4. This is most useful where the sample is thick and lossy, so the transmission signal is very low and prone to errors due to noise and small stray reflections. The equation used to calculate permittivity is given below.

$$f_2(\varepsilon_r) \equiv S_{11} + \frac{(\varepsilon_r - 1)(L-1)}{2\sqrt{\varepsilon_r}(L+1) + L(\varepsilon_r+1) - (\varepsilon_r+1)} = 0 \qquad \text{Equation 2-19}$$

where $$L = e^{i2d(\frac{\omega}{c})\sqrt{\varepsilon_r}} \qquad \text{Equation 2-20}$$

The derivative is more complicated

$$f'_2(\varepsilon_r) \equiv \frac{\frac{1}{\sqrt{\varepsilon_r}}\left((L-1)\left[\left(\sqrt{\varepsilon_r}-1\right)^2 + L\left(\sqrt{\varepsilon_r}+1\right)^2\right]\right) + 4idL\frac{\omega}{c}(\varepsilon_r - 1)}{\left(\left(\sqrt{\varepsilon_r}-1\right)^2 - L\left(\sqrt{\varepsilon_r}+1\right)^2\right)^2} \qquad \text{Equation 2-21}$$

The reflection only algorithm is less stable than the transmission only equations, but the entire frequency spectrum of 401 points can still be computed in around half a second to an accuracy level of 10^{-7}.

2.2.4. Backed reflection technique

When the sample is tested with a backing plate immediately behind the sample, the geometry is changed significantly.

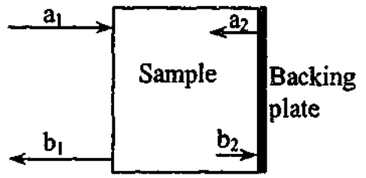

Following the normal S-matrix formulation where the signal a_1 is the source, the value of a_2 (normally zero) takes the value of $-b_2$. So the output signal b_1 is derived by

$$b_1 = S_{11}a_1 + S_{12}a_2 \qquad \text{Equation 2-22}$$

$$b_2 = S_{21}a_1 + S_{22}a_2 \qquad \text{Equation 2-23}$$

Since $a_2 = -b_2$, the equation can be rearranged to give

$$a_2 = -\frac{S_{21}a_1}{1+S_{22}} \qquad \text{Equation 2-24}$$

Substituting back into equation 2-22 gives

$$b_1 = S_{11}a_1 - \frac{S_{12}S_{21}a_1}{1+S_{22}} \qquad \text{Equation 2-25}$$

Since the input signal is defined to be unity amplitude and zero phase, $a_1 = 1$, and the sample is assumed to be homogeneous and isotropic, $S_{12} = S_{21}$ and $S_{11} = S_{22}$. Therefore

$$b_1 = S_{11} - \frac{S_{21}^2}{1+S_{11}} \qquad \text{Equation 2-26}$$

This is the signal actually measured. Putting this signal in terms of permittivity gives the following equation for use in Newton's method,

$$f_3(\varepsilon_r) \equiv b_1 - \frac{L\left(\sqrt{\varepsilon_r}-1\right)+\left(\sqrt{\varepsilon_r}+1\right)}{L\left(\sqrt{\varepsilon_r}+1\right)+\left(\sqrt{\varepsilon_r}-1\right)} = 0 \qquad \text{Equation 2-27}$$

with the derivative

$$f'_3(\varepsilon_r) \equiv \frac{c\left(1-L^2\right)+4idL\omega\sqrt{\varepsilon_r}}{c\sqrt{\varepsilon_r}\left(L\left(1+\sqrt{\varepsilon_r}\right)+\left(\sqrt{\varepsilon_r}-1\right)\right)^2} \qquad \text{Equation 2-28}$$

and L having the same value as before (Equation 2-20). This algorithm has the least stability of all the single parameter calculations but still gives fast and accurate results when the initial guess is close to the actual value.

2.3. Enhancements to network analyser measurements

2.3.1. Dielectric lenses

The solutions to many electromagnetic problems generally assume far-field behaviour for simplicity. In a free space environment it is very difficult to perform measurements in the far field since the distances involved can be quite large. In order to reduce the phase difference across a sample when measuring in the near field, it is possible to flatten out the beam with a lens. There are two main types of electromagnetic lens, delay type lenses in which a solid low-loss material is machined to an hyperboloidal shape, and advance lenses where metallic discs or slats are used to advance some parts of the wavefront. Generally, delay lenses are used since they are simpler to construct and operate over a wider frequency band.

The design of delay lenses is well known,[75] requiring knowledge of the focal length and the permittivity of the material used to make the lens. A block of material is moulded and the required shape can be cut using a computer controlled milling machine. Two lenses were used, the first made from a plastic epoxy incorporating lightweight microspheres to reduce the density and permittivity to about 500 kg/m^3 and 1.81 respectively, the second from a polyurethane (PU) foam with a density of around 250 kg/m^3 and permittivity 1.32. The focal length of the first was set at 2.8 m (the distance from the horns to the target on the range) while the second was set at 1.0 m (a reasonable working distance for the reflection/transmission wall). Both lenses had a square cross section and were over 500 mm

along each side so that large samples could be tested. Appendix A shows the formulae used in constructing the lenses.

In order to test the effectiveness of the lenses in flattening out the wavefronts, an X-Y chart recorder was modified so that a probe antenna could be mounted on the pen attachment point. In addition to this, the arms were extended to allow for movement over 500 mm in each direction. Figure 2-9 shows a photograph of the modified chart recorder.

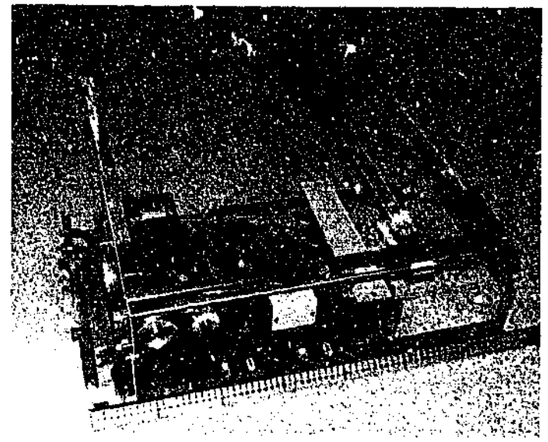

Figure 2-9. Photograph of modified chart recorder for wide area scanning measurements

The antenna used on the chart recorder was a small "probe antenna" with a nominal 8 dBi gain from 6.5-18 GHz. The position of the probe antenna was changed using a computer controllable power supply. Since the chart recorder was already set up to move to a certain position based upon an input voltage, it seemed the easiest way to position the antenna. Once the maximum range was calculated, it was simple (in theory) to position the antenna at any point in the plane to take a measurement. In practice however, it was a little more difficult, since the motors were not designed to move anything heavier than a pen. Shifting the probe antenna together with a couple of metres of cable meant that the motors could move the whole assembly left to right, but could only push the cable down towards the floor. This was not a major problem, but it meant that the scan could only go in one direction.

The normal phase variation from a microwave horn is shown in Figure 2-10. This is the measured response from a standard gain X-band horn situated 1.45 m from the scanner at 9 GHz; it corresponds to a spherical source located 1.53 m from the scanner. This "virtual source" approximately 80 mm inside the horn's throat is the phase centre of the horn, and is used to determine the focal length when the lens is in place.

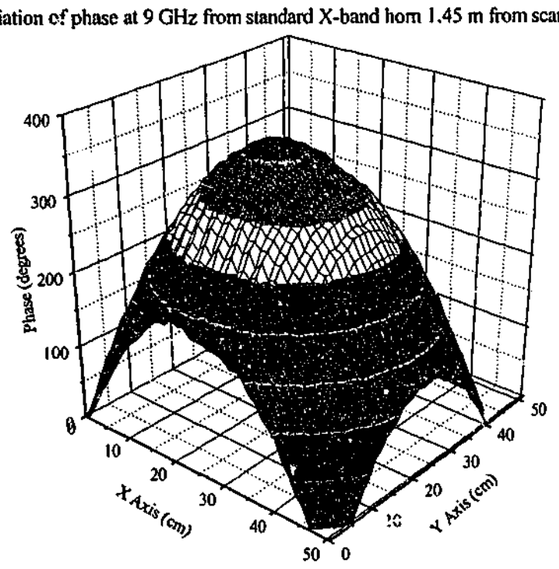

Figure 2-10. Variation of phase from a standard X-band horn 1.45 m from mouth at 9 GHz

Levelling the whole system is very difficult, as a difference of just 1 millimetre across the whole structure corresponds to a phase shift of over 20 degrees at 18 GHz. Figure 2-11 shows the effect of incorrect levelling of the chart recorder on the measured phase. These effects are relatively easy to fix with spacers; however, it can take many measurements before the levelling is correct. Once it is correct the whole structure may need to be moved again to find the correct value of focal length.

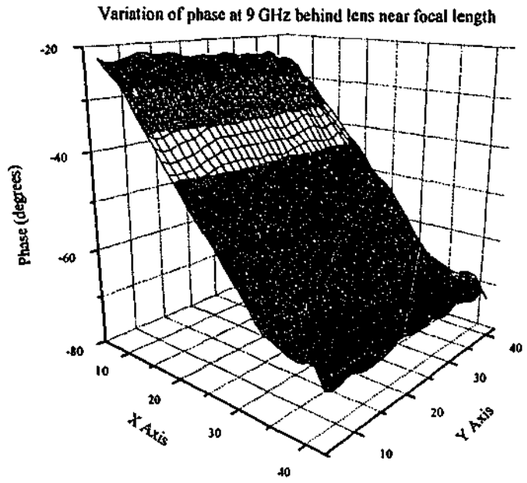

Figure 2-11. Variation of phase behind a lens where chart recorder is not flat

The bar that the antenna rested upon needed to be reinforced, as the weight of the antenna, holder and cables introduced a slight bend in the bar, resulting in a dip in the measurement of phase. The maximum phase shift was measured at about 20 degrees at 15 GHz, corresponding to a change in distance of about 1.1 mm. This effect is shown in Figure 2-12. Stiffening the bar effectively removed this artefact.

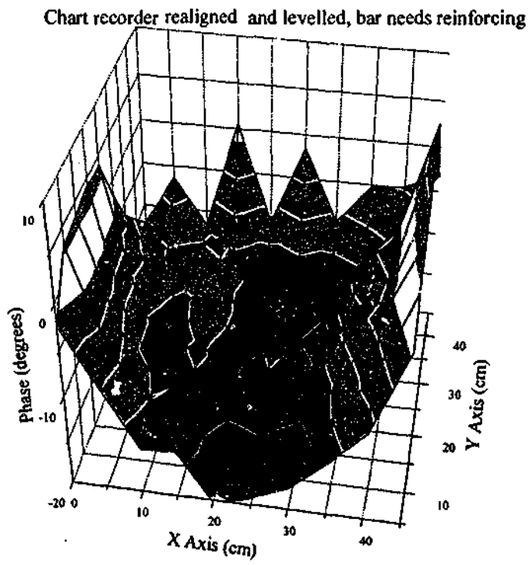

Figure 2-12. Chart recorder near focal length of lens, dip caused by bending of the crossbar.

Despite the problems encountered, the modified chart recorder performed well, giving accurate magnitude and phase measurements behind the lenses. Figure 2-13 shows the measured value of the phase behind the lens at a distance of 2.36 m from the horn mouth to the back of the lens. It can be seen the phase variation is only a few degrees, and the chart recorder or lens not being perfectly level could easily cause this error.

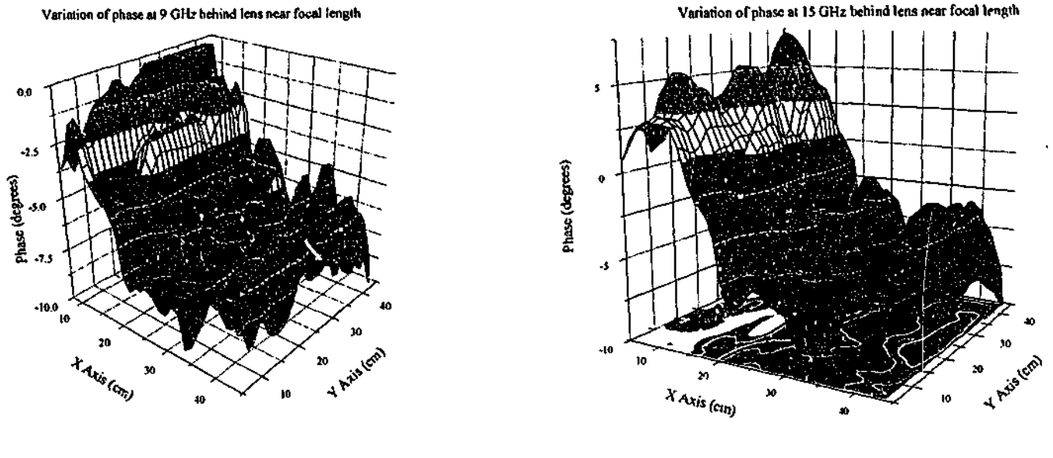

(a) (b)

Figure 2-13. Variation of phase behind lens made from syntactic foam at (a) 9 and (b) 15 GHz

A similar effect is seen with the polyurethane foam lens near its design focal length of 1 m, Figure 2-14 shows how the phase flattens out when the horn to lens distance is 0.99 m.

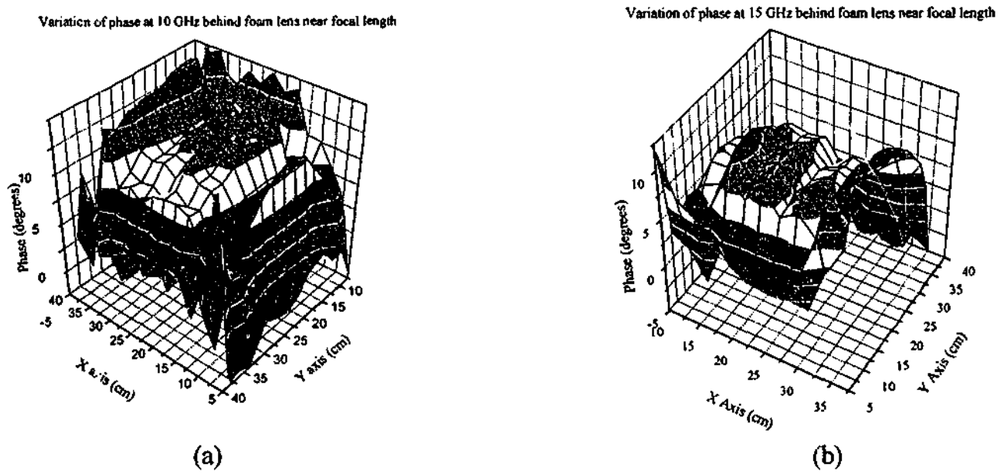

(a) (b)

Figure 2-14. Variation of phase behind lens made from PU foam at (a) 9 and (b) 15 GHz

2.3.2. Time domain and gating

One of the most effective ways to increase the accuracy of any of these techniques (especially the free space ones) is by the use of time gating. Stray reflections from parts of the measurement equipment can be identified, with those peaks removed by software if possible, or the setup can be modified if those peaks overlap those from the material under test.

Data measured in the frequency domain can be converted to the time domain by using a Fourier transform[76]. Fourier analysis in its original form is based on the assumption that any continuous periodic signal can be represented by the sum of properly chosen sinusoidal waves.

There are four categories of Fourier transform, each used for different styles of signal. Signals can be either continuous or discrete, and can be periodic or aperiodic. Since actual measured data is always discrete, only two of the Fourier transform algorithms could be used for this study. However, all Fourier transforms require the signals to extend to positive and negative infinity, and so we must made the finite data points look like an infinite signal in order to use Fourier techniques. The easiest way to do this is to assume the points lying outside of the actual measured data are equal to zero, thus making the entire series aperiodic. Unfortunately, it requires an infinite number of sinusoids to synthesize an aperiodic sequence, which means that this technique cannot be used by a computer. If we assume the measured signal repeats indefinitely in both directions, we can then use the periodic form known as the Discrete Fourier Transform.

Using sinusoids alone is not general enough for many applications, and so was extended to include both sinusoidal and exponential components. The discrete case involving both these components is known as the z-transform.

Fourier transforms of any sort require a step known as convolution, which uses a series of multiplications and additions to convert the signal from one type to another. This is a very time consuming process and limited the usefulness of Fourier transforms until the discovery of the Fast Fourier Transform[77] (FFT) algorithm. This far more efficient technique, ideally suited for use with a computer, often decreased the time taken to calculate the discrete Fourier transform by a hundreds.

The 8510C network analyser uses the Chirp-Z transform to convert frequency domain data to the time domain. This transform is especially useful for focussing in on a particular segment of the time domain one is interested in without the need to calculate the entire time span. The Chirp-Z transform was developed by Rabiner[78] and essentially involves performing

two FFT's and an inverse FFT to get to the required range in the time domain. The technique can be used to zoom in on a particular part of the time domain spectrum quicker than a standard FFT with equivalent resolution[79], or to enhance pole identification, with the added advantage that the number of points taken need not be a composite number. The details of the technique are shown in Appendix B.

As stated previously, using the Discrete Fourier Transform requires the signal to be periodic over an infinite frequency space, which means in theory the signal is repeated indefinitely. However, at the start and end-points of this repeated signal discontinuities occur. If these endpoints are not modified, then "ringing" in the time domain results. This can obscure the effect of other peaks in the time domain. To reduce this effect, a mathematical form is applied to the data to smooth the transition between the repetition points. Such a form is called a window.

There are many types of windows that have been devised to reduce the sidelobes that occur when performing a transformation from one domain to another. The starting point for any window is the so-called "rectangle" window. As shown below in Figure 2-15 as the blue line, it gives abrupt transitions at the edges of the frequency span from unity to zero, and as a result gives large sidelobes in the time domain trace. A simple way to reduce the size of the transition is to multiply the original data using a linear relationship, as shown below as the red line (the triangular window). This does indeed reduce the sidelobes compared to the rectangular window, but the discontinuities in the derivative lead to larger sidelobes than can be obtained by using a better window such as the Hanning window (shown in green). This has a $\cos^2(x)$ form and is continuous in both its function and its first derivative. This gives better sidelobes than the triangle window. It is clear that there are a number of different functions that could give smooth transitions through the frequency space. Harris[80] gives a quite complete description of various windows, with corrections to that article by Nuttall[81]. Some of the better windows are described below, which were investigated by the author for the applicability for this project.

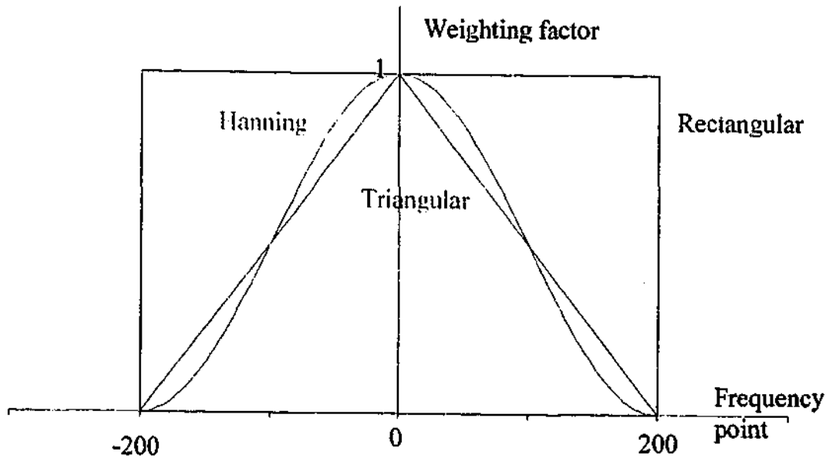

Figure 2-15. Some basic window shapes

2.3.2.1. Rectangular window

Whilst strictly not a window designed for very good sidelobe behaviour, it is nevertheless interesting to compare the rectangular window with others more suited to aiding the transition between domains. The rectangular window is simply unity across the frequency spectrum (as shown in blue in Figure 2-15 for a 401 frequency point sample) and gives rise to a transform shown in Figure 2-16. Note the first sidelobe peaks at about –13 dE and subsequent peaks fall at a rate of 6 dB per octave. A window with such high sidelobes means that these lobes may obscure smaller peaks elsewhere in the time domain. Note that the –10 dB main lobe bandwidth is 0.00732π units on the time axis. This bandwidth is the smallest of all windows, meaning that two peaks very close to each other may be able to be separated assuming the sidelobes do not obscure them. The minima occur at multiples of $2\pi/N$, where N is the number of samples in the frequency span.

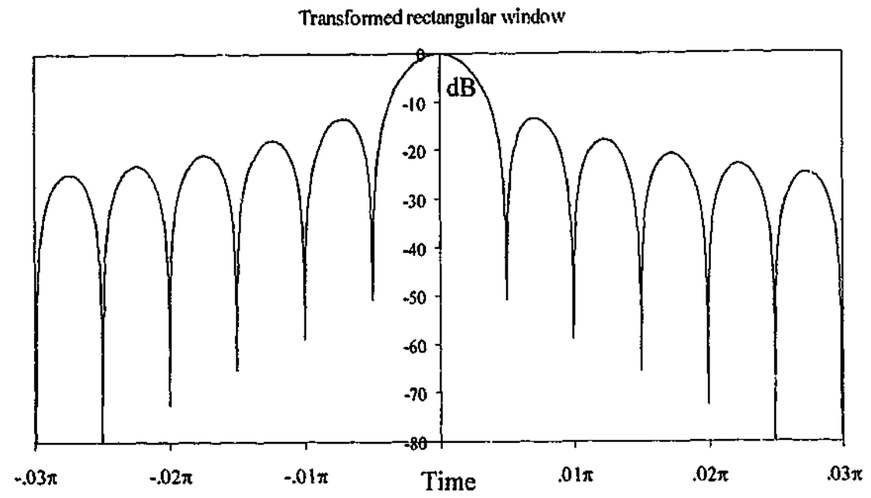

Figure 2-16. Normalised log magnitude of transformed rectangular window.

2.3.2.2. Hanning window

As stated above, this commonly used window is a form of the more general $Cos^{\alpha}(x)$ window with the parameter $\alpha=2$. The Hanning window is defined as

$$w(n) = \cos^2\left[\frac{n}{N}\pi\right] \qquad n = -N/2 \ldots -1,0,1 \ldots N/2 \qquad \text{Equation 2-29}$$

The graph of the Hanning window is shown in green in Figure 2-15. As already stated it is continuous in both its formula and its first derivative, which leads to low first sidelobes and consequent sidelobes decreasing at a rate of 18 dB per octave. The transformed window is shown in blue in Figure 2-17. Note the lower sidelobes of about –31 dB that fall off much faster than the rectangular window. Lower sidelobes come at a cost of bandwidth however, and it can easily be seen that the main lobe is much wider than that of the rectangular window. The –10 dB bandwidth for the Hanning window is 1.705 times larger than the rectangular window, and this value will be henceforth referred to as the –10dB relative bandwidth (-10dB rbw).

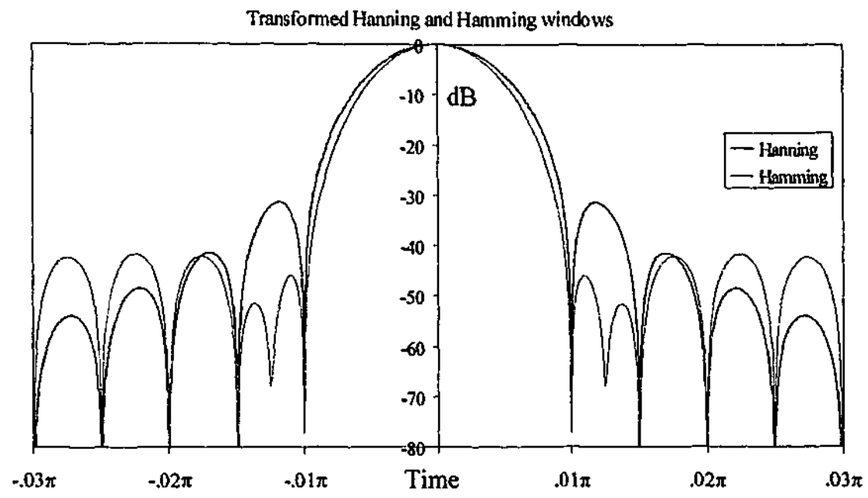

Figure 2-17. Normalised log magnitude of transformed Hanning and Hamming windows

2.3.2.3. Hamming window

The Hamming window is a modified version of the Hanning window, with parameters adjusted to achieve a much lower sidelobe level. Instead of a $\cos^2$ form, the Hamming window uses the form shown below.

$$w(n) = \frac{25}{46} - \frac{21}{46}\cos\left[\frac{2\pi}{N}n\right] \qquad n = 0,1,2,\ldots N\text{-}1 \qquad \text{Equation 2-30}$$

This window is characterised by a near cancellation of the previous first sidelobe as shown in red in Figure 2-17, resulting in a sidelobe peak of –46 dB. The –10 dB relative bandwidth is 1.548, less than the Hanning window. The higher order lobes do not reduce as quickly as for the Hanning window but are still less than –40 dB.

2.3.2.4. Blackman-Harris windows

These windows expand on the Hamming window formulation by extending the expansion to higher order terms. The family of windows has the form

$$w(n) = a_0 - a_1\cos\left(\frac{2\pi}{N}n\right) + a_2\cos\left(\frac{2\pi}{N}2n\right) - a_3\cos\left(\frac{2\pi}{N}3n\right) \qquad n = 0,1,2,\ldots N\text{-}1$$

Equation 2-31

with the parameter values calculated to achieve minimum sidelobe levels. Two have been investigated more fully, the minimum –67 dB 3-term Blackman-Harris window and the –74 dB 4-term window. These have the parameters shown in Table 2-1.

Parameter	–67dB 3-term	–74dB 4-term
a_0	0.42323	0.40217
a_1	0.49755	0.49703
a_2	0.07922	0.09892
a_3	---	0.00188

Table 2-1. Values for the parameters used for the Blackman-Harris windows

The two Blackman-Harris windows investigated have a shape shown below in Figure 2-18. The sidelobes are much lower than the previous windows, but at a cost of main lobe bandwidth. The –10 dB relative bandwidth for the 3-term window is 1.965, and for the 4-term window it is 2.063.

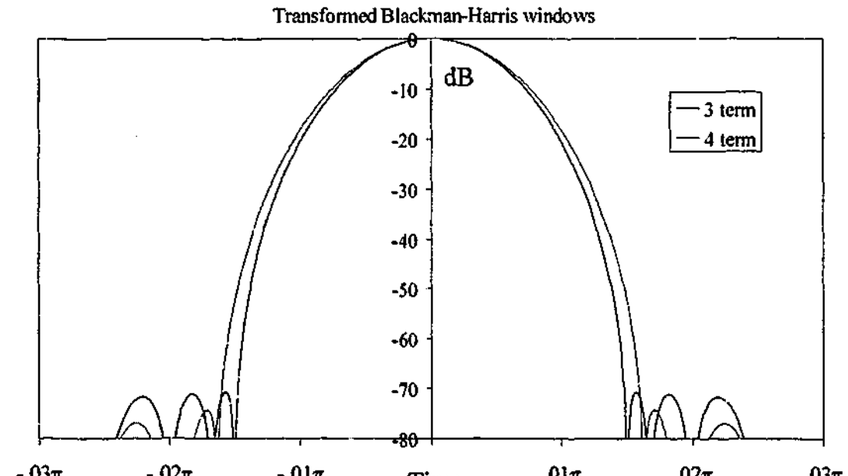

Figure 2-18. Normalised log magnitude of transformed Blackman-Harris windows

2.3.2.5. Gaussian window

The Gaussian function has a form appropriate for use as a window. It is normally used in statistical analysis with a defined mean and standard deviation. By specifying the maximum point to be the centre of the data points, the shape of the window can easily be modified by the user specifying the standard deviation. The formula for this window is

$$w(n) = e^{\left[-\frac{1}{2}\left(\alpha\frac{n-N/2}{N/2}\right)^2\right]} \qquad n=0,1,2\ldots N-1 \qquad \text{Equation 2-32}$$

By changing the value of α which is inversely proportional to the standard deviation, the window shape and therefore sidelobe level and bandwidth can be easily chosen. Some typical values of α are shown in Figure 2-19.

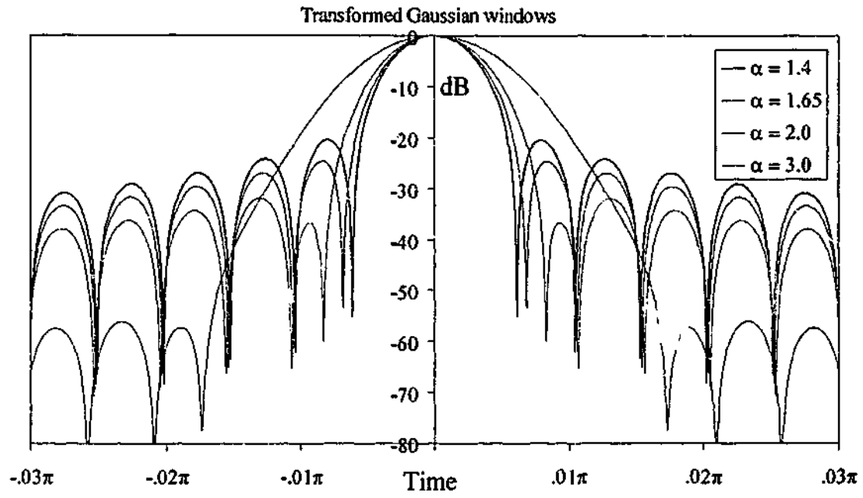

Figure 2-19. Normalised log magnitude of transformed Gaussian windows

The maximum sidelobe levels and –10 dB bandwidths are shown in Table 2-2.

α	Max sidelobe	–10 dB rbw
1.4	-20.5 dB	1.178
1.65	-24.6 dB	1.260
2.0	-31.9 dB	1.396
3.0	-56.0 dB	1.974

Table 2-2. Maximum sidelobe levels and –10 dB bandwidths of some Gaussian windows

The Gaussian window family provides a means of easily changing the sidelobe level using an adjustable parameter. For very low sidelobe levels however, the main lobe beamwidth is quite large, which may obscure peaks very close to each other. Note that setting α to zero gives the rectangular window.

2.3.2.6. Kaiser-Bessel window

An adjustable window with better performance than the Gaussian is the Kaiser-Bessel window. This window uses modified first order Bessel functions to smooth the transition. The formula is shown below

$$w(n) = \frac{I_0\left[\pi\alpha\sqrt{1-\left(\frac{n}{N/2}\right)^2}\right]}{I_0[\pi\alpha]} \qquad 0 \le |n| \le N/2$$

where

$$I_0(x) = \sum_{k=0}^{\infty}\left[\frac{(x/2)^k}{k!}\right]^2 \qquad \text{Equation 2-33}$$

This window has an adjustable parameter α which again can be used to specify the sidelobe levels and bandwidths. Some values of α are shown below in Figure 2-20, the reason for the seemingly strange values chosen will become clear shortly.

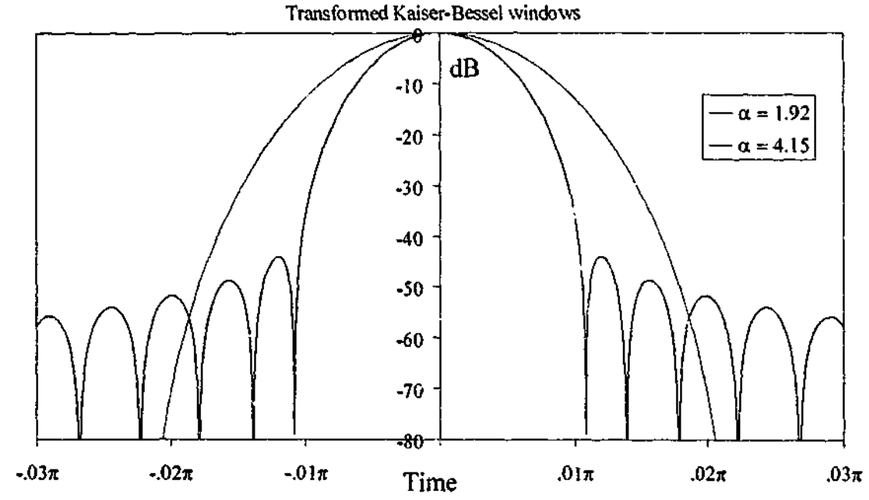

Figure 2-20. Normalised log magnitude of transformed Kaiser-Bessel windows

The corresponding sidelobe levels and –10dB bandwidths are shown below in Table 2-3.

α	Max sidelobe	–10 dB rbw
1.92	–44.0 dB	1.686
4.15	–103 dB	2.423

Table 2-3. Sidelobe levels and –10 dB bandwidths of some Kaiser-Bessel windows

It can be seen that extremely low sidelobe levels can be achieved with this window, but at the expense of bandwidth. Like the Gaussian window, setting α to zero gives the rectangular window.

The reason for the seemingly strange values chosen for α is that these values most closely mimic the behaviour of the network analyser for its time domain analysis. By chance, the author came across a frequently asked questions (FAQ) page on the Agilent Technologies website (since removed), where the question was asked of Agilent what the shape of the window applied in the time domain software was. The response was that while the actual algorithm was proprietary and patented (and at a cost of around A$30,000 well worth protecting), many windows were investigated with the final choice being the Kaiser-Bessel window. Since the author already had a working version of this window, it was a simple task of trial and error to obtain the values that closely matched that from the network analyser. Using the result of transmission through a Perspex sheet, the time domain response from the analyser using the "normal", "minimum" and "maximum" windows were compared to a Kaiser-Bessel window for data collected in the frequency domain. The results of Figure 2-21 show the values of α chosen closely match the proprietary HP window algorithm. The window labelled "minimum" corresponds to the rectangular window. The slight differences observed at very low magnitudes could be attributed to subtle changes in the measurement process that occurred between subsequent tests (the actual data was not identical, but two measurements taken, one the time domain, the other in the frequency domain).

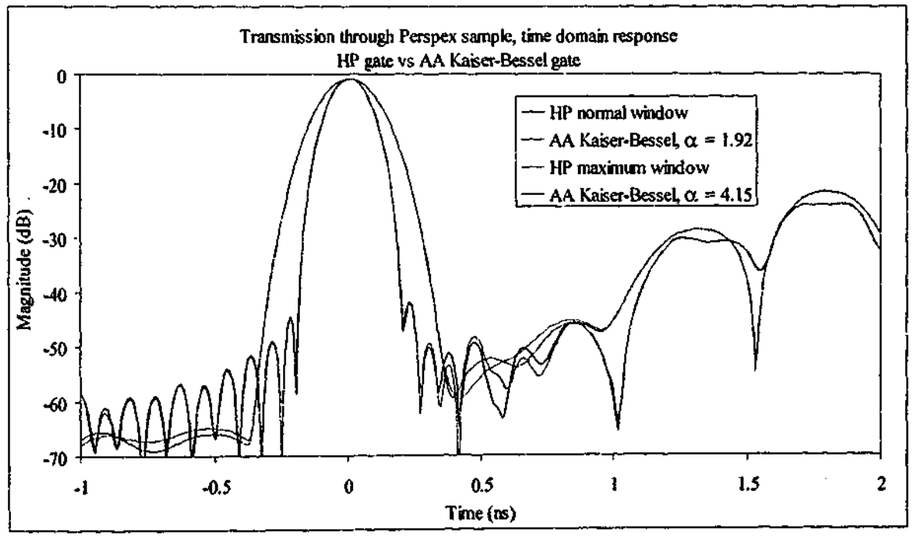

Figure 2-21. Comparison of HP and the author's (AA) windows using Kaiser-Bessel function

2.3.2.7. Time gating

Multiple reflections between the sample and the measurement equipment can lead to unwanted reflections in the measured data; however, these effects can be removed with software time gating. Time gating involves performing a Chirp-Z Fourier transform on the frequency trace, and removing the unwanted reflection peaks from the system.

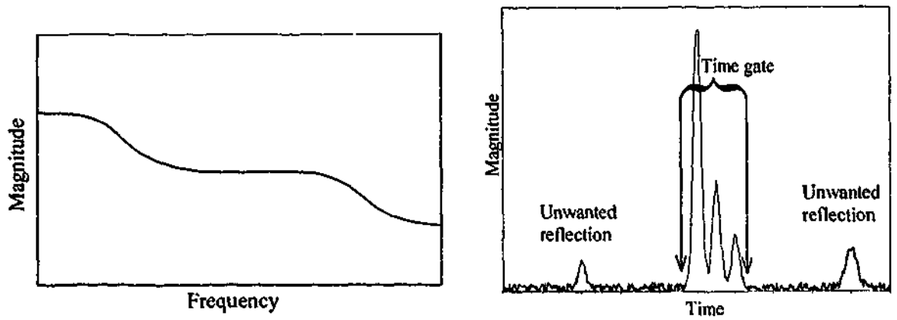

Figure 2-22. Time domain trace of a theoretical frequency spectrum.

Figure 2-22 shows a frequency and corresponding time trace of a theoretical transmission signal. The time domain trace shows peaks emanating from areas other than the sample such as the stand. These signals can be removed using a time gate leaving only the desired signal from the sample. The red trace shows the effects of the time gate being applied, which removes the two unwanted reflections that occur before and after the desired set of peaks.

The 8510C network analyser provides a proprietary and patented gating algorithm. It is described in the operating manual but little detail is given. The Agilent/HP gating technique works very well; however, they (and others[82]) note that the gated result is less accurate near the frequency endpoints than in the centre of the frequency span. The algorithm used is not available as a separate program so a gating program was developed by the author to perform post-measurement gating on ungated results. The gate used was based on the Kaiser-Bessel window, with further refinements to enhance the accuracy of the technique.

The gate was a modified filter designed to have a unity response between the gate's start and stop points and a fast reduction in areas outside the gate's passband. In this regard the gate is slightly wider than the equivalent width HP gate, which uses standard filter techniques meaning the signal is reduced by a factor of 0.5 at the start and stop values. When applied to the time domain signal, the gate adversely affects the points near the frequency start and stop points once the gated response is converted back to the frequency domain. For this reason, extra data is added to the start and stop points in the frequency domain before the first

transformation occurs. Initially the data was padded with zeroes, but this was found to have little effect. The best result was found when the extra data was the "diminishing mirror image" of the existing data around the start and stop points.

To illustrate this, we can see in Figure 2-23 and Figure 2-24 that the measured values of real and imaginary S_{21} from a large sheet of Perspex vary considerably across the frequency span 7.5-18 GHz. After the trace is converted to the time domain, the gate applied and the resultant time trace re-converted back to the frequency domain, the edges of the frequency domain show oscillatory behaviour, similar in shape to that seen in the Gibbs effect. Simply adding zeroes or fixed values in frequency space prior to gating does not sufficiently reduce the end points in the transformed signals. Instead, the number of data points is increased by performing a mirror image of the data at the end point, and applying a weighting factor to reduce the difference in amplitude of the individual point with respect to the actual value at the ends.

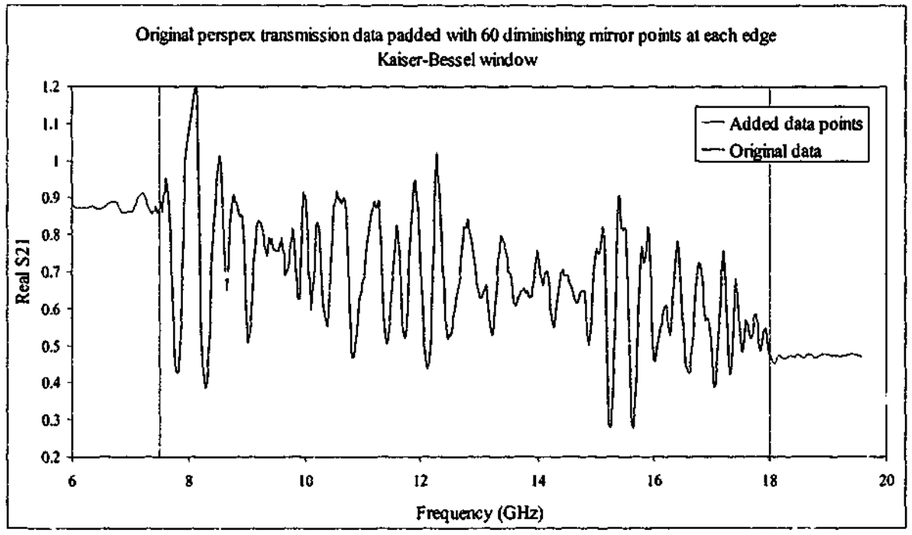

Figure 2-23. Original real S_{21} data padded with diminishing mirror points at end points

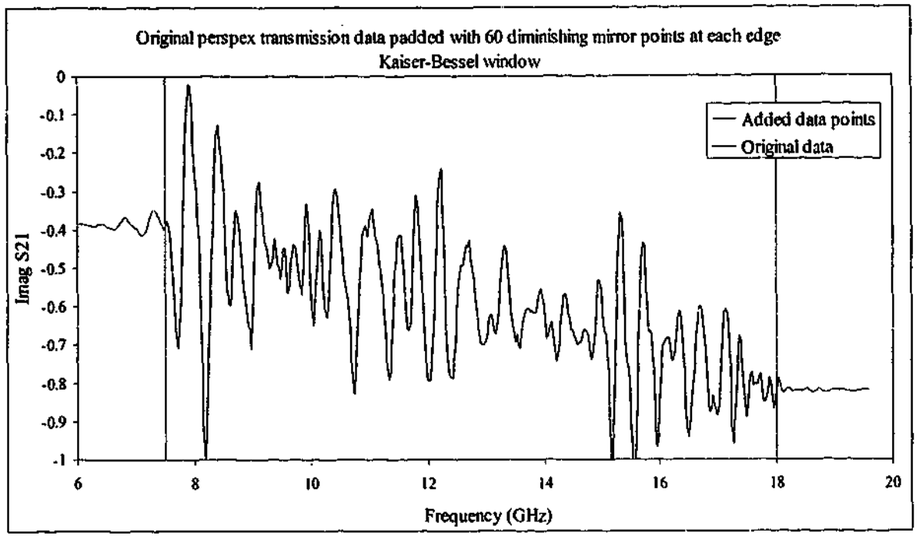

Figure 2-24. Original imaginary S_{21} data padded with diminishing mirror points at end points

Although this is difficult to describe, the implementation is easier and gives reasonably good performance at the end points. For the signal shown above, the ungated and gated responses are shown in Figure 2-25 in the time domain. The black line shows the ungated time domain data, the blue line shows the effect of the HP gate while the red line shown the gated response of the technique being described (AA). For this data set, the two gated responses are quite similar.

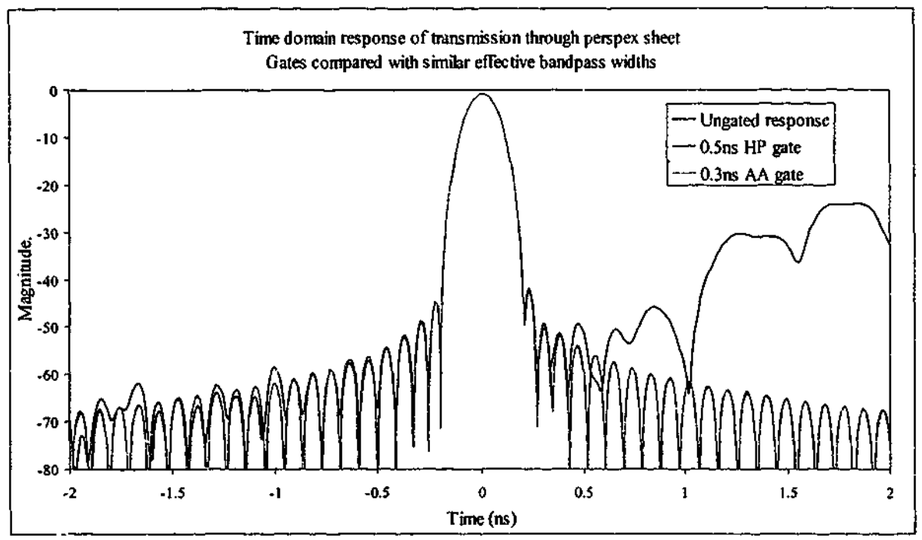

Figure 2-25. Time domain response of Perspex transmission

After the gating has been performed, the time signal is converted back to the frequency domain for further analysis. The results of the time gating can be seen in Figure 2-26 and Figure 2-27. The gated responses are very similar between the Hewlett Packard gate and the author's, except at the high frequency end in the real S_{21} value where the AA gate tends to follow the actual data a little closer.

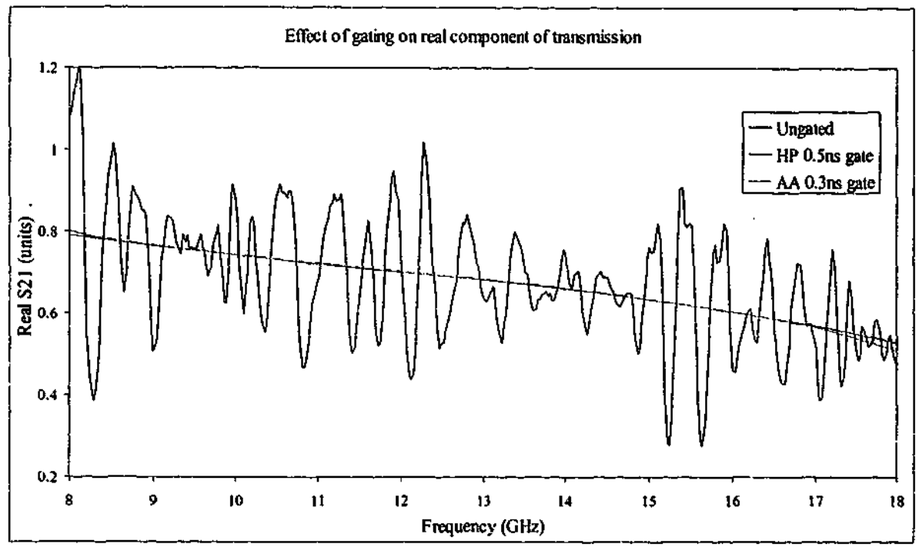

Figure 2-26. The effects of time gating on the real S_{21} signal

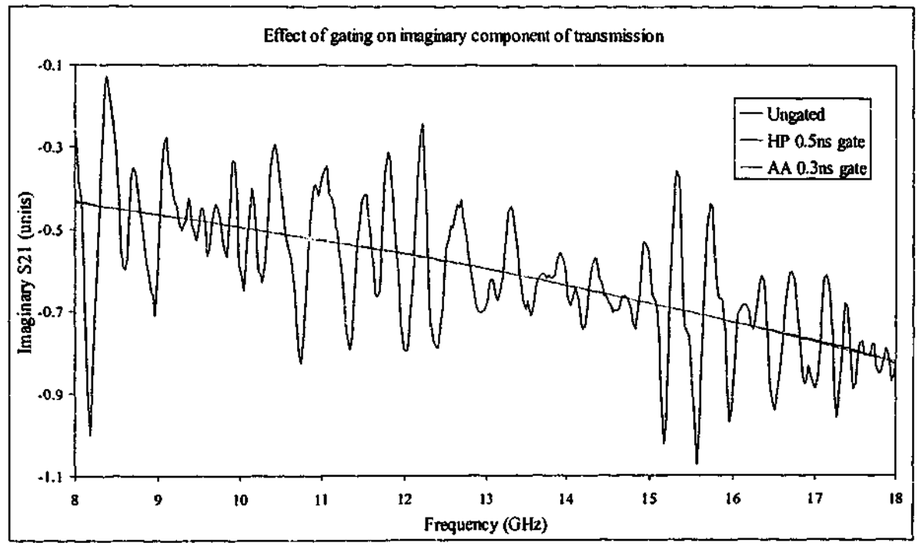

Figure 2-27. The effects of time gating on the imaginary S_{21} signal

When the permittivity was calculated from the gated data we can see how effective the gating technique is in "cleaning up" the signal. Figure 2-28 and Figure 2-29 show the values of real and imaginary permittivity calculated from the data shown above.

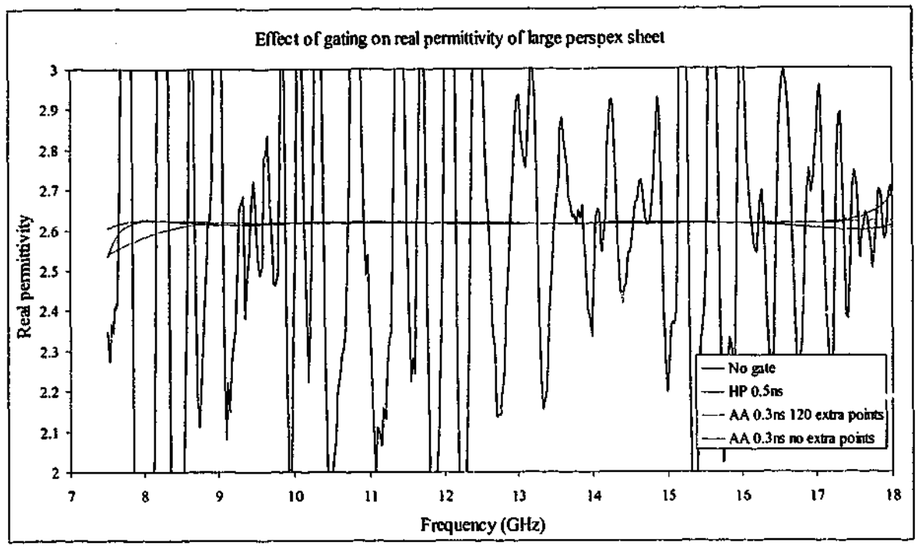

Figure 2-28. The effects of gating on the derived value of the real permittivity of Perspex

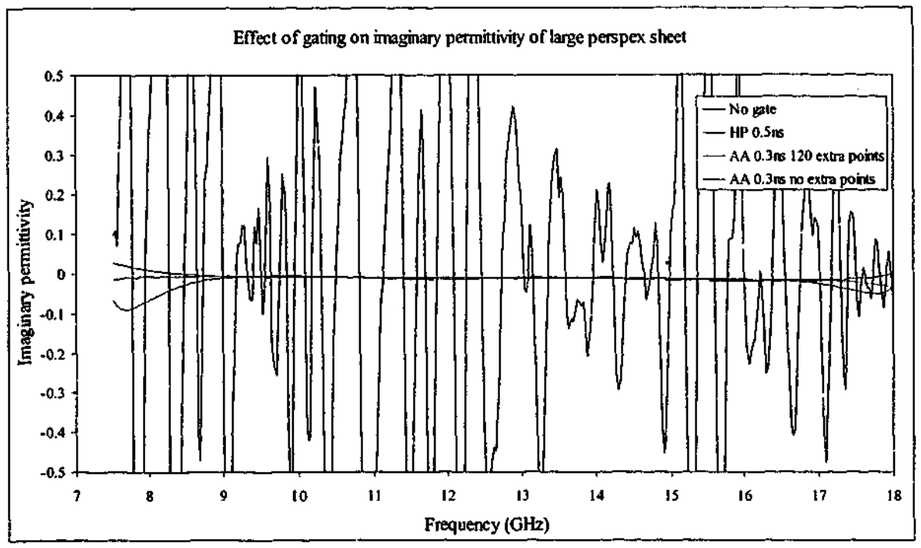

Figure 2-29. The effects of gating on the derived value of the imaginary permittivity of Perspex

It can be easily seen that time gating the signal has an enormous effect in removing the clutter in the measured signals. This leads to a corresponding increase in the accuracy of the

permittivity and/or permeability being derived. One must remember, however, that near the edges of the frequency spectrum the resulting numbers are going to be slightly in error caused by the filter technique. This can never really be reduced to zero, but the effect of adding extra points at the edges and then removing them after the transformation has occurred can lessen the impact.

Care must be taken when using time gating, however, as one may inadvertently remove peaks that are important in the permittivity/permeability extraction algorithms. Consider a lossless, non-magnetic material 10 mm thick with a real relative permittivity of 12. When the reflection and transmission is measured over the range 1-18 GHz one expects frequency responses shown in Figure 2-30 and Figure 2-31. Note how the multiple reflections inside the sample lead to constructive and destructive interferences in the total reflection and transmission responses. When the Chirp-Z transform is performed on the data over the range –1.5 ns to 2 ns, the time domain signal shows the series of peaks caused by multiple reflections inside the sample. This can be seen in Figure 2-32 and Figure 2-33.

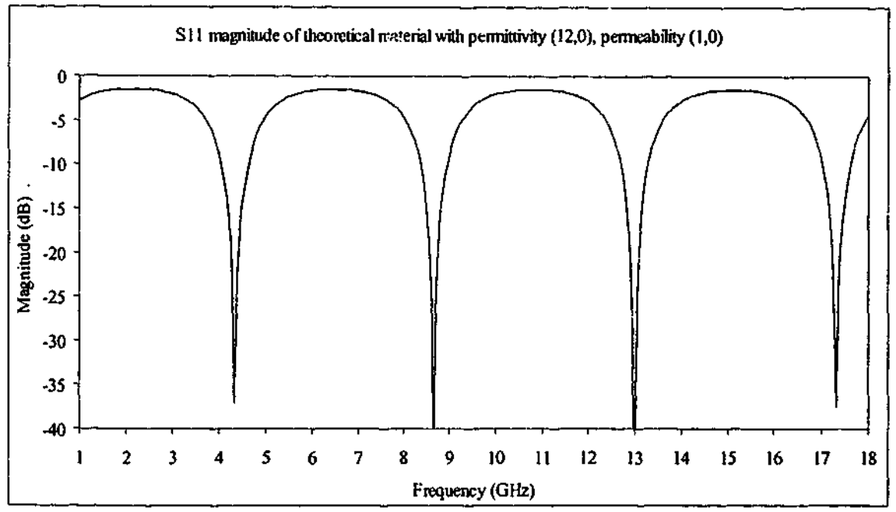

Figure 2-30. S_{11} magnitude expected from a theoretical non-magnetic material 10 mm thick with relative permittivity (12 + 0i) calculated over the range 1 – 18 GHz.

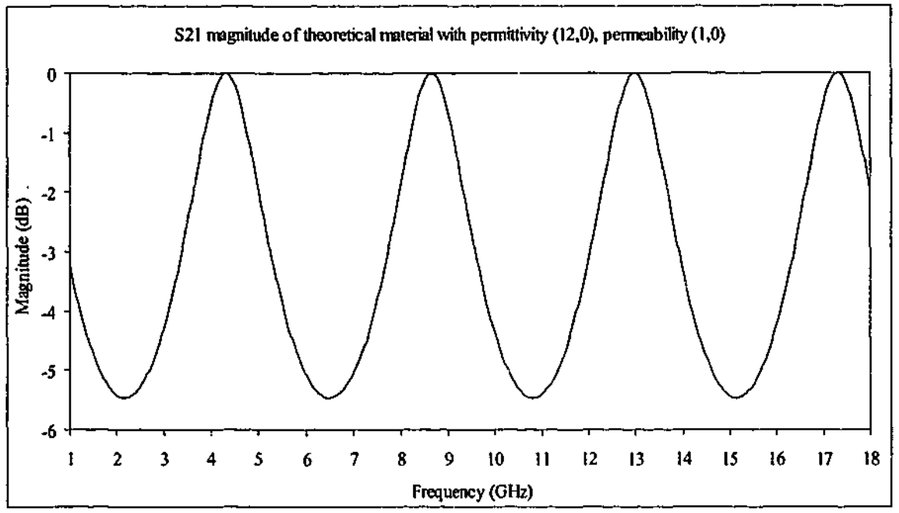

Figure 2-31. S_{21} magnitude expected from a theoretical non-magnetic material 10mm thick with relative permittivity (12 + 0i) calculated over the range 1 – 18 GHz.

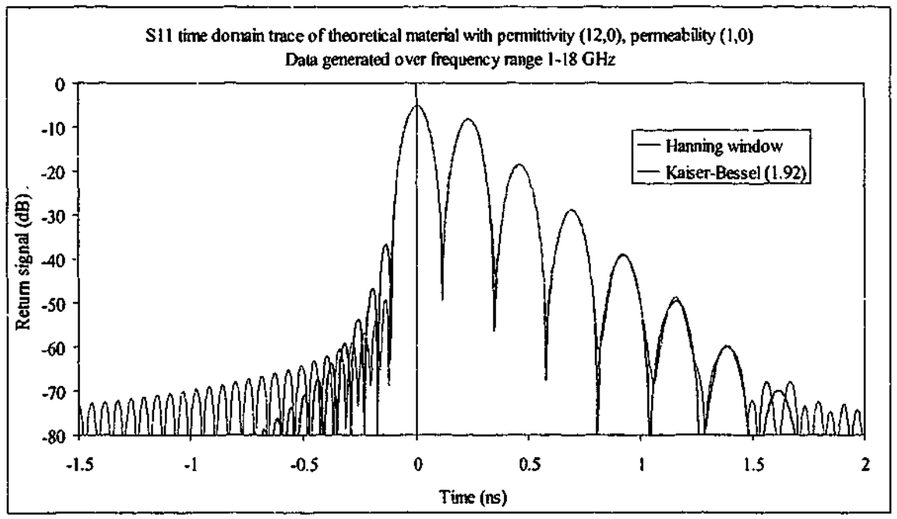

Figure 2-32. S_{11} time domain trace of a theoretical material with relative permittivity (12 + 0i) modulated with two different windows.

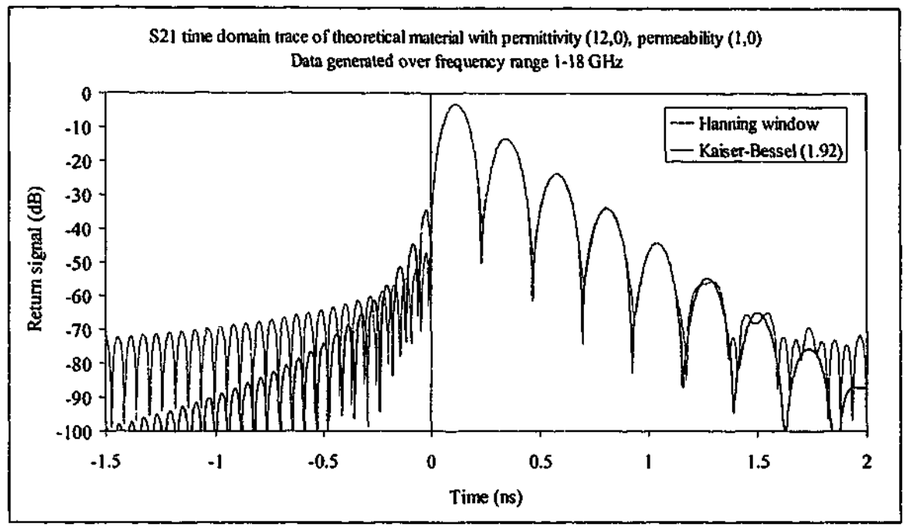

Figure 2-33. S_{21} time domain trace of a theoretical material with relative permittivity (12 + 0i) modulated with two different windows.

The extraction algorithms are expecting the data to include all such peaks. If time gating is too tight and removes some of these peaks, we may expect the derived values of permittivity and/or permeability to be in error. In order to see the effects of this, the signals were incrementally gated with software written by the author to remove some of the peaks. The centre of the gate was set at zero, and a symmetrical gate was applied to the time trace. The gate width was set so that a certain number of peaks would remain for the extraction algorithms, while the rest were removed. The result was then reconverted back to the frequency domain and the programs used to extract permittivity and permeability were run to determine the effects. The Kaiser-Bessel window was used. Note that the sample specifications of zero loss and large thickness have been chosen to accentuate the errors one encounters when removing some of the time domain data. The permittivity results using the transmission only algorithm are shown in Figure 2-34 and Figure 2-35.

It can be seen that it is very important that the number of peaks used for the extraction of permittivity is sufficiently large. Using only the first peak leads to very large errors, in fact the real permittivity calculated bears little resemblance to the actual value. Adding the second peak helps the algorithm focus in on the correct value enormously, and by the time the fifth and sixth peaks are added the consequences of the removal of higher order structure are minimal except at the lowest frequencies. The fifth and sixth peaks have maximum values of

–45 dB and –55 dB respectively, so it is reasonable to assume that once the peaks have reduced to approximately the –50 dB level, adding more peaks is not necessary.

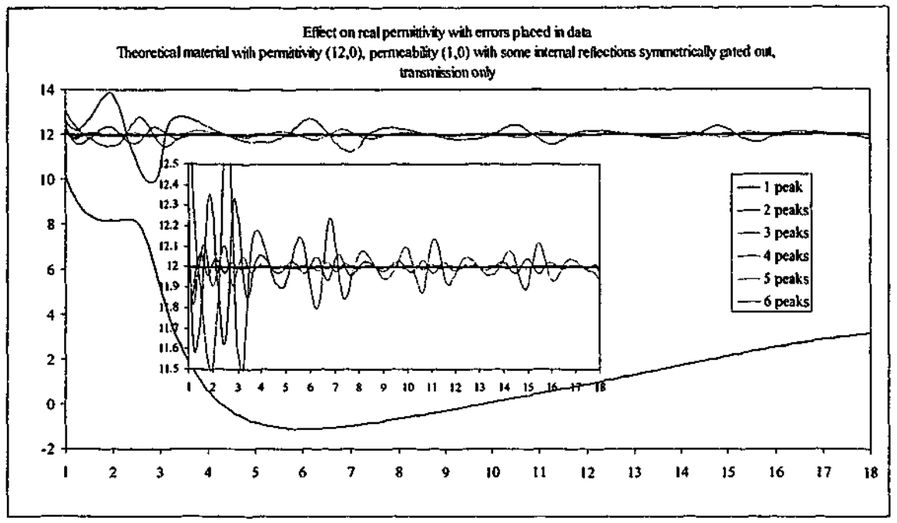

Figure 2-34. Real permittivity of theoretical material 10 mm thick with multiple reflection peaks removed with time gating using transmission only data. Note that the 1 and 2 peak results have been removed from the inset graph for ease of viewing.

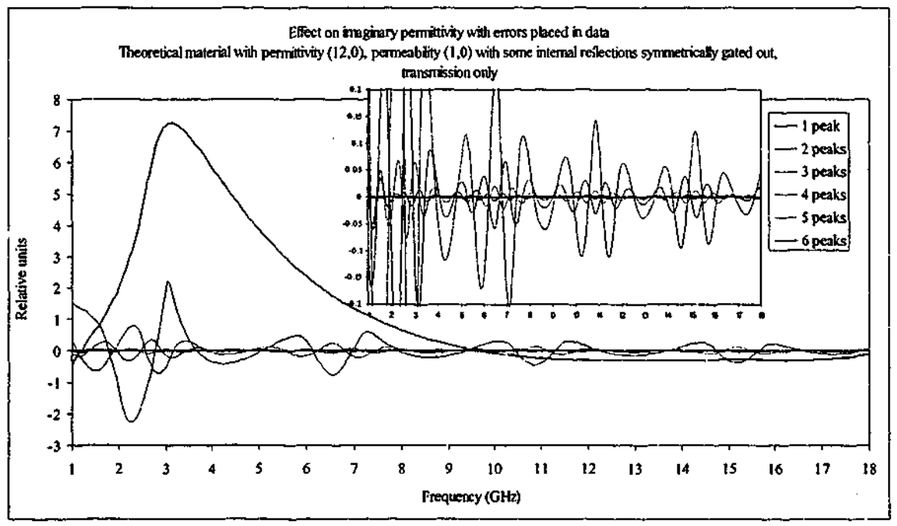

Figure 2-35. Imaginary permittivity of theoretical material 10 mm thick with multiple reflection peaks removed with time gating using transmission only data. Note that the 1 and 2 peak results have been removed from the inset graph for ease of viewing.

The procedure was repeated using the reflection only algorithm with the results shown in Figure 2-36 and Figure 2-37.

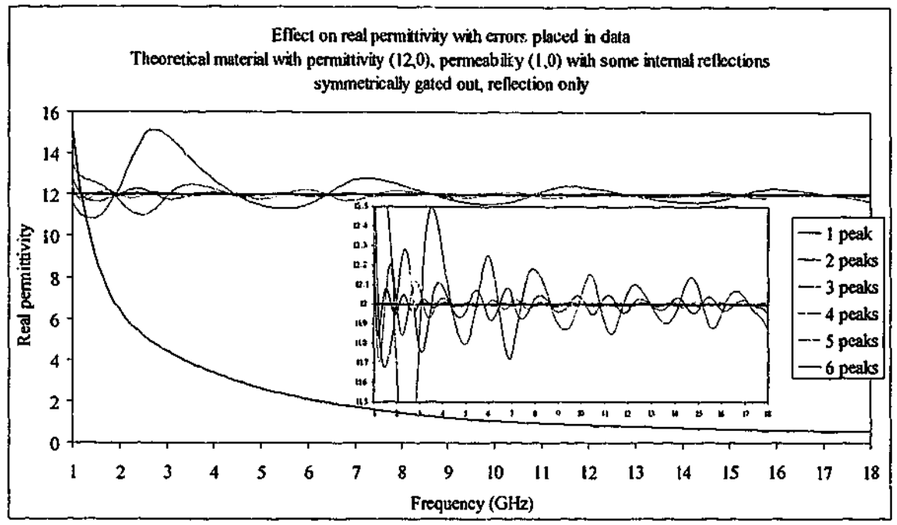

Figure 2-36. Real permittivity of theoretical material 10 mm thick with multiple reflection peaks removed with time gating using reflection only data. Note that the 1 and 2 peak results have been removed from the inset graph for ease of viewing.

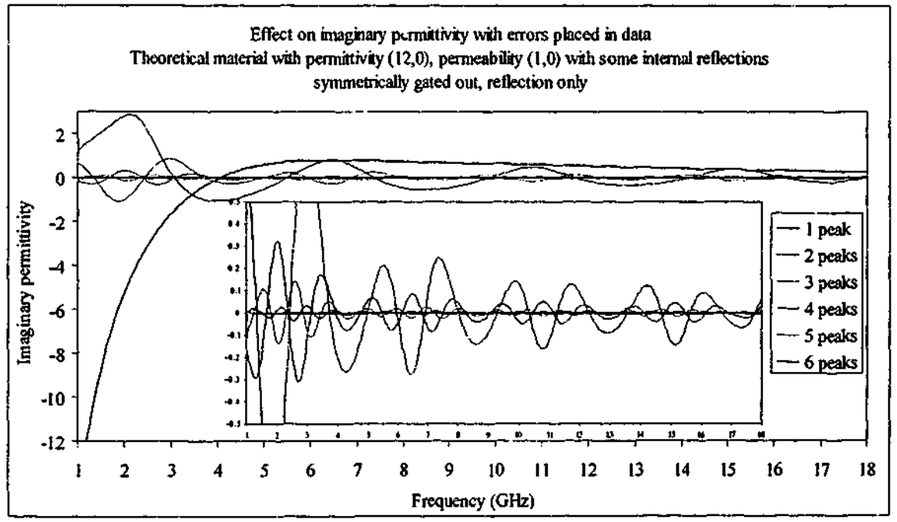

Figure 2-37. Imaginary permittivity of theoretical material 10 mm thick with multiple reflection peaks removed with time gating using reflection only data. Note that the 1 and 2 peak results have been removed from the inset graph for ease of viewing.

The process was again repeated using the reflection and transmission algorithm. This algorithm extracts both permittivity (Figure 2-38 and Figure 2-39) and permeability (Figure 2-40 and Figure 2-41).

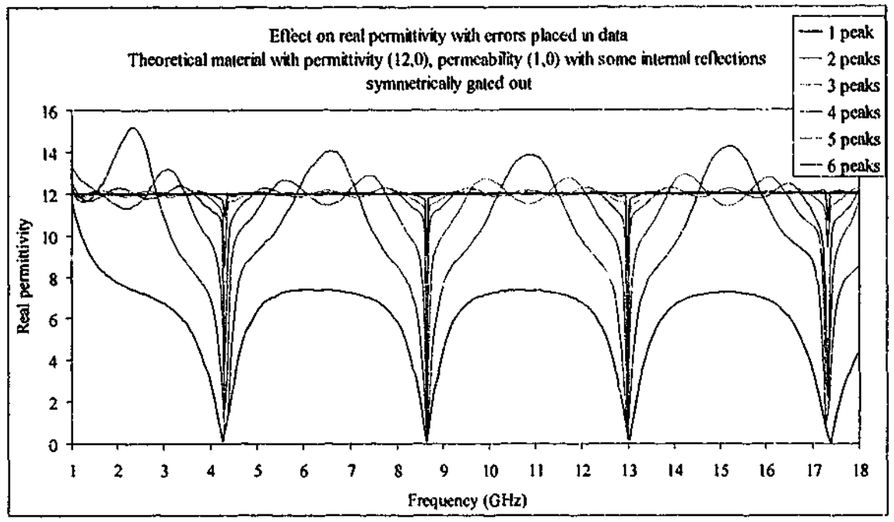

Figure 2-38. Real permittivity of theoretical material 10 mm thick with multiple reflection peaks removed with time gating using reflection and transmission data.

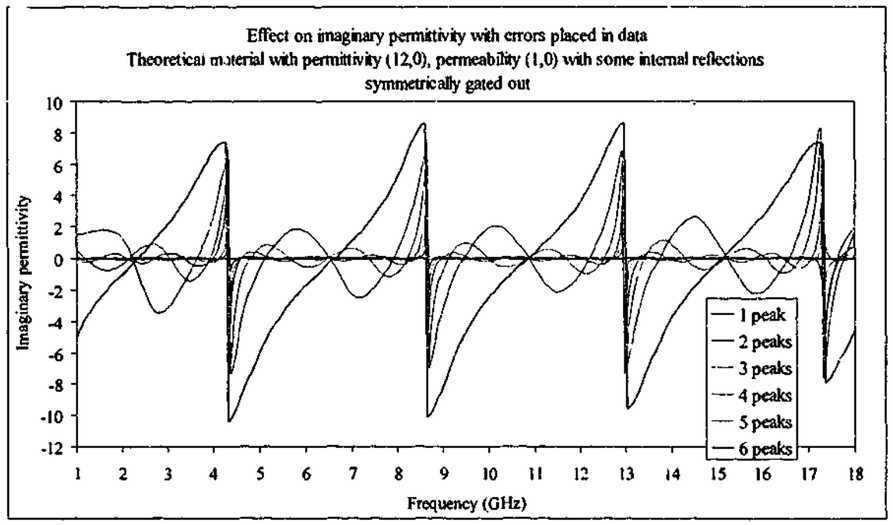

Figure 2-39. Imaginary permittivity of theoretical material 10 mm thick with multiple reflection peaks removed with time gating using reflection and transmission data.

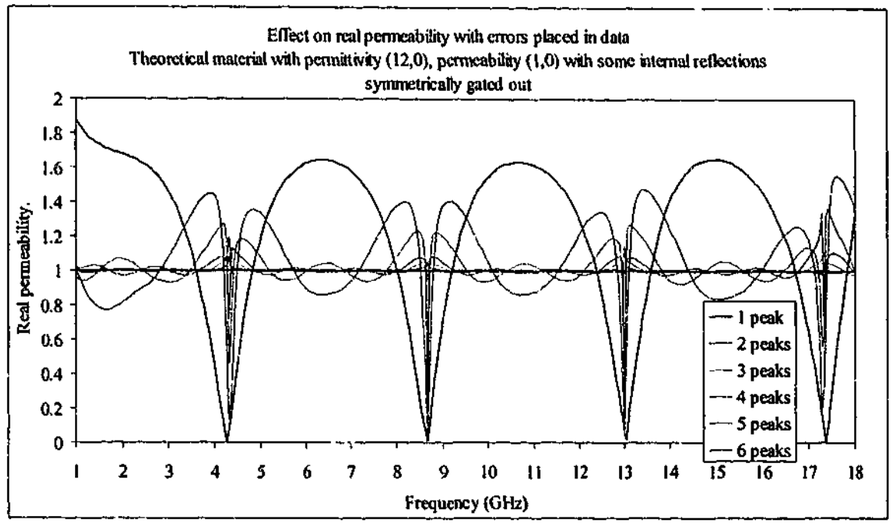

Figure 2-40. Real permeability of theoretical material 10 mm thick with multiple reflection peaks removed with time gating using reflection and transmission data.

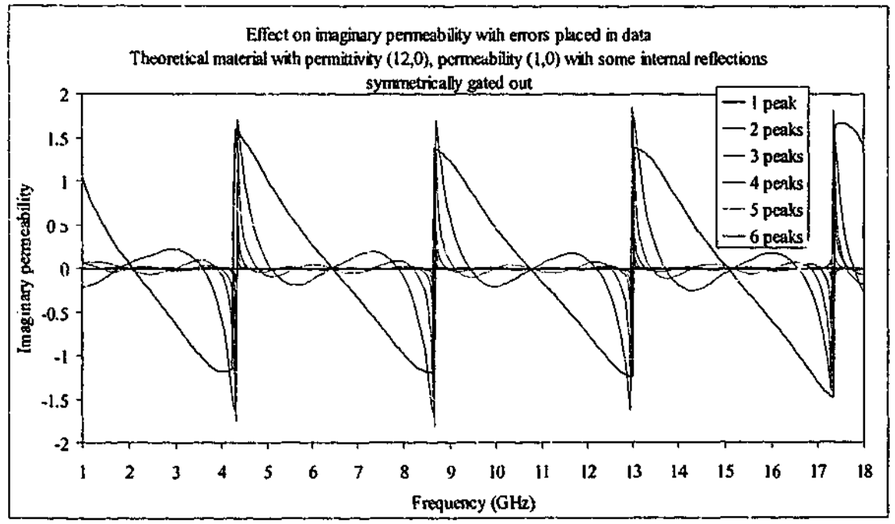

Figure 2-41. Imaginary permeability of theoretical material 10 mm thick with multiple reflection peaks removed with time gating using reflection and transmission data.

Using the reflection only data it can be seen that the effects are similar to those of the transmission only data. The first peak is not enough to give any worthwhile information about the permittivity of the material, but when the second and third peaks are added the values extracted are becoming closer to that expected. By the time the fifth and sixth peaks are

included (corresponding to –40 dB and –50 dB peak heights) the variation from the expected result is small.

However, the algorithm that uses both reflection and transmission data behaves differently to the others considered here. At the frequency points close to where destructive interference occurs in the reflected signal, large discontinuities occur in the computed permittivity and permeability results. The magnitudes of the deviation from the true values at these frequencies decrease with increasing numbers of peaks included in the calculations, but even with six peaks in both transmission and reflection, the effects are not removed.

2.3.2.8 Minimum time gate

Based on an estimate of a material's permittivity, permeability and thickness it is possible to calculate the magnitude and positions of the peaks that occur in the temporal transmission and reflection signals using a reasonably simple formula. While it is also possible to inspect these peaks by performing a transform into the time domain, it is sometimes useful to have a quick method of finding the position of any single peak without going to all the trouble of a Chirp-Z (or another) transform. By following the paths a single ray can take when incident on a slab of material, it is possible to find the time position and magnitude of any peak that can be detected by a receiver. The analysis is shown in Appendix C. The table shown below lists the equations to determine any peak from a slab of dielectric material with impedance Z_2 surrounded by a second material with impedance Z_1.

Peak #	Reflection	Transmission
1	Γ_{12}	$T_{12}T_{21}$
2	$T_{12}\Gamma_{21}T_{21}$	$T_{12}\Gamma_{21}^2T_{21}$
3	$T_{12}\Gamma_{21}^3T_{21}$	$T_{12}\Gamma_{21}^4T_{21}$
4	$T_{12}\Gamma_{21}^5T_{21}$	$T_{12}\Gamma_{21}^6T_{21}$
…	…	…
n	$T_{12}\Gamma_{21}^{(2n-3)}T_{21}$	$T_{12}\Gamma_{21}^{(2n-2)}T_{21}$

Table 2-4. Equations to determine magnitudes of any peak from a slab of material

$$\Gamma_{12} = \frac{Z_2 - Z_1}{Z_1 + Z_2}, \qquad \Gamma_{21} = \frac{Z_1 - Z_2}{Z_1 + Z_2} e^{-\gamma d}$$

where

$$T_{12} = \frac{2Z_2}{Z_1 + Z_2}, \qquad T_{21} = \frac{2Z_1}{Z_1 + Z_2} e^{-\gamma d} \qquad \text{Equation 2-34}$$

where d is the thickness of the material, and the propagation constant $\gamma = i\omega\sqrt{\varepsilon\mu}$. The time taken for each peak to reach the receiver is simply calculated by the distance travelled by the wave divided by the speed of light inside the material (relative to the calibration plane, usually set to zero at the front of the slab). The times for each peak are shown below in Table 2-5.

Peak #	Reflection	Transmission
1	0	$\frac{d\sqrt{\varepsilon\mu}}{c}$
2	$2\frac{d\sqrt{\varepsilon\mu}}{c}$	$3\frac{d\sqrt{\varepsilon\mu}}{c}$
3	$4\frac{d\sqrt{\varepsilon\mu}}{c}$	$5\frac{d\sqrt{\varepsilon\mu}}{c}$
…	…	…
n	$(2n-2)\frac{d\sqrt{\varepsilon\mu}}{c}$	$(2n-1)\frac{d\sqrt{\varepsilon\mu}}{c}$

Table 2-5. Times for each signal component to reach the receiver

These equations fit the data very well as shown in Figure 2-42 and Figure 2-43. For the purposes of the calculation, average values of permittivity and permeability at the centre frequency are used. Using the same example as before, we can see that the predicted positions and times lie exactly where they should. This example only shows a lossless, non-magnetic material so it is perhaps not surprising that the results come out so precisely.

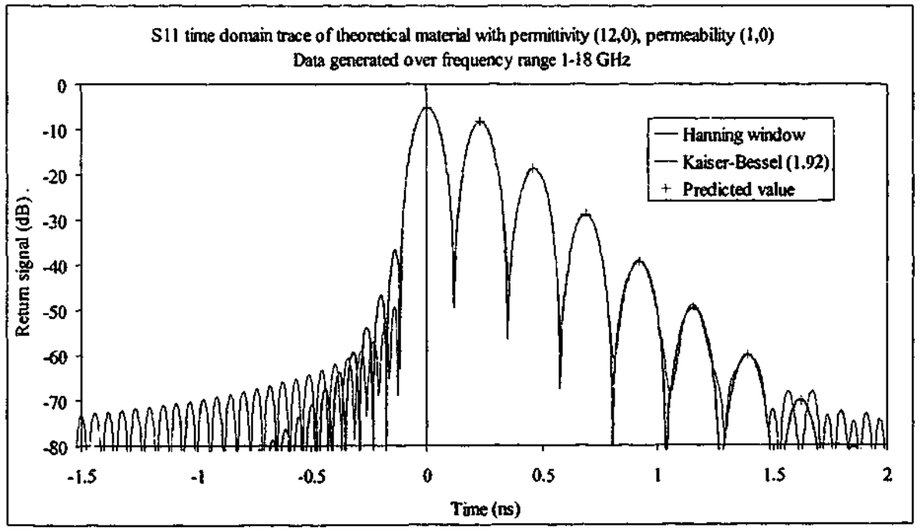

Figure 2-42. Predicted positions for reflection peaks for theoretical material 10 mm thick

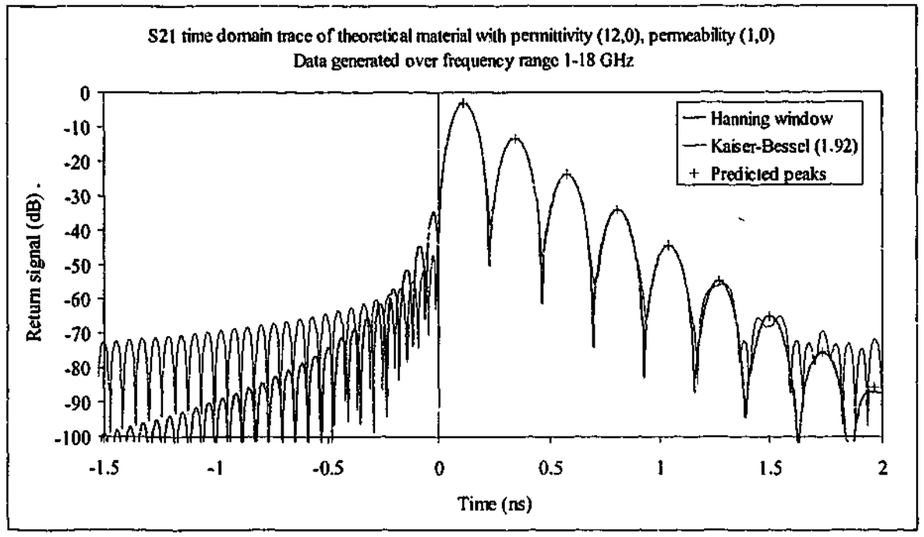

Figure 2-43. Predicted positions for transmission peaks for theoretical material 10 mm thick

Extending the prediction to lossy, magnetic materials gives the following data, shown in Figure 2-44 and Figure 2-45. These traces are for a material 5 mm thick, with a relative permittivity of 8 - 0.2i, and a relative permeability 2 – 0.2i.

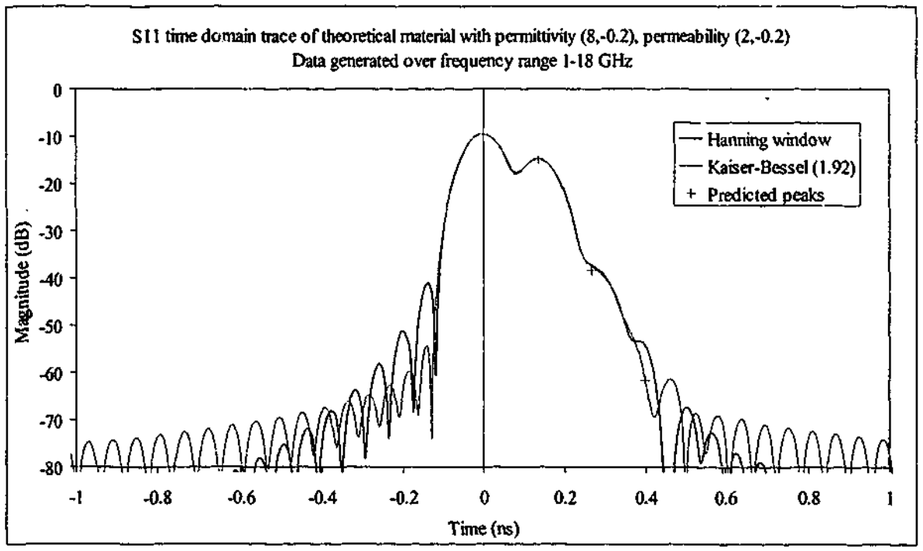

Figure 2-44. Time domain response in reflection for a lossy, magnetic material 5 mm thick

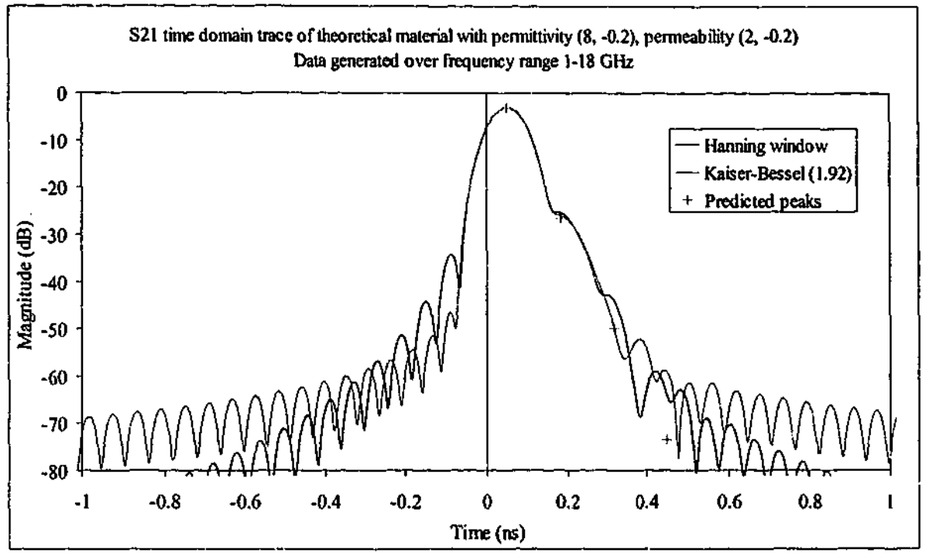

Figure 2-45. Time domain response in transmission for a lossy, magnetic material 5 mm thick

Both the reflected and transmitted signals show good correlation between the transformed data and that predicted from the previous formulae up to the point where sidelobes dominate the transformed signal.

The frequency range used also affects the minimum time gate width. In order to produce a frequency with a certain wavelength, the source needs a finite time to produce a full wave and be properly detected. For instance at 1 GHz, the wavelength is approximately 300 mm long and takes about 1 ns to completely pass a certain point in space. If the gate is set too narrow, not all the wave has had time to be properly collected and so errors in the gated signal may occur. So the lowest frequency used sets a criterion for the minimum useful span for the gate. In the case of the gold horns operating over 1 – 18 GHz, the minimum width is 1 ns. For the silver horn operating from 7.5 GHz the minimum gate width is 0.13 ns, and for the high frequency horns starting at 16 GHz the minimum gate is 0.063 ns. The time gate span should exceed that required for detection and collection of sufficient the multiple reflections.

2.4. Non-network analyser methods

2.4.1. Dielectric test fixture

At lower frequencies (up to about 100 MHz), standard capacitance techniques can be used to evaluate permittivity. A variable parallel plate capacitor is used to determine the real and imaginary permittivity of a material placed between the electrodes. An Agilent 16451B

Dielectric Test Fixture used in conjunction with a 4285A LCR meter provides a highly accurate measurement of parallel capacitance and dissipation factor for any sample tested, which can then be converted into permittivity values. In this configuration, accuracy is quoted as being ± 1% for real permittivity, and ± (5% + 0.005) for loss tangent[83]. This system operates from 75 kHz up to 30 MHz. Figure 2-46 shows the measurement system used to determine permittivity. A guarded electrode is used to minimise errors caused by stray fields at the edge of the electrodes, leading to a more accurate result.

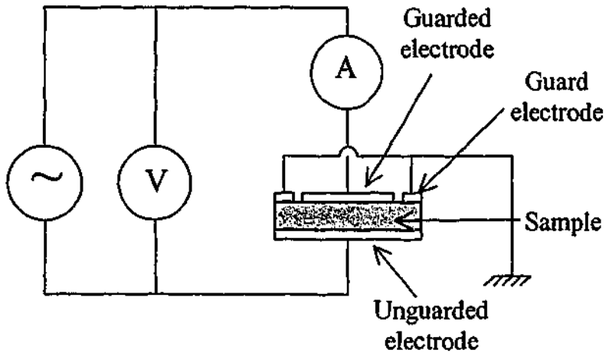

Figure 2-46. Capacitance measurement using guarded electrode system

The electrodes used have a circular cross-section, and the capacitance of the system is

$$C_p = \frac{\varepsilon_0 \varepsilon_r' A}{d} \qquad \text{Equation 2-35}$$

where C_p is the equivalent parallel capacitance, ε_r' is the relative real permittivity of the sample, ε_0 is the permittivity of free space, A is the area of electrode, and d is the thickness of the sample. This can be converted into

$$\varepsilon_r' = \frac{d\, C_p}{\pi r^2 \varepsilon_0 \alpha} \qquad \text{Equation 2-36}$$

where r is the radius of the electrode, and α is a correction factor known as the effective area constant that compensates for the fact that the guard electrode cannot fully eliminate all the stray fields at the edge of the electrode. Using the 38 mm diameter shielded electrode supplied with the 16451B, the value of α varies between 1.0005 and 1.0105 depending upon the thickness of the sample. For samples thicker than 1 mm (valid for all the samples measured), the value only changes slightly from 1.01, and so this value was used where appropriate. The loss tangent is read directly from the LCR meter, and imaginary permittivity can be determined from this.

The main problem with this technique is that since samples are never perfectly flat, an air gap between the capacitor plates and the sample will inevitably form, causing large errors in the extracted value of permittivity. It is possible to minimise this error by separating the plates slightly and measuring the capacitance of the empty fixture and comparing the result to that with the sample in place. If the parallel plate distance is known, one can use the following equations to determine the real and imaginary permittivity of the sample,

$$\varepsilon_r' = \frac{1}{1-\left(1-\frac{C_e}{C_p}\right)\left(\frac{d_s}{d_e}\right)} \qquad \text{Equation 2-37}$$

$$D_p = D_s + \varepsilon_r'\left(D_s - D_e\right)\left(\frac{d_e}{d_s} - 1\right) \qquad \text{Equation 2-38}$$

where C_p is the equivalent parallel capacitance as before, C_e is the capacitance of the empty fixture, d_s is the thickness of the sample and d_e is the distance between the parallel plates. The dissipation factor D_p is the effective loss tangent of the sample, with D_s being the measured dissipation factor with the sample present in the fixture and D_e the value with the sample absent.

Calibrating the instrument turned out to be more complicated than originally expected. Originally, the manual stated a short/open calibration at certain fixed frequencies as being sufficient for this type of measurement. Calibration factors between these fixed frequencies were calculated using interpolation. However, sudden shifts in permittivity were observed above 5 MHz, the source of which was later found to be caused by residual impedance in the device that could not be removed using the standard short/open calibration[10]. For these higher frequencies a short/open/load calibration had to be performed, but due to the limitations of the instrument, these could only be done at seven spot frequencies across the range. The load standard used was the empty test fixture with the plates held at a distance approximating the values expected from the device with the sample inserted. The frequency used to position the platens was 100 kHz, which is well below the frequency that residual impedance effects occur. This calibration had the desired effect, with consistent values across the frequency band measured.

Chapter 3. Measurement Specifics

This chapter gives details of the materials investigated, shows the effects of some of the techniques discussed in the previous chapter on actual measured data, and discusses some of the sources of measurement error that are expected to have a significant effect upon the measurements.

3.1. Details of test materials

In order to test the validity of the new techniques, standard materials were obtained from various commercial sources for testing. A wide range of materials was considered: magnetic and nonmagnetic, lossy and non-lossy, solids and liquids, thin and thick, and samples with a wide range of permittivity. Some of these materials have been used as standards by researchers for a long time because of their stability and ease of testing; others were manufactured especially for this study. These materials were required so that limitations in electromagnetic parameter extraction could be demonstrated, with any sources of error explained.

Three TiO_2 loaded plastic sheets with varying concentrations were obtained from Cuming Corporation. The product numbers for these sheets were C-Stock AK 7, AK 12 and AK 15. These were to be used as standards so that measurements could be taken with the new techniques on materials whose permittivity was known. The concentration of TiO_2 is set so that the real permittivities of these materials are indicated by the dash number, ie 7, 12 and 15. Accuracy of the permittivity is quoted[84] as ± 3% except for AK 15, which was ± 10%. The dissipation factor or loss tangent is quoted as less than 0.002, which results in the value of imaginary permittivity for all the samples being less than 0.03. Samples 305 mm square and 9.6 mm thick were purchased for this study.

Samples of lead glass normally used as a radioactive shield were also purchased for use as a comparative standard. Some sheets of LX-57B lead glass were bought from Excelray Australia, which were avaiiable with a thickness of about 7 mm. The main advantages of the glass are that it is available in a large array of sizes, and is very flat and homogeneous. The real permittivity has been measured[85] at 1 MHz with a value of 9.9, and it has been observed[86] that the permittivity for other lead glasses reduces slightly at gigahertz frequencies from those measured at megahertz frequencies. Therefore the figure of 9.9 should be seen as a maximum

at high frequencies, with a reduction in value of around 0.2 to 0.3 expected at microwave frequencies.

Polytetrafluoroethane (PTFE or Teflon as it is more commonly known) has long been used as a standard because of its stability and frequency independent properties. The real permittivity of Teflon is known to be around 2.04 at microwave frequencies and it is frequently measured when demonstrating a new technique. The sample sheet was 300 mm square and about 5.4mm thick

Polymethylmethacrylate (PMMA or Perspex) is another material with well-known properties and is cheaper than Teflon. It has a permittivity of 2.6 at microwave frequencies. For the purposes of this investigation, different sized samples of 4.5 mm thick Perspex were made.

Lossy materials with high permittivities were also required so that the methodologies could be evaluated for a range of materials. To represent these materials, a series of conductive carbon black loaded rubber samples were produced. Although the permittivities of these materials are not known, measurements of permeability can be taken as a measure of accuracy. The algorithm used for calculating permittivity and permeability calculated values of $\varepsilon\mu$ and $\frac{\mu}{\varepsilon}$, thus the error in the calculation of permittivity and permeability are connected. Since the permeability should be identical to that of free space, any deviation from this value can be seen as an error term for the permittivity. Six different samples were produced, each containing a different amount of Degussa Printex XE2, a highly conductive grade of carbon black. The concentrations and nominal thicknesses of each are shown below in Table 3-1.

Sample ID	Conc (wt%)	Thickness (mm)
A	2.5	1.6
B	5	1.6
C	10	1.1
D	12.5	1.1
E	15	1.1
F	11.6	1.6

Table 3-1. Details of carbon black loaded rubber samples

The carbon loaded rubber sheets were all originally tested when 445 mm square. Later they were cut to 305 mm and 150 mm square for testing the effects of diffraction on the measurement procedures. The materials were passed through steel rollers prior to moulding, which tended to align the secondary carbon black structures with the rolling direction, so the

materials are slightly more conductive in one direction. This necessitates testing the samples twice, once with the samples' rolling direction parallel to the electric field direction from the horn, and the other perpendicular to it. Taking an average of the two measurements gives the expected value when using the coaxial method.

One of the advantages with the technique is that specimens with large inclusions can be tested easily, so a sample containing 6 mm long carbon fibres embedded in fibreglass was investigated. Again, permeability results should give an indication of the errors in the determination. This sample was also originally 445 mm square that was later cut down to 300 and 150 mm square.

Liquids can also be useful in testing the procedure. Liquids such as water, alcohols and mono-substituted benzene compounds have a large dipole moment and so have a moderate to large permittivity at microwave frequencies. Added to this are the resonances that are observed in the frequency range of interest. Most liquids follow a Debye type relaxation curve with well-known parameters[87]. Therefore, these liquids can be used as standards for the free space technique.

The technique is useful for the characterization of magnetic materials also. For this purpose, a polyurethane paint containing 85 wt% carbonyl iron powder was cast into a mould 450 mm square and 1.3 mm thick. It was also later cut into smaller pieces for testing.

3.2. Network analyser measurements

3.2.1. Coaxial measurements

Coaxial samples of the CS-AK xx samples were made from off-cuts of the three sheets. These were difficult to machine to size accurately because they were so rigid. The inner diameter of the coaxial waveguide is 3.04 mm, and so the sample must be large enough to fit over this rod, but small enough so that no gap exists between the sample and the rod. There is a similar problem with the outer diameter of 7.00 mm. Getting an exact fit is impossible in practice and so errors caused by the gaps between the inner and outer conductors are unavoidable. These errors tend to lead to an underestimation in the permittivity.

3.2.2. Free space methods

3.2.2.1. Calibration considerations

Since the free space calibration procedure is of the simpler, "response", or "response/isolation" type, the calibration does not remove many of the error terms internal to the device. While a full 2-port calibration using waveguide components and rigid cabling could be expected to be stable for days, the response calibration in free space using flexible cables may not give adequate performance for more than a few minutes. Variations in air temperature and humidity, movement of the cables and noise in the internal electronics can all lead to errors in the calibration parameters. In order to test the stability of this free space calibration, the reflection from a 445 mm square sheet of Perspex was measured over a period without touching the instrument or the sample. The measured magnitude and phase of the reflected signal are shown below in Figure 3-1 and Figure 3-2.

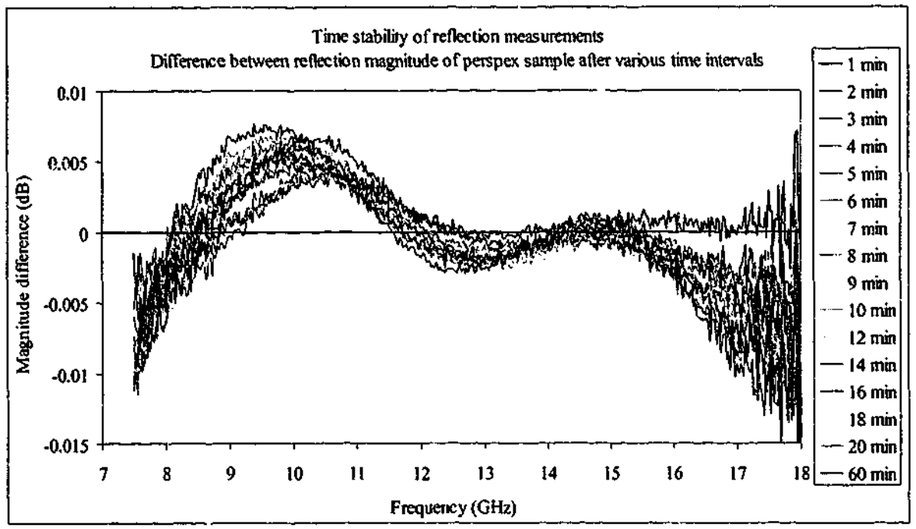

Figure 3-1. S_{11} magnitude of Perspex sheet measured at various time intervals between calibration and measurement

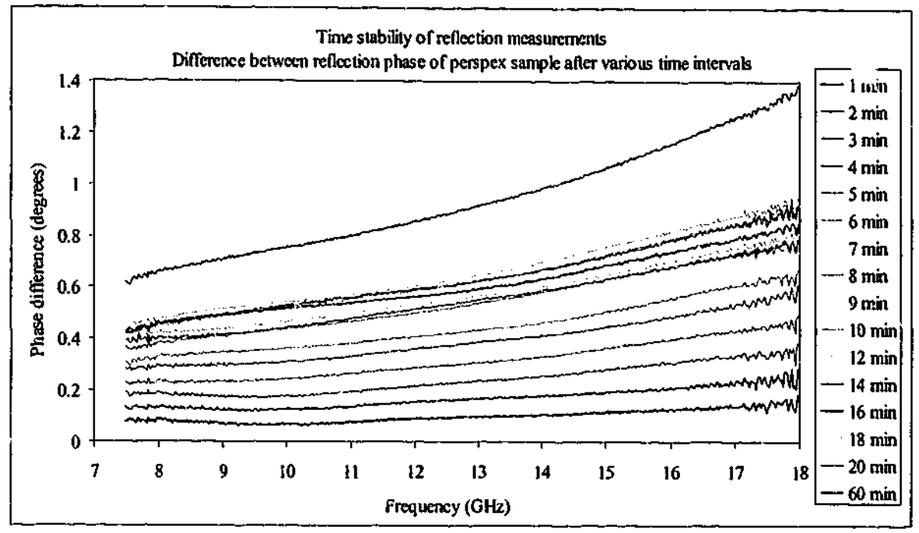

Figure 3-2. S_{11} phase of Perspex sheet measured at various time intervals between calibration and measurement

It can be seen that the magnitude stays fairly constant, while the phase tends to drift a little with time. This may simply be caused by temperature changes in the room. High frequency coaxial cables use Teflon as the dielectric spacer between the inner and outer conductors, which is known to undergo a phase change at room temperatures[88] leading to variations in the phase of the electromagnetic wave travelling through it. High quality cables such as the ones used in this study incorporate so-called "microporous Teflon", a kind of Teflon foam, to reduce this effect but one can easily account for the drift of a few tenths of a degree in phase in cables over 2 m in length as being related to the temperature of the cables. In practice this means that, for the measurement of the samples in this study, the system must be calibrated frequently. Each measurement takes between one and two minutes to firstly place the sample correctly, measure the 401 frequency points 500 times to get a good average value, transfer the data to the computer then save the data to disk. It was decided to calibrate the system after every two measurements (which usually meant after each sample was tested), thus reducing the phase error to less than a few tenths of a degree.

In order to reduce the effects of stray reflections, convoluted microwave absorbers line the metal legs of the stand, while the top of the stand has a thick layer of absorbing foam surrounding any metal parts. The arms that hold the horns are also covered in a thick layer of absorber, while the rod that the arms are attached to is protected by the convoluted absorber.

The polystyrene foam block that the samples sit on gives a phase shift in transmission, but reflects very little of the signal, and attenuation through it is very low.

The calibration procedure for the transmission measurements was very simple. The sample was removed, and the transmitted signal between the horns was measured. The reflection calibration was performed in a two step process; the reflection from a "perfect" metal sheet is measured, then the metal sheet is removed and the background signal taken. Obtaining a perfectly flat metal sheet is difficult; if the sheet is too thin then it bends easily and it is difficult to maintain its flatness. Very thick metal sheets are heavy and so introduce a bend in the polystyrene foam block, even when it is 300 mm thick. If the sample does not sit at exactly the same point in space as the reflection standard used in the calibration, the measured values of permittivity and permeability will be incorrect. When the samples are as little as 50 microns off, the effects are easily seen in the measured result. It was therefore decided to use aluminium foil lined glass sheets as reflectors for the calibration. The glass sheets would not bend and were only 3 mm thick. The foil used was about 85 microns thick, and stuck on to the glass with either a spray adhesive or a double-sided tape.

3.2.2.2. Time gating considerations

As stated previously, time gating is an important part of the measurement procedure. Because of all the stray reflections that occur in the measurement process that cannot be removed easily with a simple calibration, the signals must be time gated in order to gain a noise-free measurement. Stray reflections can occur between the sample and horns, and from parts of the measurement apparatus. The time domain response is derived via a band limited frequency sweep, with the time origin set by the calibration plane. The effects of gating an actual measurement can be seen below in Figure 3-3. The Kaiser-Bessel gate with parameter $\alpha = 1.92$ was used in the transformation.

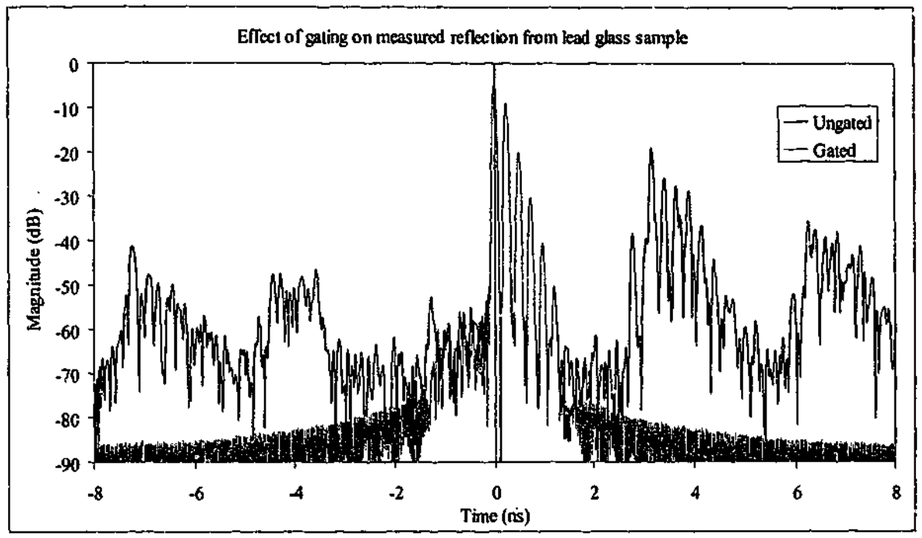

Figure 3-3. Time domain response of a typical S_{21} measurement showing effects of gating

The trace in blue shows the ungated reflection response from a 7.1 mm thick sheet of lead glass. The first reflection peak from the front of the glass is seen at $t = 0$, then the multiple reflections inside the sample occur regularly after this time. These peaks must not be removed by gating in order for the permittivity extraction algorithms to work properly. However, other clusters of peaks also appear with maximums near $t = 3.1$, 6.2, -4.5 and -7.2 ns. These echoes correspond to reflections from the send/receive horn, going back to the sample, then re-reflecting from the sample and re-entering the horn. The time of 3.1 ns corresponds to a distance of about 0.9 m, which is close to twice the horn to sample distance of 0.39 m plus the 55 mm between the horn mouth and the large metal circle used for holding the horn (see Figure 2-4 for picture of horn). Since the Fourier transform is cyclical, these reflections show up in "negative" time also. The time gate is necessary for removing the peaks that cannot be removed any other way. The red trace shows the result of applying the time gate; it has very effectively removed the horn to sample echoes while leaving the main group of peaks intact. The effect of removing these stray reflections on the frequency signal is clearly shown in Figure 3-4. The oscillations that occur in the ungated signal are completely removed, and the resulting trace gives a much more accurate result.

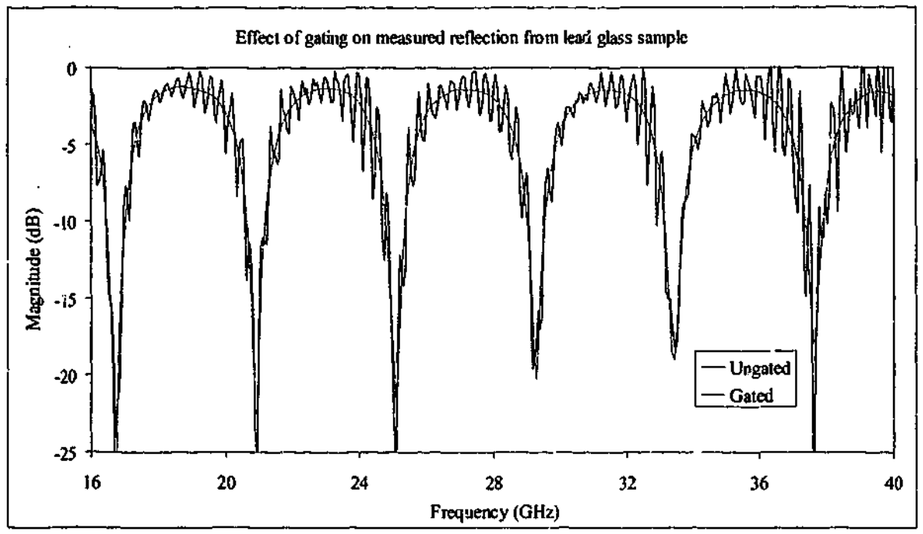

Figure 3-4. Frequency domain response of a typical S_{21} measurement showing effects of time gating

For the reasons of consistent measurement procedure, the free space measurements use a single time gate span for each frequency range where possible. In some cases, the gate widths chosen were not appropriate and so were altered accordingly, but most of the materials tested used the standard gate widths described below.

Most of the samples were made quite thin, of the order of a few millimetres. The reason for this was due to the problems observed when destructive interference in the reflection signal occurs from the sample. However, some of the samples could not be made thinner eg. the lead glass sample. It was mentioned in the previous chapter that the gate width must be kept to a minimum value depending upon the lowest frequency. For a measurement starting at 1 GHz, this corresponds to a time gate of 1 ns. Figure 3-5 and Figure 3-6 show the effects on the extracted values of real and imaginary permittivity of a Perspex sheet when the gate span is changed. These values were extracted using the transmission only algorithm. The traces with a gate width of 1 and 2 ns give values close to the expected value of 2.6 – 0.015i across the full frequency band, but as the gate span gets progressively shorter, the values shift significantly. There does not appear to be any gain to be had from increasing the gate width to 2 ns in terms of average value, only the signal becomes more noisy as additional stray reflections enter the receive horn.

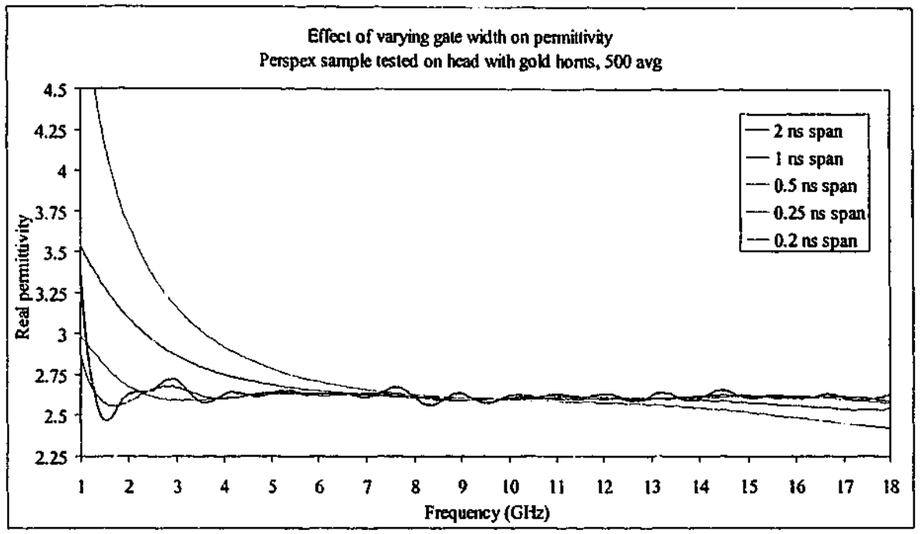

Figure 3-5. Effect of changing gate width on real permittivity for a free space transmission measurement on a 445 mm square Perspex sheet, 4.5 mm thick

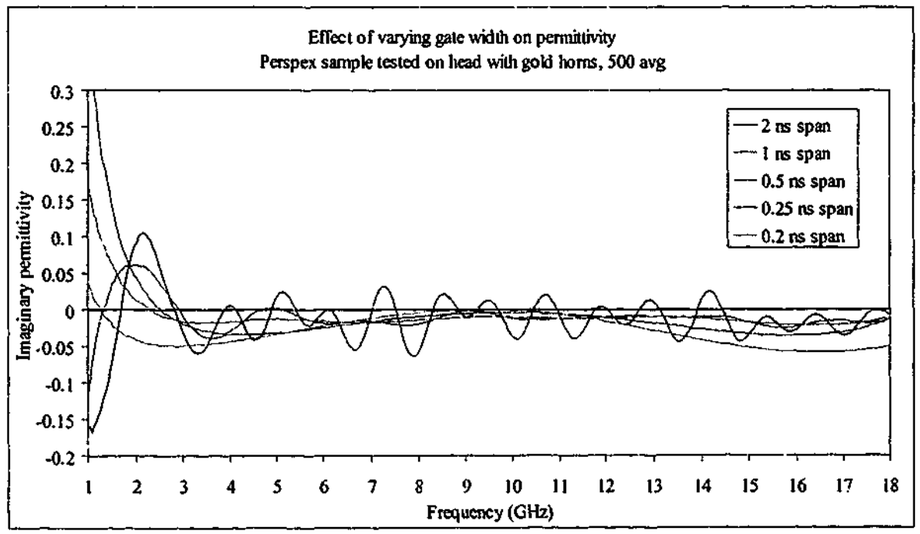

Figure 3-6. Effect of changing gate width on imaginary permittivity for a free space transmission measurement on a 445 mm square Perspex sheet, 4.5 mm thick

In order to set a standard gate width for each frequency range so that accurate comparisons could be made, the permittivity of the non-magnetic standards to be tested was measured using the transmission technique and a wide gate. The magnetic material also had its reflection tested so permeability could be estimated. Using the formula from the previous

chapter, the positions and magnitudes of the peaks were estimated. The results for the first five peaks are shown in Appendix C. A summary of these are shown below in Table 3-2, giving the time position in ns for when the magnitude drops below –50 dB.

Sample I.D.	thickness (mm)	1-18 GHz		7.5-18 GHz		16-40 GHz	
		Ref	Trans	Ref	Trans	Ref	Trans
			Thin samples				
A	1.63	0.09	0.08	0.09	0.07	0.07	0.07
B	1.61	0.11	0.12	0.11	0.09	0.08	0.09
C	1.09	0.12	0.13	0.11	0.12	0.08	0.08
D	1.10	0.14	0.12	0.10	0.12	0.09	0.07
E	1.15	0.13	0.15	0.12	0.10	0.07	0.09
F	1.66	0.16	0.13	0.15	0.12	0.09	0.11
G	1.36	0.14	0.09	0.10	0.06	0.07	0.06
Perspex	4.50	0.15	0.11	0.15	0.11	0.15	0.11
Composite	1.92	0.11	0.08	0.11	0.08	0.05	0.05
Teflon	5.40	0.15	0.11	0.15	0.11	0.15	0.11
			Thick samples				
CS-AK 7	9.63	0.90	0.78	0.90	0.78	0.72	0.78
CS-AK 12	9.62	1.06	0.92	1.05	0.92	0.83	0.70
CS-AK 15	9.78	1.44	1.28	1.44	1.28	1.44	1.29
Lead glass	7.13	0.73	0.64	0.73	0.64	0.73	0.63

Table 3-2. Positions in time in ns for when expected reflection is less than –50 dB.

The point at which the next reflection drops below –50 dB is generally the 4th or 5th peak in reflection or transmission; however, in cases where the sample is quite thick with a high real permittivity and low loss, the 6th or even 7th peaks need to be included. The peaks from the thin samples occur very close to the main peak because the wave has less distance to travel. These peaks are difficult to observe in the time domain because the width of the main lobe (influenced by the window) is usually larger than the point we are trying to see. However, the relevant peaks for the thicker samples can readily be seen, especially if the sample has low loss and a high real permittivity. The correlation of peak position and magnitude with actual ungated measured data is very good, and is shown in Figure 3-7 and Figure 3-8 for the lead glass sample over a limited range. The other thick samples show the same general shape, with the positions of the peaks shifted according to thickness and permittivity.

Based on experience and the values in Table 3-2, it was decided to choose the following gate spans to be used for the thin samples; the 1 – 18 GHz range would use a gate of 1 ns, the 7.5 – 18 GHz range would have 0.5 ns and the 16 – 40 GHz range would use a 0.25 ns gate. These spans allow the most important peaks to contribute to the overall signal while removing

the major reflections that occur in a normal measurement, such as those between the horns and the sample, or from parts of the measurement setup. The thick, low loss materials were individually gated depending on the positions of the peaks.

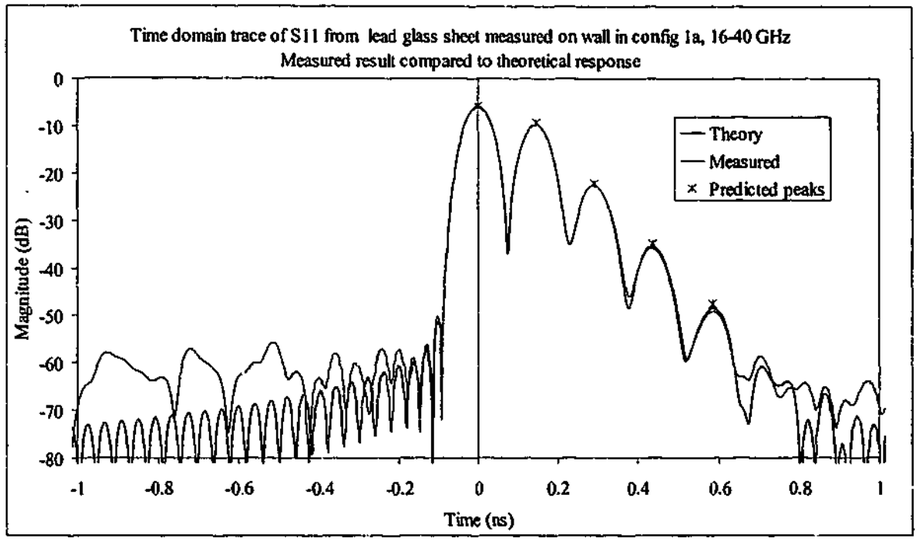

Figure 3-7. Reflection peaks of lead glass sample in the time domain over a limited range

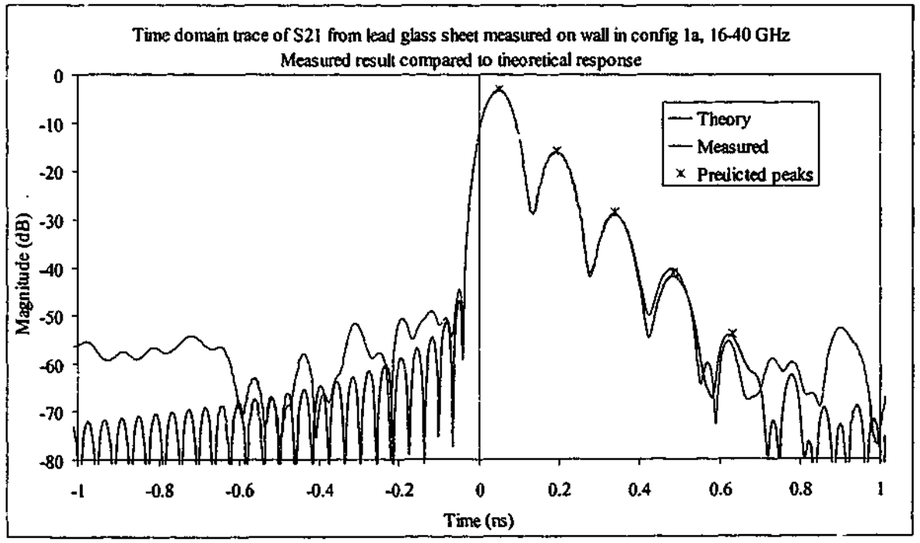

Figure 3-8. Transmission peaks of lead glass sample in the time domain over a limited range

3.2.2.3. Sample size considerations

The size of the sample has a large effect on the measurement accuracy. When performing a transmission measurement, the ideal sample has a uniform thickness that is not so large as to reduce the magnitude greatly, and is infinite in size to remove any effects due to diffraction around the edges. In reality, we desire the sample to be as large as possible and thin enough so that the magnitude transmitted through the sheet is at least two orders of magnitude larger than the diffracted signal. When this is not the case, we can instead estimate the properties of the diffracted wave by measuring the diffraction around a thin flat metal plate with the same dimensions as the sample we want to test, and then remove the effects afterwards.

For reflection measurements, it may be advantageous to use small samples. Large flat plates have much narrower reflection lobes than smaller plates, and so are more sensitive to alignment errors. Figure 3-9 shows an example of this effect, where the RCS values for a number of flat metal plates of various sizes are scaled to show the angular dependence relative to the normal incidence value. The 445 mm square sample falls off very rapidly, already 1 dB below the normal incidence value when the sample is pointing about half a degree off normal. In contrast to this, the 100 mm square sample can be more than one degree off normal and still be less than 0.2 dB from the normal value. When measuring the reflection from large samples, it is important that the sample is facing the same direction as the calibration plane.

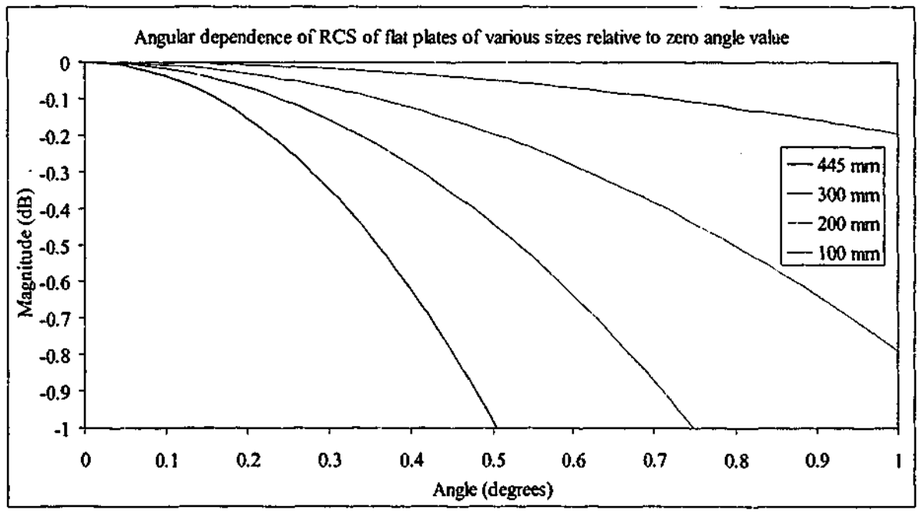

Figure 3-9. Return from flat metal plates of various sizes relative to their normal incidence values

However, if the sample is smaller than or equivalent to the wavelength of the radiation, the return signal from the material may be too low to measure accurately. A balance is therefore needed to increase the return signal but at the same time decrease misalignment effects.

3.2.2.4. Reflection/transmission configuration

Sources of error that could occur with the measurement of reflection and transmission are from near field effects caused by the horn to sample distances, sample alignment and diffraction effects. The effects from the near field could be alleviated by measuring the sample a long way from the horns, or by using a dielectric lens. The main problems with large sample-to-horn distances include maintaining source power, reducing stray reflections, and diffraction from the sample. In order to simulate far-field conditions on a sample 445 mm square in size, the horn-to-sample distance needs to be at least 2.7 m at 1 GHz, 49 m at 18 GHz and 108 m at 40 GHz. Except for the shortest distances which correspond to the lowest frequencies, these distances are difficult if not impossible to achieve inside anechoic chambers.

An effect one might anticipate of measurements taken in the near field is a slight increase in transmission magnitude compared to that of the far field. Taking a ray approach to the problem, we might expect something like that shown in Figure 3-10. The black lines show the straight paths.

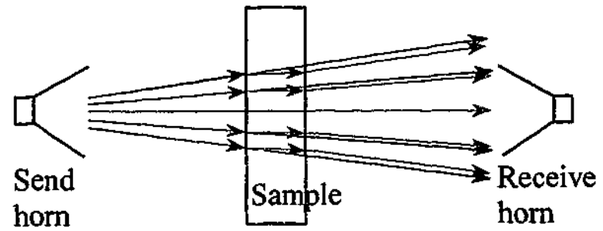

Figure 3-10. Focussing of wave due to refraction inside the sample

Rays from the send horn pass through the sample obeying the complex form of Snell's Law. The rays are bent towards the centre of the receive horn and so the receive horn sees an increased signal magnitude over what should be observed if the ray traces were all straight. It should also see a slightly increased phase shift, as the rays are not going through the sample at normal incidence.

Interference conditions are also expected to be affected by the near field effect. Since the waves are not planar, the distance covered by the rays coming in at higher angles of incidence is slightly longer, so the interference condition is no longer met.

In order to investigate the influence of sample size (diffraction) and horn position on the permittivity and permeability measurement procedure, three different positions for both send and receive horn were used. This gave a total of nine different measurements for each sample using each of the three different types of horn. The positions from the sample are shown below in Table 3-3. Because of the different sizes of the horns and the different gates each horn could operate in, the black numbers show the spacing for the silver and high frequency horns, the gold horn distances are shown in blue. The gold horn needed to be further away from the sample because the gate span needed to be large to include the entire wave at 1 GHz. Since the gate spanned the range –0.5 to +0.5 ns, the effective distance the gate operated over was 150 mm in front of the sample to 150 mm behind it. The receive horn therefore needed to be further away than that so there would be no chance of interference from reflections between the sample and the horn.

Configuration number	Send horn (m)	Receive horn (m)
1	0.39 (0.31)	0.10 (0.165)
2	0.65 (0.53)	0.10 (0.165)
3	0.905 (0.785)	0.10 (0.165)
4	0.39 (0.31)	0.55 (0.42)
5	0.65 (0.53)	0.55 (0.42)
6	0.905 (0.785)	0.55 (0.42)
7	0.39 (0.31)	1.38 (1.25)
8	0.65 (0.53)	1.38 (1.25)
9	0.905 (0.785)	1.38 (1.25)

Table 3-3. Positions of send and receive horns when testing on the reflection/ transmission configuration. Blue numbers are the gold horns' positions

Since the sample rests on a 300 mm thick block of polystyrene foam, the send horn (situated underneath the foam) is placed at almost the closest point in configurations 1, 4 and 7.

Chapter 4. Computer Programs

The computer codes used in this project were all written by the author using various versions of Visual Basic for Windows (except for one case which used Qbasic for DOS). While this allows a user-friendly interface and the coding is relatively simple, it has no inherent complex number handling ability, so all the complex functions had to be defined before they could be used. While complex addition and subtractions are of course no more difficult than simple arithmetic, maintaining branch cuts in the complex inverse circular functions can get a little wearisome at times.

4.1. Data collecting codes

4.1.1. Network analyser

The computer controlling the network analyser system is an old 486 running Windows 3.11, and since it is really only used for data collection a high-speed model is not required. It communicates to the network analyser via a GPIB board and controls all the most commonly used functions for normal measurements. The code provides a pleasing (but hardly spectacular) user interface that is familiar to most Windows users. Upon starting the program, the user is asked to select a type of measurement from a list of commonly used set-ups by clicking on a measurement type shown in Figure 4-1.

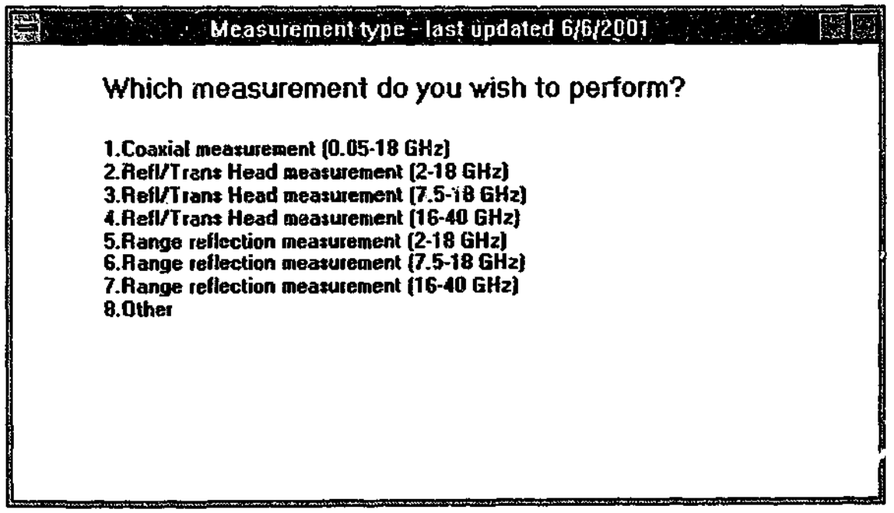

Figure 4-1. The opening window for the data collection program

Coaxial measurements are undertaken using the first selection, unbacked reflection or transmission measurements with selections 2 to 4, and backed reflection measurements use selections 5 to 7. Selection "8" allows the frequency range to be set up individually by the user. Once the user selects a measurement type, the computer sets up the frequency range, calibration parameters, and the data collection procedures to be used.

The operator is then presented with the main form, which is a screen containing a number of different buttons and check boxes, shown in Figure 4-2. From this page the whole program is run, measurements can be taken, calibration procedures begun, measurement options such as gating, averaging can be turned on or off, permittivities and permeabilities calculated and any part of the measurement can be graphed. Note that for this demonstration, option "3" was selected for transmission or unbacked reflection measurement with the silver horns.

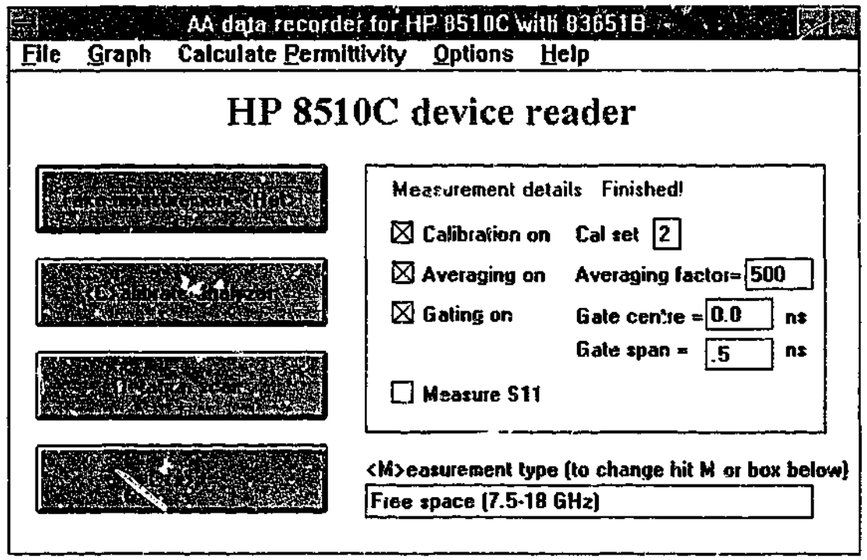

Figure 4-2. The main window of the data collection program

The buttons attempt to be self explanatory (hence their large size), with the general layout kept as simple as possible. Most of the key features can be controlled by the keyboard as well as the mouse, since it is usually much easier to hit (say) the large "Return" button on the keyboard than have to position a mouse on a screen and left-click once.

The box on the right hand side labelled "Measurement details" contains check boxes so the operator can turn a calibration set on or off, change the number of averages used, or change the time gate parameters. Since the most common measurements use S_{21} only, the reflection signal S_{11} is usually not measured. This is a time saving feature, since the measurement of S_{11} takes as long as the S_{21} measurement but will not contain any useful

information. In this case, the data file is filled with making the real part of S_{11} equal to one and the imaginary part equal to zero. However, for reflection only measurements this can be changed by clicking the check box next to "Measure S11". This tells the analyser to measure the reflected signal. When the box is checked, a second box appears to the right of the first (not visible here) asking if the user wants to measure S_{21} as well. If so, then the full S-matrix will be measured, if not the S_{21} data will be filled with ones and zeros.

The frequency range (or measurement type) can be changed by clicking on the box on the lower right of the screen. This will bring up the box shown in Figure 4-1 again and the measurement can be set up as before. The "Rotation scan" button shown in Figure 4-2 tilts and/or rotates a sample placed on the telescope mount over a set number of angles, but is not used for measurements detailed in this thesis.

Usually the first thing to do when starting a measurement is to calibrate the system. Hitting "c" on the keyboard or clicking the "Calibrate Analyser" button brings up the calibration window shown in Figure 4-3. Note that number of averages and gating parameters can also be applied here, with the values used carried over to the actual measurement.

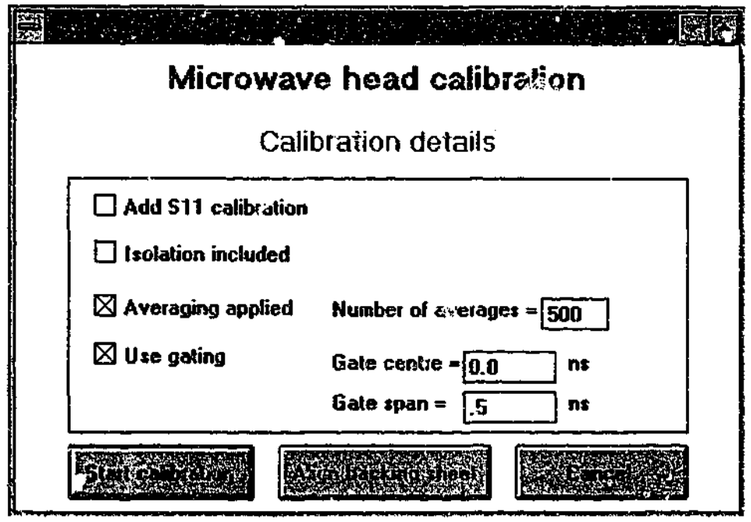

Figure 4-3. Calibration window of the data collection program

In the same way as for the main window, this window also includes all the options for calibrating reflection only measurements, with the option of calibrating S21 too. The greyed out button marked "Align backing sheet" is used, unsurprisingly, for aligning the backing plate when performing backed reflection measurements. In the case of an unbacked reflection or transmission measurement, this button is disabled. When a backed reflection calibration is to be performed, the computer is able to communicate to the telescope stand through the RS-

232 port, and tilt or swivel the stand to obtain the maximum return. This enables a more accurate measurement of the backed reflection signal. The window for aligning the backing sheet is shown in Figure 4-4.

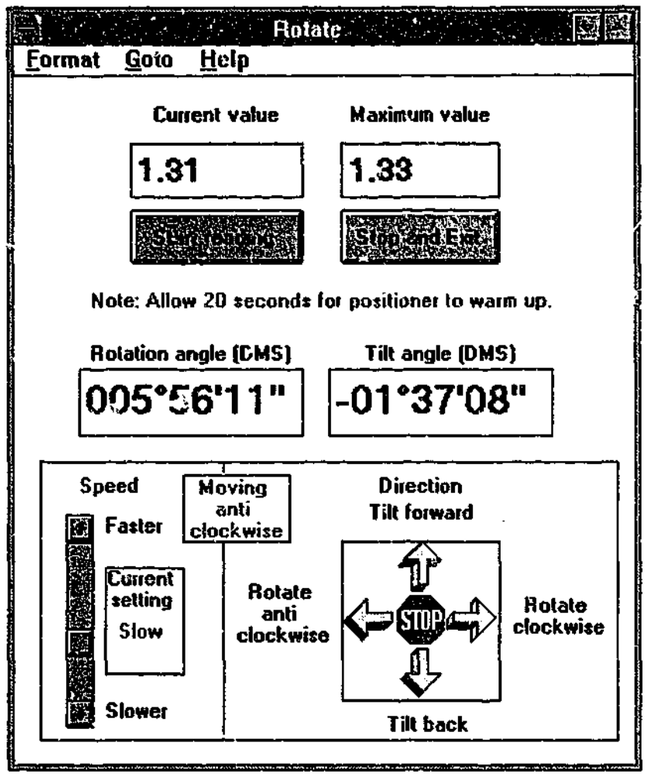

Figure 4-4. Align backing sheet window from the data collection program

When in this mode, the network analyser moves into frequency sweep mode, which allows for a much faster response than the standard stepped frequency mode. The response is not as accurate, but for the purposes of simply finding the point of maximum return, speed is not important. The analyser is also put into time domain mode, and the value of the highest peak across the full time spectrum is shown in the top left textbox. While the stand is rotated and tilted, a maximum value that has been shown in that textbox is shown in the textbox on the right. This allows the user to easily find the point of maximum return.

The angles of azimuth and altitude are shown in degrees, minutes and seconds of arc, the format can be changed to decimal degrees if desired using the "Format" drop down menu. These values are read directly from the stand. The telescope mount has four slewing speeds, from "Very Fast", to "Very Slow". The fastest speed the telescope will move is 8 degrees/second, while the slowest is 30 arcsec/second. Normally the "Slow" setting of 8

arcmin/sec is used to align the plate. The direction buttons shown as arrows at the bottom left of the window are used with the mouse; alternatively the directional keys on the keyboard can be used. The little pane with pink writing shows the current direction of the stand. This window also has a "Goto" menu that is used for positioning the stand in a certain direction – this is useful for performing a series of off-normal angle measurements (the "Rotation scan" shown in the main window).

Once the network analyser has been calibrated with either method, the measurement is taken and the data is saved to the hard disk using the window shown in Figure 4-5. Details such as sample thickness, frequency range and a detailed comments line are placed at the top of the data file, with the real and imaginary S_{11} and S_{21} data.

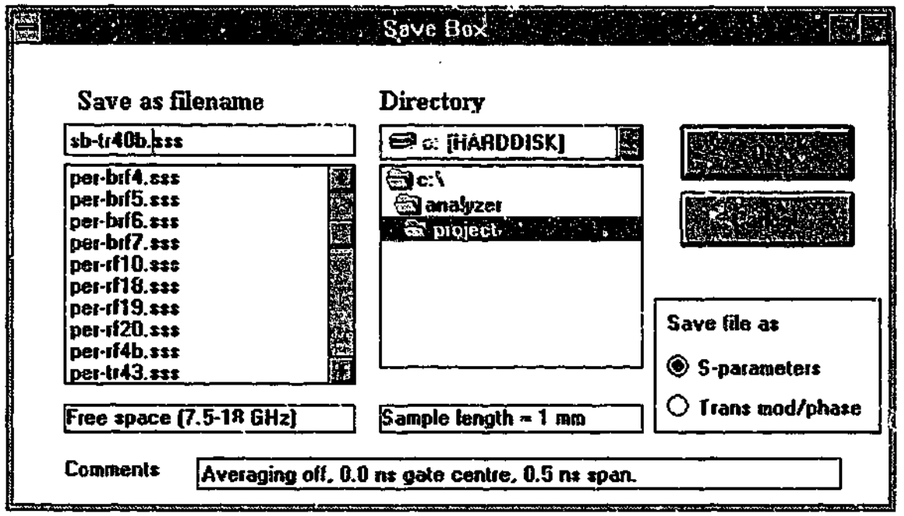

Figure 4-5. The Save file window from the data collection program

The program can also calculate the permittivity of the sample currently being measured, but because the iterative nature of the transmission only and reflection only algorithms takes a long time on the 486 (of the order of 5 – 10 seconds for all 401 data points), the permittivity calculations are usually done on a faster computer. The data collection program also allows the user to graphically display the measured responses, and the permittivity (if calculated).

4.1.2. LCR meter

A computer was used to collect data from the LCR meter and convert the raw data to permittivity values. Since the only spare GPIB board available could not be accessed via any Windows based interface, a program was written using the free QBasic program available with Microsoft DOS 6.20. While not providing the greatest user interface available (never a

feature of the author's programming style anyway), the program nevertheless does a good job of collecting the data and calculating the permittivity. The program's opening screen is shown in Figure 4-6.

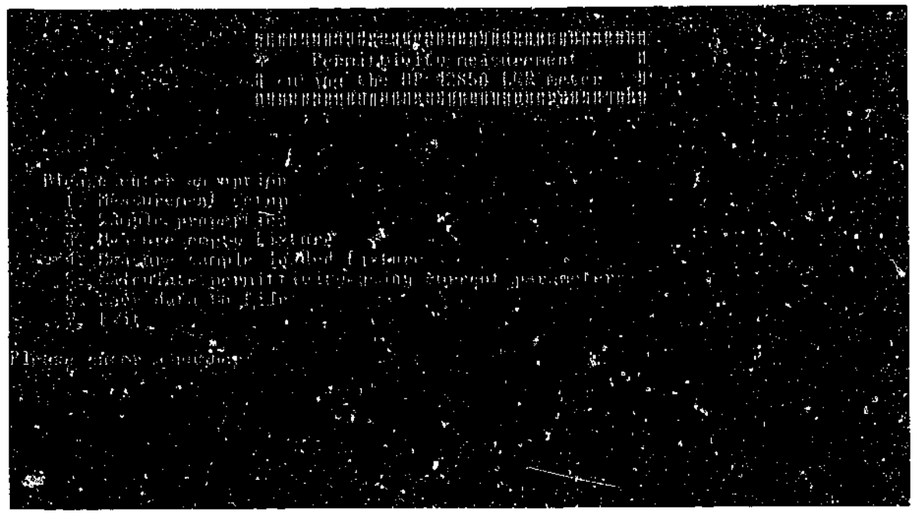

Figure 4-6. User interface of DOS based program to collect data from LCR meter

While it is a long way from the point and click Window's mentality, it is still easy to navigate using the options available from the keyboard. The important details such as sample thickness and platen size can be entered, and the automatic nature of computer-based measurement allows many time-consuming measurements to be taken while unattended.

4.2. Permittivity extraction codes

The program used to extract permittivity has progressed a long way since first conceived. The latest version contains many aids to help calculate "difficult" measurements (for instance those where diffraction had not been removed). The main screen (shown in Figure 4-7) provides the required functionality is an easy to navigate environment.

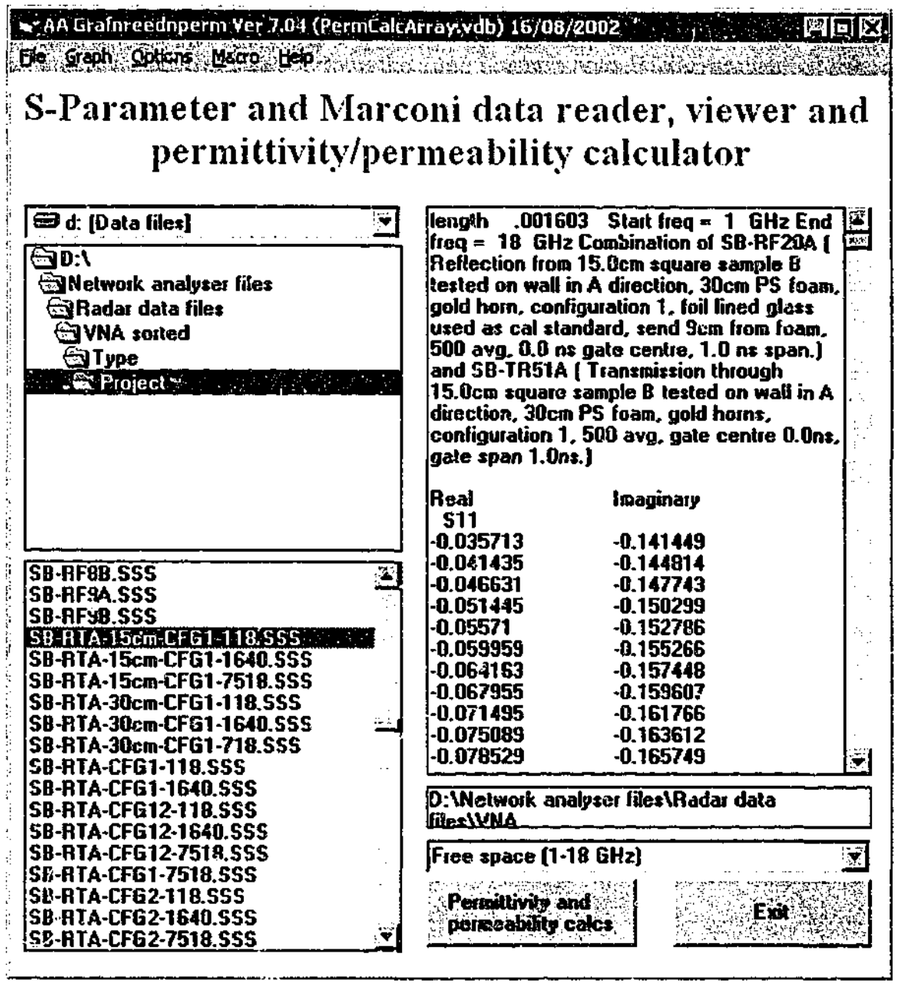

Figure 4-7. The main window of the permittivity extraction program

The main window is a basic design, showing the drive, directory and file information on the left hand side, with the file contents on the right. The large text box shows the header information of the data file as the first entry extending over a number of lines. The sample thickness (or length) in metres is shown first, the frequency range next, then the comments regarding sample position, calibration details and time gate parameters. The data file shown here is a composite of two individual measurements, the reflection and transmission responses measured separately and brought together into a single file using another program discussed later.

The raw or processed data can be graphed using the drop down menus at the top of the window. Real and imaginary parameters, or modulus and phase can be displayed as shown in

Figure 4-8, with the corresponding graph shown in Figure 4-9. The graphing routine is similar to the one used in the data collection program.

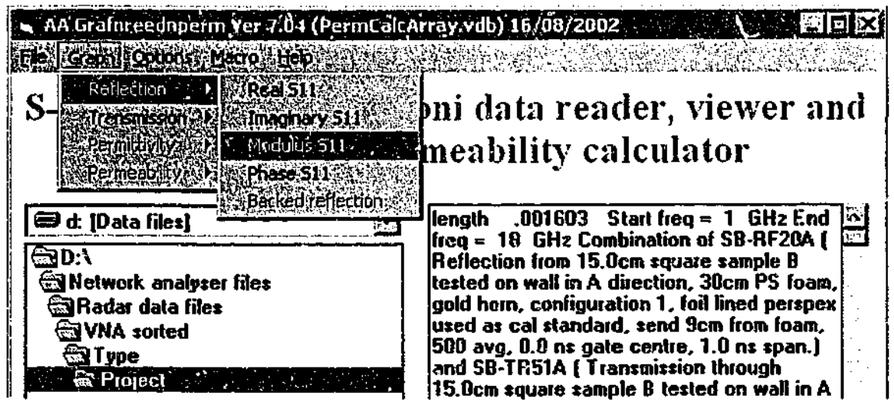

Figure 4-8. Drop down menu from the permittivity extraction main window

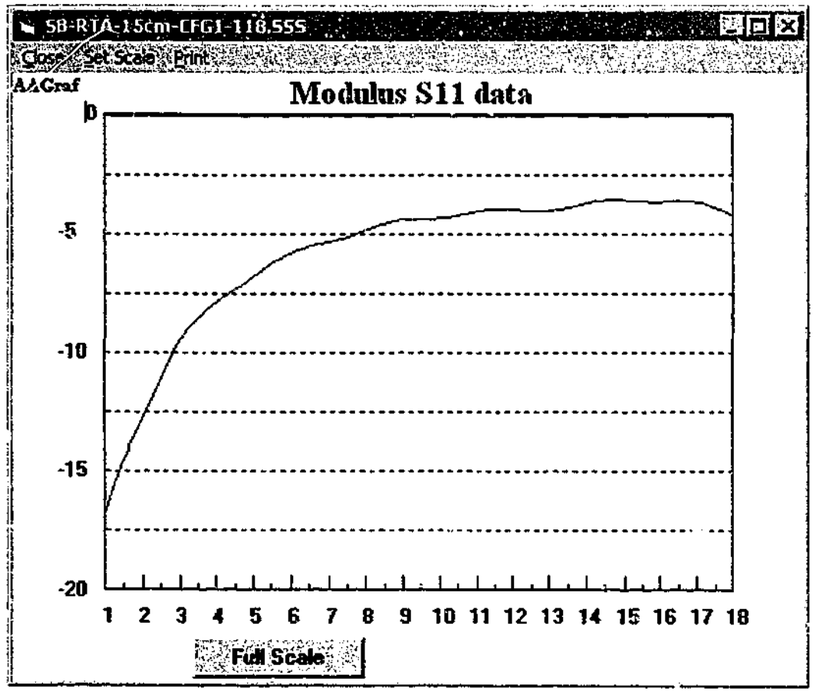

Figure 4-9. The corresponding graph of the data from Figure 4-8

The Options menu gives the user a range of techniques that may aid the permittivity extraction process. These include: changing the thickness of the sample from the one used in the data file, removing the phase shift that occurs from the glass sheet used to remove the diffraction from S_{21} measurements, or actually altering the physical data by adding or

subtracting a fixed phase or magnitude to S_{11} or S_{21}. The Macro menu allows the user to select a number of data files and perform the same operation on all of them whether it be saving the phase of the transmission response, or calculating the permittivity using the reflection only data and saving them to file.

Pressing the "Permittivity and Permeability calcs" button brings up the main extraction window, shown below in Figure 4-10.

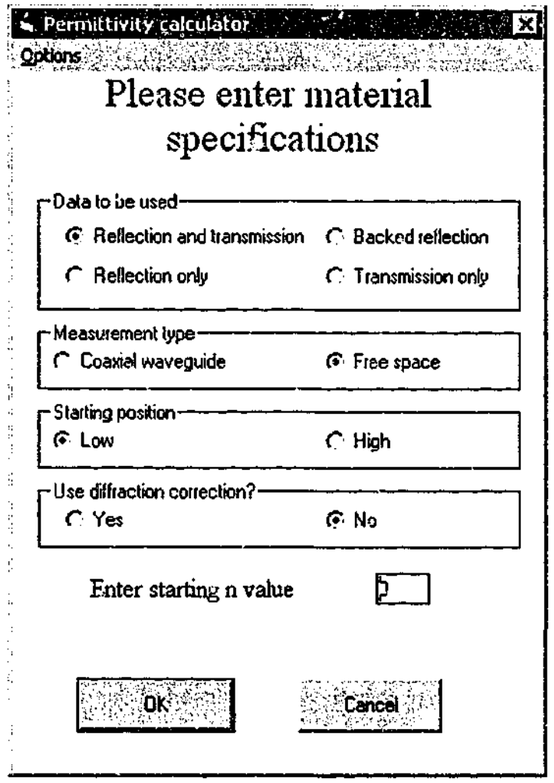

Figure 4-10. Permittivity extraction window

The top box shows which set of data should be used for permittivity or permeability extraction. It is automatically selected depending on the information found in the data file, for instance if the S11 data were all one's and zero's, the program assumes the type of measurement is transmission only. The user can of course alter this automatic selection.

The next box down shows the type of measurement being performed. This is important because transmission measurements taken in free space need a phase correction applied that is caused by the sample replacing the column of air between the horns. Measurements taken in the coaxial waveguide have this factor applied internal to the analyser and need no further correction.

The third box gives the user the option of starting the extraction process at the low or high frequency point. In cases where the diffracted signal is comparable to the material's transmission signal, the program has difficulty finding an initial solution using the transmission only extraction algorithm. Since the highest diffraction occurs at the lowest frequency, it is beneficial to start the process at the highest frequency point and step down in frequency, using the previous result as a starting point for the iteration process.

The last box asks the user if the diffraction signal should be removed from the data before performing the permittivity/permeability extraction. If this option is checked, then the appropriate file is loaded and the signal removed prior to the permittivity calculations are performed.

When performing the reflection and transmission calculations, the algorithm needs to perform a complex logarithm, which can theoretically have an infinite number of solutions. Normally the program tries the lowest solution number (n = 0), but this result is not always correct. Usually it is clear which solution is the right one with a prior knowledge of the approximate values of the permittivity and permeability of the sample tested. The value of n can and does change as frequency increases, and it is not unusual to find values of 3 or 4 at the highest frequencies in materials with large permittivities.

This complex logarithm only occurs in the reflection and transmission case, so if the transmission (or reflection) only algorithm is to be used, the boxes are replaced by the initial guesses to the iteration process. The program makes an initial guess based on the first (or last) data point which usually gives the correct result, but again this can be changed by the user. The replacement boxes are shown in Figure 4-11, where only the lower portion of the window is shown for brevity.

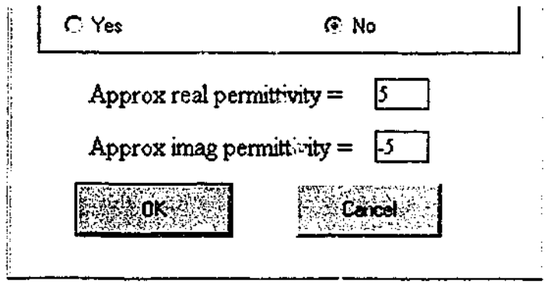

Figure 4-11. Section of the permittivity calculation window when the transmission only algorithm is to be used

The Options menu gives the user aids to improve measurement accuracy and stability. Clicking on the button brings up the menu shown in Figure 4-12 (again cropped for brevity).

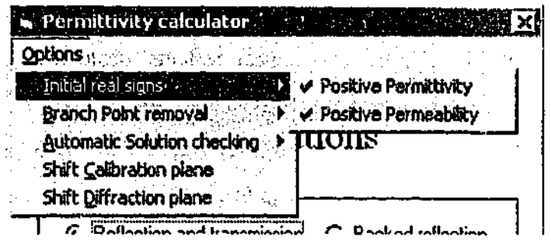

Figure 4-12. Drop down Options menu

The first option specifies whether the first data point calculated should have a positive real permittivity and/or a positive real permeability. These should of course be positive but in real measurements, especially those involving large diffraction signals, the initial values of both permittivity and permeability drop below zero before attaining realistic values at higher frequencies.

The next option gives the user the option of changing the sensitivity of the branch point removal operations in the complex analysis. When using data that is affected by diffraction signals, sometimes the extraction algorithm wants to make the real permittivity or permeability negative. The effect is shown in Figure 4-13, where the green and pink curves are showing the branch cuts in the complex permeability when the real permeability drops below zero. Using appropriate interrogation of the data these can be removed to give the blue and red traces shown below.

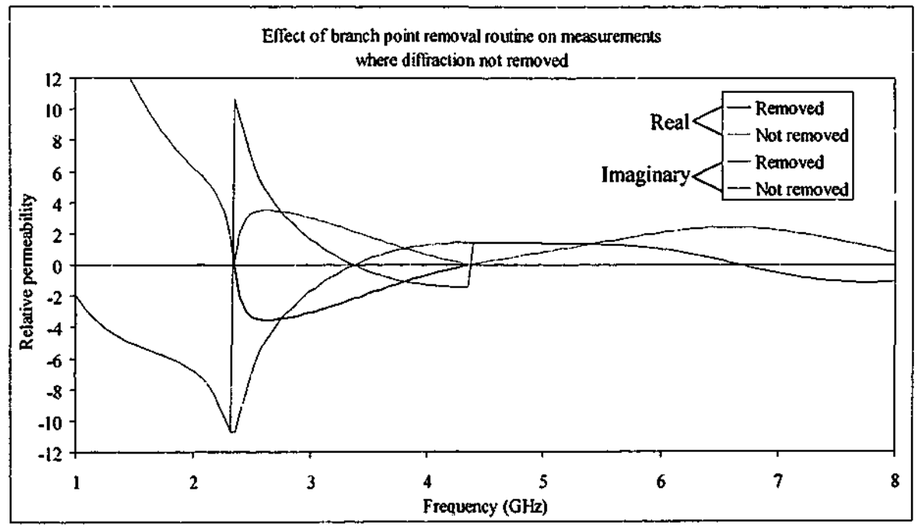

Figure 4-13. Effect of branch points on permeability calculations

When the program calculates the permeability starting at 1 GHz, it assumes the real permeability remains positive and so at about 2.3 GHz the real value "reflects" from the x axis and the imaginary component must therefore change signs. This is shown in the green and pink curves. The solution then changes back again at about 4.3 GHz across another branch cut, and the imaginary component again changes signs. When the branch cut removal option is activated, continuity of the real component is forced resulting in the blue and red curves, which is a truer picture of the solution. Of course the resulting solution is extremely inaccurate physically; however, as a mathematical solution it is a better result.

The next option examines the automatic changing of the solution number *n* as the program moves through the full frequency range. This is always enabled; however, at destructive interference points the program can sometimes get confused as to whether or not the solution number should change. Since these points frequently have permittivity and permeability values that are very different from the rest of the range, it is not necessarily an easy task to determine the correct solution. The option here is to ask the user to confirm a change in solution number; usually this option will only occur when the automatic solution changer has failed.

The fourth option allows the user to apply a calibration plane shift to the data. A calibration plane shift is required when the sample is not lying on exactly the same plane as the backing plate used for the reflection calibration. This can occur if the sample or calibration plate is not lying flat on the foam support, or if the foam support is not flat and the samples are flexible. If this is the case, a phase shift proportional to the distance entered by the user is applied to the reflected signal before extraction takes place.

One of the problems encountered with the diffraction removal was that the foil lined glass sheet had to be measured at exactly the same time as the other samples. If the horns were moved and later placed back to a position very close (the author hoped identically!) to where they were before, the diffraction removal process was not as successful. The last option was a trial to see whether changing the phase of this diffraction signal might help the diffraction removal process; however, it appeared to have little effect.

After all the options are chosen, pressing the OK button starts the appropriate extraction algorithm at either the lowest or highest frequency and then continues through the frequency span. For the reflection only, transmission only and backed reflection algorithms, the result from the previous iteration process is used as the starting point for the next. This speeds up the total time taken for all 401 frequency points to less than a second on a modern PC. Once the permittivities (and permeabilities if the full S-matrix is used) have been calculated,

average values across the full frequency span are shown in a new window, as seen in Figure 4-14.

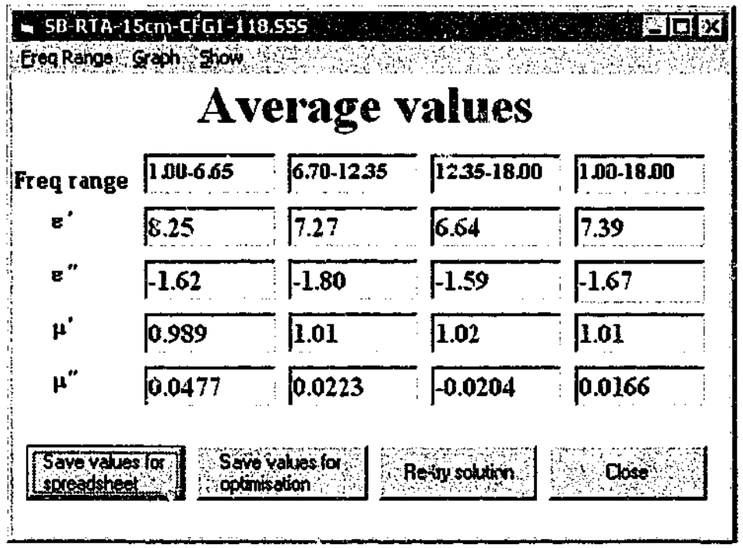

Figure 4-14. The average values across the full frequency range shown in the results window

The average values across three bands are shown as a quick check on measurement accuracy and consistency, together with the total average across all frequencies. The frequency range for these averages can be changed using the drop down menus, as can the standard deviations and all 401 data points. If the user is unhappy with the results he can press the button marked "Re-try solution" which closes this window and bring up the previous one. The graph menu (shown in Figure 4-15) allows the user to view the calculated data to ensure measurement accuracy.

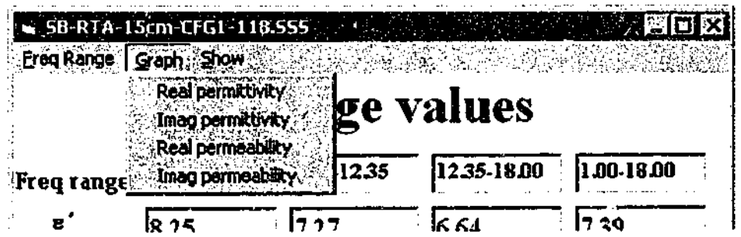

Figure 4-15. The graph menu from the results window

Selecting the real permittivity from this menu reveals the familiar graph window of Figure 4-16, with a yellow highlighted area that has been selected by the user as an area to zoom.

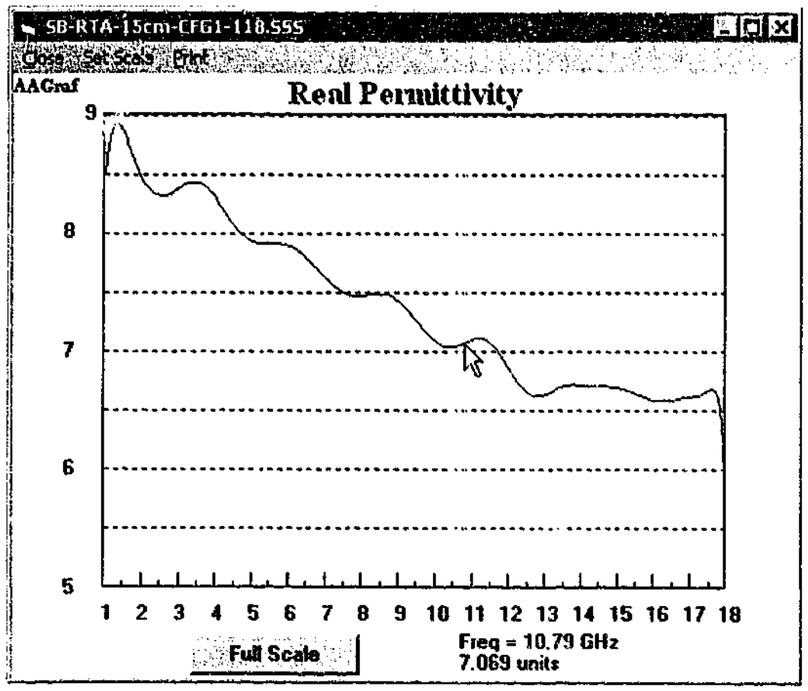

Figure 4-16. Graph window of real permittivity showing highlighted area

The user has pressed the mouse button near the frequency 5.2 GHz, and dragged the mouse across to 10.79 GHz. This area is highlighted in yellow, and once the user releases the mouse, the highlighted area is displayed to the nearest 0.5 GHz mark as a new graph, as seen in Figure 4-17.

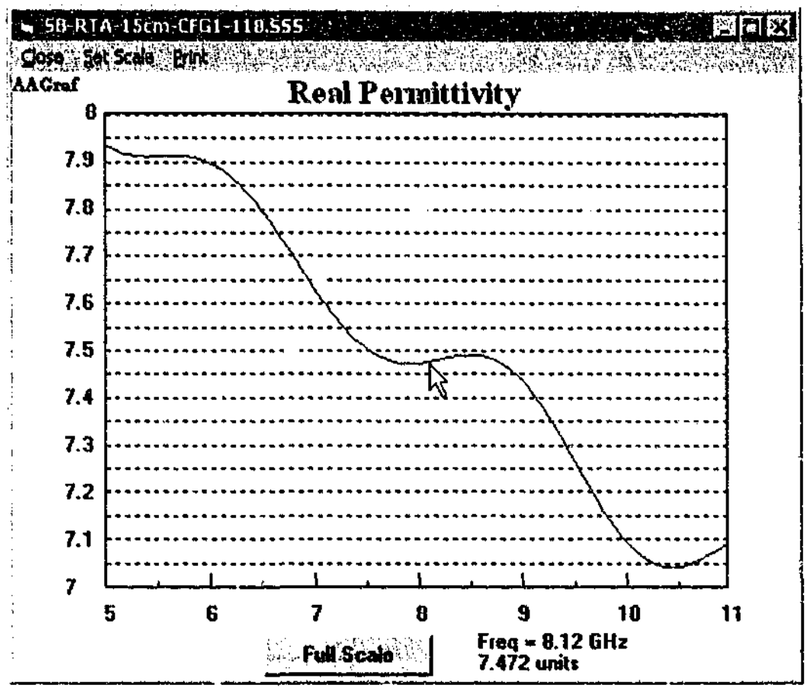

Figure 4-17. Zoomed area of the graph shown in Figure 4-16

The scale can also be set manually using the drop down menu, and a hard copy of the whole window can also be made using the print button. The bottom right of the window shows the value of the mouse pointer as it travels across the graph window to aid user identification of peak values and frequencies.

If the user is happy with the result from either the text display or graphical view, then the values can be saved to file using the other buttons on the display results window. If the diffraction signal was removed, the program automatically adds the code word "nodiff" to the filename to remind the user that the diffraction signal was removed. Likewise, if the phase of the reflected signal was altered due to calibration plane shifting, the distance the plane was shifted is noted in the comments section of the saved permittivity and permeability file.

4.3. Time gating program

Continuing with the "function over form" theme, the program used to apply the author's time gating software bears a striking similarity to the permittivity extraction program. This is hardly surprising as this piece of software was built on top of an older version of the extraction program. The front end is shown in Figure 4-18.

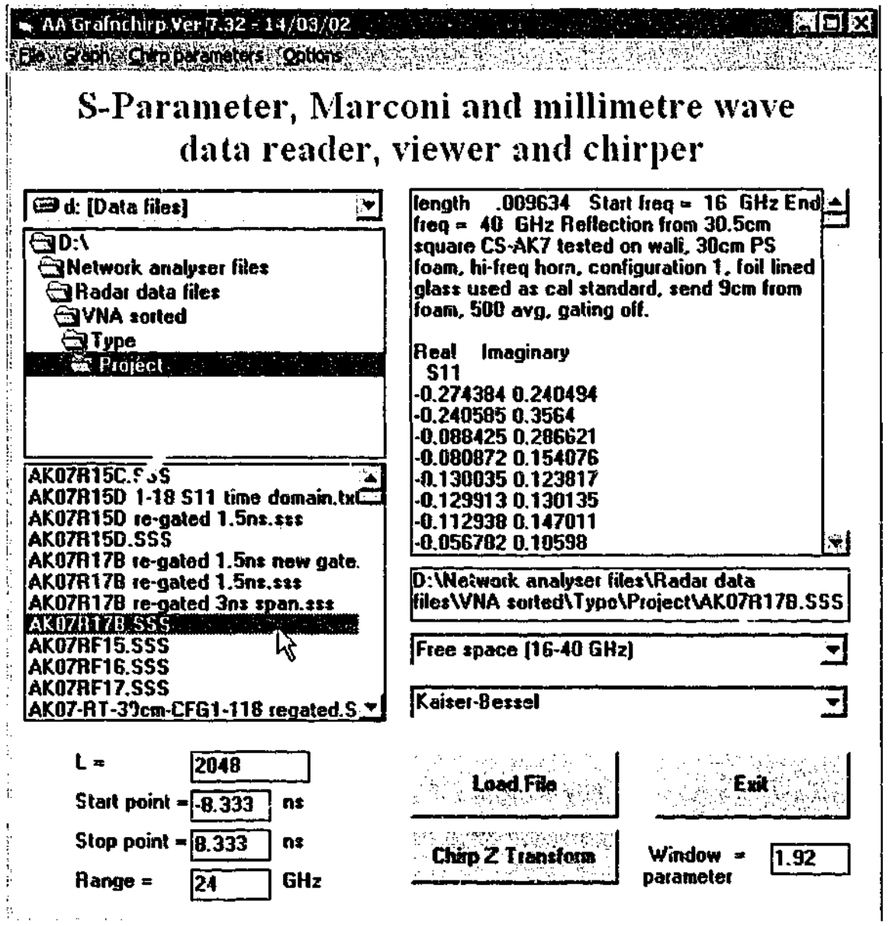

Figure 4-18. The main window of the time gating software written by the author

Once the program is loaded, the start and stop time points are calculated to show the entire time domain centred on time zero, making selection of the main peaks easier. Since the calibration places the reference signal at time zero, most of the useful peaks appear near this point. Due to the cyclical nature of the time domain, placing half of the main peak at the start of the trace with the other half at the end simply adds to the confusion of finding the correct peaks. The start and stop times can be changed by the user.

The main time gating window includes a number of additional parameters specific to the time domain application, such as the value of L that is the total number of points used in the transform. The windowing function Combo Box can be seen on the right of the main page; clicking it brings up the array of windows available to the user as shown in Figure 4-19.

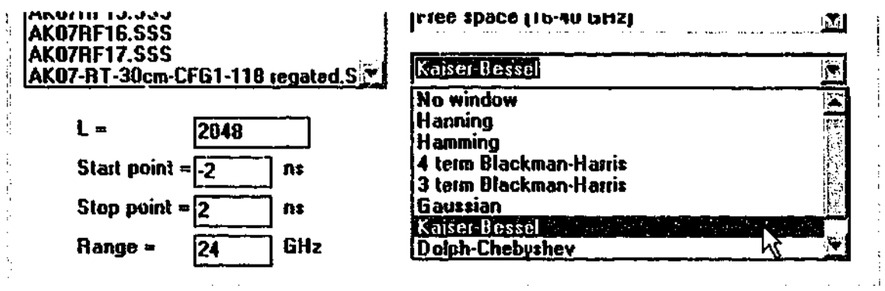

Figure 4-19. Close up of the windowing function Combo Box showing available windows

For windows that have a controllable parameter (for instance Gaussian, Kaiser-Bessel etc), the parameter can be set by a box on the bottom right of the main page.

Drop down menus allow the user to alter the number of extra points used in the transformation to smooth the edges of the data, as well as the shape and level of the time gating function. Usually these are kept at a constant value unless the user specifically desires to see what happens under different conditions.

When searching for the correct time gate to apply, it is not usually the best practice to view the entire time domain but rather a truncated version "zooming in" on the area of most interest. It is here that the Chirp-Z transform excels, allowing the user to simply calculate the points of most interest, rather than the entire spectrum. Figure 4-20 shows the full time domain of the S_{11} response from the 300 mm square sheet of C-Stock AK 7. This trace shows how many stray reflections one measures in a set-up such as this, and the importance of removing such a large number of interfering signals. When zooming in on the area of interest by setting the time span to ± 2 ns, one obtains the trace shown in Figure 4-21, with the time gating set to a value of ± 0.75 ns. The graph window used was one not written by the author, but came as an add-on package. The start and stop gate values can be set either by the user clicking on the screen similar to the graph zoom in the previous program, or by a setting in the "Options" drop down menu of the main window.

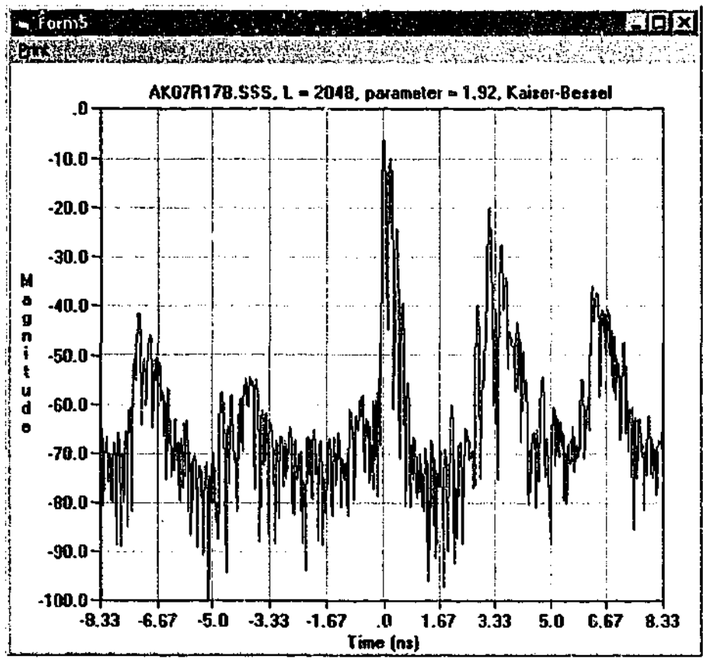

Figure 4-20. Full time domain range of measurement centred around main peaks

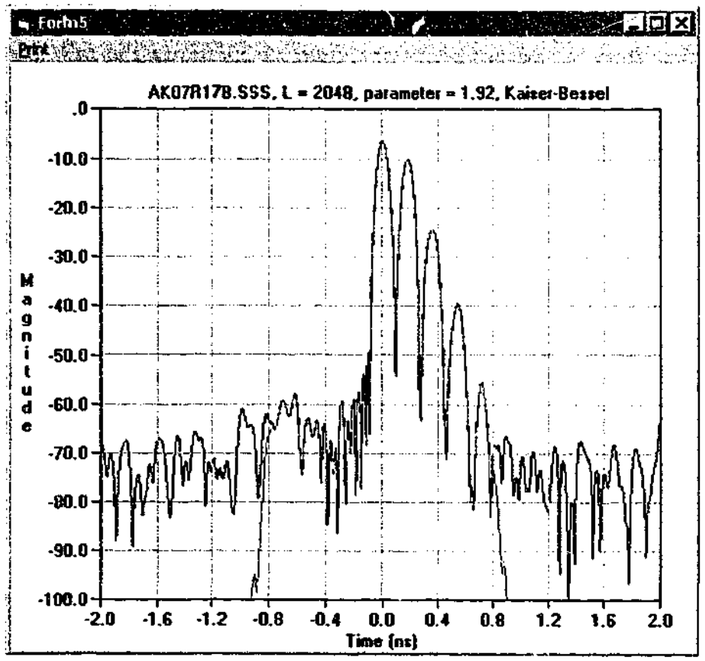

Figure 4-21. Time domain calculated over the range of ± 2 ns, with the gated signal shown in red

When a suitable time gate (such as the one shown in Figure 4-21) has been applied, the program then performs an inverse transform on the gated time data and plots the frequency result over the ungated frequency response. The appropriate graph is shown below in Figure 4-22, with the gated result shown in red.

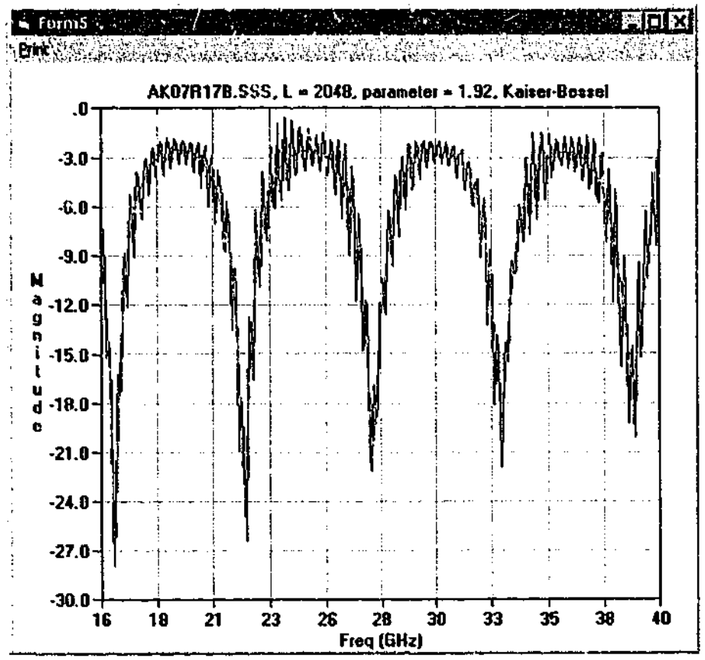

Figure 4-22. The graph of the ungated and gated frequency response

The gated signal is obviously much cleaner than ungated frequency response, which leads to a better calculation of permittivity later on.

4.4. Other ancillary programs

A good deal of time and effort was spent in creating a program that would compensate for the near field effects expected from this measurement process using a ray tracing approach. This software calculated the magnitude and phase over a flat grid from a horn antenna with known dimensions using Huygen's principle[2]. Then using knowledge of the angle of incidence of each ray striking the sample, the reflection and transmission coefficients from the lossy sample at oblique incidence were calculated. The parallel and perpendicular cases were then added vectorially for each ray before finally re-combining all the rays to form the reflection or transmission response. This complex near-field response was then compared to the far-field result (a far easier calculation to make).

It was found that the near field result did not change considerably from that of the far field due to the nature of the measurements performed. Since the samples were quite thin (usually of the order of 1 – 2 mm) and the gain of the horn antennas was not extremely high (so sensitivity was not overly affected by the ray's position), other factors such as diffraction and calibration plane shifts were far important than near field effects.

Programs were also written to calculate the near and far field patterns from a variety of horn antennas to help estimate the size of the diffraction field for a given configuration. Other programs created theoretical S-matrices for materials with constant permittivity and permeability values across a given frequency range, or combined reflection only measurement data files with their corresponding transmission data files, and a few programs were written to help catalogue and arrange the vast array of permittivity data files so that comparisons could be made.

Chapter 5. 445 mm Samples

Since diffraction was seen to be such an important factor in the transmission measurements, the largest samples (and hence least diffraction) of rubber specimens A to G, carbon fibre loaded composite, Perspex and the metal foil lined sheet were tested at all configurations to determine the best arrangement of the horns. The rubber samples A to G and the composite needed to be tested twice because of the polarisation dependence of the sheets. The samples were marked with an arrow showing a particular direction, measurements taken in the direction of the arrow have a suffix –A, and those perpendicular to the aroow direction are suffixed –B. Measuring the reflection and transmission of these sheets at nine configurations of horns over three frequency ranges gave a total of 972 individual sets of data. Each dataset (except for the foil lined sheet which was used to remove diffraction effects) can be used to extract a value of permittivity using either the reflection or the transmission algorithm. Furthermore, the reflection and transmission data can be combined to give 486 datasets containing both reflection and transmission, which when combined can be used to extract permittivity and permeability. In order to reduce the load on Amazon rainforests, this amount of data will be presented in a highly compressed form.

5.1. 1 – 18 GHz, transmission only

The transmission measurements allow for all nine configurations to be investigated. The overwhelming source of measurement error was found to be caused by the diffracted signal, even in samples 445 mm square when the horns were relatively close. Diffraction is frequency dependent of course, lower frequencies diffracting more than the higher ones. The diffracted wave was measured at each configuration using a glass sheet coated with aluminium foil cut to the same size as the samples. It was found to be very important that the configuration was exactly the same when testing the samples and testing the diffracted signal. If the horn positions had been moved after measuring the samples, simply putting the horns back to where they should have been was not repeatable enough to completely remove the effects of diffraction. The whole series needed to be measured again. When the samples were large and the distance between the horns was short, the effects were small. When either of these conditions changed it became vitally important to measure the diffraction signal before moving on to the next configuration.

The magnitude of the diffraction signal is shown below in Figure 5-1. When no obstruction is present, the response should be 0 dB. The nine configurations are detailed in Table 3-3.

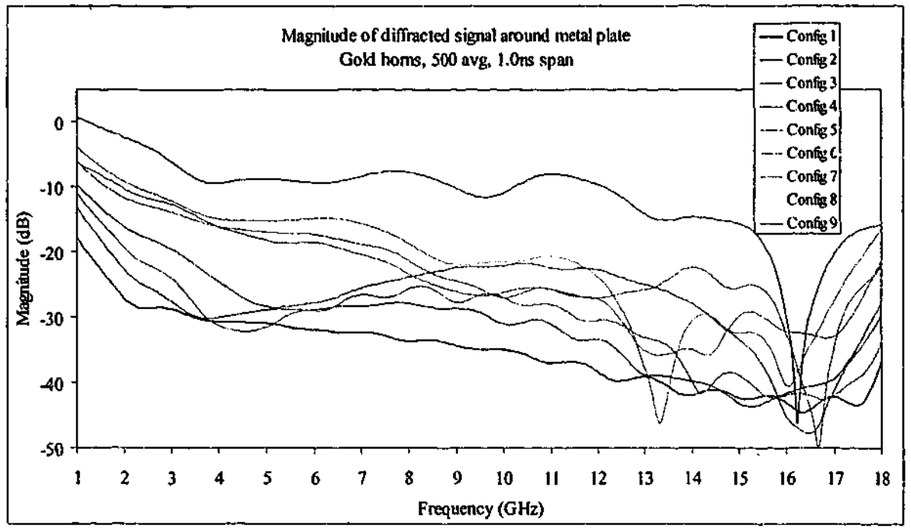

Figure 5-1. Magnitude of diffraction around 445mm square foil lined glass sample measured with gold horns

From the graph of Figure 5-1 it is clear why the diffraction signal is so important to the measurement of the samples. If the transmission through the sample is at the –10 dB level, in all but configuration 1 the diffracted wave is the same order of magnitude at least part way across the frequency spectrum. In configuration 9, the diffraction signal is even greater than the calibration signal at 1 GHz. We may be seeing the effects of Fresnel zones at this point. The fact that the diffracted signal may be equal or greater in magnitude to the actual signal desired not surprisingly leads to a highly inaccurate measurement of permittivity.

Taking the result of Perspex, we may expect to see only a small effect from diffraction. The low loss nature of Perpsex means that the wave travelling thorough the sample will be virtually unattenuated, and instead the main effect will be due to the phase shift through the sample. The transmission magnitude falls to –1 dB across the frequency span at about 9 GHz. The permittivity extracted from the transmssion measurements alone is shown below in Figure 5-2 and Figure 5-3, with the averages and standard deviations shown in Table 5-1.

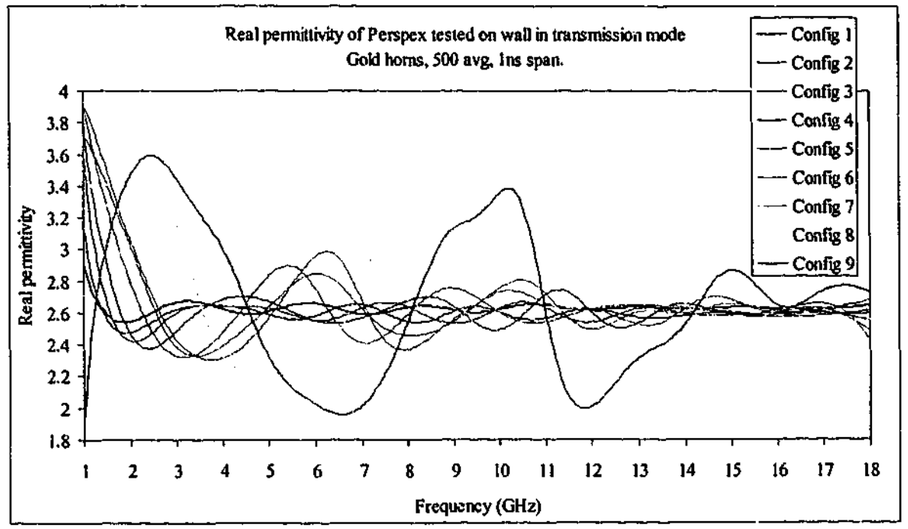

Figure 5-2. Real permittivity of Perspex measured with gold horns in free space using transmission data alone without removing diffraction

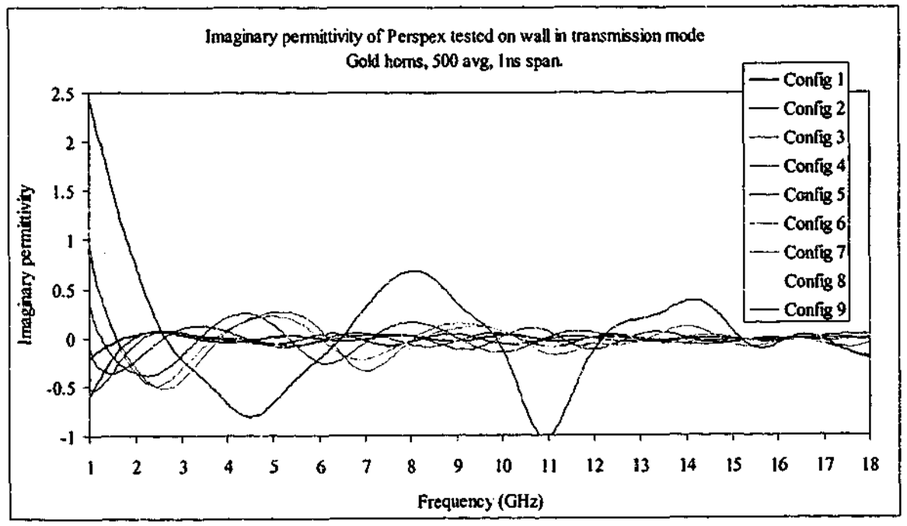

Figure 5-3. Imaginary permittivity of Perspex measured with gold horns in free space using transmission data alone without removing diffraction

Config #	Ave ε'	σ(ε')	Ave ε"	σ(ε")
1	2.627	0.034	-0.010	0.032
2	2.596	0.059	-0.028	0.079
3	2.605	0.107	-0.036	0.094
4	2.620	0.150	-0.031	0.093
5	2.644	0.221	-0.029	0.140
6	2.659	0.272	-0.035	0.201
7	2.651	0.230	-0.028	0.173
8	2.672	0.347	-0.013	0.353
9	2.683	0.469	0.036	0.581
Expected	2.60	-	-0.014	-

Table 5-1. Averages and standard deviations of permittivity measured with gold horns using transmission data alone without removing diffraction

The data from the graphs show that the permittivity of even a low loss material such as Perspex is dramatically affected by the error term caused by the diffraction signal. Although the averages across the frequency band are quite good for all configurations, only the result for configuration 1 can be said to be almost untouched by the effects of diffraction.

As the permittivity and transmission loss through the sample increases, the effects of diffraction are made much worse, especially at low frequencies. Rubber sample B is moderately lossy material with a loss tangent of approximately 0.25. Using the result of sample B, we see the large variations in permittivity as the distance between the horns increases in Figure 5-4 and Figure 5-5.

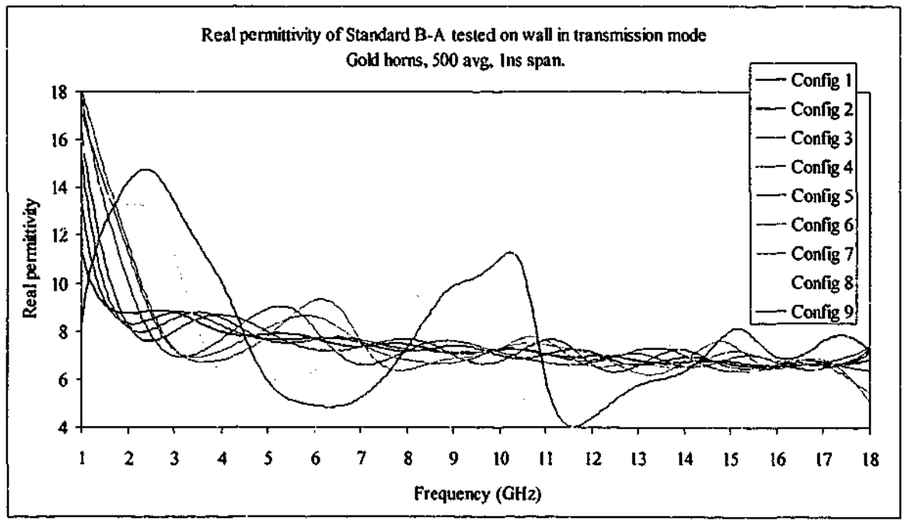

Figure 5-4. Real permittivity of sample B-A measured with gold horns in free space using transmission data alone without removing diffraction

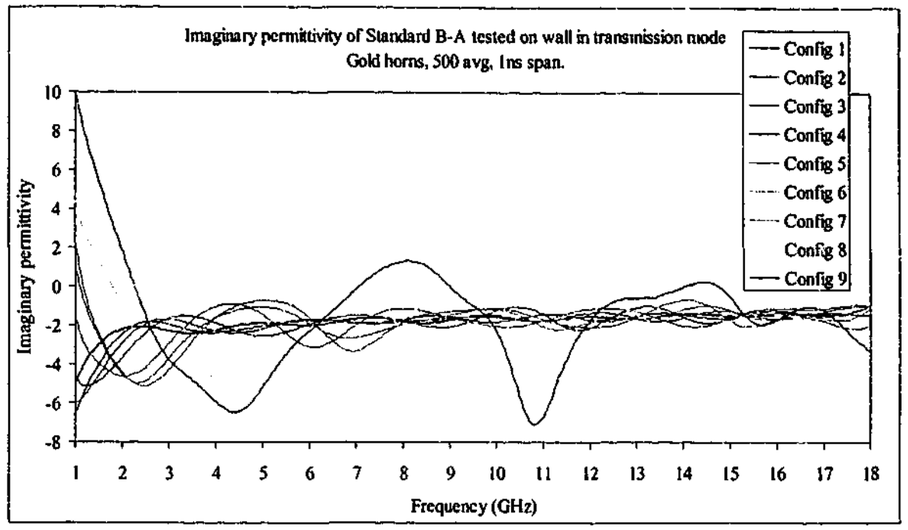

Figure 5-5. Imaginary permittivity of sample B-A measured with gold horns in free space using transmission data alone without removing diffraction

As expected, the highest permittivity materials have the greatest problems with diffraction. The transmission through sample E is about –14 dB, so at many frequencies the diffraction signal is greater than that through the sample. When the resulting signal is analysed using the extraction algorithm, the following values are returned, seen in Figure 5-6 and Figure 5-7.

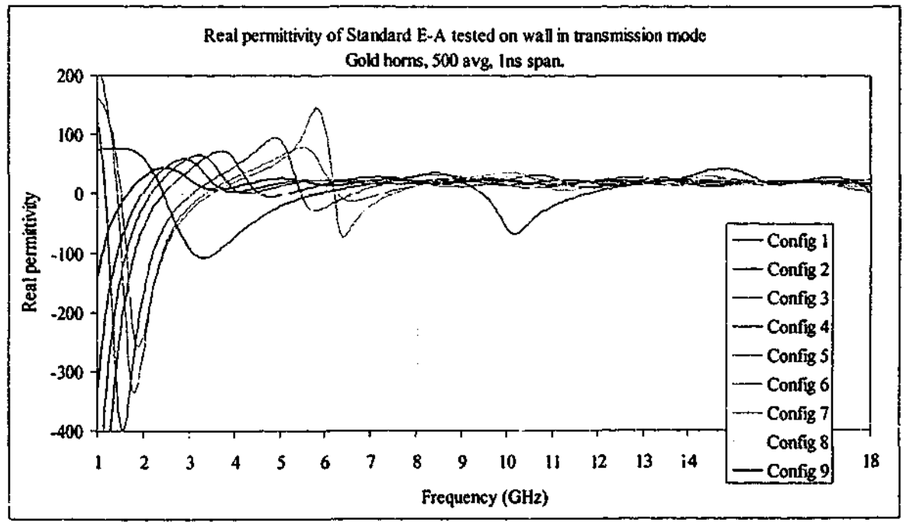

Figure 5-6. Real permittivity of sample E-A measured with gold horns in free space using transmission data alone without removing diffraction

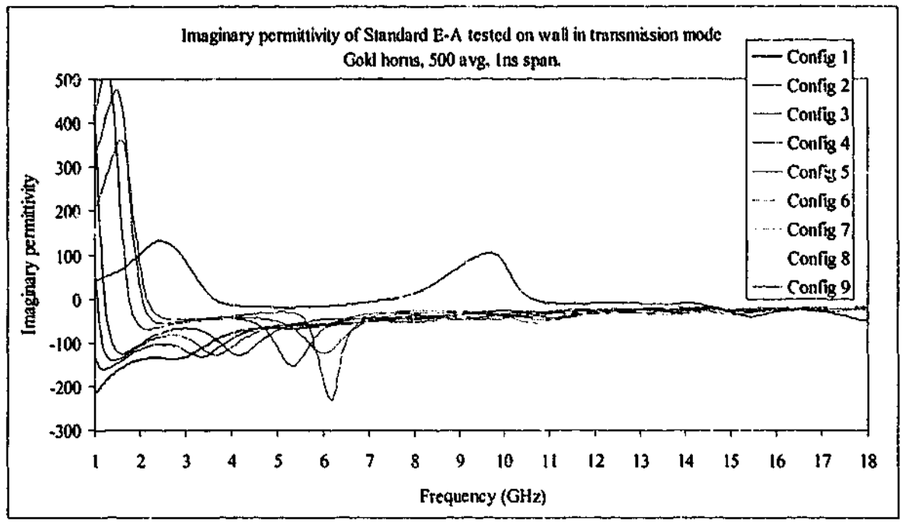

Figure 5-7. Imaginary permittivity of sample E-A measured with gold horns in free space using transmission data alone without removing diffraction

In this case, none of the configurations are spared from being adversely affected by the diffraction signal. At low frequencies the real permittivity at configuration 1 drops to below –100, and in the case of configuration 8 the program will not converge to a solution at all below 8 GHz. Clearly the diffraction signal is dominating any other adverse effects that may be occurring to the measurement.

The situation is greatly improved when the diffracted signal is removed mathematically before performing the calculation of permittivity. While the data is still in the S-parameter stage, the measured S_{21} of the diffracted field is removed vectorially from that of the sample. When this is done, the extracted values of permittivity are much improved. The permittivity of the Perspex sheet has lost most of the noise of the previous values, and the average value is also very close to that expected. Graphs of permittivity against frequency are shown in Figure 5-8 and Figure 5-9, and the average values across the frequency range are shown in Table 5-2.

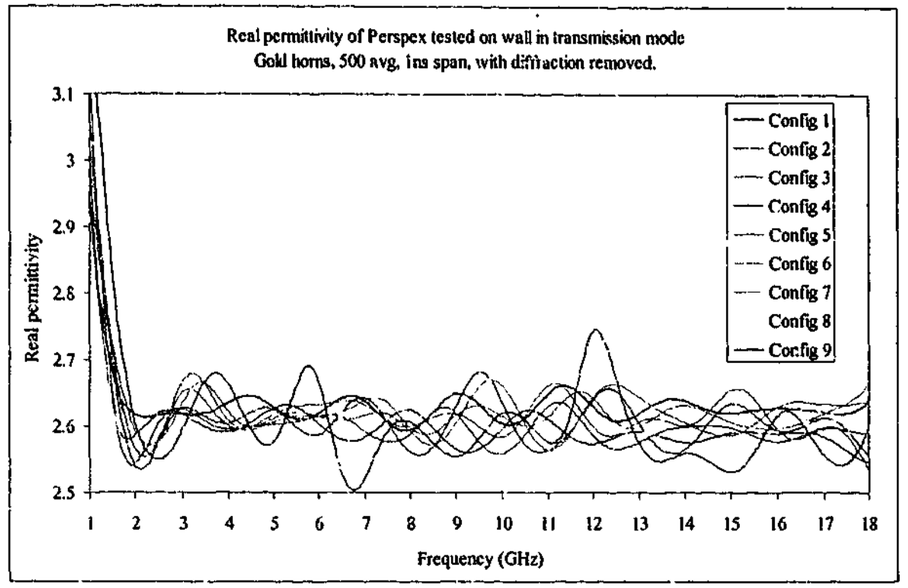

Figure 5-8. Real permittivity of Perspex measured with gold horns in free space using transmission data alone with diffraction removed

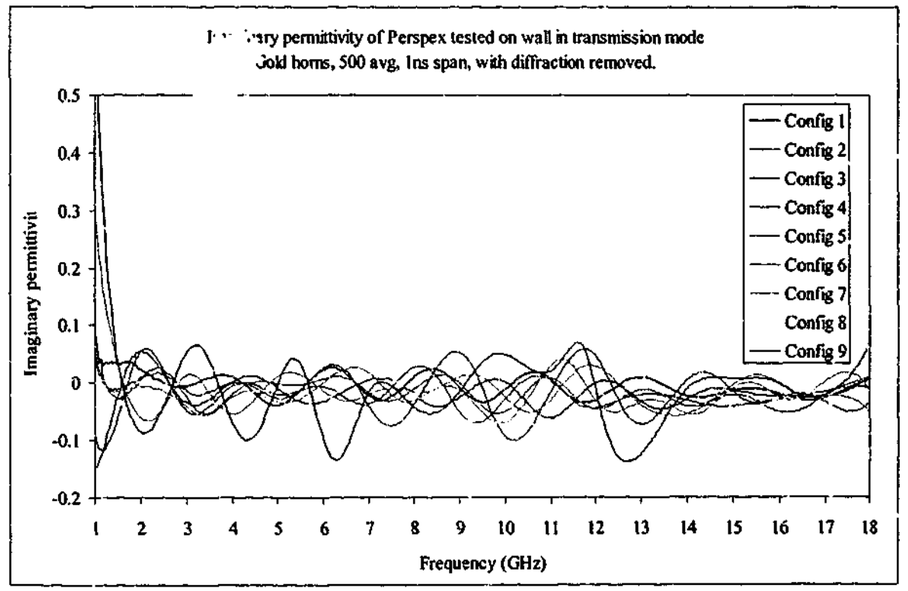

Figure 5-9. Imaginary permittivity of Perspex measured with gold horns in free space using transmission data alone with diffraction removed

Except for some minor deviations across the frequency span in configuration 9 and the area below about 2 GHz, the extracted permittivity values are extremely close to that

expected. The diffracted signal cannot be removed completely because even a minor misalignment of the sample or the metal sheet can cause small changes in phase leading to incomplete cancellation. On the whole, however, the technique of measuring the diffracted signal and then removing it gives a much better result than if it is left in.

Config #	Ave ε'	σ(ε')	Ave ε''	σ(ε'')
1	2.631	0.035	-0.006	0.020
2	2.599	0.042	-0.018	0.026
3	2.604	0.055	-0.021	0.028
4	2.613	0.058	-0.015	0.036
5	2.619	0.048	-0.017	0.020
6	2.625	0.050	-0.018	0.025
7	2.625	0.049	-0.012	0.039
8	2.624	0.046	-0.018	0.027
9	2.610	0.094	-0.010	0.080
Expected	2.60	-	-0.014	-

Table 5-2. Averages and standard deviations of permittivity of Perspex measured with gold horns using transmission data alone with diffraction removed

Similarly, the samples with higher permittivity show great improvements in the extracted values when the diffraction signal is removed.

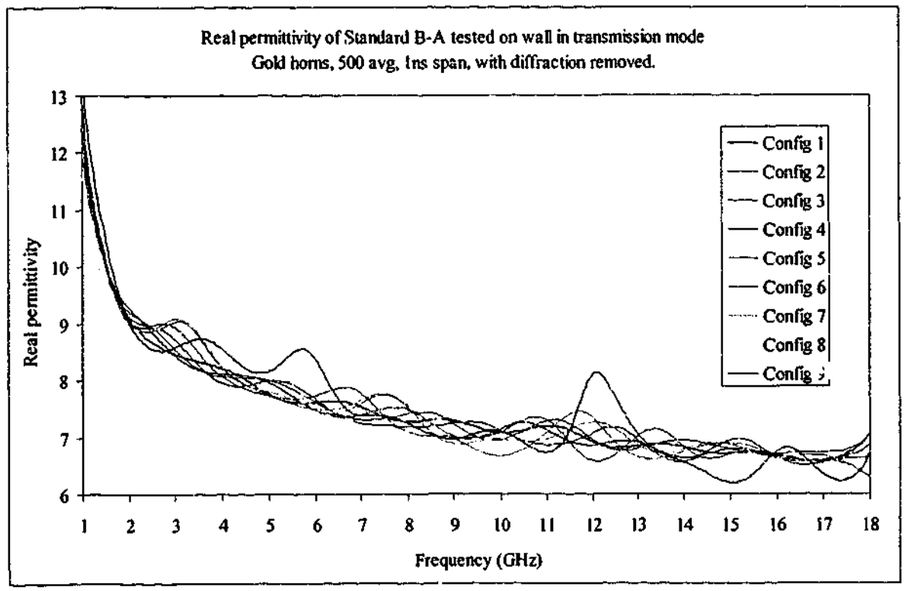

Figure 5-10. Real permittivity of Sample B-A measured in free space using transmission data alone with diffraction removed

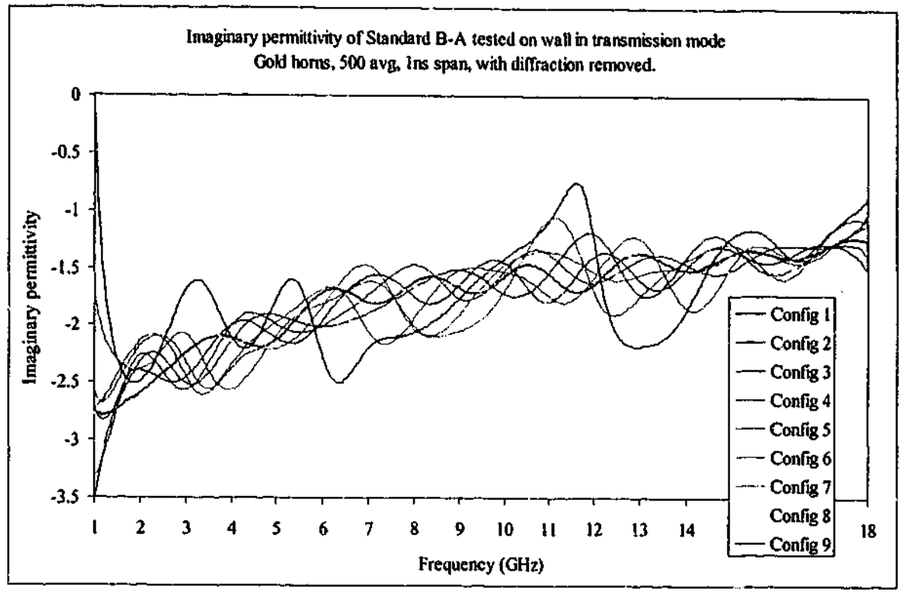

Figure 5-11. Imaginary permittivity of Sample B-A tested with gold horns in free space using transmission data alone with diffraction removed

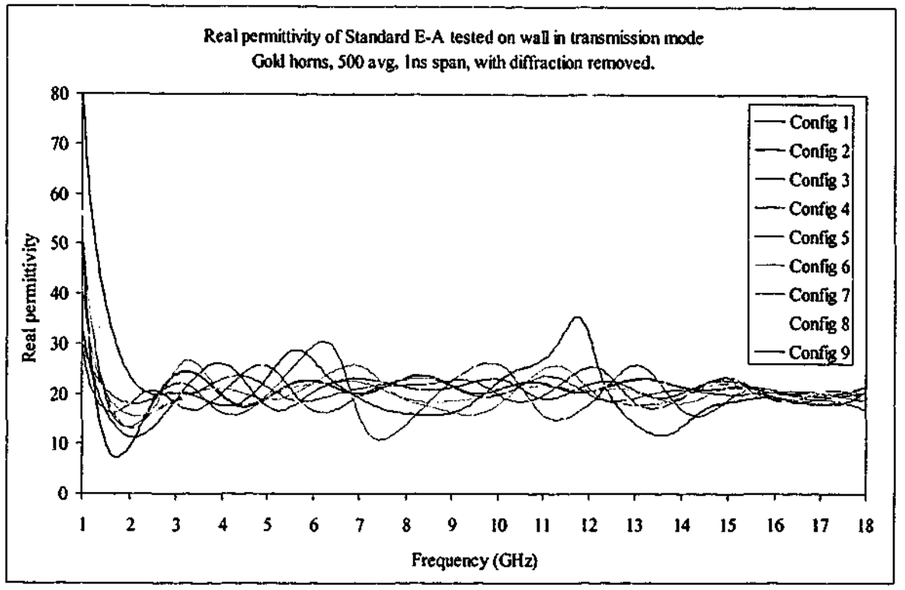

Figure 5-12. Real permittivity of Sample E-A tested with gold horns in free space using transmission data alone with diffraction removed

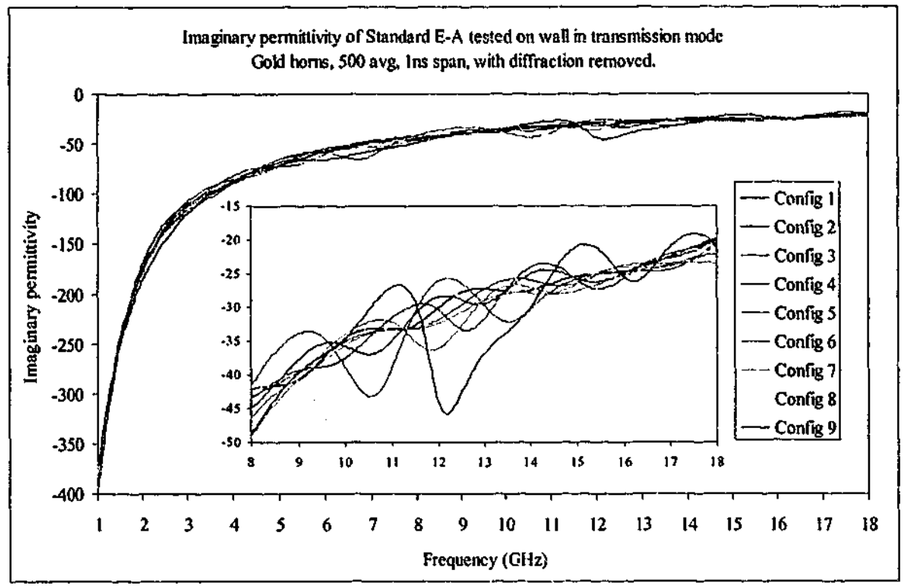

Figure 5-13. Imaginary permittivity of Sample E-A tested with gold horns in free space using transmission data alone with diffraction removed; inset shows details of high frequency response

Whilst certainly not free of undulations, the permittivity extracted from the diffraction-free data is certainly better than the diffraction-included data. Using appropriate smoothing and averaging, the actual permittivity could be quoted with reasonable certainty, even at the longest frequencies.

The range of permittivity values tested is very wide in order to determine the optimum measurement technique for a material with a given permittivity. The carbon loaded rubber samples offer a material system with a moderate to high loss tangent. Taking the average permittivity values across all nine configurations for all the samples gives the plots shown in Figure 5-14 and Figure 5-15.

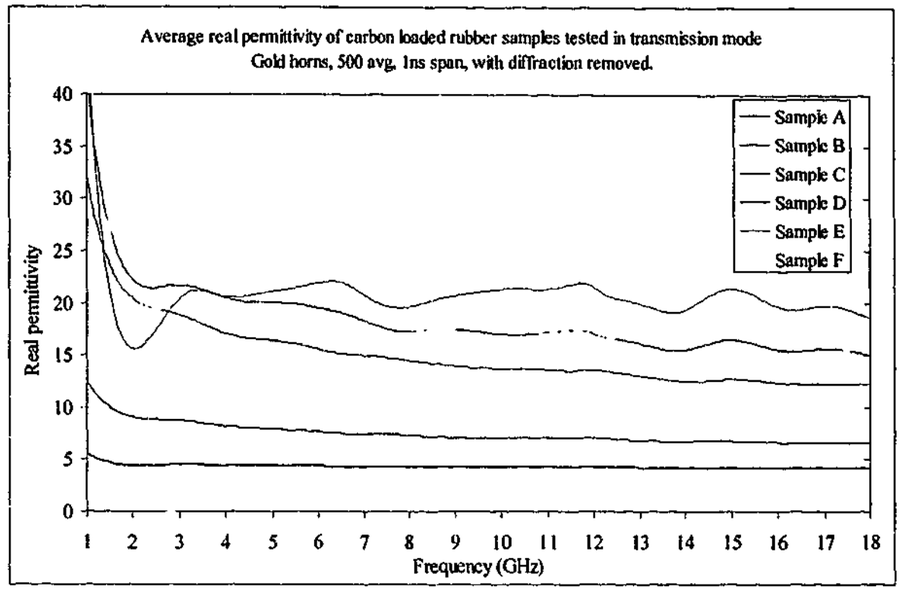

Figure 5-14. Average real permittivity of carbon loaded rubber samples tested with gold horns in free space using transmission data alone with diffraction removed

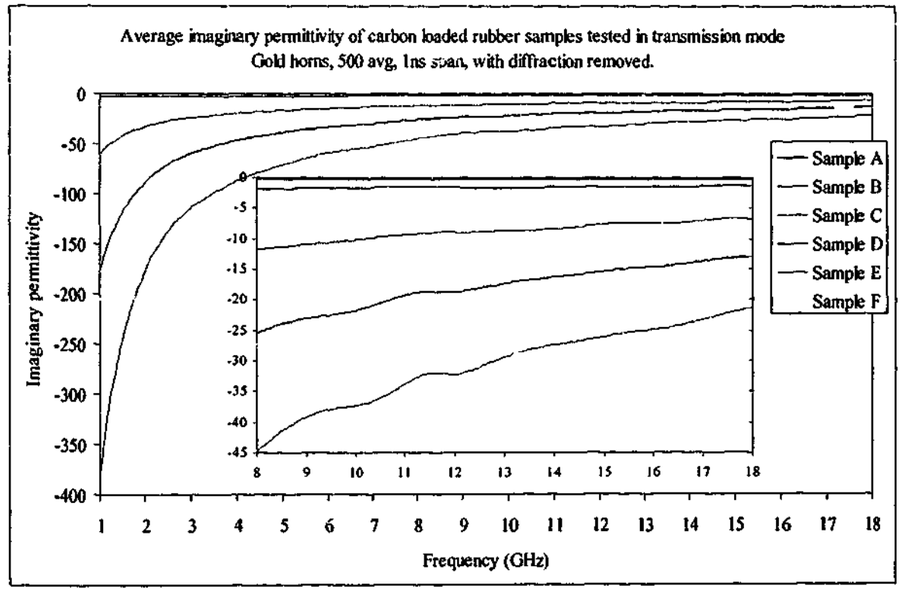

Figure 5-15. Average imaginary permittivity of carbon loaded rubber samples tested with gold horns in free space using transmission data alone with diffraction removed

For the fibreglass sample containing 6mm long carbon fibres, the permittivity shows a slightly different form to that of the carbon black loaded materials. The data does not show the same frequency dependence as the carbon black loaded samples. Instead there appears to be a Debye type resonance behaviour occurring depending on the length of the carbon fibres. The fitted curve follows the equation

$$\varepsilon = \varepsilon_\infty + \frac{\varepsilon_0 - \varepsilon_\infty}{1 + i\omega\tau} \qquad \text{Equation 5-1}$$

where the parameters $\varepsilon_0 = 52.4$, $\varepsilon_\infty = 1.38$ and $\tau = 57.92$ ps. Figure 5-16 and Figure 5-17 show the permittivity of the composite material extracted from the transmission methods.

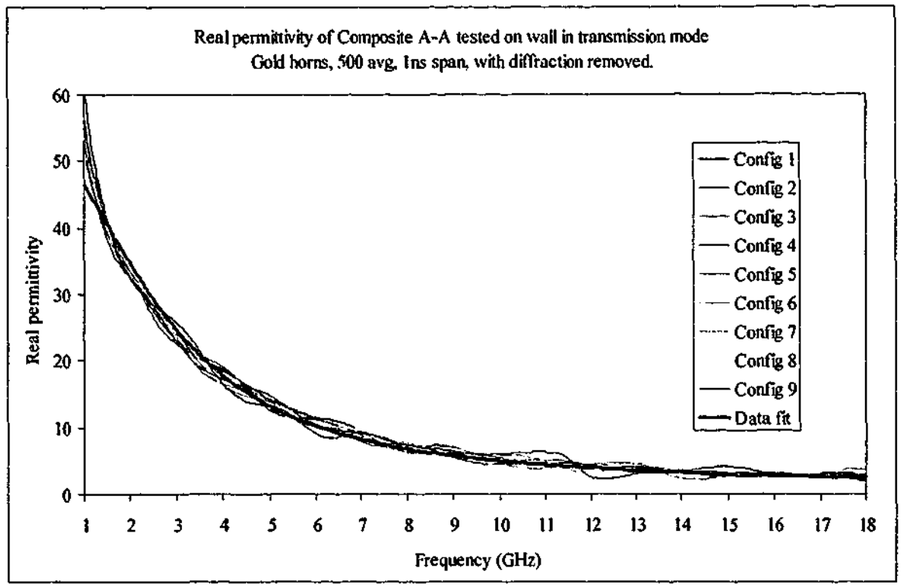

Figure 5-16. Real permittivity of Composite A-A tested with gold horns in free space using transmission data alone with diffraction removed

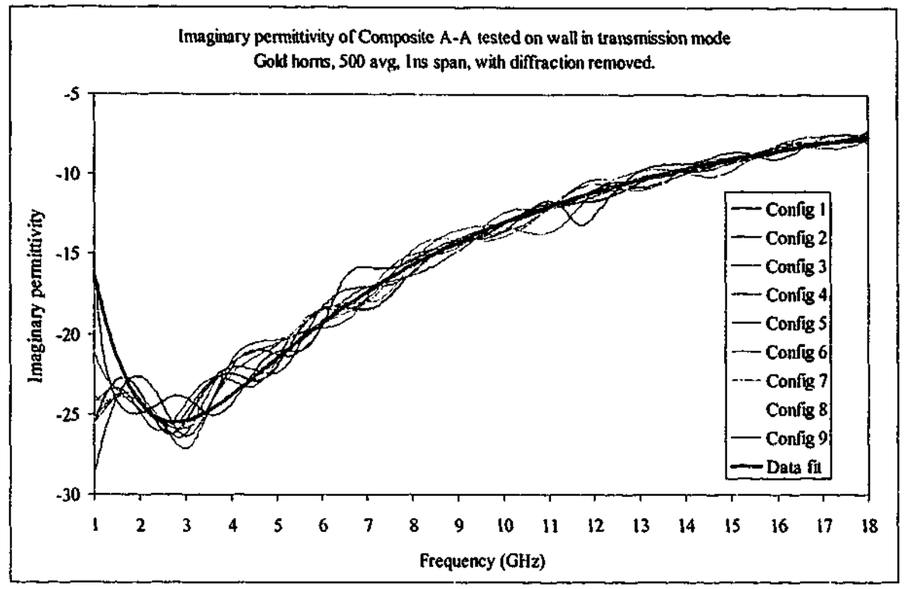

Figure 5-17. Imaginary permittivity of Composite A-A tested with gold horns in free space using transmission data alone with diffraction removed

The parameter $\tau = 57.92$ ps corresponds to a pole frequency of about 2.75 GHz. Using the values of permittivity for the material at this frequency, we find that the wavelength inside the material is about 18 mm at 2.7 GHz. It was expected that the wavelength at the resonance frequency would equal twice the length of carbon fibres in the composite, but this was not the case. However, since the permittivity of the material is increasing so rapidly at these lower frequencies, slight errors in the measurement technique may have a large effect on the measured permittivity and so affect the calculation of the wavelength inside the material. Additionally, the actual point in frequency space is close to the lowest value so effects from the ends of the gating window may be affecting the measured values.

5.2. 1 – 18 GHz, reflection only

Since reflection measurements utilize only one horn, there are only three horn positions used for reflection only measurements. It was found that in general, the position of the horn when using only the reflected signal from the samples had a very small effect on the extracted values of permittivity. The only significant difference between the values was that the permittivity calculated for configurations which have a larger sample to horn distance were slightly noisier. This is to be expected, since the return signal strength from the samples at these configurations is lower, so the noise level is more significant. The real and imaginary

permittivity from the Perspex sample is shown below in Figure 5-18 and Figure 5-19. The average values across this frequency range are very close to the expected value of 2.6 – 0.014i. A table of the real and imaginary permittivity for these measurements is shown in Table 5-3.

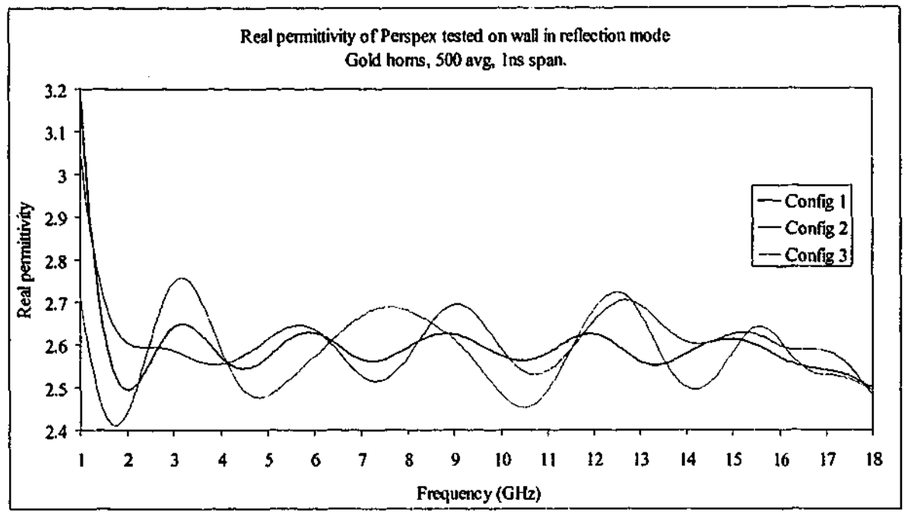

Figure 5-18. Real permittivity of Perspex tested with gold horns in free space using reflection data

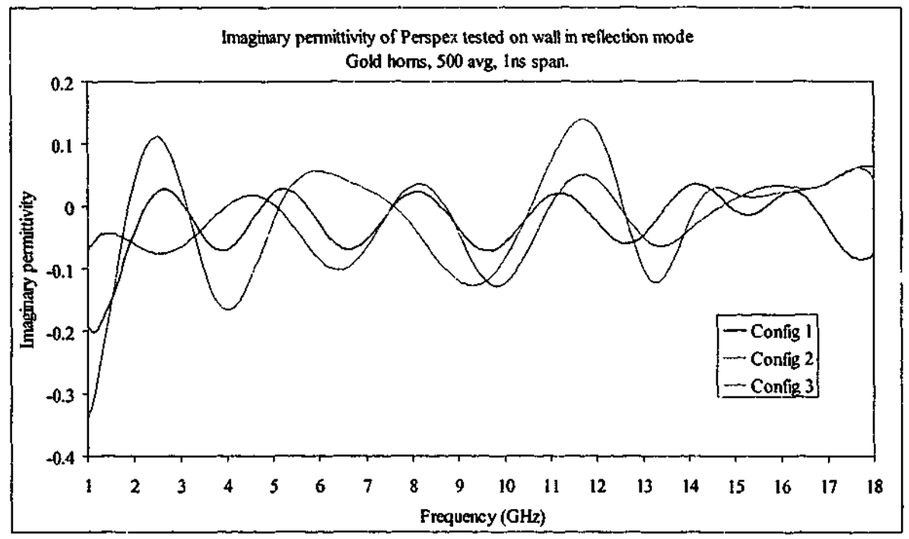

Figure 5-19. Imaginary permittivity of Perspex tested with gold horns in free space using reflection data

Config #	Ave ε'	σ(ε')	Ave ε"	σ(ε")
1	2.591	0.069	-0.025	0.046
2	2.610	0.069	-0.021	0.050
3	2.581	0.085	-0.014	0.088
Expected	2.60	-	-0.014	-

Table 5-3. Averages and standard deviations of permittivity measured using reflection data

When the permittivity of Sample B was measured in the same way as Perspex, a similar spread of values was observed between the different configurations. Figure 5-20 and Figure 5-21 show the values across 1 – 18 GHz.

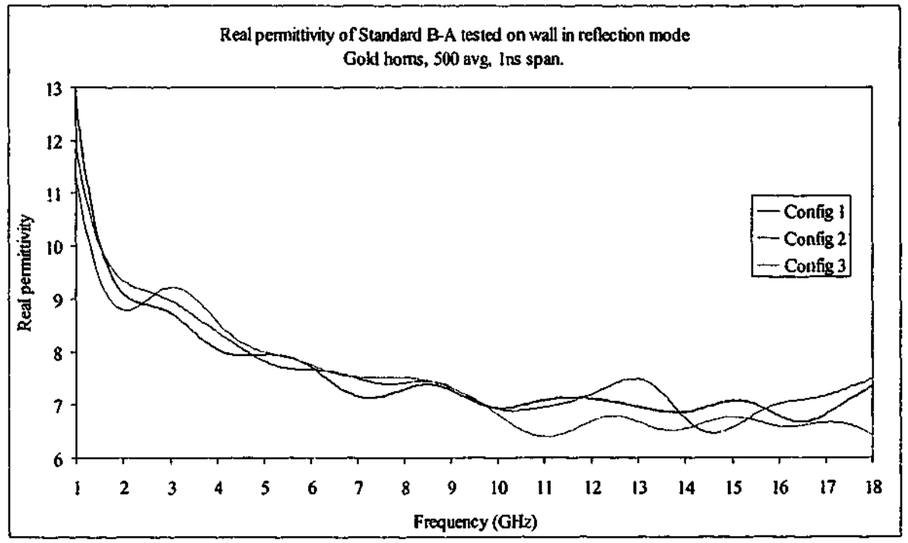

Figure 5-20. Real permittivity of rubber B-A tested with gold horns in free space using reflection data

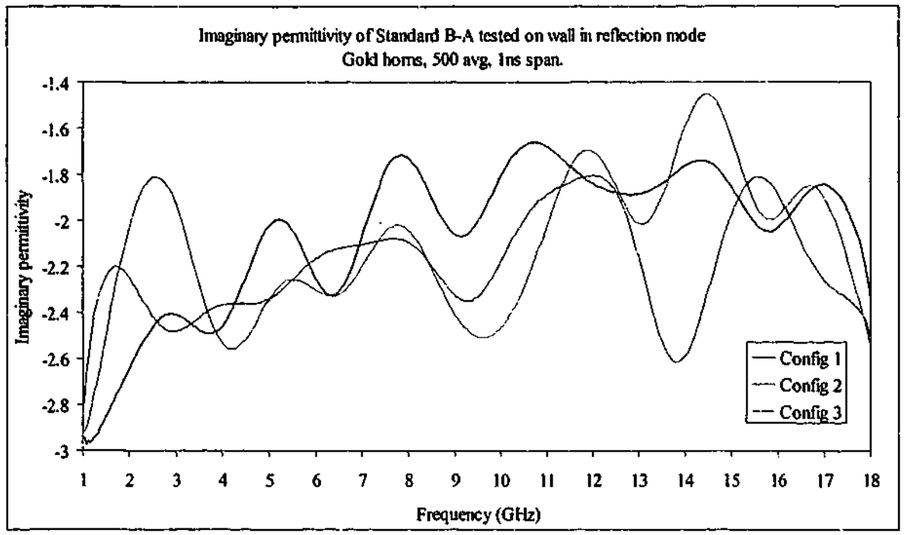

Figure 5-21. Imaginary permittivity of rubber B-A tested with gold horns in free space using reflection data

There appears to be very little difference between the results at different configurations. One may perhaps argue a slightly higher noise factor in configurations 2 and 3 over configuration 1, but the effect is slight. The average values for the three measurements are also very similar.

As permittivity increases to very high values, so do the errors in the real and imaginary permittivity. Rubber sample E has a high permittivity and a loss tangent exceeding 3. Very high imaginary permittivities are observed at the lowest frequencies which varies as 1/frequency, consistent with that expected from a material with a constant conductivitity. Figure 5-22 and Figure 5-23 show how the permittivity changes with frequency. Configuration 1 shows the real component reducing at low frequencies which may be an artefact of the extremely high imaginary values dominating the calculations, or a gating effect caused by the gate width being so close to the minimum allowed by the lowest frequency.

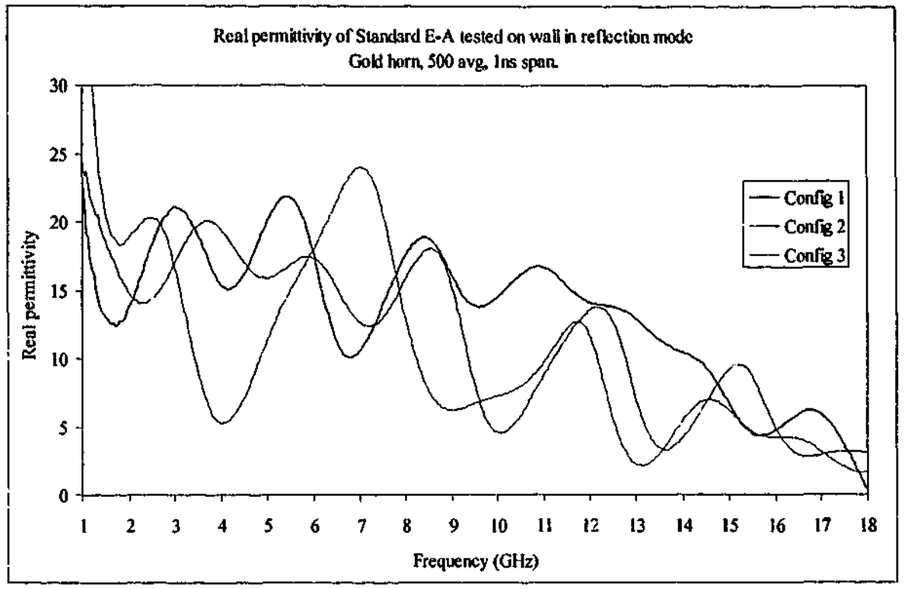

Figure 5-22. Real permittivity of rubber E-A tested with gold horns in free space using reflection data

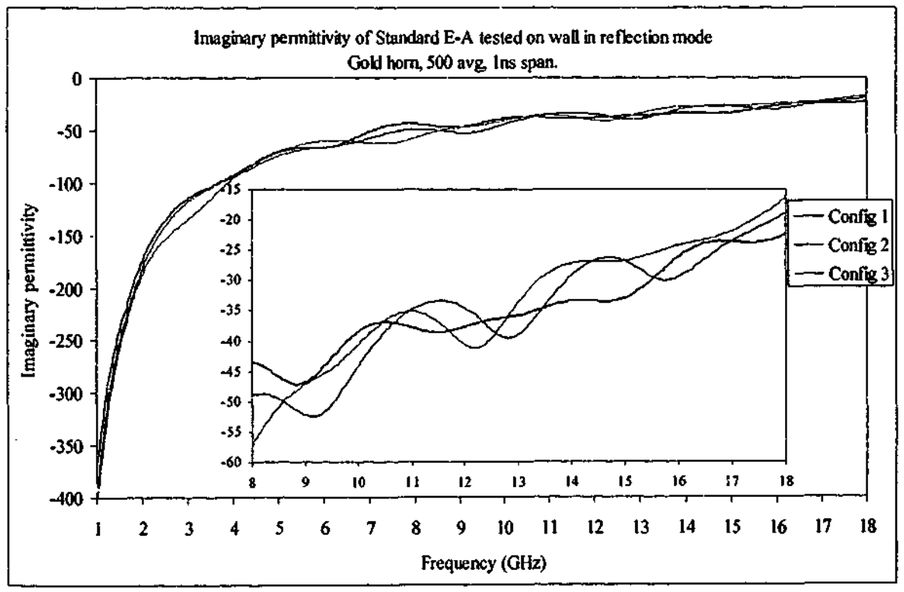

Figure 5-23. Imaginary permittivity of rubber E-A tested with gold horns in free space using reflection data

When comparing these results to the transmission only ones, we find that the values do not match, particularly for the high permittivity materials. While the imaginary permittivity

for sample E correlates reasonably well with the transmission data, the real permittivity is significantly different at higher frequencies. The reasons for this can be found by examining the raw reflection data. Using the best fit of the data for sample E as shown in Figure 5-14 and Figure 5-15, we can generate the reflection signal expected from a material with such properties and compare it to the actual signal we measure from the sample. The comparison is shown below in Figure 5-24 and Figure 5-25. The magnitude differences between the measured and expected results ("fit") are fairly small, of the order of one or two tenths of a dB for configurations 1 and 2, a little higher for configuration 3. A larger difference occurs in the phase of the reflected measurements compared to the expected curve from the permittivity data fit for transmission. There is a phase shift occurring in the reflected signal that is frequency dependent. This magnitude shift is indicative of a change in the distance between the calibration plane and the position of the sample. When a reflection calibration is taken, the position that the reflective plate was at during the calibration is called the calibration plane. The sample must be placed exactly on that plane when it is measured or the resulting shift in distance leads to a shift in the phase of the reflected signal. The phase shift is easily calculated as $360°\times 2d/\lambda$, where d is the distance between where the sample was measured to the calibration plane. A factor of 2 is present since the wave must travel to the sample and back again.

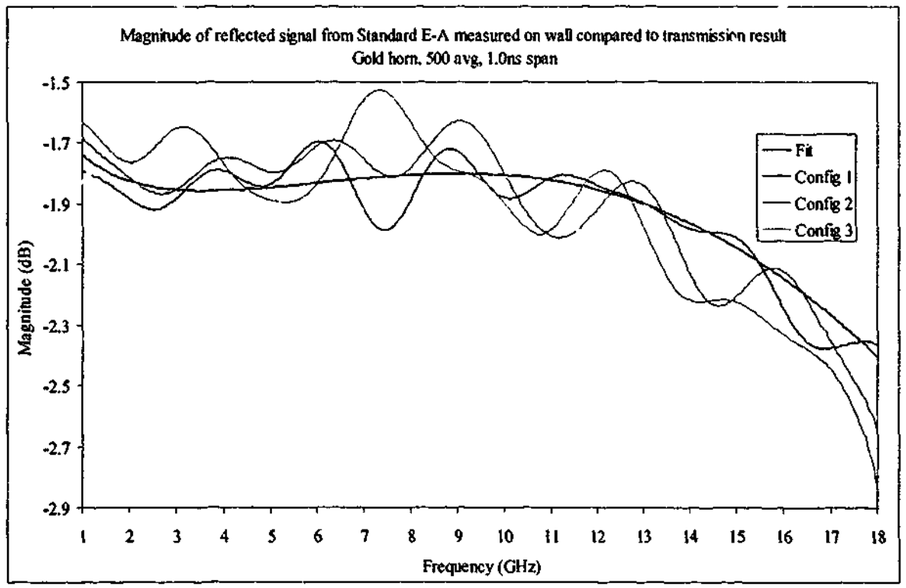

Figure 5-24. Magnitude of reflected signal expected from sample E-A using transmission results compared to measured data

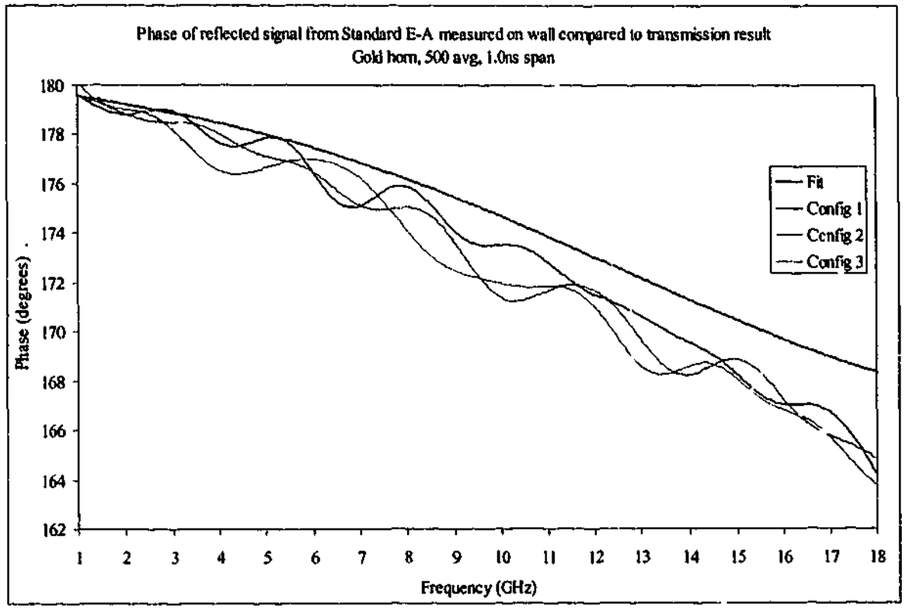

Figure 5-25. Phase of reflected signal expected from sample E-A using transmission results compared to measured data

The question of which result is the correct one should be resolved before continuing with adding a phase shift to all the reflection data. After all, it may be the transmission data that is incorrect. Since the values extracted for Perspex were similar with both measurements, and we don't know the actual permittivity of the carbon loaded rubber materials, we need some way to discriminate between the two measurements to find which is in error. It is known that the material is non-magnetic, so by combining the reflection and transmission data we can use the value of permeability to determine the correct solution. When this was done for sample E, it was found that the permeability did not average to 1.0 + 0i, but instead showed a frequency dependent shift away from this value. The values can be seen in Figure 5-26.

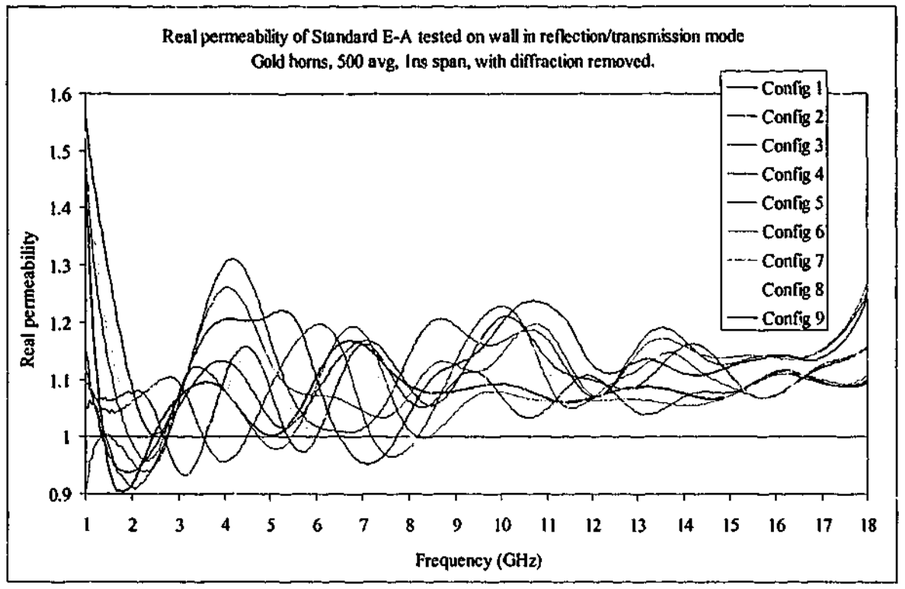

Figure 5-26. Real permeability of sample E-A tested with gold horns in free space using reflection and transmission data with diffraction removed

At high frequencies it can be seen that the permeability values are organised together in three distinct groups, which correspond to measurements taken when the send horn was fixed. Configurations 1, 4, and 7 were all taken with the send horn at its closest point, configurations 2, 5 and 8 when the horn was at the next distance, and so on. This gives an indication that the reflection result was in error, since the same error is occurring within the group. If the error was in the transmission data, we may expect a similar grouping to occur between configurations 1, 2 and 3, configurations 4, 5 and 6, and so on. By simply adding a small shift in the calibration plane for the reflection measurements, we can move the permeability values to the $\mu = 1$ line. The distance required is very small – for configurations 1, 4 and 7 we need a shift of 70 microns, 2, 5, and 8 need an 80 micron shift and 3, 6, and 9 need a 100 micron shift. These very small shifts (of the order of the author's hair breadth) can very easily be explained physically, and correct the values of the permittivity and permeability. When the shifts in the calibration plane are made, the resultant real permeability can be seen in Figure 5-27.

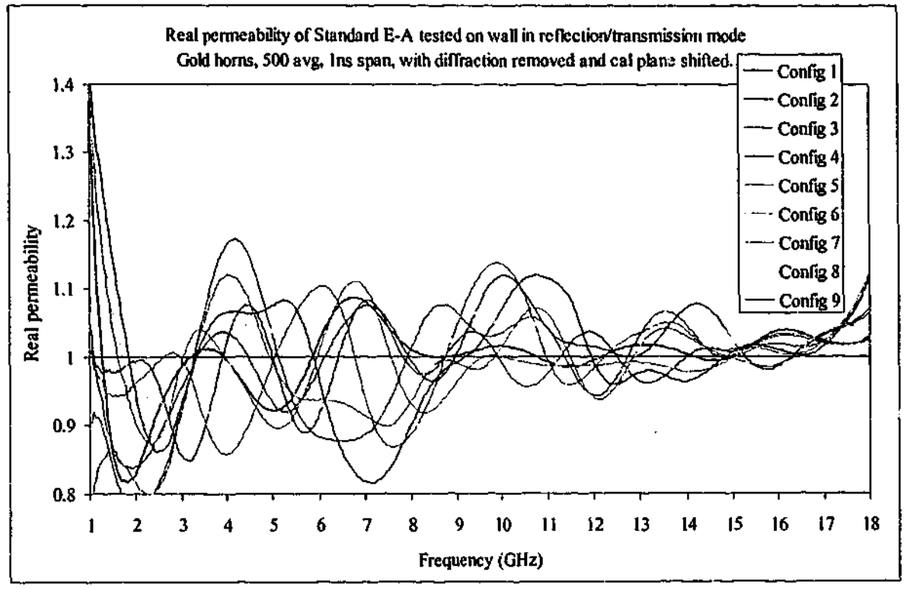

Figure 5-27. Real permeability of sample E-A tested with gold horns in free space using reflection and transmission data with diffraction removed and calibration plane shifted

Adding the calibration shift obviously doesn't affect the amount of noise in the measurement, but it does move the permeability closer to that expected. Of course the permittivity is changed also, and the values obtained more closely match those taken using transmission only measurements. Figure 5-28 and Figure 5-29 show the real and imaginary permittivity values extracted from the reflection only measurements after the calibration plane has been shifted. These values are still not precisely equal to those of the transmission only results but the difference is significantly lower.

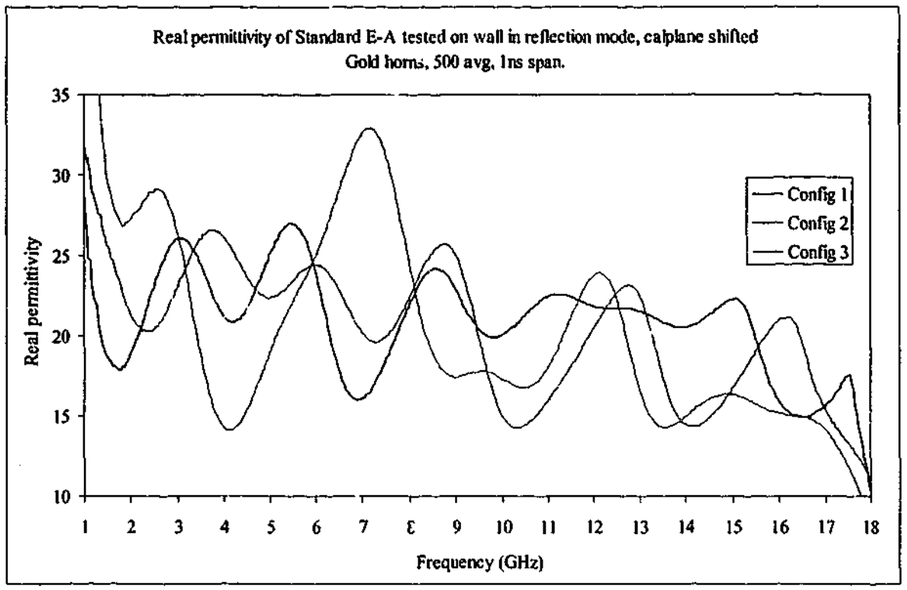

Figure 5-28. Real permittivity of sample E-A tested with gold horns in free space using reflection data with diffraction removed and the calibration plane shifted

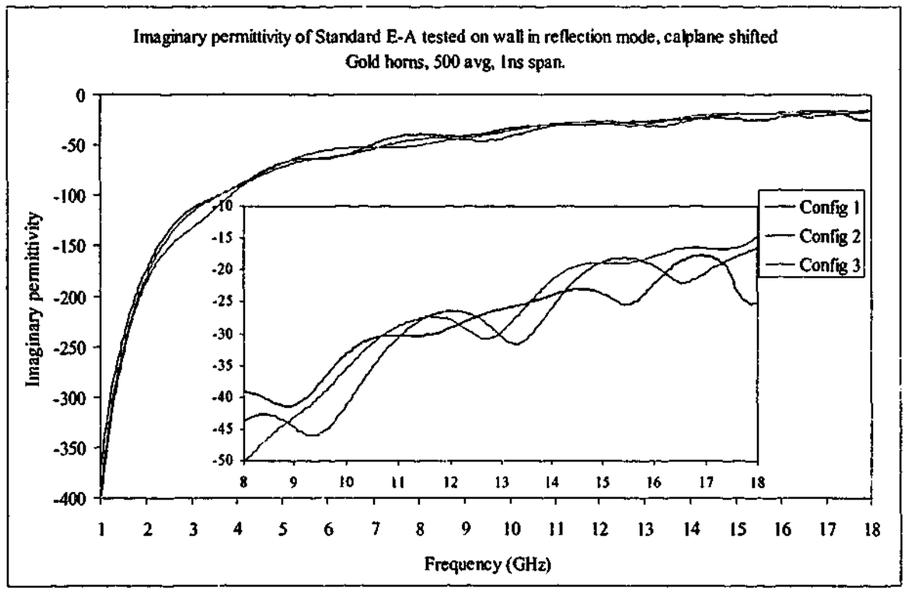

Figure 5-29. Imaginary permittivity of sample E-A tested with gold horns in free space using reflection data with diffraction removed and the calibration plane shifted

The phase shift applied to the sample measurement is positive, indicating that the sample is closer to the horn than the calibration plane. Horns are uni-directional antennas, so as the

distance between the horn and the target increases, so does the uniformity of the field emanating from the horn.

Figure 5-30 shows how the field strength varies with distance from the horn. The concentric circles indicate lines of constant field, and the colours indicate field strength.

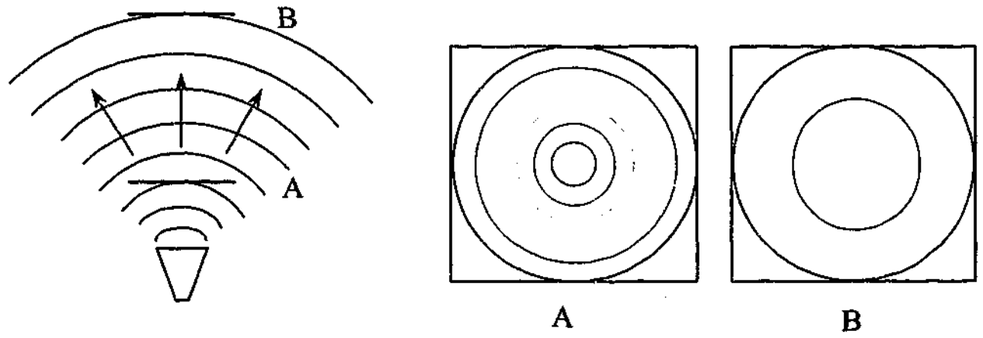

Figure 5-30. Field from a microwave horn at various distances from horn

It can be seen from the figure above that when the sheet is close to the horn, the field is concentrated near the centre. When the sample is far away, the sheet is closer to being uniformly illuminated. Therefore, variations in flatness that occur further from the centre of the sheet are less important when the sample is close to the horn, and more important when the sample is further from the horn. Since the phase shift required to correct the permeability values increases with increasing distance from the horn, the effective distance between the sample and the calibration plane must be larger. This infers that either the calibration sheet is a convex shape as viewed from the horn, or the polystyrene foam block has a concave shape. These options are shown below in Figure 5-31.

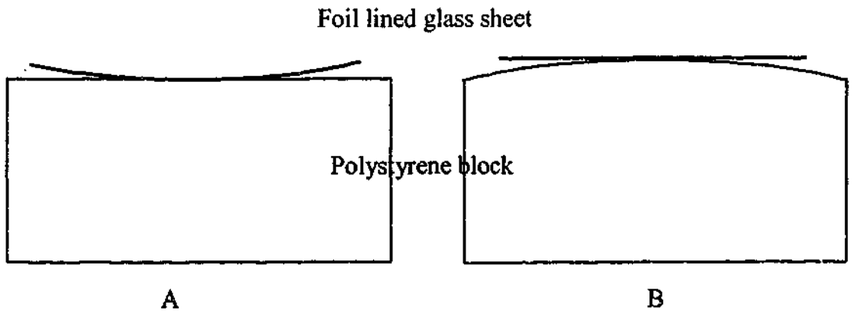

Figure 5-31. Possible sources of error for reflection measurements

We cannot be absolutely sure which configuration is correct. Since the flexible samples conform to the shape of the polystyrene block, either configuration is possible. Rigid materials will not conform to the curved polystyrene block, but may have a curvature of their own which makes comparison difficult. Close examination of the foam block revealed a surface that showed no sign of being curved.

Assuming the phase shift is constant between samples tested in the same configuration, we can then simply apply the shift measured for Sample E to all the other flexible samples. Unless otherwise stated, all data sets will be assumed to have had this correction done.

The average values of permittivity for the flexible samples are shown in Figure 5-32 and Figure 5-33. It can be seen that both real and imaginary permittivity for samples E and F are lower at high frequencies when compared to the transmission only results shown in Figure 5-14 and Figure 5-15. The samples with lower permittivity values show very similar values to the transmission only results except for sample D at frequencies above about 17 GHz, which may be due to a random error in one of the measurements.

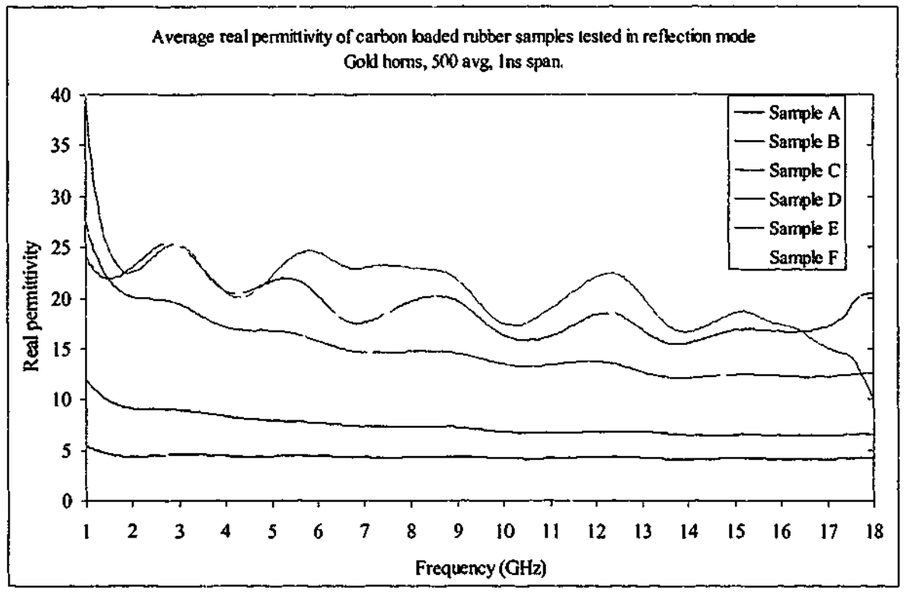

Figure 5-32. Average real permittivity of carbon loaded rubber samples tested with gold horns in free space using reflection data alone

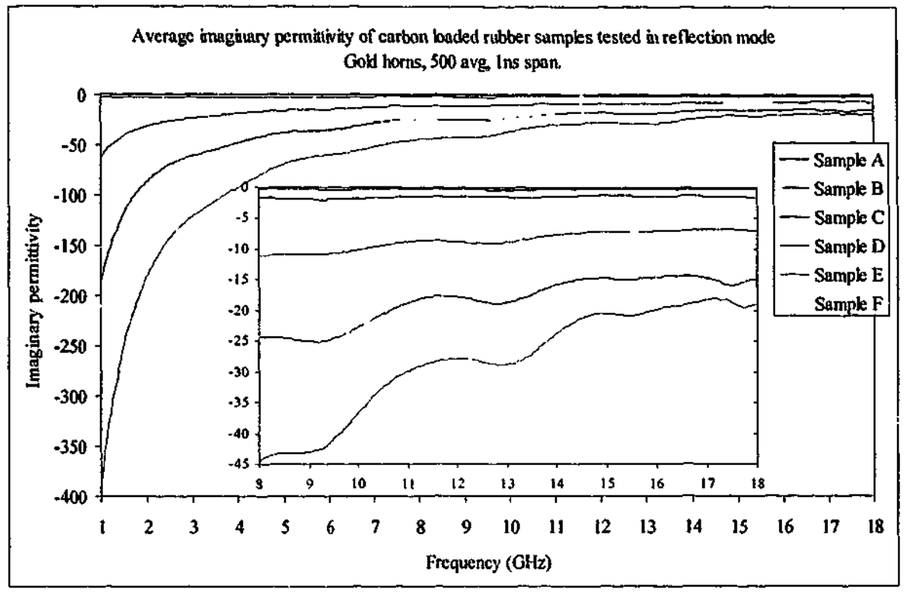

Figure 5-33. Average imaginary permittivity of carbon loaded rubber samples tested with gold horns in free space using reflection data alone

5.3. 1 – 18 GHz, reflection and transmission

Although the results using both the reflection and transmission data have been pre-empted somewhat by the discussion of phase shifts in the reflection technique, we will nevertheless present the data for the samples showing the permittivity and permeability results. Combining the data sets from the reflection and transmission measurements gives a full S-matrix of the material. This means that an iterative technique is not required to extract the permittivity, and that permeability values can also be found. For all the results shown here, the diffraction signal was removed from the transmission data.

Combining the reflection and transmission signals in the Perspex case give values very close to those expected[14]. Except for the lowest frequencies where the real permittivity rises sharply for even the closest configurations, the extracted values have high correlation to those published elsewhere in the literature.

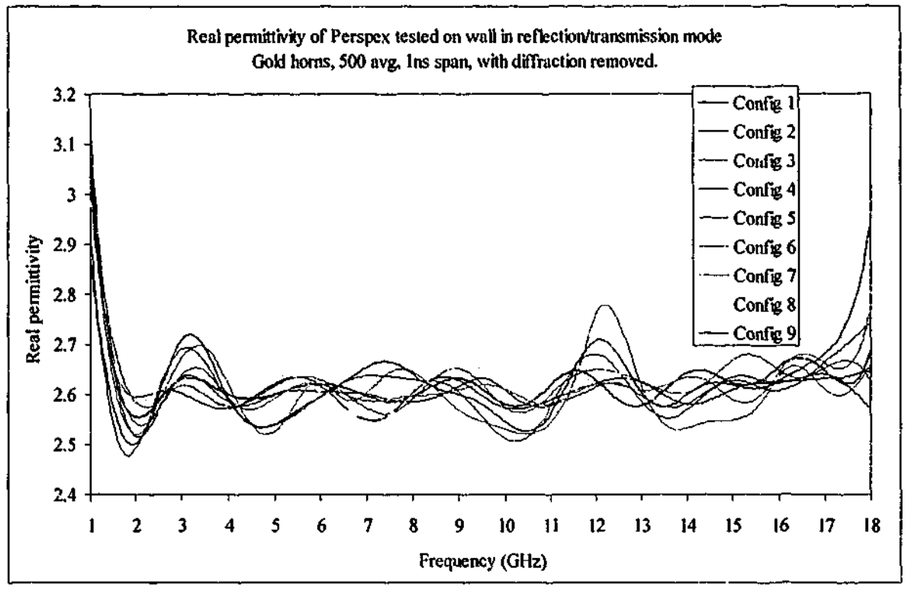

Figure 5-34. Real permittivity of Perspex tested with gold horns in free space using reflection and transmission data with diffraction removed

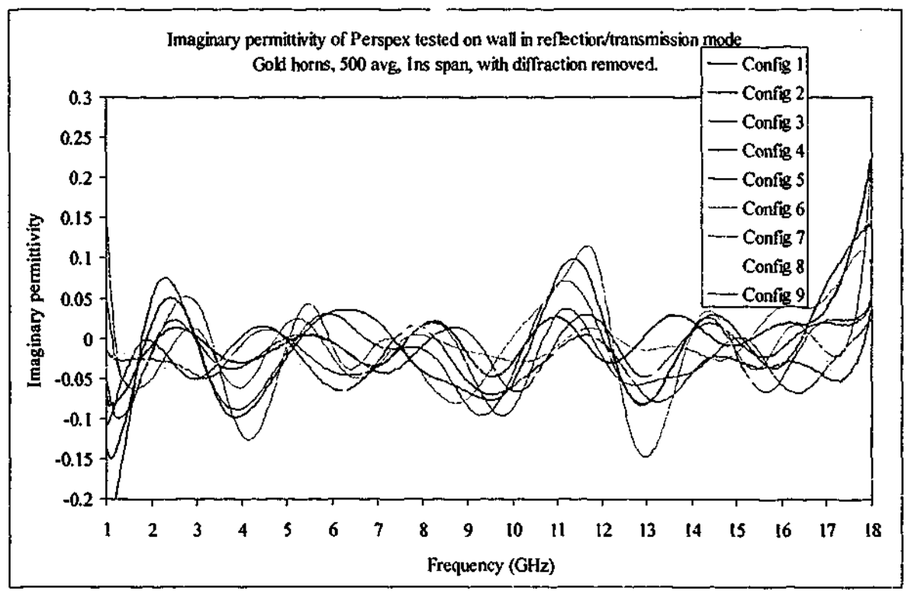

Figure 5-35. Imaginary permittivity of Perspex tested with gold horns in free space using reflection and transmission data with diffraction removed

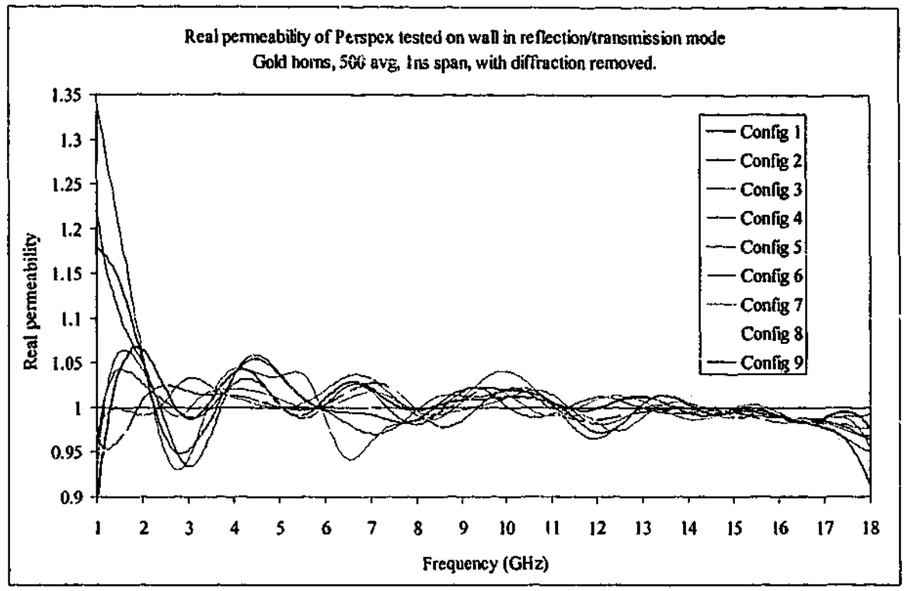

Figure 5-36. Real permeability of Perspex tested with gold horns in free space using reflection and transmission data with diffraction removed

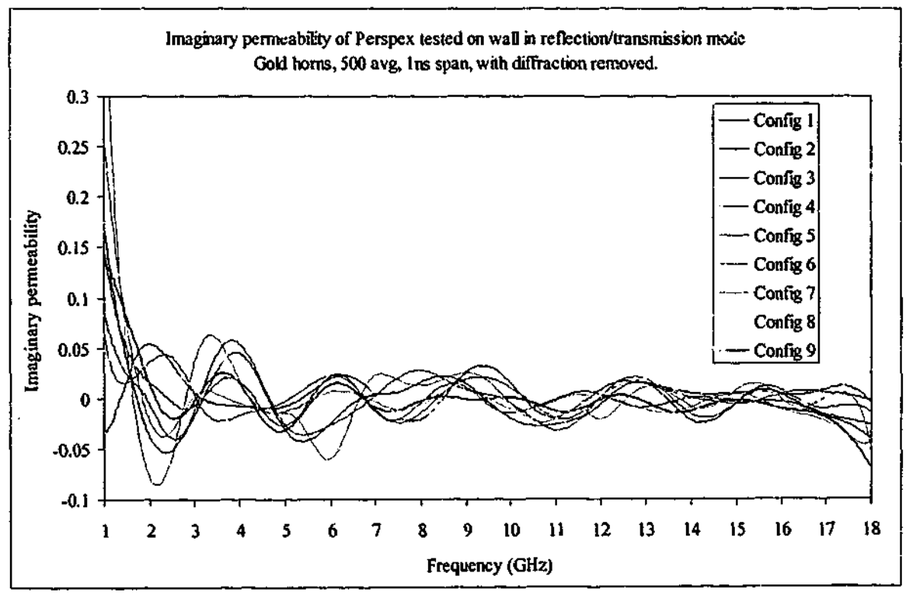

Figure 5-37. Imaginary permeability of Perspex tested with gold horns in free space using reflection and transmission data with diffraction removed

Average values across the frequency spectrum for the different configurations are shown in Table 5-4.

Config #	Ave ε'	σ(ε')	Ave ε"	σ(ε")	Ave μ'	σ(μ')	Ave μ"	σ(μ")
1	2.621	0.051	0.001	0.040	1.007	0.020	-0.002	0.027
2	2.611	0.048	-0.031	0.026	0.999	0.016	0.006	0.016
3	2.608	0.061	-0.019	0.054	1.003	0.039	0.001	0.023
4	2.611	0.059	-0.013	0.028	1.003	0.015	0.001	0.021
5	2.625	0.053	-0.026	0.029	1.002	0.016	0.004	0.016
6	2.605	0.071	-0.013	0.060	1.009	0.059	0.003	0.050
7	2.620	0.058	-0.005	0.035	1.004	0.017	-0.001	0.033
8	2.631	0.057	-0.027	0.034	1.000	0.022	0.003	0.017
9	2.622	0.069	-0.009	0.060	1.006	0.041	-0.004	0.029
Expected	2.60	-	-0.014	-	1.00	-	0.000	-

Table 5-4. Averages and standard deviations of permittivity and permeability measured with gold horns using reflection and transmission data with diffraction removed

It is clear from the graphs of both permittivity and permeability that the low frequency values (those below 2 GHz) are seriously in error. The magnitude of the reflected signal at 1 GHz is about –20 dB, so this loss in resolution combined with the fact that the diffraction is highest at low frequencies may explain this. The permeability values also start to show errors at the highest frequencies. Rather than staying at a more or less constant value of 1, the real permeability values are starting to drop. This is a prelude to what we shall see in the 16 - 40 GHz range, where destructive interference effects start to dominate the analysis. The previous chapter showed how destructive interference affects the permittivity and permeability values when some of the multiple reflections inside the sample are not included for the final analysis. The thickness of the Perspex sheet used here causes destructive interference to occur at about 20.7 GHz, and the effects of this are starting to be seen at 18 GHz. However, the total average results across the frequency range are extremely close to those expected for the Perspex sample.

The carbon loaded rubber samples fared similarly to the Perspex result. Permeability values were close to the expected result consistent with non-magnetic materials, while the permittivity values closely matched those of the transmission only results. The average permittivity values at all configurations for these samples are shown in Figure 5-38 and Figure 5-39. It is interesting to note that the permittivity reductions seen in samples E and F at high frequencies in the reflection only calculations have all but disappeared when using both reflection and transmission data.

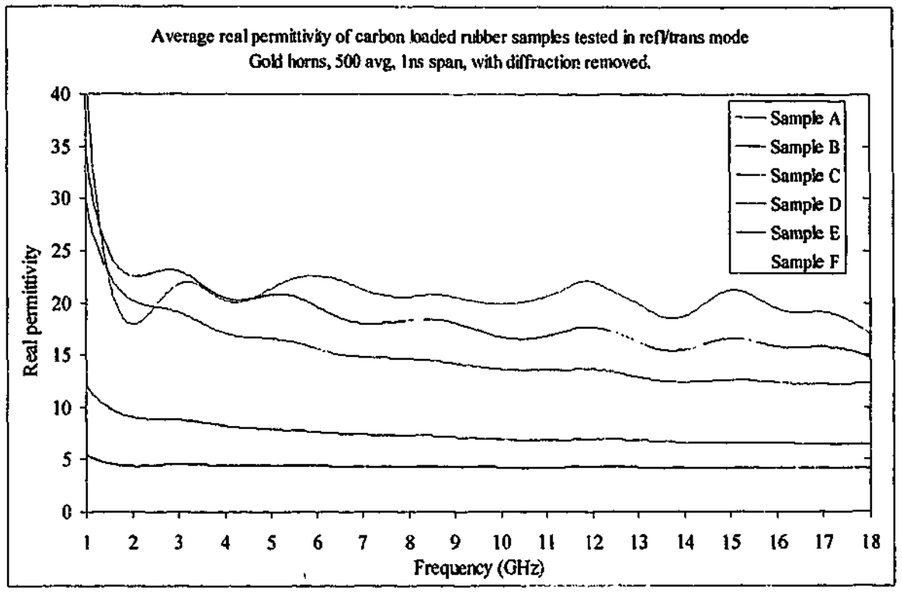

Figure 5-38. Average real permittivity of carbon loaded rubber samples tested with gold horns in free space using reflection and transmission data with diffraction removed

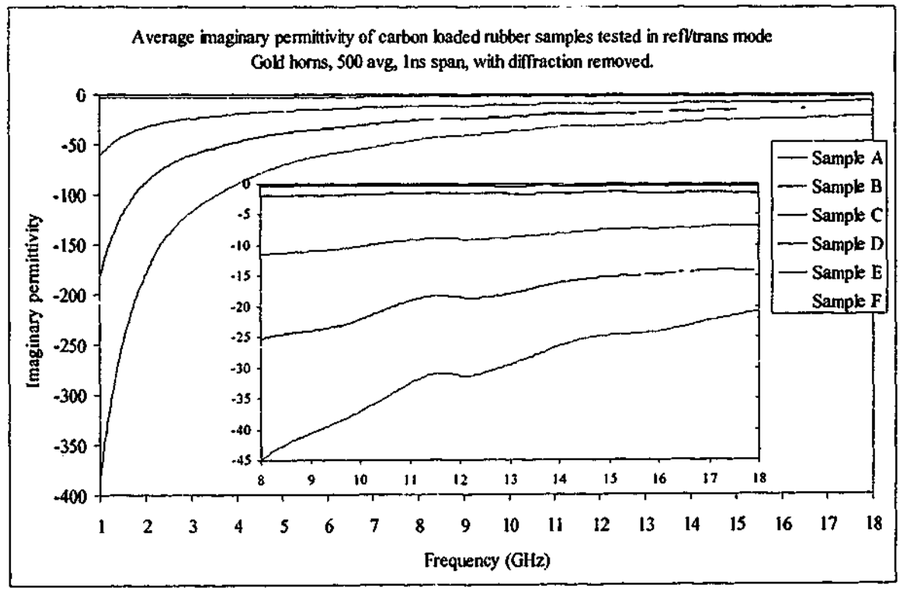

Figure 5-39. Average imaginary permittivity of carbon loaded rubber samples tested with gold horns in free space using reflection and transmission data with diffraction removed

The permeability values are very close to that expected for a non-magnetic material. There are some obvious cyclic variations across the frequency range similar to those seen in the permittivity, but in the main these do not account for more than a 5% error. The shift seen in permittivity for the reflection only result appears to manifest itself in the imaginary permeability, but the effect is quite small, much less than that seen in the permittivity. The frequency variation of permeability for the carbon loaded rubber samples is shown in Figure 5-40 and Figure 5-41.

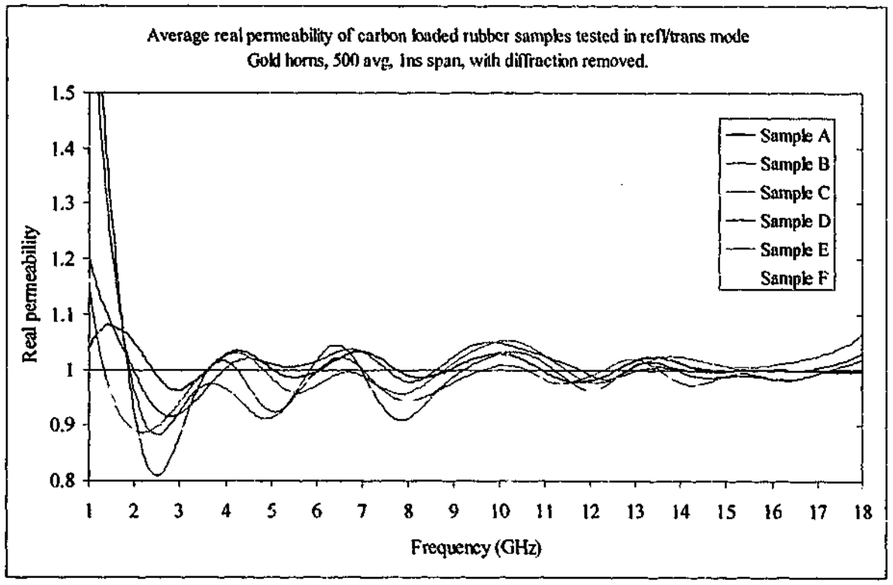

Figure 5-40. Average real permeability of carbon loaded rubber samples tested with gold horns in free space using reflection and transmission data with diffraction removed

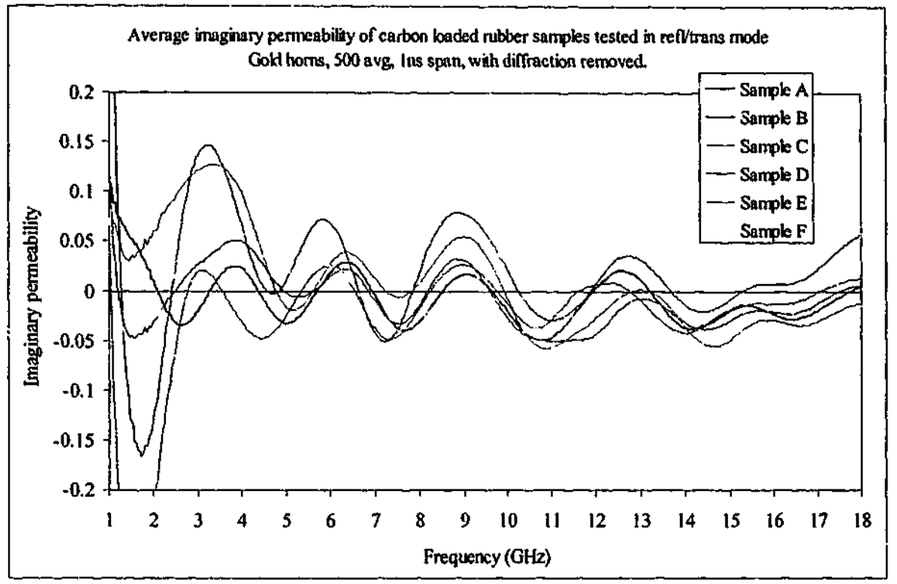

Figure 5-41. Average imaginary permeability of carbon loaded rubber samples tested with gold horns in free space using reflection and transmission data with diffraction removed

We can compare the average permeability across the whole frequency range to that of free space as a guide to the accuracy of the reflection/transmission technique. The average real and imaginary permeability for all the large non-magnetic sheets are shown below in Table 5-5 and Table 5-6.

Sample	Cfg 1	Cfg 2	Cfg 3	Cfg 4	Cfg 5	Cfg 6	Cfg 7	Cfg 8	Cfg 9
Perspex	1.01	0.999	1.00	1.00	1.00	1.01	1.00	1.00	1.01
A-A	1.01	1.00	1.02	1.01	0.99	1.01	1.00	1.01	1.03
B-A	1.01	1.01	1.01	1.01	1.01	1.00	1.01	1.01	1.03
C-A	1.00	1.00	1.01	1.01	0.996	0.984	1.00	0.998	1.01
D-A	1.00	0.998	1.02	1.01	0.996	1.01	1.01	1.00	1.03
E-A	0.999	1.01	0.992	0.994	1.00	0.981	0.995	1.01	1.00
F-A	0.976	0.967	0.960	0.976	0.960	0.944	0.969	0.973	0.974
Com A	0.977	0.990	0.954	0.971	0.971	0.952	0.969	0.979	0.984

Table 5-5. Average real permeability across the frequency range 1-18 GHz

Sample	Cfg 1	Cfg 2	Cfg 3	Cfg 4	Cfg 5	Cfg 6	Cfg 7	Cfg 8	Cfg 9
Perspex	-0.002	0.006	0.001	0.001	0.004	0.003	-0.001	0.003	-0.004
A-A	0.001	0.000	-0.030	0.004	0.003	-0.027	0.006	-0.003	-0.023
B-A	-0.002	0.002	-0.036	0.000	0.005	-0.032	0.002	0.002	-0.024
C-A	0.005	-0.012	-0.051	0.003	-0.011	-0.059	-0.006	-0.043	-0.072
D-A	0.039	0.043	-0.008	0.037	0.042	-0.015	0.028	0.026	-0.020
E-A	0.012	0.035	0.029	0.001	0.019	0.011	-0.014	-0.006	-0.010
F-A	0.005	-0.009	-0.029	0.009	-0.004	-0.026	0.006	-0.015	-0.036
Com A	0.010	0.025	-0.008	0.013	0.029	-0.003	0.011	0.026	-0.015

Table 5-6. Average imaginary permeability across the frequency range 1-18 GHz

It is apparent from these results that the lower permittivity materials have permeability values that are closer to unity and also have less variation in values. The configuration number doesn't seem to have a great influence in average values, but the standard deviation shows a general trend towards being higher with larger configuration number.

Sample G contains 85 wt% carbonyl iron powder, and is still ferromagnetic at frequencies above 1 GHz. The reflection/transmission technique is the only free space method that can give values of both permittivity and permeability since both are unknown. Since we know the phase shift that needs to be applied from the measurements of the non-magnetic materials, we can apply the same shift to the magnetic material. This gives us greater confidence in the accuracy of the electromagnetic properties of the material using this method. Over the frequency range 1-18 GHz we get the following values, shown in Figure 5-42 to Figure 5-45.

Overall the results are reasonably consistent for the different configurations. The characteristic oscillations that occur across the frequency range increase with configuration number as before, and the results should be viewed with caution below 2 GHz. However, the results are consistent with other measurements taken on carbonyl iron loaded rubber[37].

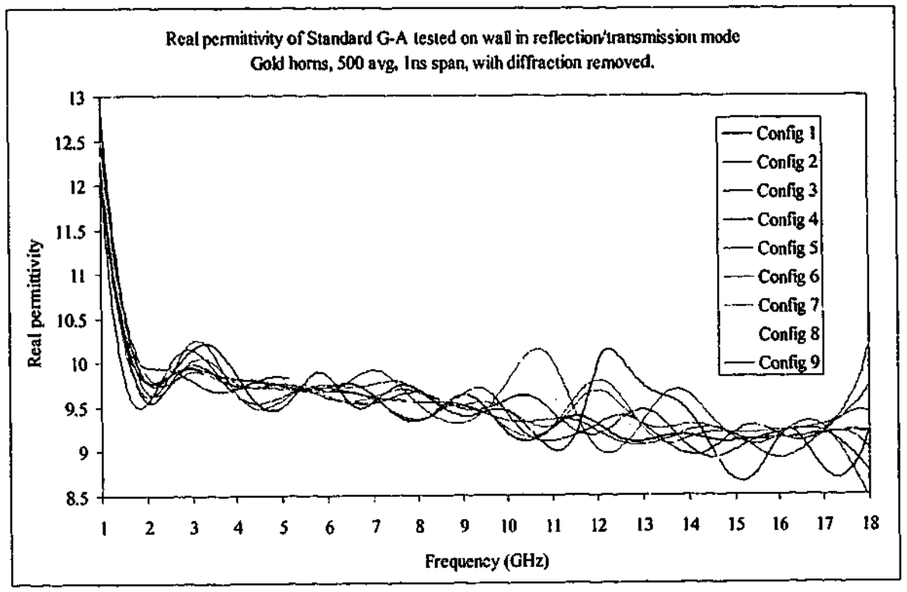

Figure 5-42. Real permittivity of sample G-A tested with gold horns in free space using reflection and transmission data with diffraction removed and phase shifted

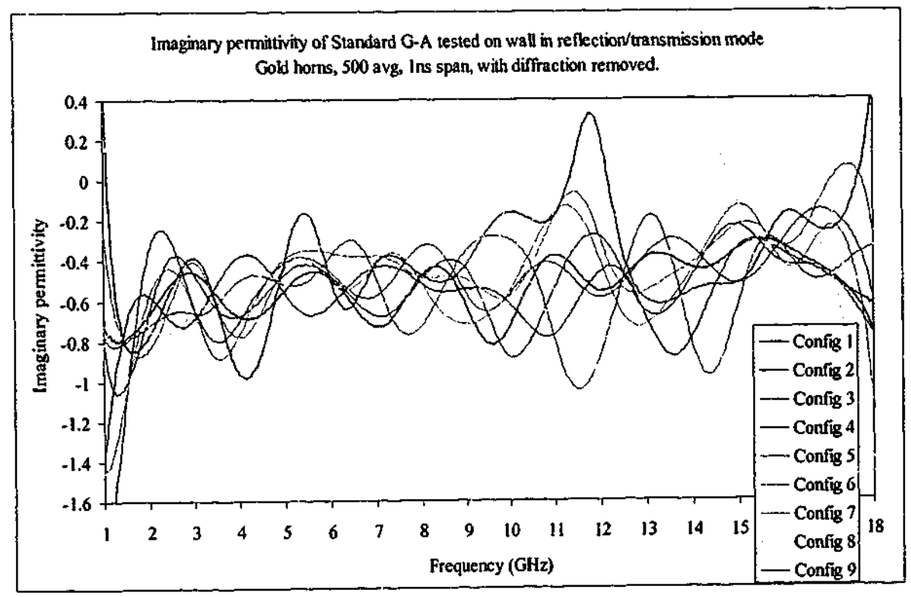

Figure 5-43. Imaginary permittivity of sample G-A tested with gold horns in free space using reflection and transmission data with diffraction removed and phase shifted

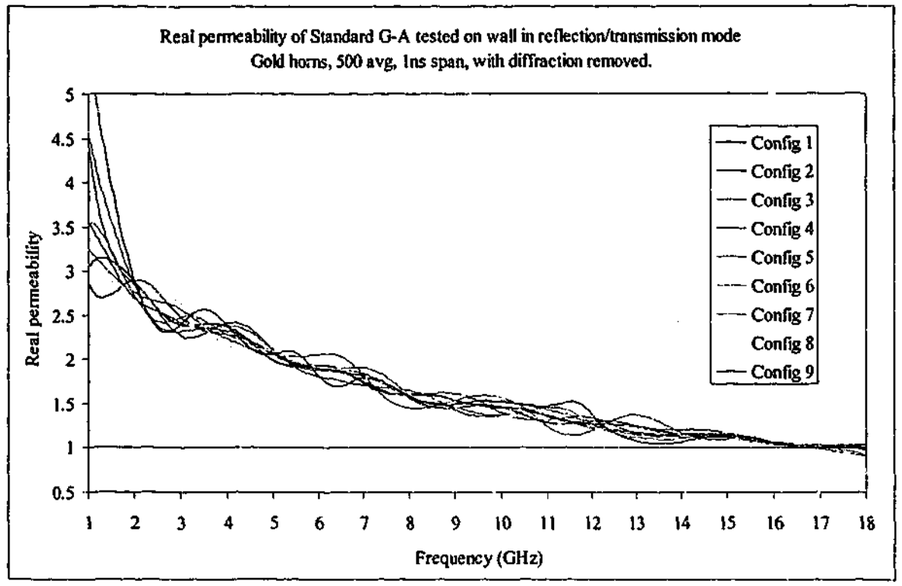

Figure 5-44. Real permeability of sample G-A tested with gold horns in free space using reflection and transmission data with diffraction removed and phase shifted

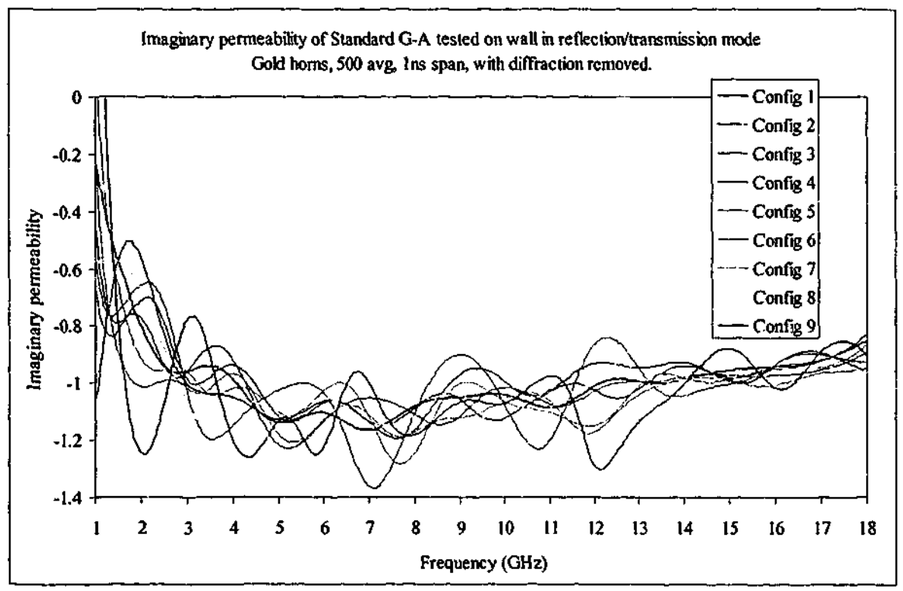

Figure 5-45. Imaginary permeability of sample G-A tested with gold horns in free space using reflection and transmission data with diffraction removed and phase shifted

5.4. 7.5 – 18 GHz, transmission only

Measurements taken with the silver horns over the frequency range 7.5 – 18 GHz are expected to have less noise and so be more accurate over the same frequency range than those taken with the gold horns. There are many reasons for this, including:

- the silver horns have higher gain so sensitivity is increased, beamwidth is reduced, and diffraction is less
- the gate span can be shorter so there is a greater likelihood that stray reflections can be eliminated
- a shorter gate span means that the horns can be placed closer to the sample so diffraction can again be reduced.

The diffraction signal was measured for each configuration using the silver horns, with the magnitude shown in Figure 5-46. The measured value is very low when the receive horn is closest to the sheet, with a intensity more than 50 dB lower than that when the foil lined glass sheet is not present. Nevertheless the signal is still considerable at longer distances, enough to cause problems especially in configurations 8 and 9. Due to an oversight in the test procedure, the reflective sheet was not measured at the same time as the samples over this frequency range. The reflective sheet was measured later, but since the positions of the horn were not precisely the same as for the samples, some errors in removing the diffraction signal have occurred, especially in the phase of the signal. These errors are lower in magnitude than those caused by diffraction. When permittivity is extracted without removing the diffraction signal the same effects occur as for the 1-18 GHz results so will not be reproduced here.

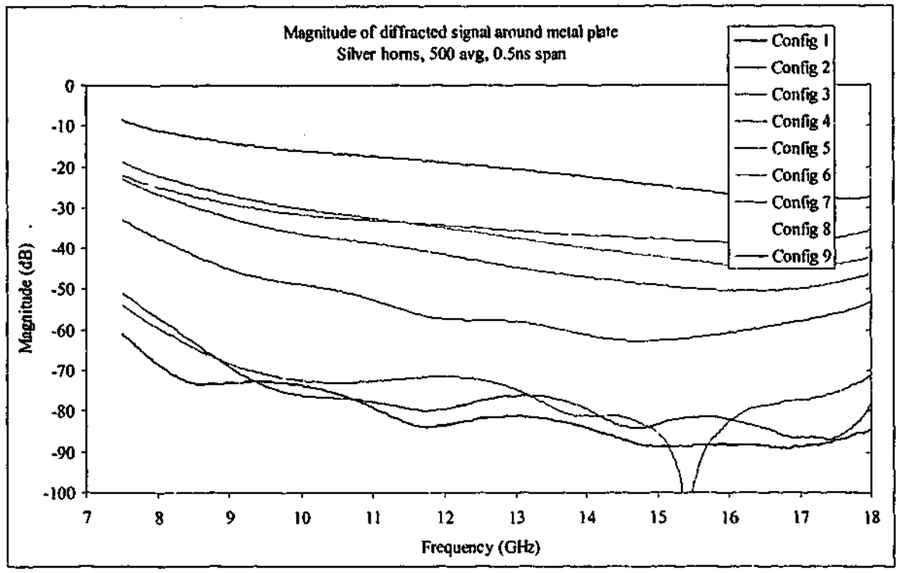

Figure 5-46. Magnitude of diffraction around 445mm square foil lined glass sample measured with silver horns

Starting as before with the Perspex sample, we expect to see less noise in the permittivity values than the gold horn result. The measurements at all nine configurations shown in Figure 5-47 and Figure 5-48 show this to be the case with variations seen only in the second decimal place. The effects of the time gating are clearly present at the frequency extremes, but do not impact greatly on the permittivity values. The average values across the frequency range are shown in Table 5-7, showing good correlation with the expected values at these frequencies.

Config #	Ave ε'	σ(ε')	Ave ε"	σ(ε")
1	2.604	0.007	-0.009	0.011
2	2.601	0.007	-0.012	0.010
3	2.605	0.007	-0.013	0.010
4	2.602	0.008	-0.016	0.005
5	2.604	0.008	-0.015	0.007
6	2.603	0.010	-0.017	0.006
7	2.597	0.007	-0.018	0.005
8	2.604	0.008	-0.016	0.004
9	2.600	0.015	-0.016	0.013
Expected	2.60	-	-0.014	-

Table 5-7. Averages and standard deviations of permittivity of Perspex measured with silver horns using transmission data alone with diffraction removed

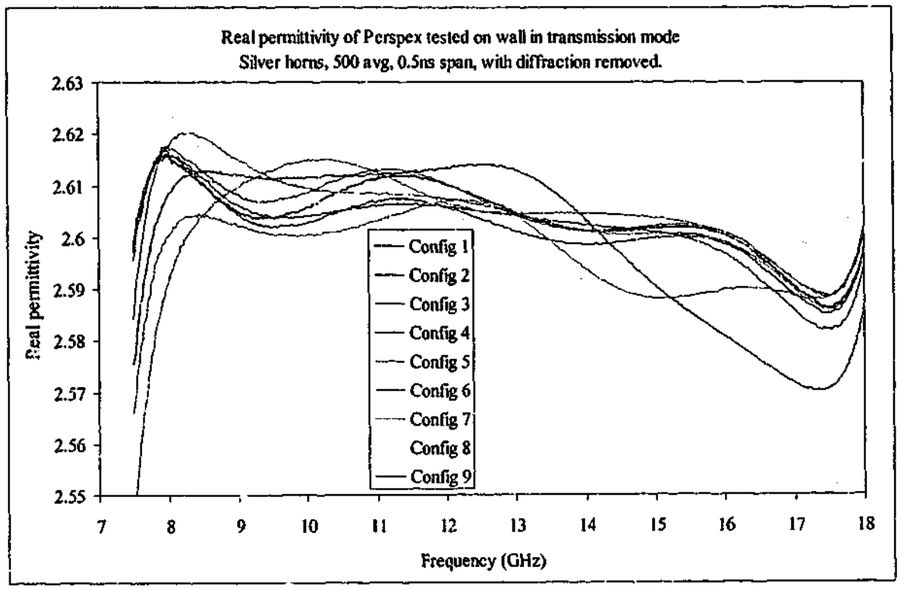

Figure 5-47. Real permittivity of Perspex measured with silver horns in free space using transmission data alone with diffraction removed

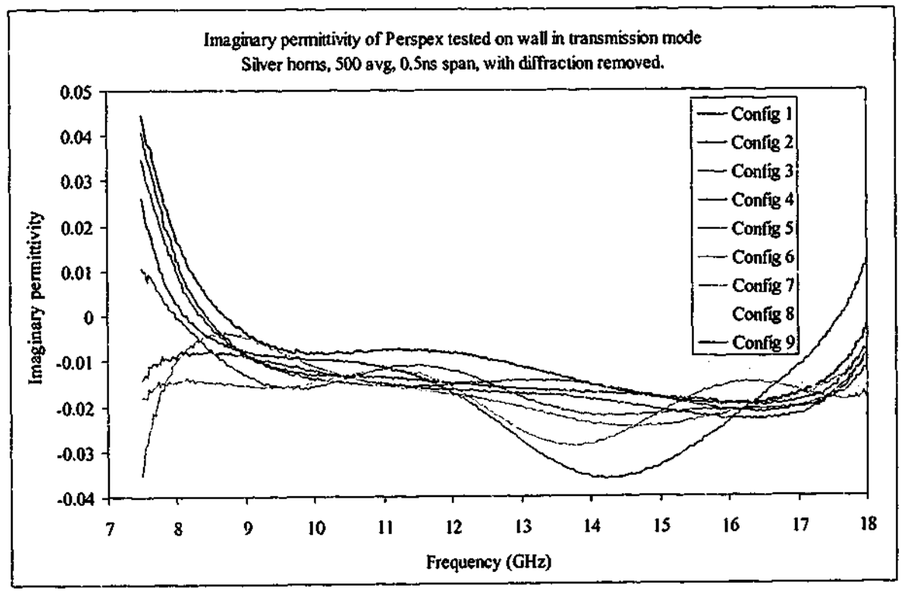

Figure 5-48. Imaginary permittivity of Perspex measured with silver horns in free space using transmission data alone with diffraction removed

A similar trend follows with the lossy rubber materials. The variations seen in the 1 – 18 GHz results are removed almost completely, leaving some slight effects due to incomplete

removal of the diffraction path for the higher configurations, and the effects of time gating at the frequency extremes.

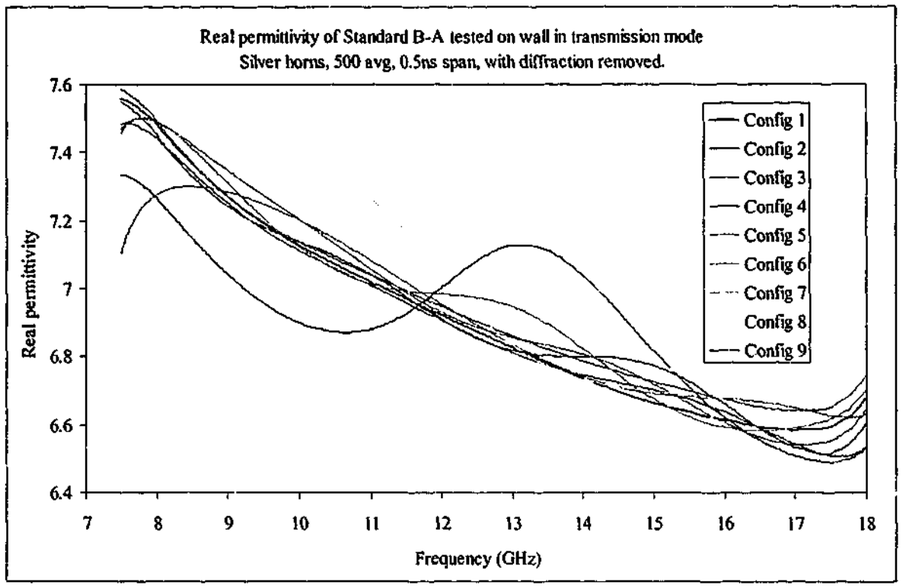

Figure 5-49. Real permittivity of Sample B-A measured with silver horns in free space using transmission data alone with diffraction removed

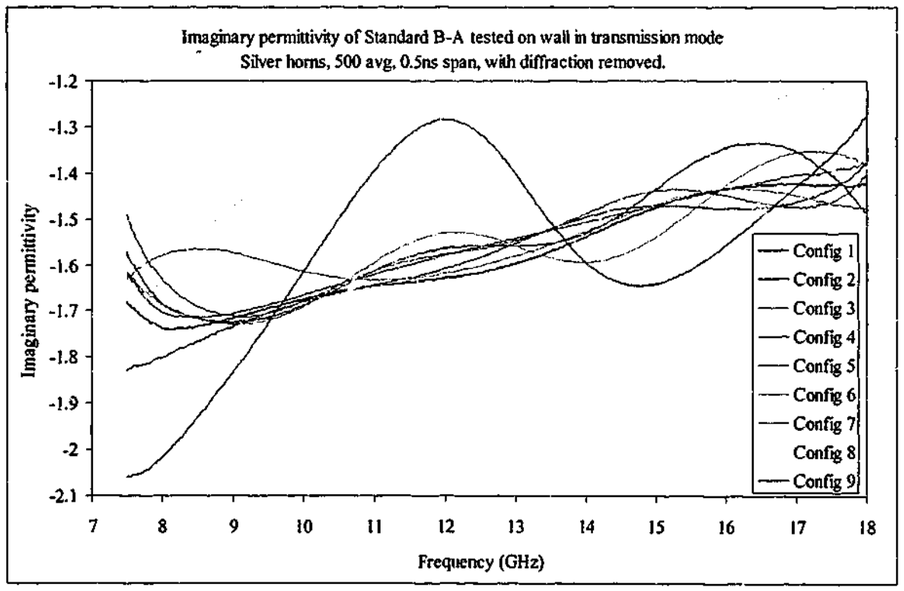

Figure 5-50. Imaginary permittivity of Sample B-A measured with silver horns in free space using transmission data alone with diffraction removed

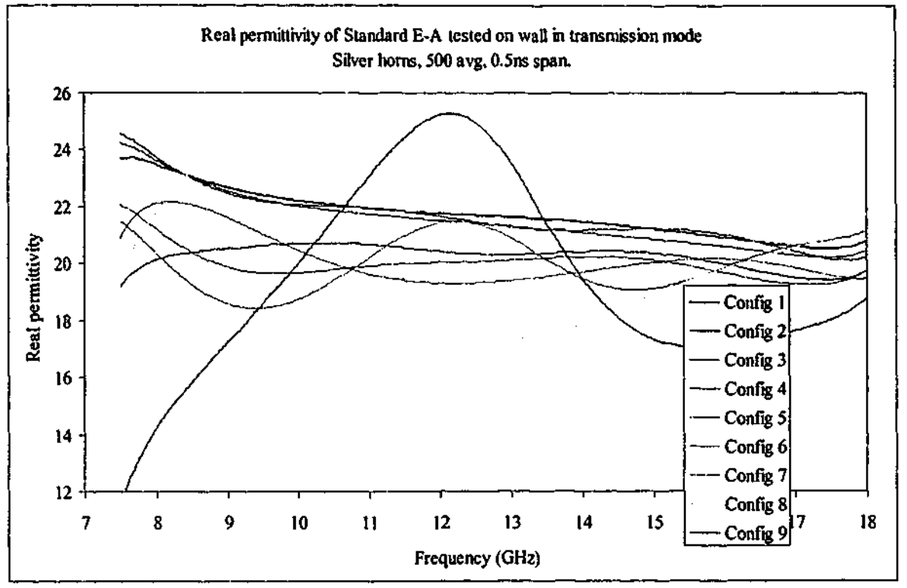

Figure 5-51. Real permittivity of Sample E-A measured with silver horns in free space using transmission data alone with diffraction removed

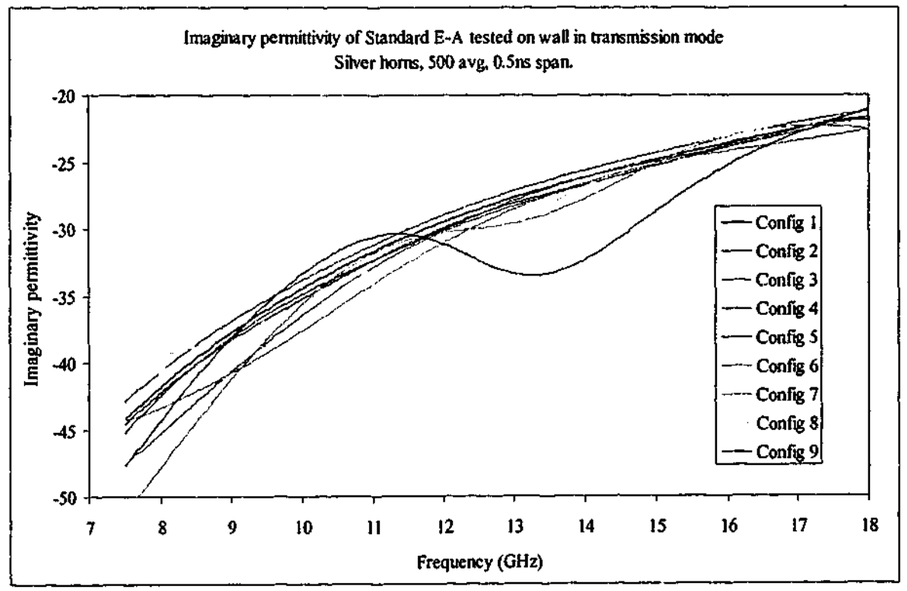

Figure 5-52. Imaginary permittivity of Sample E-A measured with silver horns in free space using transmission data alone with diffraction removed

Noise levels again increase with configuration number and sample permittivity, showing how incomplete cancellation of the diffraction wave caused by small shifts in sample

placement can affect the results. The average permittivity of all the carbon loaded samples is shown in Figure 5-53 and Figure 5-54.

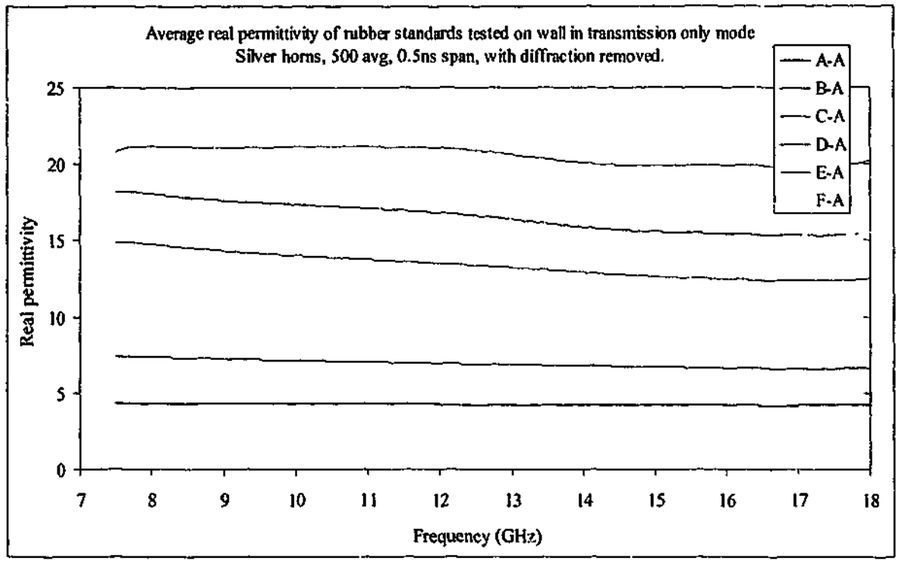

Figure 5-53. Average real permittivity of carbon loaded rubber samples tested with silver horns in free space using transmission data with diffraction removed

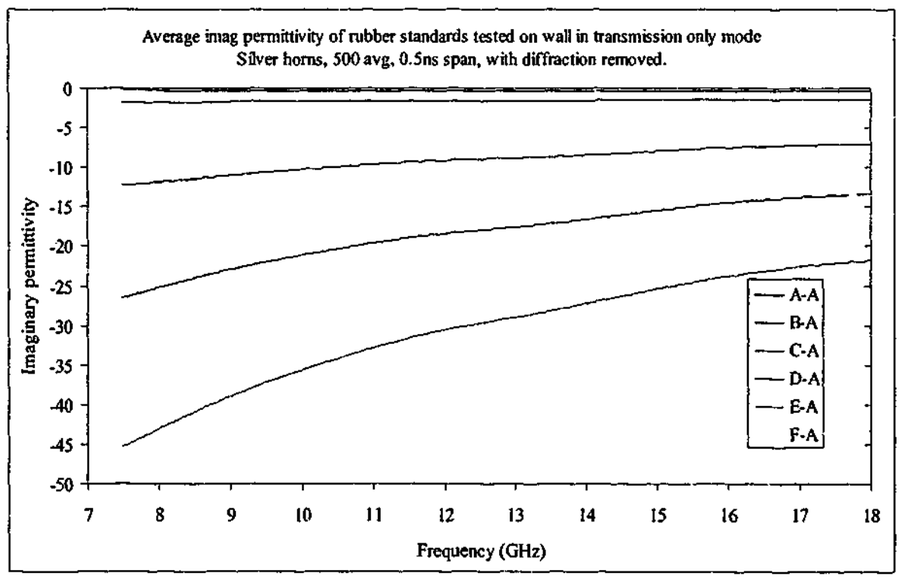

Figure 5-54. Average imaginary permittivity of carbon loaded rubber samples tested with silver horns in free space using transmission data with diffraction removed

The composite material again follows a Debye-like curve, with the resonance frequency for the fitted curve close to that seen over the 1-18 GHz range. The line of best fit has parameters of $\varepsilon_0 = 47.4$, $\varepsilon_\infty = 1.22$ and $\tau = 51.13$ ps, giving a resonance frequency of about 3.1 GHz. Even though the actual data used for the fit does not include frequencies below 7.5 GHz, the resonance frequency calculated is very close to the result of 2.75 GHz calculated over 1 -- 18 GHz. The curves of real and imaginary permittivity for the composite sample are shown in Figure 5-55 and Figure 5-56. The composite material was measured at the same time as the reflective backing sheet, so the removal of the diffracted signal was far more successful than for the carbon loaded rubber materials, especially at configuration 9. This again shows how important it is to measure the backing plate in exactly the same configuration as the samples under test.

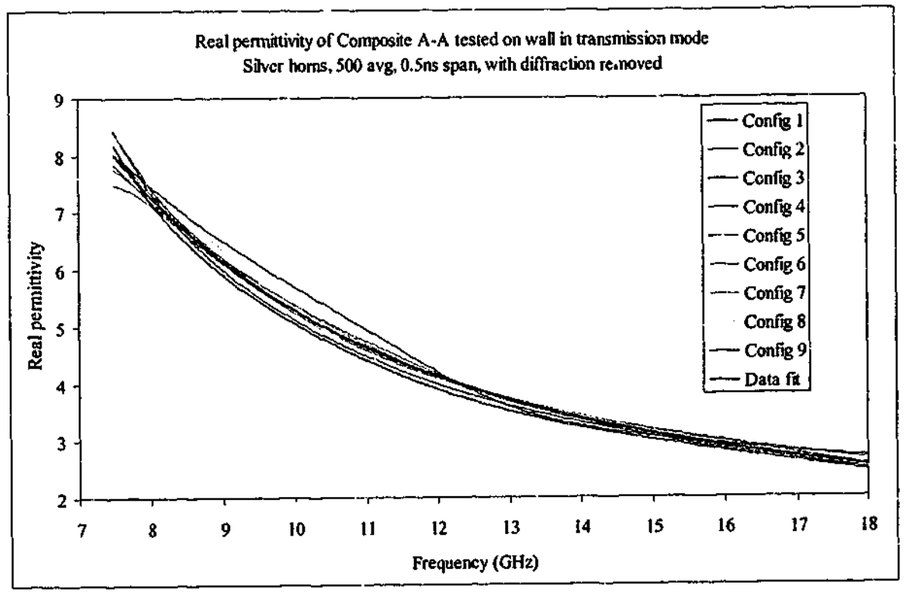

Figure 5-55. Real permittivity of Composite A-A tested with silver horns in free space using transmission data alone with diffraction removed

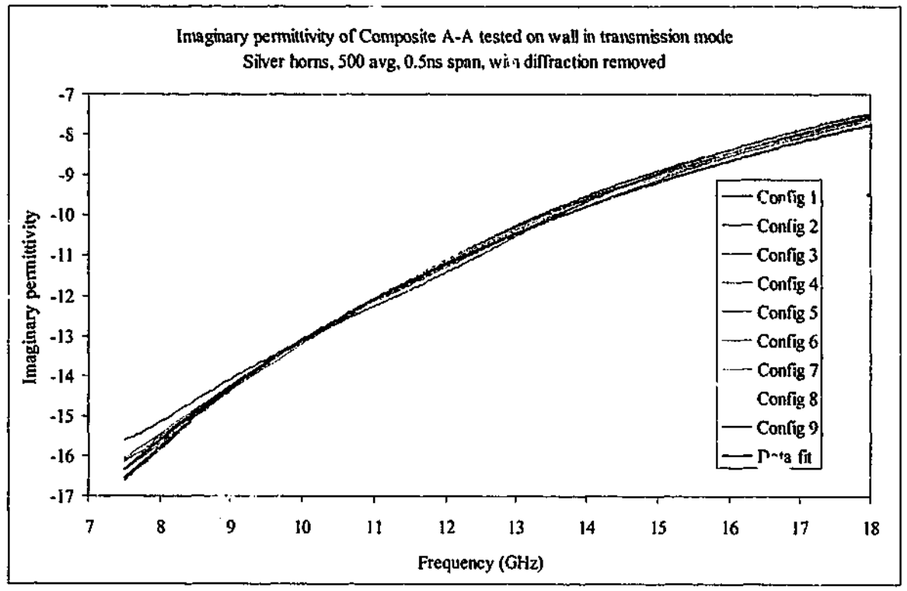

Figure 5-56. Imaginary permittivity of Composite A-A tested with silver horns in free space using transmission data alone with diffraction removed

5.5. 7.5 – 18 GHz, reflection only

As with the previous reflection measurements over the range 1 – 18 GHz, we need to investigate the amount of phase shift that needs to be applied to these measurements to ensure correct results. Since the maximum effect is seen when permittivity is highest, we shall again concentrate on the material with the highest permittivity, sample E. Using the known permeability to determine the correct phase shift as before, it was found that the optimum shift required for configuration 1 was 0.02 mm, configuration 2 needed 0.11 mm and configuration 3 required a 0.12 mm shift to bring the permeability values close to the expected value of 1. Figure 5-57 shows the real permeability of Sample E-A across the frequency band with the corresponding shifts applied.

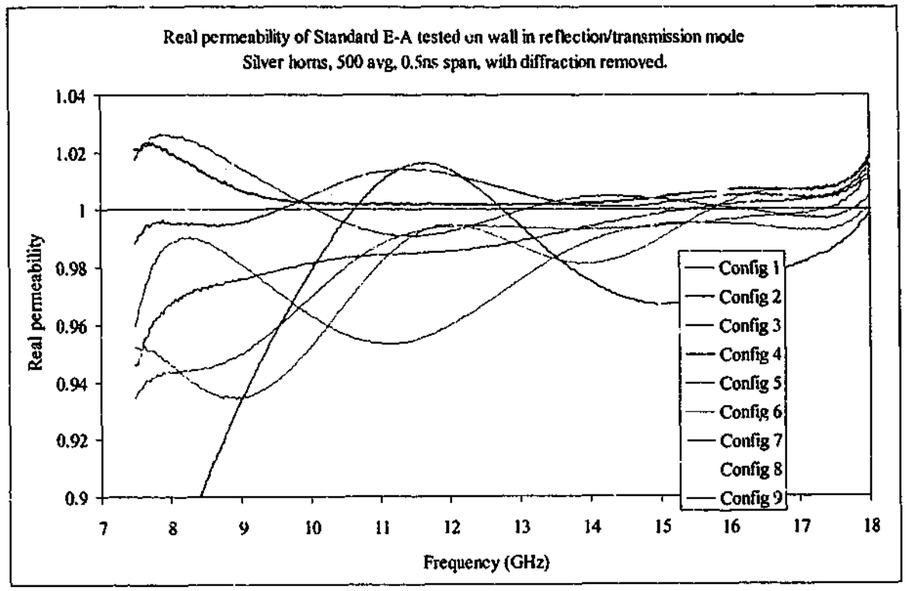

Figure 5-57. Real permeability of sample E-A tested with silver horns in free space using reflection and transmission data with diffraction removed and calibration plane shifted

Incomplete removal of the diffraction wave is responsible for the larger variations seen in Figure 5-57, and in all but configuration 9 the variation is kept to within about 6%.

With the positional shifts of the samples calculated, we can continue with the permittivity calculations from reflection data alone. Starting as before with the Perspex sample, we would expect to see the results to be better than those tested with the gold horns. Figure 5-58 and Figure 5-59 show the real and imaginary permittivity extracted from the reflection only data. Note that the positive values obtained for the imaginary permittivity are due to experimental error, as the sign convention chosen should produce negative imaginary components of both permittivity and permeability.

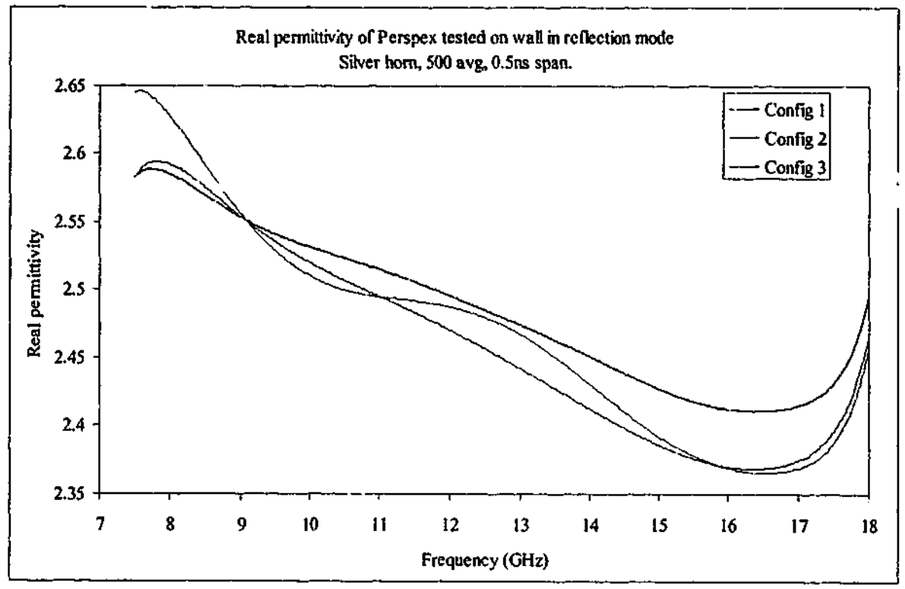

Figure 5-58. Real permittivity of Perspex sample tested with silver horns in free space using reflection only data

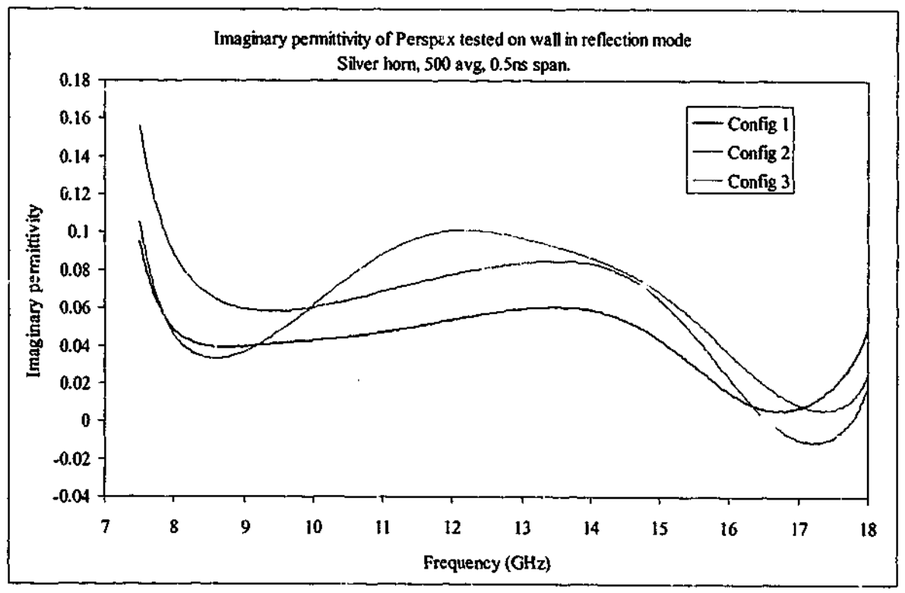

Figure 5-59. Imaginary permittivity of Perspex sample tested with silver horns in free space using reflection only data

The figures above also show the characteristic tails that occur near the start and stop frequencies caused by the time gate. This is especially obvious in the real permittivity value

for configuration 3, but the trend is apparent in all the traces. The average permittivity measured for the Perspex sample is shown in Table 5-8.

Config #	Ave ε'	σ(ε')	Ave ε''	σ(ε'')
1	2.485	0.056	0.042	0.017
2	2.460	0.072	0.058	0.033
3	2.468	0.078	0.061	0.031
Expected	2.60	-	-0.014	-

Table 5-8. Averages and standard deviations of permittivity measured using reflection data

While the oscillations are definitely reduced across the frequency range compared to the 1 – 18 GHz result, there appears to be some frequency dependence of permittivity, rather the constant value of 2.6 – 0.014i expected. Some evidence of this was observed in the 1 – 18 GHz measurement, but it is much more obvious over the narrower frequency span. Previously it was possible to remove this effect by incorporating the phase shift caused by sample movement, but over the frequency range 7.5 – 18 GHz the effect was not reduced.

The permittivity graphs of the carbon loaded rubber samples are shown in Figure 5-60 and Figure 5-61. It can be seen that the results of samples E and F in particular are quite different to those taken using transmission data, especially at the higher frequencies. The permittivities of these high concentration materials "cross over" the values observed for lower concentrations. This effect may be caused by the presence of the nearby destructive interference peak in the reflected signal for these materials, since the only major difference between samples D and F is that sample F is about 50% thicker.

Comparing these results with the transmission only ones of Figure 5-53 and Figure 5-54 we see that the results from samples A – D (ones with lower concentrations of carbon) are very similar to each other, while it is only E and F that show any marked difference.

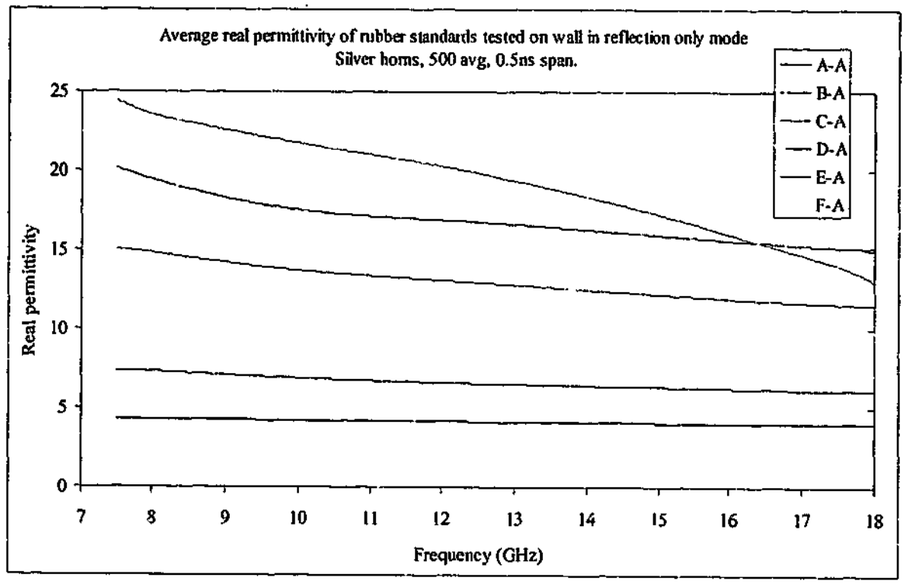

Figure 5-60. Average real permittivity of carbon loaded rubber samples tested with silver horns in free space using reflection data.

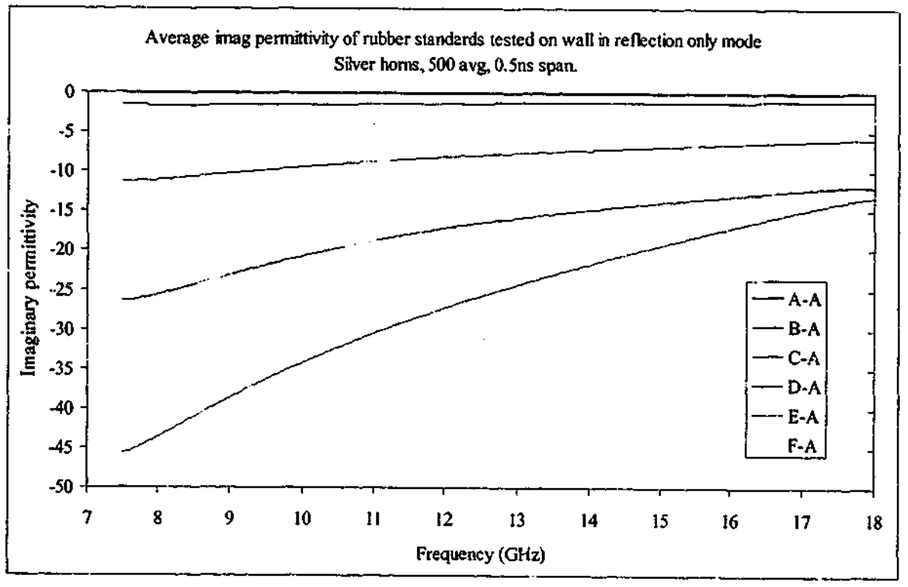

Figure 5-61. Average imaginary permittivity of carbon loaded rubber samples tested with silver horns in free space using transmission data.

The composite material requires its own phase shift since it is a stiff material and will not conform to the shape of the polystyrene foam sample holder. When phase shift was found

using the same method as for the carbon loaded rubber materials, the permittivity values extracted from the reflection data are shown in Figure 5-62 and Figure 5-63. The data fit uses the same formula as before with parameters of $\varepsilon_0 = 54.3$, $\varepsilon_\infty = 1.34$ and $\tau = 60.04$ ps, giving a resonance frequency of about 2.7 GHz.

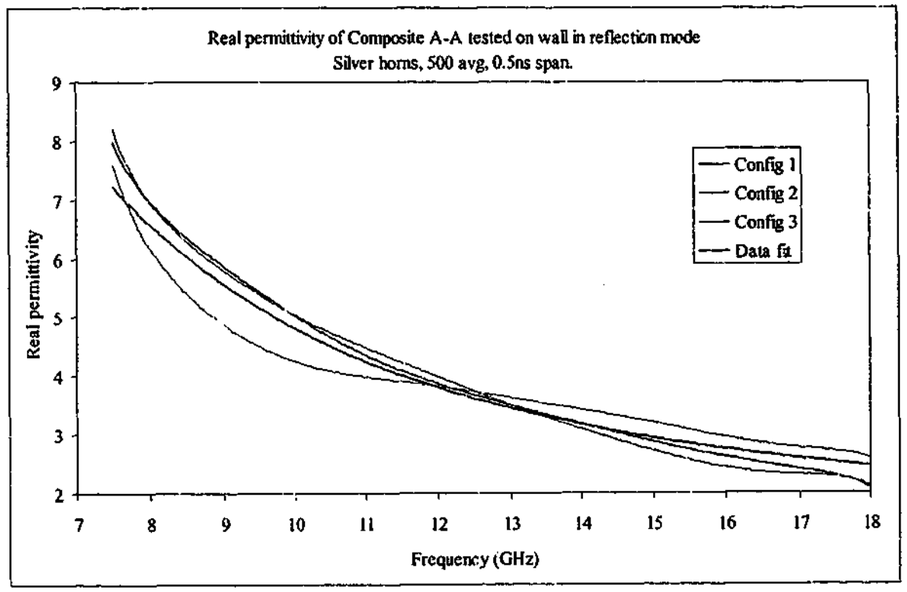

Figure 5-62. Real permittivity of Composite sample tested with silver horns in free space using reflection only data

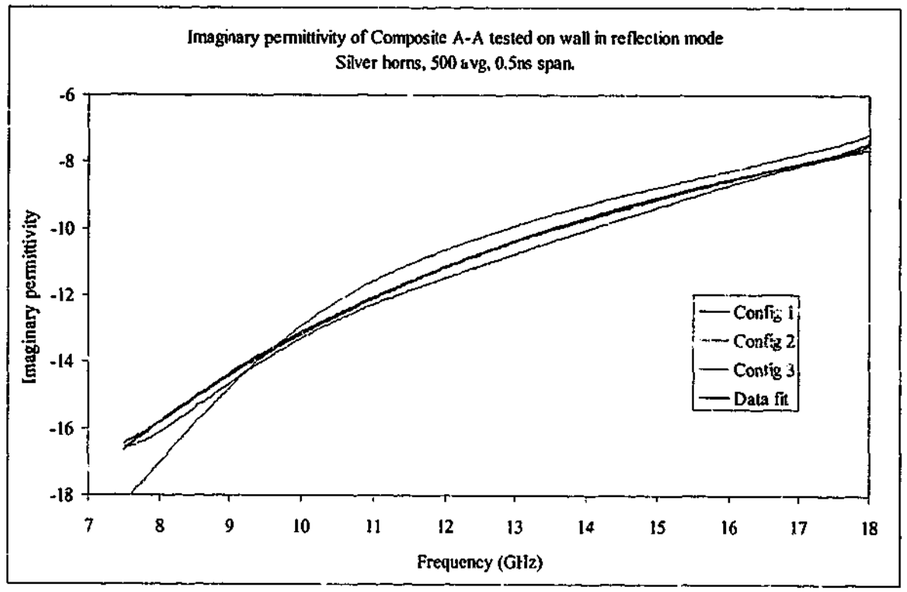

Figure 5-63. Imaginary permittivity of Composite sample tested with silver horns in free space using reflection only data

5.6. 7.5 – 18 GHz, reflection and transmission

Based upon the reflection only results over this frequency range, the extraction of permittivity and permeability using the reflection/transmission algorithm does not appear promising. However, the results come out surprising well. As seen earlier in chapter 2, destructive interference causes errors, even when many of the peaks are used in the extraction. In the Perspex case, destructive interference occurs at about 20.7 GHz, and the presence of this peak causes problems at the high end of the frequency range. Removing the diffraction signal and applying the specimen phase shift gives the following values for permittivity and permeability for Perspex, shown in Figure 5-64 to Figure 5-67. As noted before, positive values for the imaginary components are due to experimental error, rather than a change in the sign conventions.

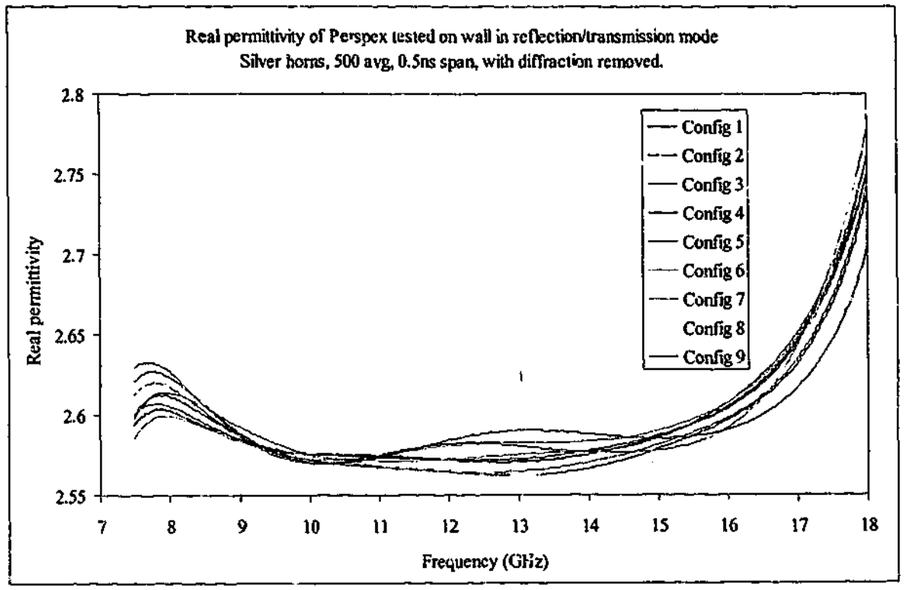

Figure 5-64. Real permittivity of Perspex tested with silver horns in free space using reflection and transmission data with diffraction removed

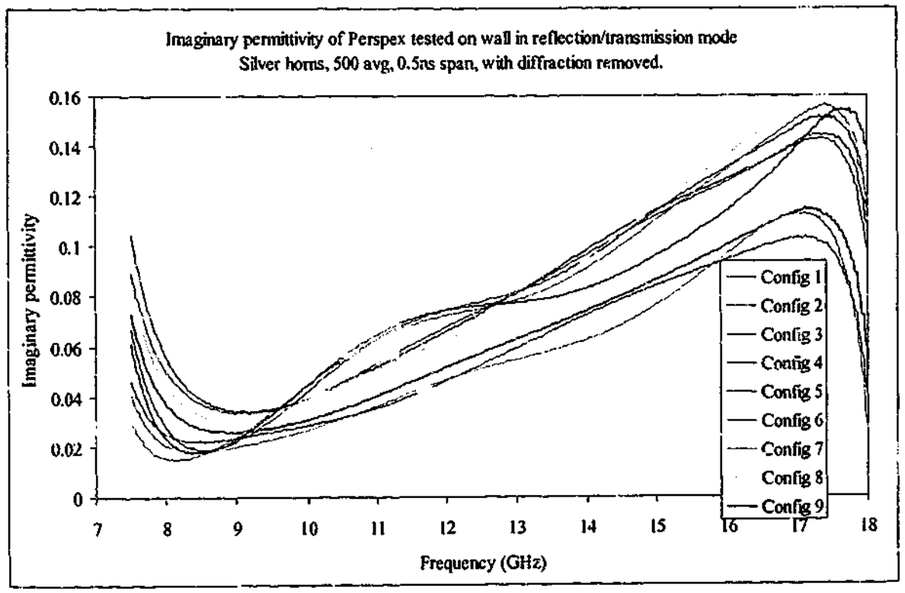

Figure 5-65. Imaginary permittivity of Perspex tested with silver horns in free space using reflection and transmission data with diffraction removed

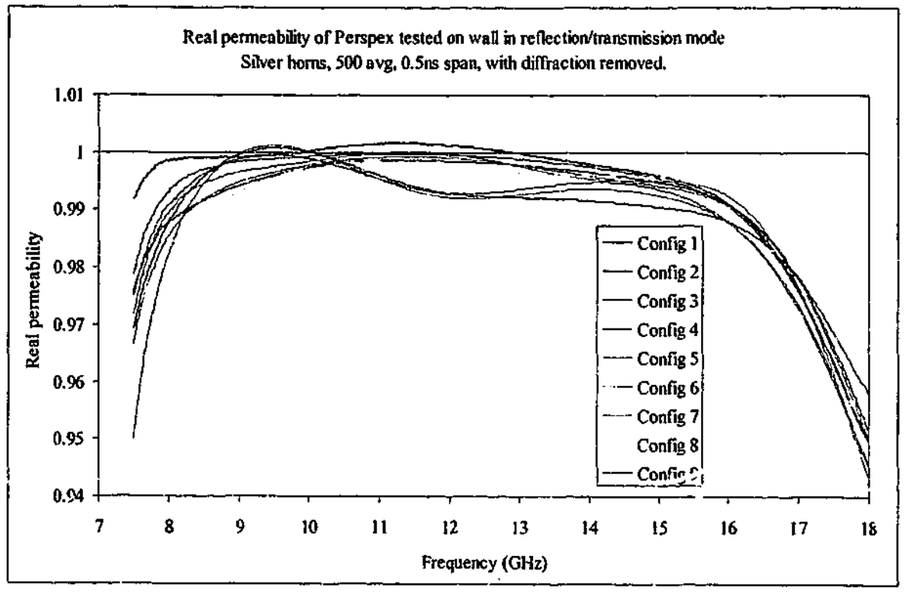

Figure 5-66. Real permeability of Perspex tested with silver horns in free space using reflection and transmission data with diffraction removed

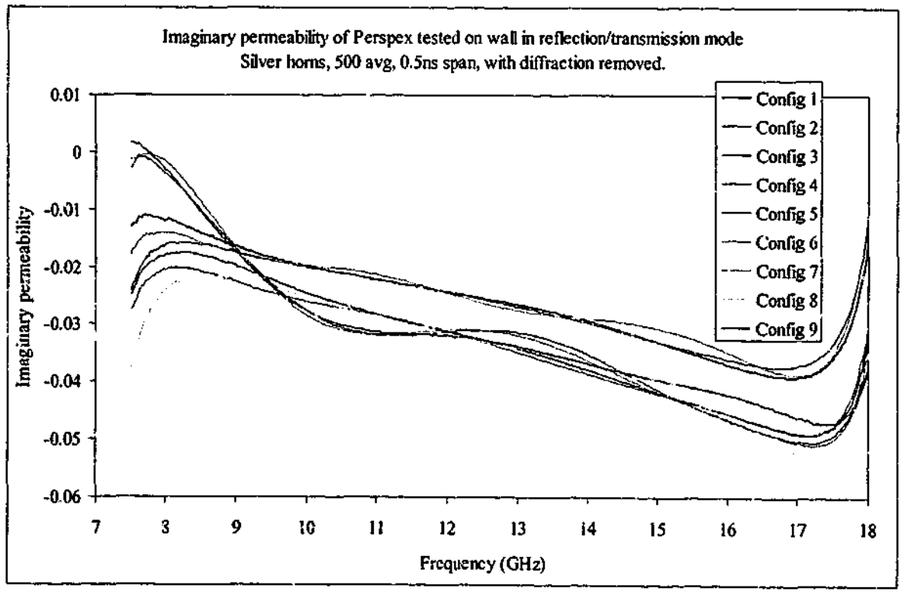

Figure 5-67. Imaginary permeability of Perspex tested with silver horns in free space using reflection and transmission data with diffraction removed

The presence of the destructive interference peak is causing problems at the high end of the frequency spectrum in the real components of permittivity and permeability as expected, but the imaginary components appear to have a linear shift with frequency across the whole band. This shift should not be present, as both imaginary components (especially in the case of permeability) should be frequency independent.

Despite these effects, the average values of the real permittivity still average very close to the expected result of 1. The average real permeability of the non-magnetic materials tested in both orientations is shown below in Table 5-9. It can be seen that the real permeability values lie reasonably close to the expected value of 1 for most samples, with deviation increasing with permittivity and horn to sample distances.

Sample	Cfg 1	Cfg 2	Cfg 3	Cfg 4	Cfg 5	Cfg 6	Cfg 7	Cfg 8	Cfg 9
Perspex	0.994	0.992	0.990	0.993	0.991	0.989	0.992	0.991	0.990
A-A	0.998	0.978	1.001	0.993	0.972	1.000	0.995	0.980	0.997
A-B	0.987	0.970	0.993	0.987	0.966	0.992	0.992	0.974	0.990
B-A	0.989	0.994	1.005	0.987	0.996	1.006	0.992	1.003	0.998
B-B	0.979	0.950	0.962	0.979	0.957	0.965	0.991	0.973	0.965
C-A	0.987	0.963	0.991	0.978	0.941	0.968	0.966	0.947	0.956
C-B	0.991	0.956	0.987	0.991	0.945	0.973	0.983	0.958	0.970
D-A	0.989	0.991	0.986	0.976	0.972	0.971	0.965	0.986	0.969
D-B	0.986	0.962	0.964	1.006	0.979	0.988	1.003	1.005	0.992
E-A	1.006	1.004	1.003	0.989	0.983	0.980	0.980	0.989	0.970
E-B	0.970	0.947	0.949	0.953	0.932	0.933	0.948	0.946	0.922
F-A	0.975	1.007	0.965	0.963	0.989	0.944	0.951	0.992	0.948
F-B	0.999	1.015	0.992	0.990	0.995	0.966	0.973	0.997	0.973
Com A	1.001	1.003	1.003	1.007	1.007	1.003	1.009	1.008	1.007
Com B	1.054	1.020	1.020	1.048	1.023	1.024	1.054	1.022	1.024
Average	0.994	0.983	0.987	0.989	0.977	0.980	0.986	0.985	0.978

Table 5-9. Average real permeability across the frequency range 7.5-18 GHz

The average permittivity for the rubber samples calculated using both reflection and transmission is shown in Figure 5-68 and Figure 5-69.

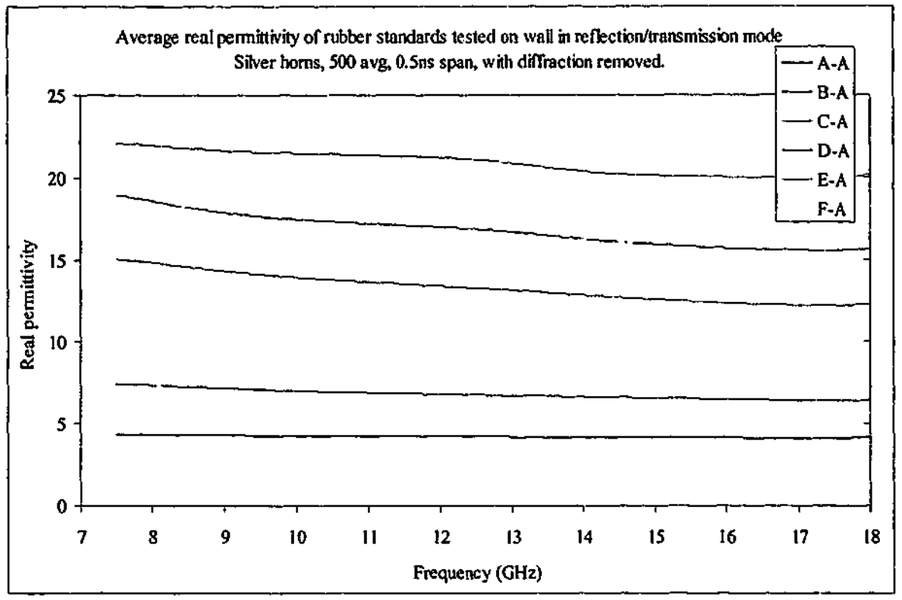

Figure 5-68. Average real permittivity of carbon loaded rubber samples tested with silver horns in free space using reflection and transmission data with diffraction removed

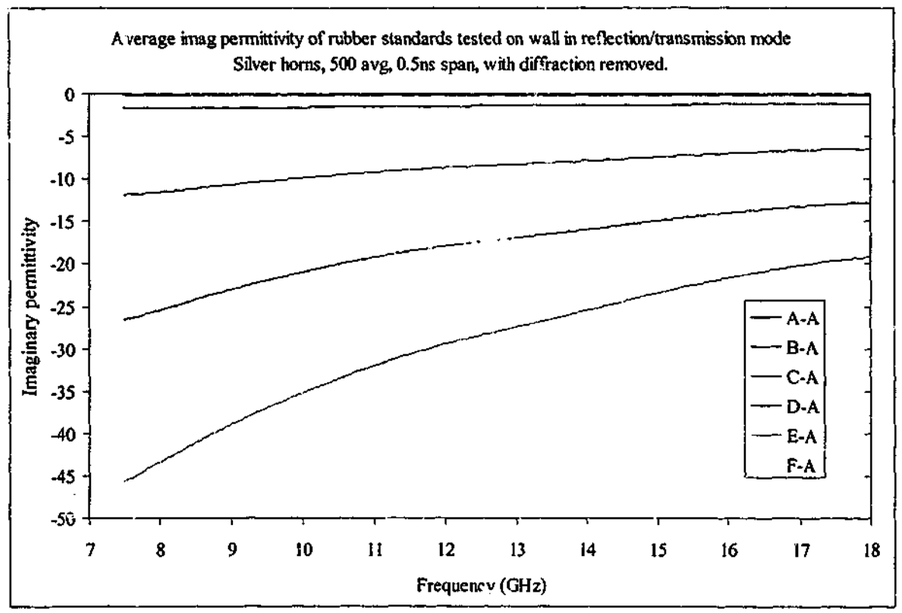

Figure 5-69. Average imaginary permittivity of carbon loaded rubber samples tested with silver horns in free space using reflection and transmission data with diffraction removed

It is interesting to note that the frequency dependence seen in the reflection only data has disappeared from the permittivity values, and that there is a high correlation between these results and the transmission only values. The frequency dependence seen in samples E and F has appeared in the imaginary permeability values as an almost linear shift with frequency. Sample D is starting to show a little shift with frequency, but samples A to C have almost constant values. The real permeability values are clustered around unity, as shown in Figure 5-70 and Figure 5-71.

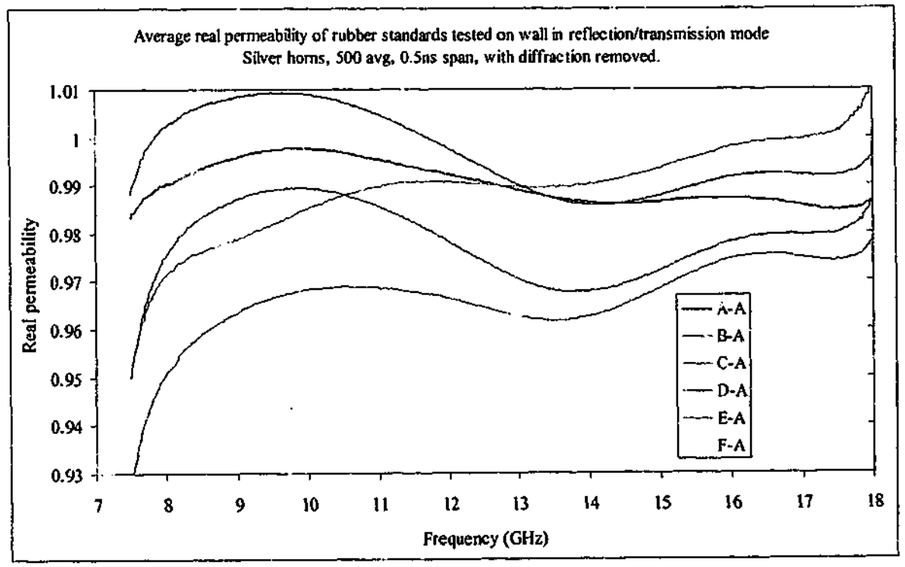

Figure 5-70. Average real permeability of carbon loaded rubber samples tested with silver horns in free space using reflection and transmission data with diffraction removed

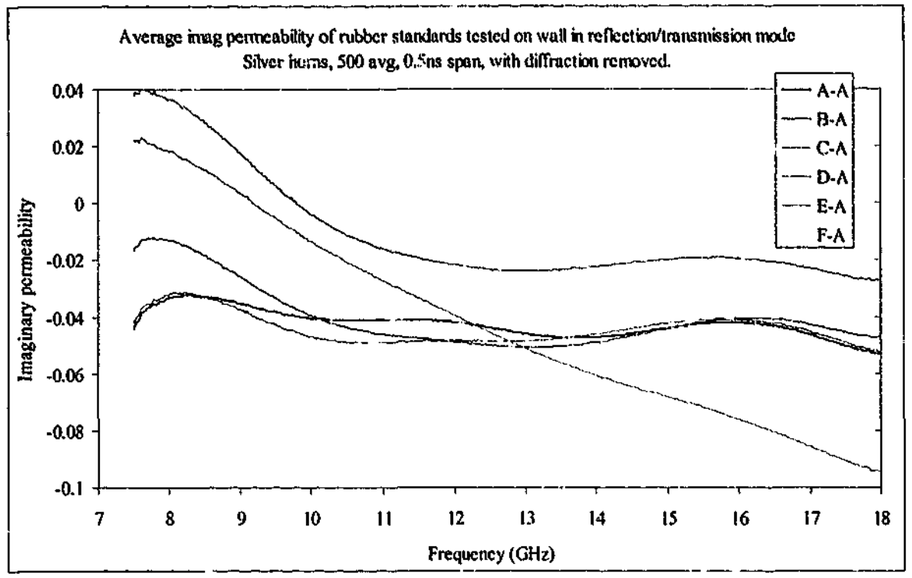

Figure 5-71. Average imaginary permeability of carbon loaded rubber samples tested with silver horns in free space using reflection and transmission data with diffraction removed

The carbonyl iron loaded PU sample shows similar results to the measurements taken over 1 – 18 GHz, only with less noise. The real permeability values are shown in Figure 5-72.

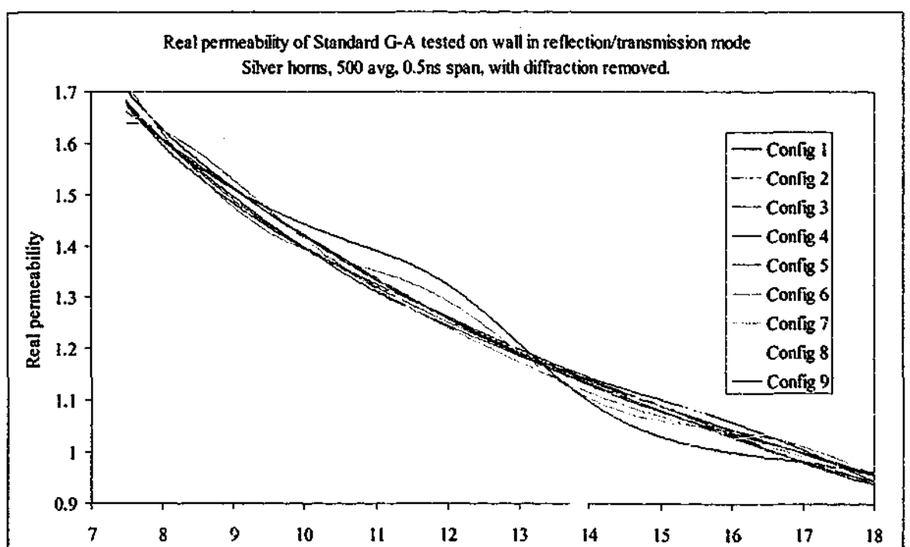

Figure 5-72. Real permeability of sample G tested with silver horns in free space using reflection and transmission data with diffraction removed

Figure 5-73 shows the imaginary permeability over the same range together with the average imaginary permeability over the range 1 – 18 GHz, indicating the shifts observed in Figure 5-71 have only a minor effect on these values.

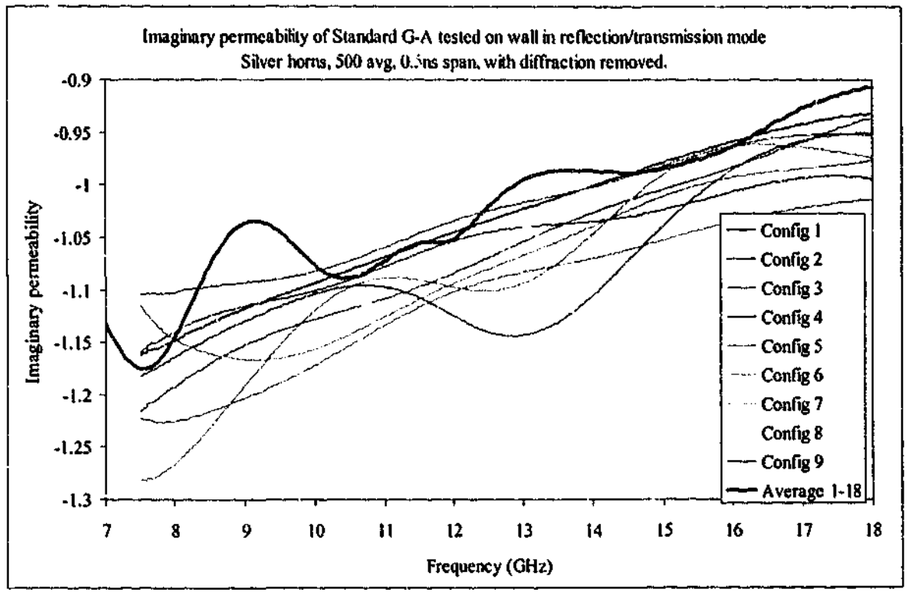

Figure 5-73. Imaginary permeability of sample G tested with silver horns in free space using reflection and transmission data with diffraction removed

The composite sample results show none of the frequency dependence of the carbon loaded rubber samples, with permeability values very close to that expected and permittivity values almost identical to those measured in transmission only mode. The permittivity values follow the Debye curve with parameters of $\varepsilon_0 = 49.5$, $\varepsilon_\infty = 1.32$ and $\tau = 54.02$ ps, giving a resonance frequency of about 2.95 GHz The full spectrum of permittivity and permeability is shown in Figure 5-74 to Figure 5-77.

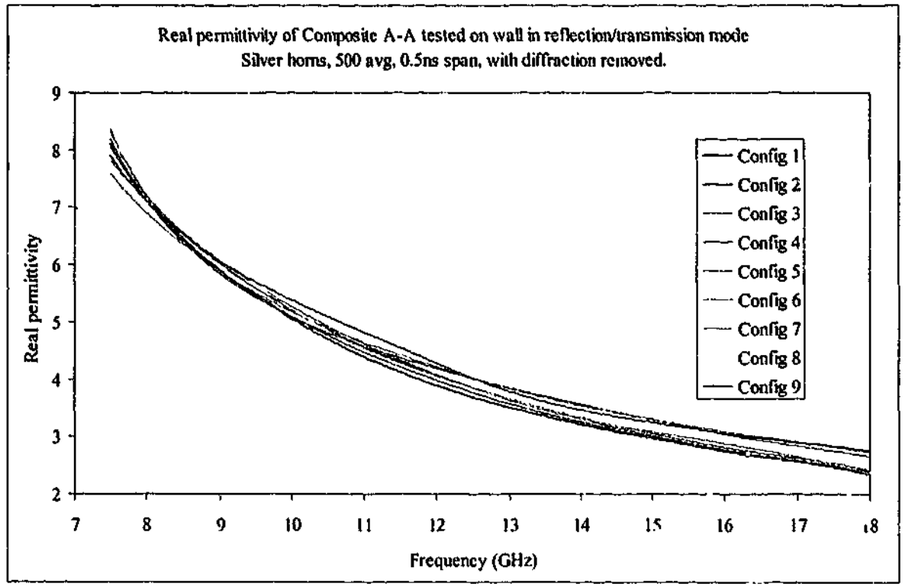

Figure 5-74. Real permittivity of composite tested with silver horns in free space using reflection and transmission data with diffraction removed

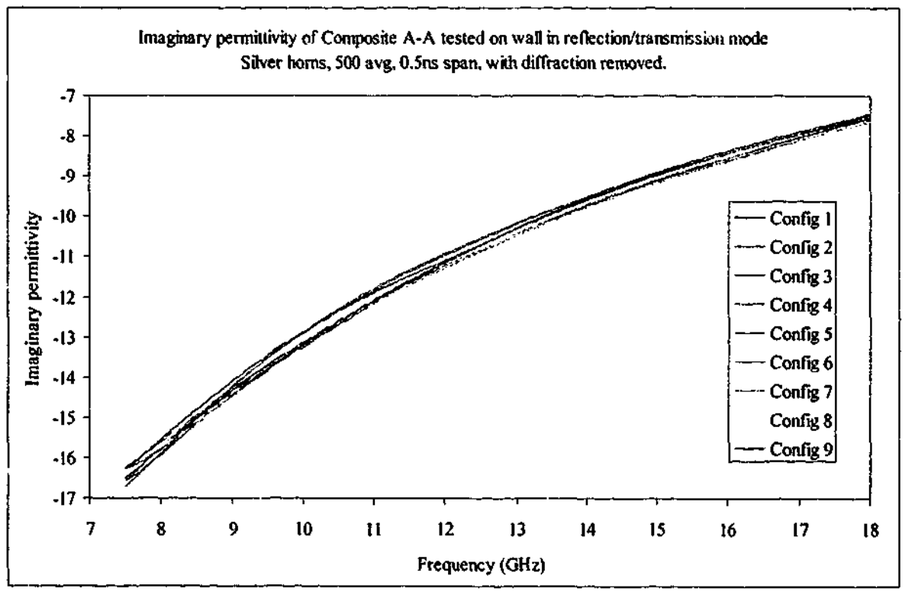

Figure 5-75. Imaginary permittivity of composite tested with silver horns in free space using reflection and transmission data with diffraction removed

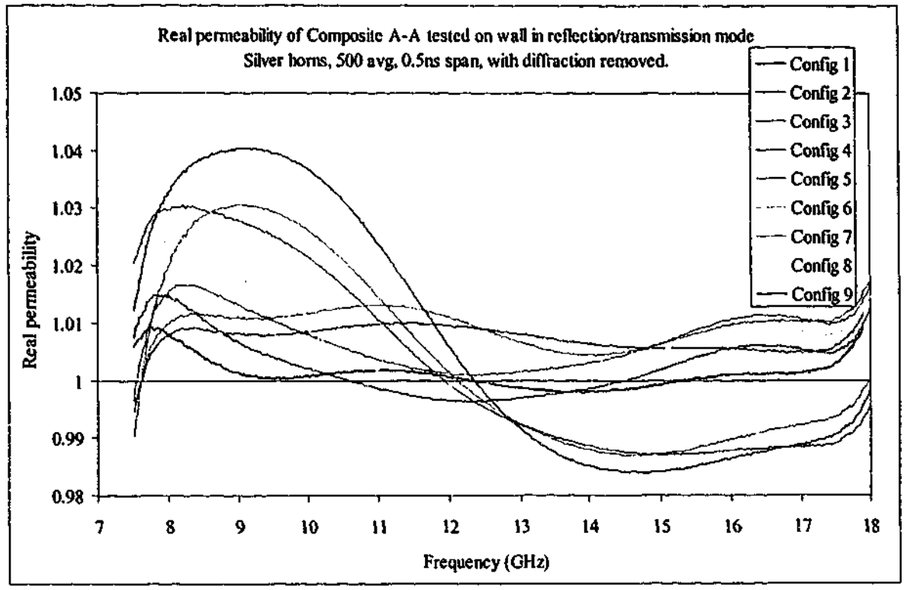

Figure 5-76. Real permeability of composite tested with silver horns in free space using reflection and transmission data with diffraction removed

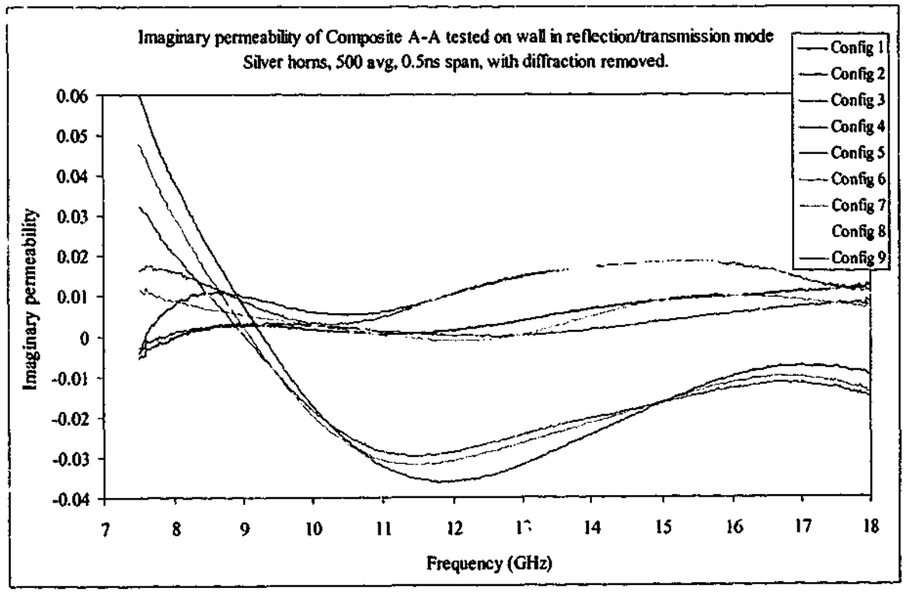

Figure 5-77. Imaginary permeability of composite tested with silver horns in free space using reflection and transmission data with diffraction removed

5.7. 16 – 40 GHz, transmission only

The high frequency horns have a very high gain, and so the area of the sample illuminated by the radiation is smaller. In addition, diffraction is reduced at higher frequencies and the time gate is shorter, so the transmission measurements were expected to be relatively free from the diffracted signal passing around the sample. Nevertheless, as was the case for the 7.5 – 18 GHz measurements, the diffraction signal was found to be large enough to cause problems in the configurations with the longest horn to sample distances. However, as was the case for the 7.5 – 18 GHz measurements, the diffraction signal was again measured later and so the subtraction was not fully successful. The magnitude of the diffracted signal across the frequency range 16 – 40 GHz is shown in Figure 5-78.

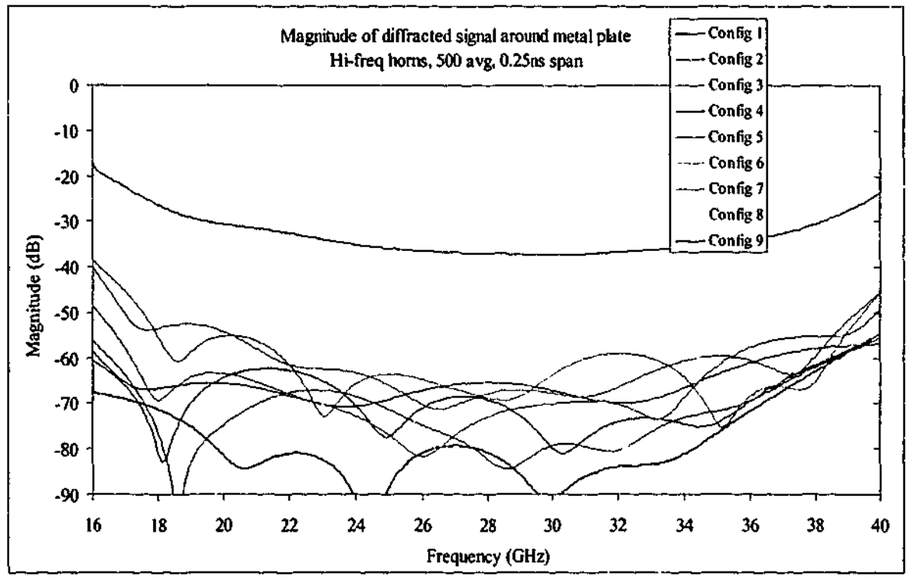

Figure 5-78. Magnitude of diffraction around 445 mm square foil lined glass sample measured with hi-freq horns

It can be seen that the only significant signal comes from the two configurations with the longest sample to horn distances; all the other configurations are greater than 40 dB below the unimpeded value.

As expected, the transmission measurement gives high accuracy for the permittivity of the Perspex sample. Since the signal is transmitted though Perspex virtually unattenuated, the signal to noise ratio is very high. The measured real and imaginary permittivities are shown in Figure 5-79 and Figure 5-80. The values measured are extremely close to those expected, with only some slight variations caused by the time gating (present in all the traces), and a small

error caused by the diffraction signal in configuration 9. This could easily be avoided if the diffraction signal was measured in the same configuration as the sample.

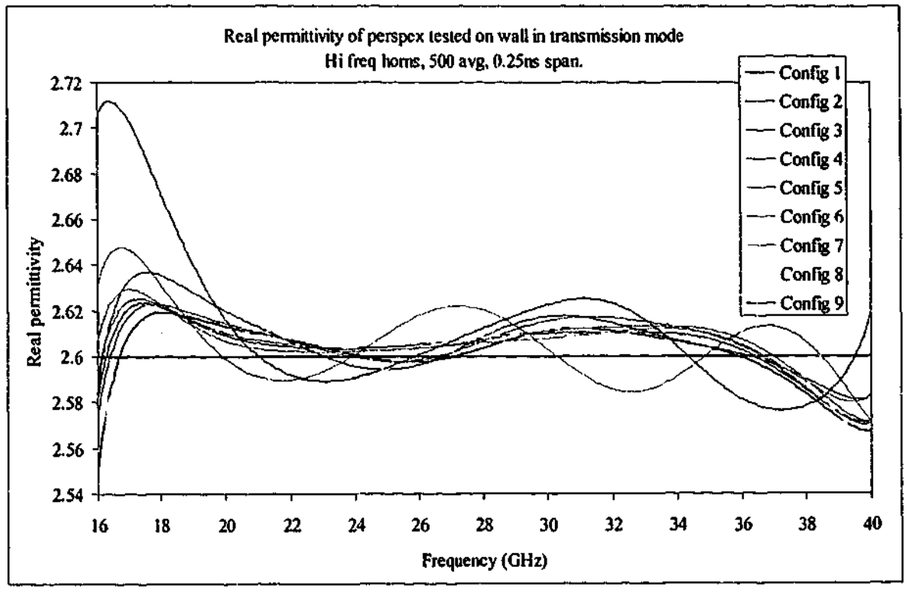

Figure 5-79. Real permittivity of Perspex measured with hi-freq horns in free space using transmission data alone without removing diffraction

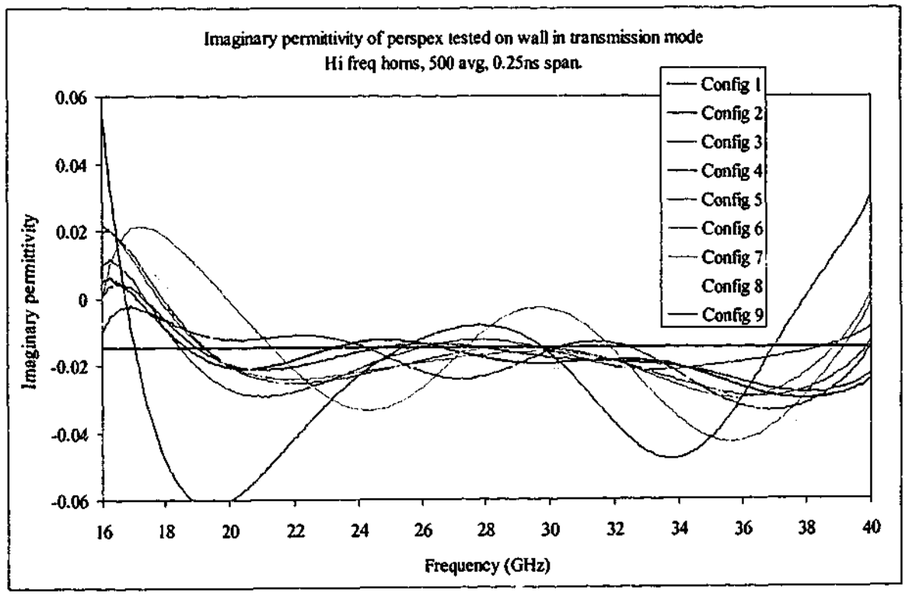

Figure 5-80. Imaginary permittivity of Perspex measured with hi-freq horns in free space using transmission data alone without removing diffraction

The carbon loaded rubber samples show behaviour very similar to the Perspex sample. Except for configuration 8 and 9, the permittivities calculated have very small deviations from each other because the diffraction signal is so small. Figure 5-81 shows the real permittivity for sample B when tested in the "A" direction, where it can be seen that all the different configurations show very similar values right across the frequency spectrum except for the lowest of frequencies in configuration 9. Even for the sample with the highest concentration of carbon black, sample E, it is seen in Figure 5-82 that the imaginary permittivity is closely matched by all the configurations despite not having the diffraction signal removed. Comparing this to the measurement over 1 – 18 GHz shown in Figure 5-7, where some configurations did not even converge on a solution because of the noise level, it is easy to see that this measurement is a vast improvement because of the very low diffraction signal.

The average values of permittivity for these samples closely match those of the previous measurements in the 16 – 18 GHz region. The average values (excluding configurations 8 and 9) are shown in Figure 5-83 and Figure 5-84.

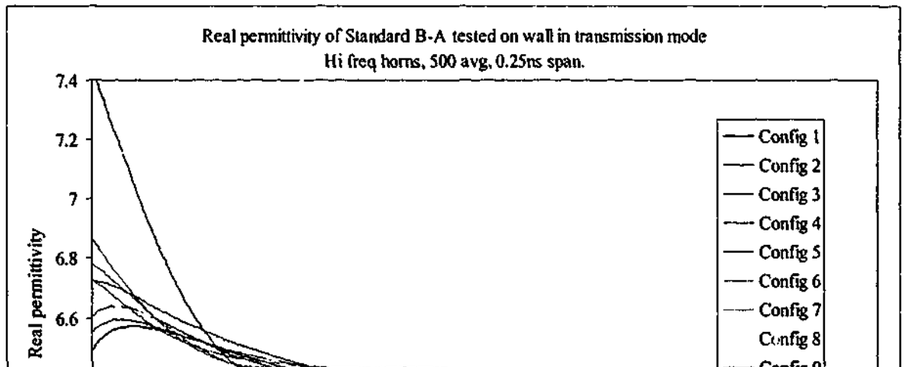

Figure 5-81. Real permittivity of Sample B-A measured with hi-freq horns in free space using transmission data alone without removing diffraction

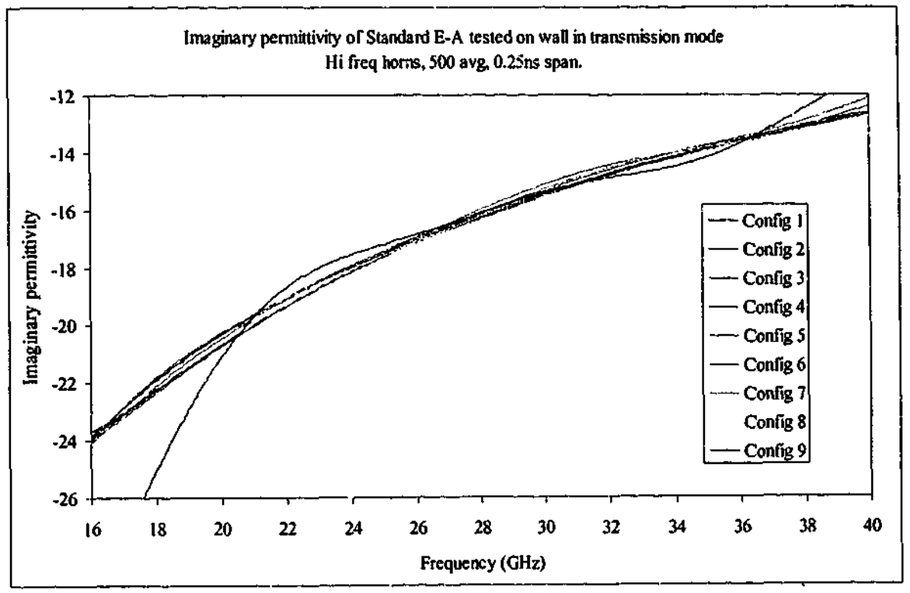

Figure 5-82. Imaginary permittivity of Sample E-A measured with hi-freq horns in free space using transmission data alone without removing diffraction

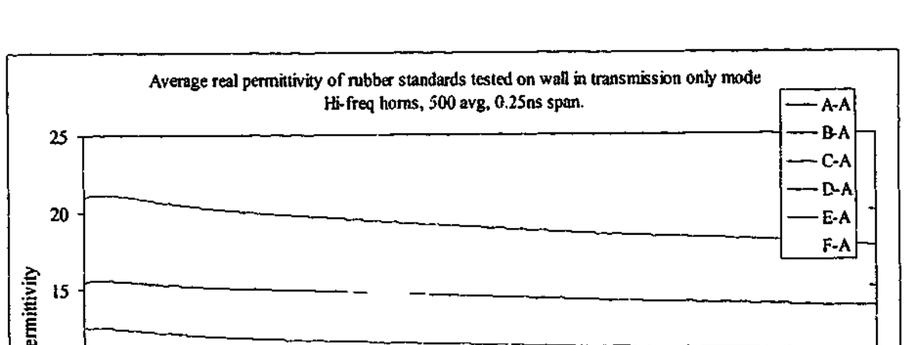

Figure 5-83. Average real permittivity of carbon loaded rubber samples tested with hi-freq horns in free space using transmission data alone (configurations 8 and 9 excluded)

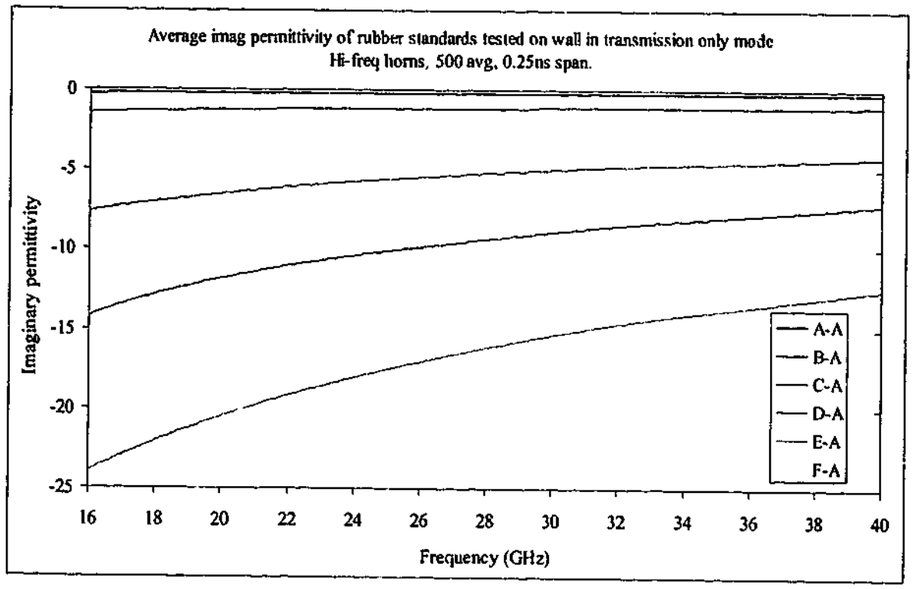

Figure 5-84. Average imaginary permittivity of carbon loaded rubber samples tested with hi-freq horns in free space using transmission data alone (configurations 8 and 9 excluded)

The composite sample also continues the trend of matching the calculated permittivity to previous results. Since the diffraction signal was measured at the same time as the composite sample, the diffraction removal is very successful and all the permittivity curves lie on more or less the same line, as seen in Figure 5-85 and Figure 5-86.

However, the Debye type relationship observed at lower frequencies no longer holds above about 30 GHz. The curves shown as "Debye fit" in Figure 5-85 and Figure 5-86 are calculated using the fitted data are from the 7.5 – 18 GHz results. The measured imaginary component reduces too quickly at high frequencies for the fitted data, indicating that the fibres are starting to behave more like conducting elements rather than resonant scatterers. This is to be expected, since the wavelengths at the higher frequencies are much shorter than the fibre lengths.

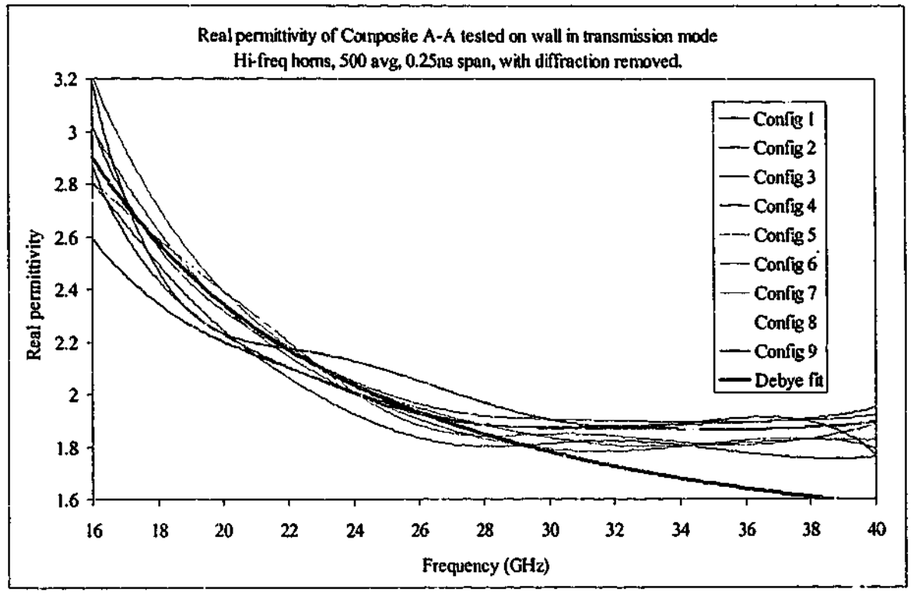

Figure 5-85. Real permittivity of composite sample tested with hi-freq horns in free space using transmission data only with diffraction removed

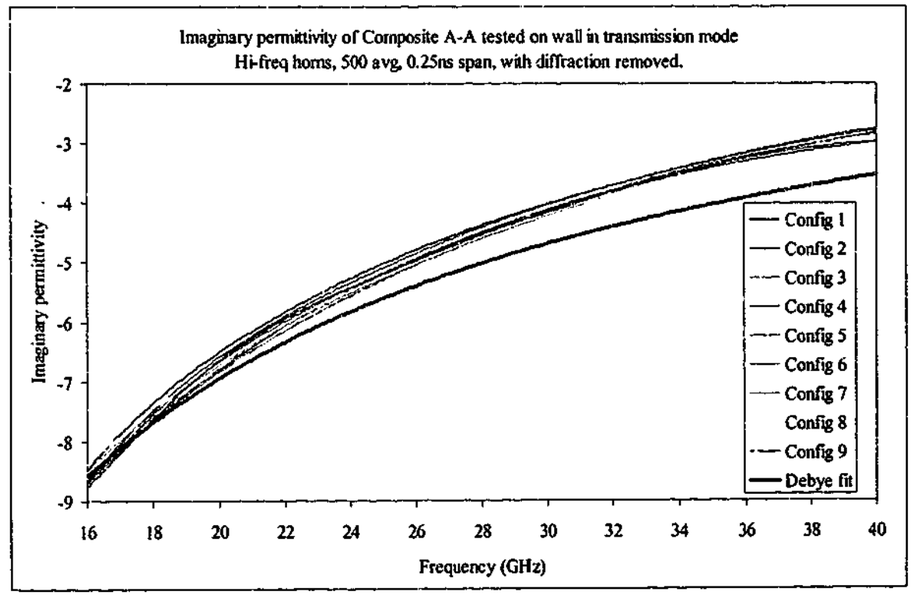

Figure 5-86. Imaginary permittivity of composite sample tested with hi-freq horns in free space using transmission data only with diffraction removed

5.8. 16 – 40 GHz, reflection only

The Perspex results over the 16 – 40 GHz range show a very similar frequency shift to that observed over the 7.5 – 18 GHz range. Instead of the real permittivity being a constant value, it decreases with frequency, as shown in Figure 5-87 and Figure 5-88. Comparing these results with the 7.5 – 18 GHz results of Figure 5-58 and Figure 5-59 one observes that the shifts are almost identical.

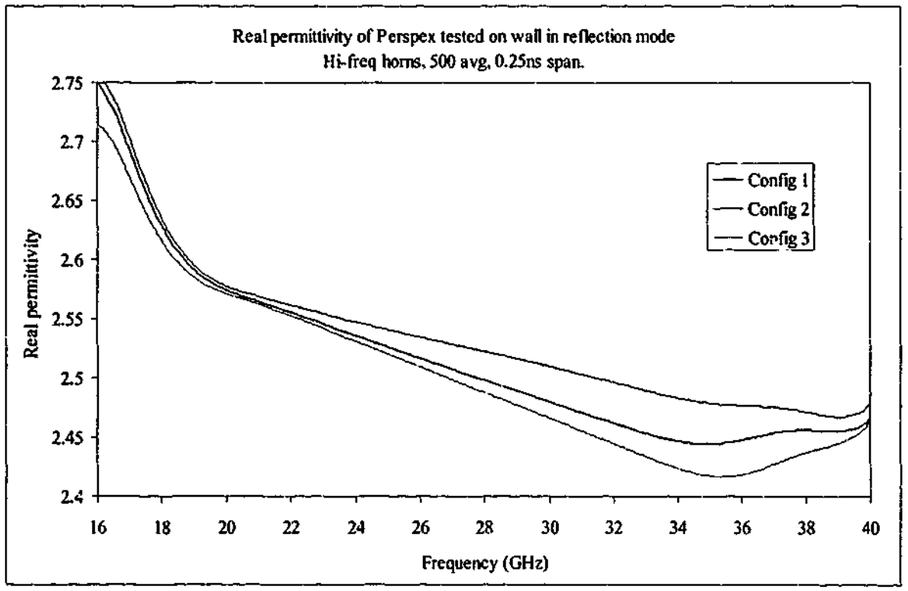

Figure 5-87. Real permittivity of Perspex measured with hi-freq horns in free space using reflection data alone

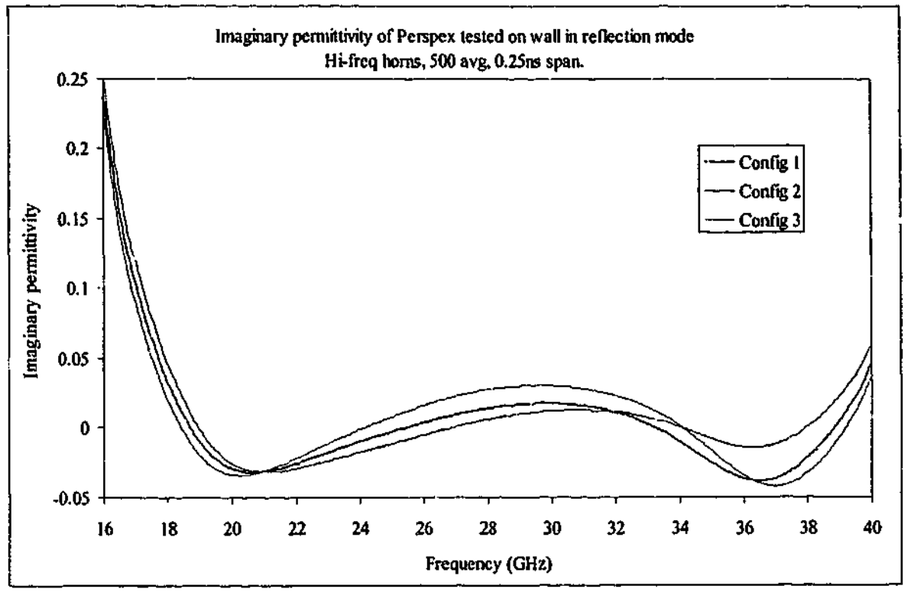

Figure 5-88. Imaginary permittivity of Perspex measured with hi-freq horns in free space using reflection data alone

To calculate the permittivity of the carbon loaded rubber samples, we use a similar technique as done for the lower frequencies to find the calibration plane shift. Using the results from sample E to work out the required shifts to the flexible rubber samples, we find the results of the carbon loaded samples are seriously in error. The average permittivity values shown in Figure 5-89 and Figure 5-90 vary wildly across the frequency band and bear little relation to the results from the transmission only measurement.

Originally it was though that testing these large specimens in the near field caused the effects observed. After all, it is only at higher frequencies that the permittivity of samples "E" and "F" crossed those of the lower permittivity samples in the 1 – 18 GHz frequency band. However, it was found that moving the send horn into each of the three configurations gave very similar results for all the rubber materials tested over 16 – 40 GHz, and so it appears the effect is due to some other effect. Since this is the frequency range in which destructive interference in the reflection signal occurs the most often, this may be the cause of the errors observed. Even though the actual signal does not drop to very low levels at the destructive interference points, the effect is observed right across the frequency band for most samples.

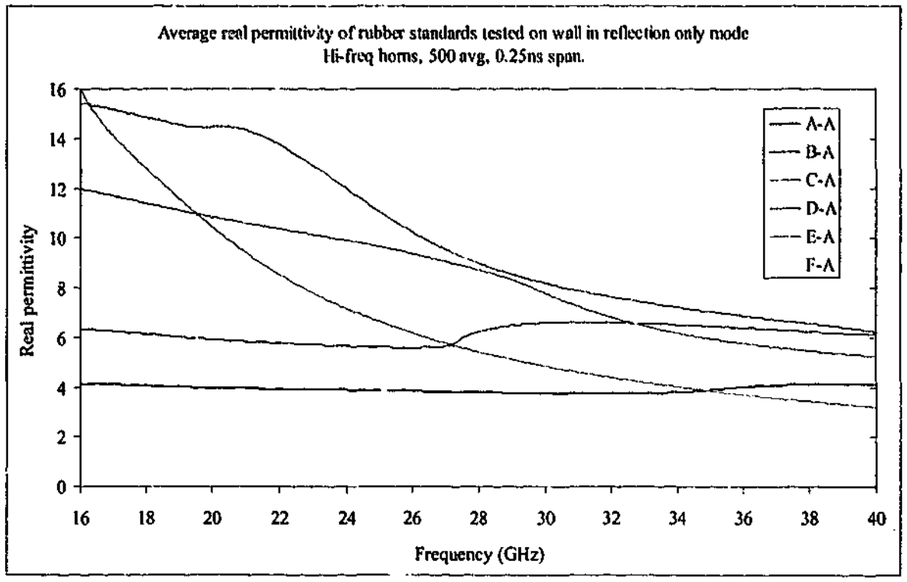

Figure 5-89. Average real permittivity of carbon loaded rubber samples tested with hi-freq horns in free space using reflection data.

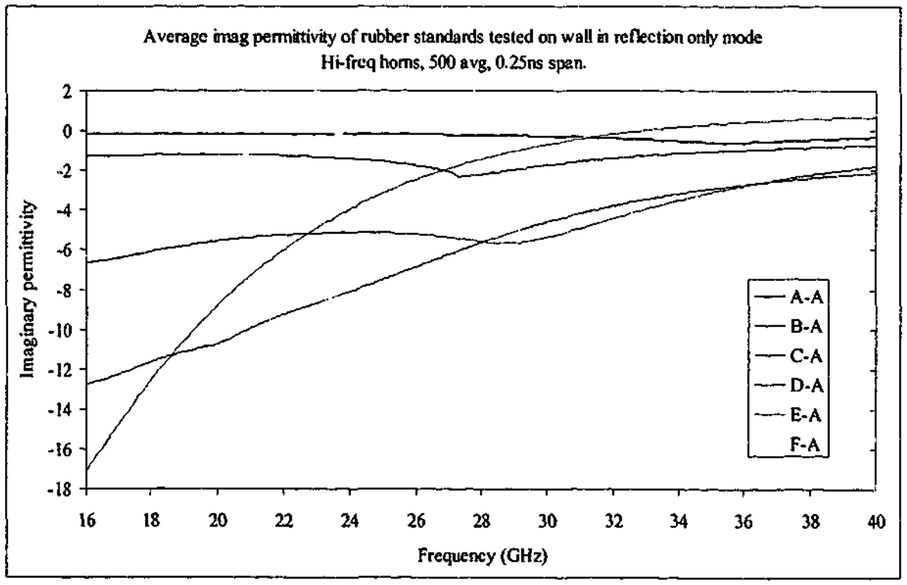

Figure 5-90. Average imaginary permittivity of carbon loaded rubber samples tested with hi-freq horns in free space using reflection data.

In contrast to the carbon loaded rubber samples, the results from the carbon fibre loaded sample has closely matched those from the transmission only measurements. Figure 5-91 and

Figure 5-92 show the permittivity of the composite sample tested in reflection only mode compared to the average result from the transmission only measurement.

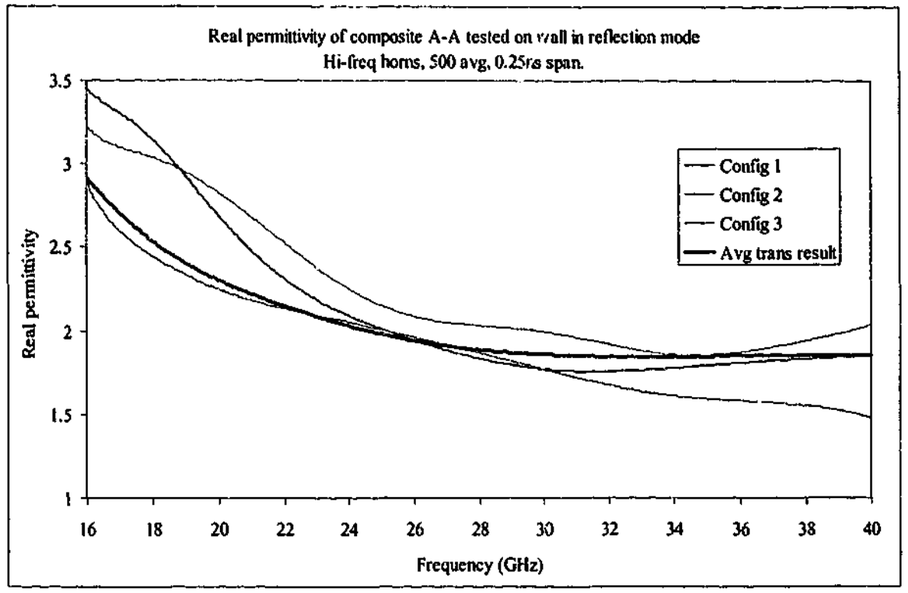

Figure 5-91. Real permittivity of composite sample measured with hi-freq horns in free space using reflection data alone

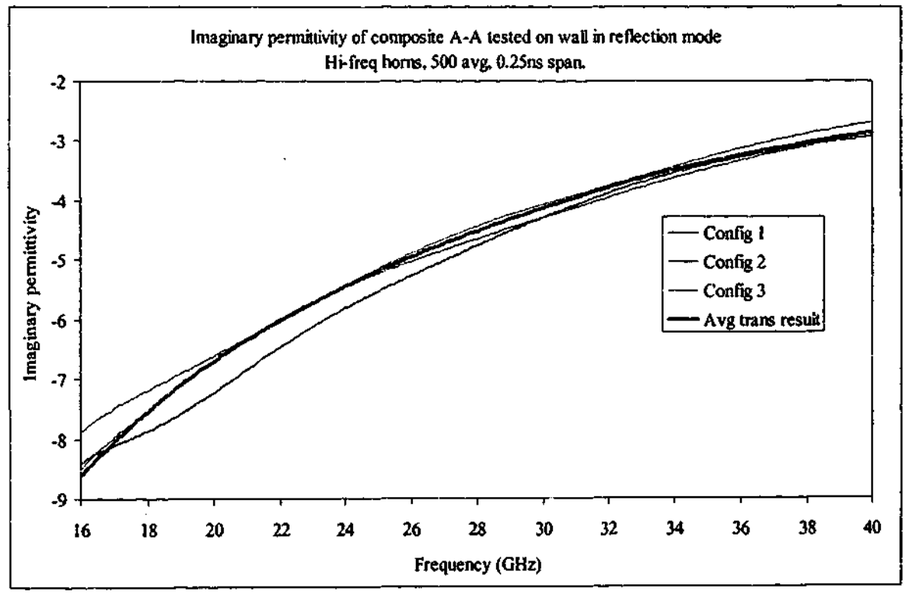

Figure 5-92. Imaginary permittivity of composite sample measured with hi-freq horns in free space using reflection data alone

5.9. 16 – 40 GHz, reflection and transmission

As the frequencies increase, the effects of destructive interference become more difficult to avoid. Whilst the single parameter extraction algorithms are affected by destructive interference to some extent, when both sets of data are used to extract both permittivity and permeability the effect is disastrous. The 4.5 mm thick Perspex sample has destructive interference peaks in the reflected signal at about 20.7 GHz and 41.3 GHz. The influence of these peaks is not confined only to those exact frequencies, but over the entire measurement range. Figure 5-93 and Figure 5-94 show how the extracted permittivity values vary across the frequency range, and never really level out to a constant value in either the real or the imaginary component. The permeability values show the same trend, with large spikes appearing at destructive interference points and a general shift of values with frequency.

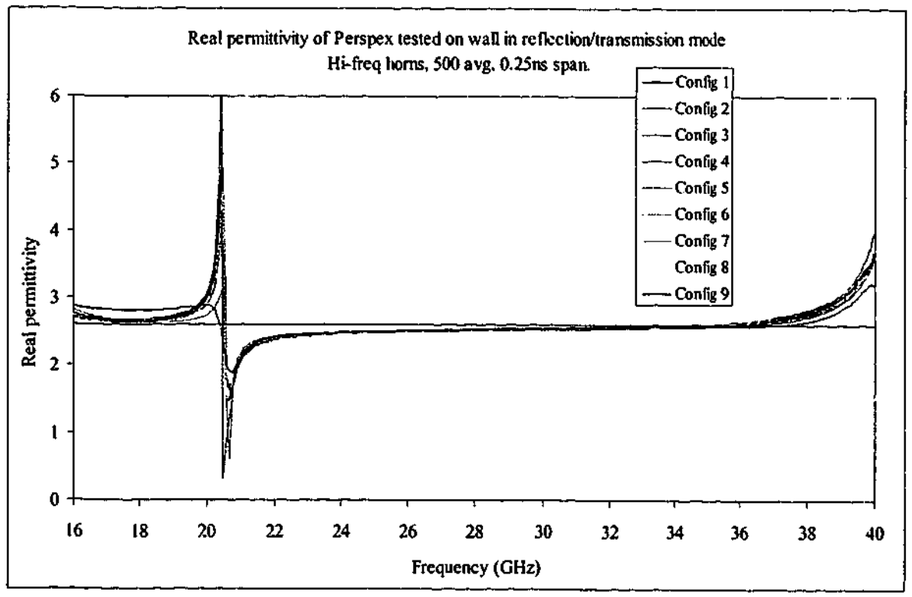

Figure 5-93. Real permittivity of Perspex measured with hi-freq horns in free space using reflection and transmission data

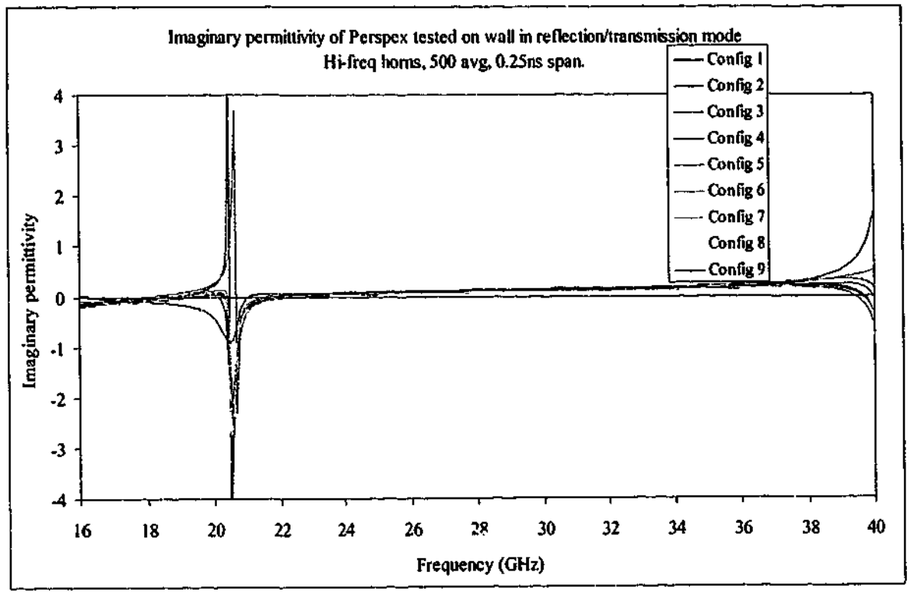

Figure 5-94. Imaginary permittivity of Perspex measured with hi-freq horns in free space using reflection and transmission data

Using the reflection data from the carbon loaded rubber samples to calculate permittivity and permeability may appear at first to be a worthless task since the permittivity values extracted from the reflection data were so different from those of the transmission only results. While the results are not as bad as the reflection only results, the values extracted are still seriously in error. The permittivity results are shown in Figure 5-95 and Figure 5-96.

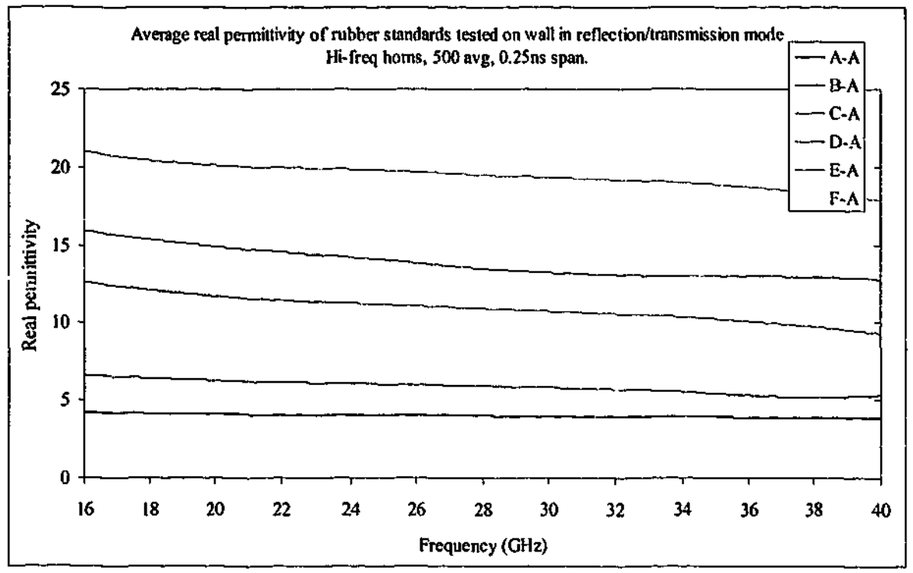

Figure 5-95. Average real permittivity of carbon loaded rubber samples tested with hi-freq horns in free space using reflection and transmission data.

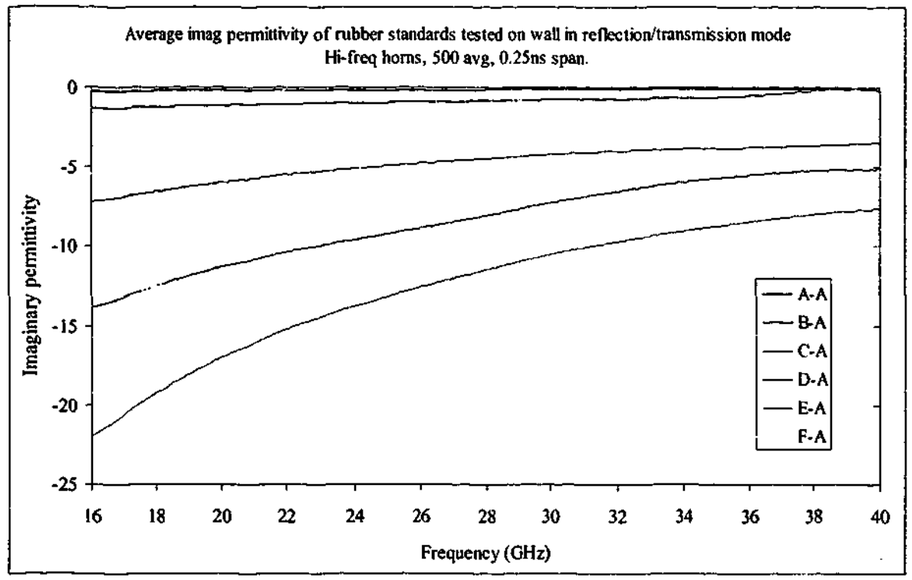

Figure 5-96. Average imaginary permittivity of carbon loaded rubber samples tested with hi-freq horns in free space using reflection and transmission data.

The imaginary permittivity for all the samples is decreasing faster with increasing frequency than what was observed in the transmission only case. This was observed in samples E and F over the range 7.5 – 18 GHz, but the difference between these results and those from the 7.5 – 18 GHz measurements is that nearly all the samples are affected, not just the high permittivity ones.

The extracted permeability values shown in Figure 5-97 and Figure 5-98 are close to that expected at low frequencies, but become less accurate as frequency increases.

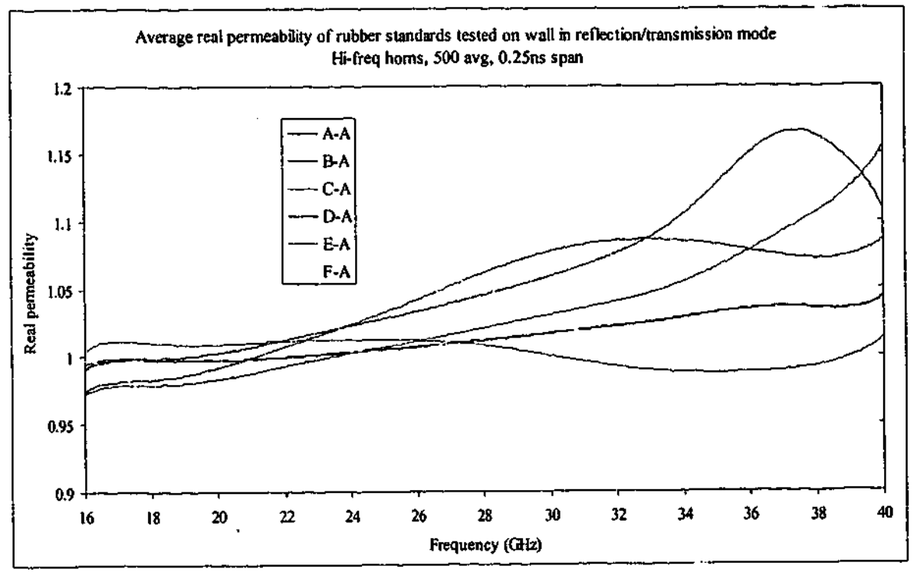

Figure 5-97. Average real permeability of carbon loaded rubber samples tested with hi-freq horns in free space using reflection and transmission data

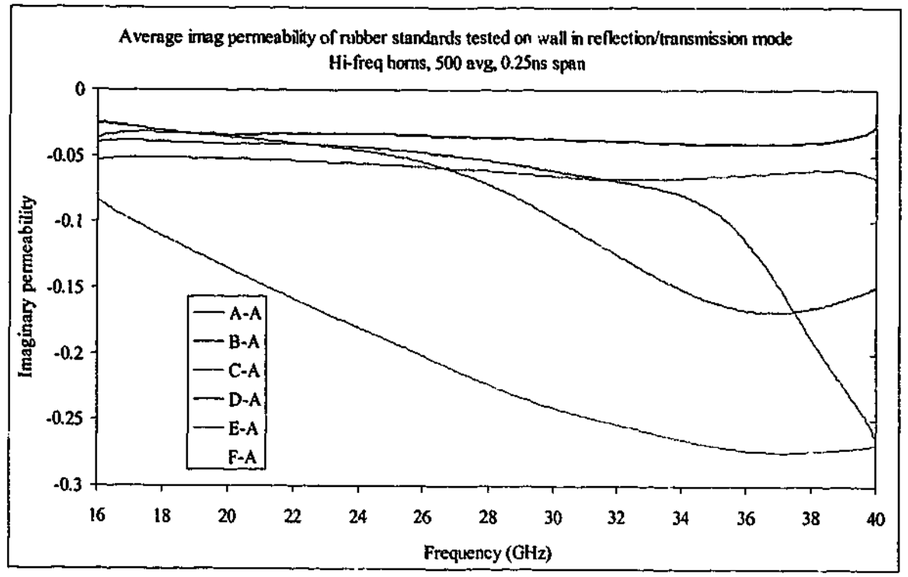

Figure 5-98. Average imaginary permeability of carbon loaded rubber samples tested with hi-freq horns in free space using reflection and transmission data

The ferromagnetic sample G is likely to have the same errors as the carbon loaded rubber samples. The real permittivity is similar to that of sample B so we might expect the errors to be of a similar magnitude. When the permittivity and permeability are calculated, we find the real permittivity over 16 – 18 GHz is very close to that of previous measurements, and decreases only slightly as frequency increases (see Figure 5-99). The errors in the imaginary permittivity (Figure 5-100) increase with the position of the receive horn and hence the diffraction magnitude. When the horns are far from the sample, the imaginary permittivity becomes positive, which is a situation that should not occur indicating that the result is in error. The real permeability drops below unity and settles at around 0.6 before showing signs of increasing back to unity at higher frequencies, while the imaginary permeability maintains a constant curve decreasing towards zero. Real permeability values very much less than unity are typical for many magnetic materials at these high frequencies, such as iron, cobalt[89] and some microwave ferrites[90, 91, 92]. The results shown in Figure 5-101 and Figure 5-102 probably show the same errors as seen in the carbon loaded rubber samples, so we can probably assume that the actual real and imaginary permeability of sample G is less than that shown in the figures below.

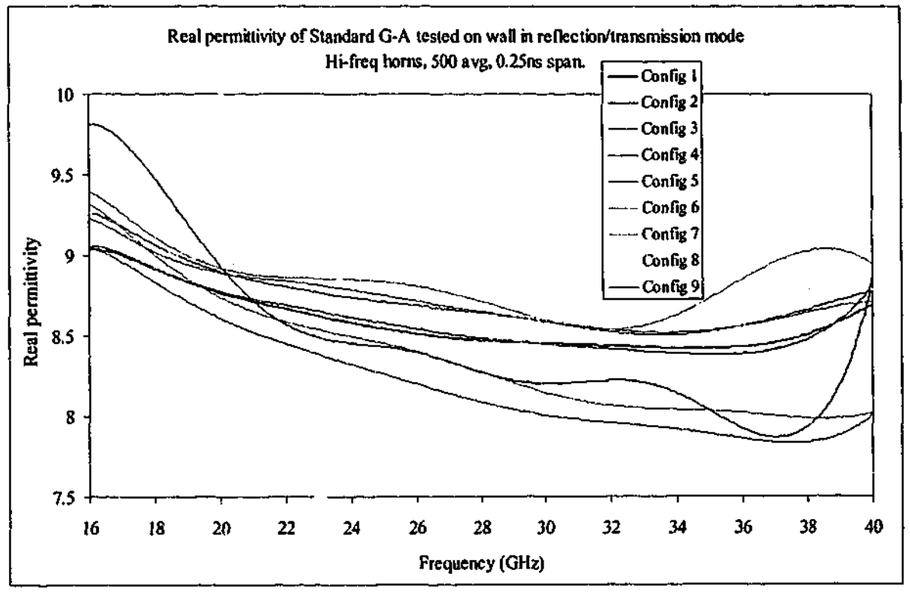

Figure 5-99. Real permittivity of sample G measured with hi-freq horns in free space using reflection and transmission data

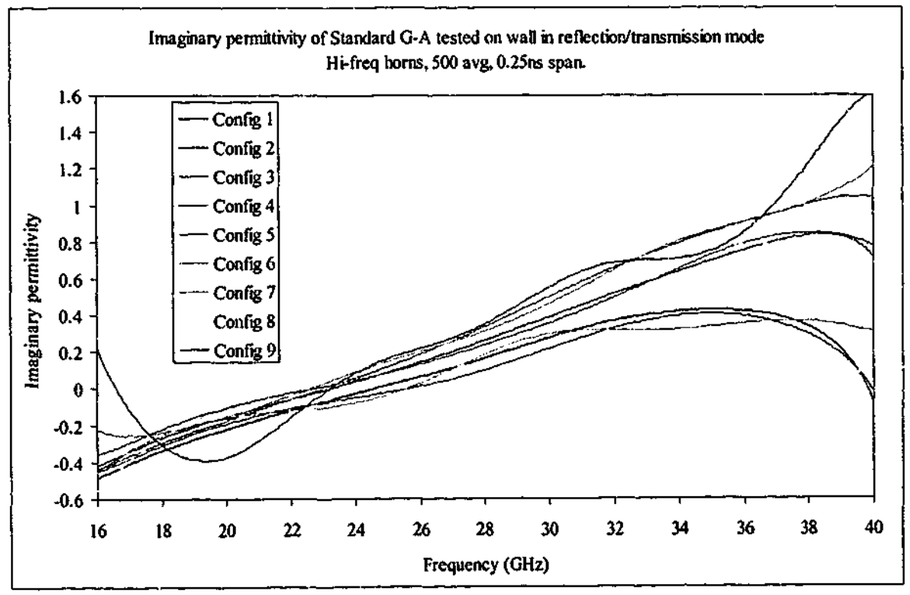

Figure 5-100. Imaginary permittivity of sample G measured with hi-freq horns in free space using reflection and transmission data

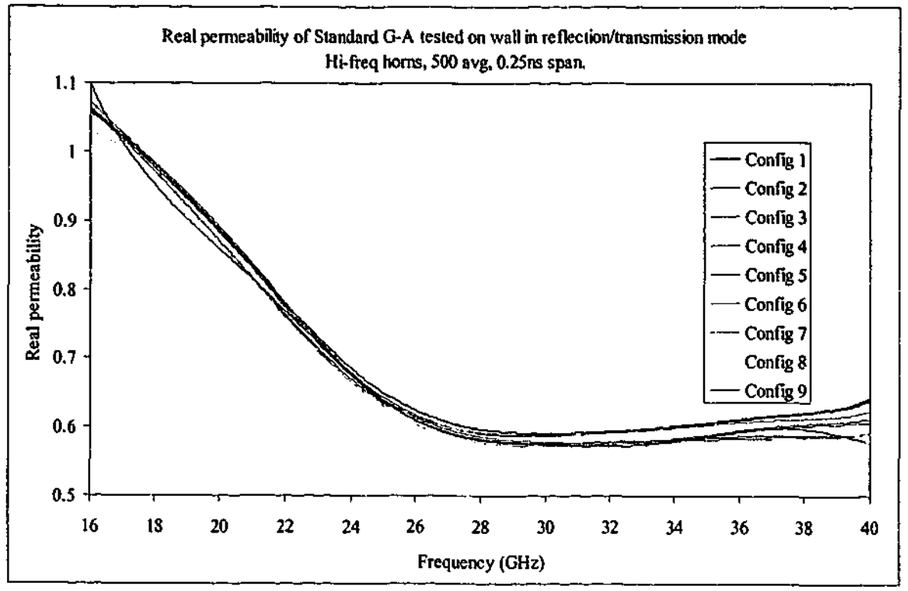

Figure 5-101. Real permeability of sample G measured with hi-freq horns in free space using reflection and transmission data

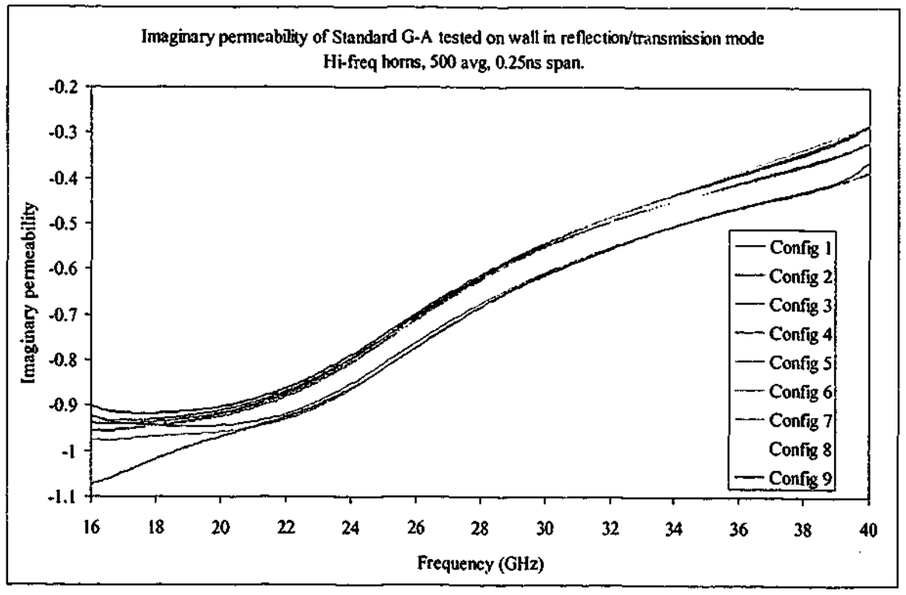

Figure 5-102. Imaginary permeability of sample G measured with hi-freq horns in free space using reflection and transmission data

The composite material shows none of the problems seen in the previous samples. The permittivity values are almost exactly the same as the transmission only results, and the

permeability shows only small deviations from the free space result. The extraction process is aided by the fact that the diffraction removal process is highly effective, but the main reason why the values obtained are so accurate is due to the accuracy of the reflected signal. The permittivity values are shown in Figure 5-103 and Figure 5-104, and the real permeability can be seen in Figure 5-105.

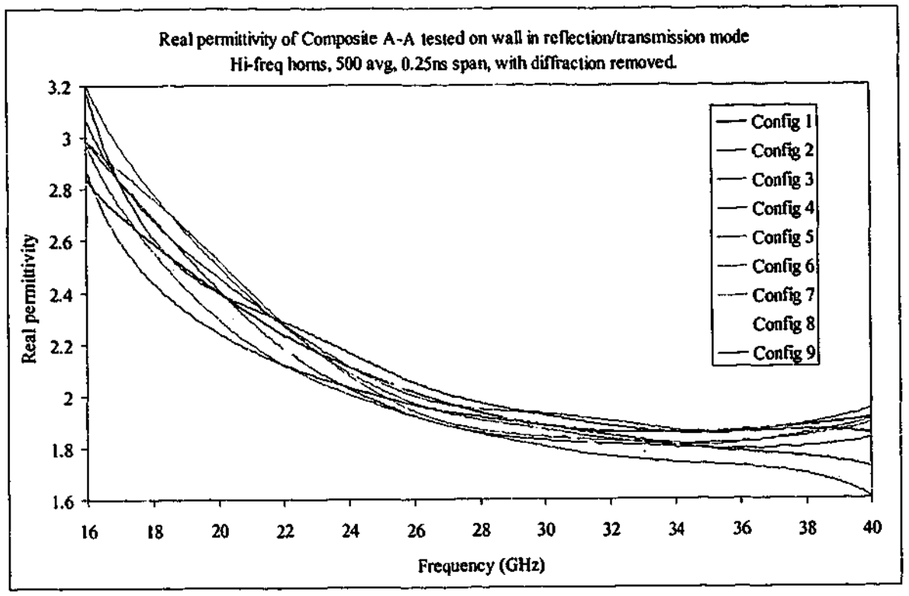

Figure 5-103. Real permittivity of composite measured with hi-freq horns in free space using reflection and transmission data, with diffraction removed

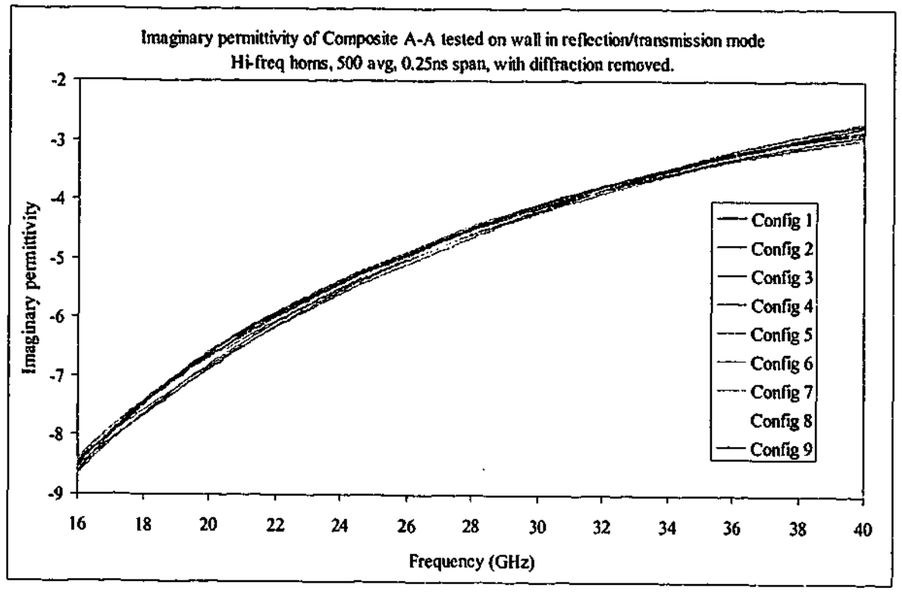

Figure 5-104. Imaginary permittivity of composite measured with hi-freq horns in free space using reflection and transmission data, with diffraction removed

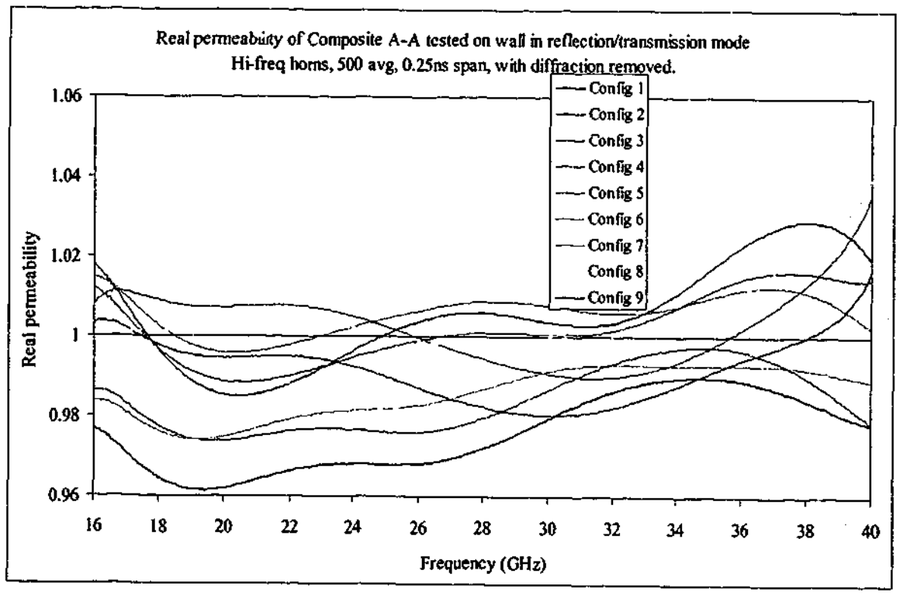

Figure 5-105. Real permeability of composite measured with hi-freq horns in free space using reflection and transmission data, with diffraction removed

5.10. Summary

The effects of diffraction were shown to have a very large effect upon the transmission signal, sometimes rendering parameter extraction impossible across the full frequency span. The solution to this was in the form of a mathematical subtraction of the measured diffraction only paths. While subtracting signals does lead to some loss of dynamic range, it nevertheless provides a simple but highly effective technique to increase measurement accuracy. While moving the horns further apart was expected to reduce effects caused by testing in the near field, it was found that the increase in the diffraction signal obscured any possible beneficial effects.

When the specimen is not at precisely the same distance from the send horn as the reflecting sheet used for calibration, the resulting phase shift in the reflection data produces errors in the extracted permittivity and permeability. If the sample, the calibration sheet or even the polystyrene foam stand is not flat, then phase errors of this sort can occur. The degree of phase shift effect is found to be dependent upon the horns, as a horn with a lower gain produces a larger lobe, effectively illuminating more of the specimen being tested. The effective phase shift is weighted according to the magnitude of the incident beam.

As the reflected signal from the specimen increased, so too did the errors when extracting permittivity using the reflection only method. The carbon loaded rubber samples marked "E" and "F" showed errors from about 16 GHz when the permittivity values crossed over those from lower permittivity samples. As frequency increased further, the permittivity of the other samples too started to vary erratically. Since this effect was consistent with configuration number, it was assumed to be caused by destructive interference effects rather than testing in the near field.

The transmission technique was by far the most stable method for determining permittivity in non-magnetic materials, once the diffraction signal was removed. Measurements were consistent across the various frequency bands and the values obtained for the standard materials were as expected. In contrast, the reflection only technique was quite unstable and required much more effort. By combining the reflection and transmission signals, the permeability could be determined accurately provided the phase shift caused by specimen position was found.

Chapter 6. 305 mm Samples

The results from the 445 mm square samples clearly show that diffraction is a major cause of error in the transmission signal. Therefore, when testing smaller samples, it is even more important to reduce the diffracted signal, either by reducing the horn-to-sample distances or by properly measuring the amount of diffraction so it can be effectively removed. Of course, the best way is to use both methods, and this was done in the measurement of the 305 mm square samples. Since the effects of diffraction would be the same for smaller samples as it was for the larger ones, it was not necessary to perform measurements in all nine configurations. The only measurement done on the smaller samples was performed in configuration 1, with the horns closest to the sample.

The specimens were cut to size and measured exactly as before. Extra materials only available in sheets 305 mm square were also tested to increase the material database. These included Teflon, lead glass and the three standards supplied by Cuming Corp. with known values of permittivity.

The range backed reflection method was also used to measure these smaller sized samples. This technique was not trialed for the larger samples due to the unavailability of a 445 mm square vacuum plate.

Because only one configuration was used for each sample, and the measurement techniques used were identical to those of the larger samples, the 305 mm data will be presented in a more compact form. The results from each measurement for a particular sample will be shown on a single set of axes, allowing comparisons to be more easily made.

The size of the samples is approximately the same as that of the longest wavelength, 300 mm at 1 GHz. It is therefore safe to assume that diffraction around the samples will be quite significant, even when the horns are very close. A foil lined glass sheet was used to measure the diffraction signal so that that part of the total measured signal for the sample could be removed. The magnitude of the diffraction component, shown in Figure 6-1, is similar to configuration 5 for the 445 mm square samples. The effect of the wider gate and lower gain of the gold horn measurement is clearly seen in the higher diffraction signal compared to that of the silver horns over the same frequency range.

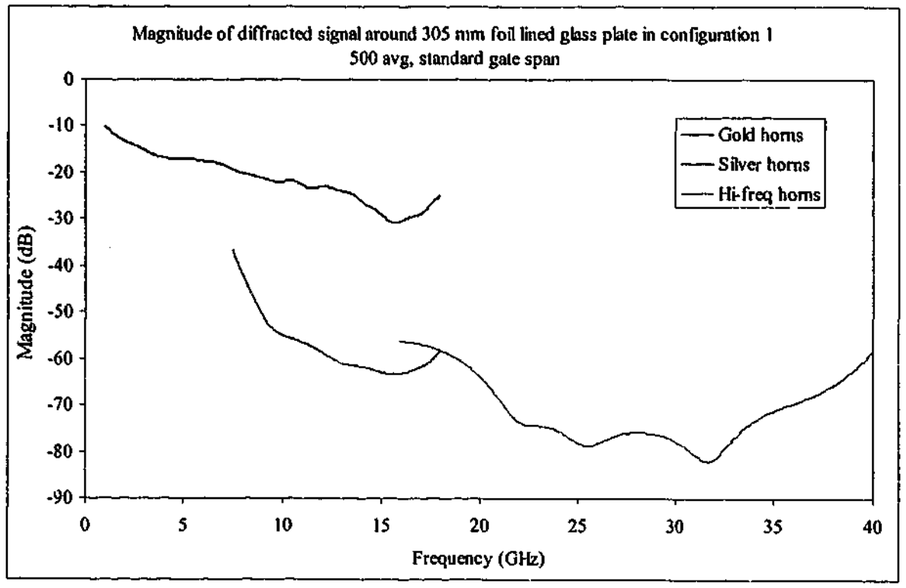

Figure 6-1. Magnitude of diffraction around 305 mm square foil lined glass sample measured in configuration 1 with standard time gates

6.1. Perspex

6.1.1. 1 – 18 GHz

The results from the Perspex sample show that the reflection, transmission and reflection/transmission algorithms all give much the same values for the smaller sample, although the average value is relatively high at about 2.65. The noise level is quite high, leading to the cyclic oscillations around the mean as could be expected from a relatively wide gate. The backed reflection method has not produced an accurate result at low frequencies either with or without the dielectric lens. The lens has marginally improved the result at higher frequencies but the low frequency values are significantly different, as can be seen in Figure 6-2. The average permeability measured with the reflection/transmission technique is $1.02 + 0.018i$ across the whole frequency band.

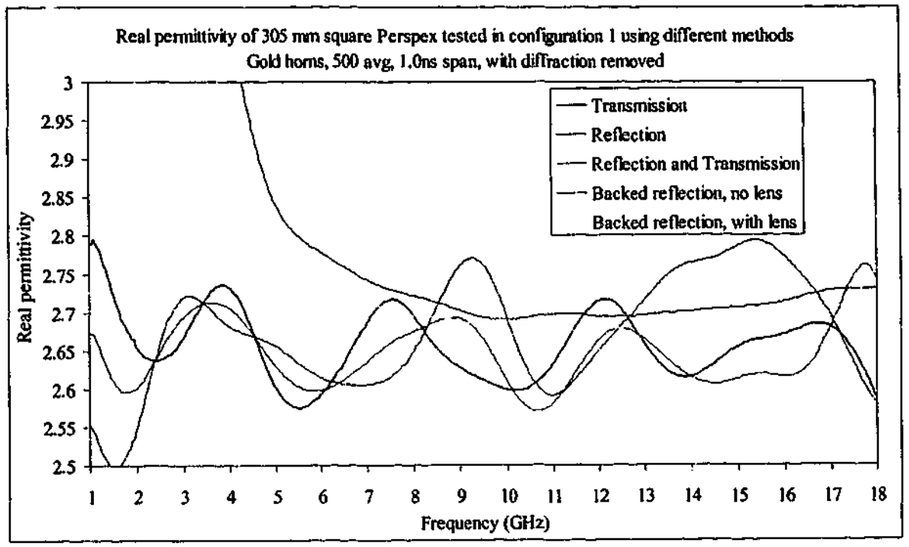

Figure 6-2. Real permittivity of Perspex measured with gold horns in free space using different methods with diffraction removed

6.1.2. 7.5 – 18 GHz

The higher frequency range shows the same values as before, with a much reduced noise level. This is due in part to the higher gain of the horns as well as the tighter gate span. The real permittivity is around the 2.60 ± 0.05 for the reflection and transmission measurements, and a little higher as before for the backed reflection configuration as is shown in Figure 6-3. The average value of permeability extracted from the reflection/transmission test is $1.01 - 0.004i$.

6.1.3. 16 – 40 GHz

Figure 6-4 shows how the techniques perform over the range 16 – 40 GHz on the 305 mm square sample. The transmission technique still gives excellent correlation to the expected value across the whole frequency range, the reflection technique is a little off at the lowest frequencies but is otherwise excellent, and the reflection/transmission technique shows the customary spikes around the destructive interference frequencies but gives good performance elsewhere. The backed reflection techniques again over-estimate the expected values. The average permeability was measured at $1.01 - 0.05i$.

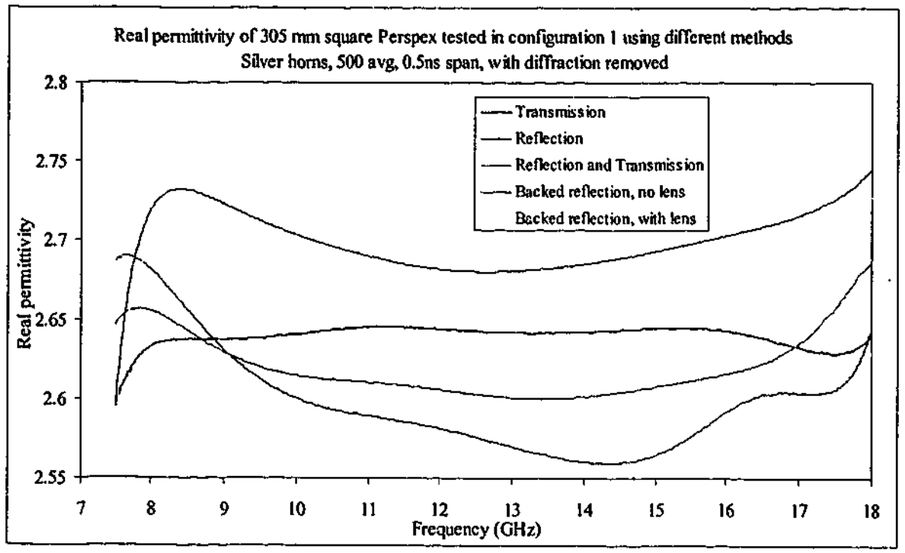

Figure 6-3. Real permittivity of Perspex measured with silver horns in free space using different methods with diffraction removed

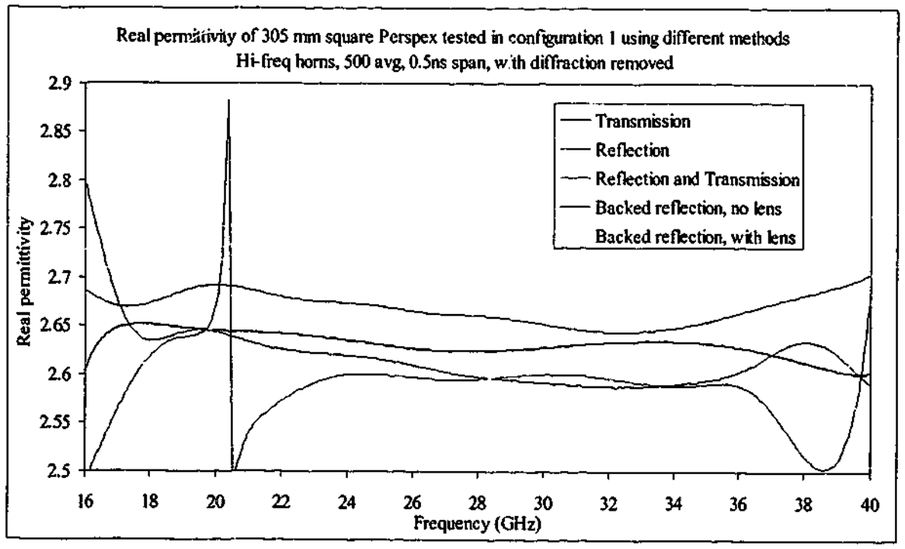

Figure 6-4. Real permittivity of Perspex measured with hi-freq horns in free space using different methods with diffraction removed

6.2. Carbon Loaded rubber

The rubber samples containing carbon black all have destructive interference peaks occurring in the 16 – 40 GHz range. While not as intense as the ones from the low loss

Perspex sample, they nevertheless cause problems in the permittivity and permeability values. Two examples will be presented in detail to show examples of the effects that occur when testing these lossy materials.

6.2.1. Sample B, 1 – 18 GHz

The moderately lossy Sample B shows good correlation between the reflection and transmission methods in both real (Figure 6-5) and imaginary (Figure 6-6) permittivity. The backed reflection technique is again over-estimating the real permittivity but gives reasonably good performance in calculating the imaginary component above 7 GHz. The average permeability was calculated to be $1.03 - 0.014i$ across the full frequency band, although the average was raised somewhat by high values in the 1 – 2 GHz band. Elsewhere, the real permeability stayed around unity.

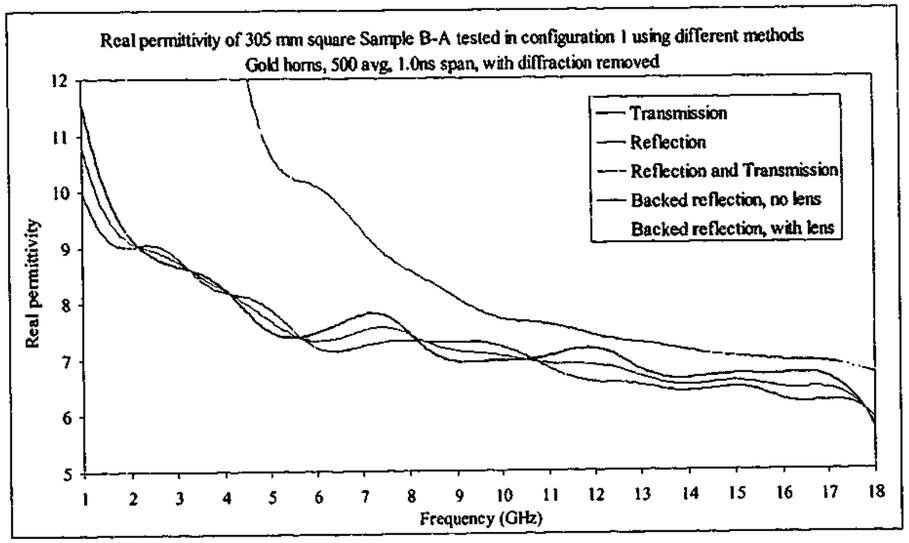

Figure 6-5. Real permittivity of Sample B measured with gold horns in free space using different methods with diffraction removed

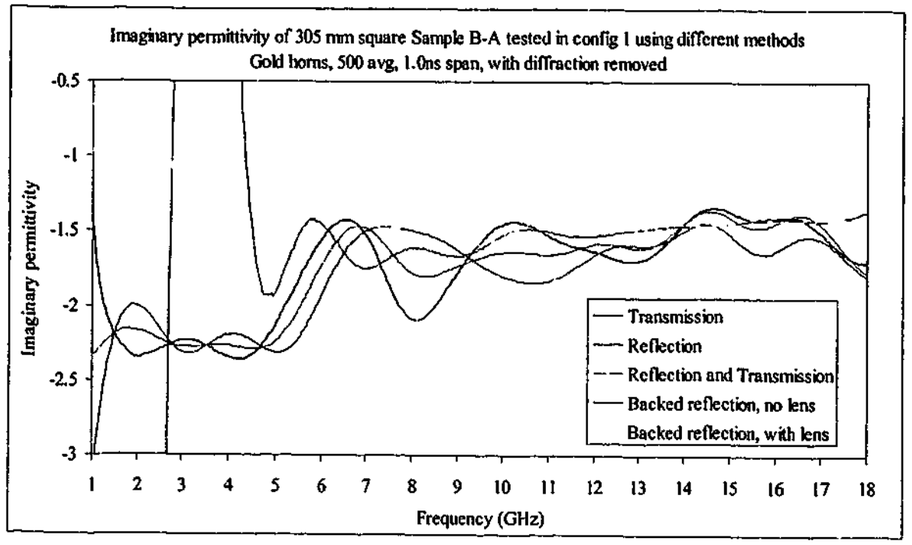

Figure 6-6. Imaginary permittivity of Sample B measured with gold horns in free space using different methods with diffraction removed

6.2.2. Sample B, 7.5 – 18 GHz

A very similar result to that of the Perspex sample was seen over the 7.5 – 18 GHz band. The reflection and transmission measurements gave very similar results with much less noise than was seen in the 1 – 18 GHz case. The presence of the dielectric lens is again aiding the backed reflection measurements but the absolute values are still significantly different from the non-backed techniques. The permittivity values are shown in Figure 6-7 and Figure 6-8. The average permeability was determined to be $1.01 - 0.018i$.

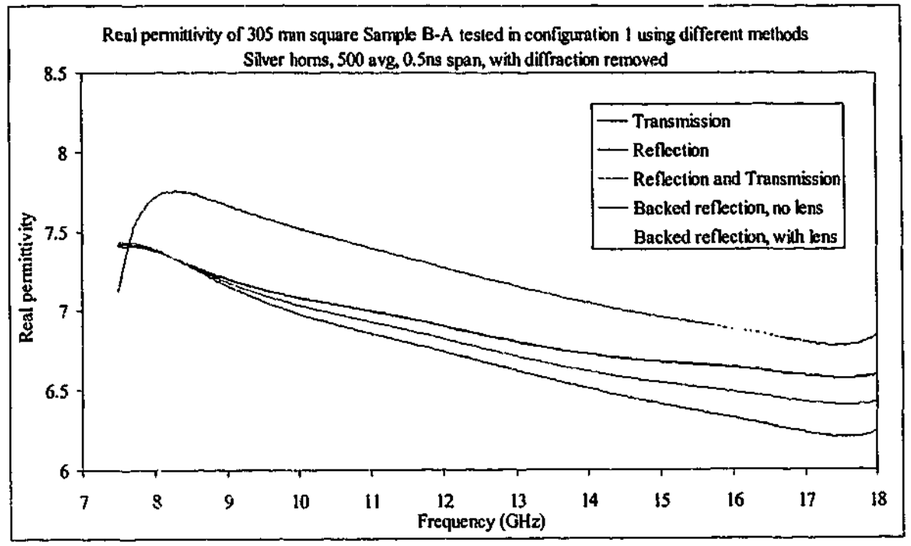

Figure 6-7. Real permittivity of Sample B measured with silver horns in free space using different methods with diffraction removed

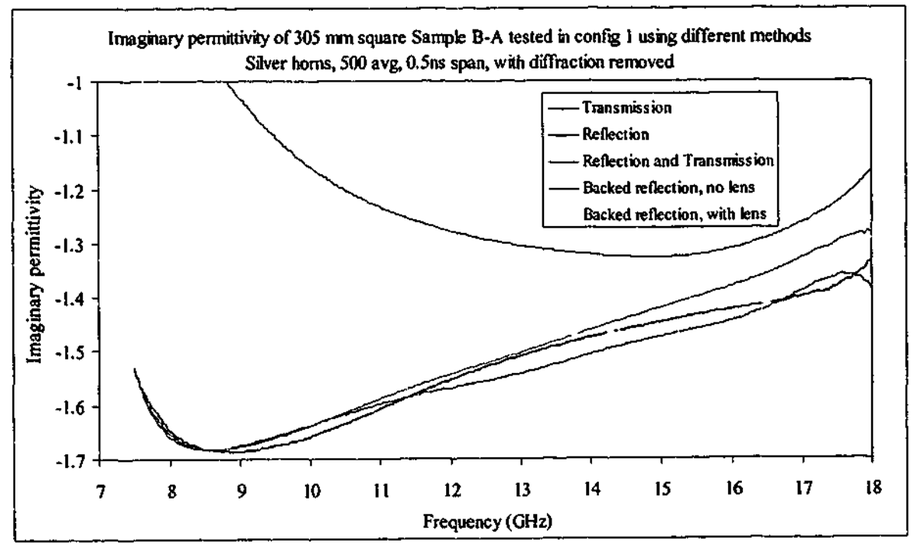

Figure 6-8. Imaginary permittivity of Sample B measured with silver horns in free space using different methods with diffraction removed

6.2.3. Sample B, 16 – 40 GHz

Destructive interference at about 38 GHz is causing some problems for the reflection/transmission technique over the 16 – 40 GHz range, but overall the results are

reasonably consistent across the frequency band. The reflection only algorithm has a little trouble in choosing the correct solution at about 27 GHz, resulting in the curves seen in Figure 6-9 and Figure 6-10.

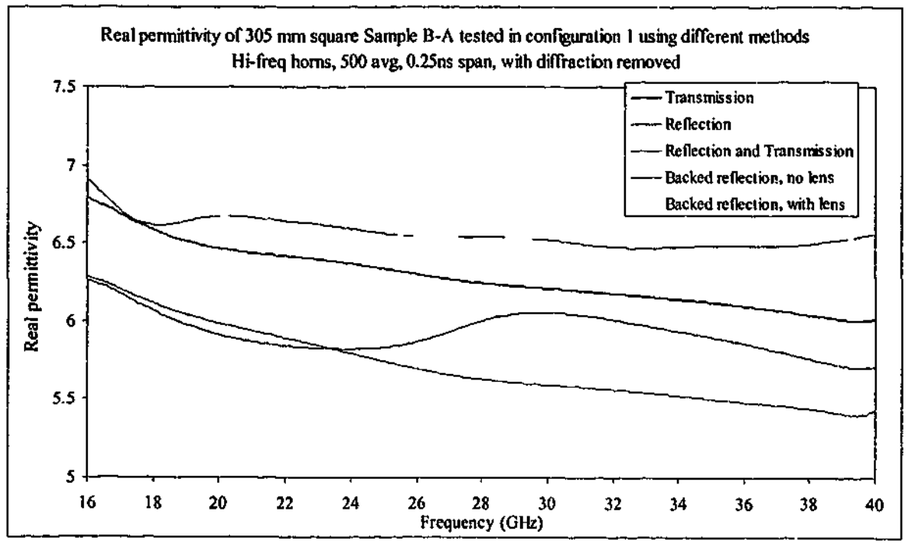

Figure 6-9. Real permittivity of Sample B measured with hi-freq horns in free space using different methods with diffraction removed

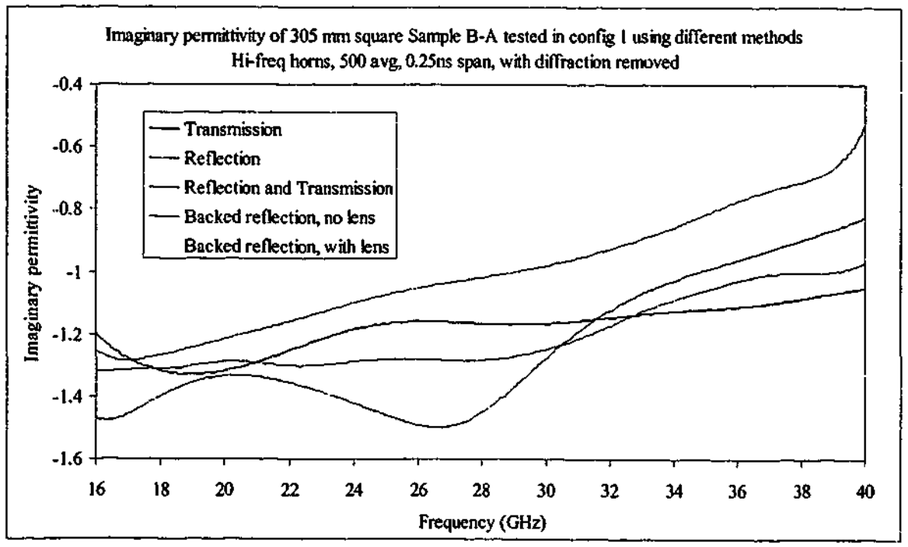

Figure 6-10. Imaginary permittivity of Sample B measured with hi-freq horns in free space using different methods with diffraction removed

We can see that the reflection and transmission result is significantly lower than the transmission only result in absolute terms, especially at high frequencies. The algorithm gives an average permeability across the range as $1.03 - 0.017i$.

The backed reflection results are similar to previous measurements; the real component is over-estimated, while the imaginary component is close to the other results.

6.2.4. Sample E, 1 – 18 GHz

As permittivity increases, the errors in the real permittivity calculations for the backed reflection technique become less. As can be seen in Figure 6-11, the values measured for real permittivity are almost the same for all techniques above 9 GHz.

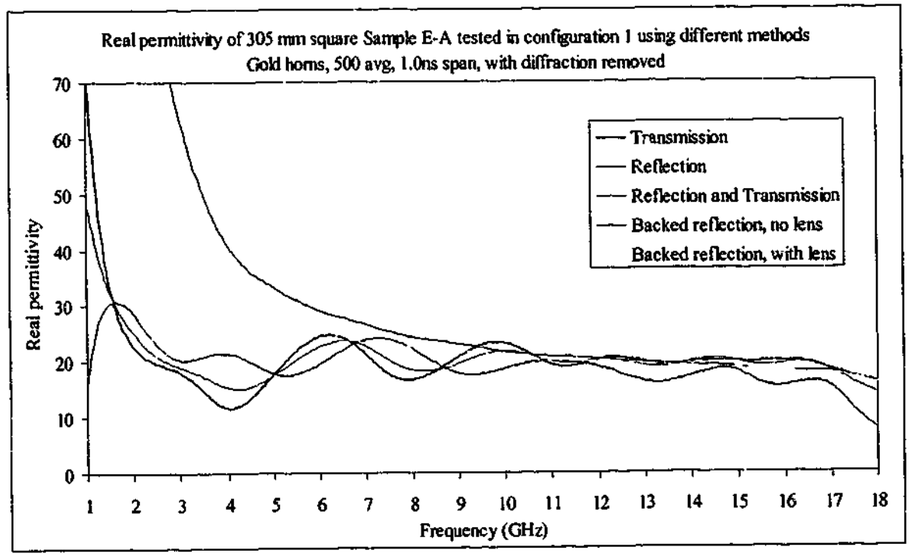

Figure 6-11. Real permittivity of Sample E measured with gold horns in free space using different methods with diffraction removed

The values of imaginary permittivity shown in Figure 6-12 are close for all unbacked materials, but the backed reflection technique gives slightly increased absolute values in the high frequency range. The average permeability across the whole frequency range is $1.00 - 0.033i$.

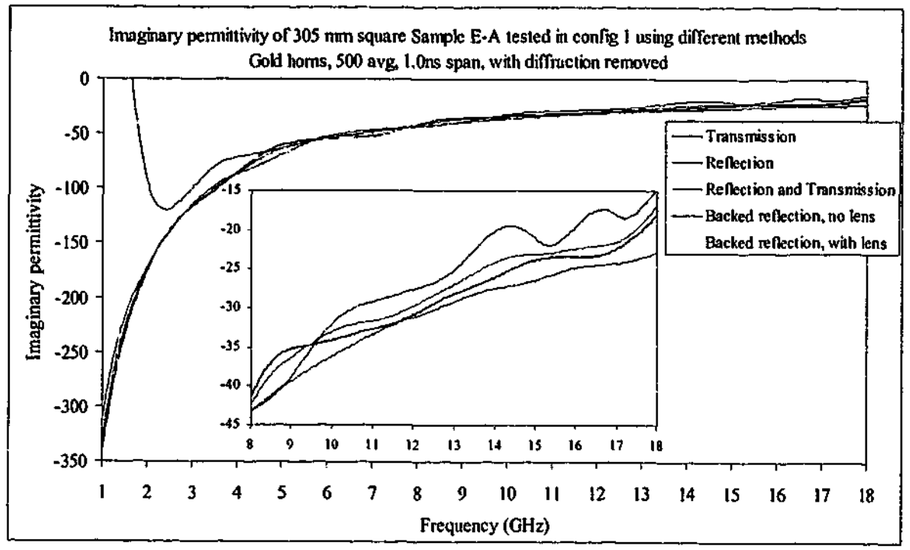

Figure 6-12. Imaginary permittivity of Sample E measured with gold horns in free space using different methods with diffraction removed

6.2.5. Sample E, 7.5 – 18 GHz

The results over the reduced frequency range for the 305 mm square sample are very similar to those of the 445 mm square sample, right down to the characteristic reduction in real permittivity using the reflection only data. Comparing the results shown in Figure 6-13 to those of Figure 5-53 and Figure 5-60, we can see that in both cases the transmission data gives a gentle reduction of permittivity with frequency, but the reflection only data shows a sharp transition. The imaginary permittivity for the 305 mm sample seen in Figure 6-14 also shows a faster reduction for the reflection only result than those of the other techniques. The result from the reflection/transmission technique closely matches the transmission only result, with an average permeability across the range of $1.00 - 0.025i$.

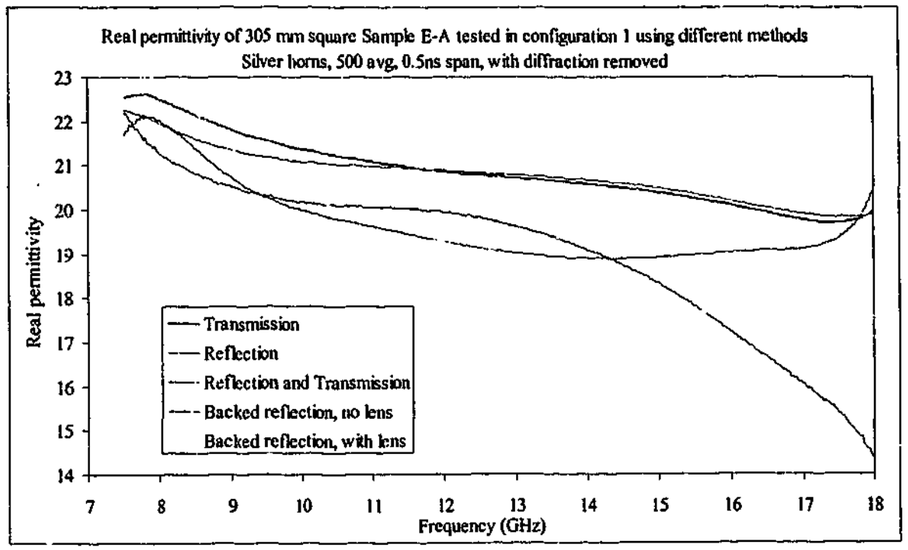

Figure 6-13. Real permittivity of Sample E measured with silver horns in free space using different methods with diffraction removed

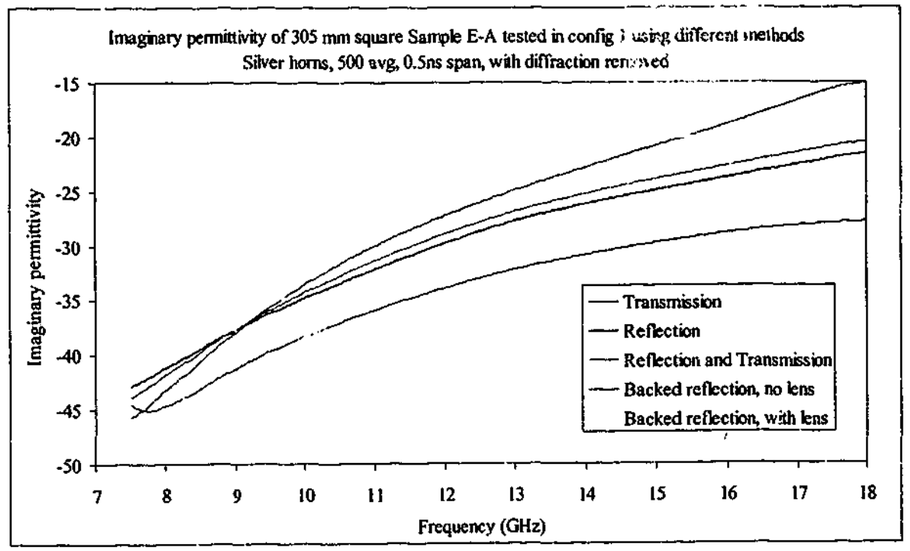

Figure 6-14. Imaginary permittivity of Sample E measured with silver horns in free space using different methods with diffraction removed

6.2.6. Sample E, 16 – 40 GHz

The trend of results from reflection only data shifting away from those of the other techniques continues in the 16 – 40 GHz result. Figure 6-15 and Figure 6-16 show the real

and imaginary permittivity extracted from the different measurements. The reflection only calculations show a marked deviation from the other results, and the effects of the errors in the reflection data are starting to affect the values from the reflection/transmission algorithm, something seen only to a minor extent in previous measurements.

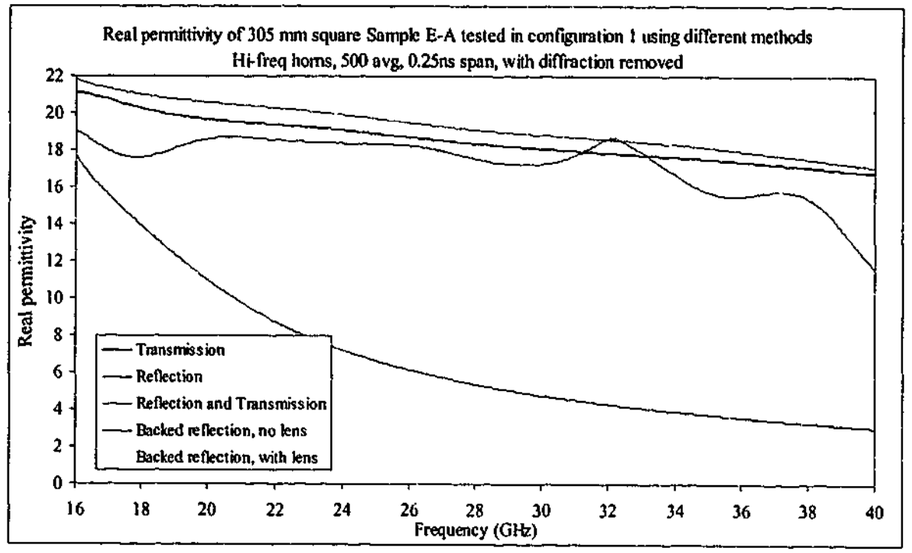

Figure 6-15. Real permittivity of Sample E measured with hi-freq horns in free space using different methods with diffraction removed

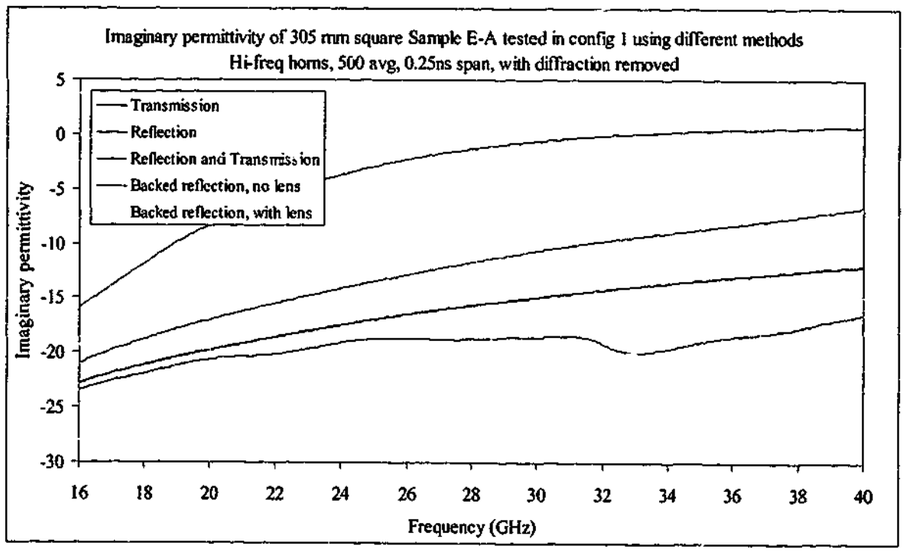

Figure 6-16. Imaginary permittivity of Sample E measured with hi-freq horns in free space using different methods with diffraction removed

The backed reflection data again shows larger magnitudes in imaginary permittivity, with the real permittivity lower than the transmission only result. The average permeability was determined to be $0.994 - 0.185i$, indicating the errors from the reflection data have manifested themselves in the permittivity and imaginary component of permeability.

6.2.7. All carbon loaded rubber samples

Placing all the carbon loaded rubber samples on the same set of axes for the 305 mm square samples produces very similar results to those taken for the large specimens. With both real and imaginary data shown in Figure 6-17 the values are a little more difficult to read, but the trend for the permittivity extraction using transmission only data can be seen to mimic the results for the larger samples (shown in Figure 5-83 and Figure 5-84).

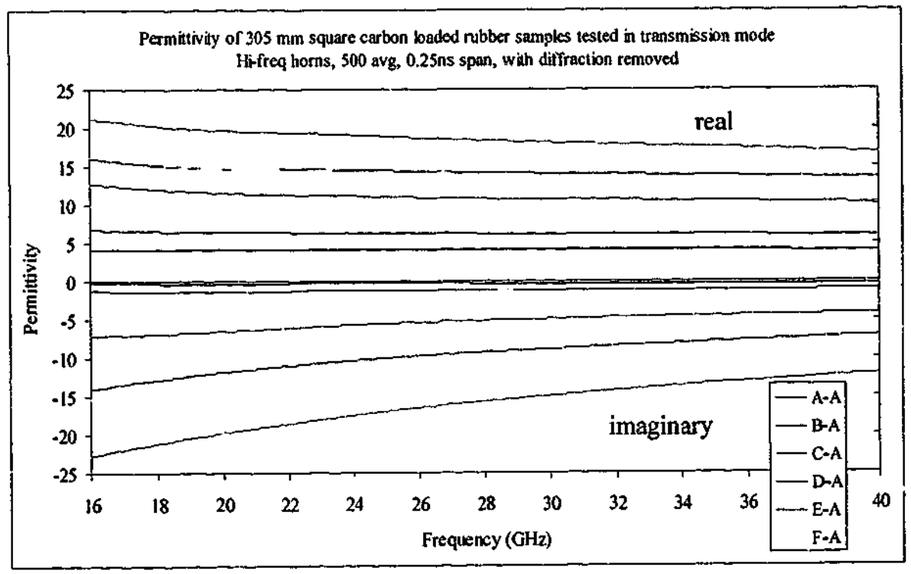

Figure 6-17. Permittivity of carbon loaded rubber samples measured with hi-freq horns in free space using transmission method with diffraction removed

In the case of the reflection only algorithm, unfortunately the trend found in the large samples given in Figure 5-89 and Figure 5-90 continues in the 305 mm square specimens. The results shown in Figure 6-18 are unpredictable over this frequency range using the reflection data alone, and do not agree with those taken with the transmission method.

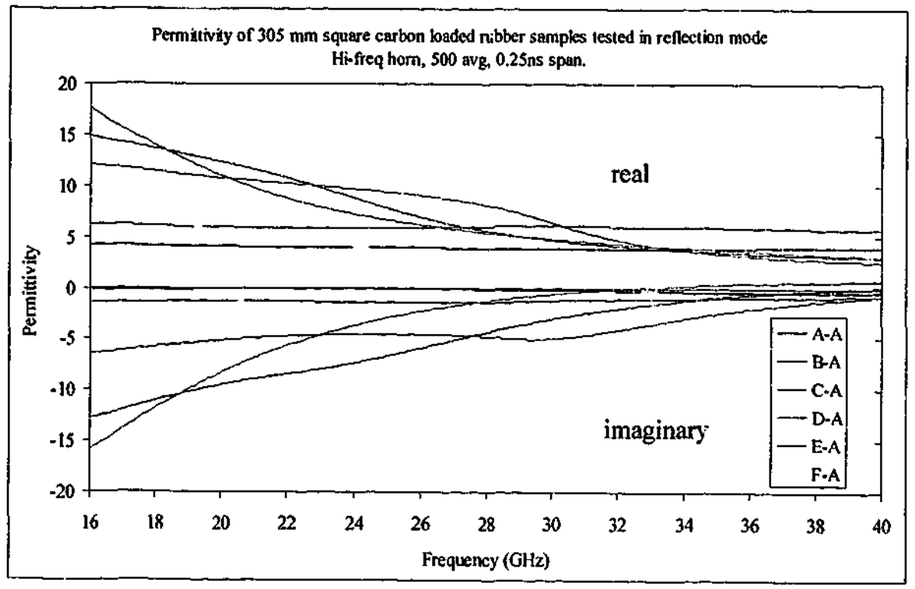

Figure 6-18. Permittivity of carbon loaded rubber samples measured with hi-freq horn in free space using reflection method

The use of 305 mm square samples has not appeared to alter the results of measurements taken with any of the algorithms, and as such it is not deemed necessary to show all the graphs over the various frequency ranges for these materials.

6.3. Carbonyl iron loaded PU

Because electromagnetic properties of the magnetic sample can only be calculated using the reflection/transmission method, the results will be presented in a different form to the non-magnetic materials. Placing the three frequency ranges on the same set of axes allows for a compact method of displaying the data and ease of comparison across frequency ranges. The measured permittivity for Sample G across 1 – 40 GHz is shown in Figure 6-19 and Figure 6-20, while the permeability values are shown in Figure 6-21 and Figure 6-22.

The first thing one notices when observing the following figures is how well the traces line up with each other in the overlapping frequency ranges. While this of course should be the case, it is nevertheless a good sign that even with all the differences between the various measurements such as horn size, gain, diffraction spread and gating effects the results still show good agreement with each other.

The high frequency results from the previous carbon loaded rubber samples B and E showed large absolute errors in the imaginary permittivity and imaginary permeability, and it

appears that sample G is no exception. While the imaginary properties of sample G are unknown, it is known that the imaginary permittivity is defined as having negative values, and should never cross the $\varepsilon'' = 0$ line. The imaginary permittivity result leads to the conclusion that the imaginary permeability result is probably also in error, and by comparing the result shown in Figure 6-22 to the result of the 445 mm square sample (Figure 5-102), we can see that the magnitude for the 305 mm sample is slightly too large. This effect is unsurprising given the larger than expected values of imaginary permeability in samples B and E.

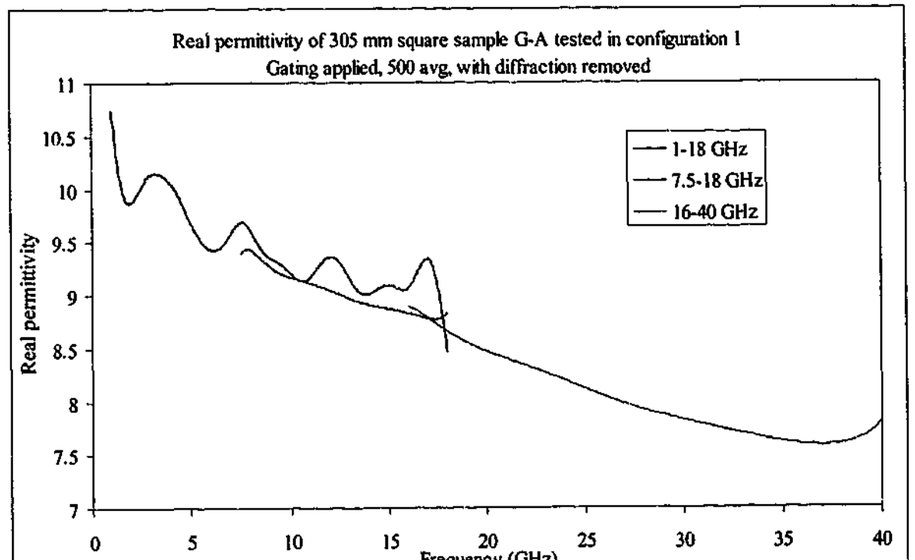

Figure 6-19. Real permittivity of Sample G measured across 1 – 40 GHz in free space using reflection/transmission method with diffraction removed

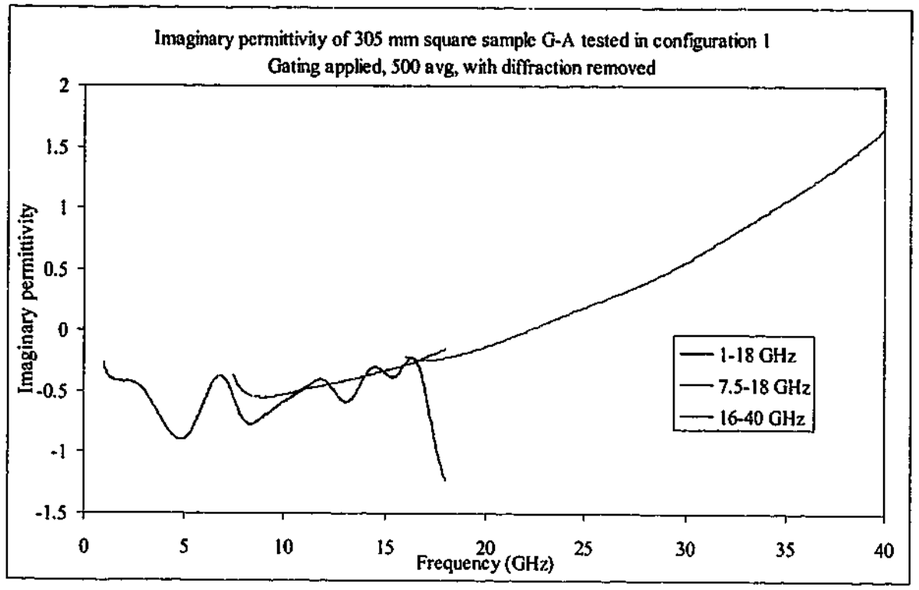

Figure 6-20. Imaginary permittivity of Sample G measured across 1 – 40 GHz in free space using reflection/transmission method with diffraction removed

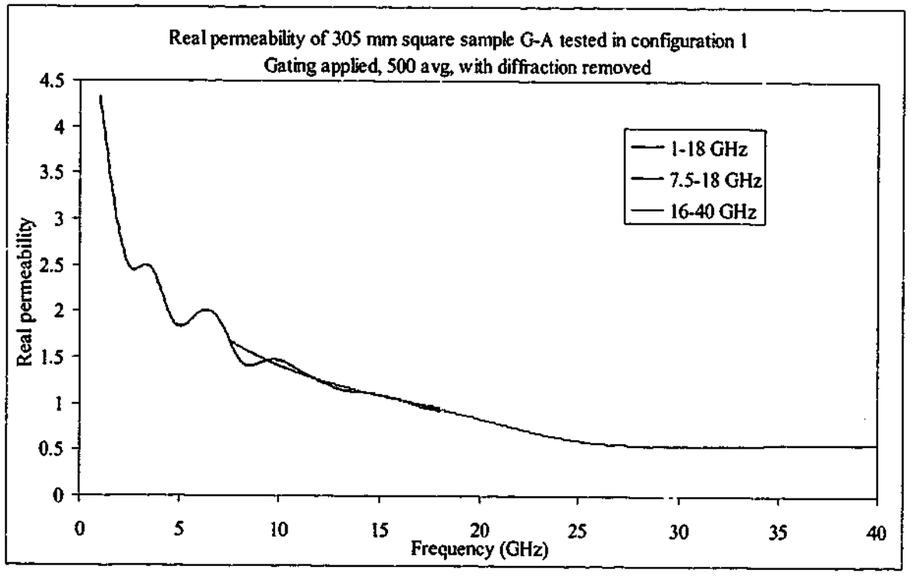

Figure 6-21. Real permeability of Sample G measured across 1 – 40 GHz in free space using reflection/transmission method with diffraction removed

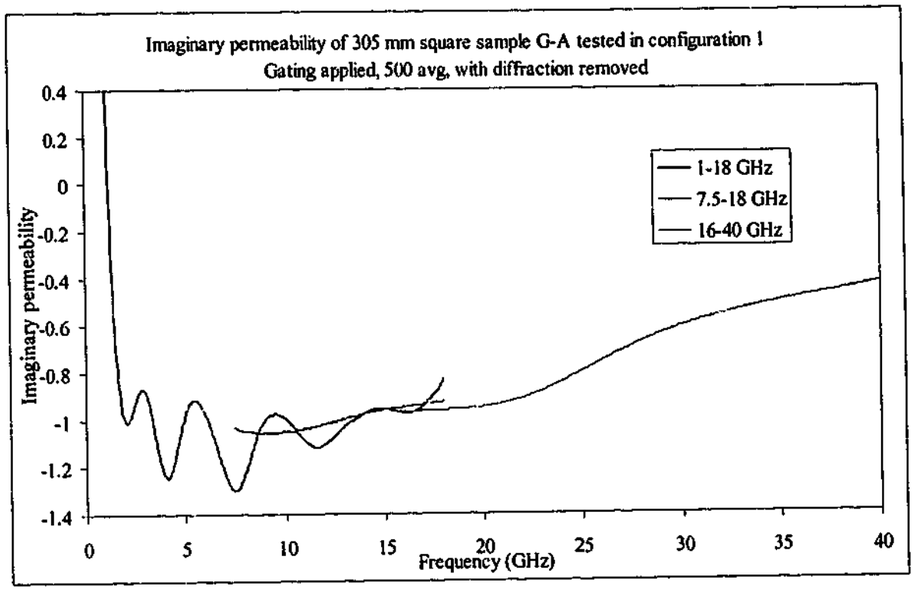

Figure 6-22. Imaginary permeability of Sample G measured across 1 – 40 GHz in free space using reflection/transmission method with diffraction removed

6.4. Composite material

6.4.1. 1 – 18 GHz

As was the case with the previous samples, the values calculated for the carbon fibre loaded composite sample show good correlation between the reflection and transmission techniques over this frequency band. The properties calculated using backed reflection techniques are similar for the real and 10% lower for the imaginary component above 5 GHz. Evidence of a resonance around 3 GHz is clear from the imaginary permittivity, and the data fit for the 300 mm square sample follows the curve given in Equation 5-1 with parameters $\varepsilon_0 = 53.56$, $\varepsilon_\infty = 1.60$ and $\tau = 59.46$ ps, corresponding to a resonance at about 2.68 GHz. These parameters are very close to those observed for the 445 mm square sample. The average permeability across the frequency range was $1.01 - 0.010i$.

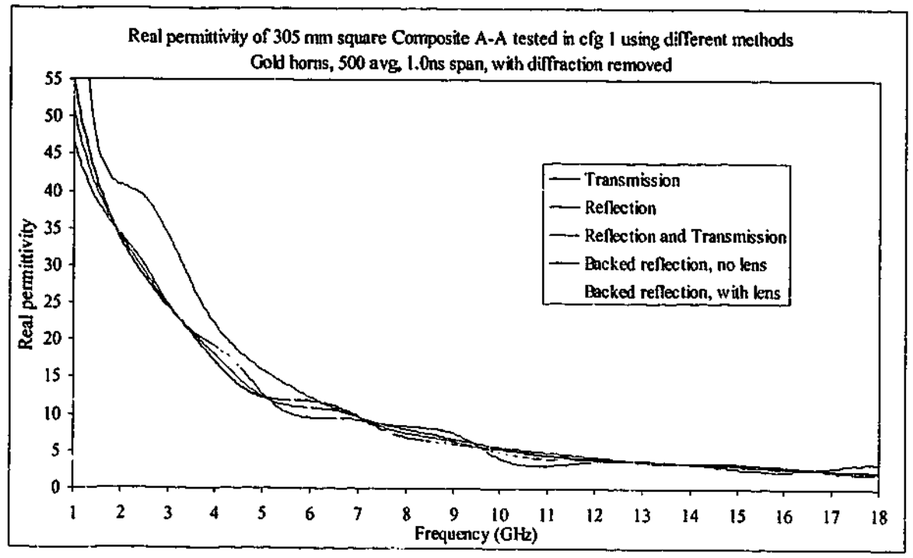

Figure 6-23. Real permittivity of composite sample measured with gold horns in free space using different methods with diffraction removed

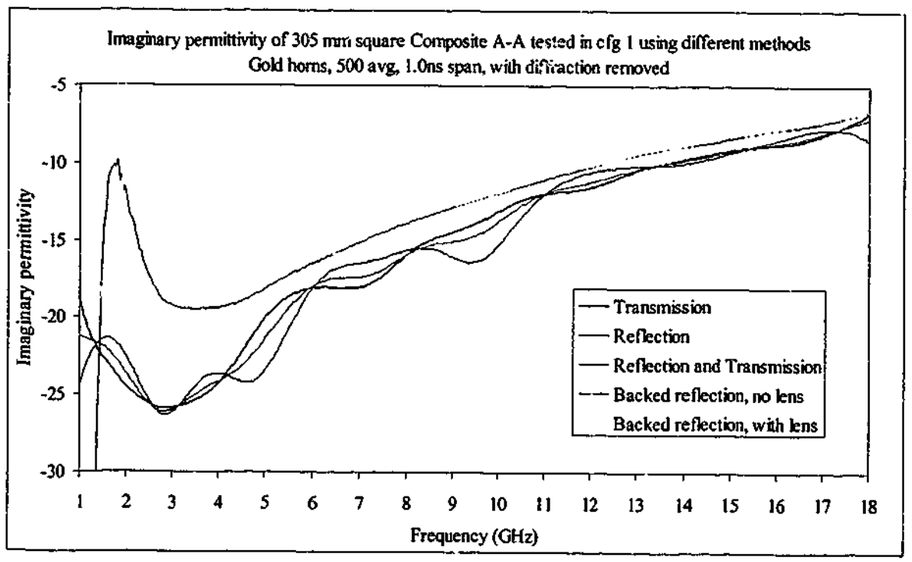

Figure 6-24. Imaginary permittivity of composite sample measured with gold horns in free space using different methods with diffraction removed

6.4.2. 7.5 – 18 GHz

The errors in reflection observed over this frequency range for other samples have failed to appear in the composite material case. The permittivity calculated from reflection and transmission techniques is the same across the whole frequency range, and the average permeability is calculated to be $1.00 + 0.000i$. Figure 6-25 and Figure 6-26 show how the real and imaginary permittivities vary with frequency for the different techniques. Only the backed reflection results show any deviation from the rest of the curves, and the errors involved with backed reflection technique have not reduced in magnitude.

6.4.3. 16 – 40 GHz

The composite material again shows different behaviour from that of the carbon loaded rubber samples over the 16 – 40 GHz range. Both reflection and transmission techniques give the same result over this range, and the average permeability using both sets of data is $0.998 - 0.006i$. The backed reflection technique is still underestimating the permittivity compared to the other techniques, as shown in Figure 6-27 and Figure 6-28.

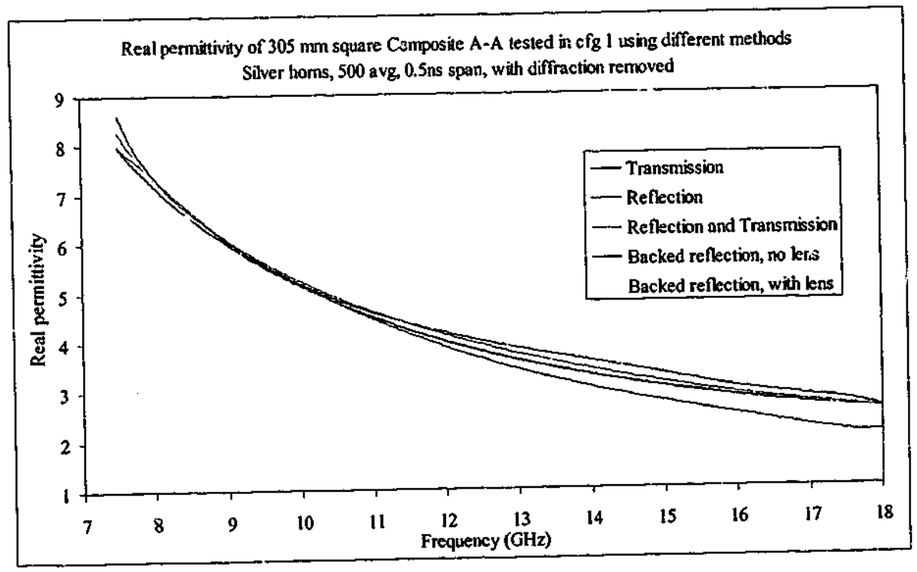

Figure 6-25. Real permittivity of composite sample measured with silver horns in free space using different methods with diffraction removed

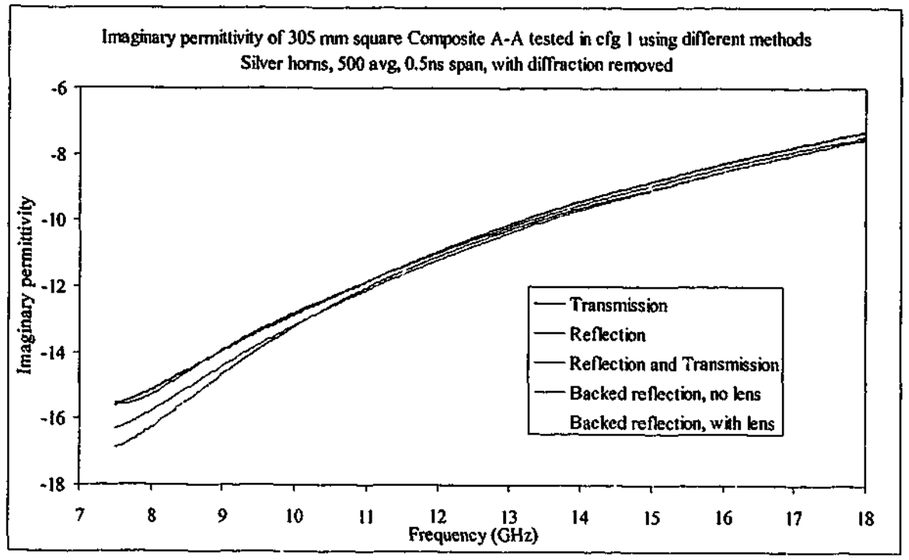

Figure 6-26. Imaginary permittivity of composite sample measured with silver horns in free space using different methods with diffraction removed

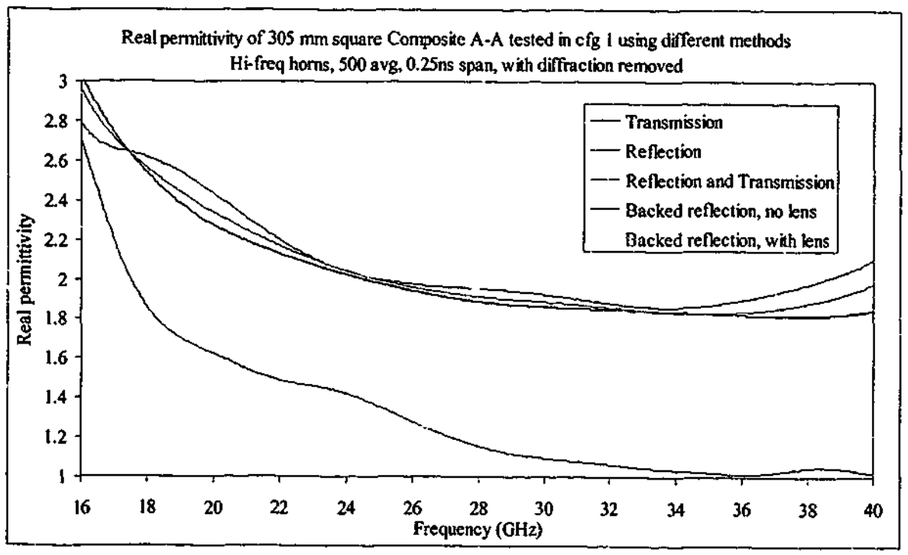

Figure 6-27. Real permittivity of composite sample measured with hi-freq horns in free space using different methods with diffraction removed

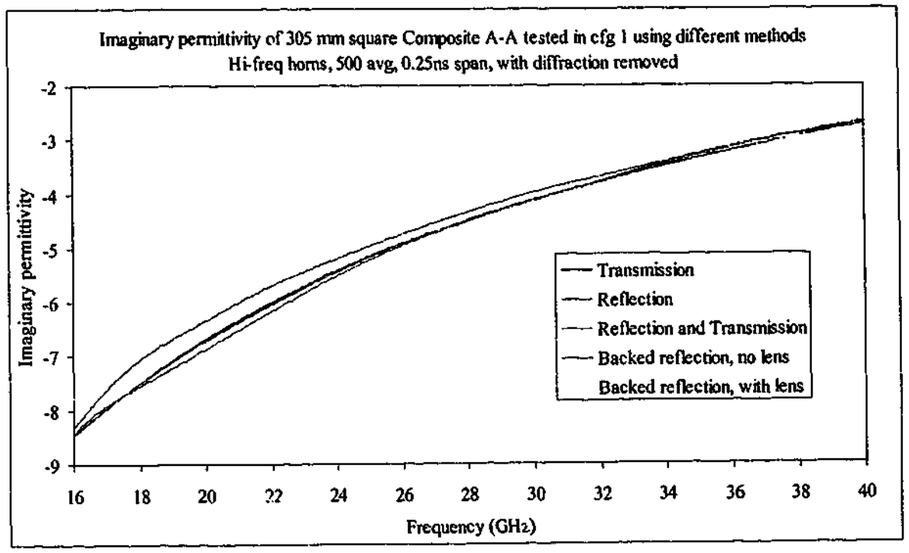

Figure 6-28. Imaginary permittivity of composite sample measured with hi-freq horns in free space using different methods with diffraction removed

6.5. Teflon

6.5.1. 1 – 18 GHz

The Teflon sample had been cut to 300 mm square for a previous measurement and so a 300 mm square metal plate was used to measure the reflection calibration and diffraction removal signals. Since the backed reflection technique uses a 305 mm square plate, the Teflon sample was not measured with this technique. The transmission only technique gives an average permittivity value of $2.03 + 0.01i$ across the whole frequency range, which is very close to the expected value of 2.04. The reflection data has errors above 10 GHz, but this does not overly affect the values from the reflection/transmission algorithm, with the average permittivity value still $2.01 + 0.048i$, with an average permeability of $1.01 - 0.019i$ calculated across the entire frequency band.

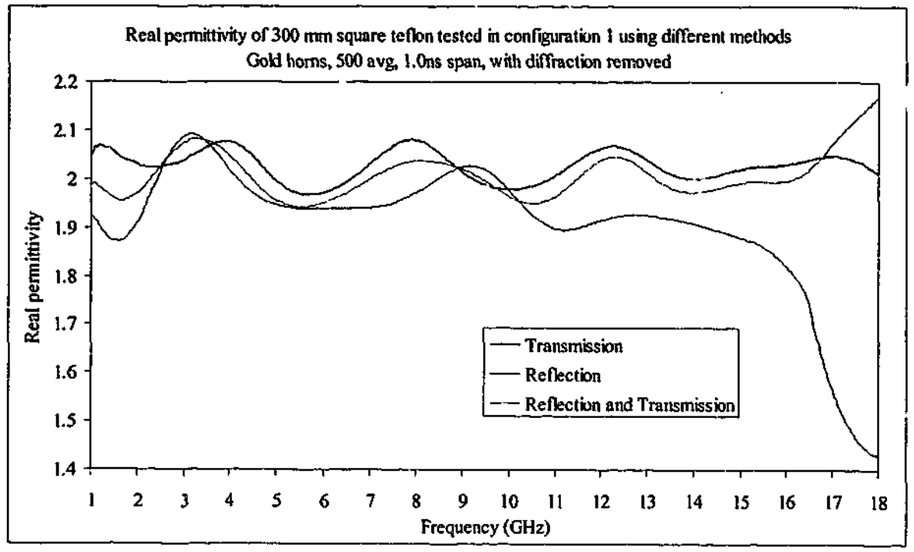

Figure 6-29. Real permittivity of Teflon sample measured with gold horns in free space using different methods with diffraction removed

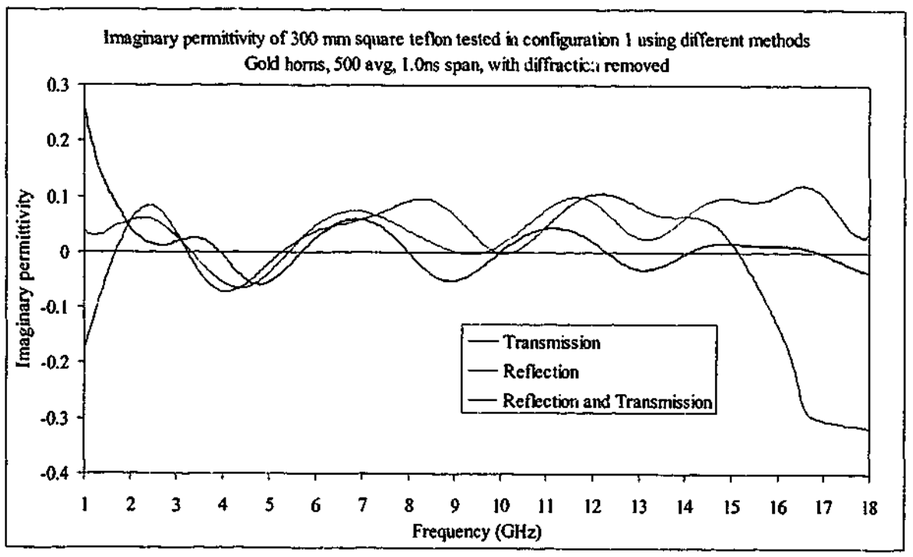

Figure 6-30. Imaginary permittivity of Teflon sample measured with gold horns in free space using different methods with diffraction removed

6.5.2. 7.5 – 18 GHz

The measurements over the reduced frequency range correlate well with each other, and the reflection only results are better using these horns than the gold ones (the opposite to previous results). The presence of a destructive interference peak at about 19.5 GHz is causing problems for the reflection/transmission algorithm above 16 GHz, but overall the average results for all techniques are very close to those expected. The results are shown in Figure 6-31 and Figure 6-32, and the average permeability is measured to be $1.00 + 0.004i$.

6.5.3. 16 – 40 GHz

Again, all three techniques give an accurate value for the permittivity and permeability of Teflon, with the transmission only result averaging 2.02 + 0.001i and the other configurations slightly less. Figure 6-33 and Figure 6-34 show the measured values, and the effects of the destructive interference peaks at 19.5 and 39 GHz on the extracted values using both reflection and transmission data. The average permeability over the range was $1.00 - 0.001i$.

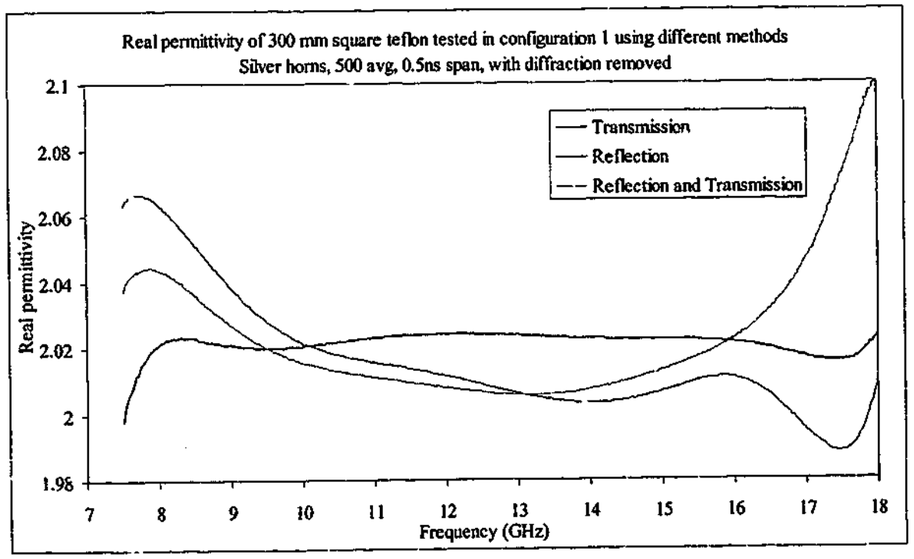

Figure 6-31. Real permittivity of Teflon sample measured with silver horns in free space using different methods with diffraction removed

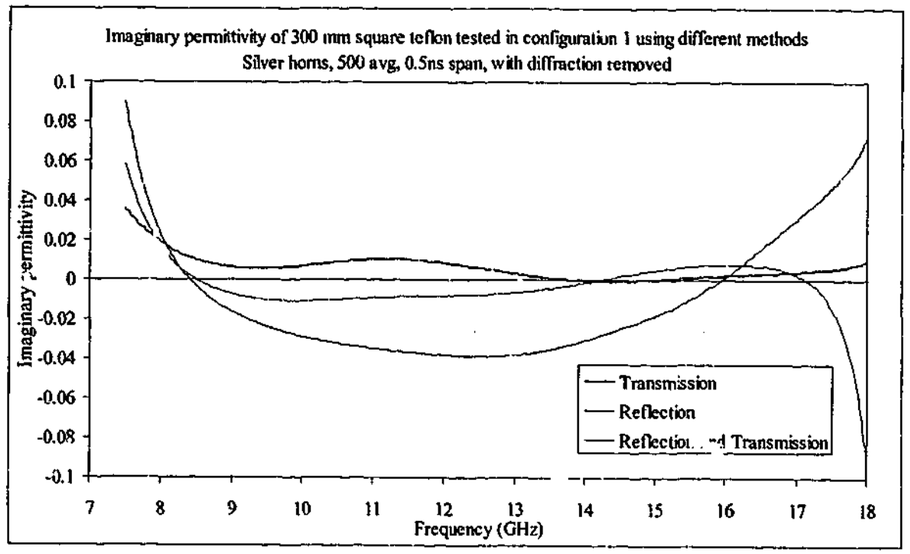

Figure 6-32. Imaginary permittivity of Teflon sample measured with silver horns in free space using different methods with diffraction removed

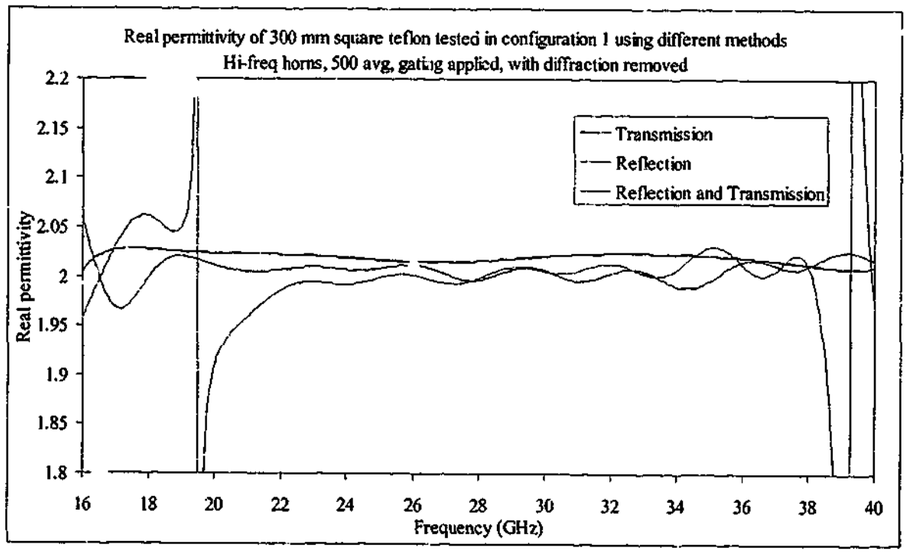

Figure 6-33. Real permittivity of Teflon sample measured with hi-freq horns in free space using different methods with diffraction removed

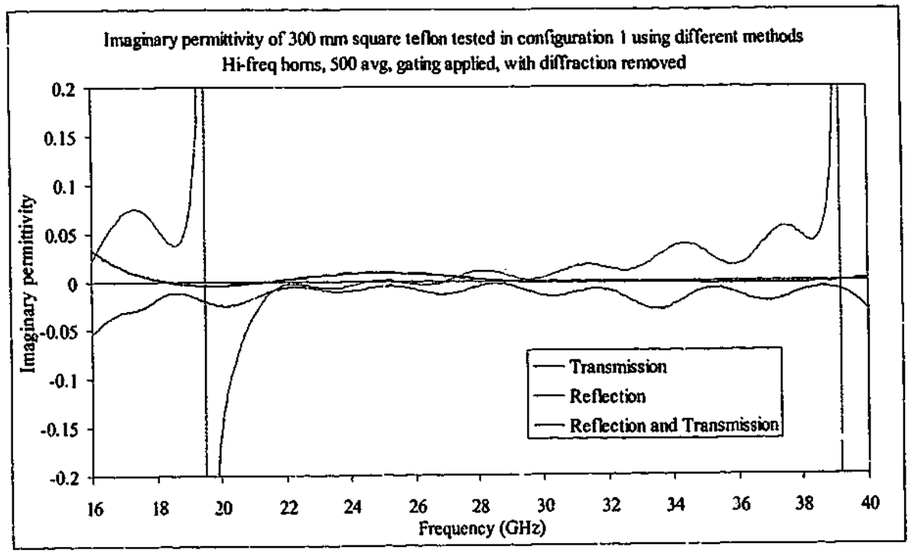

Figure 6-34. Imaginary permittivity of Teflon sample measured with hi-freq horns in free space using different methods with diffraction removed

6.6. LX-57B lead glass

The sample of lead glass used was 7 mm thick, much thicker than the previous samples tested. Combined with a low loss tangent and moderately large real permittivity, destructive interference would be a significant problem over all frequency ranges. In addition, the time gate would need to be individually set for each measurement. Rather than making multiple measurements with different gate widths, the HP gate was not used for these measurements; instead, the author's (AA) gate was applied after the measurement was taken and before the extraction algorithms were used to calculate the electromagnetic properties. Upon investigation of the time domain traces it was found that configuration 1 was not appropriate for this material, due to reflections between the receive horn and the sample overlapping the transmission signal. Figure 6-35 shows the time domain response of the transmission through the lead glass sample. Using the expected permittivity values, the position in time of the multiple internal reflections of the sample can be calculated and are shown as pink stars. The time position from multiple reflections between the sample and the receive horn are shown as green stars. The time gate required for inclusion of the most important peaks is too long to exclude these unwanted peaks, so errors in the signal would occur. The solution was to move the receive horn to a position that would not interfere with the transmission signal, whilst still

having the horn close enough that significant diffraction would be avoided. The effects of the sample to horn reflections are clearly visible in the measured signal shown in Figure 6-35.

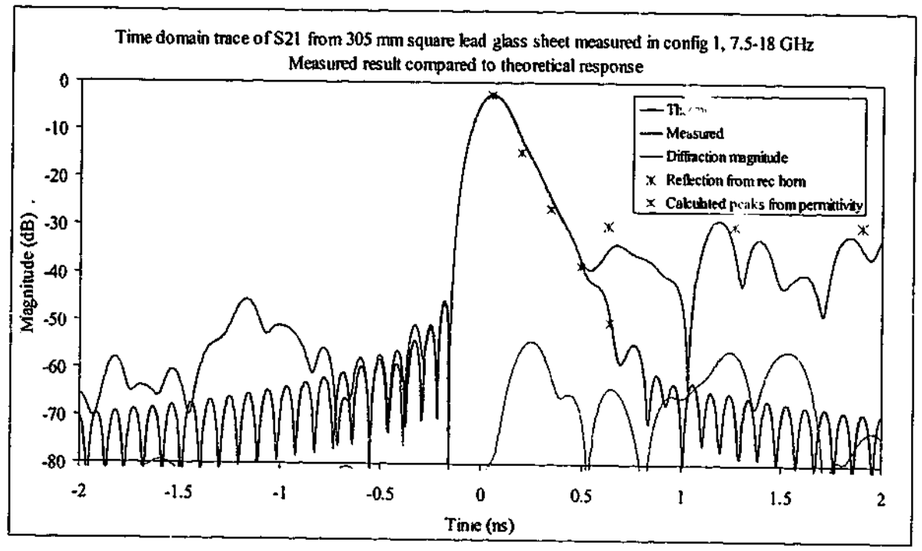

Figure 6-35. Time domain response of transmission signal through lead glass sample measured in configuration 1, over the frequency range 7.5 – 18 GHz

The receive horn was moved to a distance of 0.25 m from the foam stand that the sample rests on. This distance allows a maximum gate span of over 3 ns, which should be enough for not only the lead glass sample, but also the thick C-Stock materials. When the sample was measured in this new configuration (known as configuration 1a) the results were much closer to that expected, with the time domain trace shown in Figure 6-36. Note how the peak previously at the 0.65 ns mark has been shifted to 1.65 ns, and is no longer interfering with the multiple internal reflection signal. Note also the increase in the diffraction signal from a peak of about –55 dB to –41 dB. This is to be expected as the sample to horn distance increases, but the influence is only minor.

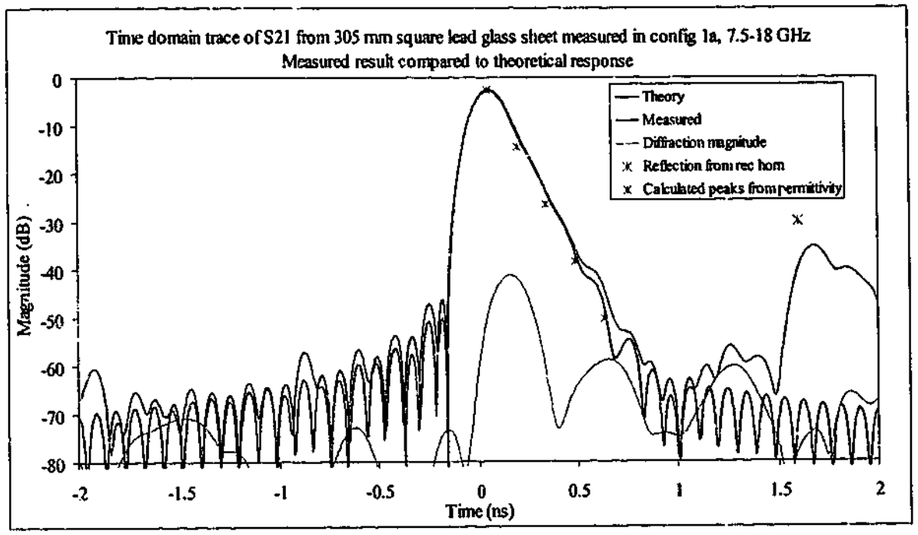

Figure 6-36. Time domain response of transmission signal through lead glass sample measured in configuration 1a, over the frequency range 7.5 – 18 GHz

The stray reflections between the sample and the horns can be removed using time gating. For the thick lead glass and C-Stock samples, the width of the AA gate was applied as deemed appropriate to allow for as many internal reflections as possible while removing stray reflections. This involved first taking an ungated measurement of S_{11} and S_{21} with the analyser, converting to the time domain and applying the optimum AA time gate before converting the time trace back to frequency space and calculating the permittivity. Doing this for each sample and each frequency range obviously takes more time and effort but the values obtained are much more accurate.

6.6.1. 1-18 GHz

Because of the thickness of the sample, destructive interference occurs throughout all frequency ranges. The S_{11} magnitude is shown in Figure 6-37 where it is clear to see destructive interference occurring at about 7 and 13.5 GHz. The AA gate width was 2.0 ns for both the transmission and reflection signals over this frequency band. The permittivity values are shown in Figure 6-38 and Figure 6-39.

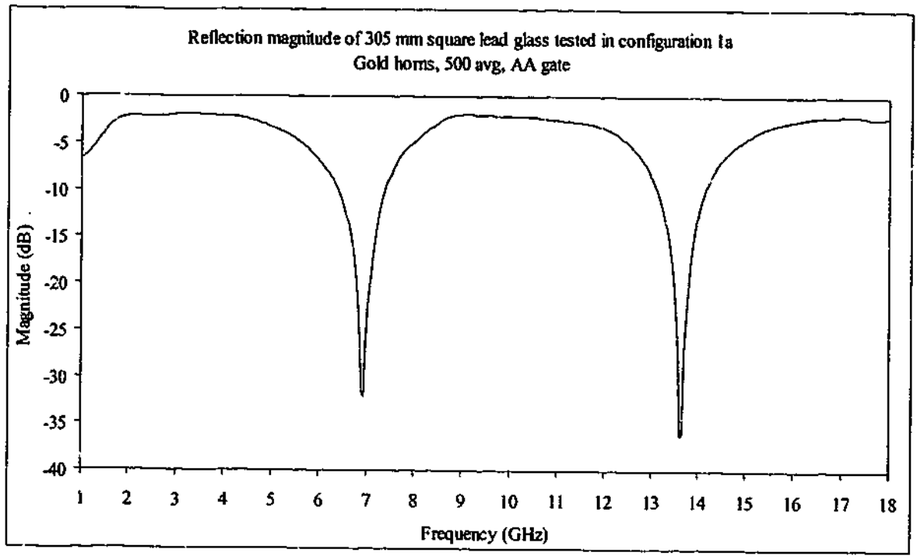

Figure 6-37. S_{11} magnitude from lead glass sample measured in configuration 1a over the frequency range 1 – 18 GHz

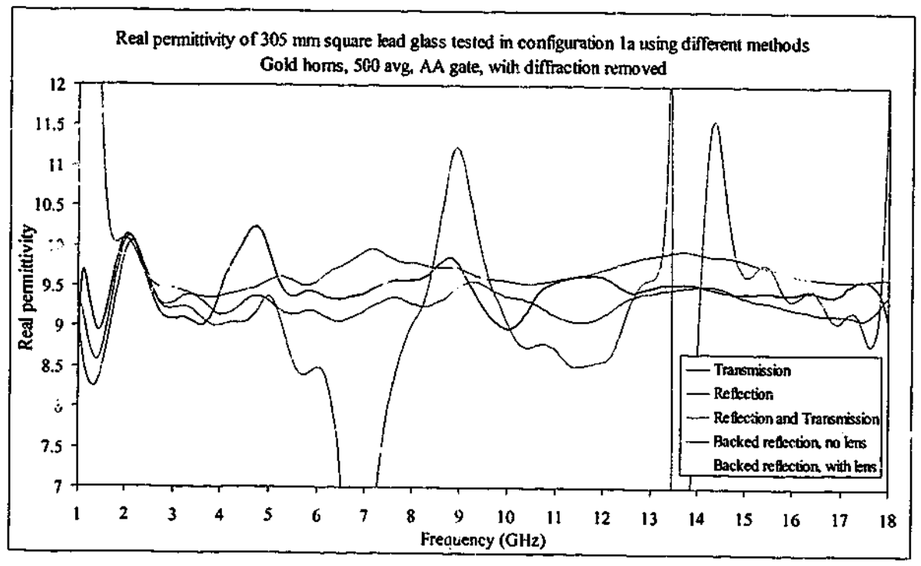

Figure 6-38. Real permittivity of lead glass sample measured with gold horns in free space using different methods with diffraction removed

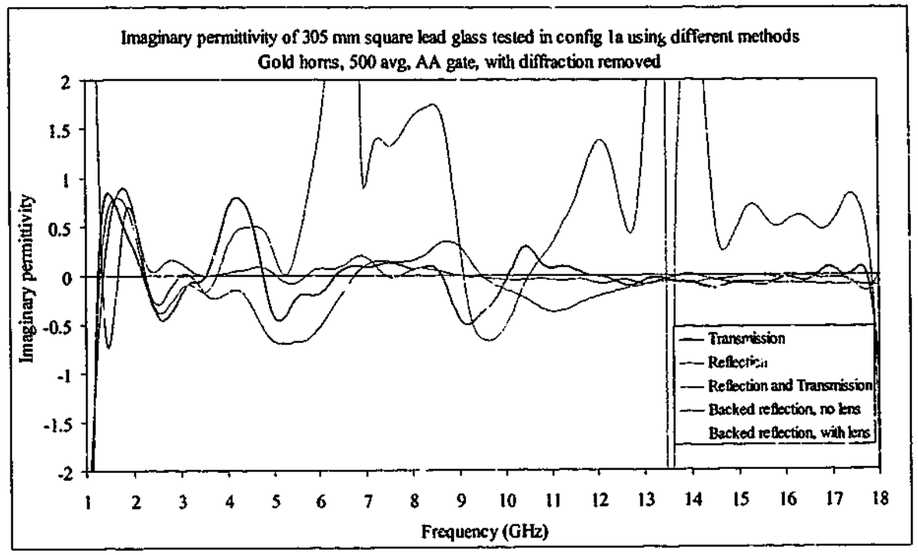

Figure 6-39. Imaginary permittivity of lead glass sample measured with gold horns in free space using different methods with diffraction removed

All methods except the reflection and transmission algorithm give similar values across the frequency band. The result from the reflection algorithm is seemingly unaffected by the strong destructive interference peaks in the reflection signal, even though they cause large errors with the same data using the reflection/transmission model. The backed reflection technique shows good performance over almost the whole band, only deviating from the expected values below 2 GHz.

6.6.2. 7.5 – 18 GHz

The trend is continued over the reduced frequency range 7.5 – 18 GHz. The destructive interference peak at about 13.5 GHz causes problems only for the reflection/transmission algorithm; the other algorithms are only slightly affected. The results of Figure 6-40 and Figure 6-41 show how the calculated values are all very close to one another except those using the reflection and transmission signals. Over this frequency range the gate width was set at 1.8 ns for the reflected signal, 1.2 ns for the transmission, and 2.0 ns for the backed reflection data.

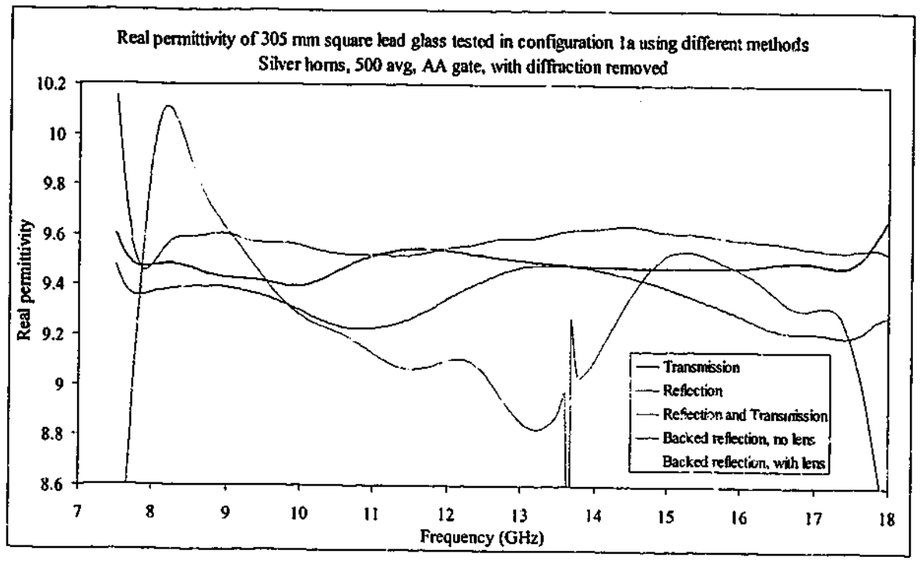

Figure 6-40. Real permittivity of lead glass sample measured with silver horns in free space using different methods with diffraction removed

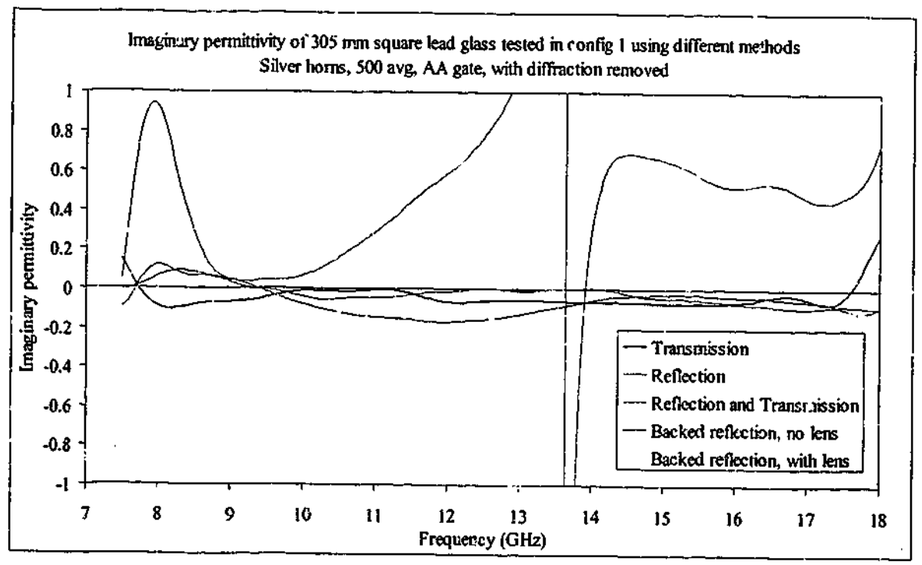

Figure 6-41. Imaginary permittivity of lead glass sample measured with silver horns in free space using different methods with diffraction removed

6.6.3. 16 – 40 GHz

Over the 16 – 40 GHz range, the reflection and transmission algorithms give almost identical results; the reflection/transmission algorithm is hampered by destructive

interferences at 20.5, 27.5, 34.2, and near 40 GHz. It can be seen in Figure 6-42 and Figure 6-43 that the backed reflection values are a little different from the reflection and transmission values but are still fairly close over a wide range.

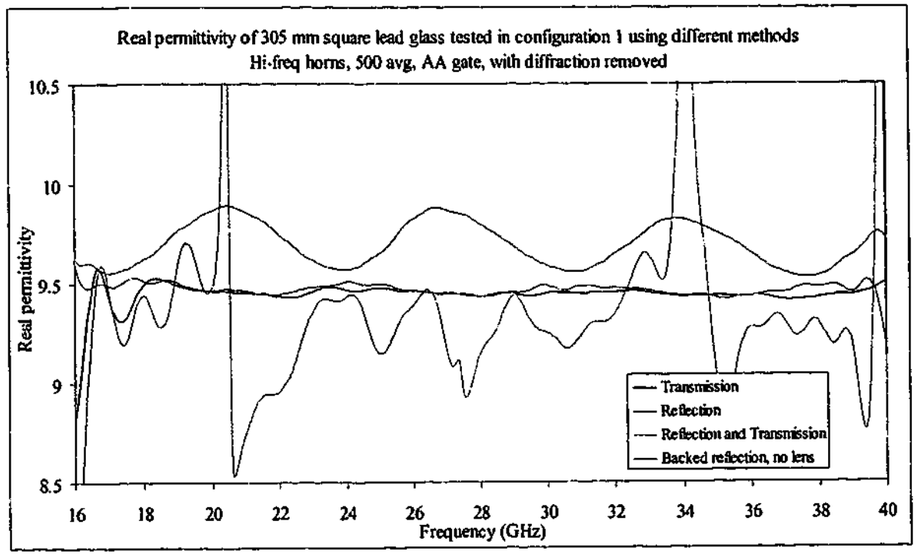

Figure 6-42. Real permittivity of lead glass sample measured with hi-freq horns in free space using different methods with diffraction removed

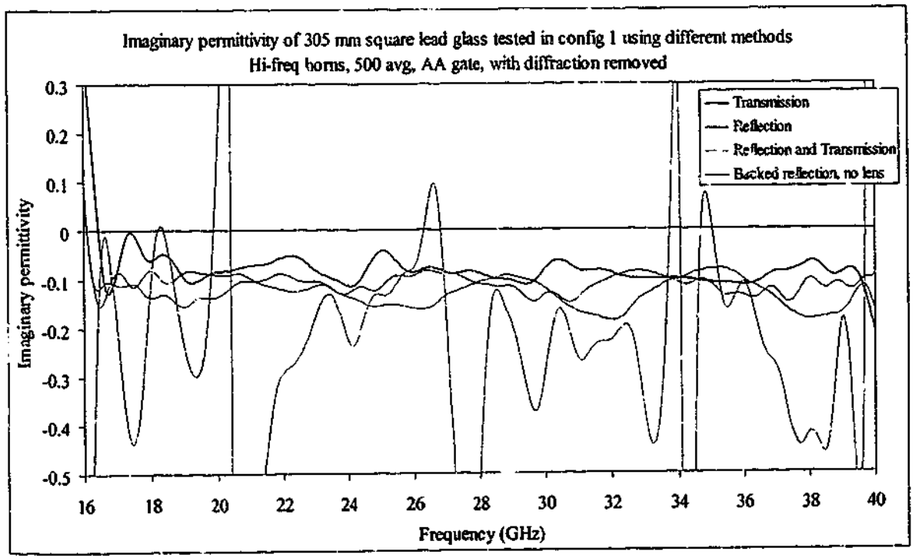

Figure 6-43. Imaginary permittivity of lead glass sample measured with hi-freq horns in free space using different methods with diffraction removed

6.7. CS-AK xx sheets

These materials were bought specifically as reference materials, since the permittivity of the samples was quoted as being accurate to ± 3% of the value required. The standard thickness that the samples were supplied was 3/8", approximately 9.6 mm. This caused destructive interference across all frequency bands making permittivity extraction difficult when the reflection/transmission algorithm was used, giving similar results to the lead glass sample. For this reason the reflection/transmission extraction will not be shown, as very little useful data can be obtained. Instead, the real permittivity results using the either transmission or reflection only algorithms are shown in Figure 6-44 and Figure 6-45. Over the full frequency range the values obtained are reasonably consistent when using either method, and there is no sign of frequency dependence. The results using the reflection only method show a little more jitter than the transmission only ones, but the averages across all frequencies (shown in black on the figures and in Table 6-1) are very similar. The gate span for these measurements ranged from 1.5 ns for the CS-AK 7 material up to 3 ns for CS-AK 15. The effect of widening the gate span can be seen as increased noise levels on the permittivity traces.

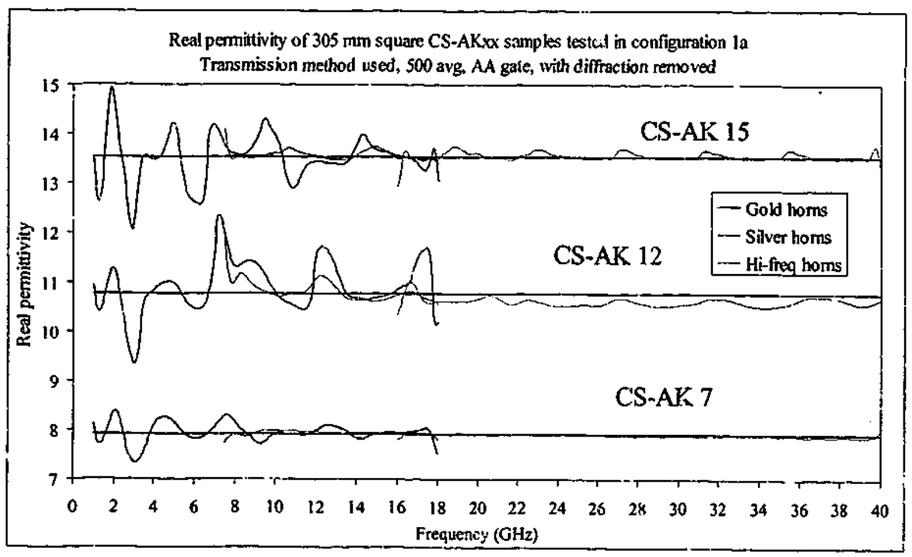

Figure 6-44. Real permittivity of CS-AK xx samples measured in free space using transmission method with diffraction removed

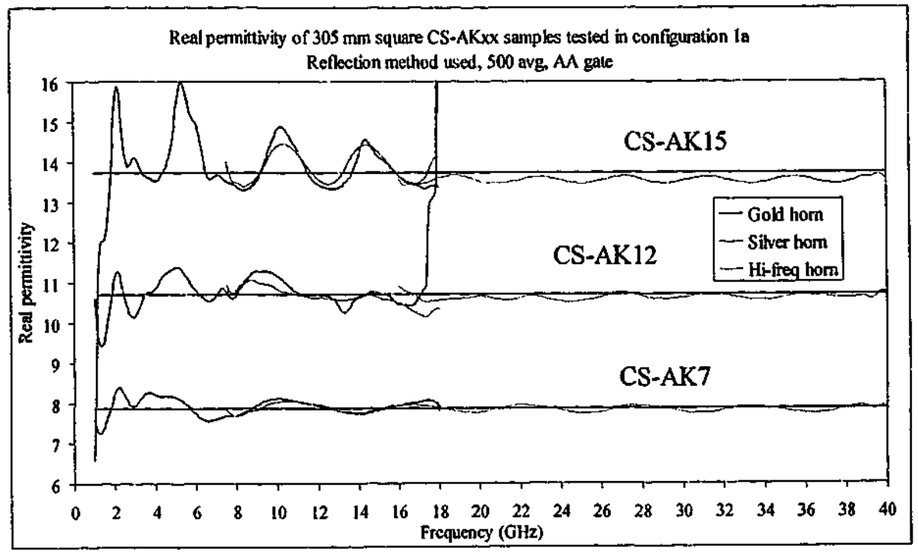

Figure 6-45. Real permittivity of C-Stock AK xx samples measured in free space using reflection method with diffraction removed

Material	Transmission	Reflection
CS-AK 7	7.92	7.88
CS-AK 12	10.77	10.69
CS-AK 15	13.55	13.75

Table 6-1. Average real permittivity of C-Stock materials measured using transmission or reflection techniques.

The measured average results are very different from those expected. The permittivity is quoted as being the number in the material's name to an accuracy of ± 3%, except for CS-AK 15 which is ± 10%. The measured values are not only in a particular direction either, the AK 12 and AK 15 results are both about 10% less than expected while the AK 7 material is about 10% greater. The imaginary components were low for all the samples.

6.8. Summary

Testing of the 305 mm square samples produced some extra information about the measurement techniques than the larger 445 mm square samples. Additional materials not available in the larger size were tested, and confirmed that the techniques were giving accurate values for the permittivity and permeability for the frequency ranges required. The results of the Teflon, Lead glass and Perspex samples all showed properties very close to that expected. Testing the CS-AK xx materials did not produce values that were expected from the

manufacturer's specifications, but were consistent across the frequency range with the various methods.

An additional technique was introduced, using the backed reflection signal to determine permittivity. This method was a little inconsistent, sometimes giving values that compared well with those from the other techniques and at other times underestimating the properties. It was clear, however, that the backed reflection technique did not perform well below about 6 GHz, which was a little surprising considering the size of the specimens were of the order of the wavelength at 1 GHz. Use of the dielectric lens appeared to have little effect on the results from the backed reflection technique, with some measurements giving results that more closely agreed with the other techniques, and at other times gave results further away.

Overall, it was shown that the measurements of the 305 mm samples did not vary greatly from those of the larger 445 mm square specimens. Since the samples were exactly the same except for their size it is perhaps not surprising that the results were similar. However, this finding does indicate that once a sample becomes larger than 305 mm, there is not much to be gained by using a larger specimen.

Chapter 7. 150 mm Samples

As sample size decreases, the frequency range over which the electromagnetic properties can be measured decreases also. Once the sample size is less than the wavelength of the microwave signal, diffraction around the sample is high and the reflection is much reduced. In order to see the effects of a smaller sample on measurement the samples were cut to 150 mm square, which is the same size as the wavelength at 2 GHz.

Diffraction around such a small sample in configuration 1 is very high, as shown by Figure 7-1, with the magnitudes shown relative to the impeded transmission signal. A flat metal plate was used to measure the diffraction signal, and even with the horns in their closest position it is clear that diffraction is going to be a problem in permittivity extraction if it is not removed completely. In particular, the magnitude of the diffraction signal in the 1 – 18 GHz configuration will be larger than that through the sample for a number of the carbon loaded rubber materials at low frequencies.

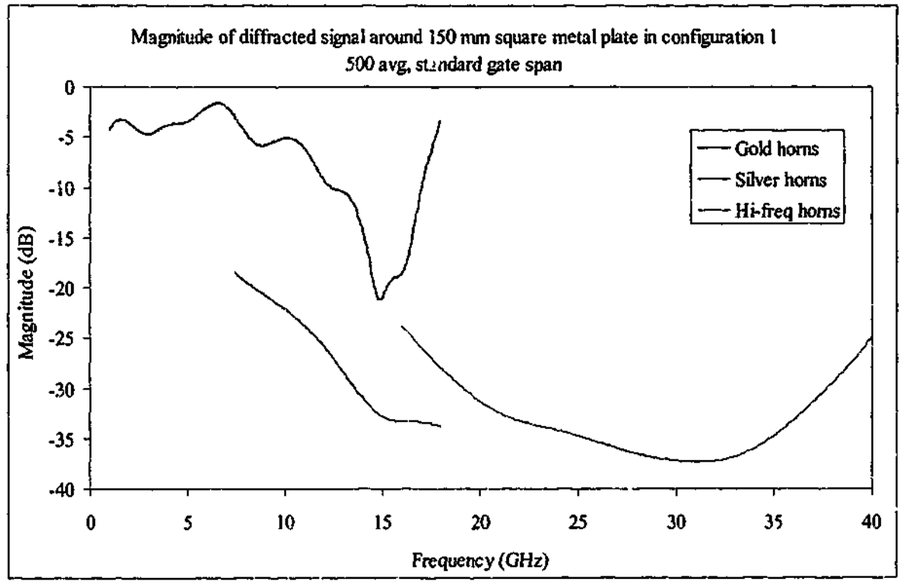

Figure 7-1. Magnitude of diffraction around 150 mm square metal sheet measured in configuration 1 with standard time gates

7.1. Perspex

7.1.1. 1 – 18 GHz

Because Perspex has such a low permittivity and loss tangent, it should be least affected by the diffracted signal. However, it also has a low reflection coefficient and the small size of the sample will reduce the reflection further. The values of permittivity extracted by the algorithms displayed in Figure 7-2 and Figure 7-3 show the effects of the reduced sample size. At frequencies above 3 GHz both the real and imaginary permittivity show good correlation to previous measurements. All the configurations give the average real permittivity at about 2.6, with the imaginary component near zero. However, below 3 GHz all the configurations start deviating away from the 2.6 mark and at the lowest frequency they are significantly different from the accepted value. One might expect this behaviour since the sample is similar to or smaller than the wavelength of the radiation. Nevertheless, despite the small sample size, the permittivity extracted from these measurements is very close to that expected for most of the frequency range. The average permeability across the range was measured at $1.00 + 0.002i$.

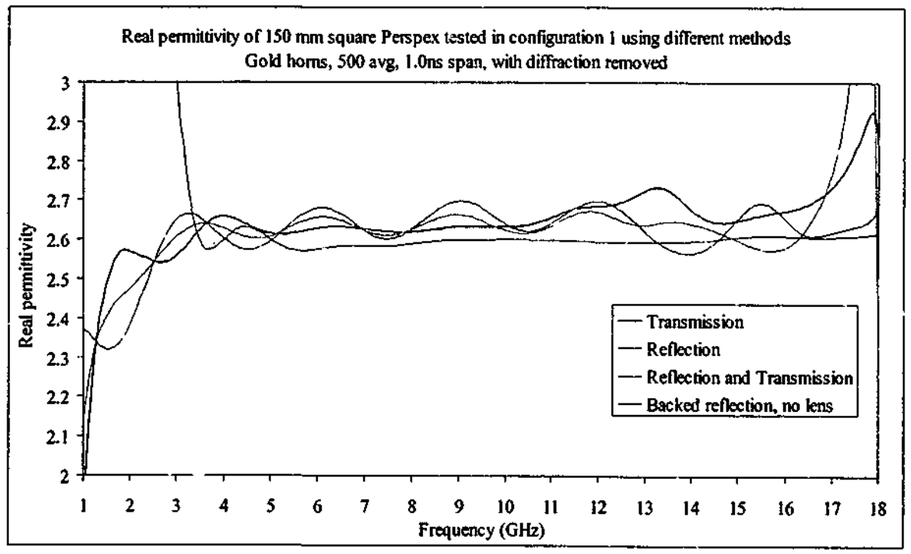

Figure 7-2. Real permittivity of Perspex measured with gold horns in free space using different methods with diffraction removed

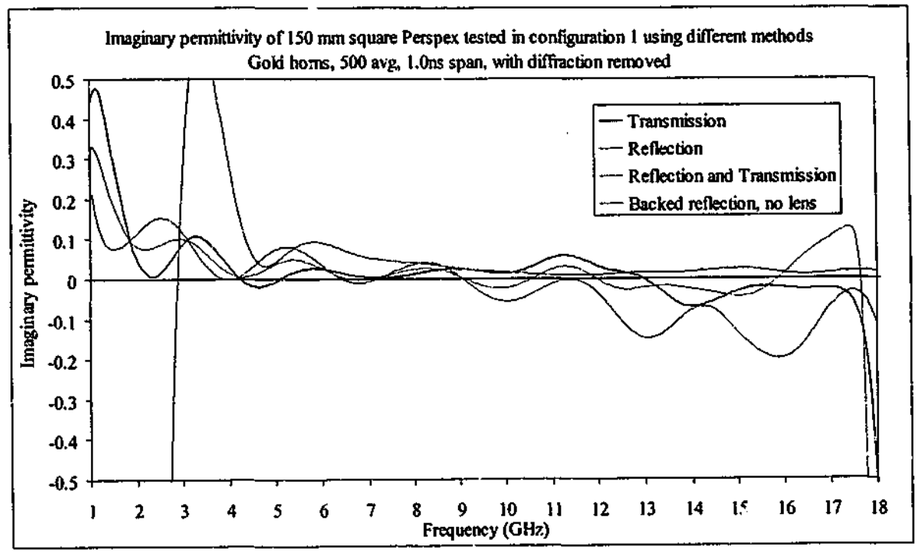

Figure 7-3. Imaginary permittivity of Perspex measured with gold horns in free space using different methods with diffraction removed

7.1.2. 7.5 – 18 GHz

The measurement with the high gain horns over the reduced frequency range shows very good performance for the small sample. Figure 7-4 and Figure 7-5 show that deviations from the accepted values are small, and noise levels are almost non-existent. Even though the sample is only about four times larger than the longest wavelength of the radiation, the techniques are able to measure the permittivity accurately at these frequencies. The average permeability across the range was $0.999 + 0.001i$.

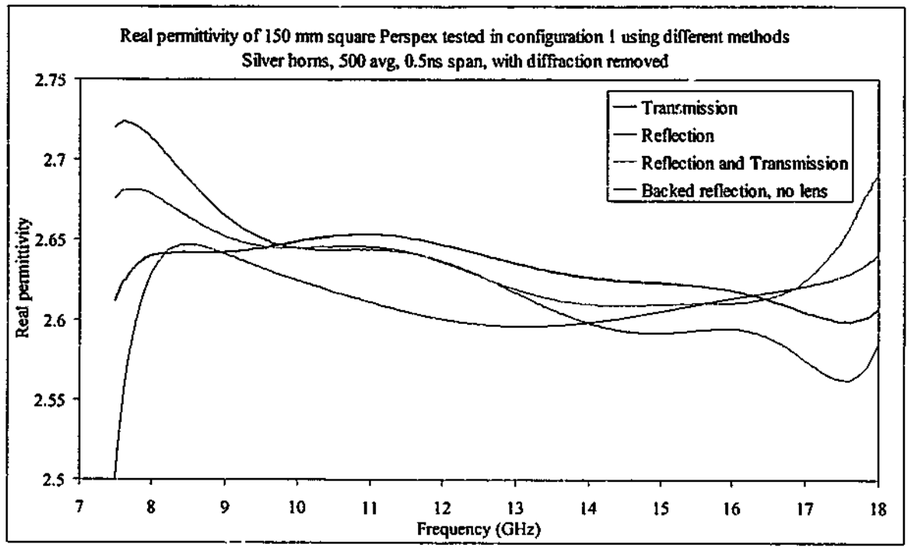

Figure 7-4. Real permittivity of Perspex measured with silver horns in free space using different methods with diffraction removed

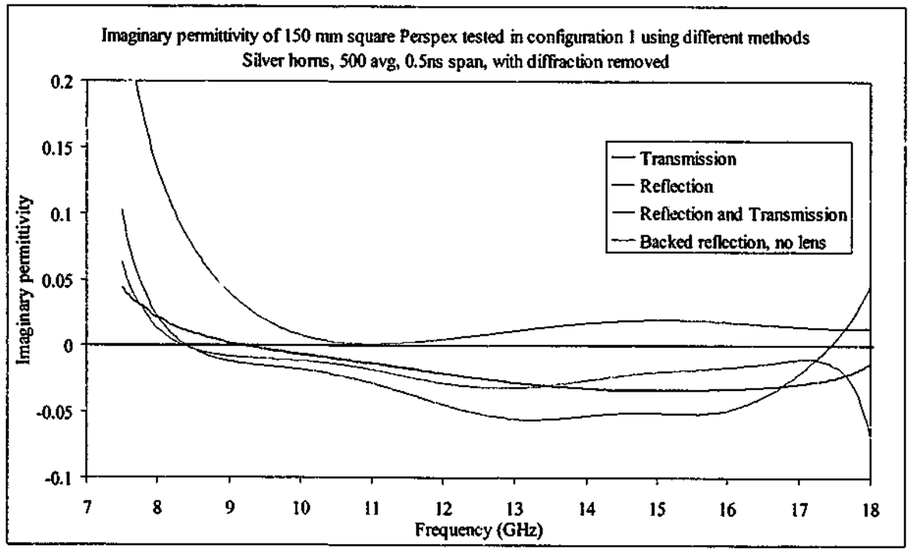

Figure 7-5. Imaginary permittivity of Perspex measured with silver horns in free space using different methods with diffraction removed

7.1.3. 16 – 40 GHz

Destructive interference conditions again dominate the high frequency region causing problems for the reflection/transmission algorithm. Figure 7-6 and Figure 7-7 show how the values obtained using both signals fluctuate near the destructive interference frequencies of 20.4 and 41 GHz. The values obtained from the reflection only measurement are also a little in error at the frequency extremes which may be an effect of the destructive interferences. The transmission and backed reflection values are very close to the expected values for Perspex. The average permeability across the range was $0.998 + 0.006i$.

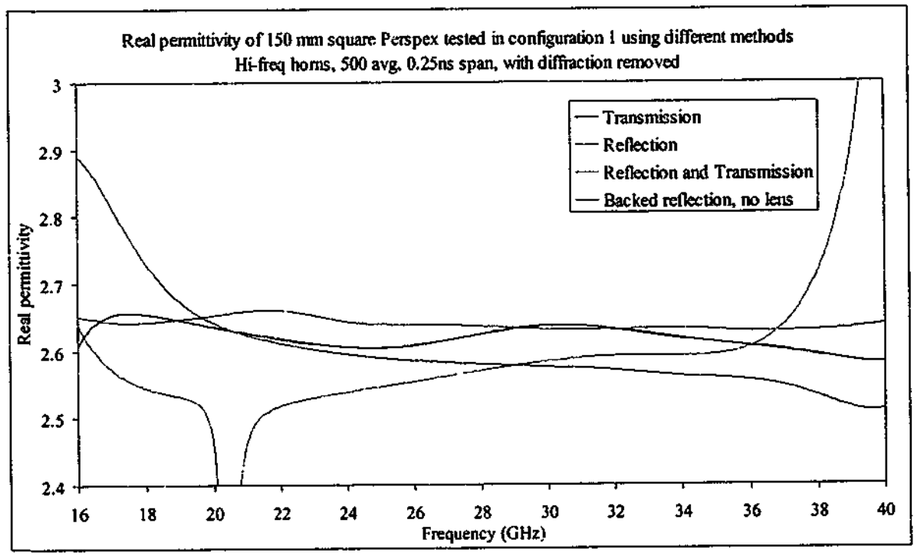

Figure 7-6. Real permittivity of Perspex measured with hi-freq horns in free space using different methods with diffraction removed

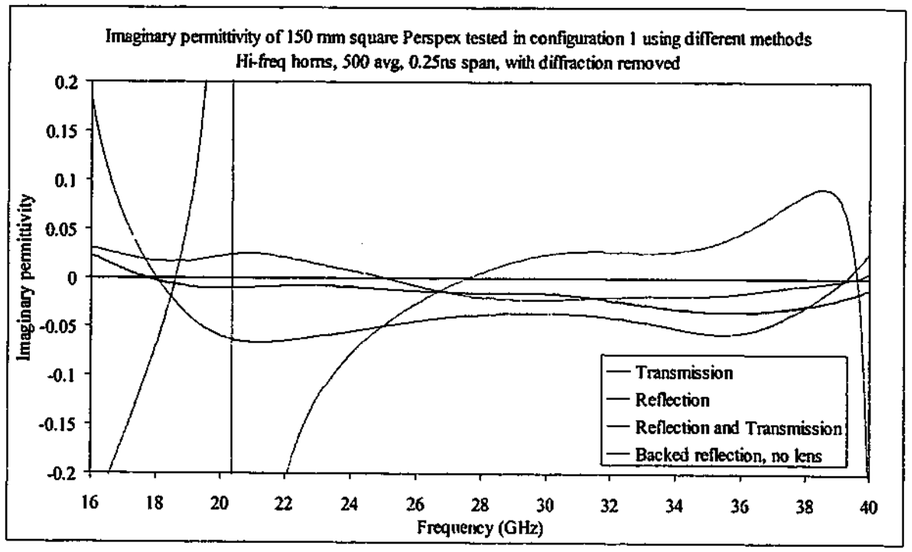

Figure 7-7. Imaginary permittivity of Perspex measured with hi-freq horns in free space using different methods with diffraction removed

7.2. Carbon loaded rubber

7.2.1. Sample B, 1 – 18 GHz

The calculated permittivity of the moderately lossy sample B is consistent across the reflection and transmission techniques, as seen in Figure 7-8 and Figure 7-9. At the frequency extremes the values start to move away from those expected, but this may be as much to do with the time gating as the small sample size. The backed reflection results are again significantly different, and the algorithm does not converge to a realistic solution below about 6 GHz. The average permeability across the range was $0.996 + 0.003i$.

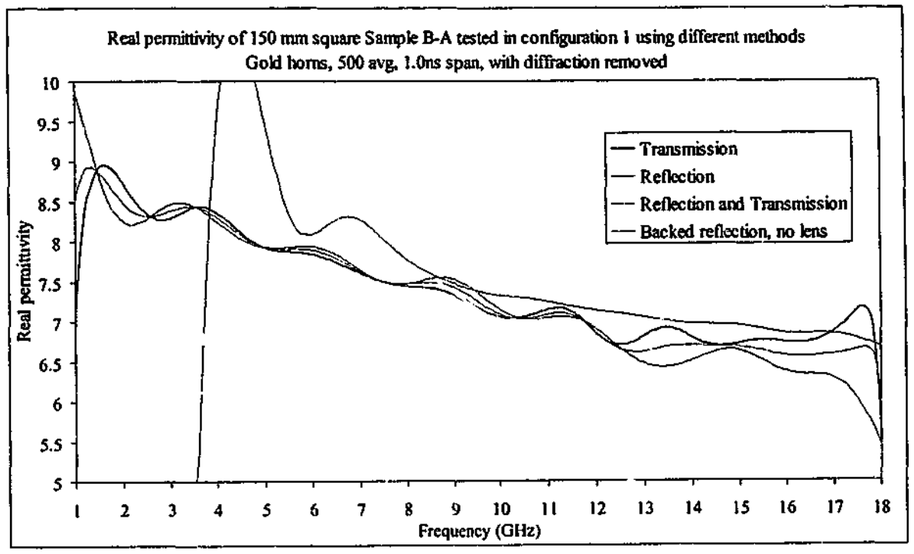

Figure 7-8. Real permittivity of Sample B measured with gold horns in free space using different methods with diffraction removed

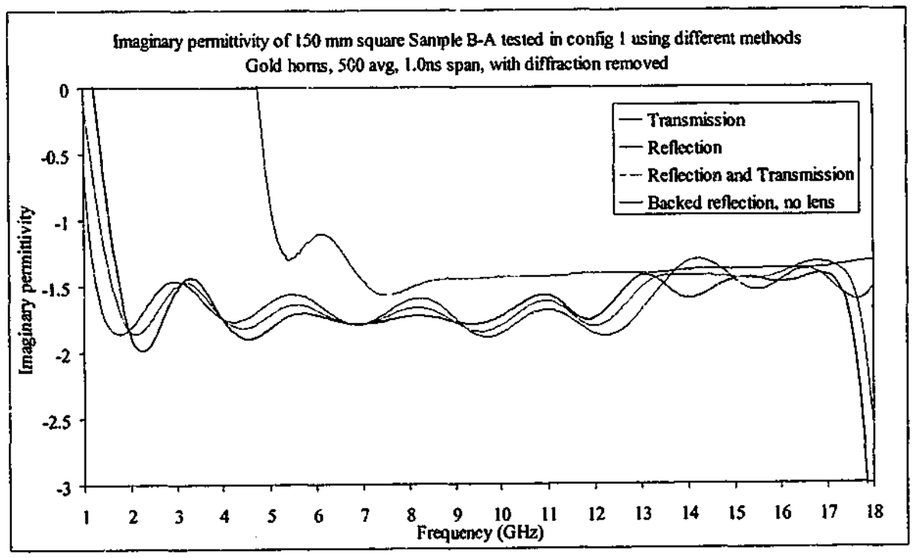

Figure 7-9. Imaginary permittivity of Sample B measured with gold horns in free space using different methods with diffraction removed

7.2.2. Sample B, 7.5-18 GHz

The reflection and transmission results over the reduced frequency span are very close to each other, with only a minor shift in the real values, and small deviations in the imaginary permittivity. The results are shown in Figure 7-10 and Figure 7-11.The backed reflection technique again shows the largest deviations from the other results, especially in the imaginary values. The technique again gives reduced values for the imaginary permittivity even though the real values are not too different from the other results. The average permeability across the range was calculated to be $0.996 + 0.024i$.

7.2.3. Sample B, 16 – 40 GHz

The presence of the destructive interference peak at about 28 GHz has an effect on the permittivity extraction for the reflection and reflection/transmission techniques. The permittivity values seen in Figure 7-12 and Figure 7-13 show that the transmission and backed reflection techniques give very similar results, while the reflection/transmission technique shows a customary reduction in real permittivity near the destructive interference point and the reflection technique shows errors near 30 GHz. The average permeability across the range was $1.003 + 0.002i$.

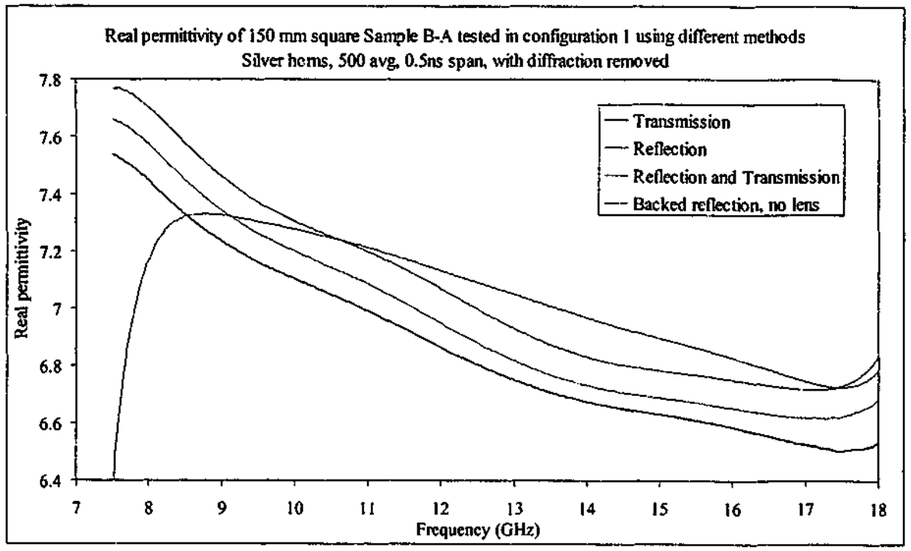

Figure 7-10. Real permittivity of Sample B measured with silver horns in free space using different methods with diffraction removed

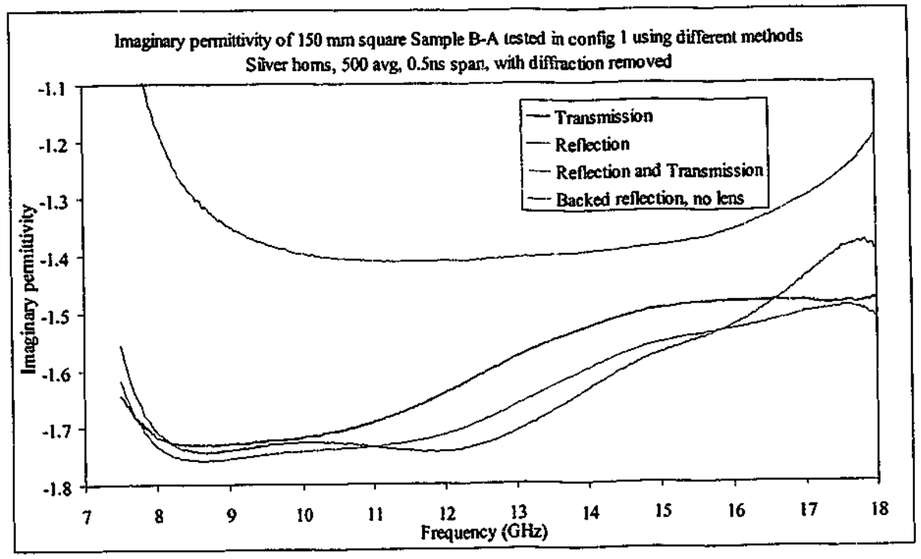

Figure 7-11. Imaginary permittivity of Sample B measured with silver horns in free space using different methods with diffraction removed

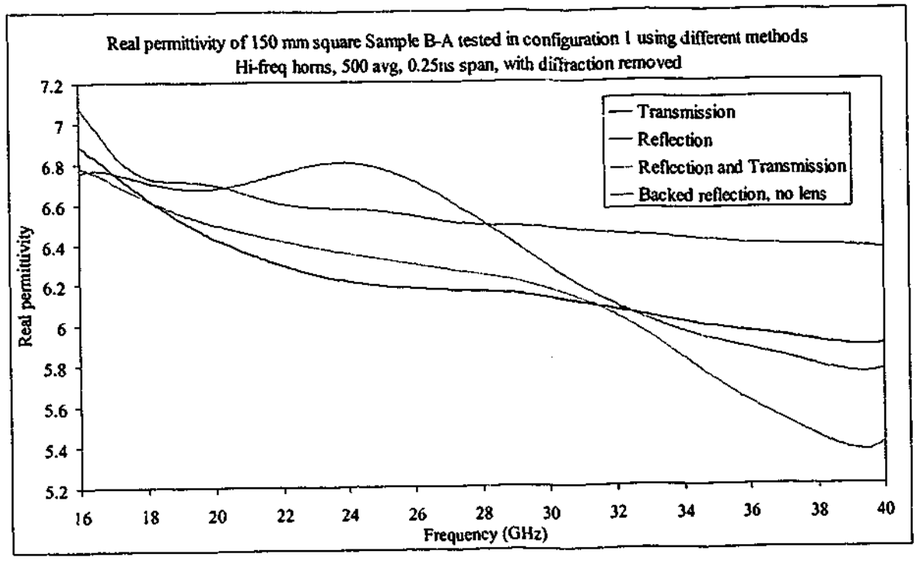

Figure 7-12. Real permittivity of Sample B measured with hi-freq horns in free space using different methods with diffraction removed

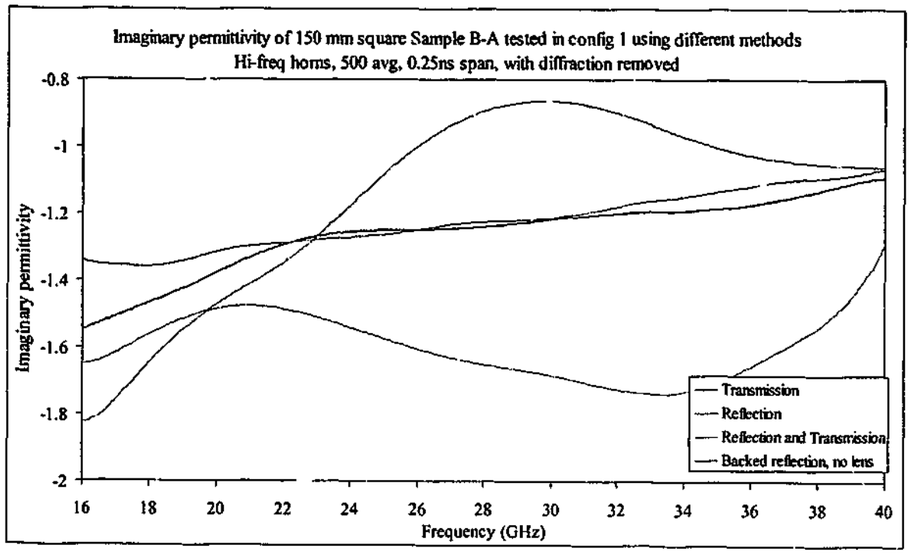

Figure 7-13. Imaginary permittivity of Sample B measured with hi-freq horns in free space using different methods with diffraction removed

7.2.4. Sample E, 1 – 18 GHz

With a low transmission magnitude and the high level of diffraction for such a small sample, we might expect the transmission algorithm to have problems in obtaining the correct values for Sample E. When examining Figure 7-14 and Figure 7-15 and comparing them to the graphs from the 445 mm square sample, we find that both the transmission and reflection techniques give a higher value for real permittivity than the larger sample at frequencies below about 6 GHz. The imaginary permittivity values are reasonably close to the larger sample down to about 2 GHz, before levelling off with values near –160 at 1 GHz. For comparison the 445 mm square sample had an imaginary permittivity of –380 at 1 GHz.

The values from the backed reflection technique match the other techniques above 6 GHz, but at frequencies below that the solution is markedly different. The average permeability measured for this sample was $0.998 + 0.020i$, and interestingly only deviated from $1 + 0i$ below about 2 GHz.

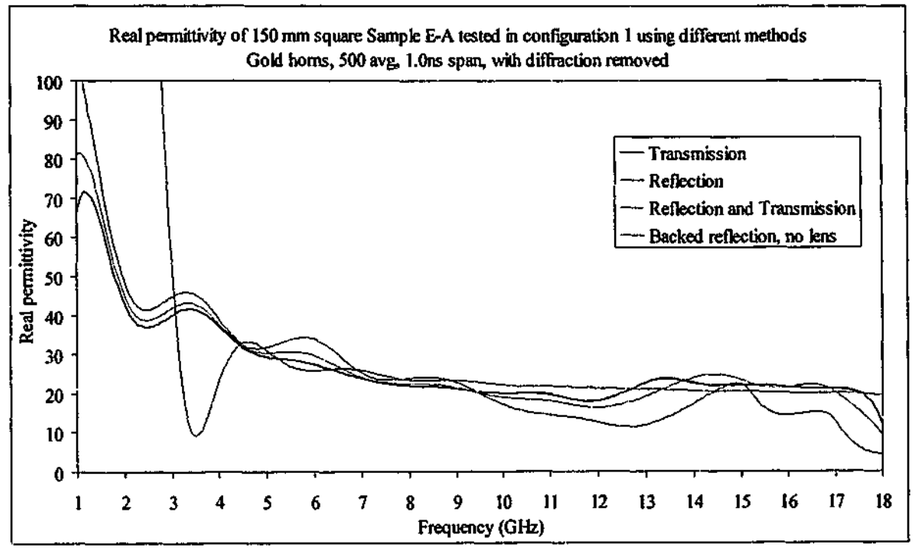

Figure 7-14. Real permittivity of Sample E measured with gold horns in free space using different methods with diffraction removed

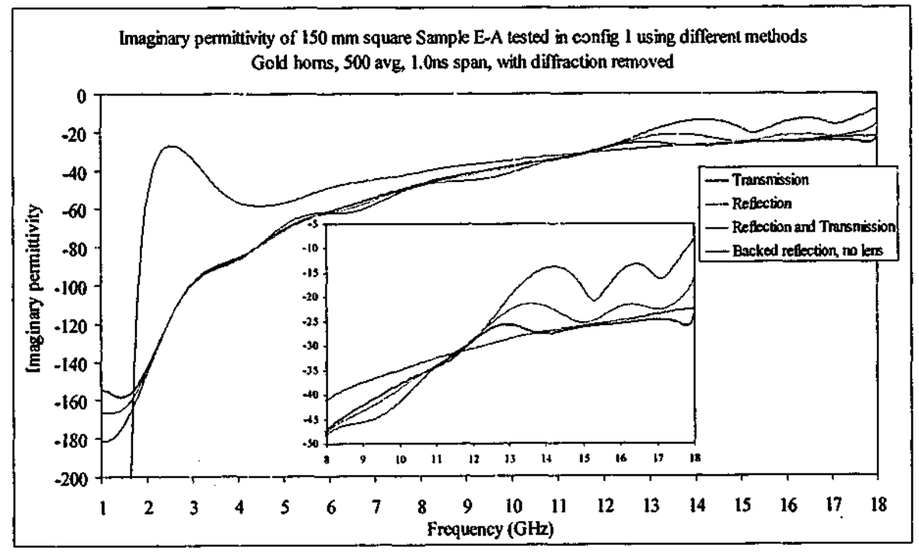

Figure 7-15. Imaginary permittivity of Sample E measured with gold horns in free space using different methods with diffraction removed

7.2.5. Sample E, 7.5 – 18 GHz

Measurements with the higher gain horns over the reduced frequency range again give a less cluttered permittivity spectrum, as can be seen in Figure 7-16 and Figure 7-17. The

transmission, reflection/transmission and backed reflection results all give very similar solutions in both real and imaginary permittivity, with the reflection result a little different across the range. There is little evidence in the raw data to suggest why the behaviour seen in the reflection data should occur, given the fact that the reflection/transmission algorithm gives permittivity values close to the transmission only result. The average permeability is 1.01 + 0.009*i*, indicating that the actual measured data is not too much in error, but that the reflection only algorithm is not as robust as it could be.

7.2.6. Sample E, 16 – 40 GHz

The problems with the reflection only algorithm continue with the 16 – 40 GHz data, as seen in Figure 7-18 and Figure 7-19. It was the only technique to show significant deviation from the other results. The average permeability across the high frequency range was 1.00 + 0.108*i*.

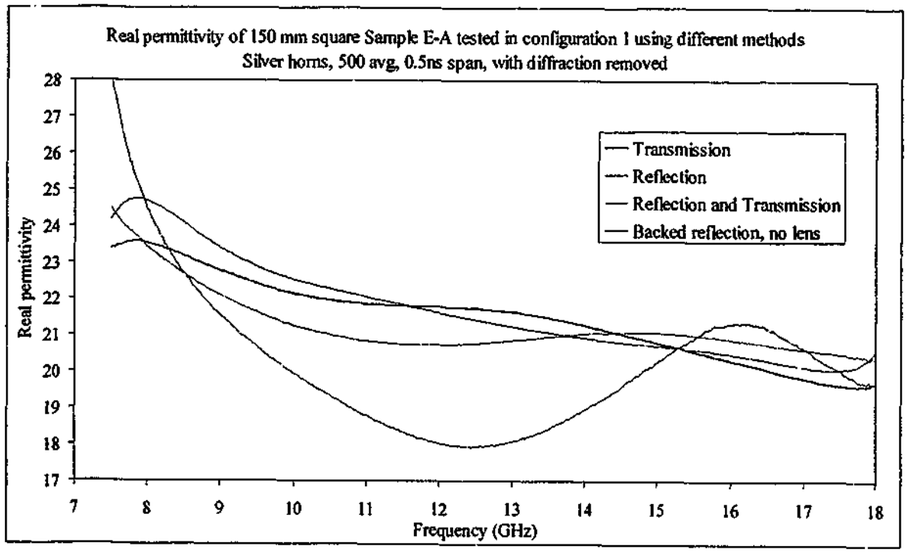

Figure 7-16. Real permittivity of Sample E measured with silver horns in free space using different methods with diffraction removed

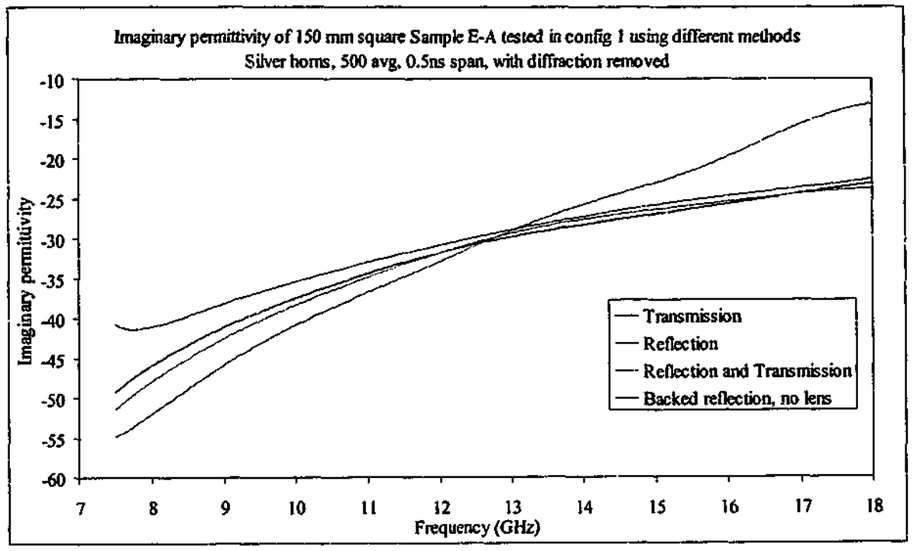

Figure 7-17. Imaginary permittivity of Sample E measured with silver horns in free space using different methods with diffraction removed

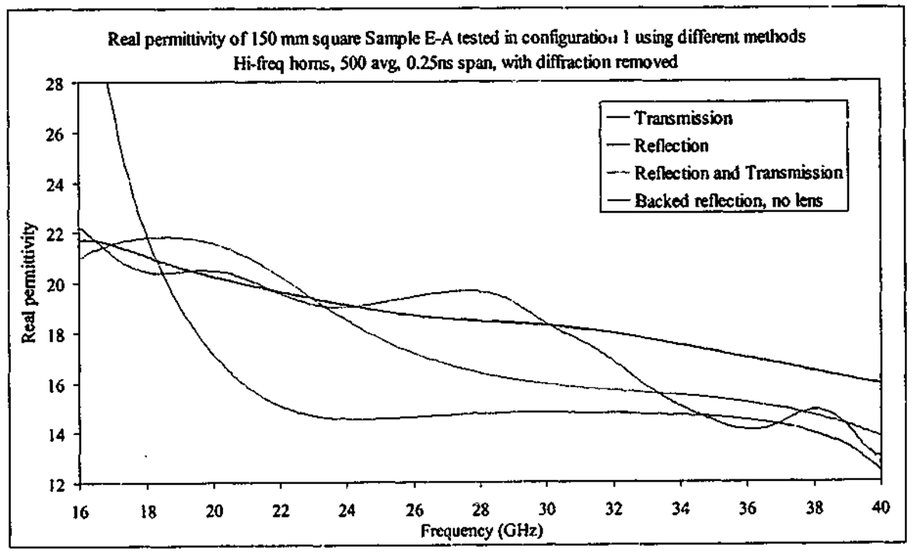

Figure 7-18. Real permittivity of Sample E measured with hi-freq horns in free space using different methods with diffraction removed

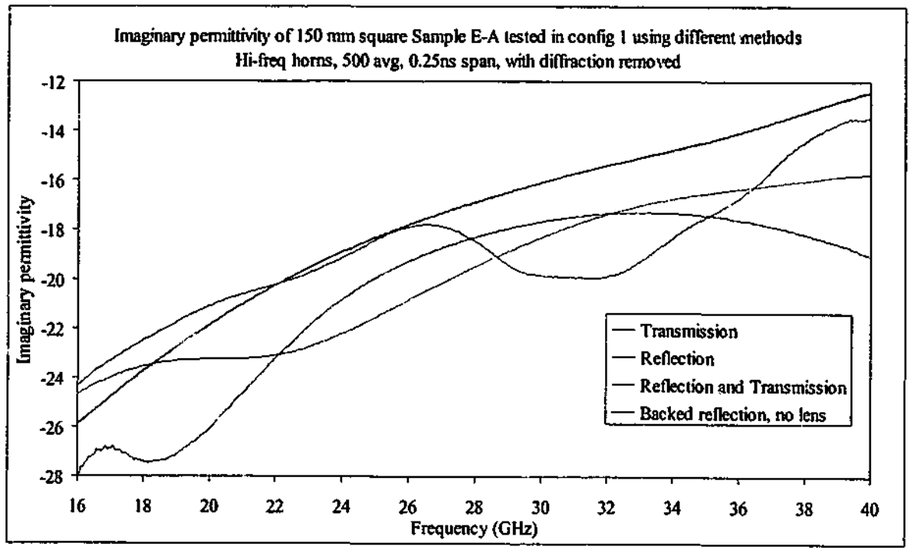

Figure 7-19. Imaginary permittivity of Sample E measured with hi-freq horns in free space using different methods with diffraction removed

It is difficult to ascertain measurement accuracy in isolation, so this section shows all the carbon loaded rubber samples on the same set of axes over a fixed frequency range. Since the effects are similar across each frequency band, only the results over the 7.5 – 18 GHz range are shown since that was deemed to be representative of all three frequency ranges.

7.2.7. All samples, transmission only

The transmission only results have usually been the most reliable of the four different techniques so we will consider them first. Over the 7.5 – 18 GHz range the diffraction is considerable without being excessive, so the diffraction removal technique is effective and leads to accurate measurements with low noise. Observing the graphs shown in Figure 7-20 and Figure 7-21 we see that the values are very close to those measured with the 445 mm square samples (see Figure 5-53 and Figure 5-54) with some small variations that could be caused by some sample inhomogeneity. There is certainly nothing shown in the graphs that immediately gives cause for any concern about the measurement accuracy.

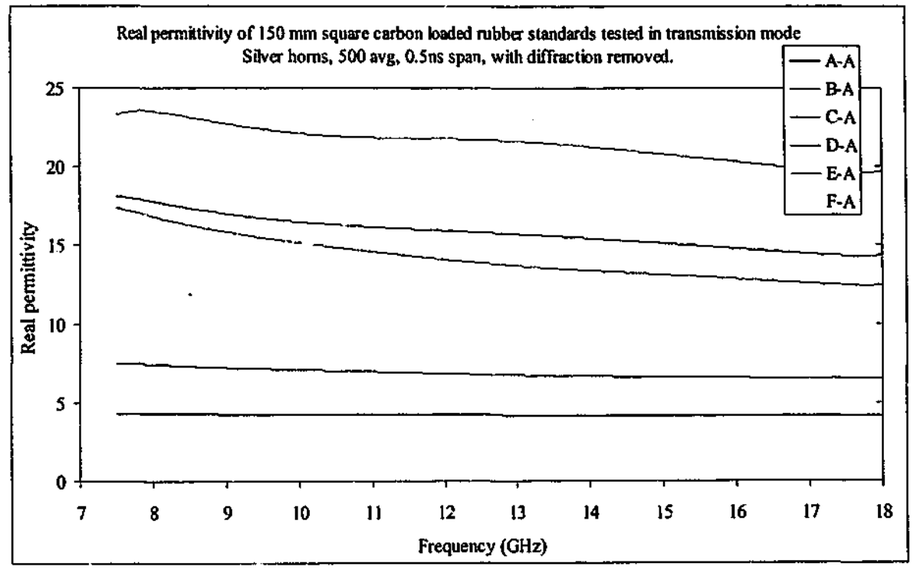

Figure 7-20. Real permittivity of carbon loaded rubber samples measured with silver horns in free space using transmission only method with diffraction removed

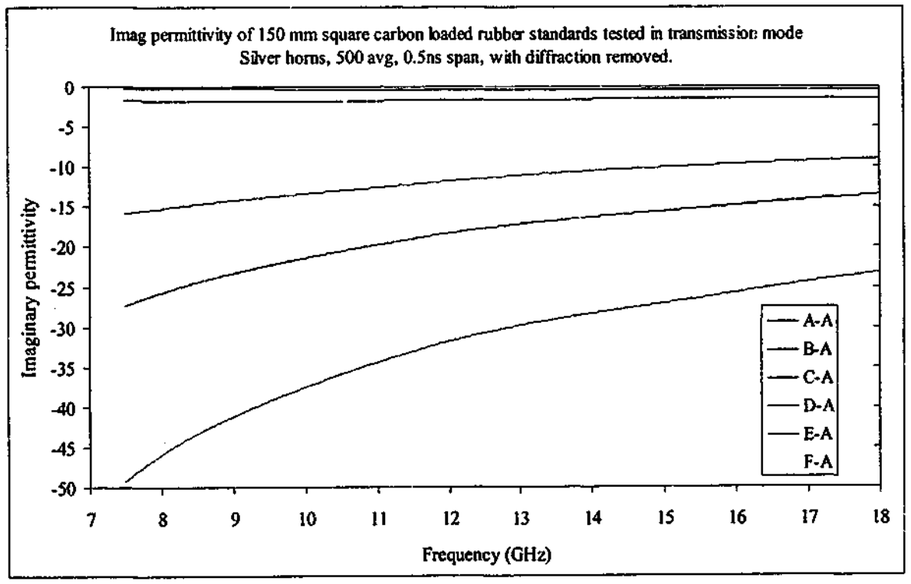

Figure 7-21. Imaginary permittivity of carbon loaded rubber samples measured with silver horns in free space using transmission only method with diffraction removed

7.2.8. All samples, reflection only

The reflection only technique is generally the least reliable of the methods used in this study, and initially it was thought that reducing the size of the samples might have had a favourable effect on the permittivity measurements. In fact this was found not to be the case, and the results from the 150 mm samples are similar to if not worse than those of the larger samples, especially as the permittivity of the samples increase. The results for all the carbon loaded rubber samples using the reflection only technique are shown in Figure 7-22 and Figure 7-23. The real permittivity values of the three lowest permittivity materials match the results for the large samples, but as permittivity increases, the results move further from the expected curves. The results from the thick, high permittivity sample F show little resemblance to the transmission only results in both real and imaginary values. Sample E also has problems in both real and especially imaginary permittivity, crossing over the curve of sample D at high frequencies. The reflection only technique is especially sensitive to small errors if the sample thickness used in the algorithm is incorrect, as will be shown in Chapter 11.

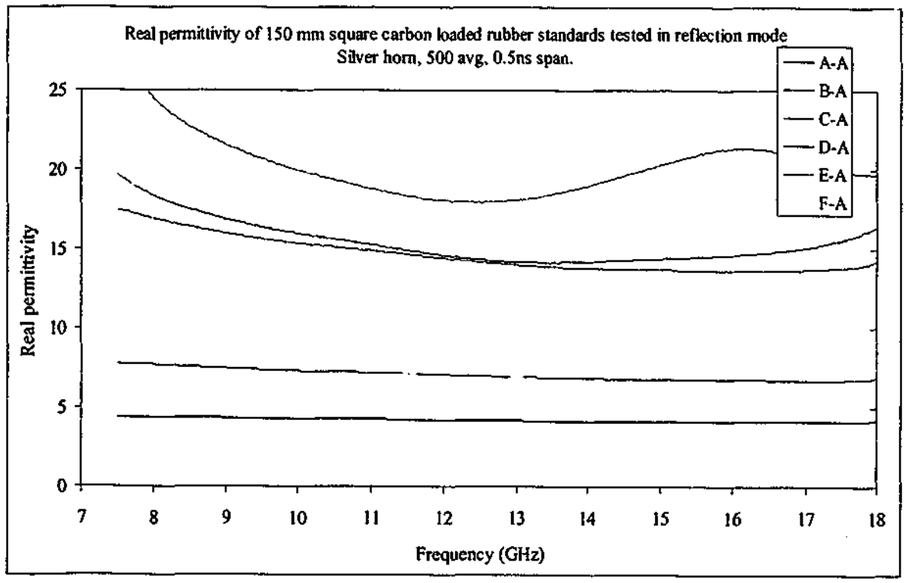

Figure 7-22. Real permittivity of carbon loaded rubber samples measured with silver horn in free space using reflection only method

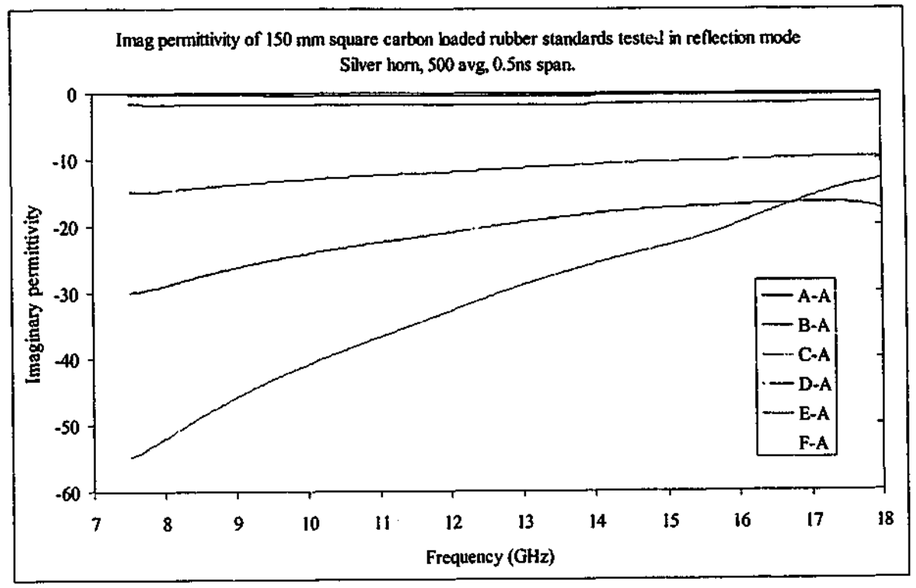

Figure 7-23. Imaginary permittivity of carbon loaded rubber samples measured with silver horn in free space using reflection only method

7.2.9. All samples, reflection/transmission technique

Combining the dubious reflection data and the more reliable transmission data gives a result that shows small errors in the permittivity and permeability values but not as excessive as for the reflection only result. The permittivity results shown in Figure 7-24 and Figure 7-25 are plausible, with the only concern being that the real permittivity of sample C and D seem a little close together, although the imaginary permittivities calculated appear correct.

The permeability values shown in Figure 7-26 and Figure 7-27 are also reasonable, with real permeability close to the accepted value of unity and the imaginary value near zero. This result may be a little unexpected considering the errors observed in the permittivity extracted from the reflection only results, but even using this rough data the error level can be estimated as less than 10%, usually better than 5%.

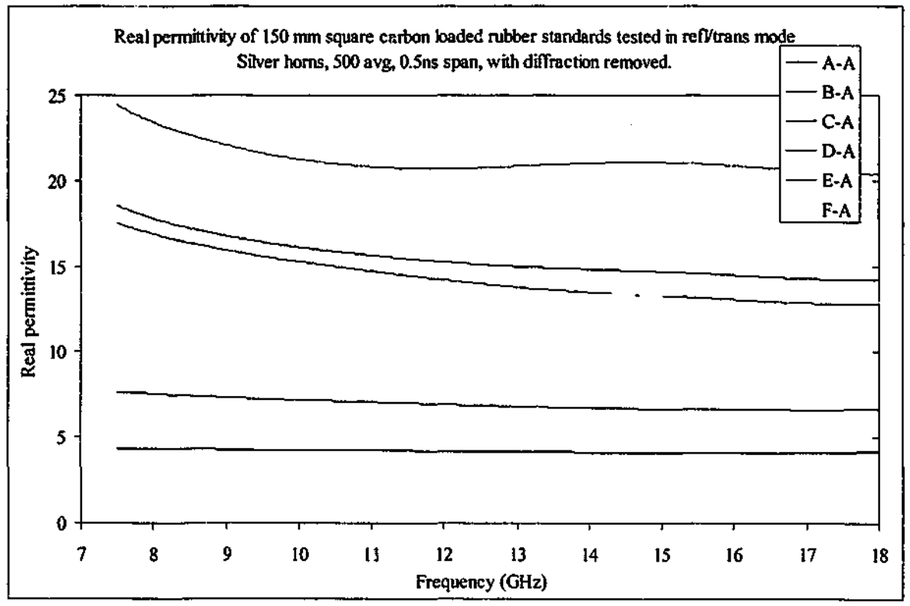

Figure 7-24. Real permittivity of carbon loaded rubber samples measured with silver horns in free space using reflection/transmission method with diffraction removed

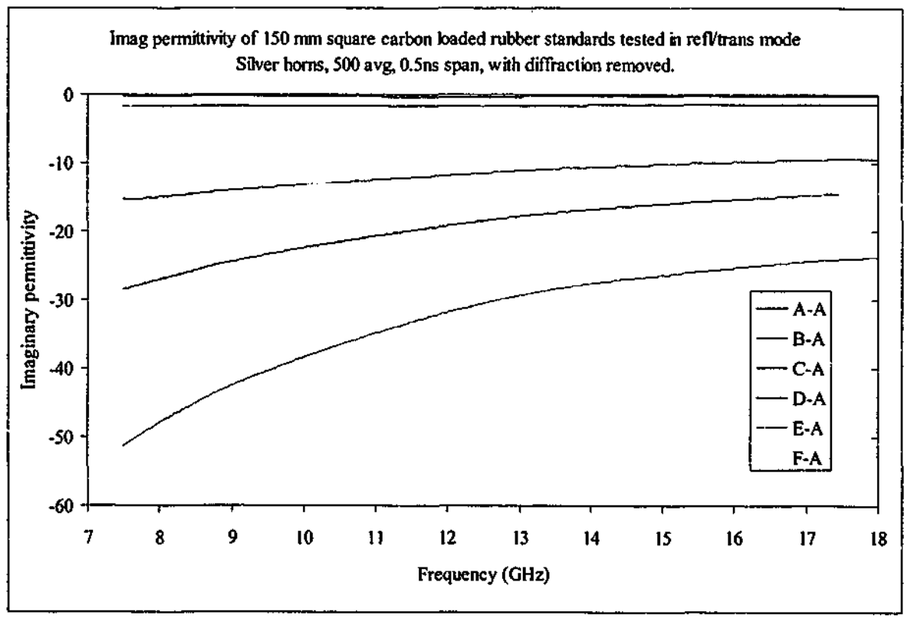

Figure 7-25. Imaginary permittivity of carbon loaded rubber samples measured with silver horns in free space using reflection/transmission method with diffraction removed

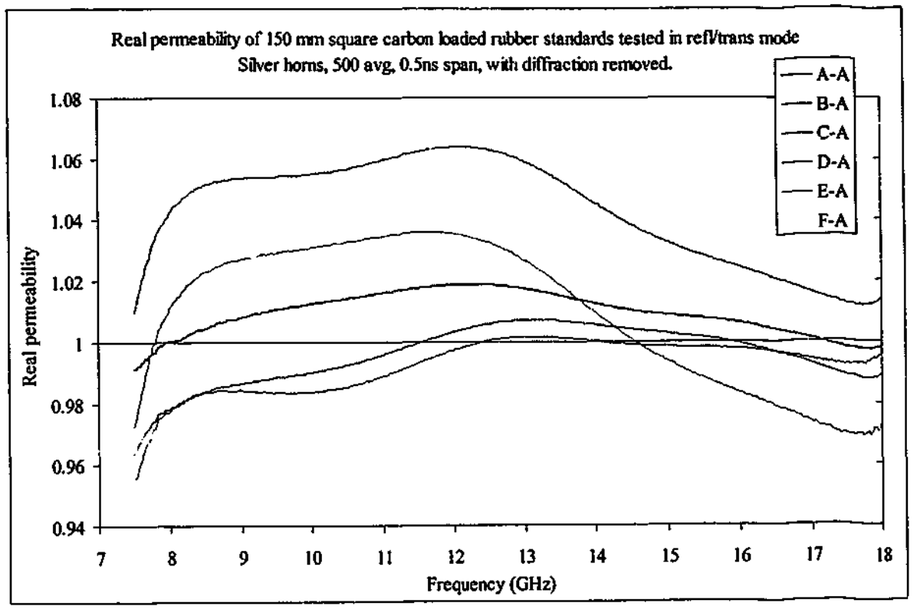

Figure 7-26. Real permeability of carbon loaded rubber samples measured with silver horns in free space using reflection/transmission method with diffraction removed

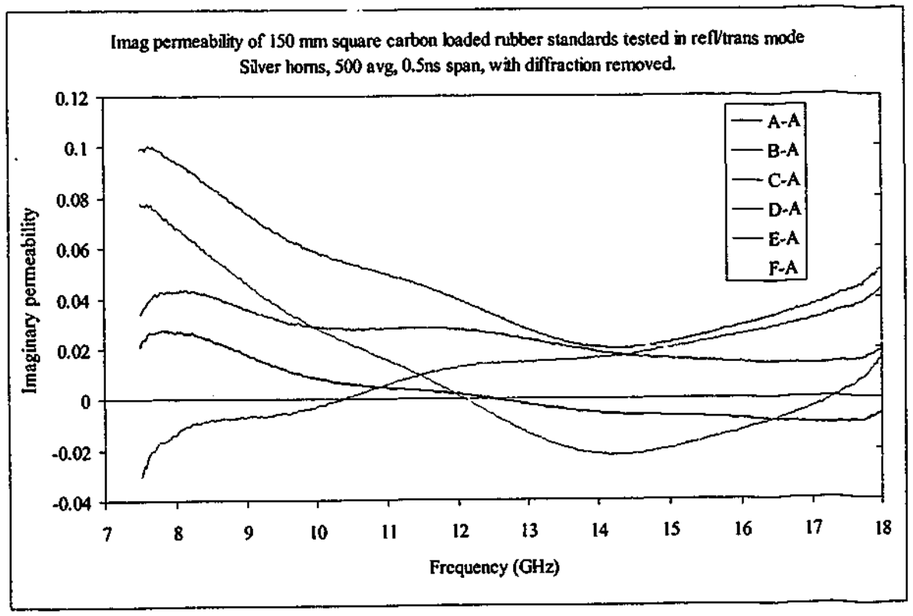

Figure 7-27. Imaginary permeability of carbon loaded rubber samples measured with silver horns in free space using reflection/transmission method with diffraction removed

7.2.10. All samples, backed reflection technique

In contrast to the unbacked reflection technique, the permittivity results from highly loaded samples do not "cross over" those of materials with lower permittivity when using the backed reflection technique. The curves seen in Figure 7-28 and Figure 7-29 show the permittivity increasing regularly with carbon concentration, and the actual values almost match those of other techniques. The reason why the backed reflection technique does not match exactly is not fully understood at this stage, but edge effects and imperfect reflection from the backing plate may be to blame. Another explanation involves the slight variation in thickness of the specimens tested. It is known that the specimens are not perfectly flat, and the alignment of the front layer is critical is determining the direction and phase of the reflected signal.

When the unbacked reflection signal is used to calculate permittivity, it was observed that the position of the front face needed to be exactly on the calibration plane in order to obtain the correct result. Since the backed reflection technique fixes the back of the sample (rather than the front as in the unbacked reflection technique), slight changes in thickness will affect the position of the front of the sheet. The resulting phase shift could easily account for the differences observed.

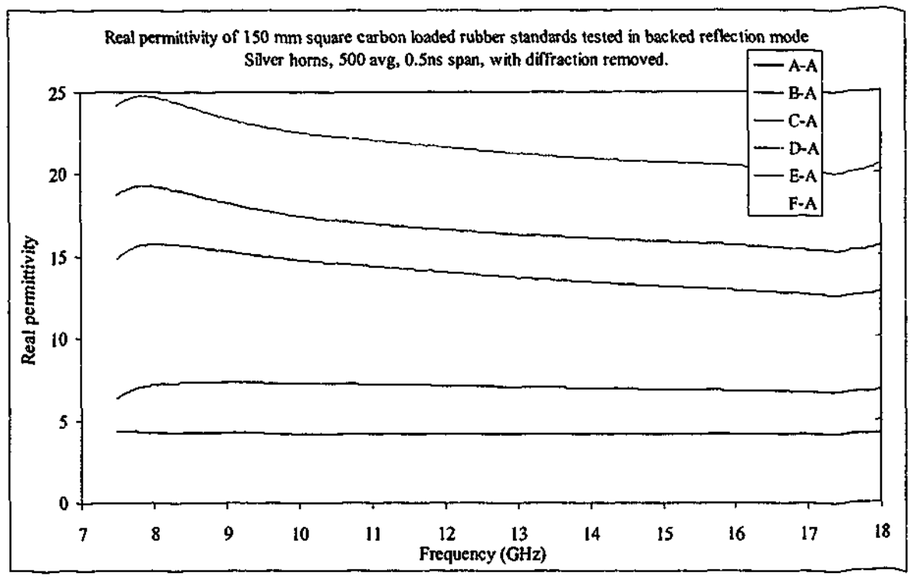

Figure 7-28. Real permeability of carbon loaded rubber samples measured with silver horns in free space using backed reflection method

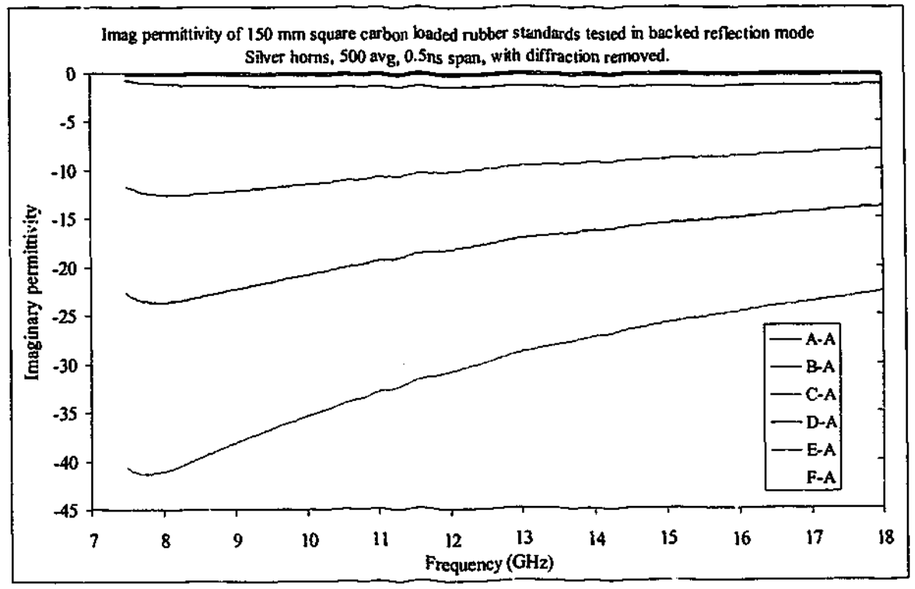

Figure 7-29. Imaginary permeability of carbon loaded rubber samples measured with silver horns in free space using backed reflection method

7.3. Carbonyl iron loaded PU

Since the properties of the magnetic sample G can only be calculated using both reflection and transmission signals, all three frequency ranges will be shown on the one set of axes. The physical attributes are similar to the carbon loaded rubber samples, and so the same phase shift for reflection is applied for this specimen as was for samples A to F. The permittivity values are shown in Figure 7-30 and Figure 7-31, and it can be seen that the traces are not as smooth as they were for the large 445 mm sample. The frequency extremes in the 1 – 18 GHz range show large errors, and the imaginary permittivity above 28 GHz crosses the frequency axis and becomes slightly positive. This behaviour was also observed in the 445 mm square sample, but in general the permittivity curves were smoother for the larger sample.

The permeability curves of Figure 7-32 and Figure 7-33 show the same trend of increased jitter across the frequency range and errors at frequency extremes, but generally the values are quite similar to those of the large sample.

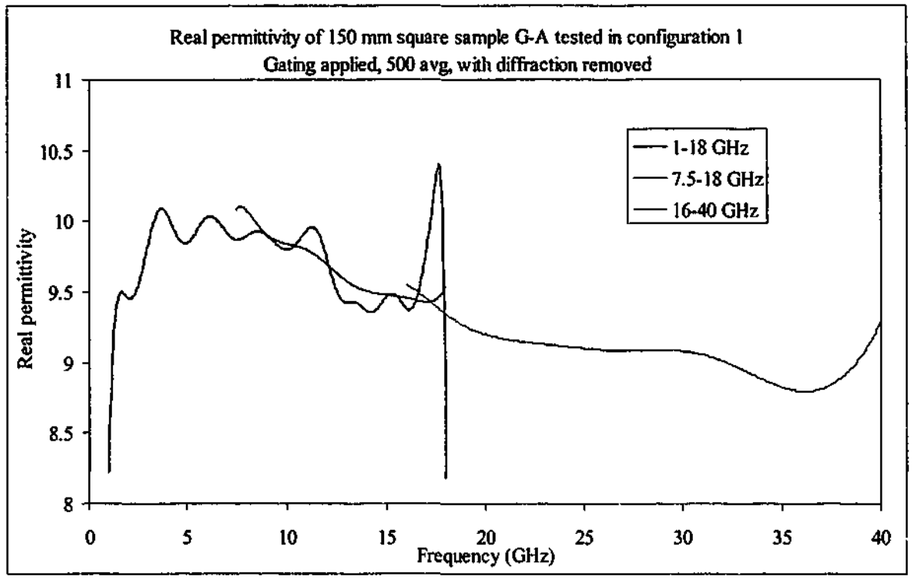

Figure 7-30. Real permittivity of Sample G measured in free space using reflection/transmission method with diffraction removed

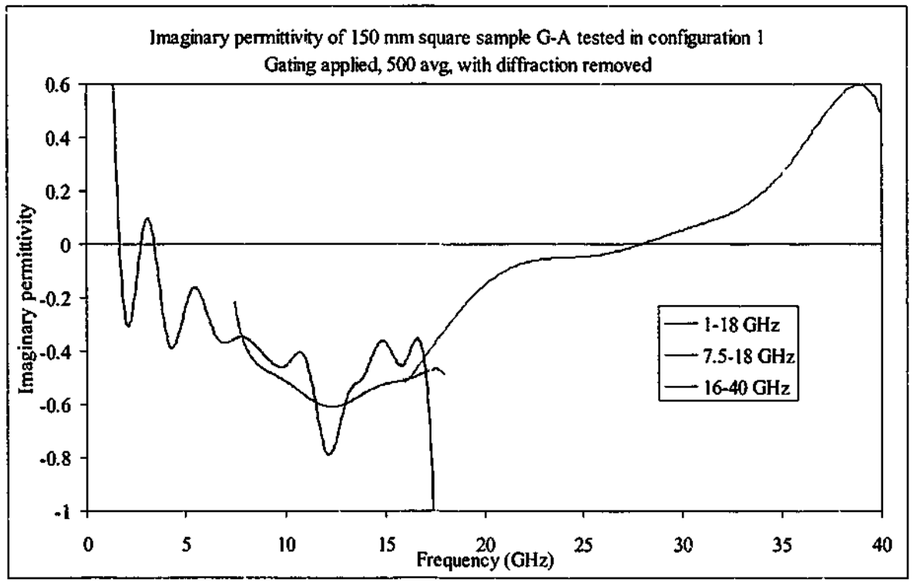

Figure 7-31. Imaginary permittivity of Sample G measured in free space using reflection/transmission method with diffraction removed

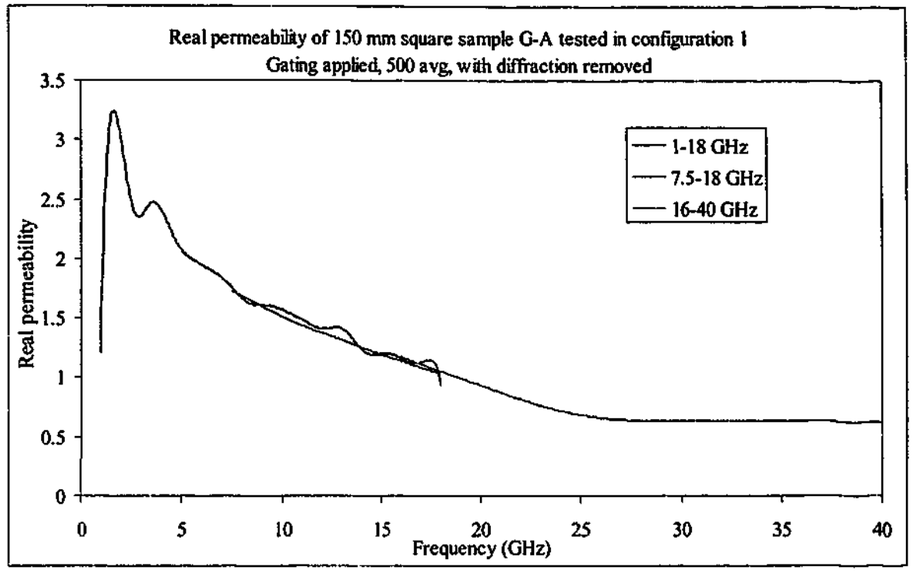

Figure 7-32. Real permeability of Sample G measured in free space using reflection/transmission method with diffraction removed

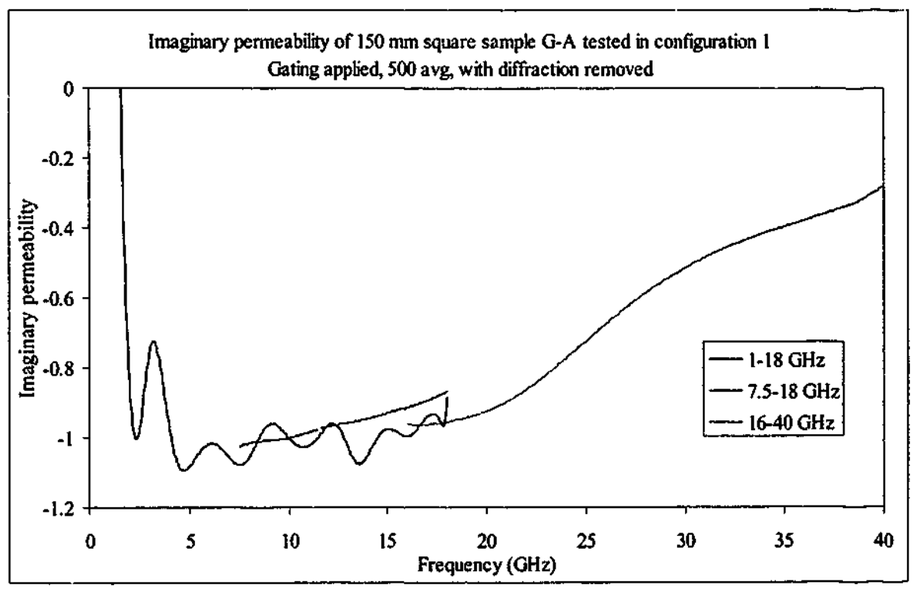

Figure 7-33. Imaginary permeability of Sample G measured in free space using reflection/transmission method with diffraction removed

7.4. Composite sample

7.4.1. 1-18 GHz

The 150 mm square composite sample shows lower permittivity values than the larger specimens below 3 GHz. This behaviour is similar to that seen in the carbon loaded rubber samples and is probably not surprising considering the wavelength of the radiation is similar to or greater than the size of the sample at these frequencies. This reduction has exaggerated the resonance effect, as shown in Figure 7-34 and Figure 7-35. The data fitted has parameters of $\varepsilon_0 = 46.00$, $\varepsilon_\infty = 0.773$ and $\tau = 48.36$ ps, corresponding to a resonance at about 3.29 GHz. Comparing these figures to those obtained for the larger samples we see that both ε_0 and ε_∞ are significantly less than previously measured, and this result is skewing the resonance frequency to a higher value than seen earlier. At higher frequencies, however, the values obtained are very similar to those measured earlier. The backed reflection method again shows difficulty in obtaining the correct values below about 7 GHz, and the reflection technique shows slightly more noise at higher frequencies. The average permeability was calculated at $0.990 - 0.015i$.

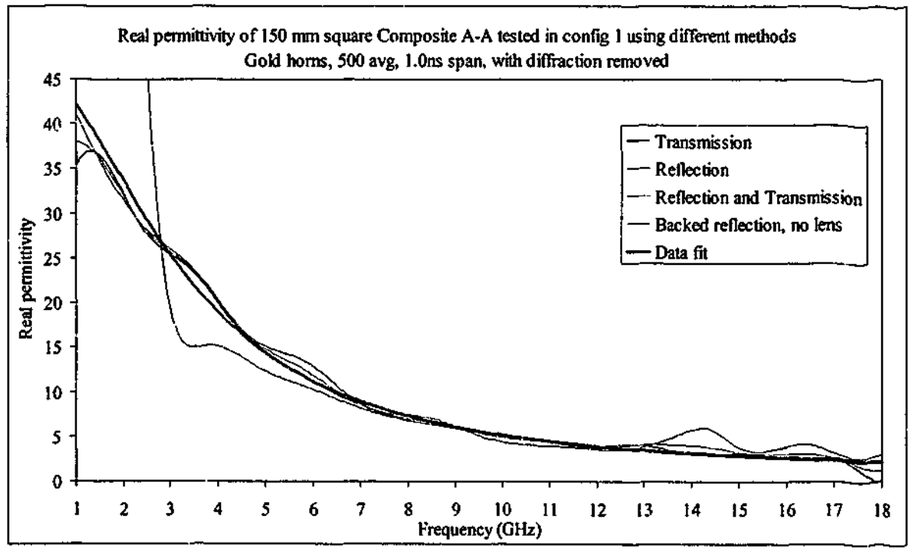

Figure 7-34. Real permittivity of Composite sample measured with gold horns in free space using different methods with diffraction removed

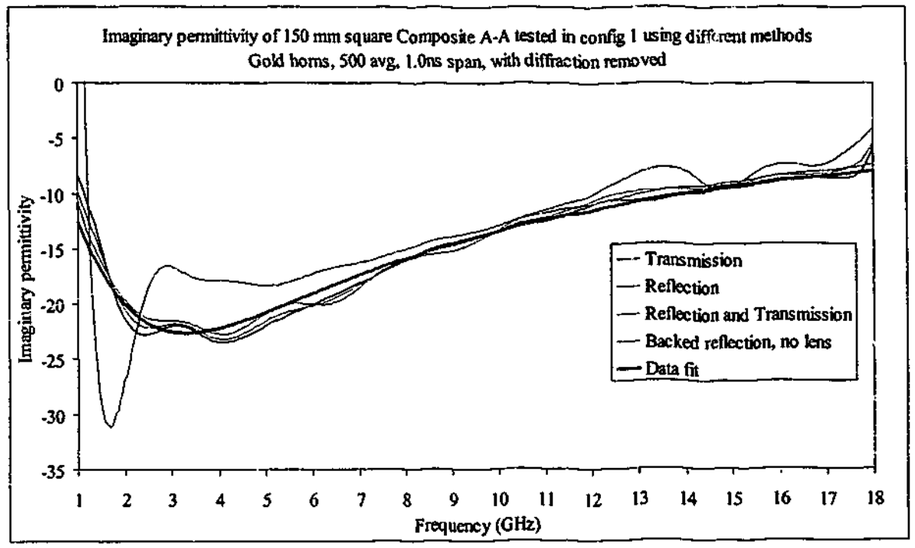

Figure 7-35. Imaginary permittivity of Composite sample measured with gold horns in free space using different methods with diffraction removed

7.4.2. 7.5 – 18 GHz

Over the reduced frequency range the results are much less noisy than the 1 – 18 GHz range, with values for the 150 mm sample almost exactly the same as the larger versions. Reflection values again show some errors at high frequencies, but in the main all the techniques show similar values, as seen in Figure 7-36 and Figure 7-37. The average permeability for this sample was $0.989 - 0.004i$.

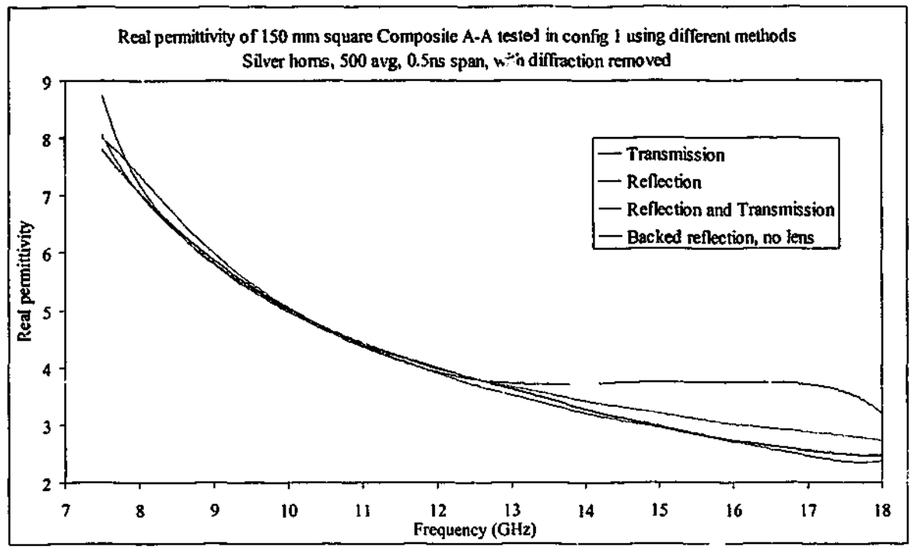

Figure 7-36. Real permittivity of Composite sample measured with silver horns in free space using different methods with diffraction removed

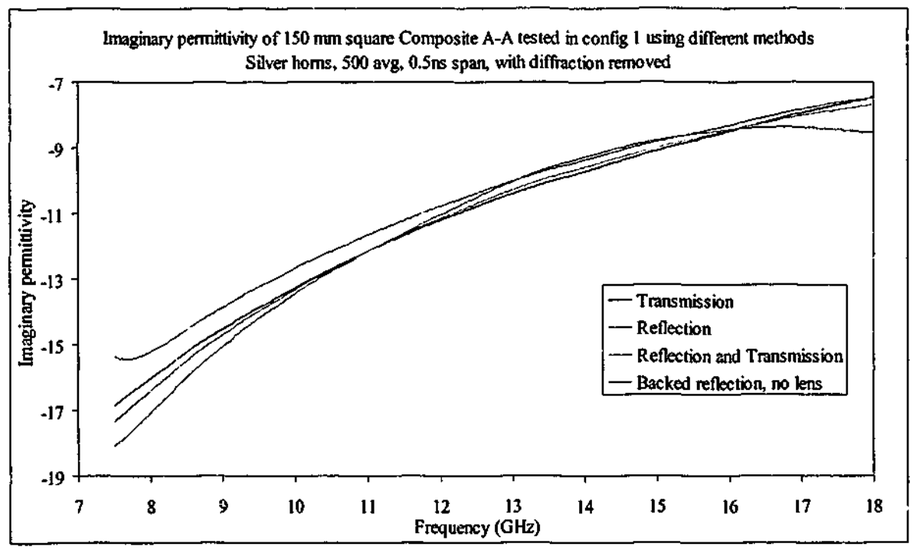

Figure 7-37. Imaginary permittivity of Composite sample measured with silver horns in free space using different methods with diffraction removed

7.4.3. 16 – 40 GHz

The high frequency result continues the trend observed in the high gain 7.5 – 18 GHz horns of consistent property evaluation across the different techniques. As can be in Figure 7-38 and Figure 7-39, all four methods give very similar values for both real and imaginary permittivity across the full frequency range. The reflection only technique again shows a little more structure across the frequency range, but only to a small degree. The average permeability across the range was $0.991 + 0.01i$.

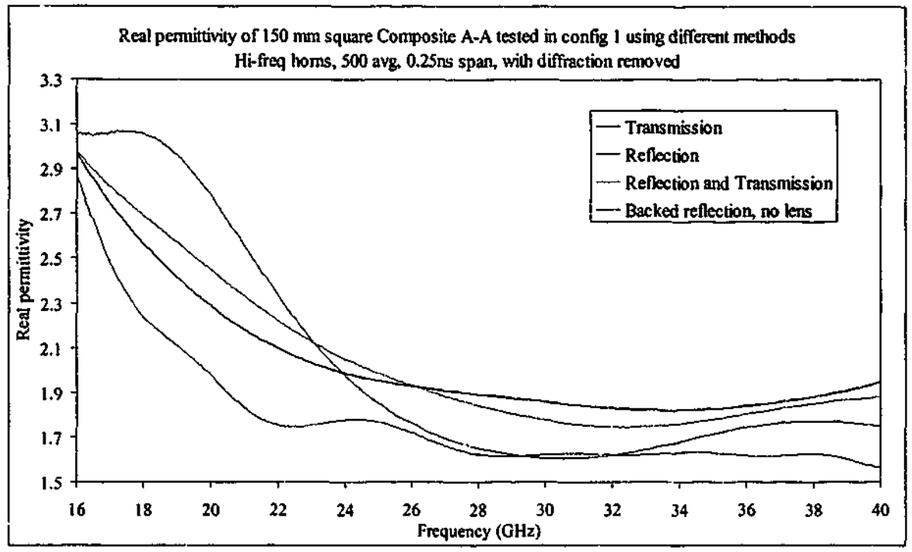

Figure 7-38. Real permittivity of Composite sample measured with hi-freq horns in free space using different methods with diffraction removed

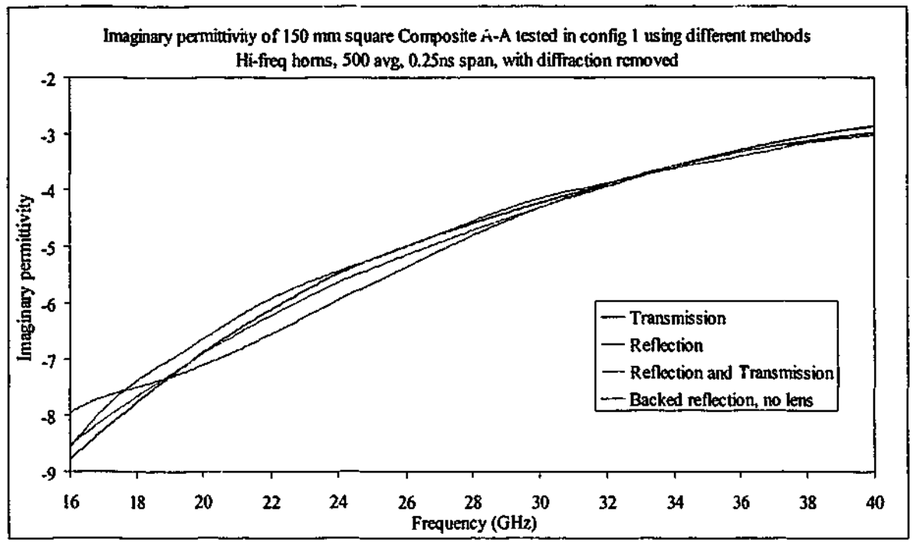

Figure 7-39. Imaginary permittivity of Composite sample measured with hi-freq horns in free space using different methods with diffraction removed

7.5. Summary

These were the smallest samples tested using free space methods, and the effect of sample size is starting to show in the results, especially at low frequencies. While the materials with lower permittivities could be measured down to about 2 GHz with reasonable accuracy, as permittivity increased so too did the level of error. For transmission measurements this crossover occurred where the magnitude of the diffraction signal was greater than that actually transmitted through the material. At frequencies above 6 GHz, the 150 mm samples have values approximately equal to those of the large samples.

Chapter 8. Dielectric Test Fixture

Since the permittivity values measured for the C-stock materials were outside the ± 3% error bounds expected, it was decided to measure the permittivity with a completely different method. An HP 4285A LCR meter was available, which used a 16451B Dielectric Test Fixture to determine complex permittivity of flat specimens. This device was used to measure capacitance and dissipation factor at seven frequency points from 1 to 30 MHz. While these frequencies are obviously not the same as used in network analyser measurements, the permittivity of the active ingredient in the C-stock material (TiO_2) does not change considerably between 1 MHz and 26.5 GHz[93]. Other standard materials that also have properties that do not vary considerably over this frequency range were also tested to confirm the accuracy of the technique.

The permittivities were measured using the non-contacting electrode method, which is considerably more accurate than the contacting electrode method with samples that are not absolutely flat. The gap between the electrodes was set to be about 0.3 mm larger than the thickness of the sample. The short/open/load calibration technique was used to remove the effects of residual capacitance above 5 MHz, with the load calibration approximating the capacitance of the fixture with the sample inserted. The real permittivity results are shown in Table 8-1, with imaginary permittivities given in Table 8-2.

Freq (MHz)	Teflon	Perspex	Lead glass	AK 7	AK 12	AK 15
1	2.017	2.764	9.972	8.577	11.31	12.99
5	2.017	2.716	9.968	8.515	11.22	12.90
10	2.018	2.702	9.989	8.501	11.20	12.88
15	2.020	2.697	10.03	8.510	11.22	12.91
20	2.022	2.696	10.10	8.539	11.27	12.99
25	2.026	2.700	10.20	8.591	11.36	13.11
30	2.031	2.707	10.35	8.680	11.50	13.32

Table 8-1. Real permittivity of materials measured with LCR meter

Freq (MHz)	Teflon	Perspex	Lead glass	AK 7	AK 12	AK 15
1	6.62×10^{-6}	-0.0538	-0.0100	-0.0574	-0.0865	-0.0869
5	-2.37×10^{-4}	-0.0406	-0.0121	-0.0674	-0.105	-0.108
10	-6.11×10^{-4}	-0.0358	-0.0132	-0.0715	-0.112	-0.113
15	-5.94×10^{-4}	-0.0339	-0.0139	-0.0731	-0.118	-0.114
20	-7.97×10^{-4}	-0.0335	-0.0136	-0.0719	-0.125	-0.112
25	-1.26×10^{-3}	-0.0352	-0.0160	-0.0698	-0.137	-0.108
30	-1.68×10^{-3}	-0.0397	-0.0200	-0.0676	-0.160	-0.101

Table 8-2. Imaginary permittivity of materials measured with LCR meter

The figures from Table 8-1 show that the measured values for the Teflon, Perspex and lead glass samples are in close agreement with the expected results. The C-Stock materials vary, with the AK 12 results showing a reasonably close match with that expected while the AK 7 and AK 15 samples are significantly different from the quoted values. All the results show a systematic increase in the real component at the highest frequencies of 25 and 30 MHz. The cause of this increase is assumed to be from incomplete removal of the residual capacitance.

Chapter 9. Coaxial Waveguide

Placing samples in the 7mm coaxial beadless airline is a standard technique used to measure permittivity and permeability of materials. The technique is one that is recommended by Agilent Technologies (Hewlett-Packard) for measuring the electromagnetic properties of materials at microwave frequencies[18]. It is especially useful for measuring materials with low permittivities and permeabilities, and can give very accurate results if the specimen tested is accurately machined.

9.1. Teflon

Teflon is a well-known dielectric material, which can be easily machined to size, and so is an ideal material to test in the coaxial waveguide. A 5.13 mm thick sample was measured with the resulting electromagnetic properties shown in Figure 9-1. The average permittivity across the full frequency band was $2.010 - 0.047i$, with an average permeability of $1.002 + 0.021i$. These values are very close to published results, except for the larger than expected imaginary permittivity value. Continual tightening and loosening of the connectors has caused the connection to degrade as can be seen in the increased error at high frequencies, in both the oscillatory behaviour and the increased imaginary permittivity.

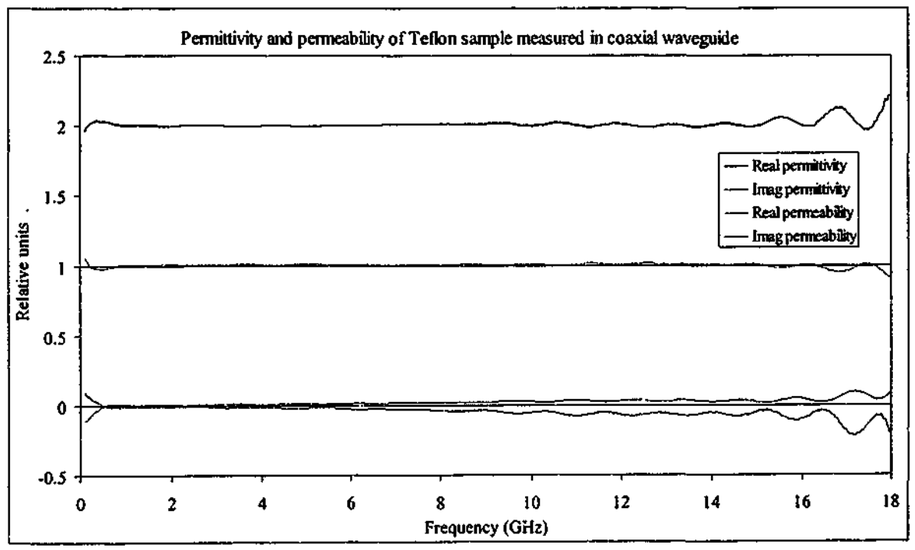

Figure 9-1. Permittivity and permeability of Teflon measured in the coaxial waveguide

9.2. CS-AK xx samples

When the coaxial specimens were made from the C-stock AK xx sheets and tested in the airline, the real permittivity values shown in Figure 9-2 were extracted. The values obtained for the higher permittivity samples are lower than that expected from the dielectric test fixture and the free space measurements, while the results of the AK 7 sample are close to those from the other techniques.

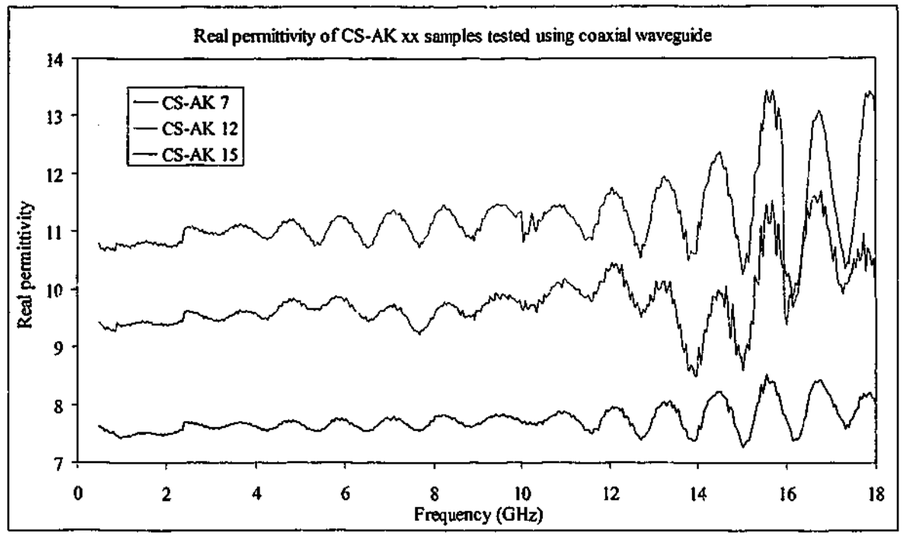

Figure 9-2. Real permittivity of CS-AK xx samples tested in the coaxial waveguide

This example highlights one of the many problems inherent with the coaxial waveguide technique. As has been stated previously, one of the disadvantages to this method is incomplete filling of the waveguide which allows some of the signal to pass around the sample untouched, leading to a lower value of effective permittivity extracted by the algorithms.

In order to investigate this effect, a specimen containing 5% by weight of charcoal in epoxy was produced and tested repeatedly in the coaxial waveguide, increasing the internal diameter between measurements. The reflection/transmission algorithm was used in the normal manner to extract the permittivity. The variation of real permittivity of the sample is shown in Figure 9-3, together with a predictive curve proposed by Peter Jewsbury[94].

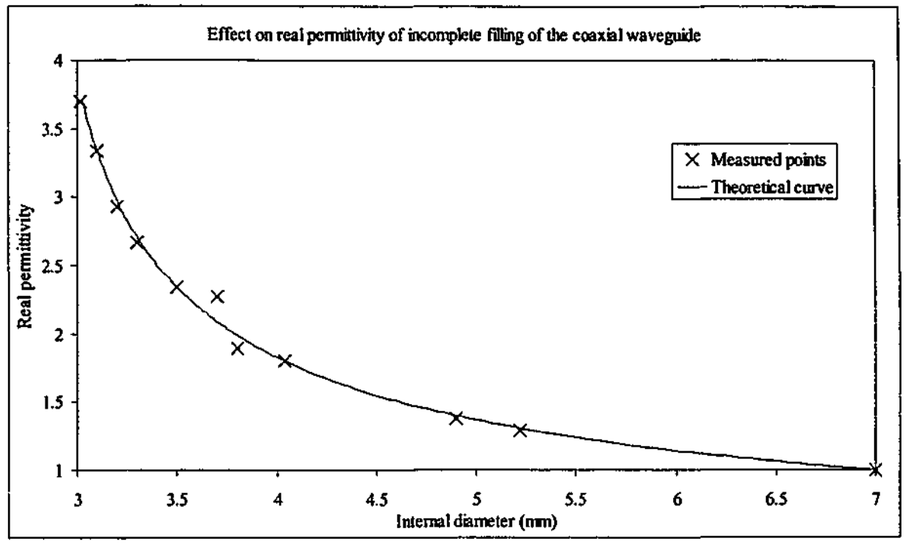

Figure 9-3. Average real permittivity of charcoal loaded epoxy sample with internal diameter increased

The curve follows the form

$$\varepsilon_m = \frac{\varepsilon_a}{\sqrt{1+\left(\varepsilon_a^2-1\right)\left(\frac{d_i-3.04}{7-3.04}\right)}} \qquad \text{Equation 9-1}$$

where ε_m is the measured permittivity, ε_a is the actual permittivity of the material and d_i is the internal diameter of the sample. This curve is based on a semi-empirical formulation using knowledge of the endpoints and describing the mean field inside the waveguide.

The curve can be used to estimate the permittivity measured by the equipment for a sample with a given permittivity and internal diameter. With high permittivity materials, it can be seen from Figure 9-4 that only very small increases in internal diameter are needed to significantly reduce the value of permittivity measured with this equipment.

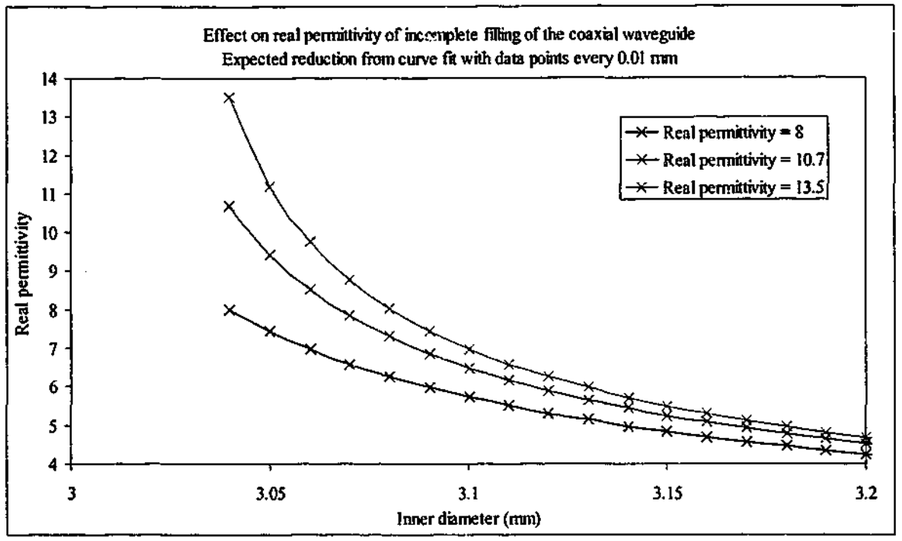

Figure 9-4. Effects of internal diameter changes on real permittivity using Equation 4-1, crosses show 10 micron increases

The permittivities used were based on the free space results of the C-stock AK xx sheets. It can be seen that with the highest permittivity sample (AK 15), it only takes a 10 micron increase in the internal diameter to reduce the measured permittivity from 13.5 to around 11.0. When the internal diameter of the sample increases above a value 0.1 mm larger than the inner conductor, the measured permittivity for all samples is very similar.

We can therefore infer from the results of Figure 9-2 that the internal diameters of the CS-AK 12 and 15 (and quite possibly the AK 7) specimens are slightly larger than the coaxial waveguide, and some of the signal is passing around the sample rather than going through it. In the case of the AK 15 material only a very slight increase in internal diameter is required to give the results observed. Although the samples felt tight on the inner and outer conductors when tested, there must nevertheless have been sufficient gaps in the sample to allow some radiation to pass unaffected.

When testing these sorts of materials in the coaxial waveguide, one is caught in a catch-22 situation. Since the specimens used are rigid they will not fit inside the waveguide if they are too small; however, if they are made large enough to fit inside the waveguide then the results are in error because they are then too large. In the absence of a fully developed correction technique, the sample needs to be measured using a better technique.

9.3. Flexible rubber samples

The flexible carbon loaded rubber samples do not have the sample problems inherent with the rigid CS-AK xx samples. Being flexible they can be slightly larger than necessary, and can then be pushed into the waveguide without causing damage to the gold plated conductors. Specimens were produced by firstly drilling a hole in the rubber on a drill press, then using a specially designed hole cutter to slice the outer ring. Previously it was found that this sample preparation technique produces good results. However, in this case it was found that the technique was causing damage to the secondary carbon black structures present in the samples, thus lowering the permittivity values measured. It is believed damage is caused both at the drilling stage and when the sample is placed onto the inner conductor when the hole is too small. Three different drill bits were used to cut the holes in the samples, with the resulting imaginary permittivity shown in Figure 9-5 (the real component showed similar effects).

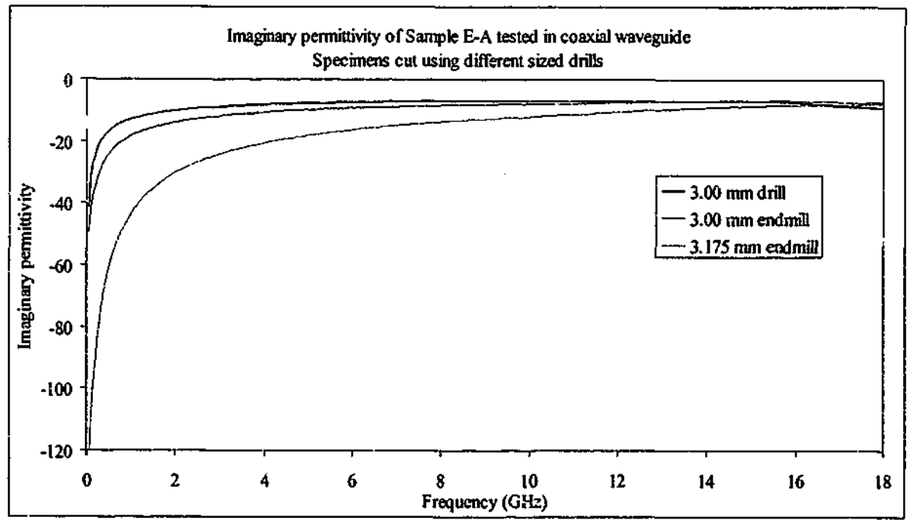

Figure 9-5. Imaginary permittivity of specimens cut from Sample E-A using different drills to cut the internal hole

Sample E shows the greatest effect with drill size because of the high loading of carbon in the system. The first attempt with the 3.00 mm drill was not very successful because the drill did not bite into the rubber, instead tending to slide through the sheet. The endmills have a flat end that cuts the rubber effectively but the 3.00 mm endmill still did not cut a hole large enough for easy placement of the specimen on the inner conductor of the coaxial waveguide. So when the specimen cut with these methods was to be placed onto the inner conductor, it

was flexed quite harshly, and so damage occurred to the sample before it was even tested. The 3.175 mm (1/8 inch) endmill provided the best solution and hence the highest permittivity measured, but it is still far below the values obtained with the free space measurements, as shown in Figure 9-6. The specimen could be positioned easily on the inner conductor, but the damage had occurred already in the drilling stage. The same effects are observed in the other carbon loaded rubber samples in both the real and imaginary components.

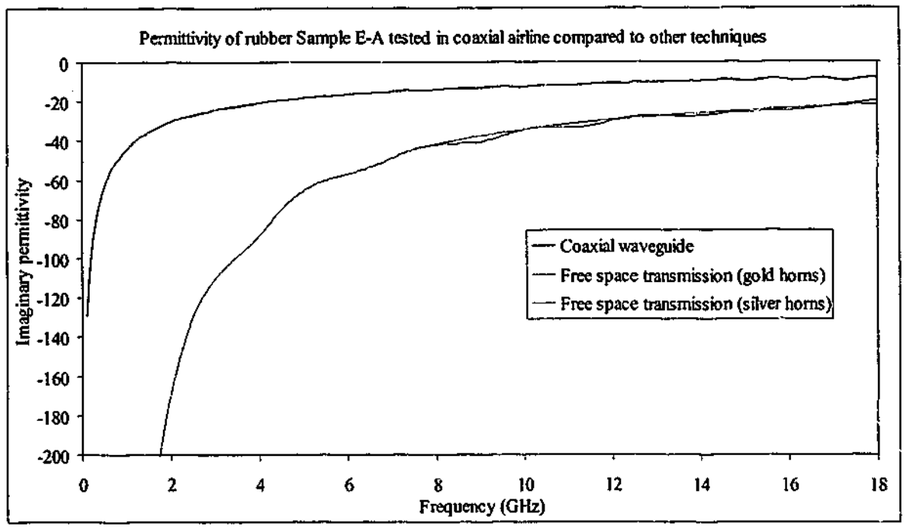

Figure 9-6. Imaginary permittivity of Sample E-A tested in coaxial waveguide compared to other techniques

A better solution would be to cut the holes in the sample with circular hole cutters on a press; however, these were not available in time for this thesis.

When it came to testing the carbonyl iron loaded polyurethane material, the results were very different. The standard technique of drilling the hole with a 3.00 mm drill cut a very neat hole in the polyurethane sheet, and since the process does not damage the additive the results from the coaxial waveguide measurement are close to those from free space testing. Adding to the ease of measurement is the fact that the specimen can be slightly oversize and still be squashed inside the waveguide, so gaps should not occur inside the line.

The permittivity and permeability results are shown in Figure 9-7 to Figure 9-10. The parameters match closely between the different techniques. Slight differences can be observed especially at low frequencies where it is known the diffraction effects are large. Overall however, the two techniques are giving consistent results for all four parameters.

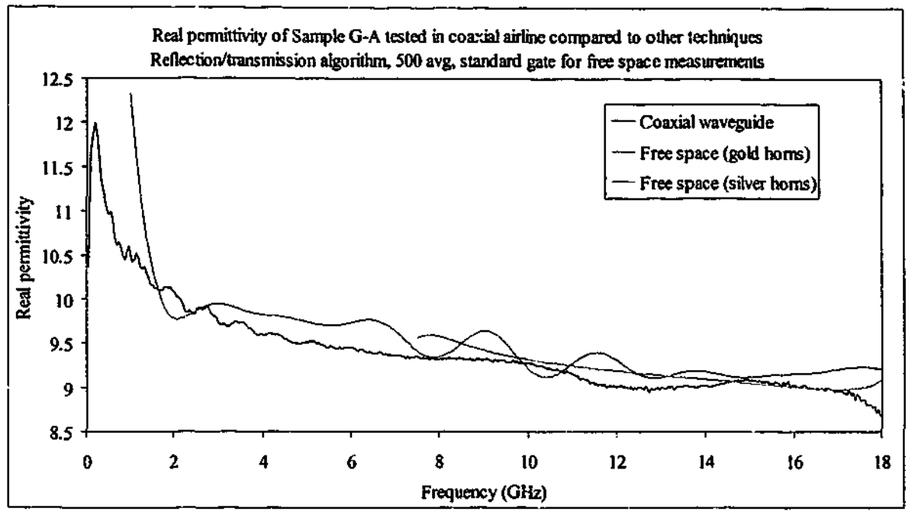

Figure 9-7. Real permittivity of Sample G-A tested in coaxial waveguide compared to free space results from 445 mm square samples

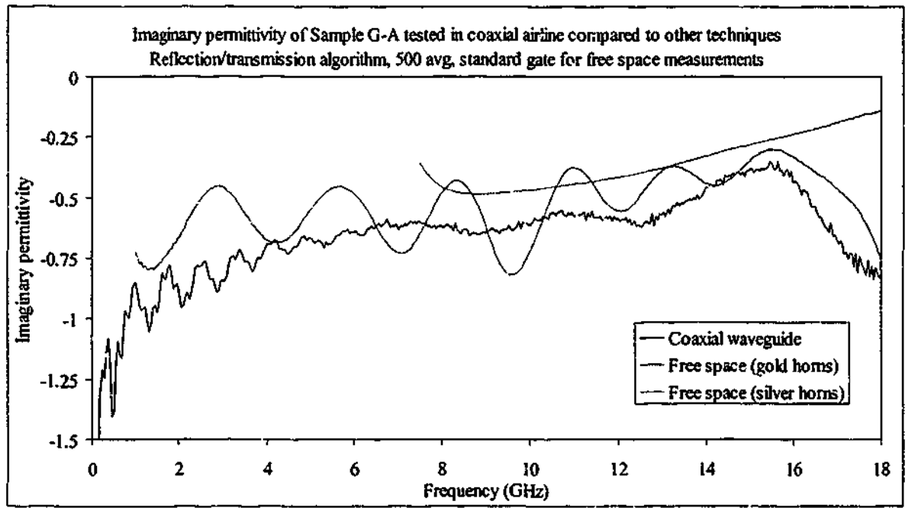

Figure 9-8. Imaginary permittivity of Sample G-A tested in coaxial waveguide compared to free space results from 445 mm square samples

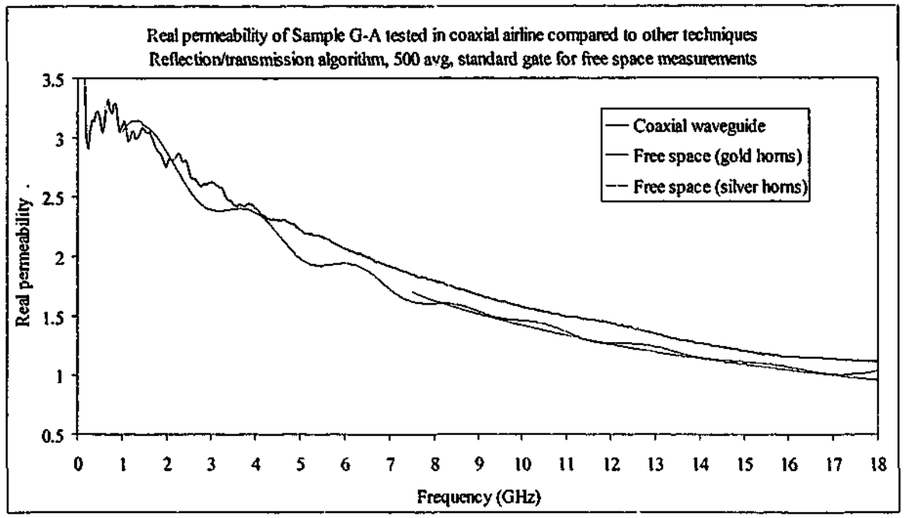

Figure 9-9. Real permeability of Sample G-A tested in coaxial waveguide compared to free space results from 445 mm square samples

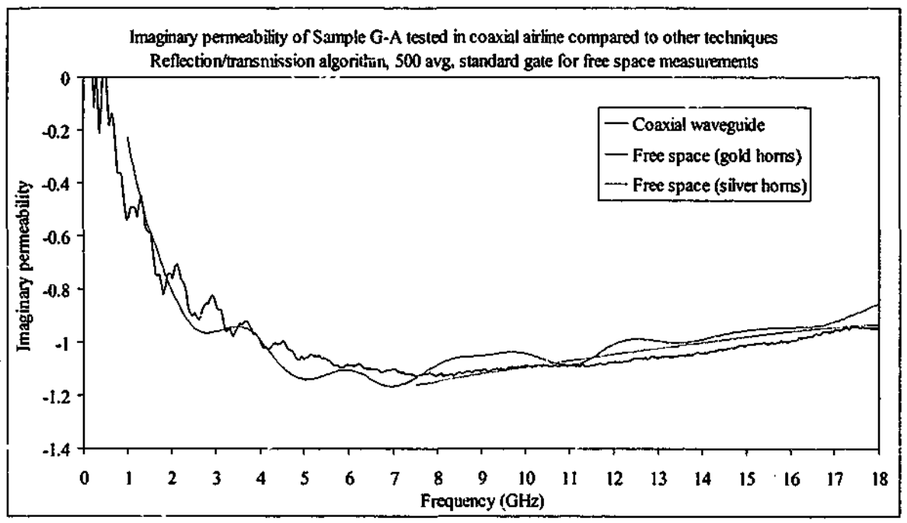

Figure 9-10. Imaginary permeability of Sample G-A tested in coaxial waveguide compared to free space results from 445 mm square samples

9.4. Fibre loaded composite

The fibreglass composite containing 6 mm long carbon fibres was expected to show the limitations of the coaxial waveguide technique; however, it was not expected to be as dramatic as it turned out to be. Since the specimen is rigid the results suffer from the same problems as the CS-AK xx samples, in that the sample must be slightly oversize to fit inside the waveguide. However, the largest effect on the permittivity of the sample is the reduction in the effective fibre length inside the specimen. Rather than being 6 mm long, the fibres have been shortened by the act of actually producing the specimen. This shortening of the fibre length has a dramatic effect upon the permittivity, as can be seen in Figure 9-11.

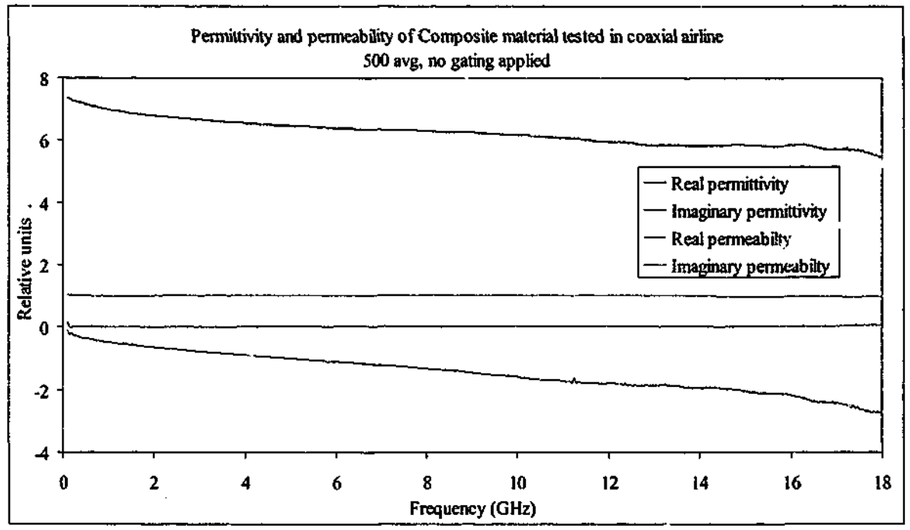

Figure 9-11. Permittivity and permeability of Composite sample tested in coaxial waveguide

When this result was first observed, the specimen was checked to see that there were actually any fibres present, and the result was not simply a fibre free region of the sheet. The fibres were observed however, and two different samples tested produced similar results so the measurement was confirmed. The permittivity has been reduced by at least an order of magnitude at low frequencies compared to the free space result (shown in Figure 5-16, Figure 5-17 and elsewhere). It is clear that the coaxial technique is not suitable for this style of material, because the sample size is too small for the 6 mm additives to be correctly measured.

9.5. Summary

The coaxial waveguide method is a standard technique that can be used to measure the permittivity and permeability of a wide range of materials; however, it does have its shortcomings. Materials like the carbon loaded rubber that are fragile, or cannot be easily machined to the correct size such as glass or the range of CS-AK xx materials need to be measured using a non-destructive technique. Other classes of materials, such as ones containing large inclusions like the carbon fibre loaded composites will produce very inaccurate values for permittivity if tested using the coaxial waveguide method.

Chapter 10. Further Measurements

In addition to the extended regimen of testing on the series of standard materials, various "one-off" measurements were taken on some other materials. These included de-ionised water (which has a well known permittivity) and a range of commercial fibreglass composite materials with various loadings of carbon fibres. Some of the results shown here were presented at the 2000 Asia-Pacific Microwave Conference[95].

10.1. Water

Water has very well known electrical properties at microwave frequencies, and has been measured many times over the years with a variety of methods[96]. The free space techniques described in this thesis are not ideal for measuring liquids; however, it is still possible if measurements are taken carefully. The main problems in measuring the permittivity of liquids in free space include making a transparent bath for the liquid to stay in, ensuring the container is flat and level and measuring the depth of the test liquid. Since the permittivity of polar liquids (such as water) change dramatically with temperature, it is also important to ensure that the temperature is constant and measured accurately.

For the purposes of this exercise a 550 mm square bath was made, consisting of a polystyrene foam base 50 mm thick with 6 mm thick MDF stuck to the sides as walls. A thin acrylic sheet was stuck to the polystyrene base and sides to make a watertight container. The acrylic sheet was sanded lightly to reduce surface tension effects with the shallow depths of water used.

The bath was placed on a stand and the heights of the legs were adjusted so that the bath was level over almost its entire base, with only a slight variation from level in some areas. The depth of liquid was to be calculated by weighing the entire bath to find the volume of water and thereby the thickness to be used in the permittivity calculations. However, it was later found that this method slightly overestimated the depth by an average of 0.1 mm, which was measured by finding the weight of water required to just cover a sanded drill bit lying in the centre of the bath. The surface tension of the water was lowered by the addition of a small amount of a surfactant (Softanol 90) to lessen meniscus effects on the drill for this test.

Transmission measurements were taken on freshly deionised water over the range 3 – 18 GHz with the gold horns, and 7.5 – 18 GHz with the silver horns. The temperature of the water was measured with a Fluke type 52 thermometer as 19.3 °C for the wide frequency

range, and 19.1 °C over the range 7.5 – 18 GHz. The permittivity results over 3 – 18 GHz are shown in Figure 10-1 and Figure 10-2.

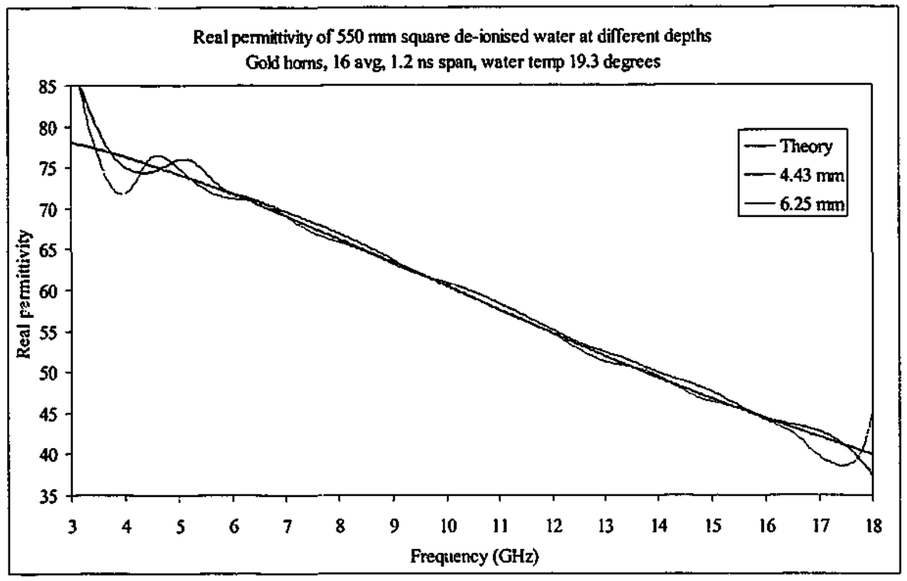

Figure 10-1. Real permittivity of de-ionised water measured with gold horns

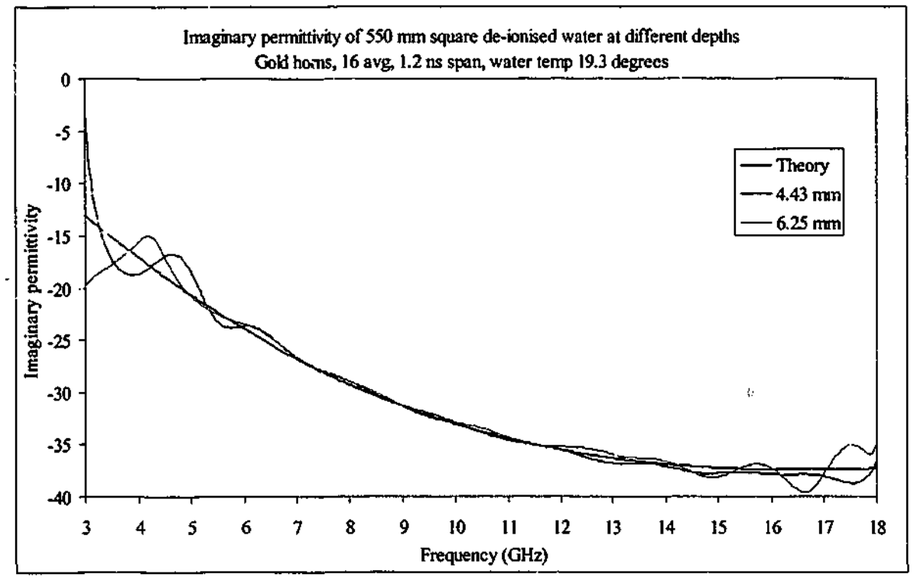

Figure 10-2. Imaginary permittivity of de-ionised water measured with gold horns

The theoretical results are taken from Kaatze[96] using the Debye relaxation spectral function shown in Equation 5-1 with parameters $\varepsilon_0 = 80.406$, $\varepsilon_\infty = 5.6$ and $\tau = 9.598$ ps.

The parameters used were taken by constructing a line of best fit between those quoted by Kaatze at 15 and 20 °C to give a value at 19.3 °C.

The send horn was 130 mm from the base of the water, with the receive horn about 250 mm away from the surface. The short horn to sample distances and large size of the sample reduces the effects of diffraction to a large degree, but as has been shown in previous results it always causes problems in transmission measurements if not properly removed. These measurements were taken before the extent of the problem was known, and as such the diffraction beam was not measured at the time. The diffraction beam is expected to be the cause of the oscillatory behaviour of the extracted permittivity values at low frequencies. At high frequencies the values again start deviating from those expected due to errors in the measurement equipment. At around 14.5 GHz the transmission signal for the 6.25 mm thick sample drops below –50 dB and as such the sensitivity of the measurement is reduced.

Over the frequency range 7.5 – 18 GHz the values extracted are a lot cleaner as would be expected from higher gain horns. The diffraction signal is much smaller at the lowest frequency, and the signal level received at the highest frequency is increased. The results are shown in Figure 10-3 and Figure 10-4. The theoretical trace shown is that calculated using water data estimated for 19.1 °C. The deepest sample again is showing signs of deviation at the high frequency end but overall the results obtained are in good agreement to those expected from the literature.

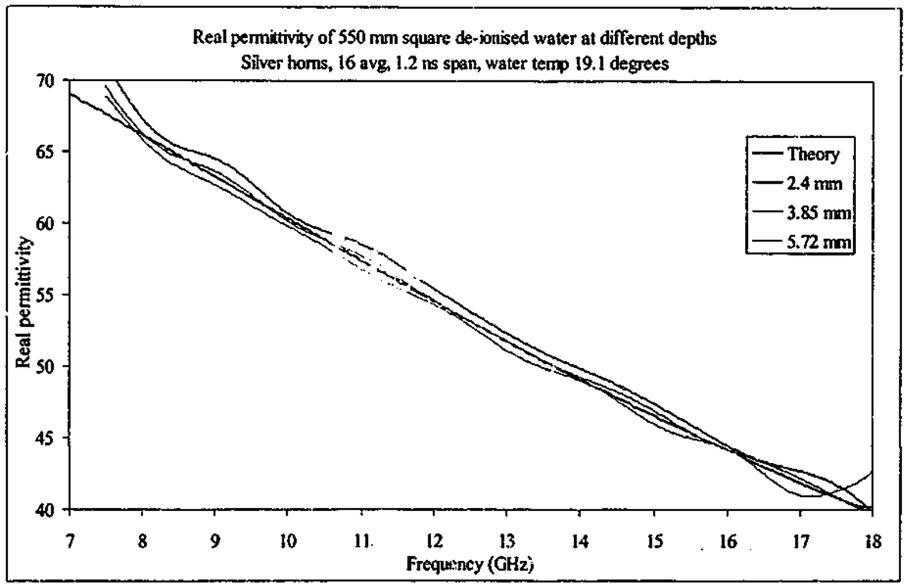

Figure 10-3. Real permittivity of de-ionised water measured with silver horns

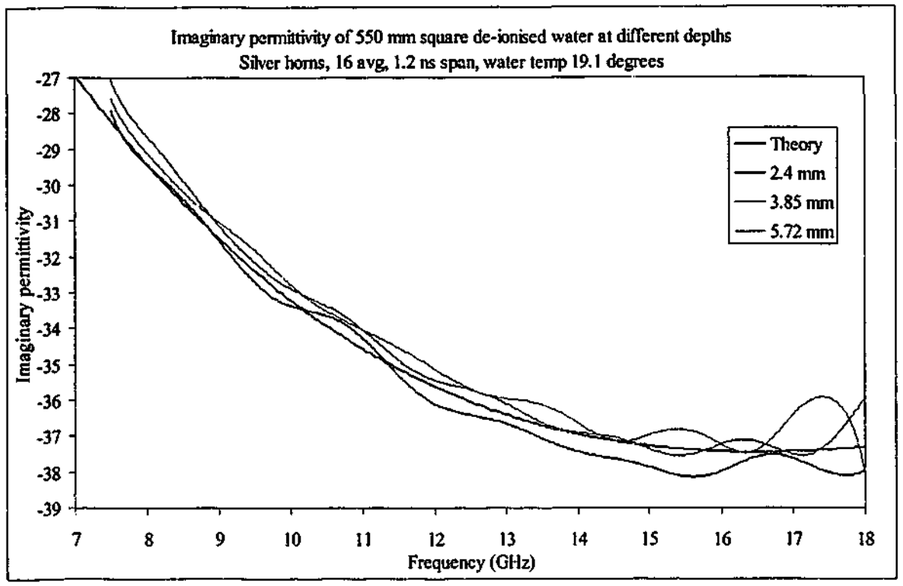

Figure 10-4. Imaginary permittivity of de-ionised water measured with silver horns

10.2. Carbon fibre loaded composite

The permittivity and permeability values from a number of fibreglass composite materials with varying loadings of carbon fibre were also tested. Like the water samples above, these samples were measured prior to the time the diffraction removal technique was developed, so to reduce the effects of diffraction on the results a foil "window" was placed on the foam stand. The aluminium foil sheet with a 200 mm square hole cut in the centre was adhered onto a piece of polystyrene foam, on which the sample was placed. Four rolls of carbon fibre impregnated fibreglass tissue were bought from Technical Fibre Products in the UK, with nominal weightings 0.05, 0.15, 0.20 and 0.25 wt% of 6.25 mm long chopped carbon fibre. A fibreglass sheet with no carbon fibre added was also measured as part of the series.

Readings were taken over 2 – 40 GHz with the time gate span set at 1.0 ns for the reflection measurements, and 0.75 ns in transmission. Using the aluminium foil window is not as effective at removing diffraction as the direct measurement of the foil lined glass sheet, but it still performs an adequate job. The results over 2 – 18 GHz are shown in Figure 10-5 and Figure 10-6. As the concentration of carbon fibre increases so too does the transmission loss through the sample and the effects of the foil window increase. The results over the 7.5 – 18 GHz range taken with the silver horns are very similar to those taken with the gold horns, only with less noise as one would expect.

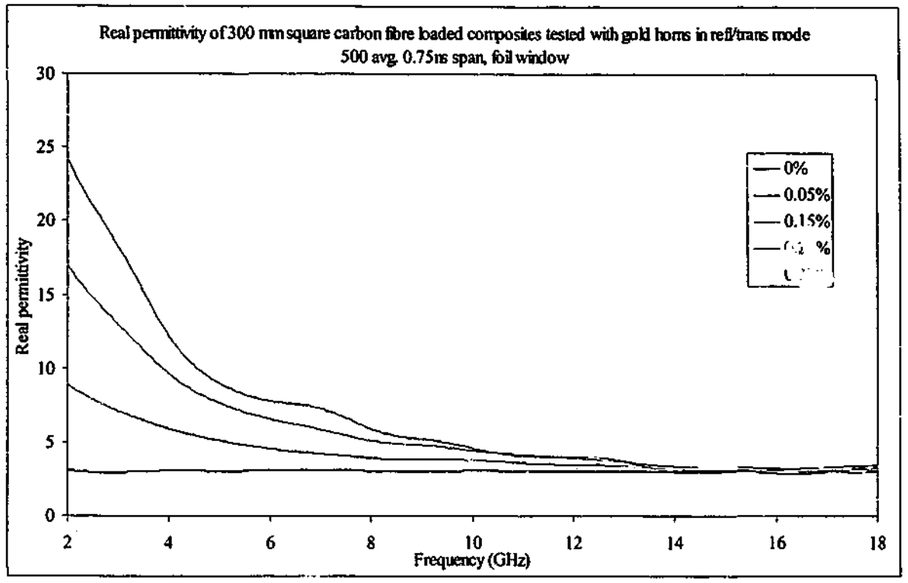

Figure 10-5. Real permittivity of carbon fibre loaded composite materials tested in reflection/transmission mode with gold horns

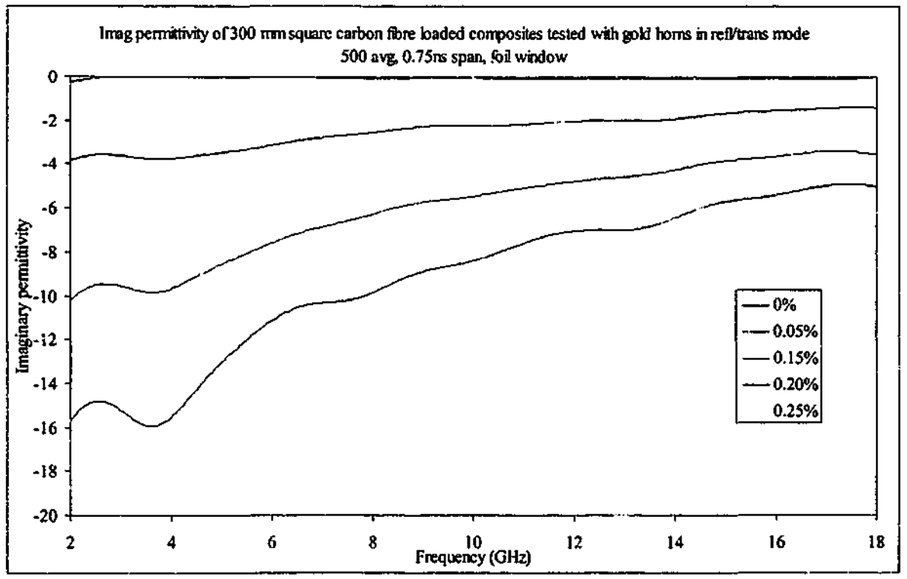

Figure 10-6. Imaginary permittivity of carbon fibre loaded composite materials tested in reflection/transmission mode with gold horns

As frequency increases, the real permittivity of the carbon fibre loaded samples drops to that of the unloaded composite material, while the imaginary component remains relatively

high. Over the frequency range 16 – 40 GHz, the real component for samples with higher loadings of carbon fibre drop slightly below the unloaded material indicating anomalous dispersion, as can be seen in Figure 10-7, with the imaginary component shown in Figure 10-8.

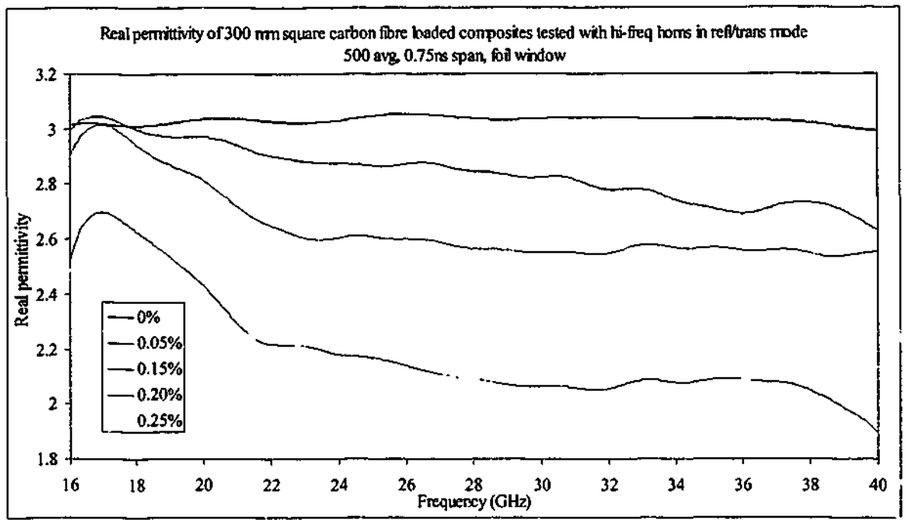

Figure 10-7. Real permittivity of carbon fibre loaded composite materials tested in reflection/transmission mode with hi-freq horns

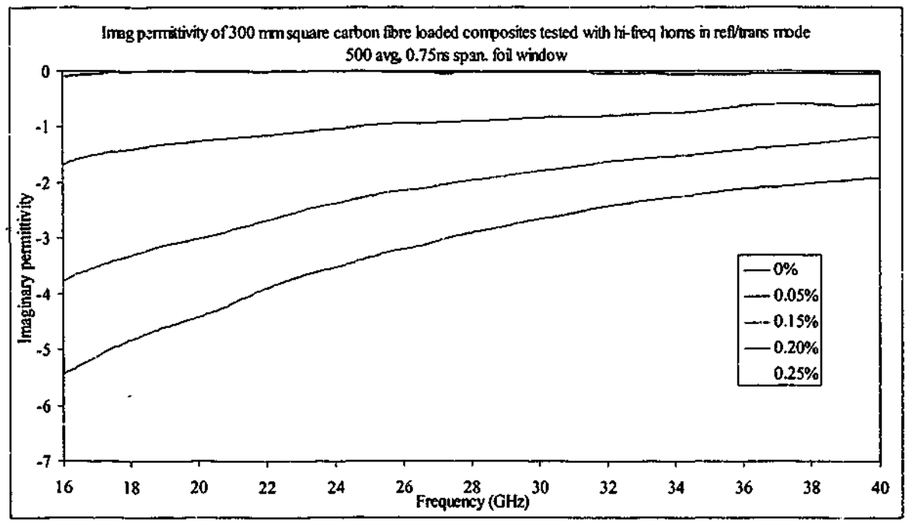

Figure 10-8. Imaginary permittivity of carbon fibre loaded composite materials tested in reflection/transmission mode with hi-freq horns

In the interests of clarity, the permittivity of the unloaded material over the range 16 – 40 GHz was calculated using the transmission only result, as destructive interference in the reflection signal caused distracting peaks at about 35.5 GHz.

The average permeability values for the samples are shown in Table 10-1. The permeability values for the unloaded sample include the effects of the destructive interference peak.

Carbon loading	2 – 18 GHz		7.5 – 18 GHz		16 – 40 GHz	
	μ'	μ"	μ'	μ"	μ'	μ"
0 %	0.992	0.001	0.999	0.007	1.025	0.002
0.05 %	0.977	0.015	0.988	0.007	1.004	0.020
0.15 %	0.952	0.018	0.965	0.002	0.988	0.007
0.20 %	0.978	0.004	0.999	0.022	1.020	0.044
0.25 %	0.951	0.009	0.968	0.022	1.011	0.031

Table 10-1. Average permeability values for the carbon fibre loaded composite materials over three frequency ranges

10.3. Diffraction removal techniques

Various techniques were investigated to remove the effects of diffraction around the samples when performing transmission measurements. The first approach used the "window" concept, where the radiation was free to pass through the centre of the window, but would be blocked from going around it by either an absorber or a reflector. The absorbing condition was arranged by cutting a square hole in the centre of a commercial available convoluted foam radar absorber. For this approach the calibration was performed with the foam absorber in place, then the sample was positioned and the transmission measured. The absorber used was optimised for the 7 – 18 GHz range and about 100 mm thick. In the case of the reflective "window", aluminium foil was adhered to a polystyrene foam sheet with a square hole in the centre as before. This was a far cheaper solution than cutting holes in RAM, and had the additional advantage of being less dependent on the frequency range used. The third approach investigated relied on removing the diffraction signal mathematically by measuring the signal of a foil lined glass sheet that was the same size as the sample.

Perspex samples 305 mm and 100 mm square were measured with the gold horns over the range 1 – 18 GHz, with both horns 190 mm from the sample. Two foil windows were used to investigate the effects of aperture size on the measurement, the sizes being 200 mm square and 90 mm square. The foam absorber had a 250 mm square hole cut in the centre. Both the foil lined foam and the absorbing foam sheets had outer dimensions of around 600 mm

square. The metal sheets used for the mathematical removal process were the same size as the sample tested.

All the methods investigated performed reasonably well at removing the diffraction signal. The time domain response of the 305 mm sample is shown in Figure 10-9, where it can be seen that the diffraction component of the transmission response occupies the region from 0.2 ns to 0.5 ns, after which time the gate removes the rest of the signal. The black line shows the expected time domain signal for the Perspex sheet. Since none of the diffraction removal processes recover the theoretical curve it is difficult to say with any certainty which technique is superior; however, the graph of the mathematical removal of the diffraction signal has the smallest peak height above 0.2 ns.

The extracted permittivity results for the 305 mm square Perspex sample are shown in Figure 10-10 and Figure 10-11, where it can be seen that the results are very similar regardless of the diffraction removal process used.

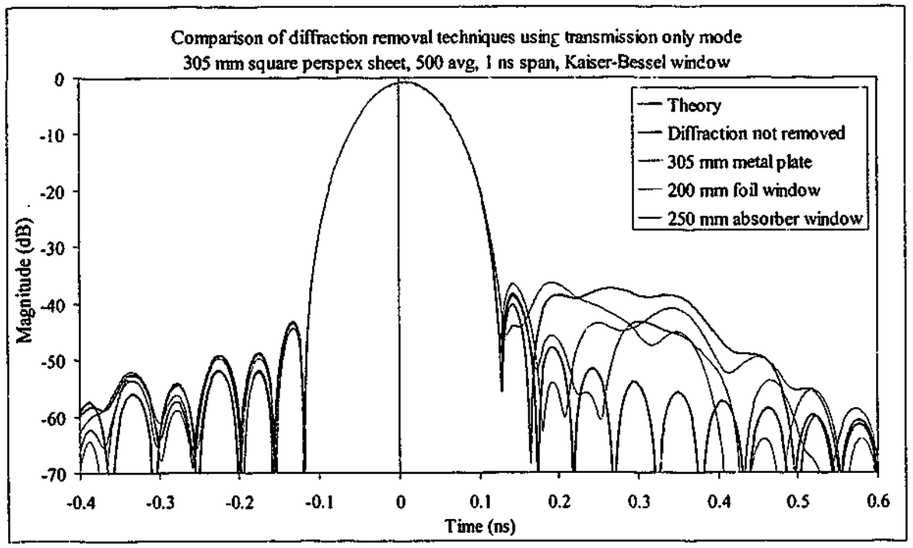

Figure 10-9. Time domain response of the transmission through the 305 mm square Perspex sample.

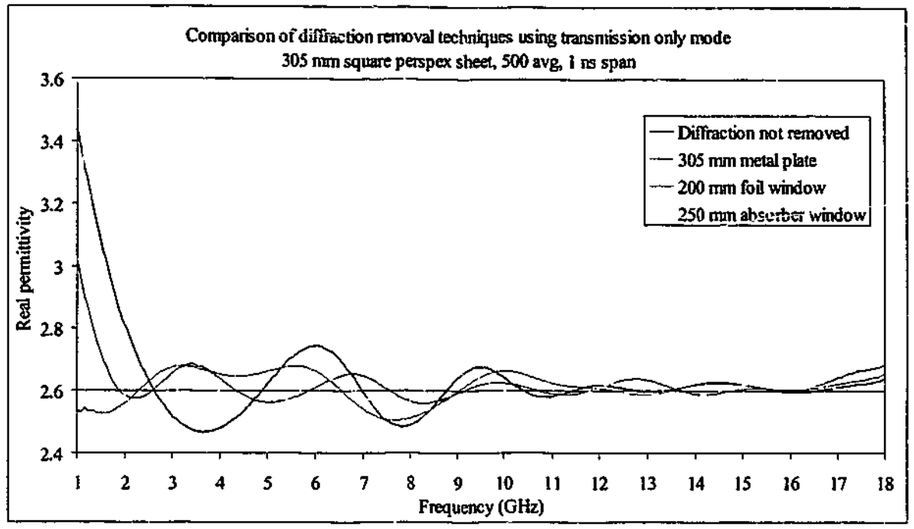

Figure 10-10. Real permittivity of 305 mm square Perspex sample measured with gold horns showing a comparison of diffraction removal processes

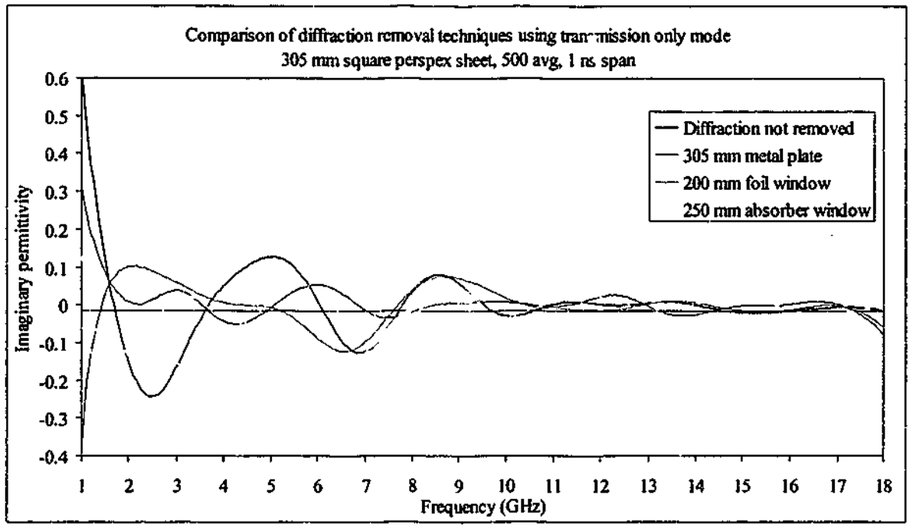

Figure 10-11. Imaginary permittivity of 305 mm square Perspex sample measured with gold horns showing a comparison of diffraction removal processes

When the 100 mm sample was measured, the results clearly showed that the mathematical diffraction removal process was superior. The diffraction signal is a lot larger for this smaller sample, and a lot less distinct in the time domain with the minimum path length difference being only 13 mm. This leads to the blue trace shown in Figure 10-12.

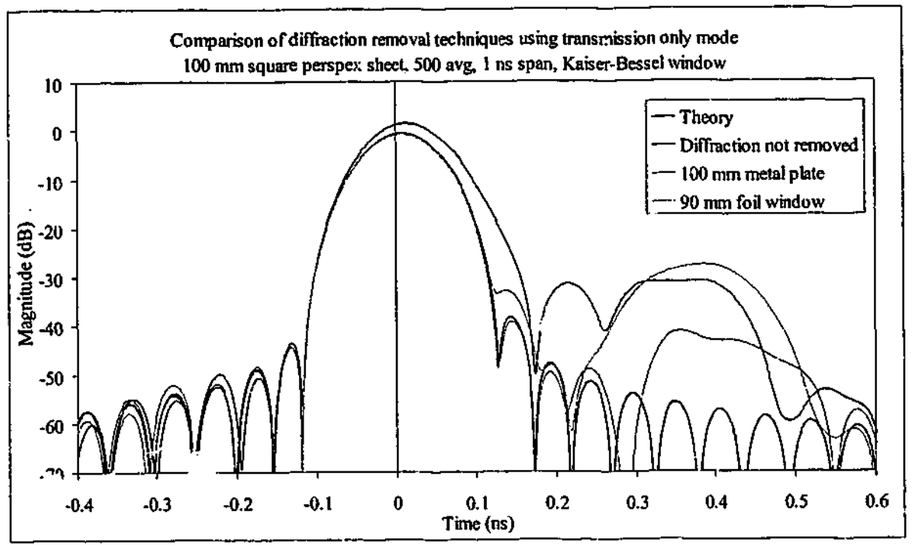

Figure 10-12. Time domain response of the transmission through the 100 mm square Perspex sample.

In contrast to the previous result, the result is much improved when the diffraction is removed mathematically when compared to the use of a much smaller foil window. Both techniques restore the signal near the calibration plane (where time = 0), but the foil window method does not remove the signal around the 0.4 ns mark. This result is reflected in the permittivity results, shown below in Figure 10-13 and Figure 10-14.

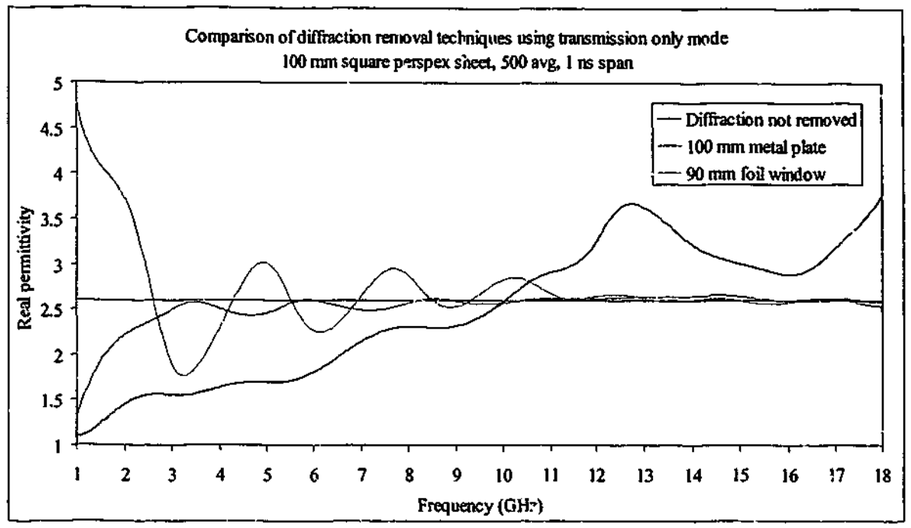

Figure 10-13. Real permittivity of 100 mm square Perspex sample measured with gold horns showing a comparison of diffraction removal processes

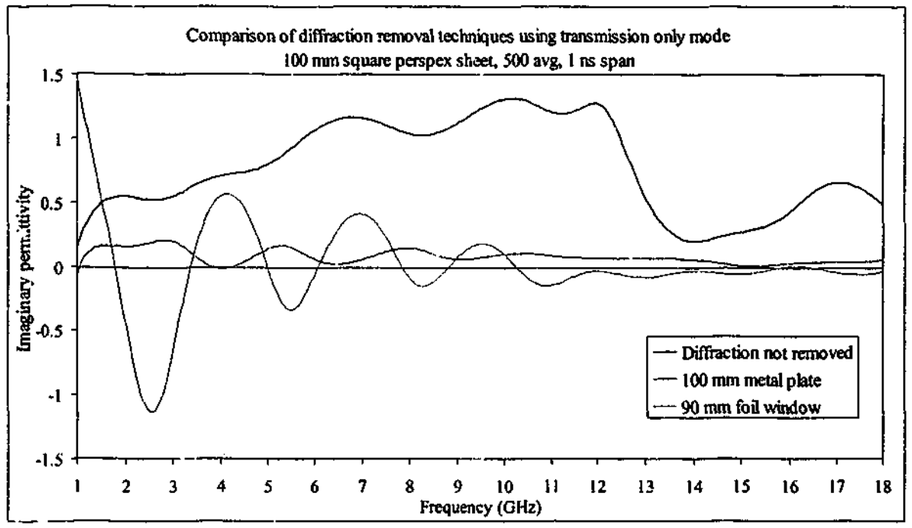

Figure 10-14. Imaginary permittivity of 100 mm square Perspex sample measured with gold horns showing a comparison of diffraction removal processes

While still not perfect, the mathematical removal of the diffraction signal is giving a relatively good estimate of permittivity above 3 GHz or so. The foil window gives oscillations around the expected values, which is still a big improvement on the permittivity result when diffraction is not removed. Measurements such as this one led to the adoption of the mathematical diffraction removal technique used in this thesis.

In order to show the effectiveness of the mathematical technique on a highly lossy material, the results of rubber sample E with different sizes are presented over the frequency range 1 – 18 GHz. The transmission loss through sample E is about –14 dB across this frequency range, while the diffraction beam is dependent upon frequency and sample size. The result from the largest sheet tested (445 mm square) in configuration 1 is shown in Figure 10-15, together with the diffraction measurement and the difference calculated using the diffraction removal technique.

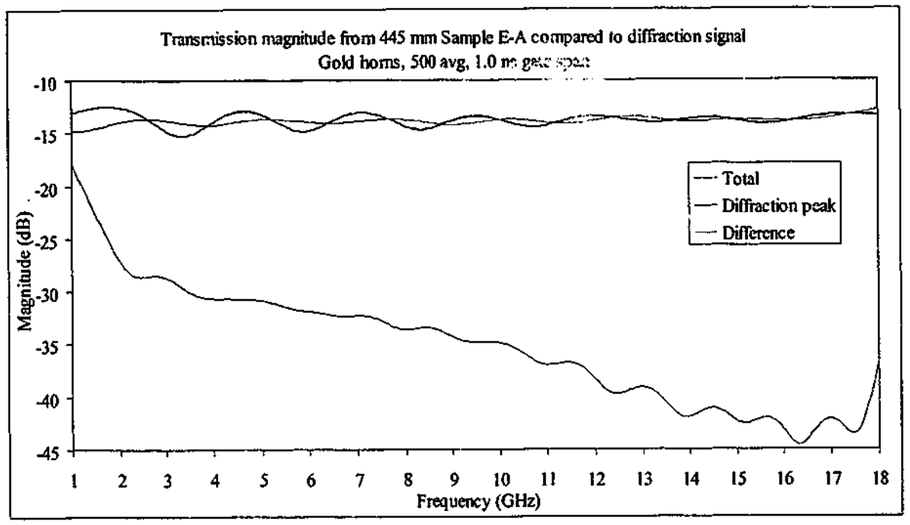

Figure 10-15. Transmission magnitude of 445 mm square Sample E-A compared to diffracted magnitude

The effect of removing the diffraction signal is relatively small in this case, since the transmission magnitude is considerably greater than the diffraction signal. As the sample size decreases to 305 mm square, the diffracted signal is of a similar magnitude to that passing through the sample which leads to the destructive interference peaks, nevertheless the diffraction removal process extracts a relatively clean signal (Figure 10-16).

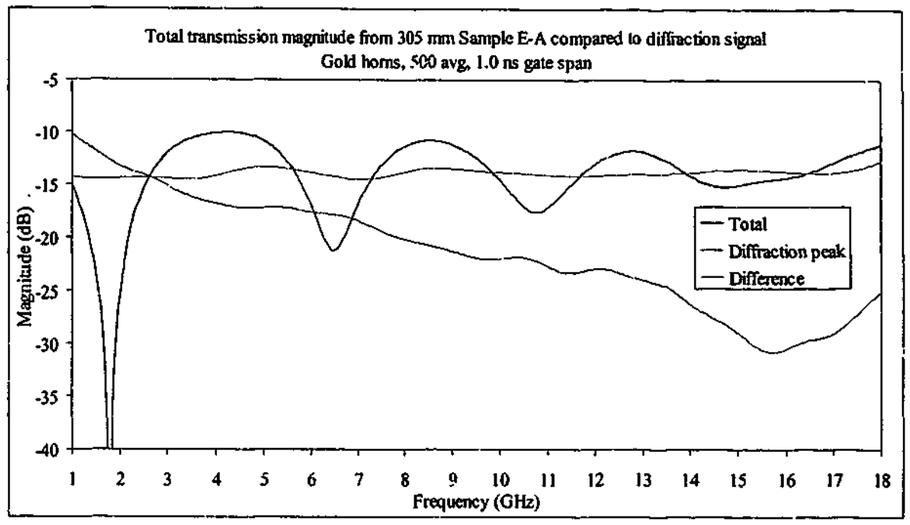

Figure 10-16. Transmission magnitude of 305 mm square Sample E-A compared to diffracted magnitude

In the case of the 150 mm square sheet, the diffraction signal dominates the total signal acquired when measuring the response from the sample. However, the diffraction removal algorithm is still able to extract useful information from the sample alone. At low frequencies the signal increases above the –14 dB level, which is not surprising considering the diffraction peak is of the order of 10 dB larger than the desired signal.

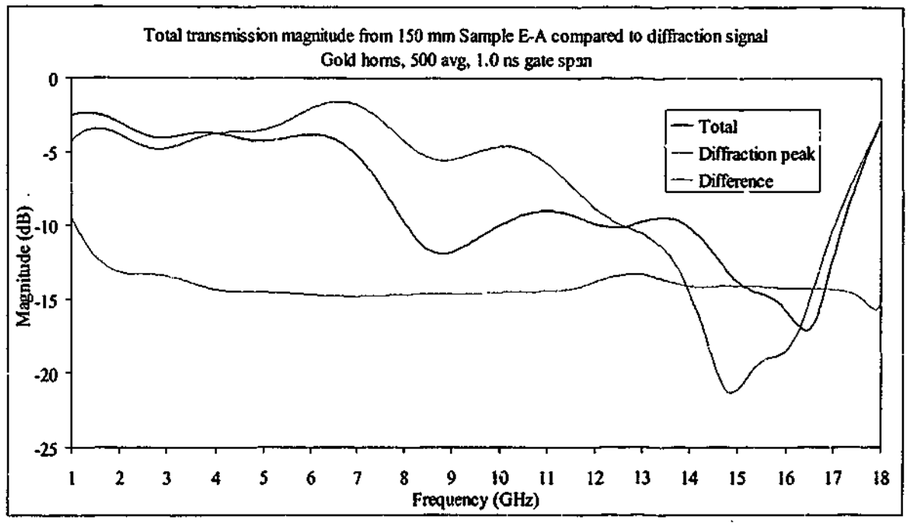

Figure 10-17. Transmission magnitude of 150 mm square Sample E-A compared to diffracted magnitude

Placing all the results on the same set of axes shows how close the magnitudes of the three different sized samples are after the diffraction removal process has taken place. When compared to the original data shown in the previous graphs, Figure 10-18 proves the worth of the technique in obtaining a more accurate measure of the material's electromagnetic properties.

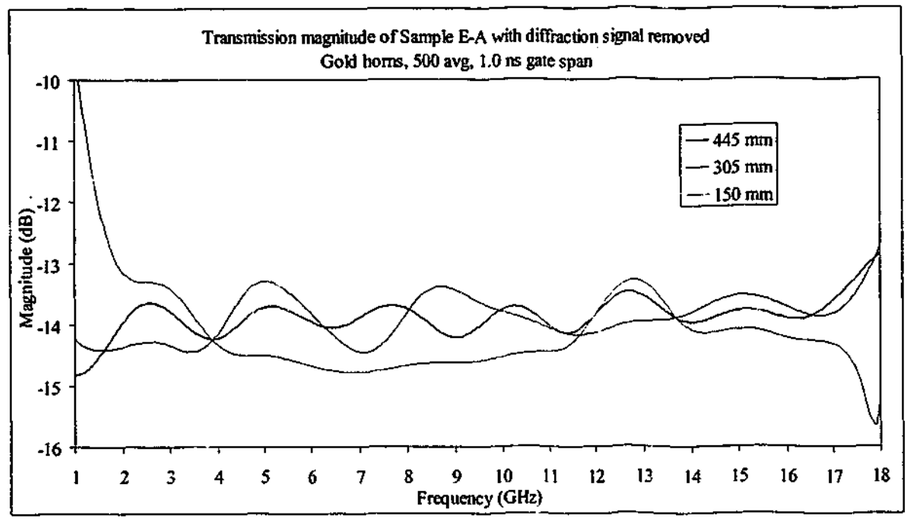

Figure 10-18. Transmission magnitude of the three sizes of Sample E-A with diffraction removed

Using the resulting magnitudes and phases of the three samples to calculate the permittivity of the material, we obtain the graph shown in Figure 10-19. The effects of stray reflections and diffraction are still present in all the traces; however, the deviations from the average values are much lower using the mathematical diffraction removal technique. None of the results can be said to be highly accurate below 2 GHz with large oscillations occurring for even the largest sample; however, an average value can be estimated for both the 445 and 305 mm square sample at these frequencies. The results from the 150 mm square sample have deviated considerably from the others at frequencies lower than about 6 GHz, and so it must be concluded that samples with this degree of loss should be considerably larger than 150 mm square to maintain accuracy. However, when one considers the original data it is somewhat remarkable that the technique converges to any value at all, and to get an acceptable result above about 6 GHz should be considered a success for the mathematical diffraction removal technique.

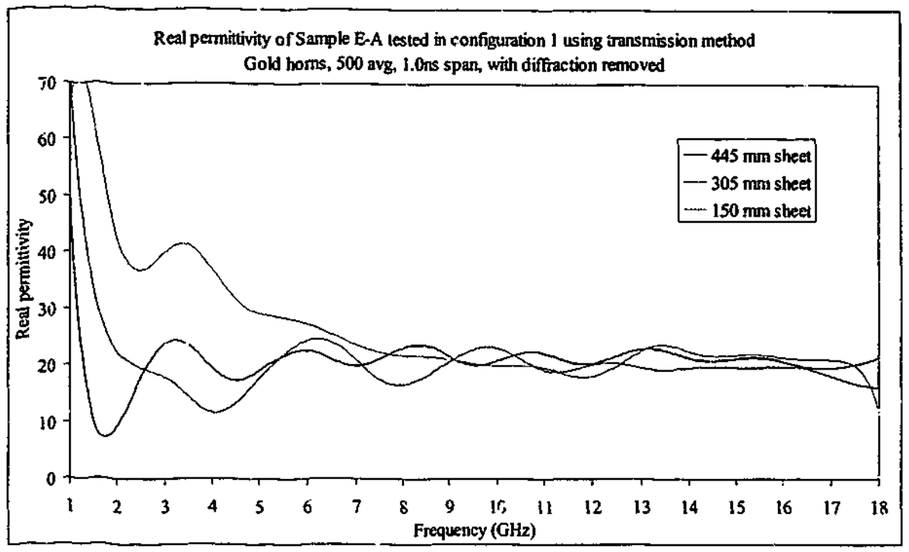

Figure 10-19. Real permittivity of different sized rubber E-A samples measured with gold horns using transmission method with diffraction removed

10.4. Lensed transmission results

The large foam lens was tested using the range of 445 mm square samples to see if its use would improve the measurements. The lens was placed on a 100 mm thick sheet of polystyrene foam, which in turn was resting on a steel frame 750 mm square attached to a steel bar running vertically along the wall. This bar is also used as the attachment point for the horns. Originally, this frame was used to hold the sample itself before it became apparent that the weight of the samples was causing the steel frame to bend slightly and so shift closer to the send horn. The shifts were only of the order of a few tenths of millimetres, but as we have seen earlier this slight shift is enough to greatly affect the reflection measurements. For this reason an aluminium frame was made to hold the samples steady. All metal parts were covered in absorbing material to minimise stray reflections.

Because the lens can only sit with its flat face down, the orientation of the measurement needed to the changed. The send horn was on top with the receive horn underneath the sample. When using this orientation reflection measurements are more difficult, as the calibration plane changes each time a sample with a different thickness is measured. While it is possible to apply a calibration shift equal to the difference between the specimen and the reflective plate's thicknesses, large errors can easily result. For the purposes of the lens test, only the transmission method was used.

The measurement setup is shown in Figure 10-20, showing the configuration when the high frequency horns are used. Because of the high transmission losses in flexible coaxial cable, the run was kept as short as possible while maintaining a reasonable distance between the cable and the area illuminated by the horn. For the lower frequency measurements the cable losses are smaller and the cables run behind the absorbing foam on the back wall. Figure 10-20(b) shows how the yellow cable runs behind the foam absorber to stay as far away as possible from the send horn. The sample slides between the 300 mm thick polystyrene foam stand and the 100 mm foam piece on which the lens is situated.

(a) (b)

Figure 10-20. Measurement setup used for lensed transmission measurements

It was found that the foam lens had very little effect on the extracted values of permittivity for the samples tested. Observing the measured S_{21} values for Perspex in Figure 10-21 and Figure 10-22 over the range 7.5 – 40 GHz, it is found that no improvement in the magnitude has been observed, and the phase traces are almost identical. Diffraction effects are prevalent across the frequency band, which are causing the deviations from the theoretical line. When these values are used to calculate permittivity, both sets of data are close to that expected with no discernable improvement caused by the lens. The permittivity values are shown in Figure 10-23 and Figure 10-24.

Very similar results were observed for all the carbon loaded rubber samples tested. Occasionally one data set would show slightly different results for the lensed measurement of the order of 5%, but the effect was not consistent across the entire set.

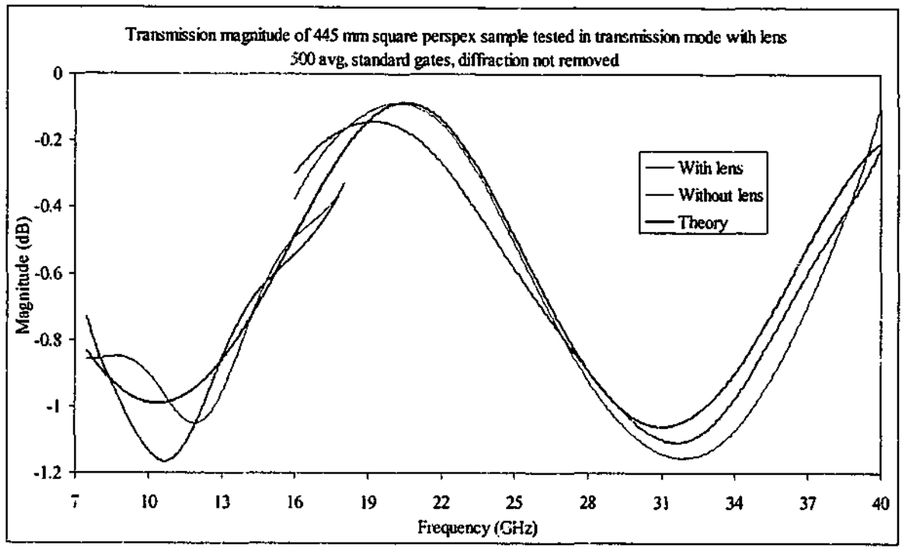

Figure 10-21. Magnitude of the S_{21} signal measured through the 445 mm square Perspex sample with and without the lens

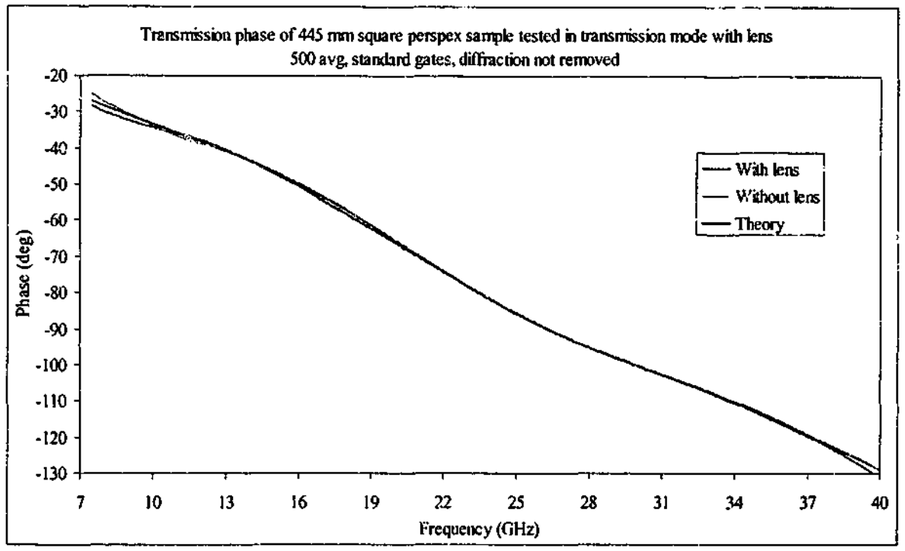

Figure 10-22. Phase of the S_{21} signal measured through the 445 mm square Perspex sample with and without the lens

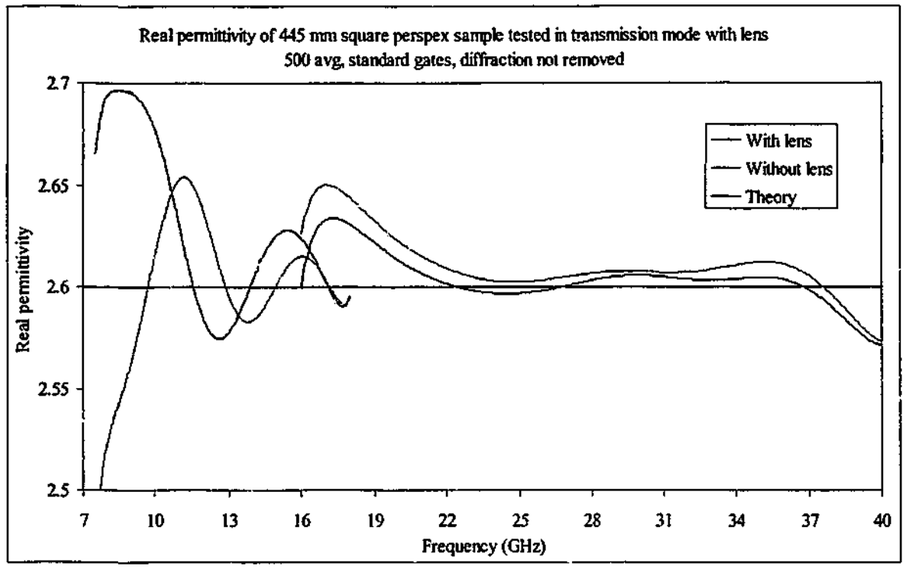

Figure 10-23. Real permittivity of 445 mm square Perspex sample tested in transmission mode with and without the lens

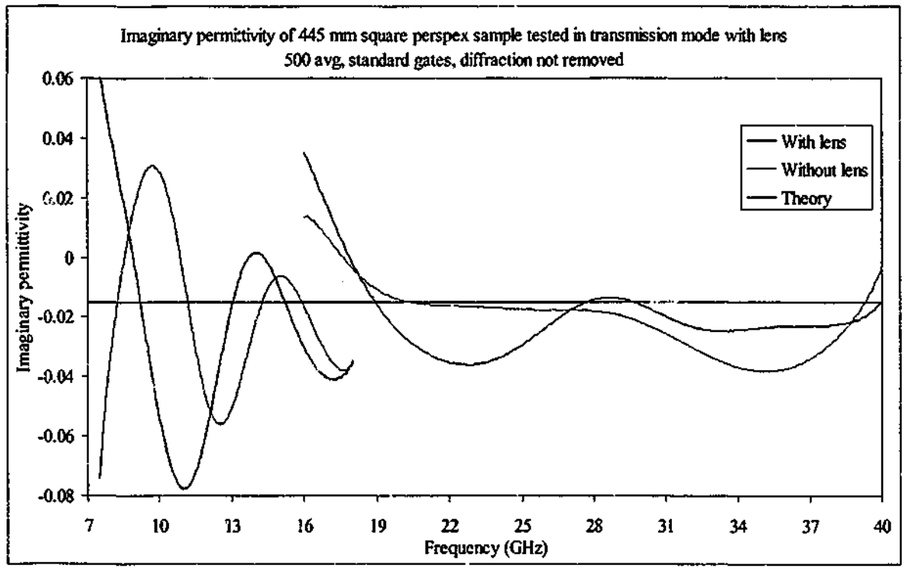

Figure 10-24. Imaginary permittivity of 445 mm square Perspex sample tested in transmission mode with and without the lens

Due to the limited effect the lens was having, the difficulties in aligning and levelling it, together with the added complications in performing reflection measurements and positioning so as to avoid multiple reflections between the lens and the sample, it was decided that use of the lens was not necessary to obtain highly accurate measurements and that its use would be discontinued.

Chapter 11. Discussion

A number of materials with very different electromagnetic properties have been examined over a wide frequency range with the purpose of discovering the optimum technique for accurate determination of the permittivity and permeability of the materials. Every technique investigated had its own strengths and weaknesses for the various samples used, with material properties often determining the best method to use.

11.1. Errors in sample thickness

The most common source of error in determining the electromagnetic properties is associated with the specimen's physical dimensions. The coaxial waveguide method relies on the sample completely filling the airline; however, both the free space and waveguide methods rely on an accurate measurement of the sample's thickness for reliable results. In order to determine the relationship between sample thickness and permittivity accuracy, a theoretical S-matrix was constructed for a non-magnetic material 1 mm thick, with a permittivity of $10 - 5i$ over the frequency range 1 – 100 GHz. The S-matrix from this hypothetical material was then used to extract permittivity and permeability while changing the thickness used in the calculations. The thickness was changed by ± 0.01, ± 0.02, ± 0.05 and ± 0.10 mm to form the graphs shown in Figure 11-1 to Figure 11-4, using the reflection/transmission algorithm.

At very low frequencies it appears that the extracted permittivity values show a simple linear relationship between the increase in thickness and the corresponding decrease in permittivity, i.e. a 5% increase in thickness leads to a 5% decrease in permittivity. The permeability values show little effect on thickness change at the lowest frequencies. However, as frequency increases, all the parameters rise and fall in a seemingly haphazard fashion with no discernable pattern. However, if one observes the reflection and transmission data shown in Figure 11-5, it becomes clear that the peaks and dips present in the extracted permittivity and permeability data line up with those of the reflection and transmission data.

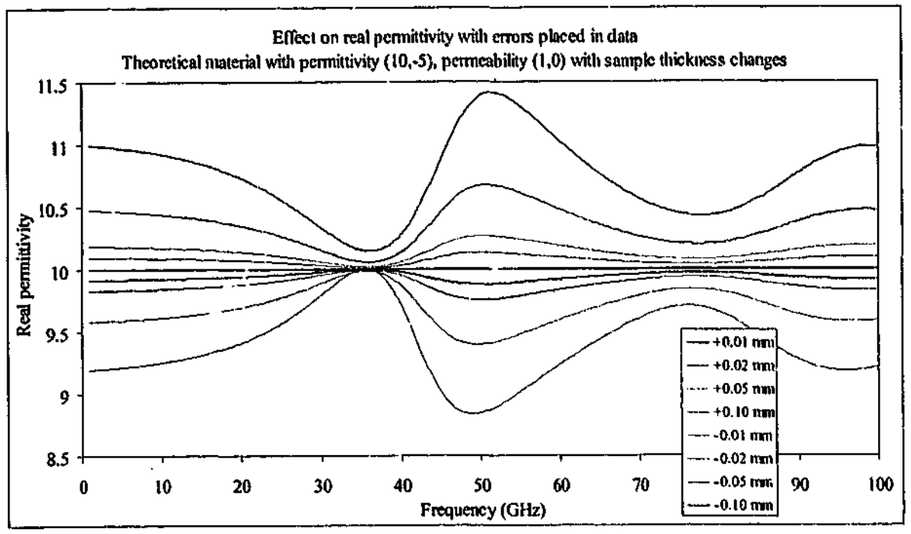

Figure 11-1. Real permittivity of theoretical material with incorrect thickness used in calculations using reflection/transmission algorithm, sample nominal thickness 1 mm

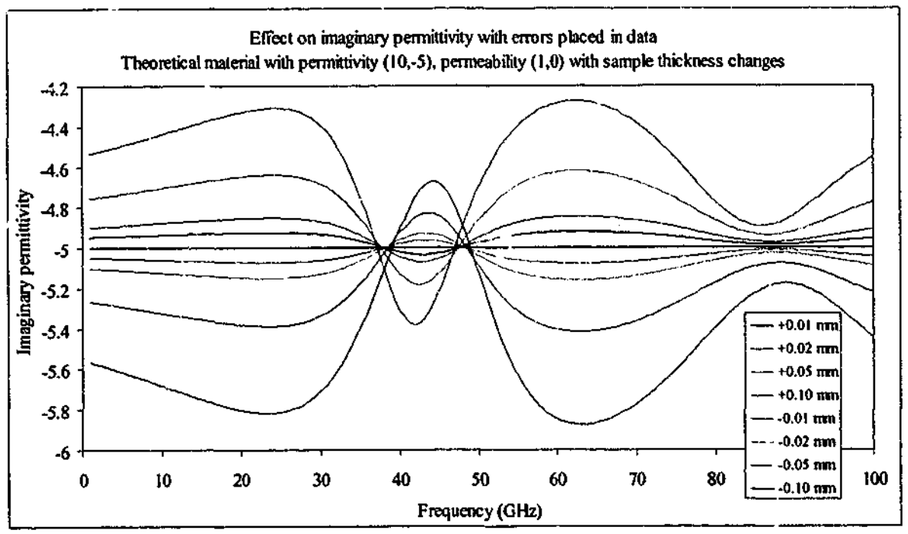

Figure 11-2. Imaginary permittivity of theoretical material with incorrect thickness used in calculations using reflection/transmission algorithm, sample nominal thickness 1 mm

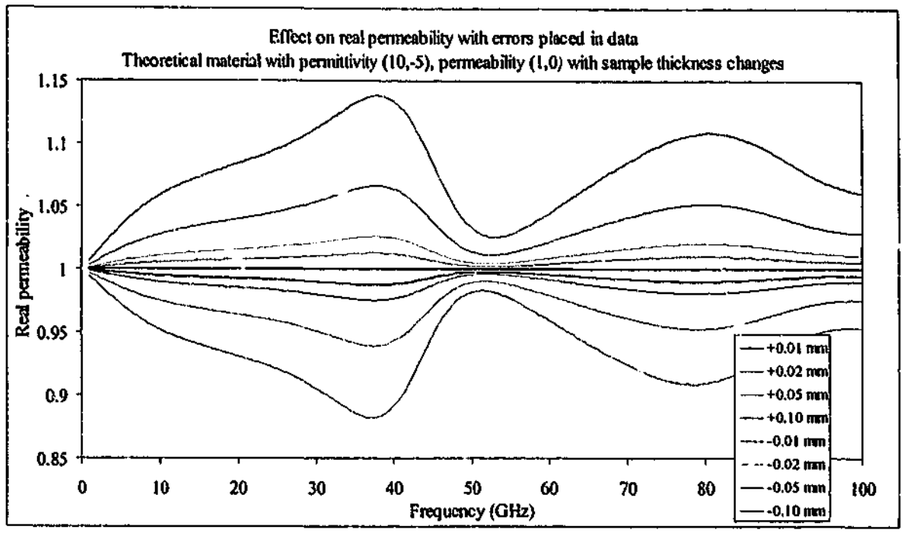

Figure 11-3. Real permeability of theoretical material with incorrect thickness used in calculations using reflection/transmission algorithm, sample nominal thickness 1 mm

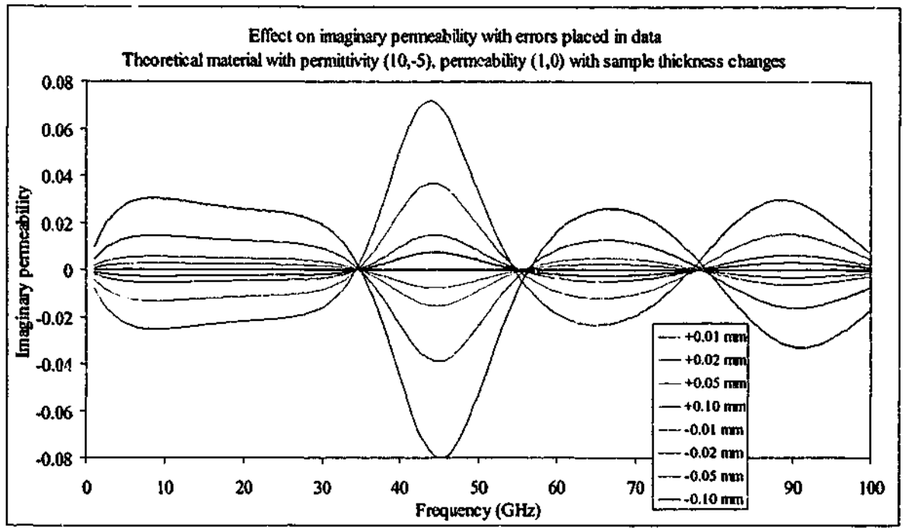

Figure 11-4. Imaginary permeability of theoretical material with incorrect thickness used in calculations using reflection/transmission algorithm, sample nominal thickness 1 mm

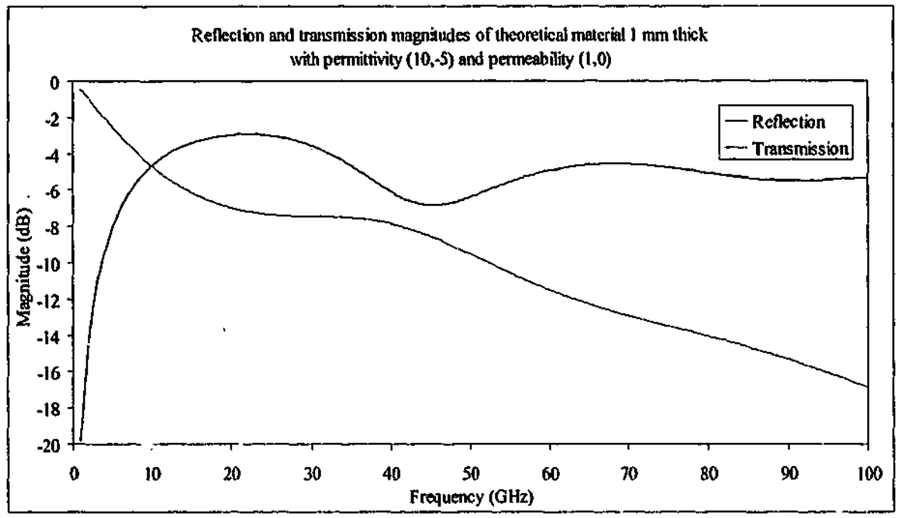

Figure 11-5. Reflection and transmission magnitudes of theoretical material with known properties

With these con- and destructive interferences removed from the trace (obtained by producing a second S-matrix with the sample 0.1 mm thick) and performing the same percentage changes in thickness as before, we obtain the results shown in Figure 11-6.

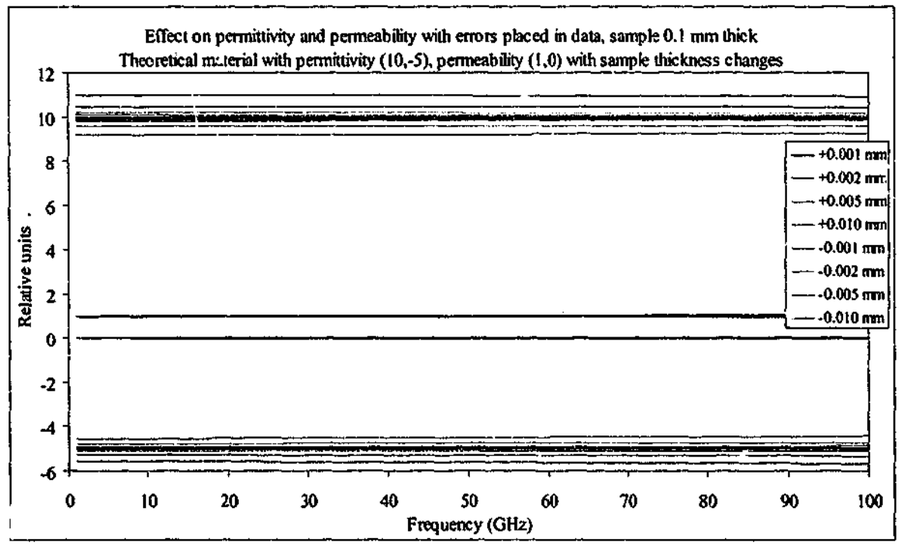

Figure 11-6. Permittivity and permeability of 0.1 mm thick theoretical material with incorrect thickness used in calculations

The conclusion from Figure 11-6 is that far from interference effects there is a one-to-one correspondence between errors in thickness determination and final permittivity results. Any error in the determination of the thickness of the sample leads to an equal percentage error in the permittivity values. Near destructive interference conditions however, the result obtained using the reflection/transmission algorithm can be quite unpredictable if thickness is not accurately known.

The reflection/transmission algorithm is able to change all four parameters (real and imaginary permittivity and permeability) to best account for an incorrect thickness when used in the calculations. The reflection only and transmission only algorithms have just the permittivity values to alter, and so respond differently to sample thickness errors. In order to investigate the effects on these algorithms, the same changes to sample thickness were applied with the results shown in Figure 11-7 to Figure 11-10.

The results from the transmission only algorithm show that errors in sample thickness have only a minor effect on the final extracted permittivity values. Of course the absolute values have been shifted by the same percentage change that was present in the thickness, but generally the extra effects are small. At around 25 GHz, the real permittivity shift increases from a value similar to the change in thickness at low frequencies, to a value about 1.5 times this value at high frequencies. Around this same frequency the imaginary values all tend towards the correct value of –5. Away from the effects observed near 25 GHz, both the real and imaginary values are relatively constant and have an error level approximately 1.5 times that of the error in the thickness.

However, the reflection only result is a completely different story. This algorithm has never been a particularly stable one when errors such as sample positional shifts are present in the data, and it can be seen that thickness variations cause this algorithm problems too. At frequencies of around 30 – 35 GHz, the algorithm has trouble staying on the correct solution and if the thickness errors are large enough, the program shifts the solution to one that has a lower permittivity. This occurs again at around 75 GHz with all the curves now shifting to a solution with lower values. Exactly what is causing these problems is not known precisely, but it probably has to do with the effects of multiple internal reflections inside the sample. Since the thicknesses are slightly incorrect, the program is expecting these effects at different frequencies to those expected, with the outcomes shown in the figures below.

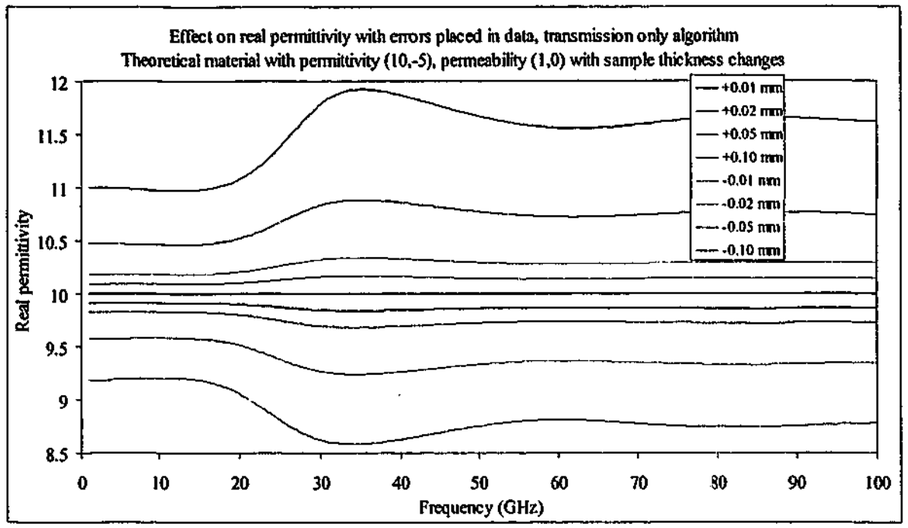

Figure 11-7. Real permittivity of theoretical material with incorrect thickness used in calculations using transmission only algorithm, sample nominal thickness 1 mm

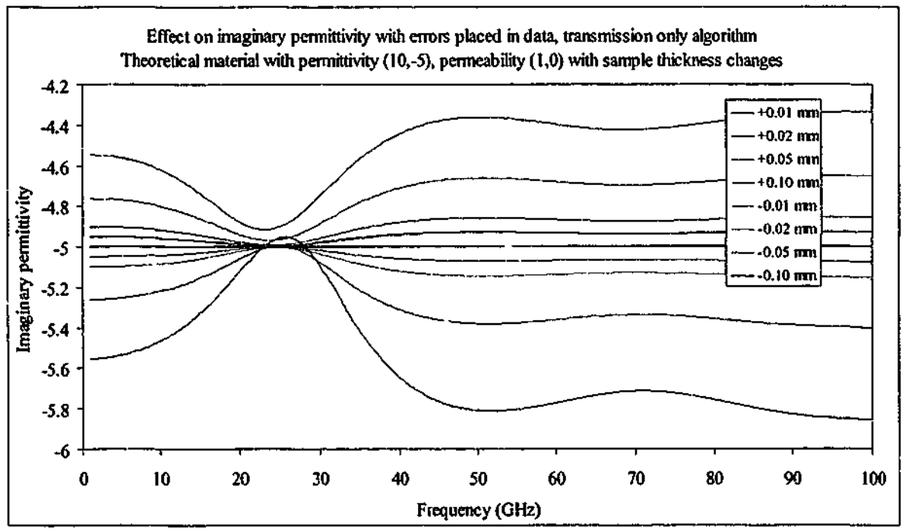

Figure 11-8. Imaginary permittivity of theoretical material with incorrect thickness used in calculations using transmission only algorithm, sample nominal thickness 1 mm

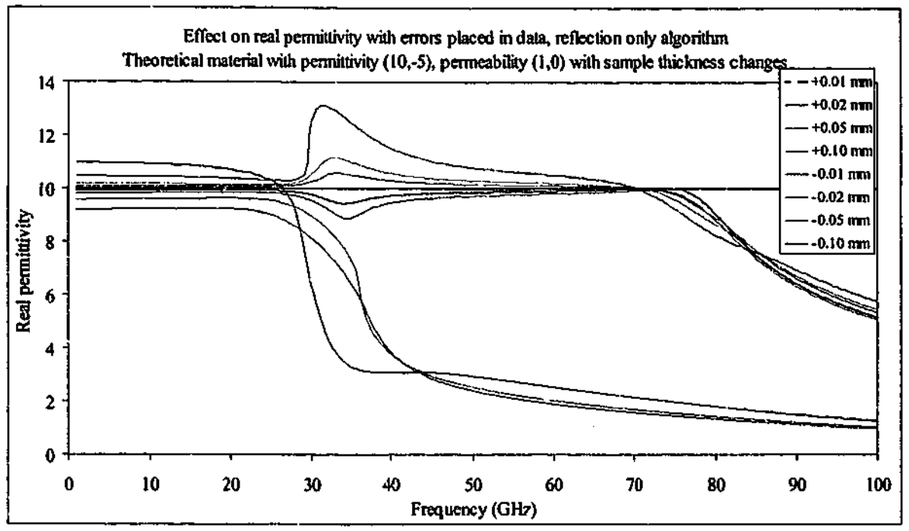

Figure 11-9. Real permeability of theoretical material with incorrect thickness used in calculations using reflection only algorithm, sample nominal thickness 1 mm

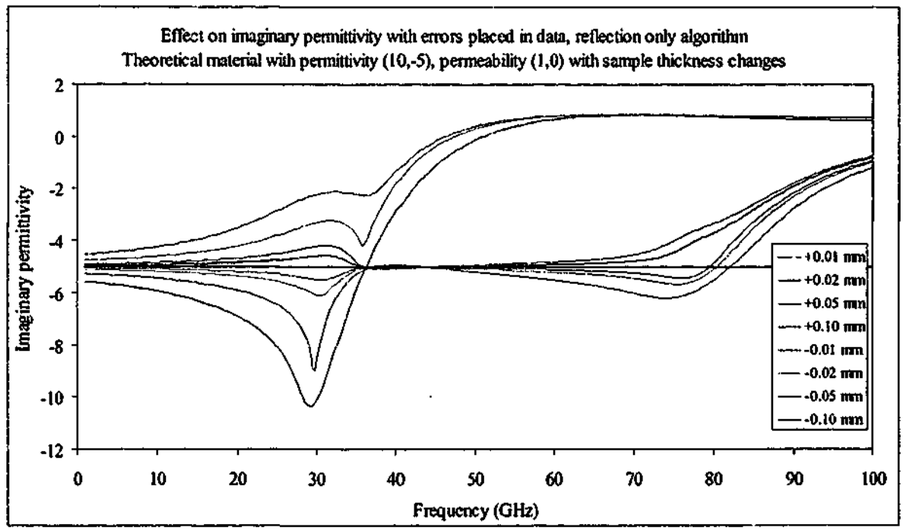

Figure 11-10. Imaginary permeability of theoretical material with incorrect thickness used in calculations using reflection only algorithm, sample nominal thickness 1 mm

When a very thin sample is used in the analysis, both single parameter algorithms show similar shifts to those observed for the reflection/transmission algorithm results of Figure 11-6. The algorithms produce similar results when the thickness used does not produce con- or destructive interference conditions.

11.2. Calibration plane shifts

The importance of sample placement on to the calibration plane when measuring reflection is critical, and is one of the major reasons why permittivity and permeability measurements are so difficult in free space. Other researchers[37] have constructed elaborate vertical stands with micrometers on worm gears to position the sample or horns to exactly the right location, but this technique is complex, only useful if the sample is rigid and requires focussing lenses to reduce the effects of the sample holder. Placing the sample horizontally on a foam stand is a much easier measurement, but the technique assumes that the sample will not compress the foam, the foam is transparent and that the surface of the foam is flat. For these reasons 300 mm thick polystyrene foam was used as a sample holder for this study. It can easily be cut reasonably flat, is almost transparent to microwaves and is stiff enough to stop the sample deforming it. The properties of flexible samples can be measured using this technique and the specimens will conform to the shape of the foam block, but rigid samples may have inbuilt stresses causing them to be deformed slightly. Since the materials used as reflection standards in this study were rigid, some slight shifting of the calibration plane is almost inevitable. However, if the shift is known (and can be measured) the effect can be countered somewhat by shifting the calibration plane in the computer program.

The effect of shifting the calibration plane by a fixed distance is frequency dependent, with higher frequencies being more affected than lower ones. This is because a fixed distance is a higher percentage of the wavelength at high frequencies than lower ones. Using the same theoretical material as before it is possible to see the effect that even a small shift in the calibration plane has on the extracted permittivity and permeability.

With the thickness of the sample set at 1 mm, the effects of altering the calibration plane on the reflection/transmission algorithm are shown in Figure 11-11 to Figure 11-14. It is interesting to note that for all but the largest shifts the real permittivity does not alter significantly until the frequency climbs above 30 GHz whereas the imaginary component moves off its correct value much earlier. When testing non-magnetic materials the permeability can be used to find the correct shift required, where it can be seen that shifts as small as 50 μm can cause the real permeability to shift by 5 % at frequencies below 20 GHz. A good method of determining the correct shift is to apply the value that removes the frequency dependence of the imaginary permeability; this usually corrects the real permeability also.

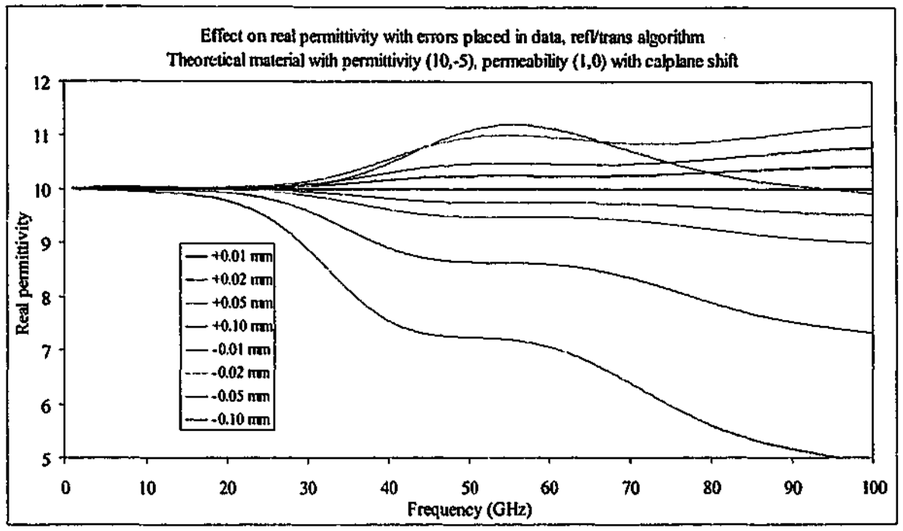

Figure 11-11. Real permittivity of theoretical material with calibration plane shifted using reflection/transmission algorithm

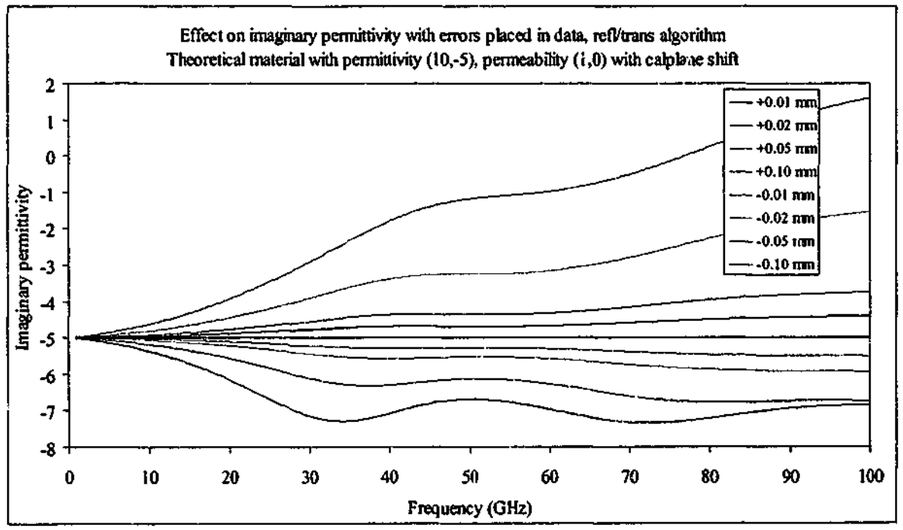

Figure 11-12. Imaginary permittivity of theoretical material with calibration plane shifted using reflection/transmission algorithm

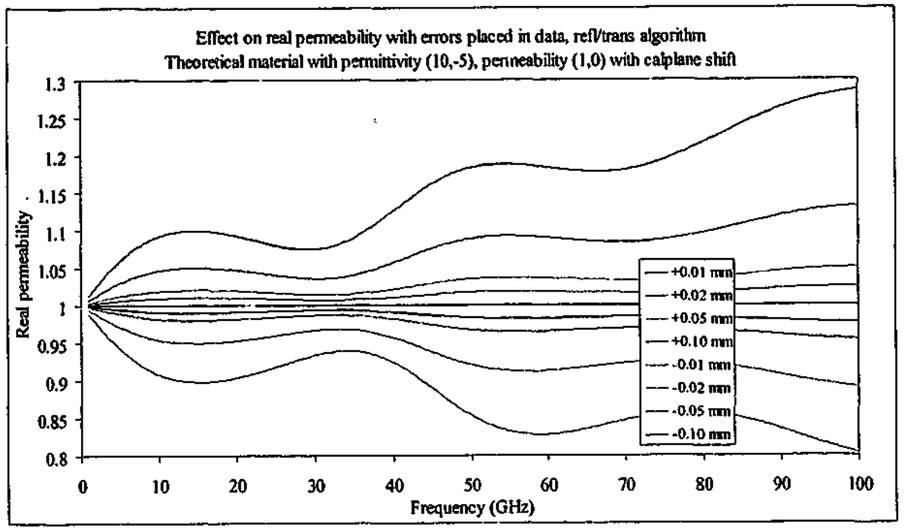

Figure 11-13. Real permeability of theoretical material with calibration plane shifted using reflection/transmission algorithm

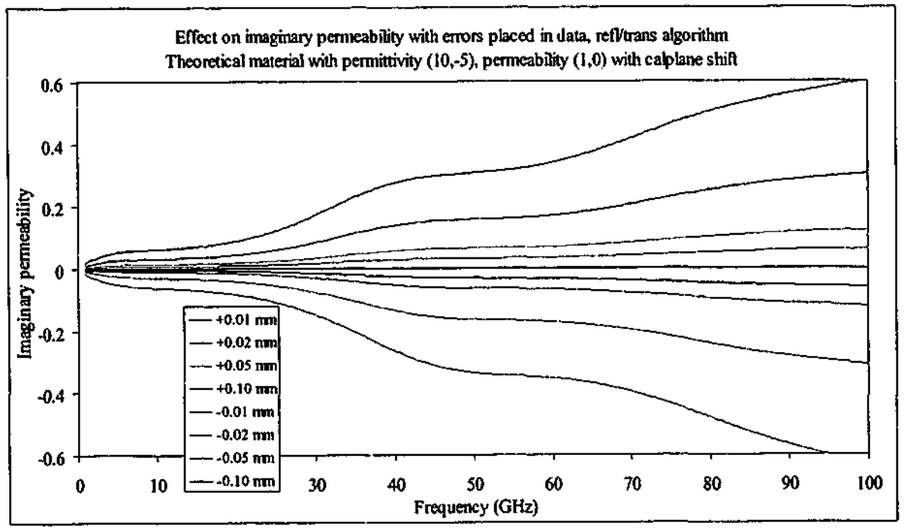

Figure 11-14. Imaginary permeability of theoretical material with calibration plane shifted using reflection/transmission algorithm

The phase shift caused by moving the calibration plane affects the permittivity evaluation differently for samples with different thicknesses. Figure 11-15 to Figure 11-18 shows how the permittivity and permeability varies with thickness after a constant phase shift corresponding to 0.1 mm of air has been applied to the data. The calibration plane shift affects

each parameter differently, with sample thickness being no reliable indicator as to whether the effect is large or small. Were a different phase shift applied, the calibration plane shift would alter the parameters differently again.

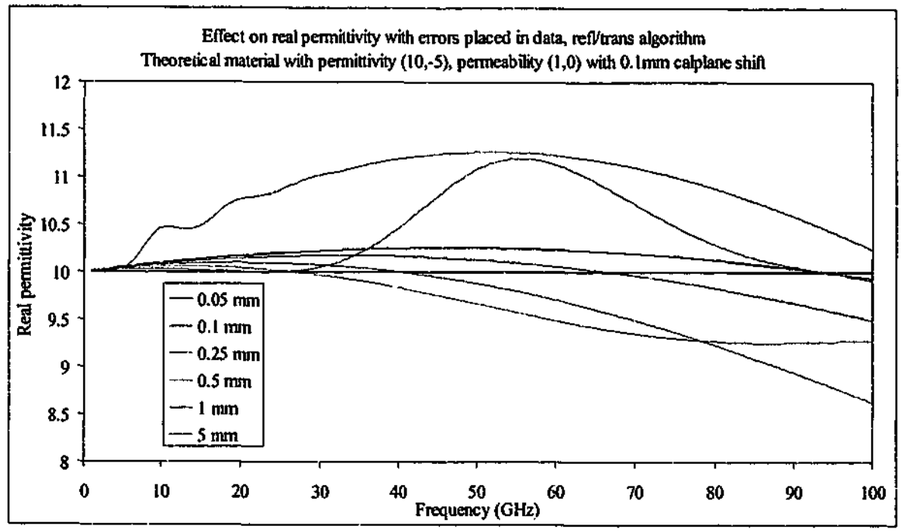

Figure 11-15. Real permittivity of theoretical material with various thicknesses and calibration plane shifted 0.1mm using reflection/transmission algorithm

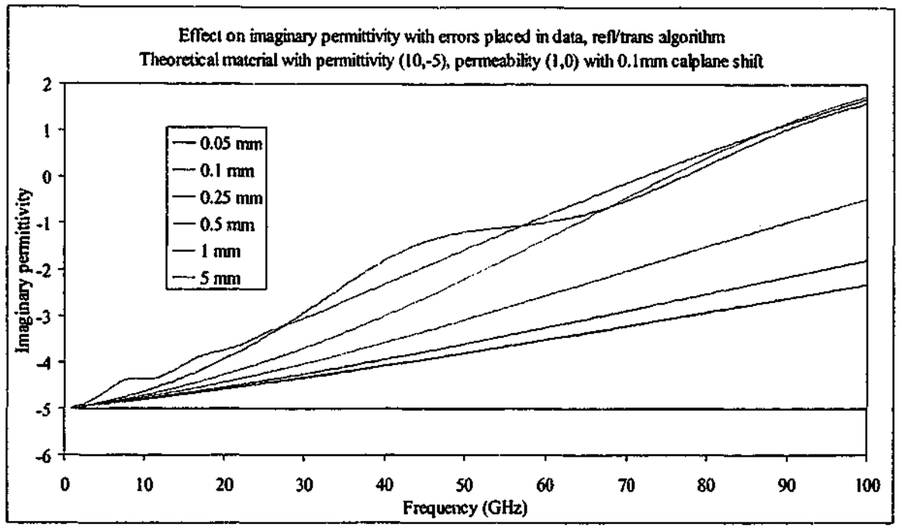

Figure 11-16. Imaginary permittivity of theoretical material with various thicknesses and calibration plane shifted 0.1mm using reflection/transmission algorithm

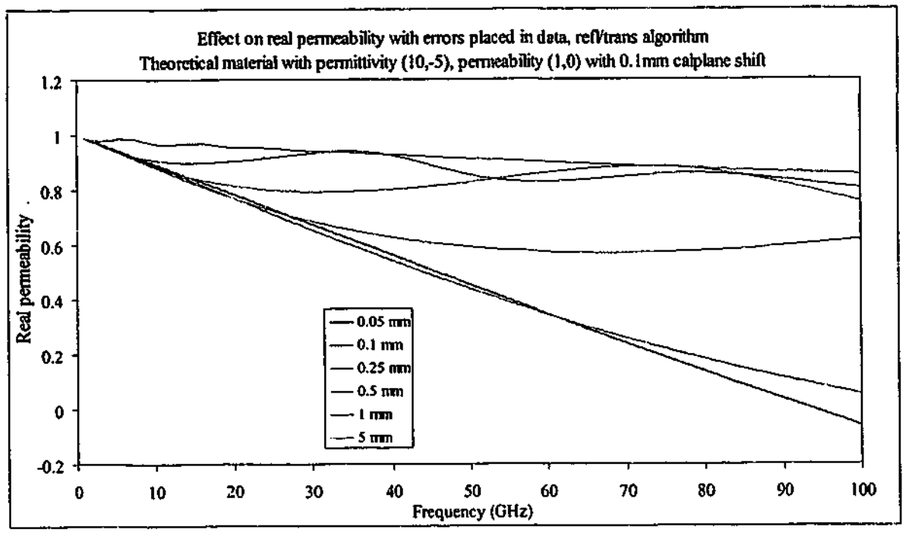

Figure 11-17. Real permeability of theoretical material with various thicknesses and calibration plane shifted 0.1mm using reflection/transmission algorithm

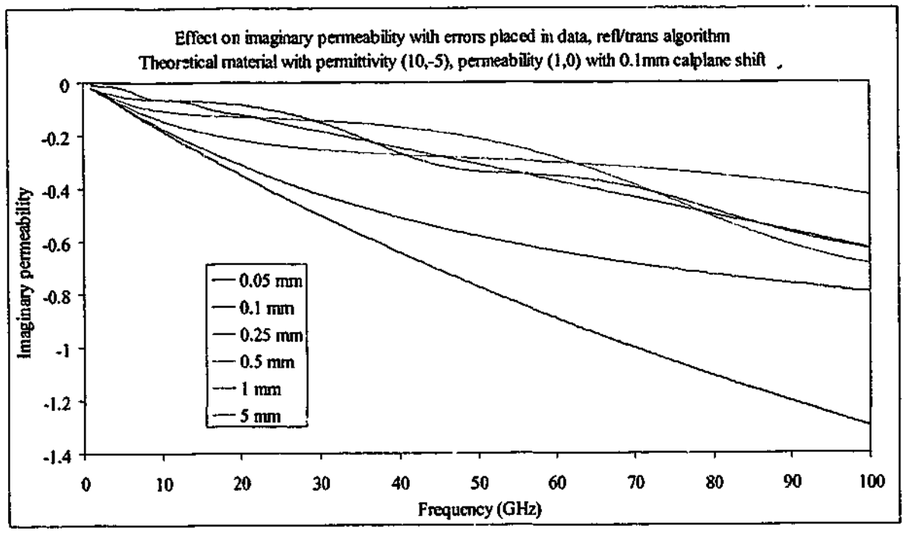

Figure 11-18. Imaginary permeability of theoretical material with various thicknesses and calibration plane shifted 0.1mm using reflection/transmission algorithm

Because the effects upon the permittivity and permeability are so sensitive to sample placement, it is good measurement practice to measure a known non-magnetic standard with similar physical properties at the same time as measuring the unknown material. If, for instance, the unknown material were flexible then this would require a flexible standard to be

measured in the same configuration. Rigid materials would be more difficult as inbuilt stresses may bend the sample in irreproducible ways; however, one should attempt to produce a non-magnetic version of the sample to be used as a standard. Failing that, the surface of the material may be machined flat in order to minimise errors. Every effort should be made to maintain a flat surface on the foam sample holder, and obtain a flat metallic sheet for calibration purposes.

11.3. Stray reflection and diffraction peaks

Extraneous signals are usually present in the measured signal, be they reflections from the test fixture or from the horns themselves. In order to gain some insight into the effects of these reflections, the time gating program was modified to add an echo with a known magnitude, phase and delay to a measured data file. The file chosen was the transmission through a Perspex sample measured with the silver horns over the range 7.5 – 18 GHz. Perspex was chosen because it has properties that are independent of frequency and because the transmission loss is low, less than 1 dB across the full frequency range. The extraneous peak (echo) applied had the following form,

$$Peak_{real} = M \times e^{-\frac{(t-s)^2}{0.007}} \cos(42t) \qquad \text{Equation 11-1}$$

$$Peak_{imag} = M \times e^{-\frac{(t-s)^2}{0.007}} \sin(42t) \qquad \text{Equation 11-2}$$

where M is the linear magnitude of the peak, t is time and s is the positional shift in time of the peak in nanoseconds. The constants in the equations maintain the correct form of the peak size and shape. When the peak is added, the effect in the time domain is shown in Figure 11-19, where the peak has a magnitude of –40 dB and a time shift of 0.5 ns. The 3-term Blackman – Harris window was used for the time domain conversion. When the time domain data is transformed back into the frequency domain the peak causes a sinusoidal error term in the measured signal for even very weak extraneous peaks. The effect on the magnitude is shown in Figure 11-20 for an added peak with a magnitude of –40 dB and time shifts of 0.2 and 0.5 ns.

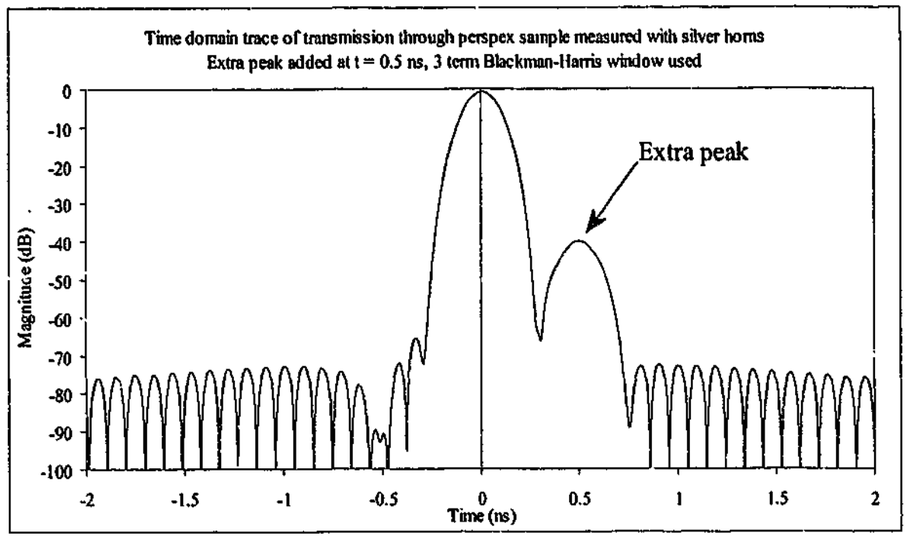

Figure 11-19. Extraneous peak added to Perspex transmission data in the time domain

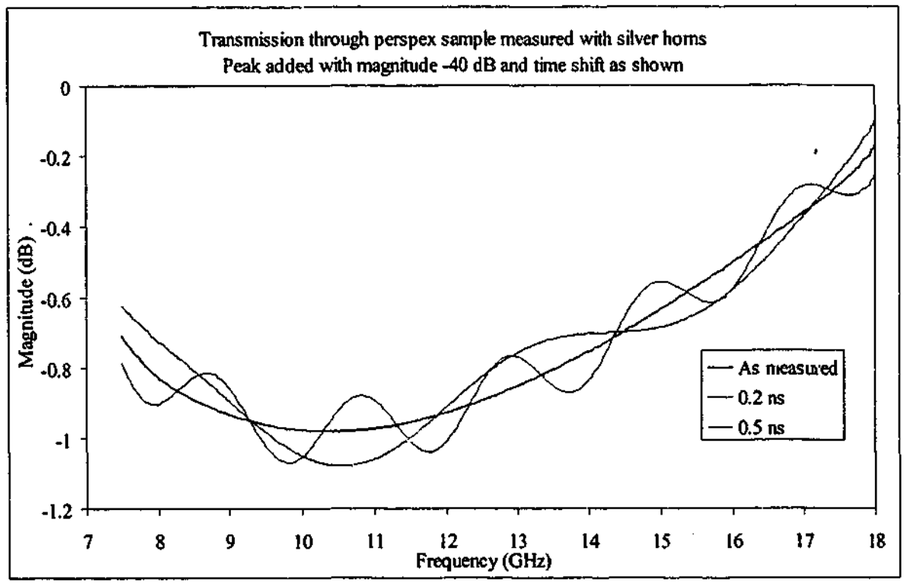

Figure 11-20. Effect of extraneous peak added to Perspex transmission data in the frequency domain

The effect on the signal is very pronounced and leads to a sinusoidal behaviour in the extracted permittivity values, with the frequency of the oscillation increasing with the displacement in time of the added peak. The extracted real permittivity values using the

transmission only method for the Perspex sample with a number of different extra peaks are shown in Figure 11-21.

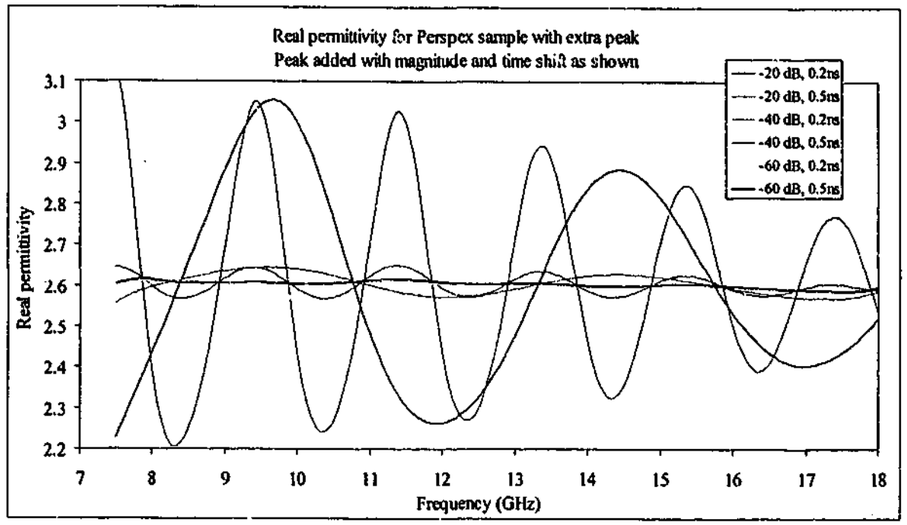

Figure 11-21. Real permittivity of Perspex sample with extra peak added

The effect on the permittivity for such low intensity peaks is quite large, considering the maximum level of the additional peak is around 1 % of the original signal. The peak 20 dB below the main signal is shown to cause error levels of ± 15% over this frequency range. Similar levels are observed in the imaginary component. One interesting point about Figure 11-21 is the time position of extraneous peaks can be inferred by the period of any oscillations in the permittivity trace. If the oscillation is rapid across the frequency span, the user can determine that a stray peak is present some distance away from the main peak. If the oscillation is slower, then the error peak may be closer to the desired one.

This effect can be seen in the measured transmission data by comparing the transmission results for the samples when the diffraction signal is not removed. In the case of the measured Perspex data when the diffraction peak is not removed, we find the time domain response shown in Figure 11-22. As the distance between the horns increases, the time difference between the diffraction peak and the main one decreases, and so we would expect to find the period of the oscillations in the frequency (and hence permittivity) spectrum increase. Sure enough, this effect is observed in the real and imaginary permittivity values across the frequency range, where the real values are shown in Figure 11-23.

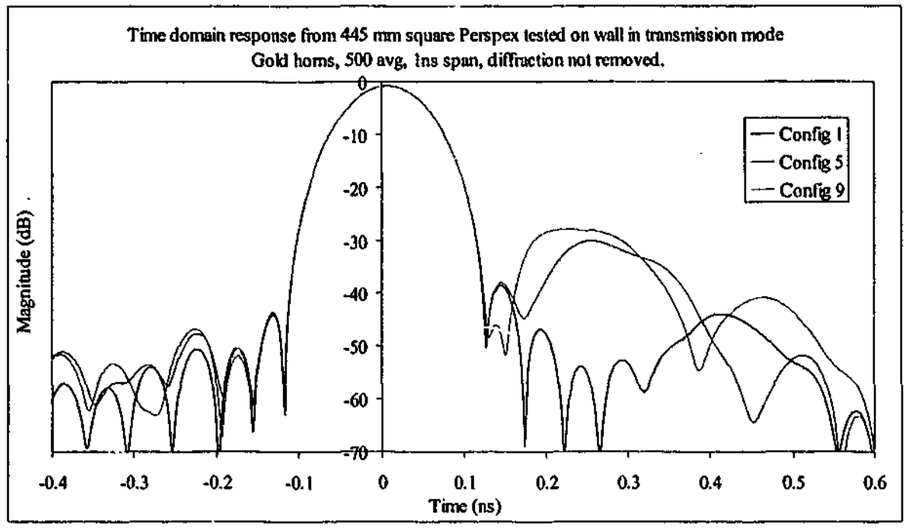

Figure 11-22. Time domain transmission response of 445 mm square Perspex sample

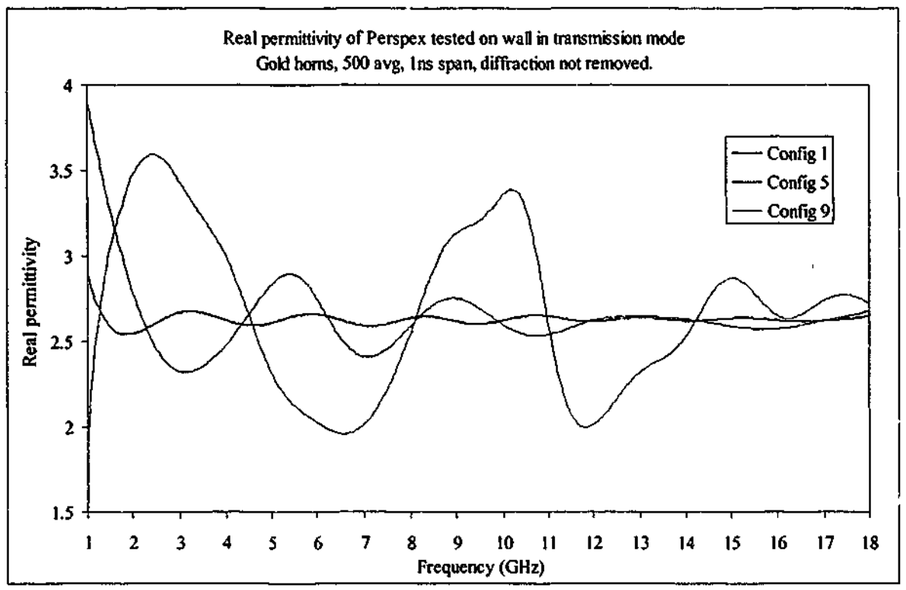

Figure 11-23. Real permittivity of 445 mm square Perspex sheet measured with gold horns using transmission only algorithm, with diffraction peak not removed

It can be seen that as the diffraction peak moves closer to the main peak, the number of dips in the trace reduces from seven in the case of configuration 1, to four when tested in configuration 5, to finally 2 or 3 when the horns were in configuration 9. It is interesting to

see the secondary structure in the configuration 9 result caused by a second peak situated at about 0.45 ns in the time domain.

The transmission data measured over 7.5 – 18 GHz with the silver horns in configuration 1 does not have a large diffraction peak interfering with the main peak. However, if we place a peak with the same magnitude, phase and time shift that was present in the measurement over 1 – 18 GHz, we would hope to measure a similar response. In the case of the configuration 1 measurement, the diffraction peak had a magnitude of about –44dB and shifted by 0.41 ns. By appropriately adjusting the phase of this peak to 100 degrees, the real permittivity values of the measurement taken with the silver horns were adjusted to those shown in Figure 11-24. There was already some structure in the measurement taken over 7.5 – 18 GHz, but the presence of the artificial peak added to the time domain data has transformed the signal to match the result over 1 – 18 GHz.

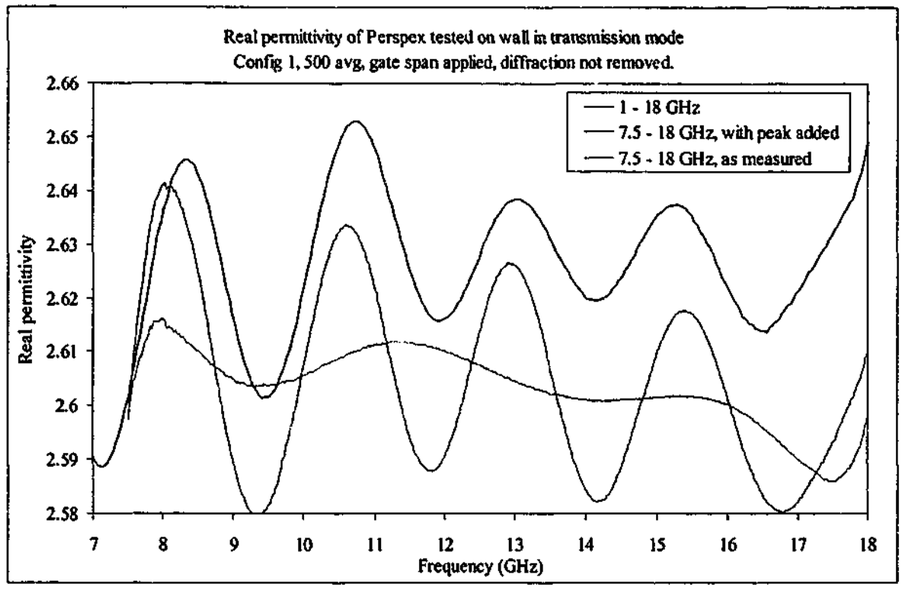

Figure 11-24. Real permittivity of 445 mm square Perspex sample measured on wall with extra diffraction peak added to transmission data

The same effect can be seen when comparing the measurements taken with the different horns (and hence gate widths). The time gate used for each measurement was set to the minimum possible whilst maintaining a full wave at the lowest frequency used. So as the gate width decreased, more of the stray reflections/diffraction peaks were excluded from the trace. This leads to a more even permittivity spectrum with the high frequency oscillations absent from the permittivity values. So when comparing the results from the gold, silver and high

frequency horns, the magnitude and period of oscillatory behaviour in the permittivity values is expected.

We can also expect this behaviour when directly comparing measurements on different sized samples. As sample size decreases, the time difference between the diffraction signal and the main signal is reduced and so the period of the oscillations across the frequency band increases. Effective removal of the diffraction peak has already been discussed, but the techniques are not 100% successful so oscillations are always present but details as to the source, size and frequency can be explained.

11.4. Sample size effects

One of the main aims of this project to find the optimum sample size for free space measurements, and the minimum size one requires for an accurate determination of permittivity and/or permeability. Naively one would expect that when performing transmission measurements that the bigger the sample, the better the measurement would be. While this statement is essentially true, it does not give an estimate of the sorts of errors one expects from a sample with a finite area. Other factors such as near field effects also come into play here, since one would expect that as the distance between the horns and the sample increases, the wavefront flattens out and the accuracy should increase. However, this means the sample must also grow in size to accommodate the increase in beamwidth from the horn, if the sample is of fixed size then the diffracted beam may introduce errors larger than those of the near field effect, which may not be able to be completely removed. As the sample size decreases, it becomes more important to effectively remove the diffraction signal.

The easiest way to directly compare the results of similar measurements on different sized samples is by placing the results on a single set of axes. Due to the amount of data involved only selected graphs will be presented here. It is useful to show how the extracted permittivity values of Perspex change with sample size over the three frequency ranges, as the other samples follow similar trends.

The real permittivity results for the three sample sizes using the transmission algorithm over the three frequency ranges are shown in Figure 11-25 to Figure 11-27. Small differences are observed in the 1 – 18 GHz range, with the largest of these occurring below 2 GHz in the 150 mm square case. In this area the wavelength of the radiation is larger than the sample so it is not surprising the results are in error; however, in this region even the 445 mm square sample is not error free. In the higher frequency ranges the size of the sample has little

discernable impact on the results, there is a slight increase in permittivity with smaller samples but the effect is less than 2 % of the actual value.

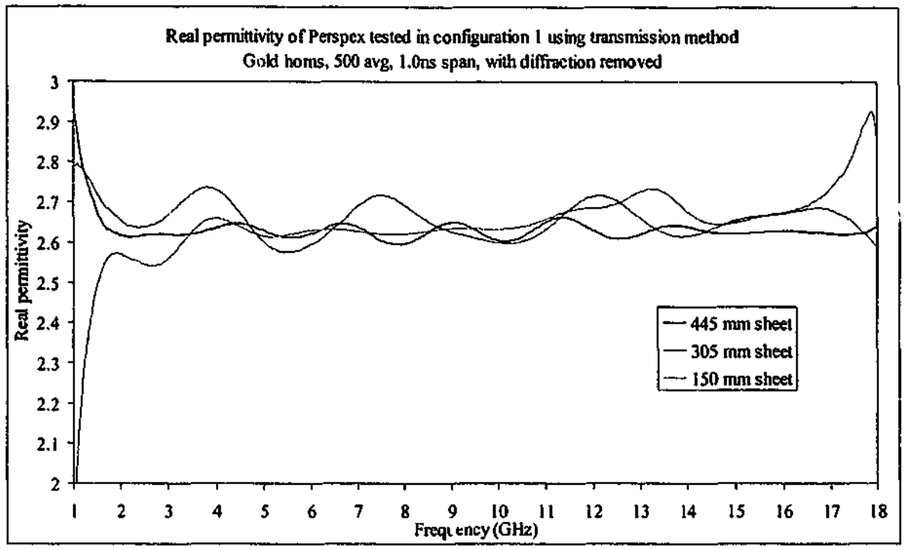

Figure 11-25. Real permittivity of different sized Perspex samples measured with gold horns using transmission only method with diffraction removed

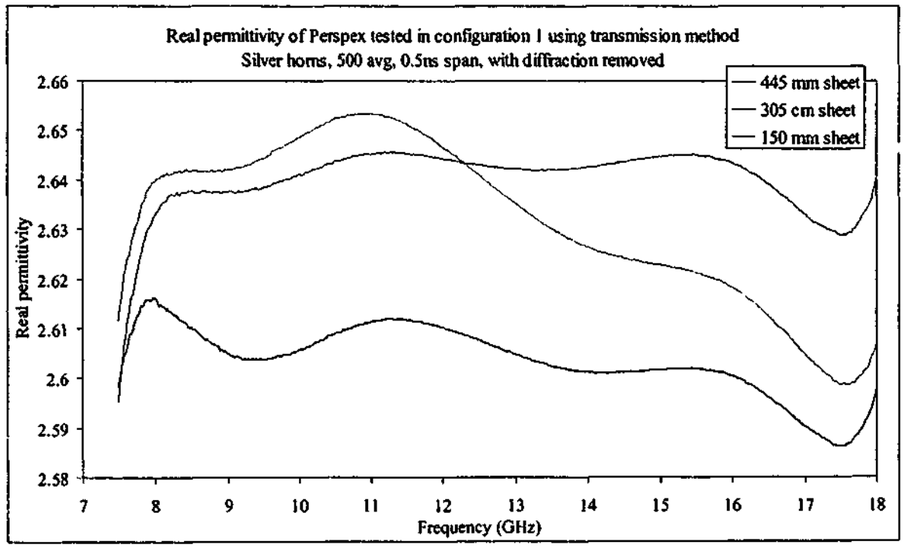

Figure 11-26. Real permittivity of different sized Perspex samples measured with silver horns using transmission only method with diffraction removed

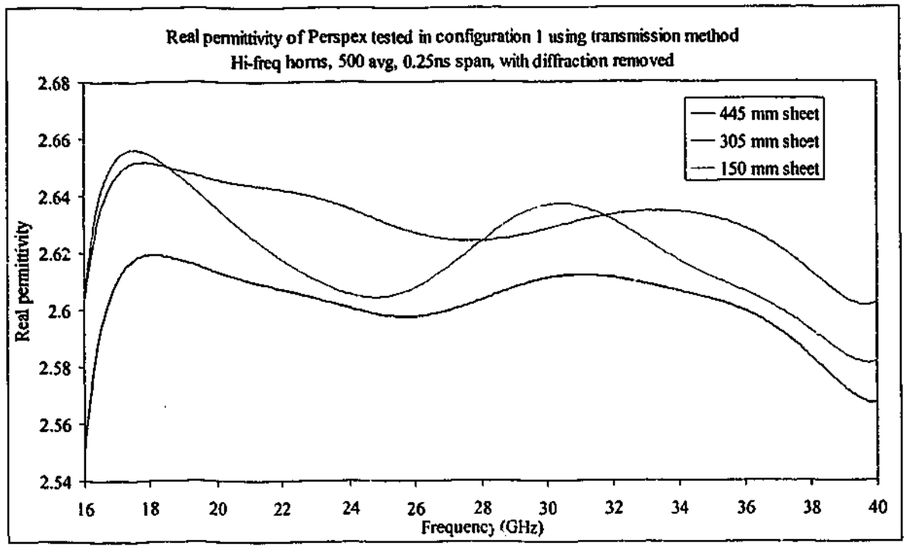

Figure 11-27. Real permittivity of different sized Perspex samples measured with hi-freq horns using transmission only method with diffraction removed

When the reflection only measurements are compared, the effects are not insignificant. Possible thickness errors in the sample may be causing problems near destructive interference points as seen earlier in the constructed material (see Figure 11-9). Sample flatness and alignment also plays a part, since large samples reflect a relatively narrow lobe that must be accurately directed back to the source. Smaller samples reflect a wider lobe that do not require the same level of pointing accuracy. So it is not surprising to see the effect of sample size on permittivity shown in Figure 11-28 and Figure 11-29. In both cases the real permittivity of the 445 mm square sheet drops below the value expected, while the 305 and 150 mm square sheets stay close to the value of 2.6 across most of the frequency band.

Due to the presence of destructive interference effects for this sample, results from the reflection and transmission algorithm are difficult to interpret since there are large spikes across the frequency bands of interest. For this reason samples other than Perspex will be used to investigate the effects of sample size on the reflection/transmission results.

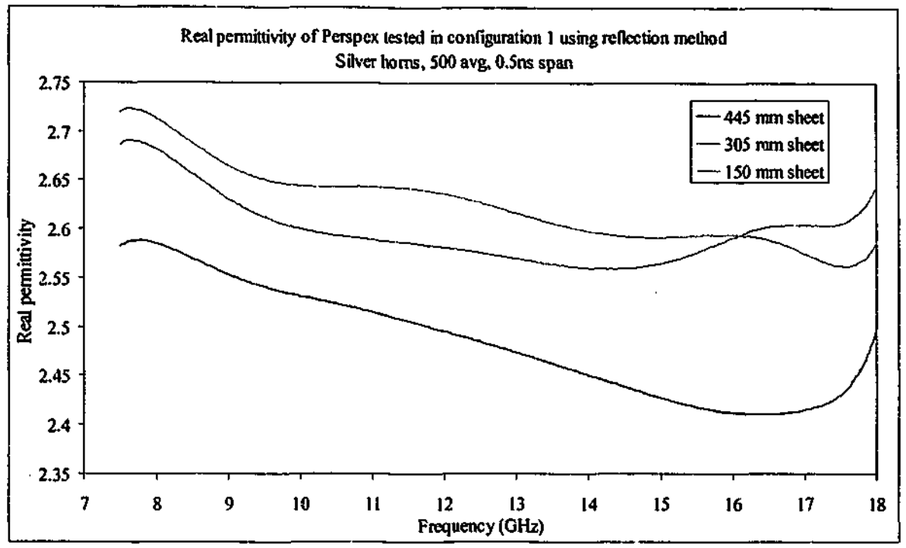

Figure 11-28. Real permittivity of different sized Perspex samples measured with silver horns using reflection only method

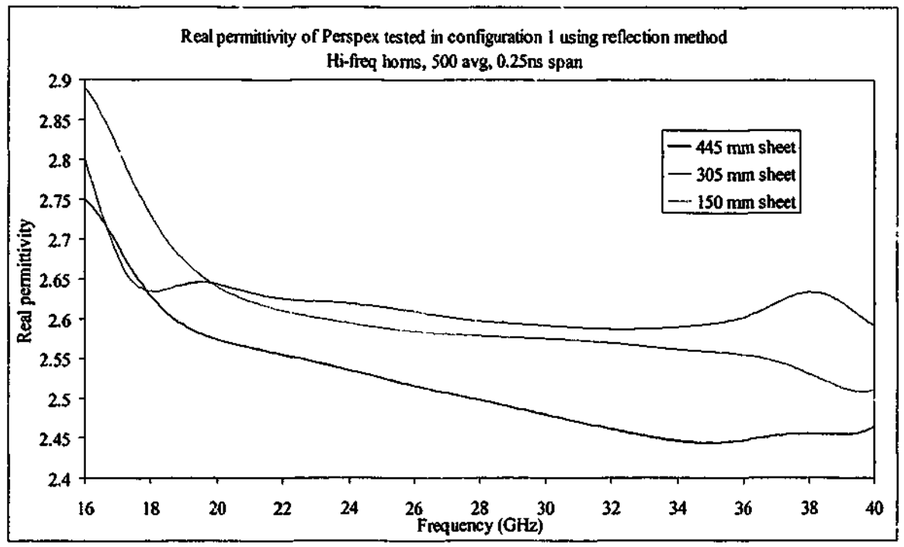

Figure 11-29. Real permittivity of different sized Perspex samples measured with hi-freq horns using reflection only method

Moving to the results of the carbon loaded rubber samples, it is possible to view all the data from a particular measurement on a single set of axes and still make sense of the results. Observing the transmission method results as before, we find that this method again gives good correlation between sample size and frequency band. The results of Figure 11-30 and

Figure 11-31 show that for all but the 1 – 18 GHz measurement of the 150 mm square sample at the frequency extremes, the size of the sample has very little effect on the permittivity values. The results from the smallest sample are in error at the lowest and highest frequencies when measured using the gold horns.

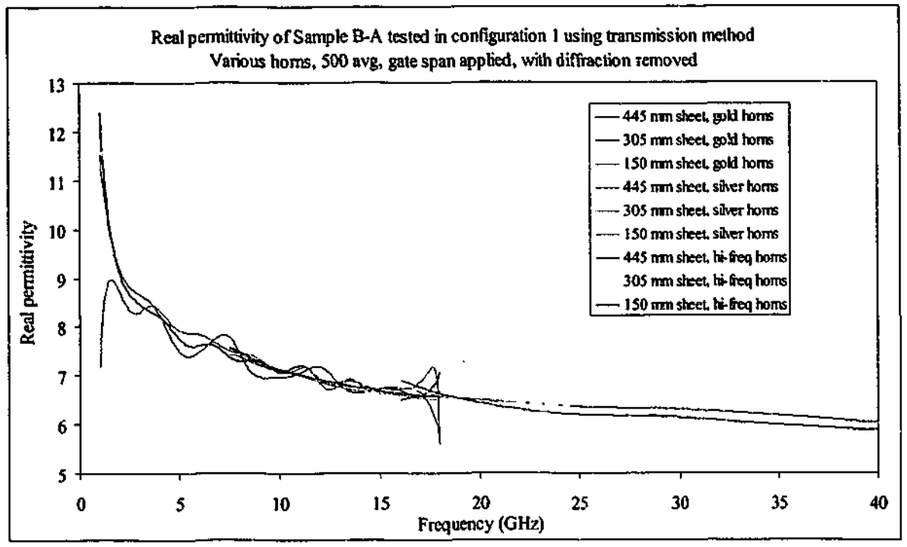

Figure 11-30. Real permittivity of different sized rubber B-A samples measured with various horns using transmission only method with diffraction removed

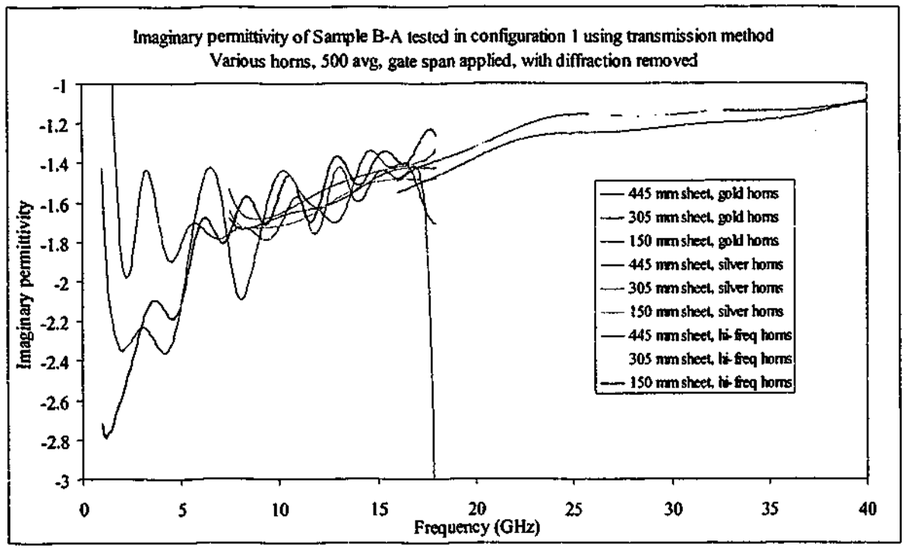

Figure 11-31. Imaginary permittivity of different sized rubber B-A samples measured with various horns using transmission only method with diffraction removed

When the reflection method is used to measure the permittivity of the samples, errors can occur because the technique has the added complication of maintaining the correct calibration plane. When the appropriate shift is applied, the results for sample B-A are shown in Figure 11-32 and Figure 11-33.

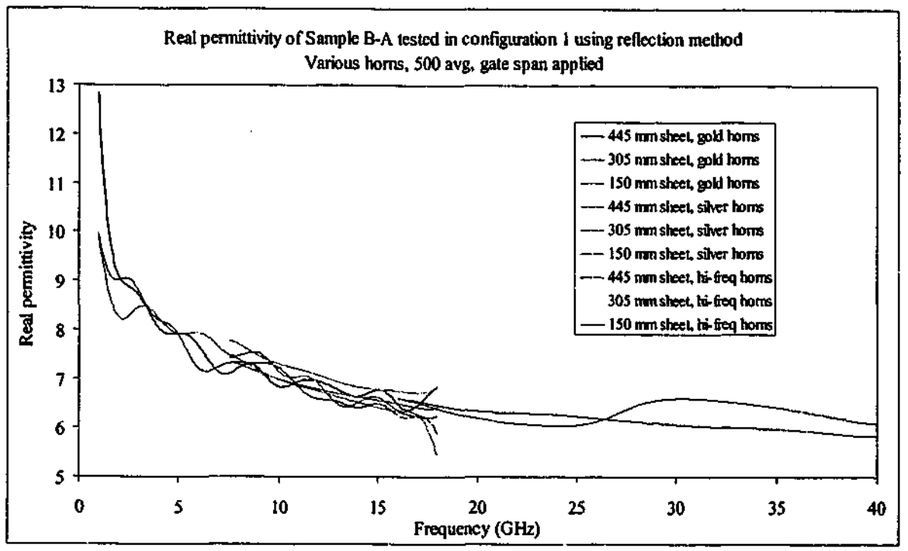

Figure 11-32. Real permittivity of different sized rubber B-A samples measured with various horns using reflection only method

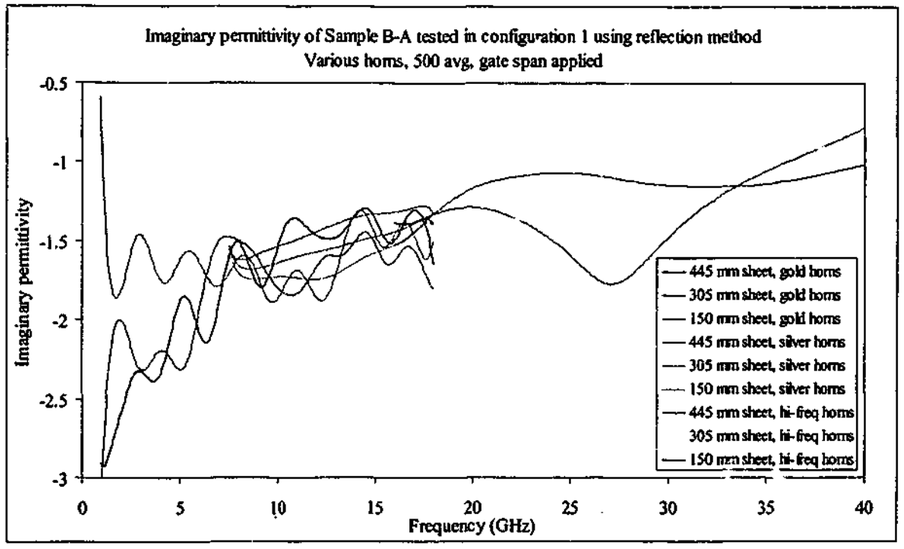

Figure 11-33. Imaginary permittivity of different sized rubber B-A samples measured with various horns using reflection only method

It can be seen that the measurements up to 18 GHz show good correlation with each other and those using the transmission only method. Only the 150 mm square sample deviates at low frequencies, where the wavelength of the radiation approaches the size of the sheet. At these low frequencies the reflection from this sample is of the order of 15 – 20 dB lower than that of the (already small) reflection from the similarly sized metal plate. This reduction in the signal causes a loss of resolution in an already error prone measurement, and so it is perhaps not surprising the results are in error.

Above 18 GHz, the reflection algorithm is introducing a peak in the imaginary component which was not present using the transmission method. This peak is more pronounced in the results taken from the larger sized samples but some evidence still remains in the 150 mm square material. Using the permittivity extracted from the transmission only result we can calculate the reflection signal expected, and compare it to the signal actually measured. These results are shown in Figure 11-34 and Figure 11-35 for the 445 and 305 mm square sheet.

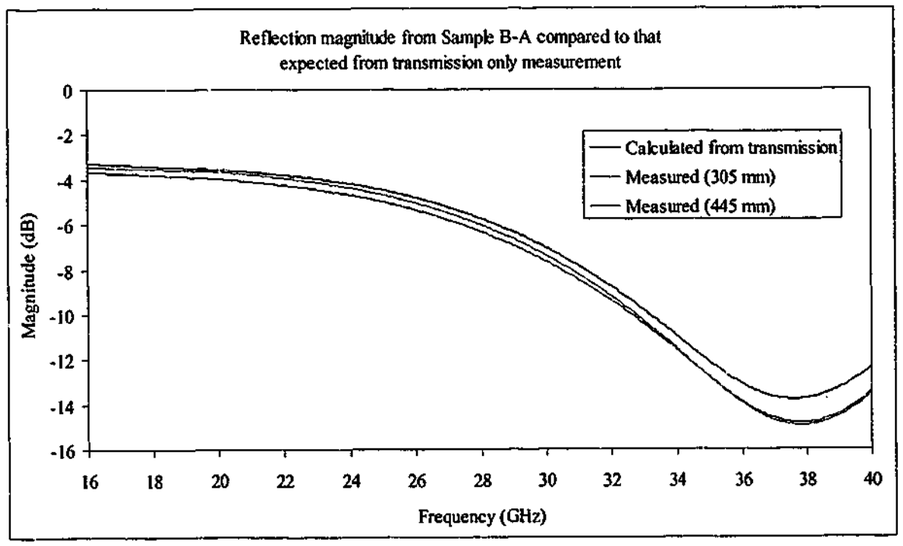

Figure 11-34. Magnitude of reflected signal from sample B compared to value calculated from transmission only result

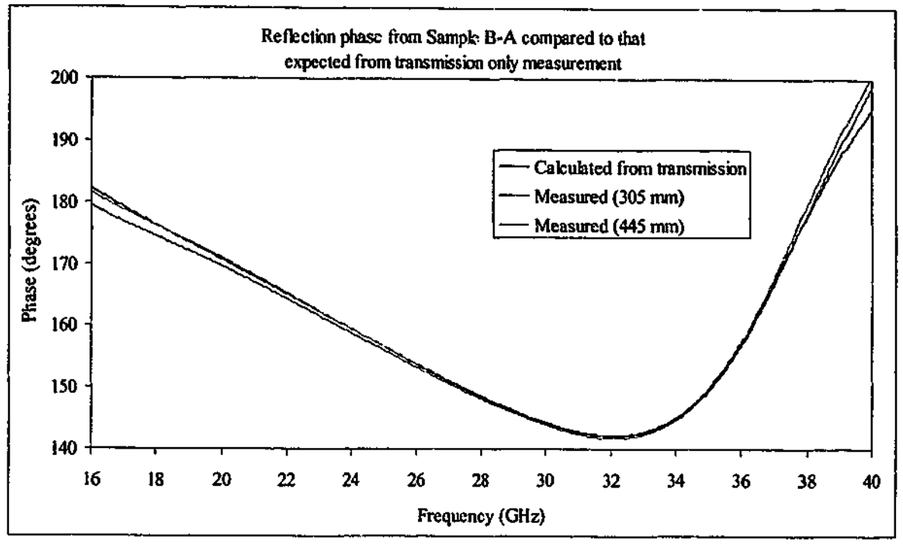

Figure 11-35. Phase of reflected signal from sample B compared to value calculated from transmission only result (phase wrapped over 180 degrees for ease of viewing)

Apart from the slightly reduced magnitude between the measured value and the expected one (which would probably tend to cause a slightly larger imaginary component to be extracted), there is very little difference between the expected and the measured values. Certainly nothing in the measured data indicates the sort of problems one sees in the derived permittivity values of Figure 11-32 and Figure 11-33. By slightly altering the value of the calibration plane shift, the magnitude of the peak in imaginary permittivity can be increased many-fold, but cannot be removed completely. The artefact is probably a feature of the sensitive nature of calculations in the complex plane.

When using both sets of data for the reflection/transmission algorithm, there is no doubt that the reduced values of reflection are causing errors in the permittivity calculations but the effect is minor. When viewing the graphs of Figure 11-36 and Figure 11-37 it is clear that the peaks present in the imaginary permittivity data when using the reflection data only have all but disappeared, being replaced by the normal variations caused by the destructive interference peak at about 38 GHz. The low frequency response of the 150 mm square sample still shows the same high frequency oscillations caused by the large diffraction signal close to the main peak, which the program cannot remove completely.

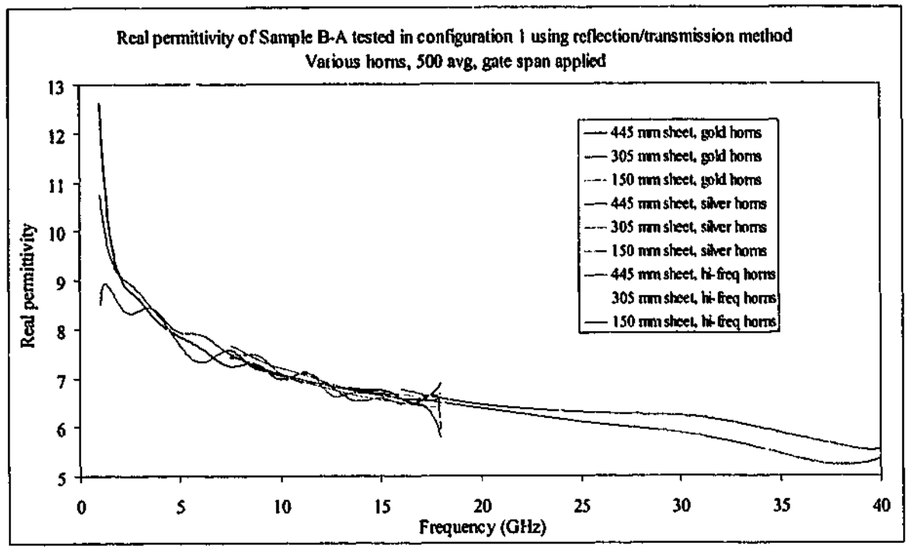

Figure 11-36. Real permittivity of different sized rubber B-A samples measured with various horns using reflection/transmission method

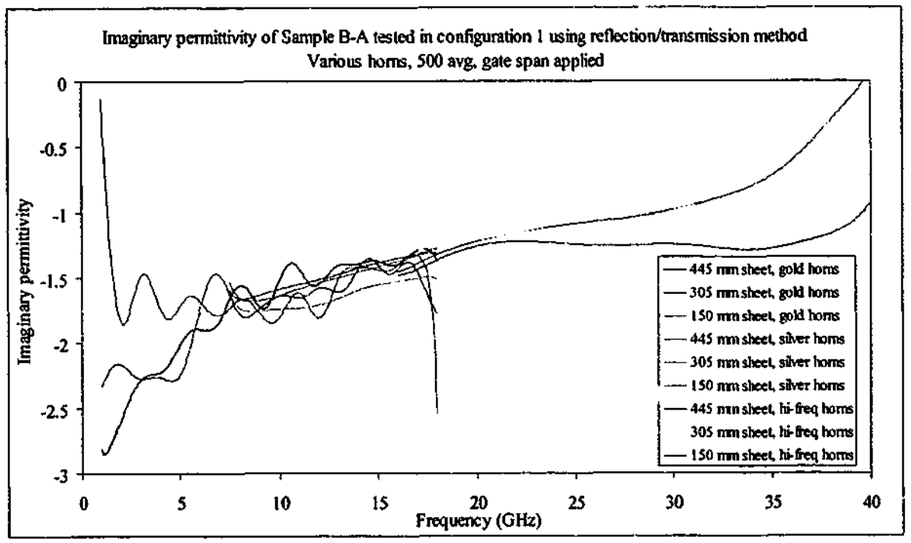

Figure 11-37. Imaginary permittivity of different sized rubber B-A samples measured with various horns using reflection/transmission method

The permeability data corresponding to the above permittivity results can be seen in Figure 11-38 and Figure 11-39. The low frequency response of the smaller samples again show oscillations caused by incomplete removal of the stray reflections and diffraction, but in the main the average values for all results stay close to the values expected for non-magnetic

materials. Only at the highest frequencies to the values stray, and this can be accounted for by the presence of the destructive interference at 38 GHz.

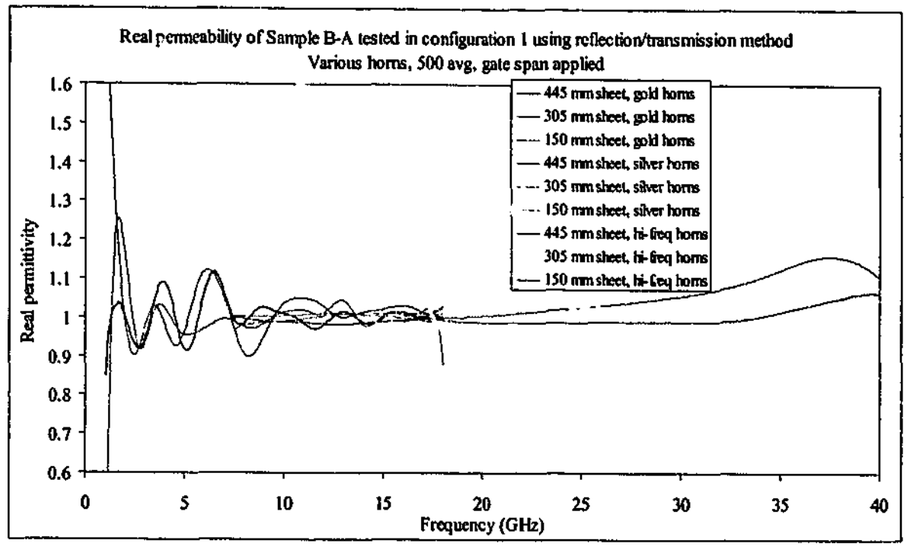

Figure 11-38. Real permeability of different sized rubber B-A samples measured with various horns using reflection/transmission method

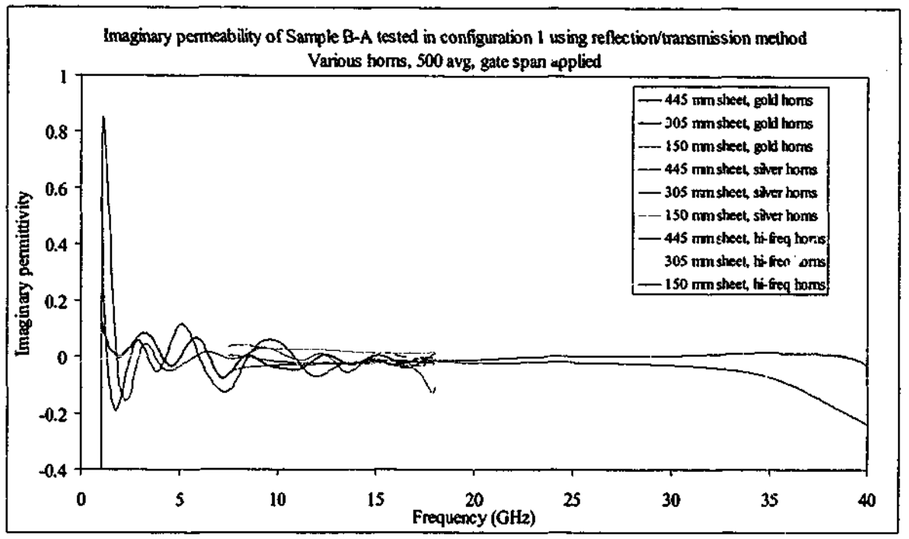

Figure 11-39. Imaginary permeability of different sized rubber B-A samples measured with various horns using reflection/transmission method

The effects noted in the discussion of rubber sample B apply more or less equally to the other carbon loaded rubber samples, with the understanding that the effects tend to increase

with sample permittivity. As permittivity increases, the transmission magnitude decreases and so the effects of diffraction increase. As can be seen from Figure 11-40 and Figure 11-41, not even the 445 mm square sheet is immune from incomplete cancellation of the diffraction wave at low frequencies, with the diffraction beam only 4 to 5 dB lower than the total transmission signal. The smaller sheets are even worse off with the diffraction beam around 10 dB *larger* than that travelling through the sample in the case of the 150 mm square sheet. When this is taken into account it is perhaps surprising that the algorithm converges at all, but the fact that it gives a consistent value is a testament to the effectiveness of the diffraction removal process. Below about 6 GHz the results from the 150 mm square sample do not follow those of the larger samples, instead the value of the real component increases markedly with a corresponding decrease in the imaginary component. In terms of constructing guidelines for good measurement practice, it should be stated that the sample should be large enough so that the magnitude of the diffraction beam be no larger than the transmission loss through the specimen. Of course one never knows for certain the transmission loss expected from a material with unknown electromagnetic properties until it is actually measured; however, after measurement procedure has taken place the user will be in a better position to state a level of accuracy for the sample. If the diffraction signal measured is large than that of the specimen, then a new sample should be produced or the diffraction removed using some other method (such as by using higher gain horns or a lens focussing technique).

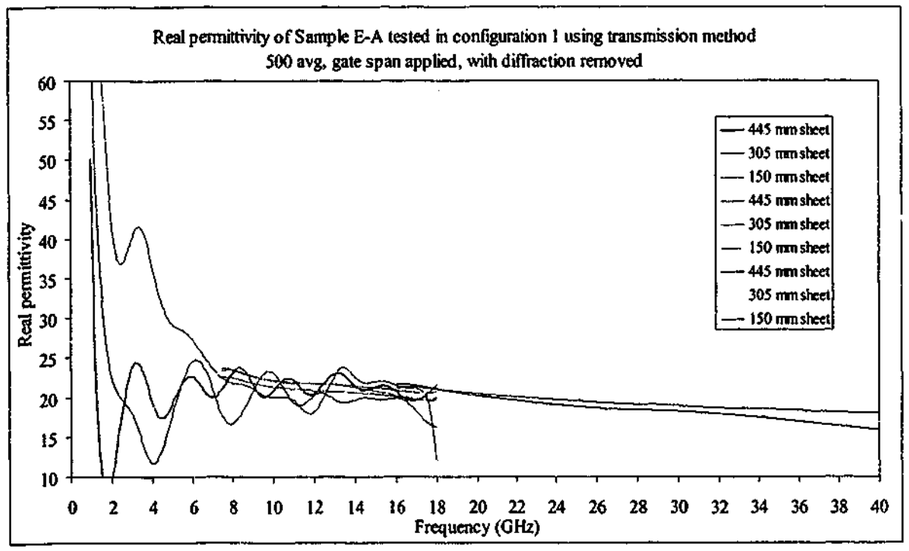

Figure 11-40. Real permittivity of different sized rubber E-A samples measured with various horns using transmission method with diffraction removed

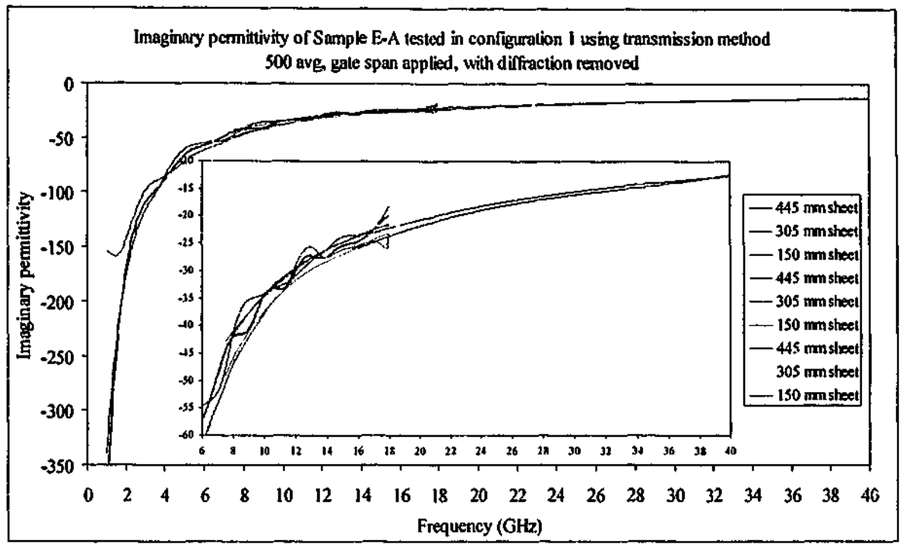

Figure 11-41. Imaginary permittivity of different sized rubber E-A samples measured with various horns using transmission method with diffraction removed

11.5. Horn to sample distances

Many results were taken in order to determine the optimum distances between the horn(s) and the sample. The effects of diffraction have already been discussed at length, and since it is the major source of error in the measurement process, every effort should be used to minimise its effects. However, there are several reasons why the sample should not be simply placed adjacent to the horns, including

- multiple reflections between the horn(s) and the sample
- multiple reflections between the two horns
- effective time gating.

The effects from multiple reflections between the horns and the sample have been presented earlier, but some further discussion is necessary. The microwave horn is a device that is designed to match the impedance between the waveguide and air at the appropriate frequencies as best as possible; however, there will always be mismatches causing reflections by the horn. Calibration techniques can remove some of these effects, but because the calibration process requires the test sample to be removed, it is not possible to completely eliminate the reflections between the sample and the horn(s). Time gating is often used to eliminate these reflections, but is only effective when the undesired signal is outside the gate width. When frequencies are high, it is possible to gate very tightly around the required signal

(within in the limits of multiple internal reflections) to remove the unwanted reflections. Of course at very high frequencies, compact high gain horns are easy to manufacture and so diffraction effects are less, which means the horns can be further from the sample to start with. At frequencies below 3 GHz, the wavelength is larger than 100 mm and many difficulties all combine to reduce measurement accuracy. High gain horns become harder to produce and are much larger, diffraction increases and the minimum time gate required to include the entire wave grows. The horns must therefore be further apart so that effective time gating can be used, the side effect being that the diffraction is increased.

Sometimes the minimum distances are fixed for other reasons, such as was the case in the reflection and transmission techniques investigated. Because the sample was positioned horizontally and the algorithms used were so sensitive to the sample's vertical position in space, a thick sheet of polystyrene foam was required to avoid the weight of the sample bending the holder. Originally, the sample was placed on a 100 mm thick sheet of polystyrene foam on a steel frame that was attached at the rear on the same vertical pole used to fix the horns. The weight of the samples caused a bending moment on the frame sufficient to extinguish any hope of measuring permeability accurately. The sheet was then adhered to a purpose built frame that was separate from the pole, but some of the samples were bending the foam sheet in the centre. The foam sheet was replaced with a 300 mm thick foam block, and the vertical position problem was solved. This meant that at least one of the horns was going to be a minimum of 300 mm from the sample, and since the send horn was positioned underneath this was the closest it could be from the sample. This increased the diffraction signal which might otherwise be smaller had the send horn been closer.

The effect of testing in the near field has been a largely unknown quantity prior to this study. Due to the complex nature of the mathematics involved in solving the equations when the incident wave is actually spherical in nature, the effect is usually just ignored and the plane wave solution used to extract the permittivity and permeability. While none of the measurements taken in the course of this study have satisfied the strictest definition of "far-field", it is nevertheless useful to note any differences in parameters when the distance between the horns and the sample is increased.

Using the reflection results of rubber sample E as an example, we find that the effect of sample to horn distance is negligible, as shown in Figure 11-42 and Figure 11-43. The results from configuration 3, where the sample to horn distance is greatest, shows more room echo clutter than the others, presumably because the actual signal strength received by the horn is lower in comparison to the fixed clutter. However, there is no indication of a systematic shift

in permittivity as the distance between the horns and the sample increases which might result from more "plane wave like" behaviour.

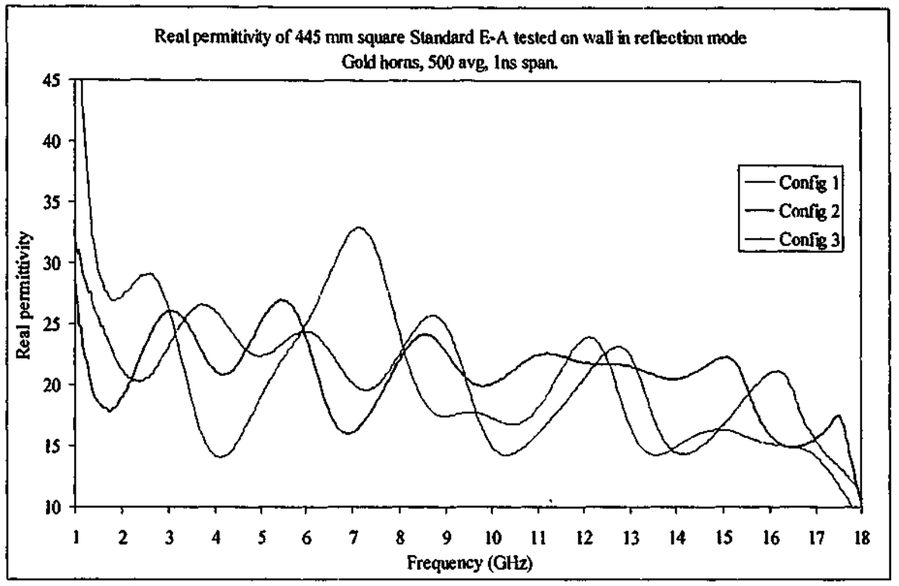

Figure 11-42. Real permittivity of 445 mm square rubber Standard E-A samples measured with gold horns using reflection method

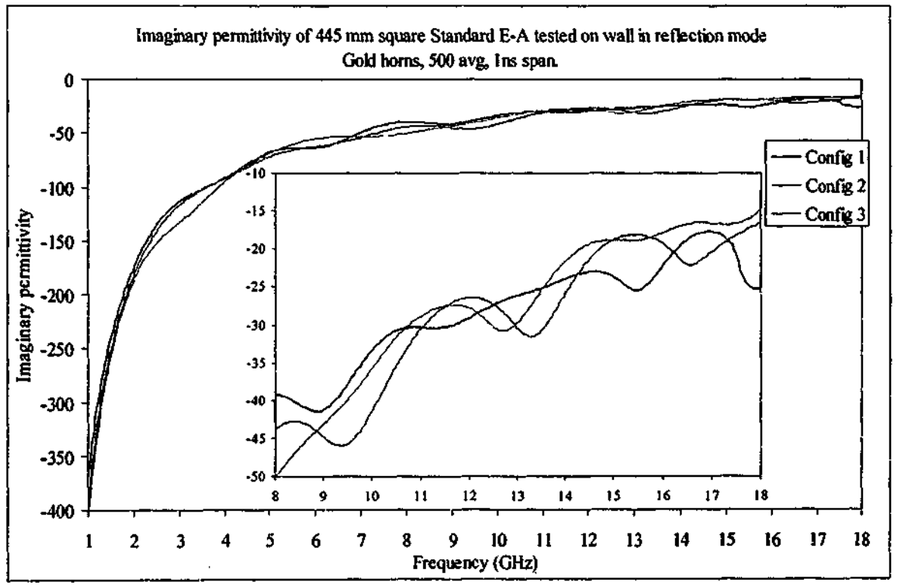

Figure 11-43. Imaginary permittivity of 445 mm square rubber Standard E-A samples measured with gold horns using reflection method

11.6. Comparison to standard techniques

One of the original aims of this project was to confirm that the free space techniques were at least of similar accuracy to the standard techniques currently employed. One common method used to measure lossy materials is with the coaxial waveguide, and results shown in Chapter 9 have shown that similar results are obtained for materials that can be measured using both techniques. The coaxial waveguide technique completely fails to accurately measure samples containing long fibres, and has difficulty measuring rigid materials with permittivities over 10 because of the problems involved in machining a sample to fit inside the waveguide without leaving gaps. The measurement of the carbon loaded rubber samples also proved troublesome for the coaxial waveguide technique due to the damage that occurs to the carbon black structure when producing a specimen for test.

The measured permittivity of Teflon is consistent over all the measurement techniques and frequencies used in this study. From the lowest frequency of 1 MHz right up to 40 GHz the properties of Teflon did not change, and so gives a good indicator as to the accuracy of the techniques. The measured values are shown in Figure 11-44.

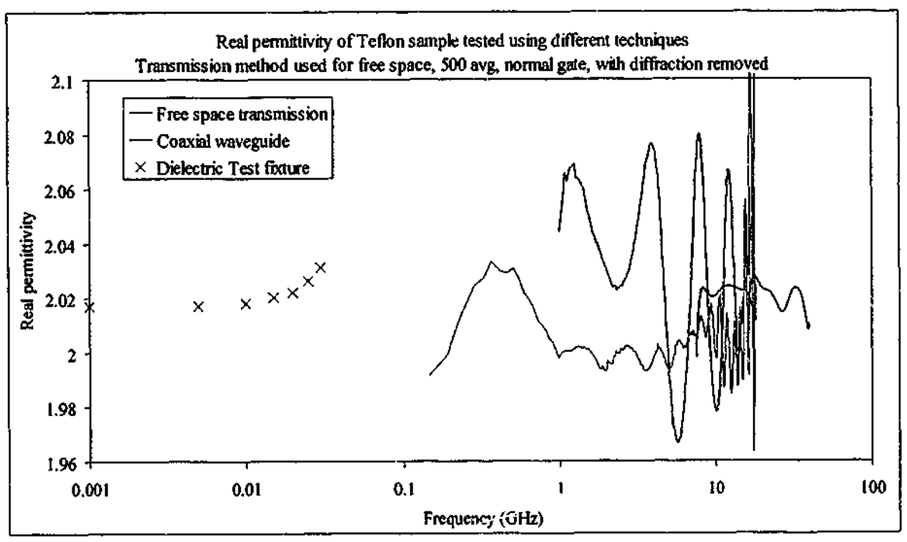

Figure 11-44. Real permittivity of Teflon measured using various techniques

The Perspex and lead glass samples also show a good match between the dielectric test fixture results and those from the free space techniques.

In the case of the CS-AK xx materials, the results from dielectric test fixture and the free space techniques closely match over the wide frequency span, whereas the coaxial method underestimates the permittivity. The extent of this underestimation is seen in Figure 11-45,

where the measured real permittivity of all the samples is shown on the same set of axes across a wide frequency band.

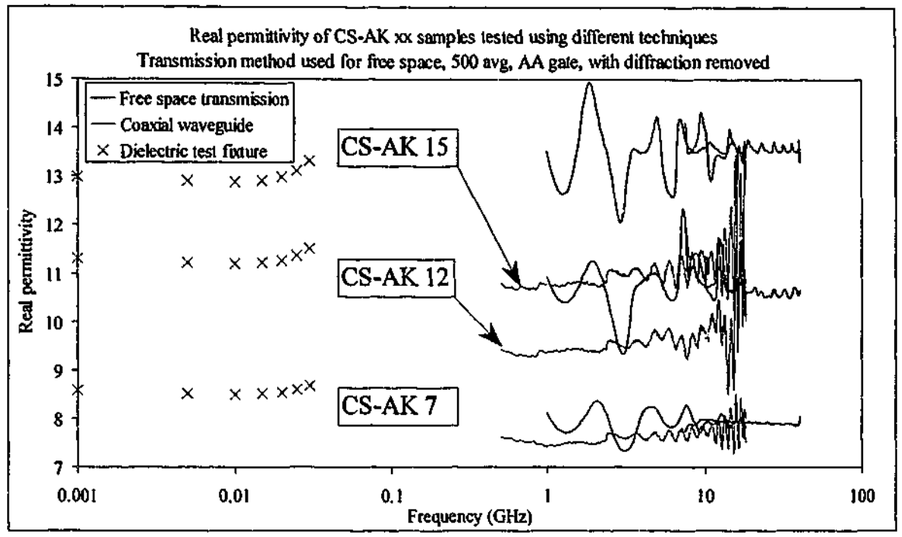

Figure 11-45. Real permittivity of CS-AK xx samples measured using various techniques

One thing that is quite clear from these measurements is that none of them match the values quoted by the manufacturer, Cuming Corporation. CS-AK 7 is higher than quoted, and AK 12 and 15 are both significantly lower. The accuracy of the dielectric constant was quoted as being ± 3% of the value in the name, except for AK 15 which had an error level of ± 10%. This sample just barely made it into the lower bound; however, based on the results it appears that the other samples may well have been mislabelled CS-AK 8 and AK 11.

It was found that the fibre loaded composite sample also couldn't be accurately measured in the coaxial waveguide. Although it is in theory possible to place a 6 mm long carbon fibre in a coaxial specimen without it being cut (the actual maximum is about 6.3 mm based on simple geometry), this would rarely happen in practice, and in any event the average length of carbon fibres would be much lower. A comparison between the values obtained from testing a specimen in the coaxial waveguide to those in free space is shown in Figure 11-46. Real and imaginary permittivity have been shown on a single set of axes, with real permittivity having positive values, and imaginary permittivity negative values.

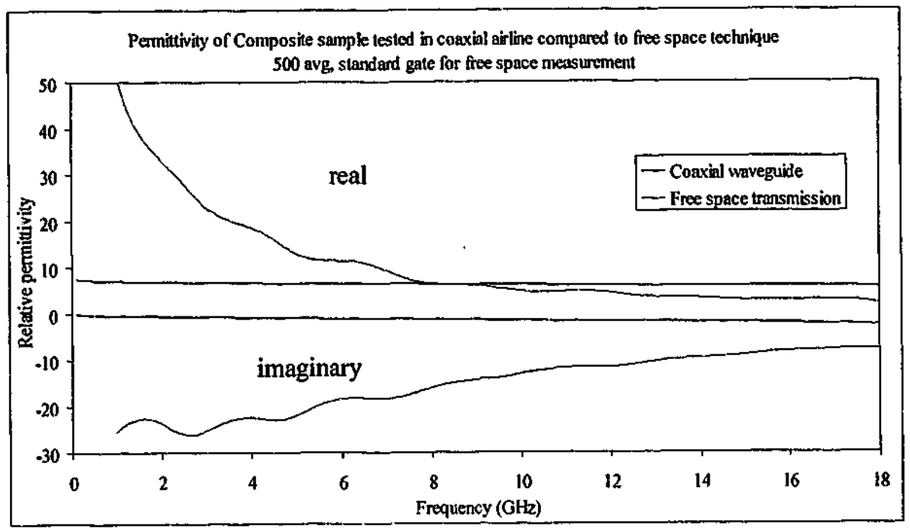

Figure 11-46. Measured permittivity of Composite sample using coaxial and free space techniques

The carbon loaded rubber samples used are particularly sensitive to damage. Just how sensitive they were was not known prior to this study, but their highly lossy behaviour is important for a number of applications. The high loss is attributed to the secondary structure of the carbon black, being almost fibrous rather than a simple sphere. This extent of this structure can be represented by a measure of the surface area of the particles. Standard filling grades of carbon black have a surface area of between 30 and 80 m^2/gram, whereas the Printex XE2 black has a surface area around 600 – 650 m^2/gram. When the coaxial specimens were produced and tested, some of this secondary structure was damaged, leading to the results shown in Figure 11-47. Real and imaginary permittivity have again been shown on a single set of axes, with real permittivity having positive values, and imaginary permittivity negative values.

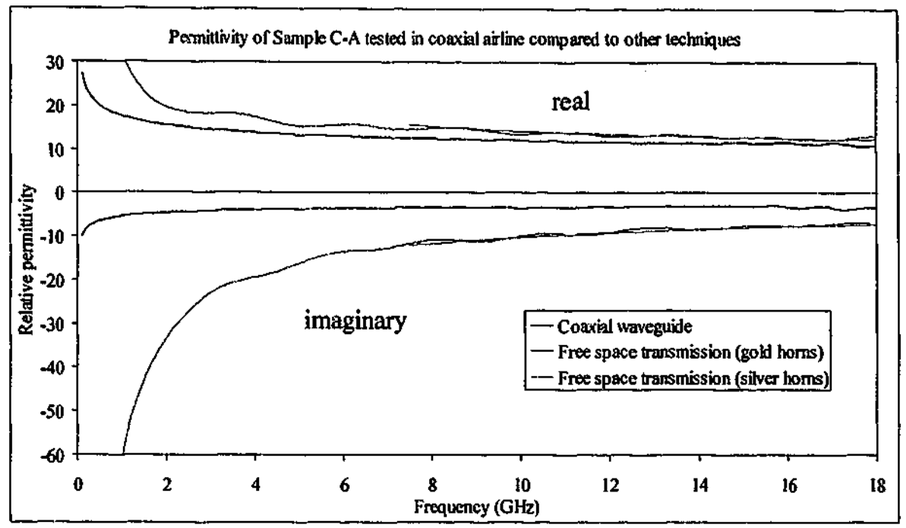

Figure 11-47. Permittivity of rubber Sample C-A measured in free space and in the coaxial waveguide (hole cut with 3.175 mm endmill).

There is an obvious difference between the two results, and the fact that the permittivity increased with greater inner hole dimension leads to the conclusion that the specimen is being damaged whilst being placed on the inner conductor. Since the cut hole is significantly smaller than the drill size, placing the smaller specimens on the inner conductor can be quite difficult and requires a fair degree of force. This action can cause damage to occur in the specimen.

11.7. The best technique?

Many techniques have been trialled and reported on in this study. While it is difficult to say precisely which method is the best, there are definitely areas where some techniques should be avoided if possible. In cases where the material to be tested has magnetic inclusions (for instance iron, cobalt and some ferrite powders), either the coaxial or free space reflection and transmission techniques could be used provided the sample is flexible. If the material is rigid or cannot be destroyed, then the free space technique is preferred due to the problems involved in accurately machining a coaxial specimen for testing. This advice should be given with the proviso that a similar non-magnetic material should be tested in the same configuration, so that any shift in the free space calibration plane can be observed and corrected. In addition to this, it is noted that the test specimen should be as large as possible so that diffraction effects can be minimised. It was shown that the uncertainties in the results

of the 150 mm square samples at frequencies lower than about 5 GHz are quite severe in materials with a large permittivity.

For non-magnetic materials the free space transmission technique is preferred for materials with a size greater than twice the longest wavelength of interest. The transmission technique is not affected by destructive interference, and providing the transmission signal through the sample is greater than the diffraction signal, highly accurate results can be obtained using the mathematical diffraction removal technique described in this thesis. Since the size of the diffraction peak is affected by the horn to sample distances, these should be reduced as much as possible whilst maintaining sufficient space so that time gating techniques can be used to remove the multiple reflections between the sample and the horns.

In cases where there is limited material available for testing, or the wavelength of the longest frequency required is greater than the sample size, then the coaxial waveguide technique is preferable. If care is taken to accurately machine the specimens for test then the results are highly accurate. The transmission or reflection only algorithms can of course be used for coaxial measurements to eliminate any destructive interference problems (assuming the sample is non-magnetic).

Frequency bands also play a part in the selection of the best technique. The horns used in this thesis have a lower limit of 1 GHz, and so should not be used below this value. The coaxial waveguide can be used down to 45 MHz with the system currently in use. Above 18 GHz however, the coaxial method cannot be used and free space techniques are the easiest ones available for measuring the electromagnetic properties. While is still possible to use rectangular waveguide at these high frequencies, the number and sizes of different specimens required make the testing difficult.

The reflection only technique suffers from problems caused by the slight shifts in position due to the specimen's weight or shape. It is vitally important that the front of the sample lies on the calibration plane, since significant errors can occur if the sample is only tens of microns from the correct position. The shift can be easily corrected for if it is accurately known, but this step adds further complications to the procedure. The size of the sample also affects the reflection only technique, and it is recommended that samples should be at least at large as the longest wavelength.

Further problems with the reflection only technique occur when the reflection signal from the sample becomes very high. It was observed in the carbon loaded rubber samples that the permittivity curve for the material with the highest loading (sample E) "crossed over" the other curves at high frequencies. The same effect occurred with the thicker rubber material (F)

that had a permittivity similar to that of sample D. In the 16 – 40 GHz range, very few of the results using the reflection only algorithm showed values similar to those from the transmission only algorithm. It appears that the reflection only algorithm is only of limited use in extracting permittivity data.

By contrast, the reflection and transmission technique is quite robust in that it can use the seemingly highly error prone reflection data to produce permittivity and permeability results that closely match the results expected. In most cases the permeability data is within ± 5% of the free space result for non-magnetic materials, and closely agrees with the results taken inside the coaxial waveguide for the magnetic material investigated. With careful sample placement and use of a known material to correct for any calibration plane shifts, the reflection/transmission technique described in this thesis should give accurate, reliable measurements.

The backed reflection technique showed some promise as an accurate measurement technique, especially at high frequencies. At frequencies below about 6 GHz this technique did not produce an accurate determination for either the 305 or 150 mm square specimens. At high frequencies, however, the technique matched the results obtained for the other techniques, giving accurate values for the materials with well-known properties. The use of the dielectric lens appeared to have little effect on the extraction process for the 305 mm square samples, with similar values obtained for lensed and unlensed measurements. This technique should only be used in cases where the transmission only technique is not appropriate, such as materials that are inhomogeneous in their thickness or have an integral backing applied that cannot be removed.

11.8. Future work

The measurements at lowest frequencies showed the greatest inaccuracy because of the low gain of the microwave horns (of the order of 6 – 8 dBi below 3 GHz) contributing to the large diffraction signal in transmission measurements, and reducing the dynamic range for reflection measurements. Larger low frequency horns have been purchased that have gain levels of the order of 17 dBi over the range 3 – 8 GHz, so measurements will be taken using these horns and then compared to those taken with the lower gain horns. It will be interesting to see if the accuracy improves using these high gain horns at the lower frequencies.

At the other end of the scale is the millimetre wave band higher than 40 GHz. The network analyser can be outfitted to measure phase and magnitude up to 110 GHz with appropriate mixers and modifications to the test set. These modifications are quite expensive

(even when compared to microwave equipment which is not cheap) but as technology advances to include the mm-wave bands, the techniques investigated here could be used to measure material properties at these frequencies.

Currently the algorithms developed here use the measured phase and magnitude of the either reflection or transmission (or both) to determine the permittivity. Since the measurement of phase is usually the most difficult part, it would be easier if permittivity extraction could be performed using scalar measurements of reflection and transmission. Assuming the material is paramagnetic, it is possible to determine the permittivity of the material based only on reflection and transmission magnitude[97]. Alternatively, the measurement of phase alone could be used to extract the values. The accuracy and stability of alternate algorithms such as these could be investigated in the future.

It had been suggested that the measurement procedure might be modelled using simulation software such as Ansoft's HFSS program. This was not attempted during this study, primarily because the program was not available (and with a price tag of A$120,000 plus A$18,000 per year for support it was too much to justify purchasing), and also because it was felt that measuring the error terms directly would lead to a better solution. Direct measurement of the diffraction signal did contribute to a highly accurate result, however if the software ever did become available it would be interesting to simulate the diffraction and error terms, and compare the results with the direct measurement approach.

Conclusion

This study has concentrated on improving the accuracy available to the free space techniques using a wide variety of methods such as time gating, antenna position, diffraction removal, specimen size and calibration plane shifts. It has also shown that the effects of testing in the near field were not as great as first imagined, which improves the ease of use of the techniques. With flat samples that are larger than about two wavelengths at the lowest frequency of testing, measurements of the electromagnetic parameters can be taken with an accuracy level of greater than ± 5%, and usually better than ± 2% over the full frequency band.

The frequency range that the measurements were performed was over 1 to 40 GHz, but theoretically the techniques used could extend in either direction provided the microwave antennas were of the correct type, and the network analyser system was able to interrogate the incoming signals.

The largest source of error in transmission measurements is caused by interference from the diffraction signal, which passes around the sample without going through it. It has been shown that the effects can be readily removed by directly measuring this path, and then mathematically subtracting it from the combined signal. This method can be successfully applied even when the magnitude of this diffraction signal is larger than the transmission signal. This very useful result allows small samples to be tested using the technique without loss of accuracy.

The overall conclusion that can be drawn from this work is that highly accurate permittivity and permeability measurements can be made on dielectric materials in free space using techniques that do not require complicated calibration methods, focussing lenses or specially designed reflectors to reduce near field or diffraction effects. The technique is less suited to materials with extremely low loss tangents when highly accurate values of imaginary permittivity are required, but will give accurate values for low to high loss materials when using the methods outlined in this thesis.

Appendix A. Microwave Lenses

Two lenses were made for use in this study. One was to be used for compact range measurements, the other on the reflection/transmission test setup. The formula used to calculate the shape of the lenses is derived below[75].

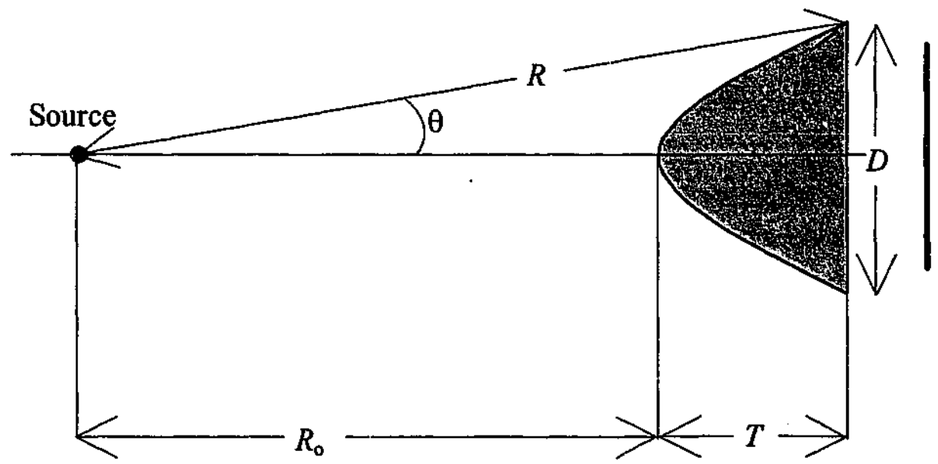

Figure A - 1 Arrangement of the lens, source and target.

The front surface of the lens is formed so as to produce a plane wave at the back (flat) surface of the lens. With the setup as shown above, the phase of the wave travelling through the lens must equal the phase of the free wave. The phase at the edge of the lens is equal to k_0R, where k_0 is the free space wave number $2\pi/\lambda$. The phase of that part of the wave that travelled through the lens equals $R_0k_0 + k_lT$ and must equal the free space wave for plane wave behaviour. Therefore

$$Rk_0 = R_0k_0 + k_1T \qquad \text{Equation A - 1}$$

For every value of D there is a corresponding thickness T that results in plane wave behaviour behind the lens. To calculate the thickness at any point on the lens we remember that the refractive index n is the ratio of the wave numbers and Pythagoras' theorem. Continuing on we obtain the following;

$$R = R_0 + nT$$

$$\sqrt{(R_0+T)^2 + (D/2)^2} = R_0 + nT$$

$$(R_0+T)^2 + (D/2)^2 = (R_0+nT)^2$$

$$R_0^2 + 2R_0T + T^2 + \frac{D^2}{4} = R_0^2 + 2R_0nT + n^2T^2$$

$$T^2(n^2-1) + 2R_0(n-1)T - \frac{D^2}{4} = 0 \qquad \text{Equation A - 2}$$

which can be solved easily with a calculator or computer.

A.1. Lens for range measurements

The lens constructed for the radar range was made from syntactic foam that incorporated lightweight microspheres in an epoxy matrix. The aim was to produce a thin, light and strong lens that would give minimal return reflection whilst producing plane wave behaviour at the target. The permittivity of the material was tested in the coaxial waveguide and was found to be $1.81 - 0.038i$, with a corresponding permeability of $1.00 + 0.006i$. The fact that the permeability was measured to be so close to that expected gives a high degree of confidence in the measured permittivity. Using a permittivity of 1.81 (giving refractive index = 1.345), R_0 = 2.4 m and the effective radius of the lens = 0.375 m (the diagonal distance of the square lens) we get the formula for the thickness T (m) of the lens at a radius R (m) from the centre as

$$T = 0.08157766 + \left(\frac{1.65774 - \sqrt{2.7481 + 3.24R^2}}{1.62}\right) \qquad \text{Equation A - 3}$$

The lens was milled on a numerical computing machine using this formula.

A.2. Lens for reflection/transmission head

This lens was made of an even more lightweight material, polyurethane foam with a density of 250 kg/m^3. This material has a permittivity of 1.32 (so n = 1.1489), R_0 = 1.0 m and the size was 520 mm square. The machining formula for this lens was

$$T = 0.33403 + 1.5615(0.298 - \sqrt{0.0888 + 1.2808R^2}) \qquad \text{Equation A - 4}$$

Because this lens had a lower permittivity and smaller focal length, the lens is much thicker than the previous lens.

Appendix B. Chirp-Z Transform

It is sometimes useful to express data measured in the frequency domain as a series of equivalent pulses in the time domain. In this way, the measurement technique can be investigated more fully as the source of contributions to the data measured can be identified. In the reflection/transmission set-up for instance, one can readily see sources of unwanted reflections of the microwave field. These include the stands holding the either the horns or the sample, reflections the horns and the sample, waves bouncing off the walls, the floor and the ceiling. Some of these possible reflections can be dealt with by a calibration technique, or by directly measuring the set-up without the sample and subtracting the result from the actual measurement of the sample. However, not all the unwanted sources can be removed in this way such as the reflections between the sample and the horns. For reflections such as these, time gating offers a solution.

In order to use time gating, the signal must first be converted to the time domain. Normally a Z-transform is used to convert a finite series of equally spaced data points from one domain to another. When converting from frequency space to time space using the Z-transform, the full time domain is generated. If the area of interest in the time domain is small, a very large number of calculations must be performed so that the required resolution is attained. The Chirp-Z transform allows the user to only calculate that part of the time domain required[78].

The Z-transform of a sequence of numbers x_n is defined as

$$X(z) = \sum_{n=-\infty}^{\infty} x_n z^{-n} \qquad \text{Equation B - 1}$$

in terms of the complex variable z. In general, both x_n and $X(z)$ can be complex. Restricting the equation to a finite series of N non-zero points we can write Equation B - 1 as

$$X(z) = \sum_{n=0}^{N-1} x_n z^{-n} \qquad \text{Equation B - 2}$$

In the same way we can calculate X for a finite series of points, say z_k

$$X_k = X(z_k) = \sum_{n=0}^{N-1} x_n z_k^{-n} \qquad \text{Equation B - 3}$$

The normal way of performing the transformation is using points equally spaced around the unit circle in the z-plane

$$z_k = e^{(i\frac{2\pi}{N}k)}, \qquad k = 0,1,2,\ldots,N\text{-}1 \qquad \text{Equation B - 4}$$

for which

$$X_k = \sum_{n=0}^{N-1} x_n e^{(-i\frac{2\pi}{N}nk)}, \qquad k = 0,1,2,\ldots,N\text{-}1 \qquad \text{Equation B - 5}$$

This is the known as the discrete Fourier transform. It has some limitations that the Chirp-Z transform can eliminate. By defining a more general curve over which the transform operates of the form,

$$z_k = AW^{-k}, \qquad k = 0,1,2,\ldots,M\text{-}1 \qquad \text{Equation B - 6}$$

where M is an arbitrary integer and both A and W are arbitrary complex numbers of the form

$$A = A_0 e^{i2\pi\theta_0}, W = W_0 e^{i2\pi\phi_0} \qquad \text{Equation B - 7}$$

The case of $A = 1$, $M = N$ and $W = e^{(-i2\pi/N)}$ corresponds to the discrete Fourier transform. The general z-plane contour begins with the point $z = A$, and depending on the value of W, spirals in or out with respect to the origin. If $W_0 = 1$, the contour is an arc of a circle. The angular spacing of the samples is $2\pi\phi_0$. Figure B - 1 shows how the arbitrary curve is described on the complex plane starting at $z = A$.

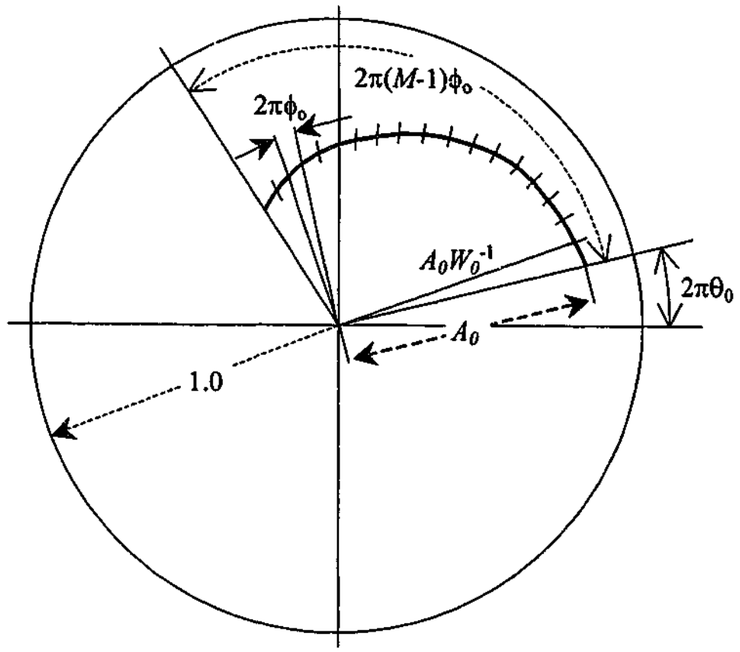

Figure B - 1 An arbitrary curve on the z-plane over which the Chirp-Z transform is calculated.

Along the contour of Equation B - 6, Equation B – 3 becomes

$$X_k = \sum_{n=0}^{N-1} x_n A^{-n} W^{nk}, \qquad k = 0,1,2,\ldots,M\text{-}1 \qquad \text{Equation B - 8}$$

which appears to need NM complex multiplications and additions thereby reducing the effectiveness of fast Fourier techniques. However, performing the substitution

$$nk = \frac{1}{2}\left(n^2 + k^2 - (k-n)^2\right) \qquad \text{Equation B - 9}$$

for the exponent of W in Equation B – 8 produces

$$X_k = \sum_{n=0}^{N-1} x_n W^{n^2/2} W^{k^2/2} W^{-(k-n)^2/2}, \qquad k = 0,1,2,\ldots,M\text{-}1 \qquad \text{Equation B - 10}$$

which looks even worse than before. However, this series can be solved using a three step process. Firstly, a new sequence y_n is formed by weighting the x_n values according to the equation

$$y_n = x_n A^{-n} W^{n^2/2}, \qquad n = 0,1,2,\ldots,N\text{-}1 \qquad \text{Equation B - 11}$$

These y_n values are convolved with the sequence v_n defined as

$$v_n = W^{-n^2/2} \qquad \text{Equation B - 12}$$

to give a sequence g_k

$$g_k = \sum_{n=0}^{N-1} y_n v_{k-n}, \qquad k = 0,1,2,\ldots,M\text{-}1 \qquad \text{Equation B - 13}$$

and then multiplying g_k by $W^{k^2/2}$ to give X_k.

$$X_k = g_k W^{k^2/2}, \qquad k = 0,1,2,\ldots, M\text{-}1 \qquad \text{Equation B - 14}$$

The first and third steps require N and M multiplications respectively; the second step is a convolution which may be computed using high speed techniques.

Some of the advantages of using the Chirp-Z transform are:

- the number of time samples does not have to equal the number of samples of the z-transform
- neither N nor M need to be composite numbers
- the angular spacing of the z_k is arbitrary.

What this means in practice is that the time domain calculated can start and stop at any point in the range without the need to calculated those points not required. Additionally, the number of points in the transform can be as many or as few as required.

Appendix C. Multiple Reflections

Whenever electromagnetic waves encounter an interface between the medium they were travelling in to a different medium, reflection and transmission can occur. Figure C - 1 shows the effect of an electromagnetic wave incident on a dielectric slab in air. Multiple reflections occur inside the sample, with each adding to the total signal received but shifted in time.

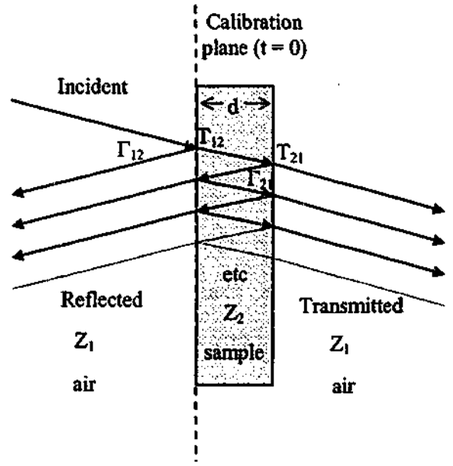

Figure C - 1. Reflection and transmission of an electromagnetic wave through a dielectric material

Based upon the material's thickness, permittivity and permeability, it is possible to estimate the position in time of each of these parts of the signal, together with their magnitude. This will enable us to determine how many reflections are required for an accurate determination of material properties. The calibration procedure usually sets the front of the slab to be at the calibration plane, meaning that time is set to be zero. All timing is calculated relative to the calibration plane, corresponding to where the incident wave arrives at time zero.

The reflection coefficient Γ is defined for semi-infinite slabs as

$$\Gamma_{ij} = \frac{Z_j - Z_i}{Z_j + Z_i} \qquad \text{Equation C - 1}$$

where the wave is travelling from medium i to medium j. Similarly the transmission coefficient T is defined as

$$T_{ij} = \frac{2Z_j}{Z_i + Z_j} \qquad \text{Equation C - 2}$$

These equations take care of the reflection and transmission at the interfaces, but as the wave travels through the medium it may be absorbed by a factor $e^{-\gamma d}$ where γ is the propagation factor and has its normal value of $i\omega\sqrt{\varepsilon\mu}$. Using the nomenclature of Figure C-1, we can see that this factor is applied to Γ_{21} and T_{21}, giving the four parameters the following form.

$$\Gamma_{12} = \frac{Z_2 - Z_1}{Z_1 + Z_2}, \qquad \Gamma_{21} = \frac{Z_1 - Z_2}{Z_1 + Z_2} e^{-\gamma d}$$
$$T_{12} = \frac{2Z_2}{Z_1 + Z_2}, \qquad T_{21} = \frac{2Z_1}{Z_1 + Z_2} e^{-\gamma d} \qquad \text{Equation C - 3}$$

Following the paths as shown in Figure C - 1 we can calculate the magnitude of the individual reflection and transmission peaks. The first reflected peak is simply Γ_{12}, having not travelled through the sample at all. The second reflected signal is first transmitted into the sample T_{12}, then reflected from the back Γ_{21}, then emerges from the sample T_{21}. The other paths can be found the same way to give the following formulae. The pattern can of course be extended for higher order peaks.

Peak #	Reflection	Transmission
1	Γ_{12}	$T_{12}T_{21}$
2	$T_{12}\Gamma_{21}T_{21}$	$T_{12}\Gamma_{21}^2T_{21}$
3	$T_{12}\Gamma_{21}^3T_{21}$	$T_{12}\Gamma_{21}^4T_{21}$
4	$T_{12}\Gamma_{21}^5T_{21}$	$T_{12}\Gamma_{21}^6T_{21}$

Table C-1. Formulae for calculating the magnitude of the multiple peaks

Calculating the position in time space is simply a matter of calculating the velocity of light in the medium (which has been slowed by an amount related to the permittivity and permeability of the medium), and then dividing by the distance the wave has travelled. For the samples tested in this study, the positions and intensities have been calculated for either the first five peaks, or that peak that has an intensity below –50 dB (whichever comes last). These values are shown in the figures below.

Transmission 1-18 GHz

Sample	A		B		C		D		E		F		G	
	Ave perm	thickness	Ave perm	thickness	Ave perm	thickness	Ave perm	thickness	Ave perm	thickness	Ave perm	thickness	Ave perm	thickness
	4.5-0.25i	1.632	7-1.5i	1.612	15-10i	1.101	17-22i	1.09	21.5-37i	1.152	16-24i	1.669	9.6-0.68i	1.356
Peak	Time (ns)	Mag (dB)	Time (ns)	Mag (dB)	Time (ns)	Mag (dB)	Time (ns)	Mag (dB)	Time (ns)	Mag (dB)	Time (ns)	Mag (dB)	Time (ns)	Mag (dB)
1st	0.01	-1.37	0.01	-2.79	0.01	-9.60	0.01	-6.39	0.02	-12.97	0.02	-12.42	0.01	-4.16
2nd	0.03	-19.45	0.04	-17.90	0.04	-24.37	0.05	-18.96	0.06	-30.56	0.08	-32.15	0.04	-35.01
3rd	0.05	-37.54	0.07	-33.00	0.06	-39.14	0.08	-31.52	0.11	-48.16	0.13	-51.89	0.07	-47.86
4th	0.08	-55.63	0.09	-48.11	0.12	-53.92	0.12	-44.09	0.15	-65.75	0.18	-71.62	0.09	-69.72
5th	0.10	-73.72	0.12	-63.21	0.15	-68.69	0.15	-55.65	0.19	-83.35	0.24	-91.36	0.12	-91.57

Sample	Perspex		Composite		Teflon		CS-AK 7		CS-AK 12		CS-AK 15		Lead glass	
	Ave perm	thickness	Ave perm	thickness	Ave perm	thickness	Ave perm	thickness	Ave perm	thickness	Ave perm	thickness	Ave perm	thickness
	2.6-1E-002i	4.5	4.1-1i	1.92	2.04-1E-002i	5.398	7.9-2E-002i	9.634	10.9-0.16i	9.616	13.5+6E-002i	9.779	9.5-5E-002i	7.134
Peak	Time (ns)	Mag (dB)	Time (ns)	Mag (dB)	Time (ns)	Mag (dB)	Time (ns)	Mag (dB)	Time (ns)	Mag (dB)	Time (ns)	Mag (dB)	Time (ns)	Mag (dB)
1st	0.01	-0.52	0.01	-9.03	0.01	-9.03	0.06	-2.28	0.07	-3.33	0.09	-3.31	0.05	-2.72
2nd	0.06	-25.76	0.05	-30.24	0.06	-30.24	0.24	-15.33	0.29	-15.00	0.33	-12.73	0.20	-14.61
3rd	0.11	-51.01	0.08	-51.45	0.11	-51.45	0.42	-29.37	0.50	-26.67	0.57	-22.15	0.34	-26.51
4th	0.15	-76.26	0.12	-72.67	0.16	-72.67	0.60	-41.42	0.71	-38.34	0.81	-31.58	0.49	-38.40
5th	0.20	-101.50	0.16	-93.88	0.21	-93.88	0.78	-54.46	0.92	-50.01	1.05	-41.00	0.64	-50.35
											1.28	-50.43		

Reflection 1-18 GHz

Sample	A		B		C		D		E		F		G	
	Ave perm	thickness	Ave perm	thickness	Ave perm	thickness	Ave perm	thickness	Ave perm	thickness	Ave perm	thickness	Ave perm	thickness
	4.5-0.25i	1.632	7-1.5i	1.612	15-10i	1.101	17-22i	1.09	21.5-37i	1.152	16-24i	1.669	9.6-0.68i	1.669
Peak	Time (ns)	Mag (dB)	Time (ns)	Mag (dB)	Time (ns)	Mag (dB)	Time (ns)	Mag (dB)	Time (ns)	Mag (dB)	Time (ns)	Mag (dB)	Time (ns)	Mag (dB)
1st	0.00	-8.88	0.00	-6.77	0.00	-6.46	0.00	-3.96	0.00	-2.30	0.00	-2.84	0.00	-8.04
2nd	0.02	-10.41	0.03	-10.34	0.03	-9.80	0.03	-12.68	0.04	-21.77	0.05	-22.29	0.05	-15.09
3rd	0.05	-28.50	0.06	-25.45	0.06	-25.24	0.07	-31.76	0.09	-39.36	0.11	-42.02	0.09	-36.94
4th	0.07	-46.59	0.09	-40.55	0.09	-37.80	0.10	-46.53	0.13	-56.96	0.16	-61.75	0.14	-58.79
5th	0.09	-64.67	0.11	-55.66	0.12	-50.37	0.14	-61.30	0.17	-74.55	0.22	-81.48	0.18	-80.64

Sample	Perspex		Composite		Teflon		CS-AK 7		CS-AK 12		CS-AK 15		Lead glass	
	Ave perm	thickness	Ave perm	thickness	Ave perm	thickness	Ave perm	thickness	Ave perm	thickness	Ave perm	thickness	Ave perm	thickness
	2.6-1E-002i	4.5	4.1-1i	1.92	2.04-1E-002i	5.398	7.9-2E-002i	9.634	10.9-0.16i	9.616	13.5+6E-002i	9.779	9.5-5E-002i	7.134
Peak	Time (ns)	Mag (dB)	Time (ns)	Mag (dB)	Time (ns)	Mag (dB)	Time (ns)	Mag (dB)	Time (ns)	Mag (dB)	Time (ns)	Mag (dB)	Time (ns)	Mag (dB)
1st	0.00	-12.60	0.00	-4.12	0.00	-5.96	0.00	-6.46	0.00	-5.43	0.00	-4.95	0.00	-5.86
2nd	0.05	-13.14	0.04	-19.63	0.05	-15.07	0.18	-9.80	0.21	-9.17	0.24	-8.02	0.15	-9.86
3rd	0.10	-38.39	0.07	-40.86	0.10	-45.62	0.36	-21.86	0.42	-20.84	0.48	-17.44	0.29	-20.56
4th	0.15	-63.63	0.11	-62.06	0.15	-75.83	0.54	-34.89	0.63	-32.30	0.72	-26.87	0.44	-32.45
5th	0.19	-88.88	0.14	-83.27	0.21	-106.03	0.72	-47.94	0.85	-44.17	0.96	-38.29	0.59	-44.36
							0.90	-60.98	1.06	-55.84	1.20	-45.72	0.73	-56.24
											1.44	-55.14		

Figure C - 2. Positions and intensities of multiple interference peaks over 1 – 18 GHz

Transmission 7.5-18 GHz

Sample	A		B		C		D		E		F		G	
	Ave perm	thickness	Ave perm	thickness	Ave perm	thickness	Ave perm	thickness	Ave perm	thickness	Ave perm	thickness	Ave perm	thickness
	4.27-0.26i	1.632	6.91-1.58i	1.612	13.5-9i	1.09	17-22i	1.101	21.6-29.6i	1.152	17.1-19.7i	1.659	9.2-0.41i	1.356
Peak	Time (ns)	Mag (dB)	Time (ns)	Mag (dB)	Time (ns)	Mag (dB)	Time (ns)	Mag (dB)	Time (ns)	Mag (dB)	Time (ns)	Mag (dB)	Time (ns)	Mag (dB)
1st	0.01	-1.36	0.01	-3.10	0.01	-6.74	0.01	-11.11	0.02	-13.35	0.02	-13.17	0.01	-5.66
2nd	0.03	-20.15	0.04	-18.93	0.04	-21.01	0.05	-28.91	0.06	-33.13	0.07	-35.69	0.04	-28.45
3rd	0.05	-38.93	0.07	-34.75	0.07	-35.29	0.08	-46.71	0.10	-52.91	0.12	-58.22	0.06	-51.23
4th	0.07	-57.72	0.09	-50.58	0.09	-49.56	0.12	-64.51	0.14	-72.69	0.17	-80.75	0.09	-74.01
5th	0.10	-76.51	0.12	-66.41	0.12	-63.83	0.15	-82.31	0.18	-92.47	0.23	-103.27	0.12	-96.79

Sample	Perspex		Composite		Teflon		CS-AK 7		CS-AK 12		CS-AK 15		Lead glass	
	Ave perm	thickness	Ave perm	thickness	Ave perm	thickness	Ave perm	thickness	Ave perm	thickness	Ave perm	thickness	Ave perm	thickness
	2.6-1E-002i	4.5	4.1-11i	1.92	2.04-1E-002i	5.398	7.9-4E-002i	9.634	10.8-0.22i	9.616	13.5+6E-002i	9.779	9.5-4E-002i	7.134
Peak	Time (ns)	Mag (dB)	Time (ns)	Mag (dB)	Time (ns)	Mag (dB)	Time (ns)	Mag (dB)	Time (ns)	Mag (dB)	Time (ns)	Mag (dB)	Time (ns)	Mag (dB)
1st	0.01	-0.52	0.01	-11.25	0.01	-0.32	0.06	-2.38	0.07	-3.65	0.09	-3.26	0.05	-2.72
2nd	0.06	-25.79	0.05	-36.90	0.06	-30.55	0.24	-15.63	0.28	-16.06	0.33	-12.59	0.20	-14.63
3rd	0.11	-51.06	0.08	-62.55	0.11	-60.78	0.42	-28.87	0.49	-28.47	0.57	-21.92	0.34	-26.54
4th	0.15	-76.31	0.12	-88.20	0.16	-91.01	0.60	-42.11	0.71	-40.88	0.81	-31.25	0.49	-38.45
5th	0.20	-101.58	0.16	-113.85	0.21	-121.24	0.78	-55.36	0.92	-53.29	1.05	-40.58	0.64	-50.36

Reflection 7.5-18 GHz

Sample	A		B		C		D		E		F		G	
	Ave perm	thickness	Ave perm	thickness	Ave perm	thickness	Ave perm	thickness	Ave perm	thickness	Ave perm	thickness	Ave perm	thickness
	4.27-0.26i	1.632	6.9[illegible]-1.58i	1.612	13.5-9i	1.09	17-22i	1.101	21.6-29.6i	1.152	17.1-19.7i	1.659	9.2-0.41i	1.356
Peak	Time (ns)	Mag (dB)	Time (ns)	Mag (dB)	Time (ns)	Mag (dB)	Time (ns)	Mag (dB)	Time (ns)	Mag (dB)	Time (ns)	Mag (dB)	Time (ns)	Mag (dB)
1st	0.00	-9.16	0.00	-6.80	0.00	-4.18	0.00	-2.96	0.00	-2.56	0.00	-3.11	0.00	-7.15
2nd	0.02	-10.75	0.03	-11.01	0.03	-13.66	0.03	-20.01	0.04	-23.24	0.05	-24.43	0.03	-17.05
3rd	0.04	-29.54	0.06	-26.84	0.06	-28.15	0.07	-37.81	0.08	-43.02	0.10	-46.96	0.07	-39.84
4th	0.07	-48.33	0.09	-42.67	0.08	-42.42	0.10	-55.61	0.12	-62.80	0.15	-69.48	0.10	-62.62
5th	0.09	-67.12	0.11	-58.49	0.11	-56.69	0.14	-73.41	0.17	-82.58	0.21	-92.01	0.13	-85.40

Sample	Perspex		Composite		Teflon		CS-AK 7		CS-AK 12		CS-AK 15		Lead glass	
	Ave perm	thickness	Ave perm	thickness	Ave perm	thickness	Ave perm	thickness	Ave perm	thickness	Ave perm	thickness	Ave perm	thickness
	2.6-1E-002i	4.5	4.1-11i	1.92	2.04-1E-002i	5.398	7.9-4E-002i	9.634	10.8-0.22i	9.616	13.5+6E-002i	9.779	9.5-4E-002i	7.134
Peak	Time (ns)	Mag (dB)	Time (ns)	Mag (dB)	Time (ns)	Mag (dB)	Time (ns)	Mag (dB)	Time (ns)	Mag (dB)	Time (ns)	Mag (dB)	Time (ns)	Mag (dB)
1st	0.00	-12.60	0.00	-4.12	0.00	-15.07	0.00	-6.46	0.00	-5.46	0.00	-4.85	0.00	-5.85
2nd	0.05	13.16	0.04	-24.07	0.05	-15.43	0.18	-9.00	0.21	-9.86	0.24	-7.92	0.15	-8.68
3rd	0.10	-39.42	0.07	-49.72	0.10	-45.66	0.36	-22.25	[illegible]	-22.27	0.48	-17.25	0.29	-20.59
4th	[illegible]15	-63.68	0.11	-75.37	0.15	-75.89	0.54	-35.49	[illegible]63	-34.68	0.72	-26.58	0.44	-32.50
5th	0.19	-88.95	0.14	-101.02	0.21	-106.12	0.72	-48.74	0.84	-47.09	0.96	-35.91	0.59	-44.41
							0.90	-61.98	1.05	-59.50	1.20	-45.24	0.73	-56.32
											1.44	-54.57		

Figure C - 3. Positions and intensities of multiple interference peaks over 7.5 – 18 GHz

Transmission 16-40 GHz

Sample	A		B		C		D		E		F		G	
	Ave perm	thickness	Ave perm	thickness	Ave perm	thickness	Ave perm	thickness	Ave perm	thickness	Ave perm	thickness	Ave perm	thickness
	4.1-0.25i	1.632	6.2-1.3i	1.612	11.5-5.5i	1.09	14.7-9.8i	1.101	19.3-16.9i	1.152	14.3-11.5i	1.659	8.8-0.15i	1.356
Peak	Time (ns)	Mag (dB)	Time (ns)	Mag (dB)	Time (ns)	Mag (dB)	Time (ns)	Mag (dB)	Time (ns)	Mag (dB)	Time (ns)	Mag (dB)	Time (ns)	Mag (dB)
1st	0.01	-1.57	0.01	-3.90	0.01	-7.61	0.01	-10.85	0.01	-15.48	0.02	-16.11	0.01	-9.32
2nd	0.03	-21.36	0.03	-22.65	0.03	-26.08	0.04	-32.52	0.05	-42.86	0.06	-47.89	0.04	-34.04
3rd	0.05	-41.15	0.06	-41.41	0.06	-44.54	0.07	-54.20	0.09	-70.24	0.11	-79.67	0.06	-58.77
4th	0.07	-60.94	0.09	-60.16	0.08	-63.01	0.10	-75.87	0.12	-97.62	0.15	-111.45	0.09	-83.49
5th	0.09	-80.73	0.12	-78.91	0.11	-81.47	0.13	-97.54	0.16	-125.00	0.20	-143.23	0.12	-106.21

Sample	Perspex		Composite		Teflon		CS-AK 7		CS-AK 12		CS-AK 15		Lead glass	
	Ave perm	thickness	Ave perm	thickness	Ave perm	thickness	Ave perm	thickness	Ave perm	thickness	Ave perm	thickness	Ave perm	thickness
	2.6-1E-002i	4.5	2-4.7i	1.92	2.04-1E-002i	5.398	7.9-8E-002i	9.634	10.6-0.28i	9.616	13.6-3E-002i	9.779	9.4-8E-002i	7.134
Peak	Time (ns)	Mag (dB)	Time (ns)	Mag (dB)	Time (ns)	Mag (dB)	Time (ns)	Mag (dB)	Time (ns)	Mag (dB)	Time (ns)	Mag (dB)	Time (ns)	Mag (dB)
1st	0.01	-0.56	0.01	-12.96	0.01	-0.37	0.06	-2.92	0.07	-4.97	0.09	-3.66	0.05	-3.07
2nd	0.06	-25.90	0.03	-49.86	0.06	-30.71	0.24	-17.24	0.28	-20.21	0.33	-13.73	0.19	-15.78
3rd	0.11	-51.24	0.05	-86.76	0.11	-61.04	0.42	-31.57	0.49	-35.44	0.57	-23.80	0.34	-28.49
4th	0.15	-76.58	0.08	-123.66	0.16	-91.37	0.60	-45.89	0.70	-50.68	0.81	-33.87	0.49	-41.20
5th	0.20	-101.93	0.10	-160.57	0.21	-121.71	0.78	-60.21	0.91	-65.92	1.05	-43.94	0.63	-53.91
											1.29	-54.00		

Reflection 16-40 GHz

Sample	A		B		C		D		E		F		G	
	Ave perm	thickness	Ave perm	thickness	Ave perm	thickness	Ave perm	thickness	Ave perm	thickness	Ave perm	thickness	Ave perm	thickness
	4.1-0.25i	1.632	6.2-1.3i	1.612	11.5-5.5i	1.09	14.7-9.8i	1.101	19.3-16.9i	1.152	14.3-11.5i	1.659	8.8-0.15i	1.356
Peak	Time (ns)	Mag (dB)	Time (ns)	Mag (dB)	Time (ns)	Mag (dB)	Time (ns)	Mag (dB)	Time (ns)	Mag (dB)	Time (ns)	Mag (dB)	Time (ns)	Mag (dB)
1st	0.00	-9.38	0.00	-7.24	0.00	-4.85	0.00	-4.01	0.00	-3.23	0.00	-3.86	0.00	-5.45
2nd	0.02	-11.47	0.03	-13.28	0.03	-16.85	0.03	-21.69	0.04	-29.17	0.04	-32.00	0.02	-21.68
3rd	0.04	-31.26	0.05	-32.03	0.05	-35.31	0.06	-43.36	0.07	-56.55	0.09	-63.78	0.05	-46.40
4th	0.07	-51.05	0.08	-50.78	0.08	-53.78	0.09	-66.03	0.11	-83.93	0.13	-95.56	0.07	-71.13
5th	0.09	-70.84	0.11	-69.53	0.10	-72.24	0.12	-86.71	0.15	-111.31	0.18	-127.34	0.10	-95.85

Sample	Perspex		Composite		Teflon		CS-AK 7		CS-AK 12		CS-AK 15		Lead glass	
	Ave perm	thickness	Ave perm	thickness	Ave perm	thickness	Ave perm	thickness	Ave perm	thickness	Ave perm	thickness	Ave perm	thickness
	2.6-1E-002i	4.5	2-4.7i	1.92	2.04-1E-002i	5.398	7.9-8E-002i	9.634	10.6-0.28i	9.616	13.6-3E-002i	9.779	9.4-8E-002i	7.134
Peak	Time (ns)	Mag (dB)	Time (ns)	Mag (dB)	Time (ns)	Mag (dB)	Time (ns)	Mag (dB)	Time (ns)	Mag (dB)	Time (ns)	Mag (dB)	Time (ns)	Mag (dB)
1st	0.00	-12.60	0.00	-6.26	0.00	-15.07	0.00	-6.46	0.00	-5.51	0.00	-4.83	0.00	-5.88
2nd	0.05	-13.23	0.02	-31.41	0.05	-15.54	0.18	-10.08	0.21	-12.59	0.24	-8.70	0.15	-9.42
3rd	0.10	-38.57	0.05	-68.31	0.10	-45.87	0.36	-24.40	0.42	-27.83	0.48	-18.77	0.29	-22.13
4th	0.15	-63.91	0.07	-105.21	0.15	-76.21	0.54	-38.73	0.63	-43.06	0.72	-28.83	0.44	-34.84
5th	0.19	-89.26	0.10	-142.11	0.21	-106.54	0.72	-53.05	0.83	-58.30	0.96	-38.90	0.58	-47.55
											1.20	-48.97	0.73	-60.26
											1.44	-59.04		

Figure C - 4. Positions and intensities of multiple interference peaks over 16 – 40 GHz

References

[1] C.A. Balanis, *Advanced Engineering Electromagnetics*, John Wiley & Sons, 1989.

[2] D.T. Paris and F.K. Hurd, *Basic Electromagnetic Theory*, McGraw-Hill, 1969.

[3] A.C. Lynch, "Precise Measurements on Dielectric and Magnetic Materials", *IEEE Trans. Instrum. Meas.*, Vol. IM-23, no. 4, pp. 425-431, Dec 1974.

[4] J.B. Birks, "The Measurement of the Permeability of Low Conductivity Ferromagnetic Materials at Centimetric Wavelengths", *Proc. Phy. Soc.*, Vol. 60, part 3, no. 339, pp. 282-92, Mar 1948.

[5] American Society of Testing and Materials, "Standard Test Methods for Complex Permittivity (Dielectric Constant) of Solid Electrical Insulating Materials at Microwave Frequencies and Temperatures to 1650°C", ASTM D 2520, 1995.

[6] H.M. Barlow and A.L. Cullen, *Micro-wave Measurements*, Constable and Co., 1950.

[7] B.C. Glancy and A. Krall, "Automated Microwave Dielectric Constant Measurement System", Naval Surface Weapons Center Report TR 86-46, Mar. 1987.

[8] Standards Association of Australia, "Methods of Test for Electrical Characteristics of Solid Plastics Insulating Materials, Method 4 – Permittivity and Dielectric Dissipation Factor", Australian Standard 1255.4-1974.

[9] S.B. Cohn and K.C. Kelly, "Microwave Measurement of High-Dielectric-Constant Materials", *IEEE Trans. Microwave Theory Tech.*, Vol. MTT-14, no. 9, pp. 406-410, Sep 1966.

[10] "Agilent Solution for Measuring Permittivity and Permeability with LCR Meters and Impedance Analyzers", Agilent Application Note 1369-1, 2001.

[11] W. Von Aulock and J.H. Rowen, "Measurement of Dielectric and Magnetic Properties of Ferromagnetic Materials at Microwave Frequencies", *Bell System Tech. J.*, pp. 427-448, Mar. 1957.

[12] J. Baker-Jarvis, R.G. Geyer, J.H. Grosvenor, M.D. Janezic, C.A. Jones, B. Riddle, C.M. Weil and J. Krupka, "Dielectric Characterization of Low-loss Materials, A Comparison of Techniques", *IEEE Trans. Dielectrics Elec. Insul.*, Vol. 5, no. 4, pp. 571-577, Aug 1998.

[13] W.E. Courtney, "Analysis and Evaluation of a Method of Measuring the Complex Permittivity and Permeability of Microwave Insulators", *IEEE Trans. Microwave Theory Tech.*, Vol. MTT-18, no. 8, pp. 476-485, Aug. 1970.

[14] A.M. Nicolson and G.F. Ross, "Measurement of the Intrinsic Properties of Materials by Time-Domain Techniques", *IEEE Trans. Instrum. Meas.*, Vol. IM-19, no. 4, pp. 377-382, Nov 1970.

[15] W.B. Weir, "Automatic Measurement of Complex Dielectric Constant and Permeability at Microwave Frequencies", *Proc. IEEE*, Vol. 62, no. 1, pp. 33-36, Jan. 1974.

[16] "S-parameter Techniques for Faster, More Accurate Network Design", Hewlett Packard application note 95-1.

[17] "S-parameter Design", Hewlett Packard application note 154, April 1972.

[18] "Measuring Dielectric Constant with the HP 8510 Network Analyzer", Hewlett Packard product note 8510-3.

[19] R.D. Hollinger, V.V. Varadan, D.K. Ghodgaonkar and V.K. Varadan, "Experimental Characterization of Isotropic Chiral Composites in Circular Waveguides", *Radio Sci.*, Vol 27, no. 2, pp. 161-168, March – April 1992.

[20] M.T. Lanagan, J.H. Kim, D.C. Dube, S.J. Jang and R.E. Newnham, "A Microwave Dielectric Measurement Technique for High Permittivity Materials", *Ferroelectrics*, Vol. 82, pp. 91-97, 1988.

[21] K.J. Bois, L.F. Handjojo, A.D. Benally, K. Mubarak and R. Zoughi, "Dielectric Plug-Loaded Two-Port Transmission Line Measurement Technique for Dielectric Property Characterization of Granular and Liquid Materials", *IEEE Trans. Instrum. Meas.*, Vol. 48, no. 6, pp. 1141-1148, Dec 1999.

[22] A. Dominek and A. Park, "Constitutive Parameter Measurements of Lossy Materials", Semi-Annual Report 721837-1, NASA-CR-183398, Ohio State University ElectroScience Laboratory, Sep 1989.

[23] H.B. Sequeira, "Extracting μ_r and ε_r of Solids from One-port Phasor Network analyser Measurements", Martin Marietta Laboratories Technical Report TR 89-83, Sep 1989.

[24] Z. Abbas, R.D. Pollard and R.W. Kelsall, "Complex Permittivity Measurements at Ka-Band Using Rectangular Dielectric Waveguide", *IEEE Trans Instrum. Meas.*, Vol 50, no. 5, pp. 1334-1342, Oct 2001.

[25] J.R. Baker-Jarvis, "Transmission / Reflection and Short-Circuit Line Permittivity Measurements", NIST Tech note 1341, July 1990.

[26] J.R. Baker-Jarvis, E.J. Vanzura and W.A. Kissick, "Improved Technique for Determining Complex Permittivity with the Transmission / Reflection Method", *IEEE Microwave Theory Tech.*, Vol. 38, no. 8, pp. 1096-1103, Aug 1990.

[27] I.J. Youngs, "NAMAS-accredited Microwave Permittivity / Permeability Measurement System", *IEE Proc. Part A Sci. Meas. Technol.*, Vol. 143, no. 4, pp. 247-253, July 1996.

[28] K. Kim, W. Kim, H. Jung and S. Jang, "Measurement Error Induced by Air Gap of Electromagnetic Wave Absorber in the Coaxial Line Method", *Jpn. J. Appl. Phys.*, Vol. 31, Part 1, no. 7, pp. 2096-2100, July 1992.

[29] K.E. Mattar, D.G. Watters and M.E. Brodwin, "Influence of Wall Contacts on Measured Complex Permittivity Spectra at Coaxial Line Frequencies", *IEEE Trans. Microwave Theory Tech.*, Vol. 39, no. 3, pp. 532-537, Mar 1991.

[30] E.J. Vanzura, J.R. Baker-Jarvis, J.H. Grosvenor and M.D. Janezic, "Intercomparison of Permittivity Measurements Using the Transmission / Reflection Method in &-mm Coaxial Transmission Lines", *IEEE Trans. Microwave Theory Tech.*, Vol. 42, no. 11, pp. 2063-2069, Nov 1994.

[31] P.K. Kadaba, "Simultaneous Measurement of Complex Permittivity and Permeability in the Millimeter Region by a Frequency-Domain Technique", *IEEE Trans. Intrum. Meas.*, Vol. IM-33, no. 4, pp. 336-340, Dec. 1984.

[32] D.G. Aguirre, "Measurement of Permittivity and Permeability of Microwave Materials", U.S. Patent 4,507,602, Mar. 1985.

[33] M.T. Hallikainen, F.T. Ulaby and M. Abdelrazik, "Dielectric Properties of Snow in the 3 to 37 GHz Range", *IEEE Trans. Antennas Propag.*, Vol. AP-34, no. 11, pp. 1329-1340, Nov 1986.

[34] M.T. Hallikainen, F.T. Ulaby, M.C. Dobson, M.A. El-Rayes and L.K. Wu, "Microwave Dielectric Behavior of Wet Soil – Part 1: Emperical Models and Experimental Observations", *IEEE Trans. Geosci. Remote Sens.*, Vol. GE-23, no. 1, pp. 25-34, Jan 1985.

[35] C.D. Capps, R.A. Falk, S.G. Ferrier and T.R. Majoch, "Broad-Band Microwave Measurement of Water Using Transient Radiation", *IEEE Trans. Microwave Theory Tech.*, Vol. 40, no. 1, pp. 96-101, Jan 1992.

[36] D.K. Ghodgaonkar, V.V. Varadan and V.K. Varadan, "A Free-Space Method for Measurement of Dielectric Constants and Loss Tangents at Microwave Frequencies", *IEEE Trans. Instrum. Meas.*, Vol. 37, no. 3, pp. 789-793, June 1989.

[37] D.K. Ghodgaonkar, V.V. Varadan and V.K. Varadan, "Free-Space Measurement of Complex Permittivity and Complex Permeability of Magnetic Materials at Microwave Frequencies", *IEEE Trans. Instrum. Meas.*, Vol. 39, no. 2, pp. 387-394, April 1990.

[38] V.V. Varadan, R.D. Hollinger, D.K. Ghodgaonkar and V.K. Varadan, "Free-Space, Broadband Measurements of High-Temperature, Complex Dielectric Properties at Microwave Frequencies", *IEEE Trans. Instrum. Meas.*, Vol. 40, no. 5, pp. 842-846, Oct 1991.

[39] V.V. Varadan, R. Ro and V.K. Varadan, "Measurement of the Electromagnetic Properties of Chiral Composite Materials in the 8 – 40 GHz Range", *Radio Sci.*, Vol. 29, no. 1, pp. 9-22, Jan – Feb 1994.

[40] R.D. Hollinger, V.V. Varadan, V.K. Varadan and D.K. Ghodgaonkar, "Free-Space Measurements of High-Temperature, Complex Dielectric Properties at Microwave Frequencies", *Ceramic Trans., Proc. Symp. on Micro. Theory and Appl. in Mat. Processing*, Vol. 21, pp. 243-250, 1992.

[41] L.L. Frasch, S.J. McLean and R.G. Olsen, "Electromagnetic Properties of Dry and Water Saturated Basalt Rock, 1 – 110 GHz", *IEEE Trans. Geosci. Remote Sens.*, Vol. 36, no. 3, pp. 754-766, May 1998.

[42] I. Cuiñas and M.G. Sánchez, "Building Material Characterization from Complex Transmissivity Measurements at 5.8 GHz", *IEEE Trans. Antennas Propag.*, Vol. 48, no. 8, pp. 1269-1271, Aug. 2000.

[43] R. Zoughi and B. Zonnefeld, "Permittivity Characteristics of Kevlar, Carbon Composites, E-Glass, and Rubber (33% Carbon) at X-Band (8 – 12 GHz)", *Rev. Prog. Quant. Nondestr. Eval.*, Vol 10B, pp. 1431-1436, 1991.

[44] J.C. Joseph, R.J. Jost and E.L. Utt, "Multiple Angle of Incidence Measurement Technique for the Permittivity and Permeability of Lossy Materials at Millimeter Wavelengths", *Ant. Prop. Soc. Int. Symp.*, Vol. 25, pp. 640-643, June 1987.

[45] J. Muñoz, M. Rojo, A. Parreño and J. Margineda, "Automatic Measurement of Permittivity and Permeability at Microwave Frequencies Using Normal and Oblique Free-Wave Incidence with Focused Beam", *IEEE Trans. Instrum. Meas.*, Vol. 47, no. 4, pp. 886-892, Aug. 1998.

[46] Z. Ma and S. Okamura, "Permittivity Determination Using Amplitudes of Transmission and Reflection Coefficients at Microwave Frequency", *IEEE Trans. Microwave Theory Tech.*, Vol. 47, no. 5, pp. 546-550, May 1999.

[47] J. Matlacz and K.D. Palmer, "Using Offset Parabolic Reflector Antennas for Free Space Material Measurement", *IEEE Trans. Instrum. Meas.*, Vol. 49, no. 4, pp. 862-866, Aug. 2000.

[48] A.L. Cullen, "A New Free-Wave Method for Ferrite Measurement at Millimeter Wavelengths", *Radio Sci.*, Vol. 22, pp. 1168-1170, Dec. 1987.

[49] F.C. Smith, B. Chambers and J.C. Bennett, "Calibration Techniques for Free Space Reflection Coefficient Measurements", *IEE Proc. Part A Sci. Meas. Technol.*, Vol. 139, no. 5, pp. 247-253, Sep. 1992.

[50] F.C. Smith, B. Chambers and J.C. Bennett, "Methodology for Accurate Free-Space Characterisation of Radar Absorbing Materials", *IEE Proc. Part A Sci. Meas, Technol.*, Vol. 141, no. 6, pp. 538-546, Nov. 1994.

[51] F.C. Smith, "A Review of UK Facilities for Characterizing the Performance of Radar Absorbing Material (RAM)", *IEE Conf. Ant. Prop # 407*, pp. 445-449, Apr. 1995.

[52] P. Blacksmith Jr. and R.B. Mack, "On Measuring the Radar Cross Sections of Ducks and Chickens", *Proc. IEEE*, Vol. 53, p 1125, Aug. 1965.

[53] I.L. Al-Qadi, D.K. Ghodgaonkar, V.K. Varadan and V.V. Varadan, "Effect of Moisture on Asphaltic Concrete at Microwave Frequencies", *IEEE Trans. Geosci. Remote Sens.*, Vol. 29, no. 5, pp. 710-717, Sep 1991.

[54] M.H. Umari, D.K. Ghodgaonkar, V.V. Varadan and V.K. Varadan, "A Free-Space Bistatic Technique for the Measurement of Parallel and Perpendicular Reflection Coefficients of Planar Samples", *IEEE Trans. Instrum. Meas.*, Vol. 40, no. 1, pp. 19-24, Feb. 1991.

[55] O. Hashimoto and Y. Shimizu, "Reflecting Characteristics of Anisotropic Rubber Sheets and Measurement of Complex Permittivity Tensor", *IEEE Trans. Microwave Theory Tech.*, Vol. MTT-34, no. 11, pp. 1202-1207, Nov. 1986.

[56] A.L. Cullen and P.K. Yu, "The Accurate Measurement of Permittivity by Means of an Open Resonator", *Proc. R. Soc. Lond.*, Vol. A325, p 493-509, 1971.

[57] P.K. Yu and A.L. Cullen, "Measurement of Permittivity by Means of an Open Resonator. I. Theoretical", *Proc. R. Soc. Lond.*, Vol. A380, pp. 49-71, 1982.

[58] A.C. Lynch, "Measurement of Permittivity by Means of an Open Resonator. II Experimental", *Proc. R. Soc. Lond.*, Vol. A380, pp. 73-76, 1982.

[59] A.C. Lynch, "Measurement of Permittivity Using an Open Resonator", *IEE Proc. Part A Sci. Meas. Technol.*, Vol. 130, no. 7, pp. 365-368, Nov 1983.

[60] W.F.P. Chan and B. Chambers, "Measurement of Nonplanar Dielectric Samples Using an Open Resonator", *IEEE Trans. Microwave Theory Tech.*, Vol. MTT-35, no. 12, pp. 1429-1434, Dec 1987.

[61] K.C. Pitman, M.W Lindley, D. Simkin and J.F. Cooper, "Radar Absorbers: Better By Design", *IEE Proc. Part F Radar Signal Process.*, Vol. 138, no. 3, pp. 223-228, Jun 1991.

[62] A.C. Lynch, H.D. Griffiths, S. Appleton, A.L. Cullen, A. Khosrowbeygi and R. Benjamin, "Free-Wave Measurement of Permeability and Permittivity of Ferrites at Millimetre-Wave

Frequencies", *IEE Proc. Part A Sci. Meas. Technol.*, Vol. 142, no. 2, pp. 169-175, March 1995.

[63] A.C. Lynch and D. Simkin, "Measurement of Permeability and Permittivity of Ferrites", *Meas. Sci. Technol.*, Vol. 1, pp. 1162-1167, 1990.

[64] A. Nishikata and Y. Simizu, "Analysis for Reflection from Coaxial End Attached to Lossy Sheet and Its Application to Nondestructive Measurement", *Electron. Commun. Jpn. Part II Electron.*, Vol. 71, no. 6, pp. 95-107, 1988.

[65] Y.Z. Wei and S. Sridhar, "Radiation-Corrected Open Ended Coax Line Technique for Dielectric Measurements of Liquids up to 20 GHz", *IEEE Trans. Microwave Theory Tech.*, Vol. 39, no. 3, pp. 526-531, March 1991.

[66] G.Q. Jiang, W.H. Wong, E.Y. Raskovich, W.G. Clark, W.A. Hines and J. Sanny, "Open-Ended Coaxial-Line Technique for the Measurement of the Microwave Dielectric Constant for Low-Loss Solids and Liquids", *Rev. Sci. Instrum.*, Vol. 64, no. 6, pp. 1614-1621, June 1993.

[67] G.Q. Jiang, W.H. Wong, E.Y. Raskovich, W.G. Clark, W.A. Hines and J. Sanny, "Measurement of the Microwave Dielectric Constant for Low-Loss Samples with Finite Thickness using Open-Ended Coaxial-Line Probes", *Rev. Sci. Instrum.*, Vol. 64, no. 6, pp. 1622-1626, June 1993.

[68] B.G. Colpitts, "Temperature Sensitivity of Coaxial Probe Complex Permittivity Measurements: Experimental Approach", *IEEE Trans. Microwave Theory Tech.*, Vol. 41, no. 2, pp. 229-233, Feb. 1993.

[69] D.V. Blackham and R.D. Pollard, "An Improved Technique for Permittivity Measurements Using a Coaxial Probe", *IEEE Trans. Instrum. Meas.*, Vol. 46, no. 5, pp. 1093-1099, Oct. 1997.

[70] S. Wang, M. Niu and D. Xu, "A Frequency-Varying Method for Simultaneous Measurement of Complex Permittivity and Permeability with an Open-Ended Coaxial Probe", *IEEE Trans. Microwave Theory Tech.*, Vol. 46, no.12, pp. 2145-2147, Dec. 1998.

[71] S.I. Ganchev, S. Bakhtiari and R. Zoughi, "A Novel Numerical Technique for Dielectric Measurement of Generally Lossy Dielectrics", *IEEE Trans. Instrum. Meas.*, Vol. 41, no. 3, pp. 361-365, June 1992.

[72] C.W. Chang, K.M. Chen and J. Qian, "Nondestructive Determination of Electromagnetic Parameters of Dielectric Materials at X-Band Frequencies Using a Waveguide Probe System", *IEEE Trans. Instrum. Meas.*, Vol. 46, no. 5, pp. 1084-1092, Oct. 1997.

[73] Hewlett Packard 8510C Network Analyzer System Operating and Programming Manual, pp. 8-16 – 8-18, 1994.

[74] C.A. Balanis, *Antenna Theory, Analysis and Design*, 2nd ed., John Wiley & Sons, pp. 616-620, 1997.

[75] J.R. Mentzer, "The use of Dielectric Lenses in Reflection Measurements", *Proc. I.R.E.*, pp. 252-256, Feb. 1953.

[76] S.W. Smith, "The Scientist and Engineer's Guide to Digital Signal Processing", California Technical Publishing, 1999.

[77] J.W. Cooley and J.W. Tukey, "An Algorithm for the Machine Calculation of Complex Fourier Series", *Math. Comp.*, Vol 19, pp. 297-301, 1965.

[78] L.R. Rabiner, R.W. Schafer and C.M. Rader, "The Chirp-Z Algorithm and Its Application", *Bell System Tech. J.*, pp. 1249-1292, May-June 1969.

[79] B. Ulriksson, "Conversion of Frequency-Domain Data to the Time Domain", *Proc. IEEE*, Vol. 74, no. 1, pp. 74-77, Jan 1986.

Frequencies", *IEE Proc. Part A Sci. Meas. Technol.*, Vol. 142, no. 2, pp. 169-175, March 1995.

[63] A.C. Lynch and D. Simkin, "Measurement of Permeability and Permittivity of Ferrites", *Meas. Sci. Technol.*, Vol. 1, pp. 1162-1167, 1990.

[64] A. Nishikata and Y. Simizu, "Analysis for Reflection from Coaxial End Attached to Lossy Sheet and Its Application to Nondestructive Measurement", *Electron. Commun. Jpn. Part II Electron.*, Vol. 71, no. 6, pp. 95-107, 1988.

[65] Y.Z. Wei and S. Sridhar, "Radiation-Corrected Open Ended Coax Line Technique for Dielectric Measurements of Liquids up to 20 GHz", *IEEE Trans. Microwave Theory Tech.*, Vol. 39, no. 3, pp. 526-531, March 1991.

[66] G.Q. Jiang, W.H. Wong, E.Y. Raskovich, W.G. Clark, W.A. Hines and J. Sanny, "Open-Ended Coaxial-Line Technique for the Measurement of the Microwave Dielectric Constant for Low-Loss Solids and Liquids", *Rev. Sci. Instrum.*, Vol. 64, no. 6, pp. 1614-1621, June 1993.

[67] G.Q. Jiang, W.H. Wong, E.Y. Raskovich, W.G. Clark, W.A. Hines and J. Sanny, "Measurement of the Microwave Dielectric Constant for Low-Loss Samples with Finite Thickness using Open-Ended Coaxial-Line Probes", *Rev. Sci. Instrum.*, Vol. 64, no. 6, pp. 1622-1626, June 1993.

[68] B.G. Colpitts, "Temperature Sensitivity of Coaxial Probe Complex Permittivity Measurements: Experimental Approach", *IEEE Trans. Microwave Theory Tech.*, Vol. 41, no. 2, pp. 229-233, Feb. 1993.

[69] D.V. Blackham and R.D. Pollard, "An Improved Technique for Permittivity Measurements Using a Coaxial Probe", *IEEE Trans. Instrum. Meas.*, Vol. 46, no. 5, pp. 1093-1099, Oct. 1997.

[70] S. Wang, M. Niu and D. Xu, "A Frequency-Varying Method for Simultaneous Measurement of Complex Permittivity and Permeability with an Open-Ended Coaxial Probe", *IEEE Trans. Microwave Theory Tech.*, Vol. 46, no.12, pp. 2145-2147, Dec. 1998.

[71] S.I. Ganchev, S. Bakhtiari and R. Zoughi, "A Novel Numerical Technique for Dielectric Measurement of Generally Lossy Dielectrics", *IEEE Trans. Instrum. Meas.*, Vol. 41, no. 3, pp. 361-365, June 1992.

[72] C.W. Chang, K.M. Chen and J. Qian, "Nondestructive Determination of Electromagnetic Parameters of Dielectric Materials at X-Band Frequencies Using a Waveguide Probe System", *IEEE Trans. Instrum. Meas.*, Vol. 46, no. 5, pp. 1084-1092, Oct. 1997.

[73] Hewlett Packard 8510C Network Analyzer System Operating and Programming Manual, pp. 8-16 – 8-18, 1994.

[74] C.A. Balanis, *Antenna Theory, Analysis and Design*, 2nd ed., John Wiley & Sons, pp. 616-620, 1997.

[75] J.R. Mentzer, "The use of Dielectric Lenses in Reflection Measurements", *Proc. I.R.E.*, pp. 252-256, Feb. 1953.

[76] S.W. Smith, "The Scientist and Engineer's Guide to Digital Signal Processing", California Technical Publishing, 1999.

[77] J.W. Cooley and J.W. Tukey, "An Algorithm for the Machine Calculation of Complex Fourier Series", *Math. Comp.*, Vol 19, pp. 297-301, 1965.

[78] L.R. Rabiner, R.W. Schafer and C.M. Rader, "The Chirp-Z Algorithm and Its Application", *Bell System Tech. J.*, pp. 1249-1292, May-June 1969.

[79] B. Ulriksson, "Conversion of Frequency-Domain Data to the Time Domain", *Proc. IEEE*, Vol. 74, no. 1, pp. 74-77, Jan 1986.

Frequencies", *IEE Proc. Part A Sci. Meas. Technol.*, Vol. 142, no. 2, pp. 169-175, March 1995.

[63] A.C. Lynch and D. Simkin, "Measurement of Permeability and Permittivity of Ferrites", *Meas. Sci. Technol.*, Vol. 1, pp. 1162-1167, 1990.

[64] A. Nishikata and Y. Simizu, "Analysis for Reflection from Coaxial End Attached to Lossy Sheet and Its Application to Nondestructive Measurement", *Electron. Commun. Jpn. Part II Electron.*, Vol. 71, no. 6, pp. 95-107, 1988.

[65] Y.Z. Wei and S. Sridhar, "Radiation-Corrected Open Ended Coax Line Technique for Dielectric Measurements of Liquids up to 20 GHz", *IEEE Trans. Microwave Theory Tech.*, Vol. 39, no. 3, pp. 526-531, March 1991.

[66] G.Q. Jiang, W.H. Wong, E.Y. Raskovich, W.G. Clark, W.A. Hines and J. Sanny, "Open-Ended Coaxial-Line Technique for the Measurement of the Microwave Dielectric Constant for Low-Loss Solids and Liquids", *Rev. Sci. Instrum.*, Vol. 64, no. 6, pp. 1614-1621, June 1993.

[67] G.Q. Jiang, W.H. Wong, E.Y. Raskovich, W.G. Clark, W.A. Hines and J. Sanny, "Measurement of the Microwave Dielectric Constant for Low-Loss Samples with Finite Thickness using Open-Ended Coaxial-Line Probes", *Rev. Sci. Instrum.*, Vol. 64, no. 6, pp. 1622-1626, June 1993.

[68] B.G. Colpitts, "Temperature Sensitivity of Coaxial Probe Complex Permittivity Measurements: Experimental Approach", *IEEE Trans. Microwave Theory Tech.*, Vol. 41, no. 2, pp. 229-233, Feb. 1993.

[69] D.V. Blackham and R.D. Pollard, "An Improved Technique for Permittivity Measurements Using a Coaxial Probe", *IEEE Trans. Instrum. Meas.*, Vol. 46, no. 5, pp. 1093-1099, Oct. 1997.

[70] S. Wang, M. Niu and D. Xu, "A Frequency-Varying Method for Simultaneous Measurement of Complex Permittivity and Permeability with an Open-Ended Coaxial Probe", *IEEE Trans. Microwave Theory Tech.*, Vol. 46, no.12, pp. 2145-2147, Dec. 1998.

[71] S.I. Ganchev, S. Bakhtiari and R. Zoughi, "A Novel Numerical Technique for Dielectric Measurement of Generally Lossy Dielectrics", *IEEE Trans. Instrum. Meas.*, Vol. 41, no. 3, pp. 361-365, June 1992.

[72] C.W. Chang, K.M. Chen and J. Qian, "Nondestructive Determination of Electromagnetic Parameters of Dielectric Materials at X-Band Frequencies Using a Waveguide Probe System", *IEEE Trans. Instrum. Meas.*, Vol. 46, no. 5, pp. 1084-1092, Oct. 1997.

[73] Hewlett Packard 8510C Network Analyzer System Operating and Programming Manual, pp. 8-16 – 8-18, 1994.

[74] C.A. Balanis, *Antenna Theory, Analysis and Design*, 2nd ed., John Wiley & Sons, pp. 616-620, 1997.

[75] J.R. Mentzer, "The use of Dielectric Lenses in Reflection Measurements", *Proc. I.R.E.*, pp. 252-256, Feb. 1953.

[76] S.W. Smith, "The Scientist and Engineer's Guide to Digital Signal Processing", California Technical Publishing, 1999.

[77] J.W. Cooley and J.W. Tukey, "An Algorithm for the Machine Calculation of Complex Fourier Series", *Math. Comp.*, Vol 19, pp. 297-301, 1965.

[78] L.R. Rabiner, R.W. Schafer and C.M. Rader, "The Chirp-Z Algorithm and Its Application", *Bell System Tech. J.*, pp. 1249-1292, May-June 1969.

[79] B. Ulriksson, "Conversion of Frequency-Domain Data to the Time Domain", *Proc. IEEE*, Vol. 74, no. 1, pp. 74-77, Jan 1986.

[80] F.J. Harris, "On the Use of Windows for Harmonic Analysis with the Discrete Fourier Transform", *Proc. IEEE*, Vol 66, n1, pp. 51-83, Jan 1978.

[81] A.H. Nuttall, "Some Windows with Very Good Sidelobe Behaviour", *IEEE Trans. Acoustics, Speech and Signal Processing*, Vol ASSP-29, n1, pp. 84-91, Feb 1981.

[82] K. Lu and T.J. Brazil, "A Systematic Error Analysis of HP8510 Time-Domain Gating Techniques with Experimental Verification", *1993 IEEE Microwave Theory Tech. Digest, KK-7*, pp. 1259-1262, 1993.

[83] Hewlett Packard 16451B Dielectric Test Fixture Operation and Service Manual, Dec 1993.

[84] Cuming Corporation Technical Bulletin 211, "C-Stock AK-500", Document control number N-01-000-137, 2 May 1992.

[85] Nippon Electric Glass Co. Ltd., "Radiation Shielding Lead Glass".

[86] R.C.Weast (ed), *Handbook of Chemistry and Physics*, C.R.C. Press, 1975-76.

[87] J. Poley, "Microwave Dispersion of Some Polar Liquids", *Appl. Sci. Res.*, Vol. 4, Section B, pp. 339-387, 1955.

[88] S.K. Dhawan, "Understanding Effect of Teflon Room Temperature Phase Transition On Coax Cable Delay in Order to Improve the Measurement of TE Signals of Deuterated Polarized Targets", *IEEE Trans. Nucl. Sci.*, Vol. 39, no. 5, pp. 1331-1335, Oct 1992.

[89] L. Olmedo, G. Chateau, C. Deleuze and J.L. Forveille, "Microwave Characterization and Modelization of Magnetic Granular Materials", *J. Appl. Phys.*, Vol. 73, no. 10, pp. 6992-6994, May 1993.

[90] W.H. von Aulock (ed.), *Handbook of Microwave Ferrite Materials*, Academic Press, 1965.

[91] H.S. Cho and S.S. Kim, "M-Hexaferrites with Planar Magnetic Anisotropy and Their Application to High-Frequency Microwave Absorbers", *IEEE Trans. Magnetics*, Vol. 35, no. 5, pp. 3151-3153, Sep. 1999.

[92] S. Sugimoto, S. Kondo, K. Okayama, H. Nakamura, D. Book, T. Kagotani and M. Homma, "M-Type Ferrite Composite as a Microwave Absorber with Wide Bandwidth in the GHz Range", *IEEE Trans. Magnetics*, Vol. 35, no. 5, pp. 3154-3156, Sep. 1999.

[93] M.T. Lanagan, J. H. Kim, Sei-Joo Jang and R.E. Newnham, "Microwave Dielectric Properties of Antiferroelectric Lead Zirconate", *J. Am. Ceram. Soc.*, Vol. 4, no. 4, pp. 311-316, 1988.

[94] P.Jewsbury (private communication)

[95] A.R. Amiet and P. Jewsbury, "Free Space Microwave Permittivity and Permeability Measurements", *2000 Asia-Pacific Microwave Conference*, pp. 445-448, Dec 2000.

[96] U. Kaatze, "Complex Permittivity of Water as a function of Frequency and Temperature", *J. Chem. Eng. Data*, Vol 34, pp. 371-374, 1989.

[97] Z. Ma and S. Okamura, "Permittivity Determination Using Amplitudes of Transmission and Reflection Coefficients at Microwave Frequency", *IEEE Trans. Microwave Theory Tech.*, Vol. 47, no. 5, pp. 546-550, May 1999.

The following poster was presented at the Monash University Electrical and Computer Systems Engineering Postgraduate Student Research Forum in September 2000.

Free Space Microwave Permittivity and Permeability Measurements

Andrew Amiet
Supervisors: Dr. Greg Cambrell and Dr. Peter Jewsbury (DSTO)

Statement of the problem

- Current measurement techniques use waveguides which require sample destruction
- Some materials can give misleading results if tested using standard techniques
- Sample preparation time consuming and very small flaws in specimen lead to large errors in deduced permittivity/permeability

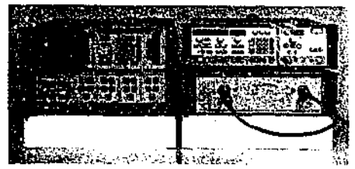

Vector Network Analyser shown using 10cm coaxial line.

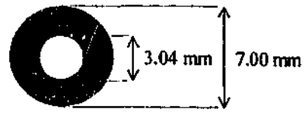

Sample size for coaxial line

Free space measurements

Advantages

- Non destructive testing of samples so can be used in a Quality Assurance role
- Requires little preparation of the sample
- Ability to test materials at very high frequencies
- Ability to test inhomogeneous materials and those with large additives (such as long fibres)

Disadvantages

- Introduces other errors to the measurement such as diffraction and near field effects
- Difficult to perform a full calibration of network analyser

Free space transmission, metal backed reflection and off normal angle reflection measurements

Results

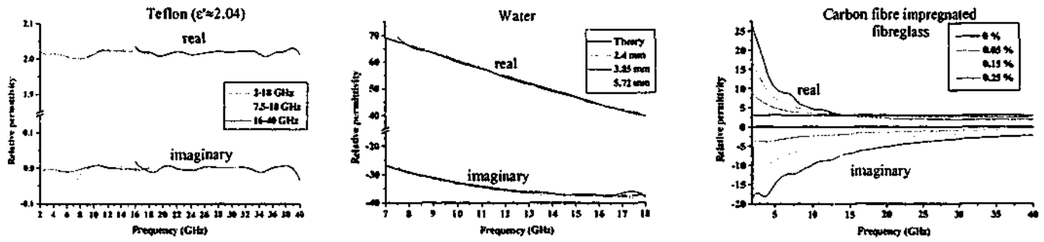

Permittivity results for Teflon, water and carbon fibre impregnated fibreglass measured in free space.

Summary

- Free space techniques can be used to measure permittivity to ±5% accuracy
- Iterative technique developed to extract permittivity values from transmission only data
- Currently investigating sources of error and their magnitudes
- Extension of technique for permeability measurements of magnetic materials

The following paper was presented at the 2000 Asia-Pacific Microwave Conference, held in Sydney, Australia in December 2000.

Free Space Microwave Permittivity and Permeability Measurements

Andrew Amiet
Supervisors: Dr. Greg Cambrell and Dr. Peter Jewsbury (DSTO)

Statement of the problem

- Current measurement techniques use waveguides which require sample destruction
- Some materials can give misleading results if tested using standard techniques
- Sample preparation time consuming and very small flaws in specimen lead to large errors in deduced permittivity/permeability

Vector Network Analyser shown using 10cm coaxial line.

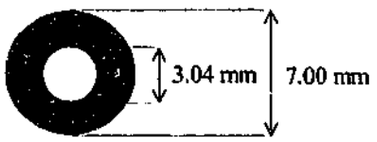

Sample size for coaxial line

Free space measurements

Advantages

- Non destructive testing of samples so can be used in a Quality Assurance role
- Requires little preparation of the sample
- Ability to test materials at very high frequencies
- Ability to test inhomogeneous materials and those with large additives (such as long fibres)

Disadvantages

- Introduces other errors to the measurement such as diffraction and near field effects
- Difficult to perform a full calibration of network analyser

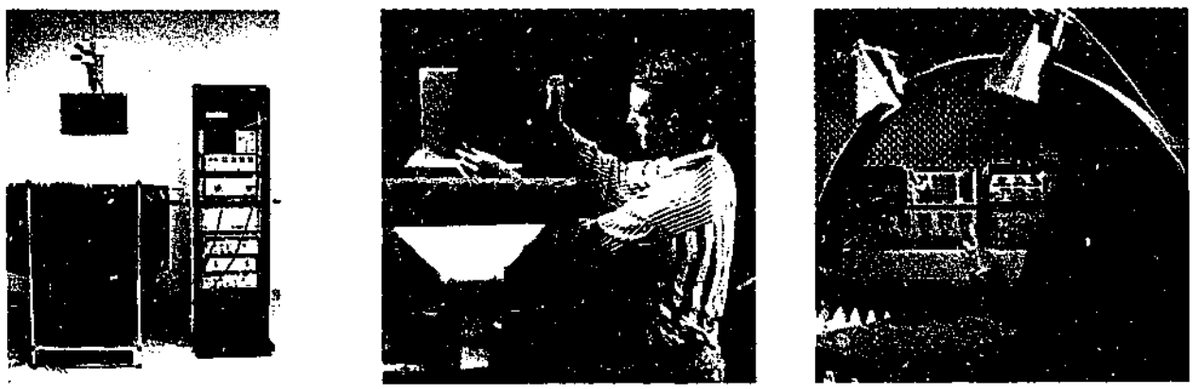

Free space transmission, metal backed reflection and off normal angle reflection measurements

Results

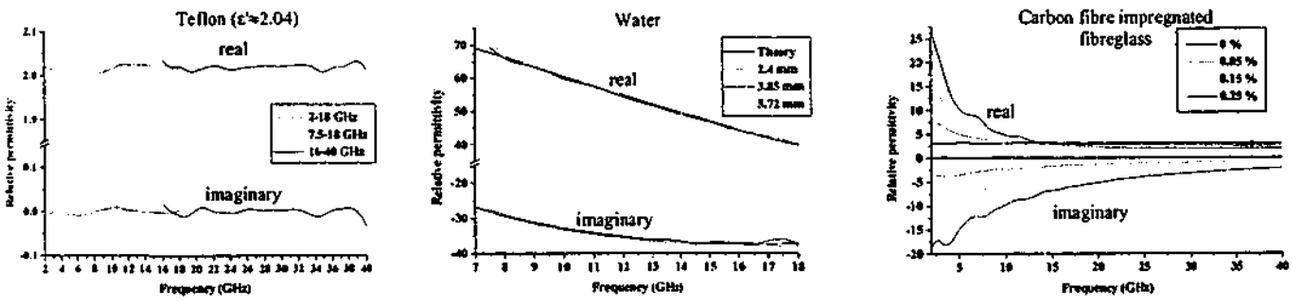

Permittivity results for Teflon, water and carbon fibre impregnated fibreglass measured in free space.

Summary

- Free space techniques can be used to measure permittivity to ±5% accuracy
- Iterative technique developed to extract permittivity values from transmission only data
- Currently investigating sources of error and their magnitudes
- Extension of technique for permeability measurements of magnetic materials

The following paper was presented at the 2000 Asia-Pacific Microwave Conference, held in Sydney, Australia in December 2000.

FREE SPACE MICROWAVE PERMITTIVITY AND PERMEABILITY MEASUREMENTS

A. AMIET
DEFENCE SCIENCE AND TECHNOLOGY ORGANISATION
P.O. Box 4331, Melbourne, 3001
E-mail: andrew.amiet@dsto.defence.gov.au

P. JEWSBURY
DEFENCE SCIENCE AND TECHNOLOGY ORGANISATION
P.O. Box 4331, Melbourne, 3001
E-mail: peter.jewsbury@dsto.defence.gov.au

Measurements of permittivity and permeability at microwave frequencies using a free space technique are presented for some well known materials and a series of absorptive samples. Free space measurements are especially useful for non-destructive evaluation, and are sometimes the most appropriate method for some composites that may contain large inclusions such as fibres, or over frequency bands where waveguide measurements are impractical to perform.

1 Introduction

The measurement of permittivity and permeability of materials at microwave frequencies can be performed in many ways. Waveguide methods are popular, where the sample is precisely machined to fit inside the waveguide. Both rectangular and coaxial waveguides are used, rectangular samples are easier to produce than coaxial ones, however they can only be used over a limited frequency range. Coaxial waveguide allows extremely wide-band measurements but sample preparation is difficult. A vector network analyser is generally used to collect the reflected and transmitted signals, and permittivity and permeability values can be extracted from the results.

Waveguide measurements suffer from errors caused by incomplete filling of the waveguide by the sample. Corrections for this have been proposed with some success [1], but are not perfect. Sample preparation is destructive and often time consuming. Some materials are not suitable for waveguide measurements, such as those containing long fibres, or foams with large voids. High frequency measurements are especially difficult due to waveguide size. Free space techniques overcome many of these problems.

Free space measurements of microwave reflection and transmission of materials have been performed for some years [2]. Dual ridged horn antennas can extend over wide frequency bands, reducing the number of measurements required. Errors associated with diffraction around the sample have been overcome by some investigators with the use of lenses to focus the beam to a small spot, however this technique requires specialised equipment and is not ideal for inhomogeneous samples. In these cases, a large area average can give a more accurate value for the material as a whole.

2 Experimental

Measurements in free space were taken using a Hewlett Packard 8510C Vector Network Analyser with an 83651B Synthesized Frequency Source and 8517A S-parameter Test Set. Data is collected by a computer controlling the system over 401 points across the frequency range of interest. Three different sets of microwave horn antennas were used to cover the frequency range of 2 – 40 GHz. The horns cover the frequency ranges 2 – 18 GHz, 7.5 – 18 GHz, and 16 – 40 GHz. The horns were mounted vertically on a table facing each other, with the sample lying between them on a thick piece of low density polystyrene foam. Reflection and transmission can be measured in this way, using the lower horn as the send/receive and the upper horn as receiver only. Measurements are taken in the near field, sample to horn distances vary with horn size, but are generally between 20 to 40 cm.

Transmission measurements are taken by placing the samples on the foam sheet and recording the magnitude and phase of the transmitted signal. The system is calibrated using the 8510C's "Response" calibration technique. Diffraction around the sample leads to small errors which can be removed either through time gating or with the use of a foil "window" surrounding the sample. The foil window introduces errors when the size of the opening is similar to the wavelength of the signal.

Reflection measurements are a little more difficult to perform. The calibration used is the "Response/Isolation" type since the reflections from the apparatus are larger than those for the transmission measurements. Convoluted Radar Absorbing Material (RAM) is used to reduce back reflections from the measurement stand. A isolation measurement is taken with only the RAM placed on the table, then the reference "short" consisting of a square metal sheet the same size as the sample is placed on the table, and the reflection measured with the RAM placed on top. In this way, reflections from behind the calibration plane are reduced. When the sample is measured, the RAM is again placed over the top of the specimen to reduce unwanted reflections.

Time gating is used when performing both reflection and transmission measurements. This removes the effects of waves rebounding from the horns to the sample and back again. Care must be taken when gating so as to not remove multiple internal reflections within the sample. The gate must be kept as wide as possible to include these effects while being small enough to reject false signals. For this reason the technique is more suited to lossy materials where the magnitude of multiple bounces is low.

Once the reflection and/or transmission signals are measured, the permittivity and/or permeability can be calculated using well known formulae [3]. For some samples, reflection measurements are too difficult to perform and so transmission only is measured. However using this technique, it is impossible to calculate both permittivity and permeability with one measurement. For non-magnetic materials, an optimisation technique can be used to extract the permittivity only.

3 Results

3.1 Teflon

The electrical properties of teflon are well known and as such it is frequently used as a standard reference material. Teflon has a real permittivity of 2.04 [1] with a very low imaginary component at microwave frequencies, and is non-magnetic. Reflection and transmission measurements were taken on a 30cm square sheet of teflon, 5.40 ± 0.08 mm thick. From these measurements permittivity (ε) and permeability (μ) values were calculated and shown in Table 1. Also shown is the average permittivity using the transmission technique only. The frequency spectrum of the permittivity using transmission measurements is shown in Fig. 1.

	ε'	ε"	μ'	μ"
Reflection / transmission				
2 – 18 GHz	2.05	-0.03	0.99	0.02
7.5 - 18 GHz	2.05	-0.05	0.99	0.03
16 -- 40 GHz	2.02	-0.14	0.99	0.10
Transmission only				
2 – 18 GHz	2.02	0.00	-	-
7.5 - 18 GHz	2.02	0.00	-	-
16 – 40 GHz	2.02	0.00	-	-

Table 1. Average permittivity and permeability of teflon measured in free space.

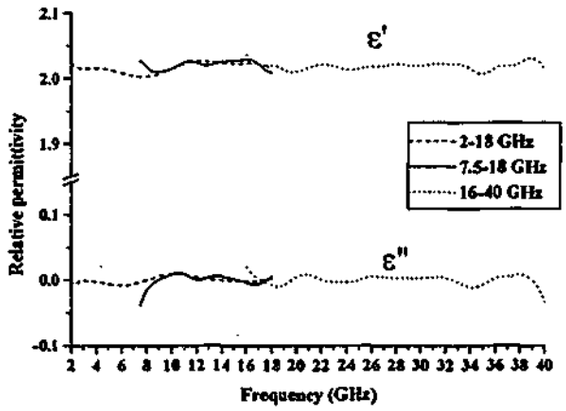

Figure 1. Frequency spectrum of permittivity for teflon using transmission alone.

Due to the thickness of the teflon sheet, destructive interference occurs at about 19.7 and 39.7 GHz and the reflected signal drops below -40 dB. This affects the calculations and is evident in the average values of ε'' and μ'' in Table 1. Transmission is not adversely affected by destructive interference and so the permittivity calculated using transmission only results is more or less constant in the 16 - 40 GHz range, as seen in Fig. 1.

3.2 Water

Another material with well known properties is water. Water has a high permittivity at microwave frequencies and shows resonant behaviour at about 17 GHz at 20 °C. The properties of water are highly temperature dependant and so this needs to be accurately measured along with the microwave readings. The water is poured into a plastic lined polystyrene foam bath, 55 cm square. The plastic lining has been roughened to minimise surface tension effects, and care has been taken to ensure the bath is flat and level. The depth of the water is calculated by measuring the weight and correcting for meniscus effects. This causes the depth in the centre of the bath to be about 0.1 mm shallower than the weight would otherwise indicate. The results for deionised water at 19.3 degrees at a number of depths compared to the theoretical result from [4] is shown in Fig. 2 and 3.

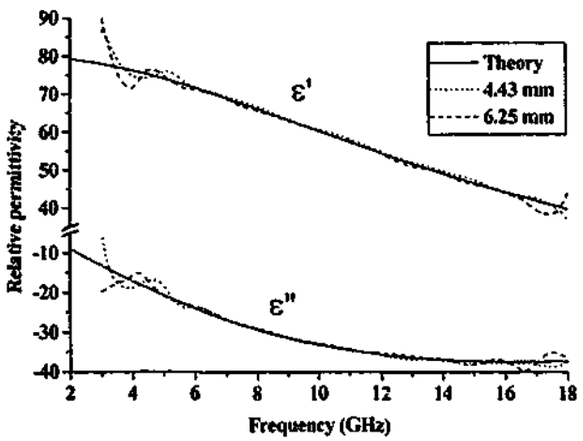

Figure 2. The permittivity of deionised water over the frequency range 2 – 18 GHz.

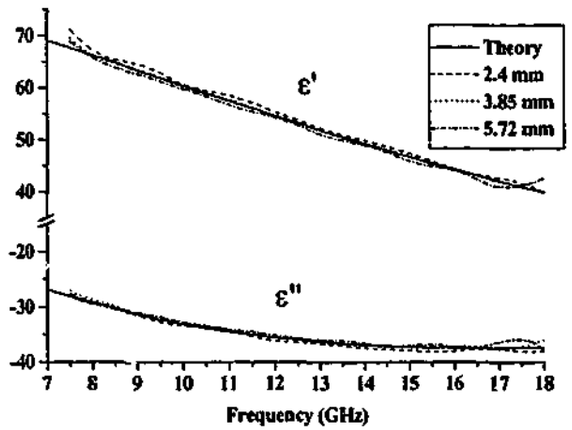

Figure 3. The permittivity of deionised water over the frequency range 7 – 18 GHz.

The results show a good agreement with a calculated curve using a Debye relaxation formula with parameters [1] $\varepsilon_0 = 80.41$, $\varepsilon_\infty = 5.6$ and $\tau = 9.598$ ps.

3.3 Absorbing material

Fibreglass tissues containing 6mm carbon fibres at various loadings were obtained from Technical Fibre Products Ltd in the UK. These were infused with resin using a vacuum process and measured over the frequency range 2 – 40 GHz. Reflection and transmission measurements were used to calculate both permittivity and permeability for these materials. The use of permeability values gives a good estimate of the accuracy of the measurement. The permittivity results are shown in Fig. 4 and average permeability results are given in Table 2. The loadings shown are weight percent carbon fibre.

The carbon fibres on the fibreglass sheet tend to lie parallel to the rolling direction, so the samples were made by alternating the orientation of each layer. To further remove any effects of alignment, the samples were tested in both orientations and the results averaged. It can seen that both real and imaginary permittivity decrease exponentially with frequency, and that the real permittivity has all but flattened out to the unloaded fibreglass result above 15 GHz.

---

[1] Values calculated fitting a straight line between values at 15 °C and 20 °C using data from [4].

Carbon loading	2 – 18 GHz		16 – 40 GHz	
	μ'	μ"	μ'	μ"
0 %	1.00	0.00	1.02	0.00
0.05 %	0.98	-0.02	1.02	0.04
0.15 %	0.95	-0.02	1.00	0.02
0.25 %	0.95	0.01	1.01	0.03

Table 2. Measured average permeabilities of loaded fibreglass across frequency bands.

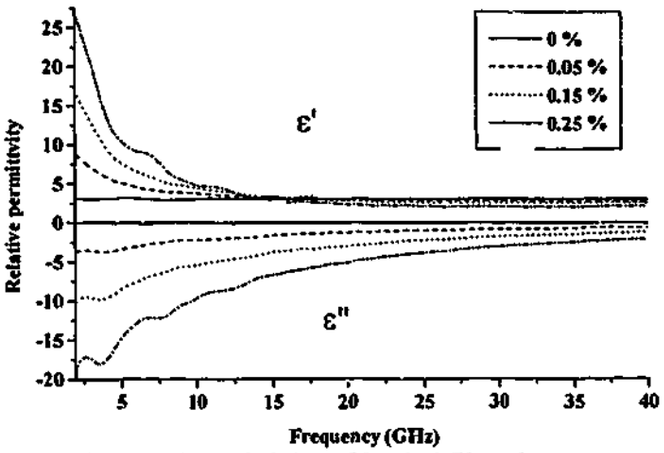

Figure 4. Permittivity of loaded fibreglass as a function of frequency.

4 Discussion

Accurate measurement of permittivity and permeability of materials is possible using this method. There is little if any sample preparation required for the test procedure other than ensuring the sample is flat and large enough to cover the foil window (if required). The effects of the foil window can be seen in Fig. 4 – results over 2-18 GHz show oscillatory behaviour especially at the lowest frequencies where the wavelength is similar to the size of the opening.

Using the transmission data alone to calculate permittivity is easy to perform and does not suffer from destructive interference effects than can occur when using reflection data. For non-magnetic materials it is an excellent method of permittivity measurement. Magnetic materials still require reflection data to be taken, however if the samples can be made thin enough to avoid destructive interference effects, permeability can still be measured accurately.

The technique is especially suited for moderate to high loss materials, where internal reflections within the sample are attenuated. Since the apparatus is not situated in an anechoic chamber, stray reflections from parts of the stand can interfere with the desired signal and need to be removed using time gating. The gate removes these unwanted signals but can also remove the reflections from inside the sample. Reducing the stray reflections using RAM will increase accuracy of the measurements.

Conclusion

The permittivity and permeability of some materials tested in free space are presented. The method yields results that are very close to those expected for some well known materials. Both electric and magnetic properties can be evaluated when reflection and transmission are measured, transmission measurements alone can be used to calculate permittivity of non-magnetic materials.

References

[1] J. Baker-Jarvis, "Transmission/Reflection and Short-Circuit Line Permittivity Measurements", NIST Tech note 1341, National Institute of Standards and Technology, July 1990.

[2] D. K. Ghodgaonkar et al, "A Free Space Method for Measurement of Dielectric Constants and Loss Tangents at Microwave Frequencies", *IEEE Trans. Instrum. Meas.*, Vol. 37, n3, pp789 – 793, June 1989.

[3] W. B. Weir, "Automatic Measurement of Complex Dielectric Constant and Permeability at Microwave Frequencies", *Proc. IEEE*, Vol. 62, n 1, pp 33 – 36, Jan 1974.

[4] U. Kaatze, "Complex Permittivity of Water as a function of Frequency and Temperature", *J. Chem. Eng. Data*, Vol. 34, n4, pp 371 – 374, 1989.

The following poster was presented at the Monash University Electrical and Computer Systems Engineering Postgraduate Student Research Forum in September 2002.

Improved free space microwave permittivity measurements

Andrew Amiet

Supervisor: Dr. Greg Cambrell Associate supervisor: Dr Peter Jewsbury (DSTO)

Introduction

Measurement of permittivity and permeability of materials in the microwave band can be performed in free space. It is a very effective non destructive method but the absence of an enclosed waveguide leads to some serious errors if the measurement is not carefully performed. Researchers have been using the technique for many years but a thorough investigation of the sources of errors, together with their resolution has not been performed. It is more difficult to calibrate a free space system because of the absence of appropriate standards. Errors can occur from stray reflections, diffraction if the sample is not sufficiently large, near-field effects, sample positioning and flatness, and destructive interference effects.

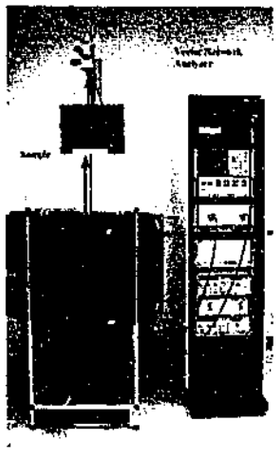

The technique involves measuring the reflection and/or transmission from a sample over the frequency range 1 to 40 GHz. The sample is placed between two microwave horn antennas as shown on the left. A vector network analyzer controls the frequency generation and data collection, the information is then sent to a PC for analysis. The network analyzer measures S-parameters, which are related to the permittivity (ε) and permeability (μ) by the formulas below.

Reflection

$$S_{11} = \frac{(1-T^2)\Gamma}{1-T^2\Gamma^2}$$

Transmission

$$S_{21} = \frac{(1-\Gamma^2)T}{1-T^2\Gamma^2}$$

where

$$\Gamma = \frac{\sqrt{\frac{\mu_r}{\varepsilon_r}}-1}{\sqrt{\frac{\mu_r}{\varepsilon_r}}+1}$$

and

$$T = \exp\left[-i\left(\frac{\omega}{c}\right)d\sqrt{\mu_r\varepsilon_r}\right]$$

d = thickness of sample, c = speed of light, ω = angular frequency

Removing errors involved with the technique

Reflection effects

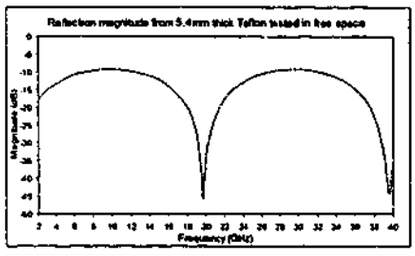

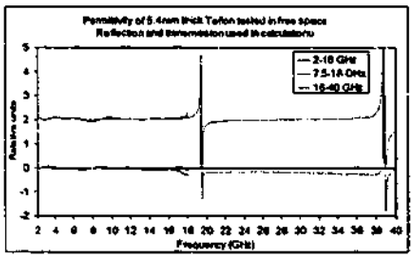

Destructive interference is common when measuring the reflection from a sample. When the microwave radiation encounters the dielectric sample under test, some is reflected from the surface and some is transmitted into the material, reflects back again from the rear of the sample and destructively interferes with the return reflection. The measured reflection from a 5.4mm thick sample of Teflon is shown in the upper left figure. When the permittivity is calculated using the formulas above using both reflected and transmitted data, the trace shows spikes at destructive interference frequencies, seen on the lower left figure. However since the permeability is known be equal to that of free space, the formulas above can be rearranged to remove S_{11} and use only the transmitted signal to extract permittivity. The equation used to extract permittivity is shown below, note that an iterative technique is used to extract the solution.

$$\varepsilon = S_{21}\left\{\varepsilon\cos\left[\frac{d\omega\sqrt{\varepsilon}}{c}\right] + i\sqrt{\frac{\varepsilon}{4}}(1+\varepsilon)\sin\left[\frac{d\omega\sqrt{\varepsilon}}{c}\right]\right\}$$

The effect of using transmission data alone can be seen in the graphs on the right. The real permittivity of Teflon is 2.04 ± 0.02 with the imaginary component being very close to zero. The transmission only technique is very effective in removing the sharp spikes.

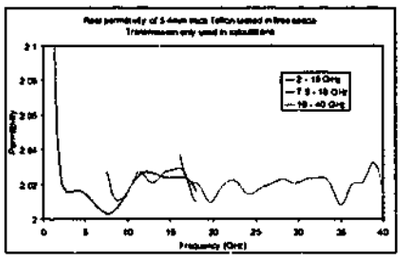

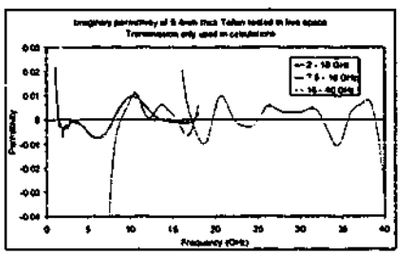

Time gating

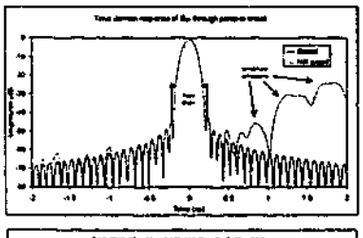

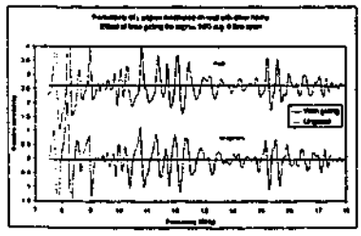

Stray reflections will always occur when measuring in free space, no matter how well the area is shielded or covered in absorbing foam. Reflections from inside the horns, the specimen holder and walls, together with multiple reflection paths from the sample to horns all add to the signal received by the horns. However some of these reflections can be removed using time gating, which involves performing a Chirp-Z transform on the frequency data, isolating the peak of interest in the time domain then converting back to the frequency domain having effectively removed all the stray peaks. The time domain trace can be seen on the upper left figure showing the effect of gating, the effect on permittivity is seen on the lower figure.

Diffraction removal

The technique assumes the sample is infinite in size ie. the only signal received by the horns travels through the sample. However real samples have a finite size, and if the horns have a wide enough spread or are a sufficient distance away from the sample then some of the wave can diffract around it and be collected by the receive horn. The diffracted wave can be measured by placing a metal plate with the same size and shape as the sample under test between the horns. The diffracted signal can be removed easily on the computer, the results of this shown in the figures to the right. Measurements of imaginary permittivity of a lossy sample with the receive horn at three locations are shown, with distance increasing as the configuration number. The lower figure shows result with diffraction removed.

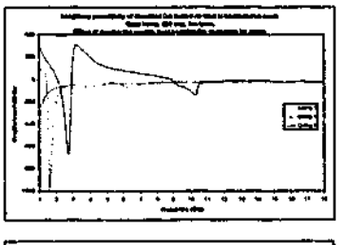

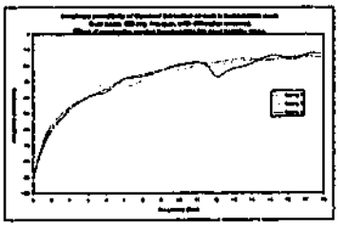

Electrical and Computer Systems Engineering
Postgraduate Student Research Forum 2002

MONASH UNIVERSITY